

THE JOURNAL OF PHYSICAL CHEMISTRY

(Registered in U. S. Patent Office)

CONTENTS

Frederick M. Fowkes: Ideal Two-Dimensional Solutions. II. A New Isotherm for Soluble and "Gaseous" Monolayers.....	385	phoretic Contribution to the Conductance of 1-1 Electrolytes.....	477
David Fleischer and Henry Freiser: The Heats of Solution of Nickel and Copper Dimethylglyoximes.....	389	J. R. Anderson and B. G. Baker: The Adsorption of Xenon and Hydrogen on Evaporated Films of Tungsten and Nickel.....	482
R. H. Valentine, G. E. Brodale, and W. F. Giauque: Trifluoromethane: Entropy, Low Temperature Heat Capacity, Heats of Fusion and Vaporization, and Vapor Pressure.....	392	Wayne E. Bell, M. Tagami, and Ulrich Merten: The Rhodium-Chlorine System at High Temperature.....	490
W. H. Slabaugh and B. C. Seiler: Interactions of Ammonia with Graphite Oxide.....	396	Leonard I. Katzin and Elsie Gulyas: Effects of Electrolytes on Rotatory Dispersion of Aqueous Tartrate Solutions.....	494
E. J. Burrell, Jr.: The Reactions of Nitric Oxide in Irradiated Cyclohexane.....	401	J. F. Shultz, L. J. E. Hofer, F. S. Karn, and R. B. Anderson: Studies of the Fischer-Tropsch Synthesis. Prepoisoning of Iron Catalysts by Sulfur Compounds.....	501
Stanley R. Sandler, Samuel Loshak, Edward Broderick, and K. C. Tsou: 1,3,5-Triaryl-2-pyrazolines as Wave Length Shifters in Scintillator Plastics.....	404	R. A. Robinson and R. H. Stokes: Activity Coefficients of Mannitol and Potassium Chloride in Mixed Aqueous Solutions at 25°.....	506
E. R. Zabolotny and H. Gesser: The Reaction of Active Nitrogen with Ammonia at -196°.....	408	M. H. Lietzke and R. W. Stoughton: The Calculation of Activity Coefficients from Osmotic Coefficient Data.....	508
Robert S. Hansen: Thermodynamics of Interfaces between Condensed Phases.....	410	Donald Graham: Activation of Metal Hydrogenation Catalysts by Irradiation.....	510
Ted B. Flanagan: The Effects of Reactor Irradiation upon the Subsequent Thermal Decomposition of Lead Styphnate.....	416	James W. Whalen: Heats of Immersion. II. Silica-Benzene and Silica-Cyclohexane.....	511
Bruno Reitzner, J. V. Richard Kaufman, and Eugene F. Bartell: Thermal Decomposition of Silver-Coated α -Lead Azide.....	421	David A. Ratkowsky and Joseph L. McCarthy: Spectrophotometric Evaluation of Activity Coefficients in Aqueous Solutions of Sulfur Dioxide.....	516
D. L. Leussing and Jerrold Jayne: Mononuclear and Polynuclear Complex Formation between Iron(II) and 2,3-Dimercapto-1-propanol.....	426	J. M. Austin and A. D. Mair: The Standard Enthalpy of Formation of Complex Sulfate Ions in Water. I. HSO_4^- , LiSO_4 , NaSO_4	519
A. O. McDougall and F. A. Long: Relative Hydrogen Bonding of Deuterium. II. Acid Ionization Constants in H_2O and D_2O	429	Alvin S. Gordon and S. Ruven Smith: A Study of the Photolysis of Cyclohexane and Acetone. I. Some Reactions of the Cyclohexyl Radical.....	521
Leonidas Petrakis: Lattice Energy and Stability of Chromium Monohalides.....	433	Shu-Sing Chang and Edgar F. Westrum, Jr.: Heat Capacities and Thermodynamic Properties of Globular Molecules. III. Two Methyl-Substituted Polytetraadamantanes.....	524
George F. Crable and Gerard L. Kearns: Effects of Substituent Groups on the Ionization Potentials of Benzenes.....	433	Richard W. Ramette, Edward A. Dratz, and Preston W. Kelly: Acid-Base Equilibria of Methyl Red.....	527
R. A. Matheson: The Conductances of Dilute Aqueous Cadmium Perchlorate Solutions at 25°.....	439	Harold S. Johnston and Julian Hecklen: Tunneling Corrections for Unsymmetrical Eckart Potential Energy Barriers.....	532
E. H. Appelman and J. C. Sullivan: Kinetics of the Vanadium(III)-Neptunium(V) Reaction in Perchlorate Solutions.....	442	John E. Gordon and S. L. Johnson: Ionization Constant of 2,2'-Dihydroxybiphenyl in Light and Heavy Water.....	534
Dan Meyerstein and Avner Treinin: The Relation between Lyotropic and Spectroscopic Properties of Anions in Solution.....	446	Richard B. De Mallie, Jr., Meyer H. Birnboim, J. E. Frederick, N. W. Tschoegl, and John D. Ferry: Viscoelastic Properties of Dilute Polystyrene Solutions and Verification of the Zimm Theory.....	536
I. E. Den Besten, P. G. Fox, and P. W. Selwood: The Mechanism of Chemisorption: Carbon Monoxide and Carbon Dioxide on Nickel.....	450	Max T. Rogers and James C. Woodbrey: A Proton Magnetic Resonance Study of Hindered Internal Rotation in Some Substituted N,N-Dimethylamides.....	540
G. Blauer and H. Linschitz: Flash-Excitation of Acridine Orange in Acidic and Basic Solvents.....	453		
William R. Ware: Oxygen Quenching of Fluorescence in Solution: An Experimental Study of the Diffusion Process.....	455	NOTES	
R. J. Gledhill: Particle-Size Distribution Determination by Turbidimetry.....	458	Harold J. Wimette and Robert H. Linnell: Thermodynamics of H-Bonding Pyrrole-Pyridines.....	546
R. C. Giberson: Oxygen Diffusion and Reaction during γ -Irradiation of Polyethylene.....	463	Martin E. Everhard and Paul M. Gross, Jr.: Solubilities of Some Strong Electrolytes in the Hydrogen Peroxide-Water System. II. Rubidium and Cesium Nitrates.....	548
H. R. Lukens, Jr., R. G. Meisenheimer, and J. N. Wilson: An Isotopic Exchange Method for Measuring the Surface Area of Supported Transition Metal Sulfides.....	469	David J. Keri and James L. Dye: The Transference Number and Activity Coefficient of Tris(ethylenediamine)-Cobalt(III) Chloride in Water at 25°.....	550
Gideon Czapski and Harold A. Schwarz: The Nature of the Reducing Radical in Water Radiolysis.....	471	H. A. Woodbury, H. Eyring, and A. F. Gabrysh: Thermoluminescence of Golden Sapphire and Fused Borax Seeded with Ni, Mg, and UO_3	551
W. C. Perkins and W. S. Koski: N^{15} -Labeled Products from C^{12} (d,n) Reactions in Alcohols.....	474	J. D. McKinley: Translational Energy Accommodation in the Nickel-Chlorine Surface Reaction.....	554
David J. Keri and James L. Dye: The Effect of the Exponential Distribution Function on the Electro-			

Contents continued on inside front cover

THE JOURNAL OF PHYSICAL CHEMISTRY

(Registered in U. S. Patent Office)

W. ALBERT NOYES, JR., EDITOR

ALLEN D. BLISS

ASSISTANT EDITORS

A. B. F. DUNCAN

EDITORIAL BOARD

A. O. ALLEN
C. E. H. BAWN
J. BIGEISEN
F. S. DAINTON

D. D. ELEY
D. H. EVERETT
S. C. LIND
F. A. LONG

J. P. McCULLOUGH
K. J. MYSELS
J. E. RICCI
R. E. RUNDLE

W. H. STOCKMAYER
E. R. VAN ARTSDALEN
M. B. WALLENSTEIN
W. WEST

Published monthly by the American Chemical Society at 20th and Northampton Sts., Easton, Pa. Second-class postage paid at Easton, Pa.

The *Journal of Physical Chemistry* is devoted to the publication of selected symposia in the broad field of physical chemistry and to other contributed papers.

Manuscripts originating in the British Isles, Europe and Africa should be sent to F. C. Tompkins, The Faraday Society, 6 Gray's Inn Square, London W. C. 1, England.

Manuscripts originating elsewhere should be sent to W. Albert Noyes, Jr., Department of Chemistry, University of Rochester, Rochester 20, N. Y.

Correspondence regarding accepted copy, proofs, and reprints should be directed to Assistant Editor, Allen D. Bliss, Department of Chemistry, Simmons College, 300 The Fenway, Boston 15, Mass.

Advertising Office: Reinhold Publishing Corporation, 430 Park Avenue, New York 22, N. Y.

Articles must be submitted in duplicate, typed, and double spaced. They should have at the beginning a brief Abstract, in no case exceeding 300 words. Original drawings should accompany the manuscript. Lettering at the sides of graphs (black on white or blue) may be pencilled in and will be typeset. Figures and tables should be held to a minimum consistent with adequate presentation of information. Photographs will not be printed on glossy paper except by special arrangement. All footnotes and references to the literature should be numbered consecutively and placed in the manuscript at the proper places. Initials of authors referred to in citations should be given. Nomenclature should conform to that used in *Chemical Abstracts*, mathematical characters be marked for italic, Greek letters carefully made or annotated, and subscripts and superscripts clearly shown. Articles should be written as briefly as possible consistent with clarity and should avoid historical background unnecessary for specialists.

Remittances and orders for subscriptions and for single copies, notices of changes of address and new professional

connections, and claims for missing numbers should be sent to the Subscription Service Department, American Chemical Society, 1155 Sixteenth St., N. W., Washington 6, D. C. Changes of address for the *Journal of Physical Chemistry* must be received on or before the 30th of the preceding month. Please include an old address label with the notification.

Claims for missing numbers will not be allowed (1) if received more than sixty days from date of issue (because of delivery hazards, no claims can be honored from subscribers in Central Europe, Asia, or Pacific Islands other than Hawaii), (2) if loss was due to failure of notice of change of address to be received before the date specified in the preceding paragraph, or (3) if the reason for the claim is "missing from files."

Subscription rates (1962): members of American Chemical Society, \$12.00 for 1 year; to non-members, \$24.00 for 1 year. Postage to countries in the Pan-American Union \$0.80; Canada, \$0.40; all other countries, \$1.20. Single copies, current volume, \$2.50; foreign postage, \$0.15; Canadian postage \$0.10; Pan-American Union, \$0.10. Back volumes (Vol. 56-65) \$30.00 per volume; foreign postage, per volume \$1.20, Canadian, \$0.40; Pan-American Union, \$0.80. Single copies: back issues, \$3.00; for current year, \$2.50; postage, single copies: foreign, \$0.15; Canadian, \$0.10; Pan-American Union, \$0.10.

The American Chemical Society and the Editors of the *Journal of Physical Chemistry* assume no responsibility for the statements and opinions advanced by contributors to THIS JOURNAL.

The American Chemical Society also publishes *Journal of the American Chemical Society*, *Chemical Abstracts*, *Industrial and Engineering Chemistry*, *International Edition of Industrial and Engineering Chemistry*, *Chemical and Engineering News*, *Analytical Chemistry*, *Journal of Agricultural and Food Chemistry*, *Journal of Organic Chemistry*, *Journal of Chemical and Engineering Data*, *Chemical Reviews*, *Chemical Titles*, *Journal of Chemical Documentation*, *Journal of Medicinal and Pharmaceutical Chemistry*, *Inorganic Chemistry*, *Biochemistry*, and *CA — Biochemical Sections*. Rates on request.

Alexander D. Kirk and Gerald B. Porter: Kinetics of Excited Molecules. III. Photooxidation of Acetone.....	556	Irwin H. Billick: The Variation of the Sedimentation Coefficient with Pressure and Concentration.....	565
I. M. Hoodless and J. A. Morrison: Ionic Transport and the Crystallographic Transition in Cesium Chloride.....	557	Rimantas Glemza and R. J. Kokes: Transient Species in Oxygen Take-up by Zinc Oxide.....	566
Mikio Tamura, Hiroshi Hada, Junpei Noguchi, and Soichi Hayashi: Infrared Spectra of Some Photographic Stabilizers Adsorbed on Silver Bromide.....	559	John H. Birely and John P. Chesick: The Kinetics of the Thermal Decomposition of [2,2,1]Bicycloheptadiene..	568
George V. D. Tiers and Donald R. Hotchkiss: Proton N.m.r. Spectroscopy. XIV. Accurate Measurement of the Spectral Position of the Formyl Peak of <i>p</i> -Anisaldehyde, Useful for Checking the Calibration of N.m.r. Spectrometers.....	560	Harold Jacobson: Preparation and Properties of a Variable Charge Ion-Exchange Membrane.....	570
Donald R. Scott and Jean B. Allison: Solvent Glasses for Low Temperature Spectroscopic Studies.....	561	A. S. Dworkin, H. R. Bronstein, and M. A. Bredig: Miscibility of Metals with Salts. VI. Lithium-Lithium Halide Systems.....	572
Asish Kumar Chandra: Ultraviolet Absorption Spectra of <i>o</i> -, <i>m</i> -, and <i>p</i> -Nitrobenzoic Acids.....	562	Ryoichi Fujishiro and J. H. Hildebrand: The Liquid-Liquid Solubility of Cyclohexane and Perfluorotri- <i>n</i> -butylamine at 25°.....	573
Ulrich Gonser: Recoil-Free γ -Ray Transition of Fe ⁵⁷ in the Blood Component Hemin.....	564	C. W. Diggias, Jr. and R. J. Bolen: Ultracentrifugal Determination of the Micellar Character of Non-ionic Detergent Solutions. III.....	574
		A. J. Ahearn and C. D. Thurmond: Mass Spectrographic Detection of Molecular Species in Group III-V Compounds.....	575

THE JOURNAL OF PHYSICAL CHEMISTRY

(Registered in U. S. Patent Office) (© Copyright, 1962, by the American Chemical Society)

VOLUME 66

MARCH 20, 1962

NUMBER 3

IDEAL TWO-DIMENSIONAL SOLUTIONS. II. A NEW ISOTHERM FOR SOLUBLE AND "GASEOUS" MONOLAYERS

BY FREDERICK M. FOWKES

Shell Development Company, Emeryville, California and Martinez Research Laboratory, Shell Oil Company, Martinez, California

Received April 24, 1961

The concept that the adsorbed monolayers on binary solutions act like an ideal two-dimensional solution has been extended to monolayers of soluble detergents and "gaseous" monolayers of substances insoluble in the substrate. In these monolayers water molecules in the surface layer are the solvent and the film pressure can be calculated as a direct result of water molecules crowding into the monolayer (or two-dimensional solution) because of a decrease in their chemical potential resulting from dilution by the surface-active molecules. From these principles a new isotherm is derived which fits pressure-area relations better than the "gas" equations, is more accurate for measuring molecular weights, and represents quantitatively the pressure-area relations for soluble detergents.

Several previous investigators of the surface tension of binary solutions have found it useful to consider the surface layer as a separate phase one molecule deep in which the composition is related to the two-dimensional tension in the same manner as the equilibrium pressure in an osmometer is related to the composition of the solution inside the membrane.¹⁻⁶ However, these examples were confined to binary systems of small molecules, such as ethanol and water. More recently the author has shown that this treatment gives quantitative relations of film pressure to mole fraction for two component monolayers on aqueous solutions of synthetic detergents with a second surface-active component.^{7,8} It is now to be shown that the film pressure on aqueous solutions of detergents (or even of very slightly soluble surface-active materials) can be related quantitatively to the mole fraction of water in the monolayer.

Theory.—The notation is the same as was used in Part I of this series.⁸ Let us consider a dilute solution of surface-active substance 1 in water 2.

(1) J. A. V. Butler, *Proc. Roy. Soc. (London)*, **A135**, 348 (1932).

(2) J. E. Verschaffelt, *Bull. classe sci., Acad. roy. Belg.*, **22**, 373, 390, 402 (1936).

(3) A. Schuchowitzky, *Acta Physicochim. U.R.S.S.*, **19**, 176, 508 (1944).

(4) J. W. Belton and M. G. Evans, *Trans. Faraday Soc.*, **41**, 1 (1945).

(5) E. A. Guggenheim, *ibid.*, **41**, 150 (1945).

(6) R. Defay and I. Prigogine, *J. Chem. Phys.*, **43**, 217 (1946).

(7) W. M. Sawyer and F. M. Fowkes, *J. Phys. Chem.*, **62**, 159 (1958).

(8) F. M. Fowkes, *ibid.*, **65**, 355 (1961).

At equilibrium, any change in the free energy of the water in the bulk phase ($kT d \ln c_2 f_2$) must equal that in the surface phase at equilibrium

$$kT d \ln c_2 f_2 = kT d \ln x_2 \phi_2 - \sigma_2 d \gamma \quad (1)$$

where c_2 and f_2 are the mole fraction and activity coefficient of the solvent (water) in the bulk, x_2 and ϕ_2 are the mole fraction and activity coefficient for the surface phase, σ_2 is the partial molecular area of the solvent in the surface film, and γ is the surface tension of the solution. Here $\sigma_2 = (\partial A / \partial n_2)_{n_1}$, where A is the total surface of the system and n_1 and n_2 are the number of molecules of solute 1 and solvent 2 in the monomolecular surface phase of area A .

Equations of State for "Gaseous" Monolayers.—

It has been customary to describe very dilute insoluble monolayers on aqueous substrates as "gaseous" because the area of surface per molecule of film-forming substance, A_1 , is such that πA_1 approaches kT at infinite dilution. The parallel has been drawn to ideal gases and it has been inferred that the pressure π is the result of collisions between molecules of the film. However, it is far more appropriate to compare dilute monolayers with a solution in an osmometer with an osmotic pressure Π , where ΠV_1 approaches kT at infinite dilution (V_1 is the volume of solution containing one molecule of solute).

In the case of an osmometer containing a solution of component 1 in solvent 2 in which molecules of the solute are localized by means of a semi-permeable membrane but the molecules of solute are

free to diffuse through the membrane, equilibration of solvent between the solution and pure solvent outside the membrane is governed by the reduction in chemical potential of the solvent in the solution, which reduces the rate of diffusion from the solution so that there is a preponderance of diffusion into the solution from the pure solvent beyond the membrane. Because of mechanical confinement, this penetration of more solvent into the solution section of the osmometer causes a rise in pressure (Π) in that section, which raises the partial molar free energy, G_2 . At equilibrium

$$dG_2 = kT d \ln c_2 f_2 + v_2 d\Pi = 0$$

where c_2 is the mole fraction of solvent in the solution, f_2 is the *pressure-independent* activity coefficient, and v_2 is the partial molecular volume of the solvent in the solution. It can be shown easily that at infinite dilution the above equation approaches in the limit

$$\Pi V_1 \doteq kT$$

In the case of a dilute monolayer on the surface of water in which the molecules of the surface-active solute 1 are solvated by water molecules 2, the surface layer behaves like a two-dimensional solution in which the solute molecules are localized by adsorption and sometimes also by insolubility. However, the solvent molecules are free to diffuse in and out of this surface layer. The solute, being concentrated in the surface, preferentially lowers the chemical potential of the water in the surface layer so that the preponderance of diffusion of water is into the surface layer and the surface film pressure (π) rises. The relation of film pressure to mole fraction of water in the surface layer (x_2) is given by equation 1. The term $kT d \ln c_2 f_2$ generally is negligibly small with the dilute solutions usually considered; consequently

$$kT d \ln x_2 \phi_2 + \sigma_2 d\pi = 0 \quad (2)$$

and the film pressure is obtained by integration

$$\pi = \frac{-kT}{\bar{\sigma}_2} \ln x_2 \phi_2, \text{ where } \bar{\sigma}_2 = \frac{\int_0^\pi \sigma_2 d\pi}{\pi} \quad (3)$$

For water σ_2 is virtually independent of film pressure, so that σ_2 (9.7 \AA^2) may be used for $\bar{\sigma}_2$. Since ϕ_2 is usually unity^{3,7,8} film pressures of soluble monolayers are calculable as

$$\pi = \frac{-kT}{\sigma_2} \ln x_2 \quad (4)$$

The value of x_2 is easily calculated from known values of σ_1 and σ_2 for each value of A_1 (the total surface A divided by n_1 , the number of molecules of component 1 in it). For water, σ_2 is invariably 9.7 \AA^2 , and for each surface-active solute there appears to be just one value of σ_1 (e.g., 26 \AA^2 for sodium dodecyl sulfate) which applied over the entire range of film pressures. This is not entirely expected, but is demonstrated in examples to follow and in the first paper of this series.⁸ For sodium dodecyl sulfate films (on salt solutions), $x_2 = 0.50$ at $A_1 = 35.7 \text{ \AA}^2$, 0.75 at 55.1 \AA^2 , 0.90 at 113.3 \AA^2 , etc. The corresponding film pressures at 25° , calculated from equation 4, are 29.3, 12.2, and 4.5 dynes/cm. Thus a complete π - A_1 isotherm can be

calculated for surface active solutes on water once σ_1 is known.

The above thermodynamic equation is far more accurate than the previously used "gas" equations. This is obvious from the steps needed to derive the "gas" equations from equation 4, by a procedure analogous to that used to derive the limiting form of the osmotic pressure equation ($\Pi V_1 = kT$) from the exact equation. For a binary solution film $\ln x_2 = \ln(1 - x_1)$. We may approximate $\ln(1 - x_1)$ by only the first term ($-x_1$) in the series expansion; this is a close approximation only when x_1 is very small. This approximation should not be used for π - A_1 isotherms at high pressures, for the error is generally about $\pi\%$ (1% at 1 dyne/cm., 10% at 10 dynes/cm., but rising to 40% error at 30 dynes/cm.). The above approximation results in

$$\pi = \frac{kT}{\bar{\sigma}_2} x_1 = \frac{kT n_1}{\bar{\sigma}_2(n_1 + n_2)} \text{ (approx.)} \quad (5)$$

Since

$$\frac{(n_1 + n_2) \bar{\sigma}_2}{n_1} = (\bar{\sigma}_2 - \bar{\sigma}_1) + \frac{n_1 \sigma_1 + n_2 \sigma_2}{n_1} = A_1 - (\sigma_1 - \sigma_2)$$

$$\pi[A_1 - (\sigma_1 - \sigma_2)] = kT \text{ (approx.)} \quad (6)$$

Variations of equation 6 have been widely used. For extremely dilute monolayers, $(\sigma_1 - \sigma_2)$ becomes negligibly small with respect to A_1 and $\pi A_1 \doteq kT$. However, this equation is of little value for finite values of π . For protein monolayers Bull⁹ and others¹⁰ have used the substitution $Nm/M = n_1$ (where N is Avogadro's number, m the mass of material spread on surface area A , and M the molecular weight) to give

$$\pi A = \frac{mRT}{M} + \frac{\pi Nm}{M} (\sigma_1 - \sigma_2) \text{ (approx.)} \quad (7)$$

A graph of πA vs. π gives a straight line with an intercept from which M is calculable and a slope from which $\sigma_1 - \sigma_2$ is calculable. When used with large molecules (proteins) the further approximation of ignoring σ_2 is quite justified. The extension of equation 6 to high pressures is clearly unjustified, and to ignore σ_2 when σ_1 is small is also incorrect. Thus, the use of equations such as¹¹

$$\pi(A_1 - \sigma_1) = kT \text{ (very approx.)}$$

for ionized monolayers at high pressures is to be avoided.

New Equation of State for "Gaseous" or Soluble Monolayers.—Spread monolayers may be "insoluble" in an aqueous substrate for the practical purpose of manipulating with a film balance and yet up to some limiting film pressure be soluble in the surface layer, as indicated by the transition from "gaseous" film to a more condensed phase. This transition has been clearly discussed by Ter Minassian-Saraga and Prigogine.¹² The greater solubility in the monolayer is illustrated by myristic acid at 20° , which shows ideal two-dimensional solution behavior up to a mole fraction of 7×10^{-3} , but is soluble in the bulk phase only up to $1.6 \times$

(9) H. B. Bull, *J. Biol. Chem.*, **185**, 27 (1950).

(10) E. Mischuck and F. Eirich in "Monomolecular Layers," Ed. by H. Sobotka, A.A.A.S., Washington, D. C., 1954.

(11) I. Langmuir, *J. Chem. Phys.*, **1**, 756 (1933).

(12) L. Ter Minassian-Saraga and I. Prigogine, *Mem. des services chim de l'etat*, **38**, 109 (1953).

10^{-6} . It appears that the activity coefficient for the water in the monolayer (ϕ_2) is unity up to this transition point, and at higher pressures, when only a more condensed phase is present, ϕ_2 is very large.

If an unknown substance is spread as a dilute monolayer under conditions that ϕ_2 is unity, its molecular weight and σ_1 may be determined with a graph of A vs. n_2/n_1 as shown in Fig. 1. The relationship of n_2/n_1 to π is calculated from equation 4 and is the same for all (except polymer) monolayers on a given substrate. It is obvious that

$$A = n_1 A_1 = n_1 \bar{\sigma}_2 \left(\frac{n_2}{n_1} \right) + n_1 \sigma_1 \quad (8)$$

so that a graph of A/m (area per mg. of film) vs. n_2/n_1 has a slope of $n_1 \bar{\sigma}_2/m$, from which the molecular weight can be determined, and the intercept is $n_1 \sigma_1/m$, from which σ_1 may be calculated. The data of Mischuck and Eirich¹⁰ for egg albumen on 2.6 M ammonium sulfate are plotted in Fig. 1 using $\bar{\sigma}_2 = 9.7 \text{ \AA}^2$. The slope gives M , the molecular weight (41,500) and a molecular area (σ_1) of 9900 \AA^2 . Tightest hexagonal packing of these molecules with a peripheral line of water molecules separating them would require n_2/n_1 to equal 50. Actually the change in slope from single molecules to more aggregated species appears to take place at about 60 molecules of water per molecule of albumen, as judged by the deviation of points from the straight line in Fig. 1.

The proposed method of plotting is easier to use in that the molecular weight is obtained from a slope rather than from a difficult extrapolation of a steep line to an intercept near the origin.¹³ Moreover there is only one approximation used, the assumption of ideal solution behavior ($\phi_2 = 1$). Furthermore, the additional information concerning n_2/n_1 is of value for it indicates the maximum film pressures at which the solute molecules actually can be separated by solvent molecules (0.7 dynes/cm. in the example cited).

Extension to Concentrated Soluble Monolayers.

—In the case of monolayers of fatty acids the surface-solution region does not extend beyond pressures of about 0.1 dyne/cm., and with protein monolayers on concentrated salt solutions the surface-solution region extends to about 0.5 dyne/cm. However, in the case of water-soluble detergents the surface layers are soluble in water at nearly all film pressures. Consequently, all the arguments and the equation of state for dilute monolayers apply for most of the pressure-area curves.

Figure 2 shows the pressure-area relation for sodium dodecyl sulfate (SDS) at 20 and 25°, using data from the literature¹⁴⁻¹⁶ obtained by Gibbs adsorption equation and surface tension measurements. In Fig. 2, the data are plotted according to the equation

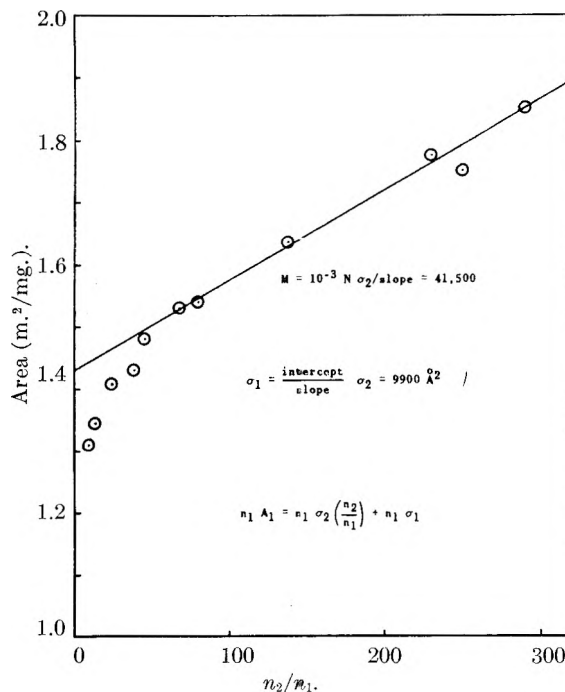


Fig. 1.—Data of Mischuck and Eirich¹⁰ for "gaseous" monolayers of egg albumen on 2.6 M ammonium sulfate plotted according to equation 3.

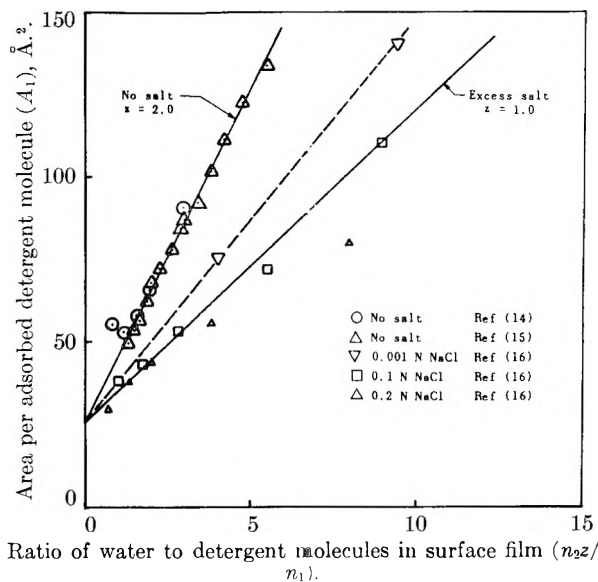


Fig. 2.—Solutions of sodium dodecyl sulfate, with and without salt. Test of proposed isotherm: $A_1 = \sigma_1 + \sigma_2 z [e^{-\pi \sigma_2/kT} / (1 - e^{-\pi \sigma_2/kT})]$.

$$A_1 = \sigma_1 + \left(\frac{n_2}{n_1 z} \right) z \sigma_2 \quad (9)$$

where z is the number of particles per molecule of SDS. If the surface solute is dissociated into z particles, this must be taken into account in using x_2 , the mole fraction of water molecules. Since equation 4 relates x_2 to π without any assumption regarding the kind of solute particles, the ratio $x_2/(1 - x_2) = n_2/n_1 z$, where n_1 is the total number of solute molecules (associated and undissociated). We may write $n_2/n_1 z$ as an exponential expression

$$\frac{n_2}{n_1 z} = \frac{x_2}{1 - x_2} = \frac{e^{-\pi \sigma_1/kT}}{1 - e^{-\pi \sigma_1/kT}} \quad (10)$$

(13) A. J. G. Allan and A. E. Alexander, *Trans. Faraday Soc.*, **50**, 863 (1954).

(14) A. P. Brady and A. G. Brown, in "Monomolecular Layers" (ref. 10).

(15) E. J. Clayfield and Matthews, "Proc. III Intern. Congr. Surface Activity," Butterworths, London, 1957, Vol. I, p. 172.

(16) E. Matijevic and B. A. Pethica *Trans. Faraday Soc.*, **54**, 1382 (1958).

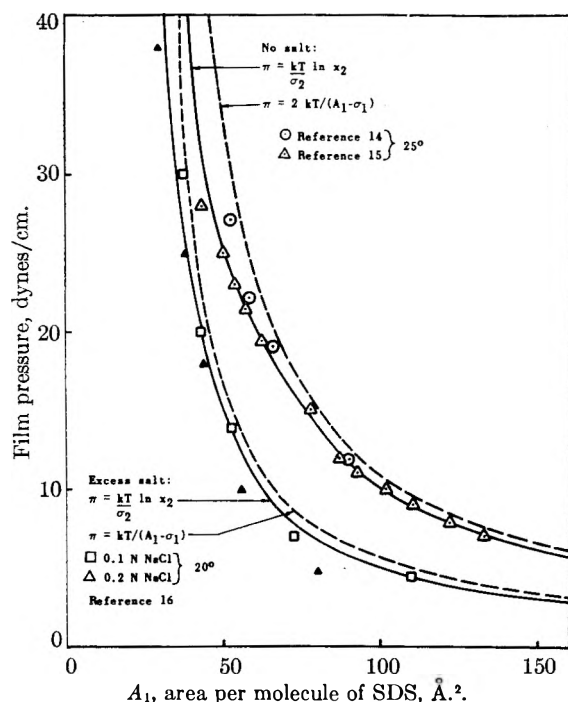


Fig. 3.—Equations of state for soluble monolayers of sodium dodecyl sulfate in the presence and absence of salt. The first eq. in both cases should read $\pi = -(kT/\sigma_2) \ln x_2$.

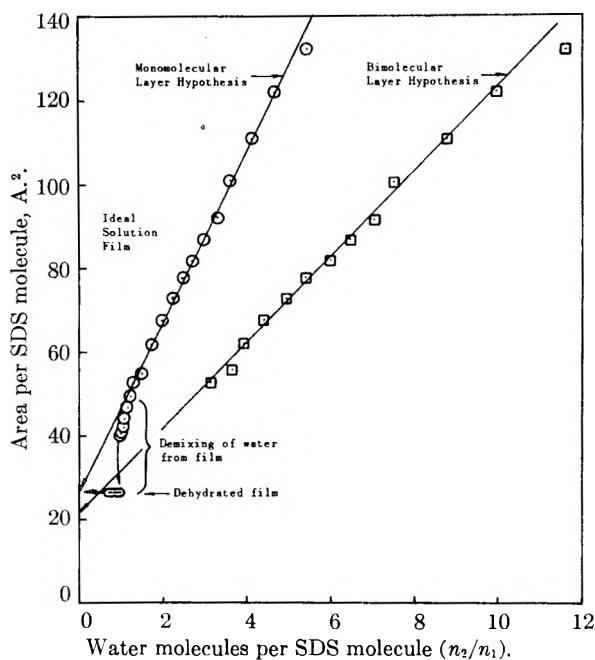


Fig. 4.—Ideal solution isotherms for sodium dodecyl sulfate adsorbed on the surface of water (ref. 15), calculated for water layers one or two molecules in depth.

The data in Fig. 2 show the effect of salt on the value of z , which is 2.0 on salt-free substrates and decreases to 1.0 with increase in salt content of the substrate. The data of Clayfield and Matthews¹⁵ were especially useful for the salt-free solutions because time-effects were taken into account better than with other studies without salt. It is obvious that these data fit equation 9 very well and the intercept at $\sigma_1 = 26 \text{ \AA}^2$ of both lines helps confirm the validity of applying the ideal two-dimensional

solution equations to soluble monolayers in the region of high film pressures. Note that σ_1 is constant over the whole pressure-area isotherm.

Figure 3 shows the same data and isotherms plotted in the customary fashion and compares them with the "gas" equations. It is obvious that the proposed ideal two-dimensional solution equations not only have a better theoretical basis than "gas" equations, but fit the data far better. At larger areas per molecule the "gas" equation gives values of A_1 which are too large by the value of σ_2 (9.7 \AA^2) as discussed earlier. However, the error in the linear approximation of $\ln x_2$ becomes quite a bit larger at high film pressures.

The main point is that concentrated soluble monolayers at high film pressures act as ideal two-dimensional solutions and that pressure-area curves for such systems may be calculated accurately using the ideal solution equations.

Some soluble monolayers have been studied by adding so much salt to the substrate that they become insoluble.¹⁷ The pressure-area isotherms, when plotted as in Fig. 2, give z -values of a few tenths. This is taken to indicate that the high salt content has so reduced the activity of water in the surface layer that it thereby has promoted the formation of dimers, trimers, and higher aggregates in the monolayer as part of the salting-out process.

Other Soluble Monolayers.—Payens¹⁸ has presented some pressure-area curves for soluble monolayers of *n*-octylamine on aqueous substrates. The data obtained on a substrate of 0.2 *M* acetate buffer at pH 6 with 1 *M* NaCl give a straight line plot according to equation 9 with a z -value of 1.0 because of the high ionic strength. The intercept gives $\sigma_1 = 20 \text{ \AA}^2$. The data for a film of the same material on a substrate of 0.2 *M* acetate buffer at pH 6 without added salt gave the same intercept and a z -value of 1.5, indicating partial conversion of the amine to octylammonium acetate. With a weaker buffer and lower pH, z should become as large as 2.0.

Data obtained on substrates other than water require a value of σ_2 for the molecular area of the solvent molecules. In the case of water and propylene carbonate¹⁹ the two-thirds power of the molecular volume (9.7 and 30 \AA^2 , respectively) has proved adequate. Jarvis and Zisman¹⁹ have measured the pressure-area isotherm for some fluorochemicals adsorbed at the surface of their solutions in polar organic solvents. One such pair is bis-(ϕ' -butyl) 3-methylglutarate in propylene carbonate. The plot of the pressure area data as A_1 vs. n_2/n_1 gives a straight line with an intercept of $\sigma_1 = 35 \text{ \AA}^2$ and a surprisingly small slope (15 \AA^2). This slope means either that σ_2 is really only half the estimated 30 \AA^2 or that there is a z -value of 0.5, indicating that this solute is associated as dimers on the surface of the propylene carbonate. Dimerization of this solute is not expected but appears more reasonable than $\sigma_2 = 15 \text{ \AA}^2$.

Depth of the Surface Phase.—The calculations of mole fraction of water in the surface solution

(17) B. A. Pethica, *Trans. Faraday Soc.*, **50**, 413 (1954).

(18) Th. A. J. Payens, *Philips Research Repts.*, **10**, 425 (1955).

(19) N. L. Jarvis and W. A. Zisman, *J. Phys. Chem.*, **64**, 157 (1960).

of monolayers all have been made by assuming that only the surface layer of water molecules is involved in the surface solutions. However, since water molecules are very small and have strong cohesive forces, it appears possible that two or more layers of water molecules could be involved in surface solutions. In the case of solutions of sodium dodecyl sulfate, where the partial molecular area σ_1 of 26 Å.² includes a contribution of the cation as well as the sulfate group, we calculate a mole fraction x_2 of 0.33 at 36 Å.². However, if two layers of water molecules were involved in surface solutions, x_2 would be 0.50; at the same time the partial molecular surface area σ_2 would be reduced to 4.85 instead of 9.7 Å.². The two effects do not quite cancel out, as is shown in Fig. 4, which makes use of the data of Clayfield and Matthews¹⁵ for salt-free solutions of sodium dodecyl sulfate (SDS) at 25°. Here the ratio of water to detergent molecules in the surface solution (n_2/n_1) was calculated (from the measured film pressure) for two cases: water layers one molecule deep or two molecules deep. The experimental slopes ($\sigma_2 = 10.0$ Å.², $\sigma_2/2 = 5.05$ Å.²) agree with theory ($\sigma_2 = 9.7$ Å.², $\sigma_2/2 = 4.85$ Å.²), but the intercepts are signifi-

cantly different and only the intercept for the monomolecular layer fits the experimental data. The intercept gives σ_1 , the partial molecular area of the solute; in the monomolecular layer calculation σ_1 is 26–27 Å.², while in the bimolecular layer calculation σ_1 is 21–22 Å.². Since it already is known that σ_1 for dehydrated monolayers (on salt solutions¹⁷) is 26–27.5 Å.², it appears entirely justified to use the monomolecular layer calculation.

In Fig. 4 the monomolecular layer plot includes (in the lower left corner) Clayfield and Matthews data at pressures over 25 dynes/cm., where the ratio of water molecules to detergent molecules approaches 1:1. It is most interesting to see that at this ratio there is a sharp transition from an ideal solution monolayer to a dehydrated monolayer (in which $A_1 = \sigma_1$). The five measurements of $A_1 = 26.3$ Å.² in this region agree well with the 26–27.5 Å.² found on salt solutions.

Acknowledgment.—The section on depth of the surface phase was inspired by the helpful criticism of Professor N. K. Adam. The advice of Dr. W. A. Zisman in revision of the manuscript is gratefully acknowledged.

THE HEATS OF SOLUTION OF NICKEL AND COPPER DIMETHYLGLYOXIMES¹

BY DAVID FLEISCHER AND HENRY FREISER²

Department of Chemistry, University of Pittsburgh, Pittsburgh 13, Pennsylvania

Received July 18, 1961

The solubilities of nickel and copper dimethylglyoximes have been determined as a function of temperature in a series of solvents. The differences in the derived heats of solution indicate that solvation effects are more important than the difference in crystal energies in determining the relative solubility of these two compounds in water, and that the crystal form of the copper compound is more stable than the crystal form of the nickel compound. The postulated nickel–nickel bond in the solid chelate would seem to be very weak.

The specificity of dimethylglyoxime for nickel(II) has been shown to be a result of a solubility effect, as copper(II) dimethylglyoxime has a larger formation constant than the less stable nickel(II) chelate.³ When comparing the solubilities of a compound there are two energy terms to be considered: the relative crystal energies and the relative energies of solvation of the species in solution. In order to examine the solubility difference of copper(II) and nickel(II) dimethylglyoximes in terms of these two energies, the heats of solution of these complexes have been determined, from the temperature dependence of the solubility, in water, chloroform, benzene, and *n*-heptane.

Experimental

Apparatus.—The solutions were contained in a double-walled glass vessel and were mixed with a magnetic stirrer. Water, maintained at constant temperature, was circulated through the vessel jacket. The vessel was sealed with a standard taper joint held in place by a metal screw clamp.

(1) Taken in part from the Ph.D. dissertation of David Fleischer, August, 1958.

(2) Department of Chemistry, University of Arizona, Tucson 25, Arizona.

(3) R. G. Charles and H. Freiser, *Anal. Chim. Acta*, **11**, 101 (1954).

A capillary tube, sealed through this joint, terminated at the bottom of the vessel in a fine glass frit. The other end of the capillary terminated in a small outer standard-taper joint to which could be fitted a short capillary take-off tube or a heated pipet.

The pipet was so constructed that its tip consisted of only the necessary inner standard taper joint. The rest of the pipet was wrapped with resistance wire and insulated with asbestos. The pipet was kept at a constant temperature by maintaining a specific voltage across its resistance.

The photometric measurements were made using a Beckman Model DU spectrophotometer. A Model E Leeds and Northrup polarograph was used for the polarographic measurements. The polarograph cell was of the conventional H-type, using a saturated calomel half cell with an agar bridge supported by a glass frit.

Reagents.—Both nickel(II) and copper(II) dimethylglyoximes were prepared from a 2:1 mole ratio of 0.1 *M* ethanolic dimethylglyoxime and reagent grade nitrate salts of the metals. The metal salts were prepared as 0.001 *M* water solutions, to which was added the alcoholic dimethylglyoxime solution. It was necessary to evaporate the copper(II) dimethylglyoxime solution before precipitation occurred. The preparation of the copper compound was very sensitive to excesses of either component, and an amorphous solid, instead of crystals, resulted unless exactly stoichiometric amounts were used. The analysis of the copper(II) dimethylglyoxime crystals gave these percentages:

	C	N	H
Calcd.:	32.7	19.1	4.8
Found:	32.9	19.1	4.8

The reagent grade chloroform was dried over sodium sulfate. Benzene, thiophene-free as determined by the isatin test, was distilled and dried over metallic sodium. The *n*-heptane was distilled and dried over metallic sodium.

Reagent grade hydroxylamine hydrochloride was obtained from Fisher Scientific Co. The 2,9-dimethyl-1,10-phenanthroline (neocuproine) was obtained from the G. F. Smith Chemical Co.

The standard metal solutions were prepared from reagent grade nitrates. The nickel nitrate solution was standardized gravimetrically with dimethylglyoxime, and the copper nitrate solution was standardized by electrodeposition.

The hydrochloric acid was distilled from stock acid by the method of Foulk and Hollingsworth.⁴

Procedure.—At each temperature, maintained within $\pm 0.05^\circ$, the first sample was withdrawn at approximately 18 hr. Subsequent samples withdrawn at 24-hr. intervals gave the same concentration, within experimental error, as did the first one.

After the highest experimental temperature was reached, some of the solubilities were redetermined as the temperature was lowered. The values obtained by approaching equilibrium from both directions agreed within the experimental error.

a. Solubility in Water.—Aliquots of standard nickel solution were diluted to 100 ml. and 5 ml. of saturated ammoniacal dimethylglyoxime was added. The solution then was extracted with 5 ml. of chloroform and the absorbance determined at 375 $m\mu$. Extraction was complete as determined by examination of a second portion of chloroform.

The experimental solution was prepared by adding an excess of nickel(II) dimethylglyoxime and of dimethylglyoxime to a 0.05 *M* ammonium acetate buffer of pH 6.9. Sandell⁵ has determined that the solubility is constant over the pH range 5.6–8.9. The 100-ml. samples were collected in the heated pipet. This was maintained at 50°, which was 5° above the highest temperature used. The samples were extracted with 5 ml. of chloroform and the absorbance determined at 375 $m\mu$.

The calibration samples for the copper solutions were prepared by adding 5 ml. of 1 *M* sulfuric acid and 0.1 ml. of Triton X-100,⁶ a maximum suppressor, to 5-ml. aliquots of standard copper solution. The concentrations were determined polarographically and a linear relationship between concentration and diffusion current was observed.

The solubility of copper(II) dimethylglyoxime was determined in the same chemical environment as was used for nickel(II) dimethylglyoxime. Five ml. of solution was collected at a very slow rate, to allow the solution to come to room temperature, in a 10-ml. volumetric flask to which 5 ml. of 1 *M* sulfuric acid had been added previously. After addition of 0.1 ml. of maximum suppressor the concentration of copper was determined as above.

b. Solubility in Chloroform.—The calibration curves described in (a) were used. Aliquots of the nickel(II) dimethylglyoxime solution were placed in volumetric flasks to which had been added previously aliquots of pure chloroform. After mixing, the absorbance was determined at 375 $m\mu$.

Ten ml. of copper(II) dimethylglyoxime solution was collected in a 25-ml. volumetric flask to which had been added previously 15 ml. of 0.5 *M* sulfuric acid. After extraction and addition of maximum suppressor the copper was determined polarographically.

c. Solubility in Benzene.—The absorption of the nickel(II) dimethylglyoxime solution was measured at 375 and 329 $m\mu$. Quantitative dilutions of the sample indicated that the 329 $m\mu$ band obeyed Beer's law. Since the absorptivity at this wave length is larger than that for the 375 $m\mu$ band, the absorbance at 329 $m\mu$ was used to establish the relative concentration of the samples. The actual concentrations were determined by comparison with the concentra-

tion of the 25° sample, which was found polarographically in the following manner.

A calibration curve was prepared by adding 5-ml. aliquots of standard nickel solutions to 5 ml. of 1 *M* distilled hydrochloric acid. The resultant solution was taken almost to dryness in a 25-ml. flask. After dilution to volume with a solution 0.5 *M* in pyridine and 1 *M* in potassium chloride the concentration of nickel was determined polarographically. A linear relationship was found between the diffusion current and the concentration.

To find the concentration of the 25° solubility sample, a 10-ml. aliquot of the benzene solution was extracted with 5 ml. of 1 *M* distilled hydrochloric acid. After the acid layer was evaporated almost to dryness, the solution was diluted to the mark with the potassium chloride-pyridine solution, and the nickel concentration was determined polarographically as above.

The calibration curve for copper was established by evaporating 5-ml. aliquots of standard solutions, almost to dryness, in a 10-ml. volumetric flask. The solution was taken to the mark with 1 *M* hydrochloric acid. After addition of 0.1 ml. Triton X-100 the copper was determined polarographically. A linear relationship was found between the diffusion current and the copper concentration.

The experimental solutions were analyzed in the following manner: Fifty-ml. aliquots of solution were collected in a volumetric flask and transferred to a separatory funnel. The flask was rinsed with 5 ml. of 1 *M* hydrochloric acid and several portions of distilled water which also were added to the separatory funnel. After extraction the acid layer was transferred to a 10-ml. volumetric flask and taken almost to dryness. The solution was taken to the mark with 1 *M* hydrochloric acid and 0.1 ml. maximum suppressor added.

d. Solubility in *n*-Heptane.—The calibration curve for nickel is described in (a).

The experimental solutions were analyzed in the following manner: Aliquots of the nickel(II) dimethylglyoxime solution were collected in volumetric flasks and transferred to a separatory funnel. To the aqueous layer was added 1 ml. of an ammoniacal solution of dimethylglyoxime and 5 ml. of chloroform. After extraction the absorbance was determined at 329 $m\mu$.

The calibration curve for copper was determined by adding 5 ml. of 10 w./v. % hydroxylamine hydrochloride and 4 ml. of 0.1 w./v. % neocuproine in absolute ethanol to aliquots of standard solution.⁷ The copper complex was extracted with 15 ml. of chloroform which then was brought to 30 ml. with ethanol. The absorbance was determined at 457 $m\mu$ in 10-cm. cells. A linear relationship between concentration and absorbance was found.

The experimental solutions were analyzed in the following manner: Portions of the copper(II) dimethylglyoxime solution were weighed into a separatory funnel and extracted with 10 ml. of 1 *M* hydrochloric acid. To the acid layer were added the same quantities of reagents as were used for the calibration determinations. After the solution was brought to a pH of 4–7 with ammonium hydroxide, it was extracted with 15 ml. of chloroform and the organic layer was diluted to 30 ml. with ethanol.

Discussion

The necessary experimental condition for separating differences in crystal energy from differences in solvation energy is to find a solvent in which the heats of solvation of both species are equal. The closer the chemical compositions and structures of two compounds are, the closer this condition can be approached.

The molecular structure of both nickel(II)⁸ and copper(II) dimethylglyoximes⁹ have been deduced from X-ray crystallographic measurements. In both complexes the central metal atom is bonded to four nitrogen atoms and hydrogen bridges exist between the glyoxime oxygen atoms of the two ligand molecules. Both the glyoxime hydroxyl

(4) I. M. Kolthoff and E. B. Sandell, "Textbook of Quantitative Inorganic Analysis," The Macmillan Co., New York, N. Y., 1952.

(5) H. Christopherson and E. B. Sandell, *Anal. Chim. Acta*, **10**, 1 (1954).

(6) Rohm and Haas Co., Philadelphia, Pennsylvania.

(7) A. R. Gahler, *Anal. Chem.*, **26**, 577 (1954).

(8) L. E. Godycki and R. E. Rundle, *Acta Cryst.*, **6**, 487 (1953).

(9) E. Frasson, R. Bardi, and S. Bezzi, *ibid.*, **12**, 201 (1959).

Solubility in water		
$t, ^\circ\text{C.}$	NiDx_2 $S \times 10^3$ (moles/l.)	CuDx_2
10.0		$568 \pm 0\%$ (2) ^a
15.0		579 (1)
20.0		$568 \pm 0\%$ (2)
25.0	$0.105 \pm 9\%$ ¹⁰ (4) ^a	$568 \pm 0\%$ (2)
30.0	$.139 \pm 4\%$ (3)	
35.0	$.184 \pm 2\%$ (3)	
40.0	$.240 \pm 2\%$ (4)	
45.0	$.307 \pm 2\%$ (3)	

^a Number of determinations.

Solubility in chloroform		
$t, ^\circ\text{C.}$	NiDx_2 $S \times 10^4$ (moles/l.)	CuDx_2
10.4	$3.03 \pm 1\%$ (2) ^a	
15.0	$3.40 \pm 0.2\%$ (4)	$11.5 \pm 1\%$ (3) ^a
20.0	$3.88 \pm .7\%$ (5)	$12.0 \pm 0\%$ (4)
25.0	$4.62 \pm .6\%$ (6)	$12.4 \pm 0\%$ (2)
30.0		$12.9 \pm 2\%$ (3)

Solubility in benzene		
$t, ^\circ\text{C.}$	NiDx_2 $S \times 10^5$ (moles/l.)	CuDx_2
20.0	$6.02 \pm 1\%$ (3) ^a	
25.0	$7.53 \pm 1\%$ (4)	$4.1 \pm 2\%$ (3) ^a
30.0	$8.88 \pm 0.5\%$ (2)	$6.1 \pm 2\%$ (3)
35.0	$11.21 \pm 1\%$ (4)	$7.8 \pm 1\%$ (5)
40.0		$10.1 \pm 2\%$ (2)

Solubility in <i>n</i> -heptane		
$t, ^\circ\text{C.}$	NiDx_2 $S \times 10^7$ (moles/l.)	CuDx_2
25.0	2.5^b	1.84^b
30.0	$3.67 \pm 6\%$ (5) ^a	
35.0	$5.72 \pm 3\%$ (2)	
40.0	$8.36 \pm 3\%$ (2)	
45.0	$11.2 \pm 2\%$ (3)	$11.8 \pm 1\%$ (4) ^a
50.0	$14.3 \pm 3\%$ (3)	$15.8 \pm 3\%$ (5)
60.0		$36.4 \pm 3\%$ (4)

Thermodynamic quantities at 25°

Solvent	Solute	ΔH° (kcal.)	ΔS° (e.u.)
H_2O	NiDx_2^c	9.0	30.2
	CuDx_2^d	0.0	0
CHCl_3	NiDx_2	4.8	16.1
	CuDx_2	1.3	4.4
C_6H_6	NiDx_2	6.6	22.2
	CuDx_2	10.0	33.6
C_7H_{16}	NiDx_2	14.8	49.7
	CuDx_2	16.6	55.6

^a Number of determinations. ^b Extrapolated value. ^c NiDx_2 —nickel(II) dimethylglyoxime. ^d CuDx_2 —copper(II) dimethylglyoxime.

groups in the nickel complex are joined by hydrogen bridges approximately 2.40 Å. long (O—O distance), which are the shortest yet determined.¹¹ The corresponding hydrogen bridges in the copper chelate are weaker, having O—O distances of 2.53 and 2.70 Å.⁹ The difference in the two hydrogen bridges in the copper chelate is attributed to the fact that one of the oxygens is coordinated to the copper atom in the adjacent molecule forming a dimer.

(10) Sandell, ref. 5, finds 0.097×10^{-5} .

(11) D. E. Williams, G. Woblawer, and R. E. Rundle, *J. Am. Chem. Soc.*, **81**, 755 (1959).

In both chelate molecules the internal hydrogen bonds would seem to be preserved in solution. Several investigators have found nickel(II) dimethylglyoxime to be unreactive with several reagents specific for active hydrogen.¹²⁻¹⁴ The most reactive of these reagents methylmagnesium iodide, was found to be unreactive with copper(II) dimethylglyoxime.¹⁵ This chemical evidence, with the physical evidence given above, would seem to establish conclusively that nickel(II) and copper(II) dimethylglyoximes have, at least in organic solution, identical structures.

Although the molecular units of these two chelates have apparently the same structure in organic solution, their crystal lattices are entirely different. The molecules of the nickel compound form an orthorhombic crystal with the nickel atoms stacked one above the other. In the monoclinic copper(II) dimethylglyoxime crystal the copper atoms alternate about a vertical axis with the organic part of adjacent layers interposed between them.

This difference in crystal structures has led to the suggestion that the solubility difference between these two chelates results from a greater crystal stability of the nickel chelate imparted by a nickel-to-nickel bond.¹¹ The structural measurements show this proposed bond to be 3.24 Å. long. When this distance is compared to a bond length of 2.30 Å., calculated from covalent radii,¹⁶ the discrepancy of 0.94 Å. seems to be rather large. The energy of this proposed bond has been estimated to be 10 kcal.,¹⁷ but the method was not indicated.

This argument for the Ni—Ni bond also has been supported by the solubility difference between nickel(II) dimethylglyoxime and nickel(II) ethylmethylglyoxime in water.¹⁸ The substitution of the ethyl group increases the C-side of the crystal, which increases the Ni—Ni distance and also increases the solubility. However, the solubilities of a series of *vic*-dioximes reported in a recent paper were found to restrict this conclusion,¹⁹ since no correlation was found between the measured Ni—Ni bond lengths and the solubilities of the respective compounds unless the nature of the ligands compared was very similar. In addition, nickel(II) diamminoglyoxime was found to have a crystal structure incompatible with Ni—Ni bonds, yet its solubilities in the same solvents as were employed with nickel(II) dimethylglyoxime were so small as to be immeasurable. Such comparisons among chelates having different organic residues cannot lead to valid conclusions concerning crystal energy, since changes in the organic residue would affect the solvation energy and it would seem that an expansion of the crystal would raise its energy regardless of the existence of a metal-to-metal bond.

(12) L. Tschugaeff, *J. Chem. Soc.*, **105**, 2192 (1914).

(13) M. F. Barker, *Chem. News*, **130**, 99 (1925).

(14) D. L. Brady and M. M. Muers, *J. Chem. Soc.*, 1599 (1930).

(15) M. Turpak, University of Pittsburgh, private communication.

(16) T. Moeller, "Inorganic Chemistry," John Wiley and Sons, Inc., New York, N. Y., 1952.

(17) R. E. Rundle, *J. Am. Chem. Soc.*, **76**, 3101 (1954).

(18) A. G. Sharpe and D. B. Wakefield, *J. Chem. Soc.*, 281 (1957).

(19) C. V. Banks and D. W. Barnum, *J. Am. Chem. Soc.*, **80**, 3579 (1958).

Without postulating the reasons for the difference in crystal energies, it would seem possible, in view of the close similarity of structure of nickel(II) and copper(II) dimethylglyoximes, to evaluate this difference by comparing their heats of solution in an appropriately chosen solvent. The solvent of choice would be one in which solvation effects would be absent. The trend observed in the experimental data indicates that this condition has been closely approached. Comparing the standard entropy changes for both chelates in water, chloroform, benzene, and heptane, it is seen that ΔS_2^0 becomes increasingly more positive. This quantity represents the entropy of fusion plus the entropy change on going from the ideal to the real solution. Since the latter term can be only zero or negative, the more positive ΔS_2^0 is, the more nearly ideal the solution, and the increasing order indicates a decreasing order of solvent-solute interaction for these chelates. Furthermore, it is seen that the quantity $\Delta(\Delta H^0) = \Delta H_{Ni}^0 - \Delta H_{Cu}^0$ decreases going from water to chloroform solution, while $\Delta(\Delta H^0)$ for benzene and heptane, -3.4 and -1.8 kcal., respectively, are equal within experimental error. Regardless of any specific solute-solvent interactions in other solvents, it is difficult to imagine any significant difference in solvation for nickel(II) and copper(II) dimethylglyoximes in such inert solvents as these two hydrocarbons. The fact that copper(II) dimethylglyoxime exhibits a significantly smaller endothermic heat of solution than the nickel chelate in both water and chloroform reflects metal-solvent interaction in keeping with the known ability of copper

to exhibit a coordination number higher than four.²⁰⁻²³

In this connection it is interesting to note that the authors found that addition of *n*-butylamine to an aqueous solution of the copper chelate permitted its quantitative extraction into chloroform, whereas a much smaller effect was observed with the nickel chelate.

An alternative explanation could be advanced in terms of a difference in ability to engage in intermolecular hydrogen bonding. There is, however, no additional evidence indicating that the copper complex would have more ability to participate in such interactions with water and chloroform than the nickel complex.

It is concluded that, although the sources of the differences are not apparent, crystalline copper(II) dimethylglyoxime is more stable by about 3 kcal. than crystalline nickel(II) dimethylglyoxime; also that the difference in hydration energies between these two compounds is more important than their difference in crystal energies in determining their relative solubilities in water. If a nickel to nickel bond does exist in the solid, it would have to be extremely weak.

Acknowledgment.—The authors gratefully acknowledge the financial assistance of the U. S. Atomic Energy Commission.

(20) J. Bjerrum and E. J. Nielson, *Acta Chem. Scand.*, **2**, 297 (1948).

(21) R. M. Keefer, *J. Am. Chem. Soc.*, **68**, 2329 (1946).

(22) H. B. Jonassen and J. R. Oliver, *ibid.*, **80**, 2347 (1958).

(23) H. A. Laitinen, E. I. Onstott, J. C. Bailar, Jr., and S. Swann, *Jr.*, *ibid.*, **71**, 1550 (1949).

TRIFLUOROMETHANE: ENTROPY, LOW TEMPERATURE HEAT CAPACITY, HEATS OF FUSION AND VAPORIZATION, AND VAPOR PRESSURE¹

BY R. H. VALENTINE, G. E. BRODALE, AND W. F. GIAUQUE

Low Temperature Laboratory, Departments of Chemistry and Chemical Engineering, University of California, Berkeley, Cal.

Received July 31, 1961

The heat capacity of trifluoromethane has been measured from 15°K. to its boiling point. The measured values of the heat of fusion and melting point were found to be 970 cal. mole⁻¹ and 117.97°K. The heat of vaporization was 3994 cal. mole⁻¹ at the boiling point, which was determined as 190.97°K. The vapor pressure of the liquid has been measured over the range 145 to 191°K. The vapor pressure of solid and liquid has been represented by an equation combining the $(F^0 - H_0^0)/T$ function with an expression for gas imperfection. A table of calculated values of vapor pressure is given for both solid and liquid. The triple point pressure was calculated to be 0.046 cm. The heat of sublimation at the absolute zero, $\Delta H_0^0 = 6013.5$ cal. mole⁻¹. The entropy of the ideal gas was evaluated from the experimental measurements as 57.18 gbs. mole⁻¹ at 190.97°K. and 1 atm. The corresponding value calculated from molecular data is 57.23 gbs. mole⁻¹ at 298.15°K., $S^0 = 62.05$ gbs. mole⁻¹, compared to 62.00 experimental. Tables of C_p^0 , S^0 , $(F^0 - H_0^0)/T$, and $(H^0 - H_0^0)/T$ are given for solid, liquid, and gas. It is pointed out that CHF₃ is so easily purified in a fractionating column, and its melting point so constant with the fraction melted, that it would be useful to compare it with a gas thermometer as a temperature standard.

This paper describes a low temperature calorimetric investigation of fluoroform, CHF₃, for the purpose of determining its entropy. The boiling points of the series CH₄, CH₃F, CH₂F₂, CHF₃, CF₄ rise in a very marked maximum at CH₂F₂, with reasonably smooth intermediate values for CH₃F and CHF₃. CH₂F₂ could form two hydrogen

bonds, whereas CH₃F and CHF₃ could form only one each, which would be in line with the above boiling point order.

The tetrahedral molecule perchloryl fluoride, ClO₃F, has been found to have residual entropy² due to exchange of atomic positions. While this effect did not seem likely to occur in the present

(1) This work was supported in part by the National Science Foundation.

(2) J. K. Koehler and W. F. Giauque, *J. Am. Chem. Soc.*, **80**, 2659 (1958).

case, especially in view of the low freezing point, there was at least a possibility of some disorder, such as the 2% detected in one crystalline form of carbonyl chloride.³ We did not, of course, consider that the energy change involved would correspond to the breaking of a possibly weak hydrogen bond but rather the difference in energy between a hydrogen bond made in either of two very similar situations. However, the measurements have shown that the crystal approaches zero entropy at limiting low temperatures.

Calorimetric Apparatus and Temperature Scale.—The measurements were made in Gold Calorimeter V.⁴ A gold resistance thermometer-heater was used for precision in temperature measurements and standard copper-constantan thermocouple No. 102 was used as a temperature reference. The thermocouple was checked at the triple and boiling points of hydrogen, and the triple point of nitrogen, by condensing these substances within the calorimeter. The thermocouple was in agreement at the triple point (63.15°K.) of nitrogen, and required a correction of about -0.08° at the triple point (13.94°K.) and -0.06 at the boiling point (20.36°K.) of hydrogen. 0°C. was taken as 273.15°K.

One defined calorie was taken as 4.1840 absolute joules.

Sample of Trifluoromethane.—The trifluoromethane was a 3-lb. lot of 98% pure material obtained from the Matheson Co. It was distilled in a vacuum jacketed, silvered, low temperature helices filled fractionating column² at a reflux ratio of about 200:1. The distillation pressure was about 55 cm. A 191.557-g. (*in vacuo*) sample was selected from the middle fraction and condensed into the calorimeter.

The heat capacity curve below the melting point, while rising rapidly, gave no indication of premelting and we infer that the sample contained less than one part in one hundred thousand on a molal basis of liquid soluble-solid insoluble impurity. This probably is to be expected in the case of such a low boiling liquid with properties considerably different from those of likely impurities.

Heat Capacity Measurements.—The heat capacity measurements are given in Table I. The

TABLE I

HEAT CAPACITY OF TRIFLUOROMETHANE

$0^\circ\text{C} = 273.15^\circ\text{K.}$, mol. wt. $\text{CHF}_3 = 70.018$, 2.73582 moles in the calorimeter; heat capacity in gibbs mole⁻¹ = defined cal. deg.⁻¹ mole⁻¹

T_{av} , °K.	$C_{meas.}$	T_{av} , °K.	$C_{meas.}$	T_{av} , °K.	$C_{meas.}$
Series I					
15.37	1.91	67.79	11.54	102.10	14.56
16.76	2.40	73.97	12.07	105.63	14.99
19.10	3.10	80.44	12.61	108.24	15.33
22.00	3.92	86.80	13.12		
24.28	4.65	92.57	13.64	122.73	20.25
28.13	5.70	97.85	14.11	129.82	20.10
30.39	6.24	102.73	14.60	137.93	20.02
33.29	6.90	107.27	15.19	146.32	20.00
36.25	7.54	111.29	15.78	154.60	20.02
39.32	8.07	115.02 ^a	16.21	163.29	20.08
42.62	8.65			171.95	20.20
46.57	9.24	80.97	12.58	180.82	20.37
50.99	9.81	89.01	13.27	189.33	20.59
56.00	10.42	93.33	13.69		
61.72	11.18	97.87	14.13		
Series II					
Series III					

^a Resistance thermometer temporarily strained. Heat capacity calculated from thermocouple.

observations were continuous in the sense that each run began where the previous one ended, thus there were no unobserved regions. An almost trivial correction to the measured heat capacity,

(3) W. F. Giauque and J. B. Ott, *J. Am. Chem. Soc.*, **82**, 2089 (1960).
 (4) J. B. Ott and W. F. Giauque, *ibid.*, **82**, 1308 (1960).

under saturation pressure, was made on the results for liquid fluoroform in computing the smoothed values of C_p which are given later.

The Melting Point and Heat of Fusion of Trifluoromethane.—The melting point was observed as a function of the fraction melted. There was essentially no change. Trifluoromethane appears to be so easily purified that it would make a good temperature reference if it were compared directly with a gas thermometer. Other desirable characteristics in this connection are that it is non-flammable, non-toxic, and can be readily condensed into suitable pressure vessels for storage or transportation.

The melting point observations are given in Table II. The resistance thermometer gave very high precision, demonstrating the constancy of the melting point to 0.001° , however, the resistance thermometer was calibrated in terms of the standard thermocouple and the temperature given is $\pm 0.05^\circ$ in an absolute sense.

TABLE II
MELTING POINT OF TRIFLUOROMETHANE
 $0^\circ\text{C.} = 273.15^\circ\text{K.}$

Time, min.	% Melted	T , °K., resistance thermometer
0	Heat added	
39	3	117.970
59	Heat added	
71	12	117.971
119	Heat added	
214	49	117.971
354	49	117.971
1394	49	117.971
Accepted value		117.97 \pm 0.05°K.

The heat of fusion was determined in the usual manner of starting heat input below the melting point and ending above it, with appropriate corrections for the $\int C_p dT$. The data are given in Table III.

TABLE III
HEAT OF FUSION OF TRIFLUOROMETHANE
Cal. mole⁻¹, triple point = 117.97°K.

T_1 , °K.	T_2 , °K.	Total heat input (cor.)	$\int C_p dT$	ΔH
116.806	121.472	1061.7	89.1	973
117.149	122.990	1083.2	115.8	967
117.079	120.884	1043.0	74.3	969
				Av. 970 \pm 3

Heat of Vaporization of Trifluoromethane.—The method used for measuring the heat of vaporization was essentially that described earlier,⁵ except that the 5-l. bulb which accepted the gas at constant pressure was not thermostated or calibrated. The amount of fluoroform was determined later by condensation in a stainless steel pressure vessel. The amounts of about 0.1 mole were determined to 0.02%. The weighings were corrected for the buoyancy of the weights. The heats of vaporization were measured within about 0.2° of the boiling point and an appropriate correction was made. The results are given in Table IV.

(5) W. F. Giauque and H. L. Johnston, *ibid.*, **51**, 2300 (1929).

TABLE IV

HEAT OF VAPORIZATION OF TRIFLUOROMETHANE
Cal. mole⁻¹, boiling point = 190.97°K.

Moles evap.	Time of heat input, min.	ΔH
0.11399	30	3993.5
.11215	34	3992.8
.08612	34	3995.5
		Av. 3994 ± 4

Thermodynamic Properties of Solid and Liquid Trifluoromethane.—The thermodynamic properties of solid and liquid trifluoromethane are given in Table V. The extrapolation below 15°K. could be done only by recognizing Einstein contributions to the heat capacity in the region 15–30°K. in addition to the expected Debye term. The properties of the gas are given in Table VI. The moments of inertia were taken from Bernstein and Herzberg.⁶ $I_{A^{\circ}} = I_{B^{\circ}} = 81.08 \times 10^{-40}$, $I_{C^{\circ}} = 148.67 \times 10^{-40}$ g. cm.². The fundamental frequencies were taken from Plyler and Benedict.⁷ The values used were 507(2), 700(1), 1150(1), 1152(2), 1372(2), and 3031(1).

Values of the thermodynamic properties of the gas at higher temperatures are given at 100° intervals to 1500°K. by Gelles and Pitzer.⁸

TABLE V

THERMODYNAMIC PROPERTIES OF SOLID AND LIQUID TRIFLUOROMETHANE IN GIBBS MOLE⁻¹
1 gbs. = 1 defined cal. deg.⁻¹

T, °K.	C_p°	S°	$-(F^{\circ} - H_0^{\circ})/T$	$(H^{\circ} - H_0^{\circ})/T$
15	2.601	0.668	0.174	0.494
20	3.370	1.400	.384	1.016
25	4.870	2.315	.676	1.639
30	6.146	3.320	1.033	2.287
35	7.268	4.354	1.433	2.921
40	8.229	5.389	1.860	3.529
45	9.012	6.405	2.309	4.096
50	9.697	7.390	2.768	4.622
55	10.309	8.344	3.232	5.112
60	10.854	9.265	3.697	5.568
70	11.750	11.008	4.618	6.390
80	12.541	12.629	5.519	7.110
90	13.390	14.154	6.395	7.759
100	14.331	15.613	7.244	8.369
110	15.583	17.034	8.070	8.964
117.97	16.853	18.167	8.714	9.453
liquid				
117.97	20.410	26.389	8.714	17.675
120	20.340	26.737	9.012	17.725
130	20.094	28.354	10.442	17.912
140	20.016	29.839	11.775	18.064
150	20.005	31.219	13.026	18.193
160	20.049	32.512	14.204	18.308
170	20.176	33.730	15.317	18.413
180	20.369	34.889	16.372	18.517
190	20.632	35.997	17.376	18.621
190.97	20.662	36.102	17.471	18.631

TABLE VI

THERMODYNAMIC PROPERTIES OF TRIFLUOROMETHANE GAS
IN GIBBS MOLE⁻¹

T, °K.	C_p°	S°	$-(F^{\circ} - H_0^{\circ})/T$	$(H^{\circ} - H_0^{\circ})/T$
15	7.949	36.501	28.552	7.949
20	7.949	38.788	30.839	7.949
25	7.949	40.562	32.613	7.949
30	7.949	42.011	34.062	7.949
35	7.949	43.236	35.287	7.949
40	7.949	44.298	36.349	7.949
45	7.949	45.234	37.285	7.949
50	7.949	46.072	38.123	7.949
55	7.950	46.829	38.880	7.949
60	7.952	47.521	39.572	7.949
70	7.962	48.748	40.797	7.951
80	7.986	49.812	41.859	7.953
90	8.031	50.755	42.796	7.959
100	8.102	51.605	43.635	7.970
110	8.198	52.381	44.395	7.986
117.97	8.293	52.958	44.955	8.003
120	8.320	53.100	45.091	8.009
130	8.465	53.771	45.733	8.038
140	8.629	54.404	46.330	8.074
150	8.809	55.006	46.889	8.117
160	9.002	55.580	47.414	8.166
170	9.205	56.132	47.911	8.221
180	9.416	56.664	48.382	8.282
190	9.634	57.179	48.832	8.347
190.97	9.657	57.228	48.875	8.353
200	9.858	57.679	49.262	8.417
210	10.085	58.165	49.674	8.491
220	10.317	58.640	50.071	8.569
230	10.552	59.104	50.454	8.650
240	10.789	59.558	50.824	8.734
250	11.029	60.003	51.182	8.821
260	11.270	60.440	51.530	8.910
270	11.513	60.870	51.868	9.002
273.15	11.589	61.004	51.972	9.032
280	11.756	61.293	52.197	9.096
290	11.999	61.710	52.518	9.192
298.15	12.198	62.045	52.774	9.271
300	12.243	62.121	52.831	9.290
310	12.485	62.526	53.137	9.389
320	12.727	62.927	53.437	9.490
330	12.967	63.322	53.730	9.592
340	13.205	63.713	54.018	9.695
350	13.441	64.099	54.301	9.798
360	13.674	64.481	54.578	9.903
370	13.905	64.859	54.851	10.008
380	14.132	65.232	55.119	10.113
390	14.356	65.602	55.383	10.219
400	14.576	65.969	55.643	10.326
450	15.617	67.746	56.890	10.856
500	16.554	69.441	58.061	11.380

The Vapor Pressure and Gas Imperfection of Trifluoromethane.—The vapor pressure was measured from 145°K. to the boiling point. A cathetometer was used to compare a 16-mm. diameter mercury manometer with a standard meter bar.

Corrections were applied for the meniscus depression⁹ and also for the weight of the column of fluoroform in the tube leading to the calorimeter. g was taken as 979.973¹⁰

(6) H. J. Bernstein and G. Herzberg, *J. Chem. Phys.*, **16**, 30 (1948).(7) E. K. Plyler and W. S. Benedict, *J. Research Natl. Bur. Standards*, **47**, 202 (1951).(8) E. Gelles and K. S. Pitzer, *J. Am. Chem. Soc.*, **75**, 5259 (1953).(9) W. Cawood and H. S. Patterson, *Trans. Faraday Soc.*, **29**, 514 (1933).

(10) Landolt-Börnstein-Roth, "Physikalische-Chemische Tabellen," Verlag Julius Springer, Berlin, 1923.

for this location and $g_0 = 980.665 \text{ cm. sec.}^{-2}$. The density of mercury was taken from the I.C.T.¹¹

We have analyzed the vapor pressure data by a method which previously^{12,13} has been shown to be very sensitive in showing errors in such measurements. For pressures near or below one atmosphere Berthelot's equation may be written in the approximate form

$$PV = RT + bP/T^2 \quad (1)$$

$$\Delta F_0/T = -R \ln f/a_{(l)} = -R \ln P - b'P/T^3 - V_{(l)}(1 - P)/T \quad (2)$$

where b' (cal. deg.² atm.⁻¹ mole⁻¹) corresponds to b (cm.³ deg.² mole⁻¹), f represents the fugacity of the gas, and $a_{(l)}$ the activity of the liquid referred to the standard state at one atmosphere.

$$\frac{\Delta F_0}{T} = \left(\frac{F^0 - H_0^0}{T}\right)_{(g)} - \left(\frac{F^0 - H_0^0}{T}\right)_{(l)} + \frac{\Delta H_0^0}{T} \quad (3)$$

Let

$$\frac{\Delta H_0^0'}{T} = - \left(\frac{F^0 - H_0^0}{T}\right)_{(g)} + \left(\frac{F^0 - H_0^0}{T}\right)_{(l)} - R \ln P - \left(\frac{V_{(l)}(1 - P)}{T}\right) \quad (4)$$

where $\Delta H_0^0'$ is an approximate value of the heat of sublimation of trifluoromethane at the absolute zero, obtained by ignoring gas imperfection.

The values of $\Delta H_0^0'$ are plotted against P/T^2 , and the intercept should give the true $\Delta H_0^0'$ for sublimation at the absolute zero. The above plot is found to be a straight line, which gives a reasonable basis for the use of the form b/T^2 in estimating temperature coefficients for use in correcting entropy and heat content for gas imperfection.

The value of ΔH_0^0 was found to be 6013.5 cal. mole⁻¹ for the heat of sublimation at 0°K. $b' = -6.0 \times 10^5 \text{ cal. atm.}^{-1} \text{ deg.}^2 \text{ mole}^{-1}$.

There is another method of evaluating the second virial coefficient at the boiling point, where the heat of vaporization was measured

$$V_{(g)} = \frac{\Delta H}{T} \times \frac{dT}{dP} + V_{(l)} = \frac{RT}{P} + \frac{b}{T^2} \quad (5)$$

ΔH is the heat of vaporization

$\frac{dT}{dP}$ corresponds to the boiling point

$V_{(l)} = 48 \text{ cm.}^3$ estimated for CHF_3 at 190.97°K. (b.p.)

b' is found to be $-6.67 \times 10^5 \text{ cal. atm.}^{-1} \text{ deg.}^{-1} \text{ mole}^{-1}$

Although the above value $b' = -6.67 \times 10^5$ has less uncertainty in its evaluation, it depends on the assumed $1/T^2$ form. We prefer to use the value -6.0×10^5 obtained from the vapor pressure data, because it is more intimately connected with temperature coefficients, and the value of b which is obtained by that method will to some extent correct for an error in the assumed temperature dependence. Values of the vapor pressure at even temperatures for solid and liquid are given in Table VIII. They were calculated from the equation

$$R \ln P_{(\text{atm})} =$$

$$4.5758 \log P = - \left(\frac{F^0 - H_0^0}{T}\right)_{(g)} + \left(\frac{F^0 - H_0^0}{T}\right)_{(l)} - \frac{\Delta H_0^0'}{T} - \frac{b'P}{T^3} - \left(\frac{V_{(l)}(1 - P)}{41.29T}\right) \text{ gbs.} \quad (6)$$

where $\Delta H_0^0 = 6,013.5$, $b' = -6.0 \times 10^5$, $V_{(l)} = 48 \text{ cm.}^3$ estimated. The experimental observations are compared with equation 6 in Table VII.

TABLE VII

OBSERVED VAPOR PRESSURES OF TRIFLUOROMETHANE

T, °K.	Inter. cm. $F_{\text{obs.}}$	$P_{\text{calcd.}}$
145.348	2.04	2.03
158.080	7.10	7.13
164.511	12.34	12.36
169.182	17.88	17.85
172.824	23.45	23.43
176.426	30.25	30.26
179.349	33.88	36.88
182.000	43.93	43.94
183.882	49.51	49.53
185.917	53.12	56.20
187.889	63.34	63.33
189.551	63.92	69.91
191.177	73.89	76.93

TABLE VIII

VAPOR PRESSURE OF SOLID AND LIQUID TRIFLUOROMETHANE

T, °K.	Inter. cm. P_{Solid}	T, °K.	P_{Liquid}
40	3.62×10^{-24}	120	6.49×10^{-2}
50	2.09×10^{-17}	130	3.04×10^{-1}
60	6.51×10^{-13}	140	1.11
70	1.02×10^{-9}	150	3.31
80	2.47×10^{-7}	160	8.45
90	1.70×10^{-5}	170	19.01
100	4.90×10^{-4}	180	38.54
110	7.42×10^{-3}	190	71.85
	Triple point	Boiling point	
117.97	4.56×10^{-2}	190.97	76.00

The Entropy of Trifluoromethane from Calorimetric Data.—A summary of the entropy calculation is given in Table IX.

TABLE IX

THE ENTROPY OF TRIFLUOROMETHANE IN GIBBS MOLE⁻¹

1 gbs. = 1 defined cal. deg. ⁻¹

0-15°K. (extrapolation)	0.67
15-117.97° (graphical integration)	17.50
Fusion, 970/117.97	8.22
117.97-190.97 (graphical integration)	9.71
Vaporization, 3994/190.97	20.91
Entropy of CHF_3 gas at b.p. 190.97°K.	57.01
Corr. to ideal gas, $\Delta S = -25'P/T^3$	0.17
Entropy of ideal CHF_3 gas at b.p.	57.18 gbs. mole ⁻¹
S^0 from molecular data at 190.97°K.	57.23
At 298.15°K., $S^0_{\text{mol data}} =$	
62.045 $S^0_{\text{exp.}} = 62.00 \text{ gbs. mole}^{-1}$	

In computing the value of S^0 given as experimental at 298.15°K., the increment above the boiling point has been taken from the spectroscopic data.

We thank John P. Clan for assistance with the measurements and calculations.

(11) "International Critical Tables," Vol. 2, McGraw-Hill Book Co., New York, N. Y., 1926, p. 457.

(12) R. H. Busey and W. F. Giaque, *J. Am. Chem. Soc.*, **75**, 806 (1953).

(13) R. H. Sherman and W. F. Giaque, *ibid.*, **77**, 2154 (1955).

INTERACTIONS OF AMMONIA WITH GRAPHITE OXIDE

BY W. H. SLABAUGH AND B. C. SEILER

*Department of Chemistry, Oregon State University, Corvallis, Oregon**Received August 2, 1961*

Certain aspects of the structure of graphite oxide and the mechanism by which it adsorbs ammonia have been investigated through observation of the phenomena: adsorption isotherms and isobars, infrared absorption spectroscopy, and X-ray diffraction. From the apparent stepwise process of adsorption and intercalation of ammonia, the graphite oxide is shown to consist of laminar platelets that are populated by enol and keto groups. The resulting rough surface possesses holes or cavities that accommodate the early portions of adsorbed ammonia. Further adsorption produces a monolayer that separates the platelets by distances proportional to the size of the ammonia molecule. The adsorption process is not simple, but involves condensation of the film, chemical interaction with the acidic sites, and physical adsorption.

Introduction

Although graphite oxide has been known since 1859, when Brodie¹ first oxidized graphite with fuming HNO₃ and KClO₃, little has been reported about its gaseous adsorption properties. Graphite oxide has two features which make it a potentially good adsorbing agent. First, graphite oxide retains a laminar structure similar to graphite itself,² and therefore, it should have approximately the same surface area as graphite. Second, graphite oxide has been found by Thiele,³ Hoffman,⁴ and others to have radicals such as carboxyl, hydroxyl, epoxy, and possibly other groups attached to the hexagonal platelets. These groups constitute energetic sites for chemical adsorption, especially for polar molecules.

The adsorption of water and certain non-polar gases, such as nitrogen and hexane, on graphite oxide has been studied by several investigators.^{5,6} They found that, while there was considerable water adsorption, the adsorption of non-polar gases was comparatively small. The adsorption of water is attributed to the intercalation of water molecules between the graphite oxide platelets, which is possible because of the high dipole moment of water and the hydrophilic nature of graphite oxide.

Because of the acidic nature of graphite oxide and the high polarizability of NH₃, the adsorption of this gas should be even more interesting than that of water. This paper shows the results of an investigation of the graphite-NH₃ system, involving adsorption and desorption isotherms, infrared absorption spectra, and X-ray diffraction. An examination of the adsorption properties of graphite oxide salts also is included.

Experimental

Sample Preparation.—The graphite oxides were prepared from Canadian graphite No. 5, which was supplied by the Asbury Mills, Asbury, New Jersey. The material was 99% pure and its particle size was less than 35 μ in diameter. No preliminary treatment of the graphite was made.

Samples of graphite oxide were prepared by the conventional Brodie method,¹ and by a modified Brodie method suggested by Maire.⁷ After the final oxidation step for all

samples, the graphite oxide was electrolyzed for approximately 48 hr. in a Mattson type cell. The electrode polarity was reversed periodically to prevent excessive accumulation of material on the cellophane membranes. The dialyzed products were freeze-dried and stored at ambient temperatures in clear glass bottles. The compositions of the graphite oxides are given in Table I.

TABLE I
COMPOSITION OF GRAPHITE OXIDE

%C	%O	%H	%ash	C:O ratio
Conventional Brodie method (vacuum dried)				
50.05	46.92	3.03	0.1	1.43:1
50.71	46.19	3.09	.1	1.46:1
51.71	45.70	3.13	.1	1.51:1
51.15	45.97	2.87	.1	1.48:1
Modified Brodie method (vacuum dried)				
55.53	42.24	2.23	0.01	1.75:1
55.48	42.00	2.52	.01	1.76:1

In early experiments the basis of weight was graphite oxide vacuum dried for 24 hr. at less than 0.1 mm. pressure. However, this basis was subject to error although the weight remained constant after this period. Therefore, the graphite oxide was stored over a saturated Ca(NO₃)₂ solution, the relative humidity of which was 51%. The moisture content of graphite oxide kept in this manner was approximately 18–19%. This percentage in turn was based on samples oven-dried for 3 hr. at 160°. The temperature, 160°, was chosen as the standard drying temperature because differential thermal analysis⁸ revealed that graphite oxide appears to lose all of its adsorbed water between 115–130°, while complete decomposition does not occur below 200°. Furthermore, X-ray diffraction⁹ showed that the basal spacing reaches a minimum at approximately 140 to 150°. Finally, pyrolysis¹⁰ of graphite oxide had shown a definite break in the loss of weight when graphite oxide was heated to 150–160°. Little difference appeared between the structure and composition of vacuum-dried and oven-dried graphite oxide. This was demonstrated by infrared analysis in the present study and by C and H determinations.

The graphite oxide salts were prepared by batch ion-exchange of the graphite oxide prepared above, using 10% salt solutions. The concentrations in meq. of metal ions per g. of the graphite salts were 2.00, 1.61, 1.09, and 0.83 for the Li, Na, K, and Rb salts, respectively.

Adsorption.—The NH₃ adsorption isotherms were determined gravimetrically with quartz helixes maintained at constant temperature. Changes in weight of a 0.3000-g. sample could be detected with an accuracy of ± 0.02 mg. Samples were thermostated during the adsorption measurements to $\pm 0.2^\circ$.

Weighed samples of graphite oxide were suspended from the helixes and evacuated slowly for 24 hr. Then the pressure was lowered to 0.1 μ or less, and outgassing was continued for two more days at room temperature before measurements were taken. The samples then were brought to the desired temperature, and appropriate increments of NH₃

- (1) B. C. Brodie, *Trans. Royal Soc. (London)*, **149**, 249 (1859).
- (2) H. L. Riley, *Fuel*, **24**, 43 (1954).
- (3) H. Thiele, *Kolloid-Z.*, **80**, 1 (1937); **115**, 167 (1949); **116**, 1 (1950); **117**, 144 (1950).
- (4) U. Hoffman and E. Konig, *Z. anorg. u. allgem. Chem.*, **234**, 311 (1937).
- (5) J. H. de Boer and A. B. C. van Doorn, *Proc. Koninkl. Ned. Akad. Wetenschap.*, **61B**, 242 (1958).
- (6) W. H. Slabaugh and Conrad Hatch, *J. Chem. Eng. Data*, **5**, 453 (1960).
- (7) J. Maire, *Compt. rend.*, **232**, 61 (1951).

- (8) C. V. Hatch, Ph.D. thesis, Oregon State College, 1960.
- (9) J. Cano-Ruiz and D. M. C. MacEwan, *Tercera Reunion Internacional Sobre Reactividad De Los Solidos*, April, 227 (1956).
- (10) E. Matuyama, *J. Phys. Chem.*, **58**, 215 (1954).

TABLE II
ADSORPTION BEHAVIOR OF GRAPHITE OXIDES AND SALTS WITH NH₃

W_m -B.E.T. (mg./g.) (meq./g.)	Graphite oxides at -36° (Conventional Brodie samples)				Graphite oxide salts at -35°			
	Li	Na	K	Rb	Li	Na	K	Rb
164	170	175	167	142	143	144	144	144
9.7	10.0	10.3	9.8
Area (m. ² /g.)	750	778	799	764	649	657	658	658
Residual NH ₃ after desorption at 25°								
mg./g.	42.3	42.8	34.6	35.1	47.9	..	33.8	31.4
meq./g.	2.49	2.52	2.04	2.06	2.82	..	1.98	1.85
Residual NH ₃ after desorption at 70°								
mg./g.	..	21.7	13.4	13.8	42.8	..	27.4	25.0
meq./g.	..	1.28	0.79	0.81	2.52	..	1.61	1.47

were added. Equilibrium was obtained in 2 to 10 hr. depending on the sample, temperature, and pressure.

Infrared Absorption.—Infrared absorption spectra of graphite oxide were obtained by the pressed KBr pellet technique with a Perkin-Elmer Model 21 double beam instrument. Both LiF and NaCl prisms covering the range from 4,000 to 2,000 cm.⁻¹ were employed, but the difference in the spectra from these two prisms was negligible in this region. Only the NaCl prism was used in the 2,000-650 cm.⁻¹ region. Samples also were examined by Lippincott¹¹ by means of a diamond cell in a Model IR4 Beckman spectrophotometer with a NaCl prism.

X-Ray Diffraction.—X-Ray diffraction studies were made on graphite oxide with NH₃ adsorbed at room temperature. Other temperatures were not used because the proper equipment was not available to maintain the sample at constant temperature while making the X-ray analysis. The X-ray diffraction samples were mounted in Plexiglas sample holders and were protected with a covering of 0.012-mm. polyethylene film. The sample holders were placed in glass tubes which were attached to the vacuum system. The tubes could be readily sealed off from the system at appropriate pressures. A minute hole in the Plexiglas holder allowed NH₃ to reach the sample, and this hole then was sealed with a silicone grease immediately after the glass tube was broken in an inert atmosphere. Within a few minutes the X-ray diffraction measurement was made.

Discussion of Experimental Results

Adsorption.—NH₃ adsorption isotherms were obtained for graphite oxide at -45 , -35 , and -25° for the conventional Brodie samples. The isotherms for the four samples were almost identical in shape, although their vertical displacement varied over a range of 6%. Relatively little difference was noticed between isotherms at -35 and -25° . Because of their similarities only the isotherms for the fourth sample are shown in Fig. 1 for -45 and -35° . An isotherm of a modified Brodie sample at -35° also is shown in Fig. 1, demonstrating the similarity of NH₃ isotherms for graphite oxide made by the conventional and the modified Brodie methods.

From B.E.T. plots which were regularly linear up to P/P_0 of 0.25, the surface areas were calculated on the basis of an area of 12.9 Å.² for the NH₃ molecule. The areas shown in Table II are much higher than the 358 m.²/g. observed by de Boer and van Doorn⁶ for the adsorption of water vapor. de Boer and van Doorn calculated a theoretical area for both sides of the laminar platelets of graphite oxide of 1477 m.²/g. If the experimental area of 773 m.²/g. found in this study is the result of adsorption of a single layer of NH₃ molecules between each pair of platelets plus their outer edges, then the area of 773 m.²/g. is equal to one-half of the 1477 m.²/g. plus the area of the edges of the platelets.

(11) E. R. Lippincott, F. E. Welsh, and C. F. Weir, *Anal. Chem.*, **33**, 137 (1961).

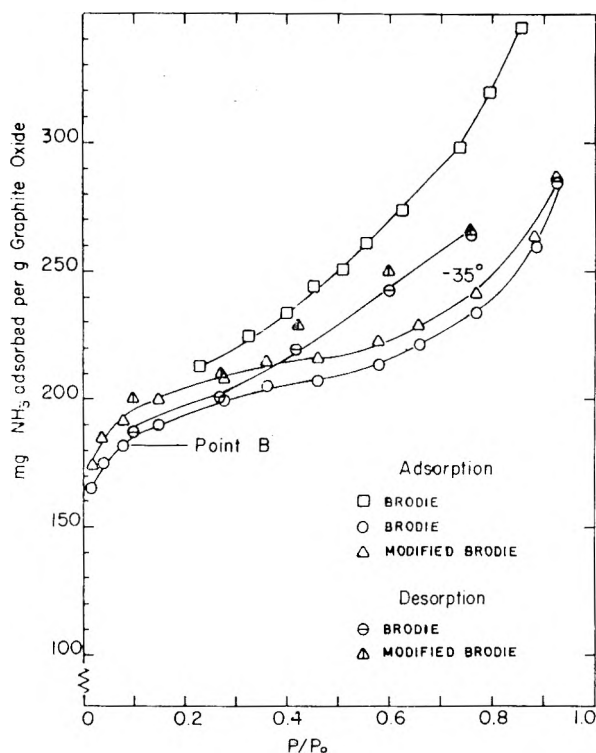


Fig. 1.—Adsorption isotherms of NH₃ on graphite oxide made by conventional Brodie method and modified Brodie method.

This leaves 70 mg.²/g. attributed to the areas of the outer edges of the platelets.

The break in the isotherms (point B) appears at approximately 175-180 mg./g. of NH₃, compared to an average of 169 mg./g. for W_m , which is calculated from the B.E.T. equation. The average amount of NH₃, 9.95 meq./g., corresponds fairly closely to the value of 11.0 meq./g. obtained by Clauss, *et al.*,¹² for the exchangeable hydrogen. This factor is an indication that initial adsorption is influenced primarily by the acidic sites on the graphite oxide.

The NH₃ isotherms of graphite oxide salts (Li, Na, K, and Rb) gave B.E.T. surface areas as shown in Table II. These areas are lower than those for graphite oxide itself, probably because the metal ions are larger than hydrogen and they occupy more space on the laminar surface. In addition the possibility remains that the metal ions restrict the expansion of the laminar crystals, as compared to

(12) A. Clauss, A. Plas, H. P. Boehm, and U. Hoffmann, *Z. anorg. u. allgem. Chem.*, **291**, 205 (1957).

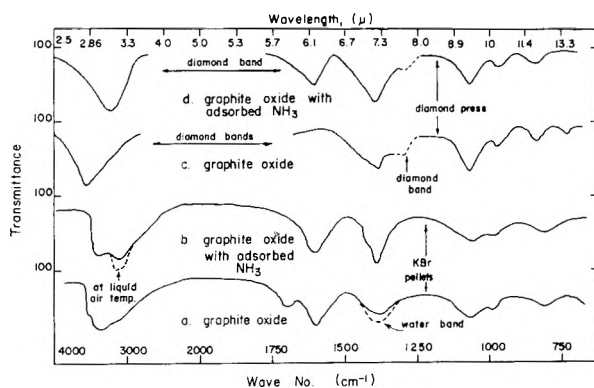


Fig. 2.—Infrared absorption of graphite oxide.

the extent that they expand when hydrogen ions are present.

All of the ammonia could not be desorbed from graphite oxides and their salts even after outgassing for six days at less than 1μ pressure. The weights of NH_3 remaining are shown in Table II. These values were lowered, as also shown in the table, by heating the samples to 70° .

On the basis of incomplete outgassing in adsorption systems the exchange capacity or number of acidic sites can be assessed. For example, Zettlemoyer, *et al.*,¹³ noticed this phenomenon on the outgassing of NH_3 from stearic and succinic acids, and Cornet¹⁴ in his studies with NH_3 on Montmorillonite clays found, while outgassing hydrogen ben-tonite, that the residual NH_3 corresponded to the ion-exchange capacity of the clay. If this were the case, then the number of readily exchangeable hydrogen ions in graphite oxide would be between 2.0 to 2.5 meq./g., as determined from the data on residual NH_3 given in Table II.

Infrared Absorption.—The infrared absorption spectrum of graphite oxide is characterized by a relatively broad band in the $3300\text{--}3500 \text{ cm}^{-1}$ region when the graphite oxide contains adsorbed water. The shoulder develops into a well defined peak as the water content increases. This peak is clearly the result of the O-H stretching motion of the water molecule. In the present case the band in this region retains some semblance of a shoulder, even for samples dried at 160° for 3 hr. or dried under pressure of less than 0.1μ . Enough moisture may possibly have been adsorbed from the atmosphere to show some traces of water. Hadzi and Novak^{14a} did not describe their method of treating the sample after drying, so one does not know if the samples were run in an inert or a dry atmosphere.

A well defined shoulder also appears at 3250 cm^{-1} for graphite oxide with adsorbed NH_3 (Fig. 2b) at room temperature. This peak was intensified considerably by cooling the sample to liquid air temperature and using a LiF prism. The assignment of this band may be made to the hydrogen stretching motion (N-H) from either the NH_4^+ or the

NH_3 itself.¹⁵ This band is too diffused to distinguish between any particular bands.

The spectrum obtained from vacuum-dried graphite oxide compressed between diamond crystals shows a relatively sharp peak at 3530 cm^{-1} . This peak was shifted to a lower frequency, 3250 cm^{-1} , upon the adsorption of NH_3 . The shift may be caused by hydrogen bonding of NH_3 with a hydroxyl group. The band at this frequency is a little broader, which may mean that it is a combination of two peaks, although the intensity is approximately the same.

The small band at 1720 cm^{-1} may be assigned to free carboxylic carbonyl groups. The adsorption of NH_3 either destroys this band or shifts it to a region already masked by another band, such as the region near 1610 or 1375 cm^{-1} . A band shift is more probable because of the formation of an ammonium salt. Strangely, this band and the one at 1610 cm^{-1} do not appear in the spectrum obtained from graphite oxide in the diamond cell. The high pressures used in compressing the sample between the diamond crystals may be sufficient to destroy these groups. For example, graphite oxide will decompose when ground in a mortar and pestle.¹⁶

The sharp band at 1610 cm^{-1} is present in every spectrum obtained from graphite oxide using the pressed salt technique. This peak seemed unaffected by the adsorption of H_2O or NH_3 . However, Hadzi and Novak found this peak only in moist graphite oxide. In this work, the peak seemed just as intense with graphite oxide dried for 3 hr. at 160° as with wet graphite oxide. As mentioned above, a trace of moisture possibly was adsorbed from the atmosphere to give a peak in this region, although this peak did not increase in intensity with increased water content. The spectrum obtained from the oxide compressed between diamonds showed a peak in this region only with adsorbed NH_3 . This particular band may be assigned to the unsymmetrical bending vibration of NH_3 .

Hadzi and Novak assigned the band at approximately 1400 cm^{-1} to the deformation of the O-H groups. The band, intensified with adsorbed water, meets this theory. This peak also is intensified to a larger degree with adsorbed NH_3 . According to Pliskin and Eischens,¹⁷ a band appears in the 1400 cm^{-1} region due to the N-H bending vibration of the NH_4^+ , which has exchanged with the potassium ion in the KBr pellet. This postulation is, however, unlikely in the present case because the KBr and graphite oxide were mixed after adsorption took place. Also, this band shows an increase of intensity in the spectrum obtained with the diamond cell. Therefore, this band can be attributed to the formation of NH_4^+ ions in the graphite oxide.

The other bands at lower frequency were not changed by the adsorption of NH_3 . These bands were somewhat intensified when obtained from the diamond cell and also when the spectrum was determined in samples at liquid air temperature. One small band, 740 cm^{-1} , appears in Fig. 2a and 2c and disappears in the spectrum in Fig. 2d.

(13) A. C. Zettlemoyer, J. J. Chessick, and A. Chand, *J. Phys. Chem.*, **59**, 375 (1955).

(14) I. Cornet, *J. Chem. Phys.*, **11**, 217 (1943).

(14a) D. Hadzi and A. Novak, *Trans. Faraday Soc.*, **51**, 1614 (1955).

(15) J. E. Mapes and R. P. Eischens, *J. Phys. Chem.*, **58**, 1059 (1954).

(16) H. Thiele, *Kolloid-Z.*, **80**, 1 (1937).

(17) W. A. Pliskin and R. P. Eischens, *J. Phys. Chem.*, **59**, 1156 (1955).

Adsorption in this region may be due to the skeletal vibrations of the solid lattice. The NH_3 is between the graphite oxide platelets could change the nature of the lattice and influence its vibrational frequency, causing this band to shift.

X-Ray Diffraction.—The change in c -spacing of graphite oxide in relation to the weight of NH_3 adsorbed is shown in Fig. 3. The discrepancy between the two graphs reflects the effect of variations in preparation of the samples on the c -spacing. The difference in drying may have had some effect on the orientation of the atoms or groups of atoms in the graphite oxide, which could have changed the c -spacing.

The values shown in Fig. 3 with asterisks are the maximum possible weights of NH_3 adsorbed by the particular samples in question and not necessarily the true weights adsorbed at the time the X-ray diffractions were made. The reason for this is that in order to adsorb quantities of NH_3 above 180 mg./g., the NH_3 pressure had to be increased above one atmosphere. Therefore, some gas leakage from the sample holder during the time the X-rays were made was possible.

Three major breaks occur at 67, 122, and 175 mg./g. of sample. The difference in c -spacing for the minor plateaus is 0.57 Å. for sample 3b and 0.65 Å. for sample 3a. For the major plateaus the values are 1.19 and 1.22 Å., respectively. These latter values may be considered as the distance the platelets were expanded by a monolayer of NH_3 . The c -spacing for NH_3 -saturated graphite oxide always decreased on exposure to the atmosphere to a constant value of 7.37 Å. for sample 3a. Apparently, the graphite oxide expelled the excess NH_3 until only a monolayer remained. This factor indicates that the force of attraction between the graphite oxide platelets and the NH_3 monolayer is quite large, probably because of hydrogen bonding.

In every case the maximum intensity of X-ray diffraction was obtained at 175 mg./g. The relative intensities of X-ray diffraction were estimated from the heights of the tracings obtained for the c -spacing in the spectrometer, and these intensities for sample 3a are shown in Fig. 4. This figure shows both a maximum at the W_m value and a smaller maximum at 80 mg./g., which corresponds to the first plateau in Fig. 3. Significant conclusions in this respect are that the maximum intensity was obtained at 175 mg./g. (W_m), and ammonia-free samples and samples with relatively little ammonia adsorbed on them always had the lowest intensity and were the most diffuse in a particular run. This change in intensity is attributed to a change in crystallinity in the sample. The low intensity of dried graphite oxide also may be the result of its warped structure as postulated by Ruess,¹⁸ where two planes of carbon atoms approximately 0.5 Å. apart cause interference and diminution of the resultant intensity.

The stepwise X-ray curves also have been found in other systems, particularly in the studies of clays.^{14,19,20} However, these plateaus always were

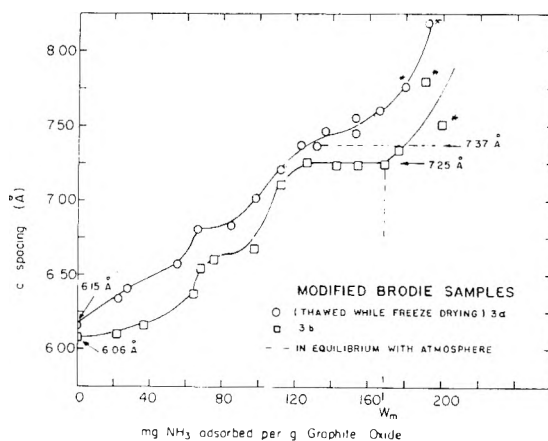


Fig. 3.—X-Ray diffraction c -spacings in the adsorption of NH_3 by graphite oxide.

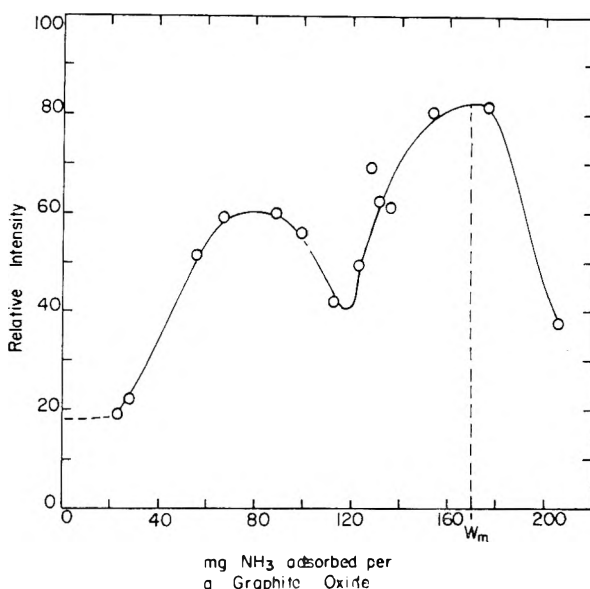


Fig. 4.—Relative intensity of X-ray diffraction for graphite oxide with adsorbed NH_3 .

attributed to the respective formation of layers of adsorbate between adsorbent platelets. In the present case only the higher plateau, starting at 122 mg./g. of graphite oxide, may be considered as corresponding to a single layer formation; the lower plateau is caused by another phenomenon proposed later in this discussion. de Boer and van Doorn⁹ in their X-ray diffraction studies of graphite oxide with adsorbed water found very little change in the c -spacing until the sample contained over 16.2% water (162 meq./g.). If one compares the calculated area of NH_3 (12.9 Å.) with that of water (10.8 Å.), the 162 meq./g. would roughly compare with the 122 meq./g. in Fig. 3, where the plateau in the c -spacing begins. de Boer and van Doorn found that the c -spacing had expanded to at least 6.8 Å. However, these investigators claimed that this expansion was insufficient to account for all the adsorbed water. This indicates that an adsorbed molecule such as water or ammonia may fit into the graphite oxide lattice without much effect on the c -spacing.

According to Cano-Ruiz and MacEwan in their

(18) G. Ruess, *Monatsh. Chem.*, **76**, 381 (1947).

(19) A. C. Zettlemoyer, G. J. Young, and J. J. Chessick, *J. Phys. Chem.*, **59**, 962 (1955).

(20) J. W. Jordan, *ibid.*, **53**, 294 (1949).

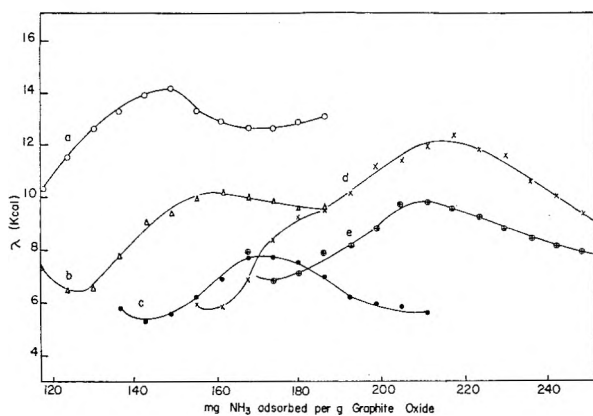


Fig. 5.—Isosteric heats of adsorption on graphite oxide calculated from adjacent isobars. Curve a is based on the two isobars at 1.34 and 4.95 cm., curve b is based on the two isobars at 4.95 and 10.15 cm., etc.

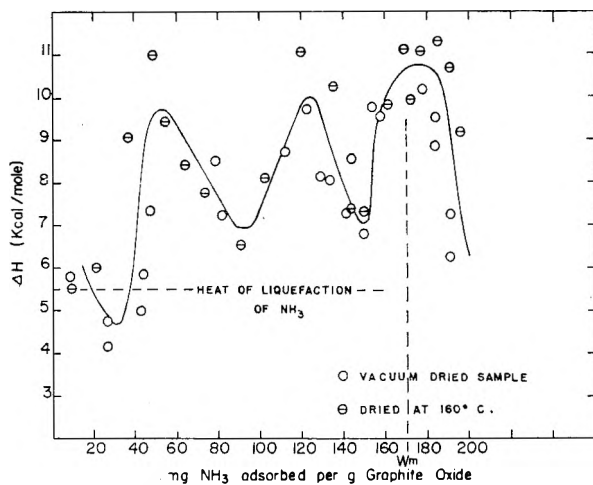


Fig. 6.—Calorimetrically determined heats of absorption of ammonia on graphite oxide at 0°.

review of the model of graphite oxide proposed by Ruess¹⁸ the carbon atoms in a tetrahedral "chair" configuration form two layers with a perpendicular separation of 0.5 Å.; the oxygen atom in the ether linkages extends out from the center of the plane 2.4 Å., and the O-H groups extend 3.05 Å. from the center of the plane. Consequently, the latter group would cause the graphite oxide layers to expand to 6.1 instead of 3.4 Å. for the original graphite. Now, if one assumes that the effective van der Waals radius of the carbon atom in graphite oxide is the same as it is in graphite, its effective radius is 1.71 Å. Thus, the free space between carbon layers in graphite oxide is 6.1 minus 3.4, or 2.7 Å.

The van der Waals diameter of nitrogen is 3.0 Å., which could be quite close to the effective diameter of NH₃. This assumption may be considered valid if one considers NH₃ analogous to water. In the clay systems referred to above the effective diameter of water is approximately 2.6 to 2.8 Å. This agrees quite well with 2.8 Å., which is the van der Waals diameter of oxygen and which should be similar in effect to the nitrogen in NH₃.

The difference between the diameter of NH₃ and the free space is approximately 0.3 Å.; the difference between 6.10 and 6.65 Å. for the first plateau

is 0.55 Å., which is in good agreement, considering the assumptions that were made. This means that up to the first plateau, NH₃ was admitted to the system with little expansion of the *c*-spacing. This also explains the small expansion of the *c*-spacing found by de Boer and van Doorn. If the oxygen from the ether linkage extends from the center of the carbon plane 2.4 Å., then any NH₃ molecule between the oxygen and the next carbon plane should expand the *c*-spacing to 7.1 Å. This corresponds closely to the 7.25 Å. found at the second plateau. This information suggests that the initial adsorption of NH₃ is in the open spaces surrounding the oxygen and the O-H groups, while the next addition is between the ether groups and the carbon planes. If the 162 mg./g. of water found by de Boer and van Doorn is a true value for *W_m*, and if the 122 mg./g. of NH₃ at the start of the plateau is a comparable value for *W_m*, then the difference between the H₂O monolayer and the NH₃ monolayer would be the area covered by the ether linkage between the platelets. The difference between the areas for NH₃ at 122 mg./g. and at 175 mg./g. of graphite oxide is 245 m.²/g. The difference between the area found from NH₃ isotherms and that found from water isotherms is approximately 190 m.²/g., which is in only fair agreement with the other difference.

Heats of Adsorption.—Adsorption isobars were made experimentally in order to calculate the isosteric heats of adsorption. Calculation of these heats is possible from the isotherms, although to determine them very accurately in the region at point B is difficult because the isotherms are quite close together. The isosteric heats of adsorption, λ , were calculated from these isobars by means of the Clausius-Clapeyron equation

$$\log \frac{P_1}{P_2} = \frac{\lambda}{2.3R} (1/T_2 - 1/T_1)$$

Some controversy exists on the validity of the use of this equation on non-reversible systems, such as the graphite oxide-NH₃ system. Therefore, even though these values are only apparent isosteric heats, at least a qualitative representation of the energy associated with the adsorption process is indicated by them.

The calculated isosteric heats are shown in Fig. 5, and Fig. 6 gives the direct calorimetrically measured heats of adsorption measured by a method after Beebe.²¹ The accumulation of errors inherent in the latter method produces a considerable amount of scatter in the data, but these two methods of measurement are consistent with each other to the extent that, along with the X-ray data, a mechanism of adsorption may be postulated.

Contrary to what generally is found, these data do not correspond with the usual trend of heats of adsorption. Instead they show almost no heat of adsorption beyond the heat of liquefaction of NH₃ at low coverage. This is attributed to the prying apart of the platelets, which is an endothermic process. Subsequently, adsorption takes place with increasing ease, and less energy is used up in

(21) R. A. Beebe, B. Millard, and J. Cynarski, *J. Am. Chem. Soc.*, **75**, 839 (1953).

mechanically prying the layers apart. The fluctuations in heat of adsorption, though reproducibly measured, are probably the result of several factors whose combined effect produces a complex mechanism. It seems clear that at the W_m region, complete saturation of the active sites has occurred, the platelets now are separated, and the heat of adsorption becomes a maximum. In this region other factors must be considered, such as condensation of the adsorbed NH_3 as the result of lateral interaction of NH_3 molecules in the completed mono-

layer and the formation of additional layers. This step would involve considerable energy because of the probability of hydrogen bonding between the NH_3 molecules and the active sites on the two adjacent platelets.

Acknowledgments.—The authors gratefully acknowledge the support of the National Science Foundation for this study. This material was submitted in partial fulfillment of requirements for the doctoral thesis of B.C.S. at Oregon State University.

THE REACTIONS OF NITRIC OXIDE IN IRRADIATED CYCLOHEXANE

BY E. J. BURRELL, JR.

Radiation Physics Laboratory, Engineering Dept., E. I. du Pont de Nemours & Company, Wilmington, Delaware

Received August 3, 1961

Specific rate constants have been measured for the reaction of nitric oxide with nitrosocyclohexane monomer and for the dimerization of nitrosocyclohexane monomer. The implications of these reactions for nitric oxide scavenging reactions are discussed.

Introduction

Nitric oxide long has been used to suppress free radical reactions and leave undisturbed the so-called molecular processes in various thermal and radiation reactions.^{1,2} Some attempts also have been made to use nitric oxide as a free radical trap to characterize the products of these reactions as an aid in the kinetic analysis of such reactions.³⁻⁵ The expected primary product is the nitroso compound of the radical in question.

On the other hand, Donaruma and Carmody⁶ have shown that in the chemical reaction of nitrosocyclohexane and nitric oxide the major products are cyclohexyl nitrate and nitrocyclohexane in the ratio of about 3:1 at moderate temperatures. It thus is apparent that the expected nitroso product can be at least partially consumed in further reactions.

It is, therefore, of interest to determine whether nitrosocyclohexane monomer is formed in the radiation reaction of cyclohexane and nitric oxide⁷ and, if it is, to measure the specific rate constants of the further reactions of nitrosocyclohexane monomer.

Experimental

Chemicals.—The following chemicals were used without further purification: Eastman spectro grade cyclohexane, Matheson nitric oxide (99% min. purity), Linde argon (99.995% min.), Aldrich Chemical Company cyclohexanone oxime, and Matheson chlorine.

1-Chloronitrosocyclohexane was prepared⁸ *in situ* by

(1) J. Jach, F. J. Stubbs, and C. Hinshelwood, *Proc. Roy. Soc. (London)*, **224A**, 283 (1954).

(2) K. Yang, *J. Phys. Chem.*, **65**, 42 (1961).

(3) W. A. Bryce and K. U. Ingold, *J. Chem. Phys.*, **23**, 1968 (1955).

(4) J. G. Calvert, S. S. Thomas, and P. L. Hanst, *J. Am. Chem. Soc.*, **82**, 1 (1960).

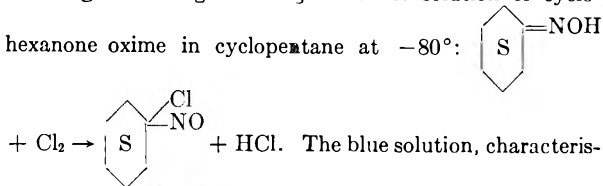
(5) A. Henglein, *Intern. J. Appl. Radiation and Isotopes*, **8**, 149 (1960).

(6) L. G. Donaruma and D. J. Carmody, *J. Org. Chem.*, **22**, 635 (1957).

(7) E. Müller and G. Schmid, *Chem. Ber.*, **94**, 1364 (1961), have just reported the radiation-synthesis of nitrosocyclohexane dimer.

(8) N. V. Sidgwick, "The Organic Chemistry of Nitrogen," Oxford Univ. Press, 1937, p. 207.

bubbling chlorine gas through a dilute solution of cyclohexanone oxime in cyclopentane at -80° :



of monomeric nitroso compounds, showed an infrared absorption at 6.34μ attributed to the monomeric nitroso group.⁹ This infrared band disappeared rapidly on subsequent reaction with nitric oxide at -80° and a new band appeared at 6.0μ which was attributed to 1-chlorocyclohexyl nitrate.

Linear Irradiations.—A Varian Linear Accelerator (Lineac) delivers high-intensity bursts of 6-Mev. electrons in 5- μ sec. pulses. An optical system, placed at right angles to the electron beam entering the cell, detects the absorption of 7000 Å. light due to the presence of the transient nitrosocyclohexane monomer formed in the cyclohexane-nitric oxide solution by the electron pulse. The absorption as a function of time is presented as an oscilloscope trace. Electrons enter the side of the 1.4-ml. sample cell through a 0.005-in. metal window. The "Spectrosil" fused silica windows (available from Thermal American Fused Quartz Company, Dover, New Jersey) used in the cell show no transient or permanent absorption due to electron or X-ray irradiation at the intensities used here. For further details see reference 10.

Infrared Analysis.—Irradiated samples typically were evaporated down to about 1/50th of the initial volume by bubbling argon through the samples. The samples then were analyzed on a Perkin-Elmer Model 137 infrared spectrometer.

Extinction Coefficient of Nitrosocyclohexane Monomer.—A 0.02 M solution of nitrosocyclohexane in decane in a 0.10-mm. quartz cell was heated in a Primol D oil-bath in the Cary Model 14M spectrophotometer. The optical density at 2900 Å. was measured as a function of temperature.

$$OD = \log I_0/I = \epsilon cd$$

As the temperature increases more dimer molecules dissociate reversibly to form monomer molecules. The optical density is then a measure of the fraction of dimer dissociated at any temperature.

The same nitrosocyclohexane solution was placed in a 5.00-cm. quartz cell and the optical density at 7000 Å. was

(9) W. Lüttke, *Z. Elektrochem.*, **61**, 302 (1957).

(10) R. L. McCarthy and A. MacLachlan, *Trans. Faraday Soc.*, **56**, 1187 (1960).

The predominant radical formed by the radiation in Step 1 is the cyclohexyl radical. The e.p.r. spectrum of irradiated frozen cyclohexane indicates the presence of a single radical (less than $\sim 5\%$ of a second species), and the splittings of the spectrum are consistent with the cyclohexyl structure.

The reaction of a cyclohexyl radical with nitric oxide (Step 2) has been assumed to be very rapid compared to Steps 3 and 4.

The qualitative observation that chloronitrosocyclohexane reacts rapidly at -80° with nitric oxide suggests a low activation energy process leading to the formation of nitrate. Chloronitrosocyclohexane is known to be monomeric in solution.⁸

Nitrosocyclohexane, which exists as the dimer at room temperature, reacts very slowly with nitric oxide⁶ in a non-radiation reaction. In fact, it will be seen that only insofar as the nitrosocyclohexane dimer dissociates to monomer at higher temperatures does it react with nitric oxide. Thus, monomeric nitrosocyclohexane reacts rapidly with nitric oxide whereas the dimer does not react noticeably.

The N-nitroso-N-alkyl-hydroxylamine nitrite intermediate in Step 3 has been postulated by Brown,¹² by Donaruma and Carmody,⁶ and by Batt and Gowenlock.¹³ The present study accepts this postulated intermediate and obtains a measure of its decay. In the transient measurements with the Lineac the half-period for disappearance of the nitrosocyclohexane monomer in the presence of nitric oxide was approximately constant even though the nitric oxide concentration was varied by a factor of ten. The nitric oxide was present in large excess compared to the monomer concentration, and if most of the monomer forms the unstable intermediate (Step 3a) the fraction of monomer entering this equilibrium is relatively insensitive to nitric oxide concentration. The resulting low concentration of "free" monomer remaining together with the low optical extinction coefficient of the monomer substantiates the high amplification necessary to detect the transient nitroso absorption. Donaruma and Carmody⁶ find a similar non-dependence on nitric oxide concentration in the thermal reaction of nitric oxide with nitrosocyclohexane although different reasons are advanced to explain it.

The nitrosocyclohexane monomer was the species observed, but since it is believed to be in equilibrium with the unstable intermediate, its rate of disappearance should be equal to that of the intermediate. Thus, the half-period of 0.2 sec. observed for disappearance of nitrosocyclohexane monomer is also the half-period for the breakup of the intermediate. In other words, Step 3c is rate-controlling and the nitroso monomer feeds into the intermediate to maintain the rapidly attained equilibrium (Step 3a, 3b).

If one nitrosocyclohexane monomer molecule meets another the dimer is formed (Step 4). The rate of this reaction (in the absence of nitric oxide) was measured directly in a non-radiation reaction. Once the dimer has formed it is immune to attack

by nitric oxide unless the dimer dissociates again. If the dimer dissociates, the reaction sequence of Step 3 becomes operative. It is interesting to note here that the nitroso dimerization reaction could not be studied under Lineac conditions in a way analogous to nitrate formation. At best one could form by a Lineac pulse cyclohexyl radicals in just the quantity required to react completely with nitric oxide molecules available (allowing for $H \cdot + NO$ reaction). Even so the nitrosocyclohexane monomer will intercept some of those radicals which otherwise would combine with each other. Nitric oxide reacts with monomer as in Step 3. Radicals also are known to react rapidly with other nitroso monomers¹⁴ to give dialkyl and trialkyl nitrogen compounds.

The half-period for simple dissociation of nitrosocyclohexane dimer (in the absence of nitric oxide) at 51° has been calculated to be 13.5 sec. Donaruma and Carmody⁶ have found for the thermal reaction of nitric oxide and nitrosocyclohexane a half-period for disappearance of nitrosocyclohexane of 90 sec. at 51° . Their results are consistent with our measurements. The major factor in the disappearance of nitrosocyclohexane dimer is its rate of dissociation into monomer. The monomer then reacts rapidly with nitric oxide as in Step 3. However, the cyclohexyl radical produced in Step 3 may escape the liquid cage and react again with nitric oxide. The monomer so formed can either enter the monomer-dimer equilibrium or enter reaction Step 3 again. The "lifetime" of the monomer, and therefore of the dimer, thus is prolonged. Donaruma and Carmody's half-period value for the over-all reaction is expected to be somewhat larger than our half-period value for the simple dissociation of nitrosocyclohexane measured more directly. The agreement is considered satisfactory, particularly in view of the very different methods of observation.

For high temperatures the half-period for dissociation of the dimer is very short. The calculated value of 2 msec. at 120° is in good agreement with our observations on the dissociation of nitrosocyclohexane dimer. A solution of the dimer (no nitric oxide) was turbulently mixed with hot solvent in the stopped-flow apparatus. The resulting solution at 120° required some 5 msec. to reach the observation port, at which time the dissociation reaction was largely complete. Thus it became necessary to calculate the dissociation rate constant from the dimerization rate constant (obtained at lower temperatures) and the equilibrium constant.

Thus it is seen that nitric oxide does indeed scavenge free radicals. It also is evident, however, that more than one nitric oxide molecule disappears per radical consumed whenever cyclohexyl nitrate is formed. Furthermore, stringent conditions are necessary in order to obtain only nitrosocyclohexane dimer by precluding formation of cyclohexyl nitrate. It also will be noted that some cyclohexyl radicals may escape from the solvent cage when the N-nitroso-N-cyclohexylhydroxylamine nitrite intermediate breaks up (Step 3). That some of these radicals

(12) J. F. Brown, *J. Am. Chem. Soc.*, **79**, 2480 (1957).

(13) L. Batt and B. G. Gowenlock, *Trans. Faraday Soc.*, **56**, 682 (1960).

(14) R. N. Haszeldine and B. I. H. Mattinson, *J. Chem. Soc.*, 1741 (1947); B. Gingras and W. A. Waters, *Chem. & Ind. (London)*, 615 (1953).

probably do escape primary "recombination," *i.e.*, nitrate formation, is evidenced by the fact that nitrocyclohexane is a significant product in a typical radiation reaction. The NO_3 radicals which escape concurrently with the cyclohexyl radicals react with nitric oxide to form nitrogen dioxide (Step 5). Nitrogen dioxide then combines with any cyclohexyl radical to give the observed nitrocyclohexane (Step 6).

While cyclohexyl radicals in the liquid phase have been shown to undergo a well-defined set of

reactions with nitric oxide at moderate temperatures, extreme care must be exercised in interpreting the scavenging (or non-scavenging) action of nitric oxide.

Acknowledgment.—The assistance of V. F. Hanson in designing the double-wave length photomultiplier detector, of V. F. Damme in constructing some of the equipment, and of H. D. Williams of Eastern Laboratory, Explosives Department, for preparation of bisnitrosocyclohexane samples is gratefully acknowledged.

1,3,5-TRIARYL-2-PYRAZOLINES AS WAVE LENGTH SHIFTERS IN SCINTILLATION PLASTICS^{1a}

BY STANLEY R. SANDLER, SAMUEL LOSHAEK, EDWARD BRODERICK, AND K. C. TSOU^{1b}

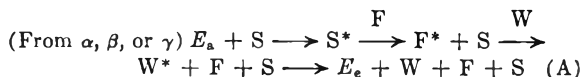
Central Research Laboratory of The Borden Chemical Company, Philadelphia 24, Pennsylvania

Received August 11, 1961

A series of substituted 1,3,5-triaryl-2-pyrazolines has been shown to be a good wave length shifter in plastic scintillators. The importance of the aryl group in position 3 is shown by the fact that 1,5-diphenyl-3-methyl-2-pyrazoline is not an effective wave length shifter. The 5-position, on the other hand, can be replaced by a methyl group without affecting its efficiency as a wave length shifter. The substituent effects and their relationship to the excited state of the 2-pyrazoline nucleus are discussed.

Introduction

In the scintillation mechanism, radiation energy (α , β , or γ) is absorbed by the plastic solvent, transferred first to the (fluor) solute and then to a secondary solute. The secondary solute functions as a wave length shifter since it emits the energy as fluorescent light at a wave length which corresponds to the wave length of maximum sensitivity of the photomultiplier tube. These processes can be pictured briefly as



where E_a is the energy absorbed, S, F, W, and E_e are the plastic solvent, fluor, wave length shifter and energy emitted, respectively.

The present work reports the use of a series of 1,3,5-triaryl-2-pyrazolines as wave length shifters in plastic scintillators and the effect of substitution in 1, 3, 4, and 5-positions of the 2-pyrazoline ring on the wave length shifter efficiency.

Results

In previous publications,² the effect of ring substitution on the efficiency of the aromatic solvent and fluor in plastic and liquid scintillators was shown to be related either to the inductive effect of the substituents or ionization potential.³ It was of interest to determine whether the wave length shifting efficiency of the 2-pyrazolines could be related to similar parameters. The 1,3,5-triaryl-2-pyrazolines with substituents in the 1, 3, 4,

and 5-positions therefore were chosen as wave length shifters in polyvinyltoluene scintillation plastics. The results are presented in Tables I and II. In Table III some 1,3,5-triaryl-2-pyrazolines were tested for their ability to act as fluors. The pulse heights in all cases are reported relative to an anthracene crystal of the same dimensions, using a Pa^{234} β source (0.01 mc., 2.3 Mev.) for irradiation.

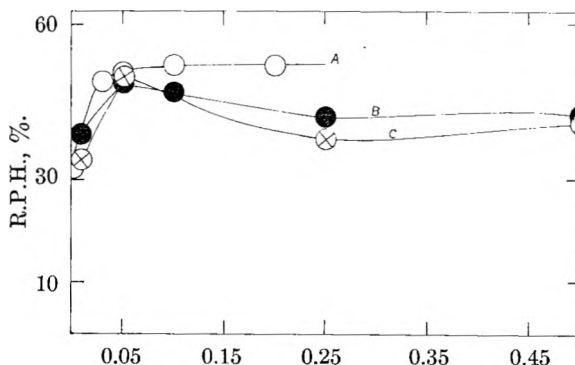


Fig. 1.—Relative pulse heights of polyvinyltoluene-3% *p*-terphenyl scintillators containing varying concentration of 1,3,5-trisubstituted-2-pyrazolines as wave length shifters: A, 1,3-diphenyl-5-methyl-2-pyrazoline; B, 1,3,5-triphenyl-2-pyrazoline; C, 1,5-diphenyl-3-*p*-methoxyphenyl-2-pyrazoline.

It was found that 0.05% of the pyrazoline was sufficient to give the maximum pulse height. This is illustrated for 1,5-diphenyl-3-*p*-methoxyphenyl-2-pyrazoline, 1,3,5-triphenyl-2-pyrazoline, and 1,3-diphenyl-5-methyl-2-pyrazoline. The results are shown in Table IV and are plotted in Fig. 1.

(1) (a) This work was supported by the U. S. Atomic Energy Commission under Contract No. AT-(30-1)-1931; (b) to whom inquiry concerning this article should be addressed.

(2) S. R. Sandler and S. Loshaek, *J. Chem. Phys.*, **34**, 439 (1961); **34**, 445 (1961).

(3) S. R. Sandler, P. J. McGonigal, and K. C. Tsou, *J. Phys. Chem.*, **66**, 166 (1962).

TABLE I

RELATIVE PULSE HEIGHT OF POLYVINYLTOLUENE SCINTILLATORS CONTAINING 3% *p*-TERPHERYL AND 0.05% 2-PYRAZOLINES

$\begin{array}{c} R_4-CH-C-R_3 \\ \quad \\ R_5-CH \quad N \\ \quad / \quad \backslash \\ \quad \quad N-R_1 \end{array}$					
R ₁	R ₃	R ₄	R ₅	R.P.H. ± 2	
C ₆ H ₅	CH ₃	H	C ₆ H ₅	22	
C ₆ H ₅	C ₆ H ₅	H	CH ₃	51	
C ₆ H ₅	C ₆ H ₅	H	C ₆ H ₅	49	
<i>p</i> -CH ₃ -C ₆ H ₄	C ₆ H ₅	H	C ₆ H ₅	51	
C ₆ H ₅	<i>p</i> -CH ₃ O-C ₆ H ₄	H	C ₆ H ₅	50	
C ₆ H ₅	<i>p</i> -Cl-C ₆ H ₄	H	C ₆ H ₅	52	
C ₆ H ₅	<i>p</i> -CH ₃ -C ₆ H ₄	H	C ₆ H ₅	51	
C ₆ H ₅	<i>p</i> -(CH=CH)-C ₆ H ₄	H	C ₆ H ₅	41	
C ₆ H ₅	C ₆ H ₅	<i>p</i> -C ₆ H ₅ -CH ₂ NH-C ₆ H ₄	C ₆ H ₅ ^a	52	
C ₆ H ₅	C ₆ H ₅	CH ₃ -NH-	C ₆ H ₅ ^a	52	
C ₆ H ₅	<i>p</i> -CH ₃ -C ₆ H ₄	H	<i>p</i> -(CF ₃) ₂ N-C ₆ H ₅	51	
C ₆ H ₅	<i>p</i> -CH ₃ -C ₆ H ₄	C ₆ H ₅ -CH ₂ -NH	C ₆ H ₅ ^a	51	
C ₆ H ₅	C ₆ H ₅	H	<i>p</i> -(CF ₃) ₂ N-C ₆ H ₄	45	

^a These compounds were obtained through the courtesy of Prof. N. H. Cromwell of the University of Nebraska and are described in *J. Am. Chem. Soc.*, **71**, 716 (1949); **73**, 1044 (1951). ^b R.P.H. is the relative pulse height and it is measured in per cent. when compared with an anthracene crystal of the same dimensions as 100.

TABLE II

RELATIVE PULSE HEIGHT OF POLYVINYLTOLUENE SCINTILLATORS CONTAINING 1% *p*-TERPHERYL AND SUBSTITUTED 1,3,5-TRIARYL-2-PYRAZOLINES

$\begin{array}{c} CH_2-C-R_3 \\ \quad \\ R_5-CH \quad N \\ \quad / \quad \backslash \\ \quad \quad N-R_1 \end{array}$					
R ₁	R ₃	R ₅	%	R.P.H. ± 2	
C ₆ H ₅	C ₆ H ₅	C ₆ H ₅	0.10	38	
C ₆ H ₅	C ₆ H ₅	C ₆ H ₅	.25	42	
C ₆ H ₅	C ₆ H ₅	<i>p</i> -CH ₃ CONH-C ₆ H ₄ ^a	.10	39	
C ₆ H ₅	C ₆ H ₅	<i>p</i> -CH ₃ CONH-C ₆ H ₄ ^a	.25	37	
C ₆ H ₅	C ₆ H ₅	<i>p</i> -HO-C ₆ H ₄ ^a	.10	36	
C ₆ H ₅	C ₆ H ₅	<i>p</i> -HO-C ₆ H ₄ ^a	.25	34	
C ₆ H ₅	C ₆ H ₅	<i>p</i> -CH ₃ O-C ₆ H ₄ ^a	.10	41	
C ₆ H ₅	C ₆ H ₅	<i>p</i> -CH ₃ O-C ₆ H ₄ ^a	.25	40	
C ₆ H ₅	C ₆ H ₅	<i>p</i> -C ₆ H ₅ -C ₆ H ₄ ^a	.10	41	
C ₆ H ₅	C ₆ H ₅	<i>p</i> -C ₆ H ₅ -C ₆ H ₄ ^a	.25	37	
C ₆ H ₅	<i>p</i> -CH ₃ O-C ₆ H ₄	C ₆ H ₅	.10	36	
C ₆ H ₅	<i>p</i> -CH ₃ O-C ₆ H ₄	C ₆ H ₅	.25	42	
C ₆ H ₅	<i>p</i> -CH ₃ O-C ₆ H ₄	<i>p</i> -CH ₃ O-C ₆ H ₄ ^a	.10	41	
C ₆ H ₅	<i>p</i> -CH ₃ O-C ₆ H ₄	<i>p</i> -CH ₃ O-C ₆ H ₄ ^a	.25	40	
C ₆ H ₅	<i>p</i> -C ₆ H ₅ -C ₆ H ₄	2-Naphthyl ^a	.50	35	
C ₆ H ₅	<i>p</i> -C ₆ H ₅ -C ₆ H ₄	<i>p</i> -CH ₃ O-C ₆ H ₄ ^a	.50	39	

^a These compounds were obtained through the courtesy of Drs. R. H. Wiley and C. H. Jarboe of the University of Louisville.

The ultraviolet and infrared absorption data that were used to characterize the substituted 2-pyrazolines prepared in this study are shown in Table V.

For comparison some 1,3,5-triarylpyrazoles were tested for their efficiency as wave length shifters in polyvinyltoluene. The effect of another double bond in the pyrazoline ring can be seen in Table VI.

Discussion

From the results obtained in this work a large number of 1,3,5-triaryl- and 1,3-diaryl-2-pyrazo-

TABLE III

RELATIVE PULSE HEIGHT OF POLYVINYLTOLUENE SCINTILLATORS CONTAINING SUBSTITUTED 1,3,5-TRIARYL-2-PYRAZOLINES AS FLUORS

$\begin{array}{c} CH_2-C-R_3 \\ \quad \\ R_5-CH \quad N \\ \quad / \quad \backslash \\ \quad \quad N-R_1 \end{array}$				R.P.H. ± 2		
R ₁	R ₃	R ₅	% 0.1	0.5	1.0	
C ₆ H ₅	C ₆ H ₅	C ₆ H ₅	20	30	34	
C ₆ H ₅	C ₆ H ₅	<i>p</i> -HO-C ₆ H ₄	16	24	..	
C ₆ H ₅	C ₆ H ₅	<i>p</i> -CH O-C ₆ H ₄	20	26	..	
C ₆ H ₅	C ₆ H ₅	<i>p</i> -C ₆ H ₅ -C ₆ H ₄ ^a	14	26	..	
C ₆ H ₅	<i>p</i> -CH ₃ O-C ₆ H ₄	C ₆ H ₅	15	31	..	
C ₆ H ₅	<i>p</i> -CH ₃ O-C ₆ H ₄	<i>p</i> -CH O-C ₆ H ₄	18	27	..	
C ₆ H ₅	<i>p</i> -C ₆ H ₅ -C ₆ H ₄	2-Naphthyl ^a	15	27	..	
C ₆ H ₅	<i>p</i> -C ₆ H ₅ -C ₆ H ₄	<i>p</i> -CH O-C ₆ H ₄ ^a	27	30	..	

^a See footnote a, Table II.

TABLE IV

RELATIVE PULSE HEIGHTS OF POLYVINYLTOLUENE-3% *p*-TERPHERYL SCINTILLATORS CONTAINING VARYING CONCENTRATIONS OF 1,3,5-TRISUBSTITUTED-2-PYRAZOLINES AS WAVE LENGTH SHIFTER

%	R.P.H. ± 2		
	1,3,5-Triphenyl-2-pyrazoline	1,5-Diphenyl-3- <i>p</i> -tolyl-2-pyrazoline	1,3-Diphenyl-5-methyl-2-pyrazoline
0	35	35	35
0.02	39	34	..
.03	49
.05	49	50	51
.10	47	..	52
.20	52
.25	42	38	..
.50	..	41	..

lines can be used as efficient wave length shifters in plastic scintillators.⁴ In some cases these pyrazolines are more efficient than POPOP, a conventional wave length shifter. The 2-pyrazoline ring was substituted at all available positions (1, 3, 4, and 5) with substituents that differed greatly

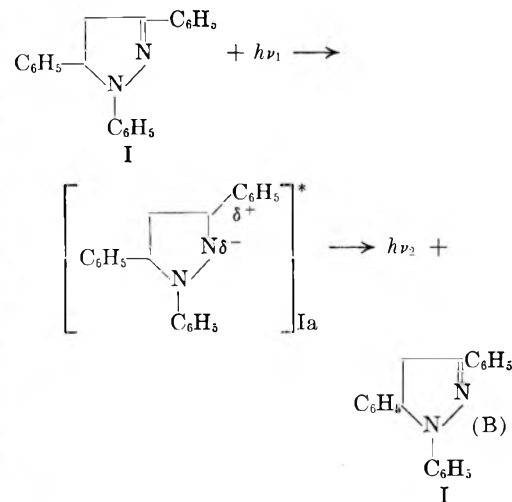
TABLE V
SPECTRAL CHARACTERISTICS OF SUBSTITUTED 2-PYRAZOLINES

R_3	R_4	R_5	λ_{max}	Ultraviolet ($m\mu$), CH ₃ OH ϵ_{max}	ϵ_{max}	C=N— Infrared (μ), KBr pellet CH_2	Ar—N	CH—N	—C—H
$p\text{-(CH}_3\text{=CH)-C}_6\text{H}_4$	H	C_6H_5	259	3,550	380	6.24(s)	7.12(m)	7.54(s)	14.45(m)
C_6H_5	H	C_6H_5	241	6,650	276	6.25(s)	7.13(s)	7.60(s)	14.42(s)
C_1H_5	H	CH_3	235	13,900	358	6.24(s)	7.18(s)	7.51(s)	14.45(s)
C_6H_5	H	C_6H_5	240	13,620	355	6.25(s)	7.17(m)	7.55(m)	14.45(s)
$p\text{-CH}_3\text{-O-C}_6\text{H}_4$	H	C_6H_5	247	10,300	350	6.25(s)	7.22(s)	7.50(m)	14.53(s)
$p\text{-Cl-C}_6\text{H}_4$	H	C_6H_5	242	16,200	360	6.27(s)	7.22(s)	7.58(s)	14.48(s)
$p\text{-CH}_3\text{-C}_6\text{H}_4$	H	C_6H_5	255	18,140	358	6.26(s)	7.19(s)	7.57(s)	14.54(s)
			(255)	(13,500)	(360)				14.32(s)
C_6H_5	$\text{CH}_3\text{-NH-}$	C_6H_5	242	14,800	360	6.24(s)	7.18(s)	7.50(m)	14.48(s)
$p\text{-CH}_3\text{-C}_6\text{H}_4$	H	$p\text{-(CH}_3\text{)}_2\text{N-C}_6\text{H}_4$	241	15,900	352	6.24(s)	7.21(s)	7.51(s)	14.58(s)
			(246)	(11,060)	(360)				
$p\text{-CH}_3\text{-C}_6\text{H}_4$	$\text{C}_6\text{H}_5\text{CH}_2\text{-NH}$	C_6H_5	244	15,400	358	6.24(s)	7.20(s)	7.60(m)	14.44(s)
C_6H_5	H	$p\text{-(CH}_3\text{)}_2\text{N-C}_6\text{H}_4$	254	22,500	355	6.17(ms)	7.25(m)	7.50(m)	14.52(s)
			(255)	(15,300)	(360)				
C_6H_5	H^e	C_6H_5	241	15,400	359	6.17(s)	7.20(s)	7.57(s)	14.50(s)
						6.27(m)			

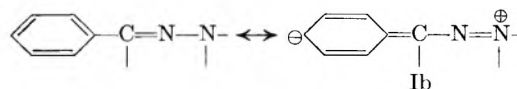
^a In chloroform solution. ^b Did not dissolve completely in methanol. ^c *p*-Tolyl substituted at 1-position.

in electronegativity. From Tables I and II it is seen that substituents on the aryl group at the 1, 3, and 5-positions and substituents at the 4-position have no significant effect on the efficiency compared to 1,3,5-triphenyl-2-pyrazoline. It is significant to note, however, that when a methyl group replaces a phenyl group at position 3 the system loses its ability to act as a wave length shifter. Furthermore, when a methyl group replaces the phenyl group at position 5 of 1,3,5-triphenyl-2-pyrazoline the efficiency is not altered. These results lead to the conclusion that the Ar—C=N—N group is important in the pyrazoline ring in order to provide a system capable of acting as a wave length shifter. The latter group cannot be effective as a wave length shifter in an acyclic form as in benzophenone phenylhydrazone or benzal-phenylhydrazone since the hydrazones are fluorescent quenchers.⁶

On the basis of these results a possible excited state for 1,3,5-triphenyl-2-pyrazoline is as follows (W^* in equation A)



It was suggested by one of the referees of our paper that it is probably the Ar—C=N—N< group that is the essential chromophore for the 358 $m\mu$ absorption. This group can resonate thus



(4) While this paper was in preparation, there appeared similar work on the use of 1,3,5-triphenyl-2-pyrazolines as efficient wave length shifters in plastic scintillators.⁵

(5) (a) E. A. Andreevich, E. E. Baroni, K. A. Kovyrzina, I. M. Rozman, and V. M. Shonya, *Izvest. Akad. Nauk. S.S.S.R. Series Fiz.*, **1**, 67 (1958); (b) I. M. Rozman and S. F. Kilin, *Soviet Phys. Uspekhi*, **2**, 856 (1960); (c) E. E. Baroni, K. A. Kovyrzina, I. M. Rozman, E. E. Andreevich, and V. M. Shonya, *Zhur. Phys. Chim.*, **34**, 665 (1960).

(6) Benzophenone phenylhydrazone and benzal phenylhydrazone give a R.P.H. of 6 and 7, respectively, when used at 0.05% in polyvinyltoluene with 3% *p*-terphenyl as fluor.

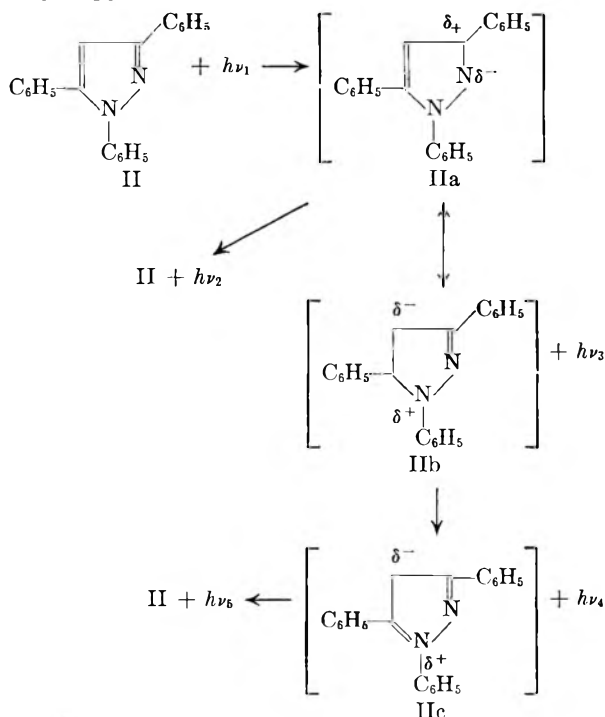
TABLE VI
RELATIVE PULSE HEIGHTS OF POLYVINYLTOLENE SCINTILLATORS CONTAINING SUBSTITUTED PYRAZOLES (0.05%) AS WAVE LENGTH SHIFTERS^a

R ₁	R ₃	R ₅	R.P.H. ±2
C ₆ H ₅	C ₆ H ₅	C ₆ H ₅	21
C ₆ H ₅	<i>p</i> -C ₆ H ₅ -C ₆ H ₄	C ₆ H ₅	34
C ₆ H ₅	<i>p</i> -CH ₃ -C ₆ H ₄	C ₆ H ₅	29

^a These scintillators contain 3% PTP. The pyrazoles were generously provided by Prof. N. H. Cromwell of the University of Nebraska.

and this chromophore is consistent with absorption at a wave length as long as 358 mμ. This also was proposed by Neunhoeffer, *et al.*⁷ We believe that Ib does contribute to the absorption process but in order for the emission process to take place Ia is sufficient. This is supported by the fact that the 3-methyl derivative does fluoresce in the greenish-yellow region. A detailed fluorescence spectra study is currently in progress to further clarify this phase of the mechanism.

Introducing another double bond at positions 4 and 5 in the pyrazoline ring and thereby converting it to a pyrazole reduces greatly the wave length shifter property of the 1,3,5-triaryl-2-pyrazolines (see Table VI). This fact probably can be explained by the ease of energy transfer of the excited state IIa to IIb or IIc because of the overlap of the π orbital with the p orbital of the nitrogen at position 1. The excited state IIa is similar to Ia and for that reason it is probably the most important one contributing to the wave length shifting property of pyrazoles.



(7) O. Neunhoeffer, G. Allsdorf, and H. Ulrich, *Ber.*, **92**, 252 (1959).

Thus part of the energy $h\nu_3$ and $h\nu_4$ is lost as self quenching of the wave length shifter itself.

1,3-Diphenyl-5-methyl-2-pyrazoline (III) shows brilliant blue fluorescence and is a wave length shifter, whereas 1,5-diphenyl-3-methyl-2-pyrazoline (IV) shows greenish yellow fluorescence and is not a good wave length shifter. The latter fact is similar to the observation by Wiley and co-workers⁸ that IV cannot be excited to a fluorescent state which is essential for a wave length shifter.

The fluorescence spectra of some 2-pyrazolines were published recently⁸ and all show maxima between 440 and 466 mμ. For example, I has a maximum at 440 mμ. Substitution in the 1, 3, or 5-aryl groups showed little change in the position of the maximum. Since the wave length shifting property depends on the fluorescent emission spectra the latter observation accounts for the fact that the efficiency of the substituted pyrazolines showed practically no change with aryl substitution as seen in Tables I and II.

The ultraviolet spectra of the 2-pyrazolines are summarized in Table V. The substitution of a methyl for a phenyl group at the 3-position causes a hypsochromic shift of almost 79 units of the 355 mμ max. This difference in absorption max. accounts for the difference in fluorescent properties and the low efficiency of the 3-methyl derivative. The substitution of a methyl group for a phenyl group at the 5-position, on the other hand, causes a bathochromic shift of only 3 units to 358 mμ with a higher ϵ -value. The presence of the absorption band at 355 ± 5 mμ therefore seems to be necessary for a good wave length shifter. The relatively little difference in wave length shifting efficiency between substitution of a methoxy (hypsochromic effect of 5 units) and a chloro group on the 3-phenyl group (bathochromic effect of 5 units) illustrates clearly the negligible substituent effect on the phenyl ring when the ultraviolet max. is within this region. The 3-styryl derivative, however, shifts the λ_{max} to 380 mμ and as a result, its wave length shifting efficiency drops almost 20% (Table I). Methyl substitution on the 1-phenyl group causes a bathochromic shift of only 4 units (to 359 mμ). Consequently, no significant improvement in wave length shifting properties was observed. The resonance effect of the *p*-styryl group and the inductive effect of a CH₃ group exert a different influence on the excited state Ia but both have the effective emission step which is required for good wave length shifting efficiency. Neunhoeffer, Allsdorf, and Ulrich⁷ earlier had attributed a hyperconjugation effect to the CH₃ group in order to account for its fluorescent property. However, since 1-phenyl-2-pyrazoline has an ultraviolet max. at 280 mμ,⁹ one would not attach too much significance to this effect at least from the small difference in ultraviolet spectra.

The ultraviolet spectra (Table V) indicate that the substitution of a methyl group for a phenyl at the 5-position shifts the 355 mμ max. in I only to

(8) R. H. Wiley, C. H. Jarboe, F. N. Hayes, E. Hansbury, J. T. Nielson, P. X. Callahan, and M. C. Sellars, *J. Org. Chem.*, **23**, 732 (1958).

(9) G. F. Duffin and J. D. Kendall, *J. Chem. Soc.*, 408 (1954).

358 $m\mu$, whereas at the 3-position it shifts the 355 $m\mu$ max. to 278 $m\mu$. The band at 355 $m\mu$ varies little with substitution, and the band at 240 $m\mu$ varies from 235–252 with substitution. Electron donating groups on the aryl groups in the pyrazoline ring shift the 240 $m\mu$ maximum to longer wave lengths.

Introduction of another double bond in the 1,3,5-triphenyl-2-pyrazoline nucleus leads to a pyrazole which does not absorb at 350–360 $m\mu$ but has only one strong band at 250 $m\mu$ (ϵ_{\max} 30,800). It is significant to note here that the ultraviolet λ_{\max} of 240 $m\mu$ is present in unsubstituted 2-pyrazoline.¹⁰

The infrared spectra of the 2-pyrazolines were examined in the 2–15 μ region and the results are shown in Table V. The single strong band at 6.25 to 6.27 μ probably is due to both the C=N and aromatic C=C stretching vibration, as also has been noted in an earlier report.⁸ In general, the fingerprint regions of the 2-pyrazolines are very similar.

The triaryl-2-pyrazolines also can be used as fluors in plastic^{11,5a} and liquid⁸ scintillators. Our results for plastics are reported in Table III. There it is seen that 1,3,5-triphenyl-2-pyrazoline at 1.0% concentration in polyvinyltoluene gives a R.P.H. of 34 whereas *p*-terphenyl (PTP) at the same concentration gives a R.P.H. of 30. A possible excited state for the pyrazoline fluor probably would be similar to that shown for it as a wave length shifter in equation B.

(10) K. Dimroth and K. Luderite, *Ber.*, **81**, 243 (1948).

(11) E. A. Andreeshchev, E. E. Baroni, K. A. Kovyrzina, I. E. Pani, I. M. Rozmen, and V. M. Shomya, *Priboiy i. Tekh. Ezperimenta*, **1**, 32 (1956).

Experimental

The 1,3,5-triaryl-2-pyrazolines were synthesized by the reaction of the appropriate chalcone and arylhydrazine in glacial acetic acid at water-bath temperatures.¹² The preparations of the new pyrazolines are described below.

3,5-Diphenyl-1-*p*-tolyl-2-pyrazoline.—A solution of 42.6 g. of benzalacetophenone and 25.0 g. of 4-methylphenylhydrazine hydrochloride (Aldrich Chemical Co.) in 500 ml. of glacial acetic acid was heated on a water-bath at 100° for 4 hours. The 2-pyrazoline crystallized when the solution was cooled to room temperature. The product was filtered, washed with methanol, and recrystallized from a mixture of benzene and methanol to give 15.0 g. (30%) of yellow crystals, m.p. 165–166°.

*Anal.*¹³ Calcd. for C₂₂H₂₀N₂: N, 8.97; Found: N, 9.04.

1-Phenyl-3-*p*-tolyl-5-dimethylaminophenyl-2-pyrazoline.—A solution of 50.0 g. of *p*-(dimethylamino)-benzal(*p*-methyl)-acetophenone and 21.0 g. of phenylhydrazine in 600 ml. of glacial acetic acid was heated in a water-bath at 100° for 4 hours and then cooled to room temperature. The crystalline product was filtered and washed with cold methanol and recrystallized from a benzene-methanol mixture to yield 24.3 g. (36%) of canary yellow needles, m.p. 143–145°.

*Anal.*¹³ Calcd. for C₂₄H₂₈N₃: C, 81.06; H, 7.16. Found: C, 80.28; H, 7.16.

Determination of Relative Pulse Heights.—The R.P.H. values were determined as previously described for plastic scintillators^{2,3} relative to an anthracene crystal of the same dimensions (13/16 × 1/2 in.) using a Pa²³⁴ β source (0.01 mc., 2.3 Mev.).

Acknowledgment.—We are grateful to Mr. Paul J. McGonigal and Mr. Heinz Günter Dickens for their help in carrying out some of the experiments, and to Dr. B. D. Halpern for his encouragement in this work.

(12) K. V. Auwers and H. Hollmann, *Ber.*, **59B**, 601 (1926).

(13) Analyses were performed by Dr. Stephen M. Nagy, Microchemical Laboratory, 78 Oliver Road, Belmont, Massachusetts.

THE REACTION OF ACTIVE NITROGEN WITH AMMONIA AT -196°

BY E. R. ZABOLOTNY AND H. GESSER

Parker Chemistry Laboratory, University of Manitoba, Winnipeg, Canada

Received August 14, 1961

Active nitrogen has been found to destroy ammonia at -196° to produce hydrazine which in turn is destroyed. Possible reaction sequences are proposed to account for the results.

Introduction

The gas phase reaction of active nitrogen with ammonia was studied recently by Freeman and Winkler² over a temperature range of -5 to about 440° . Hydrazine was not detected as a product and it therefore was assumed that only hydrogen and nitrogen were produced in the reaction. It also was found that the extent of reaction was greater at -5 than at 440° . This was attributed to secondary hydrogen atom attack on the basis of a parallel behavior in the hydrogen atom-ammonia reaction. Under similar experimental conditions the HCN produced from the active nitrogen-ethylene reaction was about six times greater than the ammonia destroyed. This was

interpreted to indicate the presence of at least two active species in active nitrogen. The reaction of active nitrogen with hydrazine was similarly investigated³ and shown to yield ammonia by secondary reactions. The present investigation was undertaken in an attempt to determine the mechanism by which ammonia is destroyed by active nitrogen.

Experimental

The apparatus was essentially that described by Winkler and co-workers,⁴ the main difference being that the discharge tube and reaction system were not poisoned and the reaction chamber was immersed in liquid nitrogen. The reactant was condensed slowly at -196° in a U-trap 40 cm. from the discharge tube (1 in. below the liquid nitrogen level)

(1) This research was supported by the Defence Research Board of Canada under Grant Number 9530-28, Project D46-9530-28.

(2) G. R. Freeman and C. A. Winkler, *J. Phys. Chem.*, **59**, 371 (1955).

(3) G. R. Freeman and C. A. Winkler, *Can. J. Chem.*, **33**, 692 (1955).

(4) D. A. Armstrong and C. A. Winkler, *J. Phys. Chem.*, **60**, 1100 (1956).

before the discharge was started. In order to leave "thick" deposits a 15-cm. section of 8-mm. tubing was inserted 35 cm. from the discharge tube as the inlet arm of the U trap. The connecting tubing between the discharge, trap and pump was 16 cm.

Anhydrous ammonia (Matheson) and redistilled hydrazine (Eastman) were used. The molecular nitrogen flow rate was 6.4×10^{-3} mole/min., corresponding to a pressure of 1.45 mm. in the reaction zone.

Condensable products and reactant were separated by a LeRoy still and the amounts measured in a combined Toepler pump and gas buret.

Hydrazine was identified by its vapor pressure, infrared analysis, and the identification of ammonia among the products of its decomposition. The potassium iodate, carbon tetrachloride test also was used but with limited success.

Results and Discussion

The yellow nitrogen afterglow was partly quenched by the solid ammonia deposit and the reaction under almost all conditions was accompanied by an intense blue reaction flame. When the discharge was turned off the blue luminescence disappeared immediately. The results of many experiments indicated that the reaction was extremely dependent on the conditions of the walls, the amount of reaction and the surface area of the reactant. For example there was a threefold decrease in the extent of reaction when the deposit was just below the level of liquid nitrogen as compared with experiments in which the ammonia was deposited at the liquid nitrogen level in the surrounding dewar vessel. The extent of decomposition of ammonia varied with the amount of reactant as shown in Table I.

TABLE I
DECOMPOSITION OF AMMONIA AT -196° BY ACTIVE NITROGEN

Reaction time, 5 min.; all quantities in micromoles		
NH ₃ reactant	NH ₃ decomposed	N ₂ H ₄ formed
37.8	8.4	2.4
78.0	11.6	2.6
117	20.4	14.4
152	14	2.5
192	17.5	4.2

When constant quantities of ammonia were used the decomposition showed a regular time depend-

TABLE II
DECOMPOSITION OF AMMONIA AT -196° BY ACTIVE NITROGEN

NH ₃ reactant, μ moles	Reaction time, min.	NH ₃ decomposed, μ moles	N ₂ H ₄ produced, μ moles
63.0	2.5	6.6	4.5
62.4	5.0	18.6	7.8
62.6	5.0	12.4	2.0
63.2	7.5	28.4	1.7
61.8	7.5	16.2	5.0
62.6	10.0	18.3	1.7
63.2	10.0	17.5	1.3
63.5	15.0	28.0	1.6
62.3	20.0	43.9	0.5
188.2	2.5	37.7	3.9
186.3	5.0	48.1	15.8
186.3	7.5	70.1	5.6
187.1	10.0	87.8	6.3
187.3	15.0	111.6	4.5
186.3	20.0	117.9	4.0

ency. The results for two different initial quantities of ammonia are recorded in Table II.

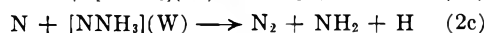
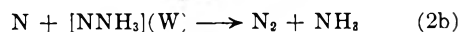
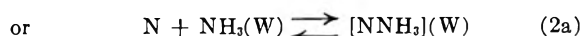
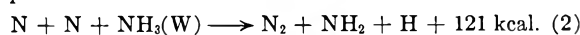
The hydrazine production goes through a maximum where a large percentage of the ammonia destroyed appears as hydrazine, thus indicating that the hydrazine is produced and subsequently destroyed by active nitrogen. This was verified by reacting active nitrogen with hydrazine at -196° . Ammonia was produced but the rate of decomposition of hydrazine was not significantly greater than the rate of decomposition of ammonia, indicating that the weak nitrogen-nitrogen bond probably plays no important part in the reaction scheme. Hydrogen atoms failed to decompose NH₃ at -196° but reacted with N₂H₄ to yield ammonia to about the same extent as did active nitrogen.

The flow rate of nitrogen atoms as determined by the yield of HCN from ethylene was 250×10^{-6} mole/min. Hence only a small percentage (about 1 to 15%) of the available nitrogen atoms leads to ammonia destruction.

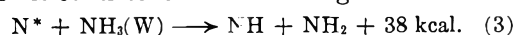
Several possible reactions can be considered as responsible for the decomposition of ammonia by active nitrogen⁵



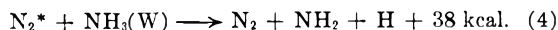
This reaction can be definitely eliminated since it would have a minimum activation energy of 17 kcal. and would not occur to a significant extent at -196° . This is in agreement with the gas phase reaction.^{2,6}



These reactions probably occur on the walls where ammonia can be destroyed by the energy of recombination of nitrogen atoms. The reactivity of hydrogen atoms with ammonia and hydrazine at -196° is consistent with the energetics involved.



This reaction could proceed quite readily with ²D and ²P excited nitrogen atoms, but the low concentration of these species in active nitrogen precludes their importance. Metastable A³Σ nitrogen



molecules have been postulated⁷ as the species in active nitrogen which is responsible for the destruc-

(5) Heats of reaction are based on

$D(\text{N}-\text{H}) = 87 \text{ kcal.}$ G. Pannetier and A. G. Gaydon, *J. chim. phys.*, **48**, 221 (1951).

$D(\text{NH}-\text{H}) = 90 \text{ kcal.}$ A. P. A'tschuller, *J. Chem. Phys.*, **22**, 1947 (1954).

$D(\text{NH}_2-\text{H}) = 104 \text{ kcal.}$ M. Szwarc, *Chem. Revs.*, **47**, 75 (1950).

$D(\text{N}_2) = 225 \text{ kcal.}$ J. M. Handrie, *J. Chem. Phys.*, **22**, 1503 (1954).

$D(\text{NH}_2-\text{NH}_2) = 60 \text{ kcal.}$ M. Szwarc, *Proc. Roy. Soc. (London)*, **A198**, 267 (1949).

$A^3\Sigma(\text{N}_2^*) = 142 \text{ kcal.}$ K. D. Bayes, *Can. J. Chem.*, **39**, 1074 (1961).

$\text{N}(^2\text{D}) = 55 \text{ kcal.}$ } Atomic Energy Levels. National Bureau of
 $\text{N}(^2\text{P}) = 82.5 \text{ kcal.}$ } Standards. Circular 467.

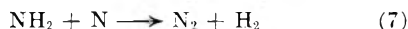
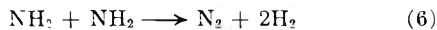
(6) G. B. Kistiakowsky and G. G. Volpi, *J. Chem. Phys.*, **28**, 665 (1958).

(7) (a) K. D. Bayes, *Can. J. Chem.*, **39**, 1074 (1961); (b) R. L. Nelson, A. N. Wright, and C. A. Winkler, Symposium on Some Fundamental Aspects of Atomic Reactions, Sept., 1960, McGill University, Montreal.

tion of ammonia in the gas phase, and probably accounts for the major process by which ammonia is decomposed at -196° . Hydrazine undoubtedly is formed by the recombination of NH_2 radicals on the walls.

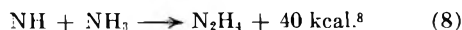


These radicals also are destroyed by the reactions



In some cases it is noted that more N_2H_4 is pro-

duced than is equivalent to one-half of the ammonia decomposed. This would seem to indicate that hydrazine may be formed by some process, other than reaction 5, which incorporates nitrogen from the discharge, possibly by a reaction such as



where the NH radical could be formed by atom recombination or by reaction 3.

(8) See G. R. Freeman and C. A. Winkler, *Can. J. Chem.*, **33**, 692 (1955), for appropriate energy values.

THERMODYNAMICS OF INTERFACES BETWEEN CONDENSED PHASES¹

BY ROBERT S. HANSEN

Institute for Atomic Research and Department of Chemistry, Iowa State University, Ames, Iowa

Received August 16, 1961

Measurements of properties of plane interfaces between condensed phases generally are conducted at constant pressure. The Gibbs surface excess convention, which eliminates pressure as an independent variable, is not the natural convention for such measurements. A convention eliminating chemical potentials of two components is discussed and shown to be particularly appropriate for condensed phase interfaces. The physical interpretation of this convention and formulas for evaluation of thermodynamic quantities from experimental data are presented. An approach to the evaluation of statistical theories of adsorption from solution in terms of experimental thermodynamic information is illustrated.

Theoretical

Interfacial thermodynamics has received broad study and the basic approach to this subject can be considered well known. The classic work is that of Gibbs²; an excellent paper by Guggenheim and Adam³ discusses the physical interpretation of surface excesses, and Guggenheim⁴ has given a good summary of interfacial thermodynamics emphasizing a viewpoint somewhat different from that of Gibbs. A very brief presentation by Guggenheim (ref. 4, p. 221) has a result which would be equivalent to that obtained by the convention suggested here, and another very brief treatment by Overbeek⁵ is similar in concept. An introduction to the present thermodynamic problem therefore can be briefly stated.

Consider two phases α and β containing n_1, n_2, \dots, n_k moles of components 1, 2, \dots , k ; let σ denote the plane interface between them. Let E, S and V be the energy, entropy and volume of the system; A the area of σ ; c_i^α and c_i^β the concentrations of i in α and β at great distance from σ ; $E^\alpha, E^\beta, s^\alpha$, and s^β the energies and entropies per unit volume in α and β ; and let γ be the boundary tension. At equilibrium the temperature T , pressure P , and chemical potential μ_i are uniform throughout the system. Then three equations apply to the system

$$0 = -S dT + V dp - A d\gamma - \sum_{i=1}^k n_i d\mu_i \quad (1)$$

$$0 = -s^\alpha dT + dp - \sum_{i=1}^k c_i^\alpha d\mu_i \quad (2)$$

$$0 = -s^\beta dT + dp - \sum_{i=1}^k c_i^\beta d\mu_i \quad (3)$$

Equation 1 can be considered to express a functional relation between γ and the $k+2$ variables $T, p, \mu_1, \dots, \mu_k$; eq. 2 and 3 indicate that only k of these variables are independent. Equations 2 and 3 can be used to express any two of the variables $T, p, \mu_1, \dots, \mu_k$ in terms of the remaining k to obtain in eq. 1 a relation between one dependent and k independent variables. Multiply eq. 2 by λ^α , eq. 3 by λ^β , and subtract from eq. 1 to obtain

$$A d\gamma = -(S - \lambda^\alpha S^\alpha - \lambda^\beta S^\beta) dT + (V - \lambda^\alpha V^\alpha - \lambda^\beta V^\beta) dP - \sum_{i=1}^k (n_i - \lambda^\alpha c_i^\alpha - \lambda^\beta c_i^\beta) d\mu_i \quad (4)$$

Elimination of two differentials is simply achieved by choosing λ^α and λ^β to make their coefficients zero; the same result is obtained in more cumbersome fashion by using eq. 2 and 3 to eliminate them algebraically.

Define the quantities $E_d^s, S_d^s, V_d^s, n_{id}^s$ by $E_d^s = E - \lambda^\alpha E^\alpha - \lambda^\beta E^\beta$; $S_d^s = S - \lambda^\alpha S^\alpha - \lambda^\beta S^\beta$; $V_d^s = V - \lambda^\alpha V^\alpha - \lambda^\beta V^\beta$; $n_{id}^s = n_i - \lambda^\alpha c_i^\alpha - \lambda^\beta c_i^\beta$, and the quantities $E_{id}^s, S_{id}^s, \tau_{id}^s, \Gamma_{id}$ by $A E_d^s = E_{id}^s, A S_d^s = S_{id}^s, A \tau_{id}^s = V_{id}^s, A \Gamma_{id} = n_{id}^s$, then

$$d\gamma = -s_d^s dT + \tau_d^s dP - \sum_{i=1}^k \Gamma_{id} d\mu_i \quad (5)$$

and this equation is basic in the sense that only independent differentials appear on the right hand side if λ^α and λ^β are chosen to make any two of the

(1) Contribution No. 1052. Work was performed in the Ames Laboratory of the U. S. Atomic Energy Commission.

(2) J. W. Gibbs, "Collected Works," Vol. I, Yale University Press, New Haven, Conn., 1948, pp. 219-237.

(3) E. A. Guggenheim and N. K. Adam, *Proc. Roy. Soc. (London)*, **A139**, 218 (1933).

(4) E. A. Guggenheim, "Thermodynamics," 2nd Ed., pp. 35-45, 214-226, 255-57, Interscience Publishers, Inc., New York, N. Y., 1950.

(5) J. Th. G. Overbeek in H. R. Kruyt, Ed., "Colloid Science," Vol. I, Elsevier Publishing Co., Amsterdam, 1952, pp. 116-118.

quantities $s_d^s, \tau_d^s, \Gamma_{id} \dots \Gamma_{kd}$ equal to zero. The form of eq. 5 will depend on the convention d exercised in this choice. Now γ is a property of the interface, independent of the amounts of phases α and β present so long as these amounts are sufficient to extend to appreciable distances away from the interface. Its partial derivatives after the independent variables on which it depends, and therefore such quantities as s_d^s, τ_d^s and Γ_{id}^s for a given convention d, also must be independent of the amounts of α and β present. This physically obvious result is easily confirmed mathematically; changes in amounts of α and β present correspond to replacing S by $S + as^\alpha + bs^\beta, V$ by $V + a + b, n_i$ by $n_i + ac_i^\alpha + bc_i^\beta, \epsilon$ and it is readily shown that, if λ^α and λ^β are chosen to make two specified differential coefficients vanish, the remaining coefficients are independent of a and b . The properties $S_d^s, \tau_d^s, \Gamma_{id}, \text{etc.}$, are hence properties of the interface and the convention used to define them, and can be considered specific surface excess quantities.

In the Gibbs convention, λ^α and λ^β are chosen to make the coefficients of dp and one chemical potential differential, say $d\mu_1$, vanish (*i.e.*, to eliminate P and μ_1 as independent variables). In this convention, therefore, τ_d^s and Γ_{id} are zero. Effectively, the same choice is used by Guggenheim in his general treatment.⁴ Any two of the surface excess quantities (*e.g.*, s_d^s and τ_d^s, s_d^s and Γ_{id} , or Γ_{id} and Γ_{2d}) could equally well have been chosen as zero; the choice is purely conventional but the Gibbs choice is the classic one. Physically, however, it is desirable to retain as independent any variables which we intend to control experimentally. For this reason it is not desirable to eliminate temperature as an independent variable. In experiments dealing with interfaces between condensed phases (*e.g.*, liquid-liquid or solid-liquid interfaces) it appears equally undesirable to eliminate pressure as an independent variable. In fixed temperature, fixed pressure experiments it is convenient to eliminate two chemical potentials, which we shall choose as μ_1 and μ_2 , as independent variables by setting Γ_{1d} and Γ_{2d} equal to zero. We denote by E^s, S^s, τ^s and Γ_i the specific surface excess quantities, $\bar{E}^s, S^s, V^s, n_i^s$, the total surface excess quantities established by this convention. Then

$$d\gamma = -s^s dT + \tau^s dP - \sum_{i=3}^k \Gamma_i d\mu_i \quad (6)$$

The equations $\Gamma_1 = \Gamma_2 = 0$ establish λ^α and λ^β

$$\lambda^\alpha = \frac{n_1 c_2^\beta - n_2 c_1^\beta}{c_1^\alpha c_2^\beta - c_2^\alpha c_1^\beta} \quad \lambda^\beta = \frac{n_2 c_1^\alpha - n_1 c_2^\alpha}{c_1^\alpha c_2^\beta - c_2^\alpha c_1^\beta}$$

Physically, λ^α and λ^β are the volumes of phases α and β (considered homogeneous with compositions as they exist far from σ) which would together contain the amounts of components 1 and 2 in the system.

We now consider two propositions concerning the specific surface excess quantities.

(1) If the partial molal volume of each component in the system is independent of location (*i.e.*, $\bar{v}_i^\alpha = \bar{v}_i^\beta = \bar{v}_i^\sigma = \bar{v}_i$) then, since $\sum \bar{v}_i^\alpha c_i^\alpha = \sum \bar{v}_i^\beta c_i^\beta = 1$ we have

$$A \sum_{i=1}^k \bar{v}_i \Gamma_{id} = \sum_{i=1}^k n_i \bar{v}_i - \lambda^\alpha - \lambda^\beta = V - \lambda^\alpha - \lambda^\beta = A \tau_d^s$$

i.e.,

$$\sum_{i=1}^k \bar{v}_i \Gamma_{id} = \tau_d^s$$

regardless of the convention d. If the concentration of a component j in a phase α is such that $\bar{v}_j^\alpha c_j^\alpha \ll 1$ the above conclusion is negligibly altered if $\bar{v}_j^\alpha \neq \bar{v}_j^\beta = \bar{v}_j^\sigma$. In a two-phase three-component condensed system (*e.g.*, water-benzene-heptanol) we would expect $\tau_d^s \sim 10^{-7}$ cm. For such a system $(\partial\gamma/\partial p)_{T,\mu_3} \sim 10^{-7}$ cm., or about 0.1 dyne/cm. atmosphere. Evidently studies over large pressure ranges will be necessary for accurate documentation of the pressure dependence of properties of interfaces between condensed phases, including τ_d^s . For most practical purposes properties of interfaces between condensed phases are pressure independent and information derivable from a pressure dependence is unavailable. This fact is obscured when pressure is eliminated as an independent variable.

(2) The proposed convention seems well suited to a discussion of the interface between an inert gas (component 1) and a solution of slightly volatile components (2, 3...). Choosing $\Gamma_1 = \Gamma_2 = 0$, values of λ^α and λ^β have been given, and we have $\lambda^\alpha + \lambda^\beta = V - A\tau_s, c_2^\alpha \lambda^\alpha + c_2^\beta \lambda^\beta = n_2$. Suppose that the inert gas has negligible surface activity and solubility in the solution phase; then its removal from the system, keeping $n_2, n_3 \dots, V$ and T fixed should negligibly affect $c_2^\alpha, c_3^\alpha \dots c_2^\beta, c_3^\beta \dots$. To this modified system the Gibbs convention is appropriate. Denoting quantities in this convention by primes, we have $\tau_s' = 0, \Gamma_2' = 0$, so $\lambda'^\alpha + \lambda'^\beta = V, c_1^\alpha \lambda'^\alpha + c_2^\beta \lambda'^\beta = n_2$. So

$$\lambda'^\alpha - \lambda^\alpha = \frac{A\tau_s c_2^\beta}{c_2^\beta - c_2^\alpha}, \lambda'^\beta - \lambda^\beta = -\frac{A\tau_s c_2^\alpha}{(c_2^\beta - c_2^\alpha)}$$

and

$$A(\Gamma_1' - \Gamma_1) = -(\lambda'^\alpha - \lambda^\alpha)c_1^\alpha - (\lambda'^\beta - \lambda^\beta)c_1^\beta = \frac{A\tau_s}{c_2^\beta - c_2^\alpha} (c_2^\alpha c_1^\beta - c_2^\beta c_1^\alpha)$$

Let α denote the gas phase, 2 the major component of the solution. Then $A\tau_s c_2^\beta$ is in order of magnitude the number of moles in a monolayer. In an aqueous 1 molar solution, for example, $c_2^\beta - c_2^\alpha \sim 50$ moles per liter, and if the vapor pressure of no component exceeds 100 mm. at room temperature $(c_2^\alpha/c_2^\beta)(c_1^\beta - c_1^\alpha) \sim 0.006$. Hence $\Gamma_1' - \Gamma_1 \sim 10^{-4}$ monolayer, *i.e.*, Γ_1' and Γ_1 differ negligibly if vapor pressures are small and component 2 is the major component of the solution.

We now consider some general thermodynamic relations in terms of the proposed convention. From the first and second laws of thermodynamics together with the definitions of surface excess quantities ($\Gamma_1 = \Gamma_2 = 0$ convention) we have

$$dE^s = T dS^s - p dV^s + \gamma dA + \sum_{i=3}^k \mu_i dn_i^s \quad (7)$$

We define the accessory functions $3C^s, H^s, F^s$ and G^s by

$$\mathcal{H}^s = E^s + pV^s \quad (8)$$

$$H^s = E^s + pV^s - \gamma A = \mathcal{H}^s - \gamma A \quad (9)$$

$$F^s = E^s + pV^s - TS^s = \mathcal{H}^s - TS^s \quad (10)$$

$$G^s = E^s + pV^s - TS^s - \gamma A = H^s - TS^s = F^s - \gamma A \quad (11)$$

and the corresponding specific quantities $\bar{\mathcal{H}}^s$, \bar{H}^s , \bar{F}^s , \bar{G}^s by $A\bar{\mathcal{H}}^s = \mathcal{H}^s$, $A\bar{H}^s = H^s$, $A\bar{F}^s = F^s$, $A\bar{G}^s = G^s$. Note also that $\bar{\mathcal{H}}^s = (\partial\mathcal{H}^s/\partial A)_{T,p,\gamma,\mu_i}$, etc. (subscript μ_i means that $\mu_3, \mu_4 \dots \mu_k$ are all held constant, *i.e.*, all $k-2$ independent chemical potentials). Where X^s is any extensive surface excess thermodynamic quantity, define \bar{x}^s by

$$\bar{x}_i^s = \left(\frac{\partial X^s}{\partial n_i^s} \right)_{T,p,\gamma,n_j^s} \quad (12)$$

the subscript n_j^s meaning that all of the quantities $n_3^s, n_4^s, \dots, n_k^s$ except n_i^s are held constant, \bar{x}_i^s is the surface analog of a bulk partial molal quantity;

X^s is homogeneous of degree 1 in n^s , so $\sum_{i=3}^k n_i^s \bar{x}_i^s = X^s$. (Note: X^s will in general have a non-zero value even when $n_3^s, n_4^s, \dots, n_k^s$ are all zero,

$$X_0^s = \lim_{\text{all } n_i^s \rightarrow 0} \sum_{i=3}^k n_i^s \bar{x}_i^s \neq 0 \text{ in general}$$

With these definitions

$$G^s = \sum_{i=3}^k \mu_i n_i^s; \quad G^s = \sum_{i=3}^k \mu_i \Gamma_i \quad (13)$$

$$\bar{G}_i^s = \mu_i = \left(\frac{\partial F^s}{\partial n_i^s} \right)_{T,p,A,n_j^s} \quad (14)$$

$$\bar{H}_i^s = \mu_i + T\bar{s}_i^s = -T^2 \left[\frac{\partial}{\partial T} \left(\frac{\mu_i}{T} \right) \right]_{p,\gamma,n_i^s,n_j^s} \quad (15)$$

$$\left(\frac{\partial \mathcal{H}^s}{\partial n_i^s} \right)_{T,p,A,n_j^s} = \mu_i + T \left(\frac{\partial S^s}{\partial n_i^s} \right)_{T,p,A,n_j^s} = -T^2 \left[\frac{\partial}{\partial T} \left(\frac{\mu_i}{T} \right) \right]_{p,A,n_i^s,n_j^s} \quad (16)$$

$$\gamma \bar{A}_i = \bar{F}_i^s - \mu_i = \bar{\mathcal{H}}_i^s - \bar{H}_i^s \quad (17)$$

$$s^s = - \left(\frac{\partial \gamma}{\partial T} \right)_{p,\mu_i} \quad (18)$$

$$\left(\frac{\partial S^s}{\partial A} \right)_{T,p,n_i^s} = - \left(\frac{\partial \gamma}{\partial T} \right)_{p,A,n_i^s} = - \left(\frac{\partial \gamma}{\partial T} \right)_{p,\Gamma_i} \quad (19)$$

$$\bar{s}_i^s = \left(\frac{\partial S^s}{\partial n_i^s} \right)_{T,p,A,n_j^s} - \bar{A}_i \left(\frac{\partial \gamma}{\partial T} \right)_{p,\Gamma_i,\Gamma_j} \quad (20)$$

$$\bar{\mathcal{H}}^s = \sum_{i=3}^k \mu_i \Gamma_i + \gamma - T \left(\frac{\partial \gamma}{\partial T} \right)_{p,\mu_i} \quad (21)$$

$$\mathcal{H}^s = \sum_{i=3}^k n_i^s \left(\frac{\partial \mathcal{H}^s}{\partial n_i^s} \right)_{T,p,A,n_j^s} + A \left[\gamma - T \left(\frac{\partial \gamma}{\partial T} \right)_{p,\Gamma_i} \right] \quad (22)$$

Suppose activities of components in one phase are known, then $\mu_i = \mu_i^0 + RT \ln a_i$, where μ_i^0 is the chemical potential of component i in its reference state. Let $\bar{H}_i^1 = -T^2 d/dT (\mu_i^0/T)$ and $\bar{s}_i^0 = 1/T (\bar{H}_i^0 - \mu_i^0)$ be the partial molal enthalpy and entropy of i in its reference state. Then

$$\bar{H}_i^s - \bar{H}_i^0 = -RT^2 \left(\frac{\partial \ln a_i}{\partial T} \right)_{p,\gamma,n_i^s,n_j^s} \quad (23)$$

$$\left(\frac{\partial \mathcal{H}^s}{\partial n_i^s} \right)_{T,p,A,n_j^s} - \bar{H}_i^0 = -RT^2 \left(\frac{\partial \ln a_i}{\partial T} \right)_{p,A,n_i^s,n_j^s} = -RT^2 \left(\frac{\partial \ln a_i}{\partial T} \right)_{p,\Gamma_i,\Gamma_j} \quad (24)$$

$$\left(\frac{\partial \ln a_i}{\partial T} \right)_{p,\Gamma_i,\Gamma_j} = \left(\frac{\partial \ln a_i}{\partial T} \right)_{p,\gamma,n_i^s,n_j^s} - \frac{\bar{A}_i}{RT} \left(\frac{\partial \gamma}{\partial T} \right)_{p,\Gamma_i,\Gamma_j} \quad (25)$$

Evidently numerous other relations could be derived; those given appear most likely to be useful.

Derivation of Surface Excess Thermodynamic Functions from Experimental Data. Boundary Tension Measurements.—The boundary tension is the thermodynamic potential appropriate to the variables $p, T, \mu_3, \mu_4 \dots$ (*i.e.*, given the function $\gamma(p, T, \mu_3, \mu_4 \dots)$ all surface excess quantities can be obtained by differentiation. Thus (see eq. 6)

$$s^s = - \left(\frac{\partial \gamma}{\partial T} \right)_{p,\mu_i} \quad (26)$$

$$\tau^s = \left(\frac{\partial \gamma}{\partial p} \right)_{T,\mu_i} \quad (27)$$

$$\Gamma_i = - \left(\frac{\partial \gamma}{\partial \mu_i} \right)_{T,p,\mu_j} \quad (28)$$

whence other thermodynamic functions can be obtained from their definitions.

Experimental information can readily provide instead the function $\gamma(T, p, a_3, a_4 \dots)$, from which

$$s^s = - \left(\frac{\partial \gamma}{\partial T} \right)_{p,a_i} - \sum_{i=3}^k \Gamma_i \left(\frac{\partial \mu_i}{\partial T} \right)_{p,a_i,a_j} = - \left(\frac{\partial \gamma}{\partial T} \right)_{p,a} + \sum_{i=3}^k \Gamma_i (\bar{s}_i^0 - R \ln a_i) \quad (29)$$

$$\tau^s = \left(\frac{\partial \gamma}{\partial p} \right)_{T,a_i} \quad (30)$$

$$\Gamma_i = - \frac{1}{RT} \left(\frac{\partial \gamma}{\partial \ln a_i} \right)_{T,p,a_j} \quad (31)$$

$$G^s = \sum_{i=3}^k \Gamma_i (\mu_i^0 + RT \ln a_i) \quad (32)$$

$$F^s = \sum_{i=3}^k \Gamma_i (\mu_i^0 + RT \ln a_i) + \gamma \quad (33)$$

$$H^s = -T \left(\frac{\partial \gamma}{\partial T} \right)_{p,a_i} + \sum_{i=3}^k \Gamma_i \bar{H}_i^0 \quad (34)$$

$$\mathcal{H}^s = \gamma - T \left(\frac{\partial \gamma}{\partial T} \right)_{p,a_i} + \sum_{i=3}^k \Gamma_i \bar{H}_i^0 \quad (35)$$

These are illustrative and are probably the most useful thermodynamic quantities obtainable from boundary tension measurements (experimental information generally will not suffice for the calculation of τ^s ; the quantities $\bar{s}_i^0, \bar{H}_i^0 - \bar{H}_i^0$, and $\mu_i^0 - \bar{\mathcal{H}}_{i0}^0$, where $\bar{\mathcal{H}}_{i0}^0$ is the enthalpy of pure i at absolute zero, are obtainable but may be unknown).

Adsorption Isotherms from Concentration Change.—Isotherms of concentration change generally are determined for a solid adsorbent and liquid solution having negligible mutual solubility. Let V ml. of solution (phase β) containing $n_2, n_3 \dots$ moles of components 2, 3, \dots with initial concentrations $c_2', c_3' \dots$ be added to n_1 moles of adsorbent (component 1, phase α). At equilibrium the concentrations in phase β are $c_2, c_3 \dots$. Con-

centrations of component 1 in phase β , and of components 2, 3 . . . in α all are assumed to be zero at equilibrium. All initial and final concentrations are subject to determination. Then

$$\lambda_\alpha = \frac{n_1}{c_1^\alpha} \lambda_\beta = \frac{n_2}{c_2} = \frac{Vc_2'}{c_2}$$

$$n_i^s = n_i - \lambda_\alpha c_i^\alpha - \lambda_\beta c_i^\beta =$$

$$Vc_i' - V \frac{c_2'}{c_2} c_i = V(c_i' - c_i) + V \left(\frac{c_2 - c_2'}{c_2} \right) c_i \quad (36)$$

The function $V(c_i' - c_i) = f(c_3, c_4 \dots)$ is the commonly presented isotherm of concentration change, the quantity $V[(c_2 - c_2'/c_2)c_i]$ an accessible modifying term, small if component 2 is the major component of β . Let $\bar{v}_2, \bar{v}_3 \dots$ be the partial molar volumes of components 2, 3 . . . in the equilibrium solution, then

$$\sum_{i=3}^k n_i^s \bar{v}_i = V \sum_{i=3}^k \bar{v}_i (c_i' - c_i) + V \frac{c_2 - c_2'}{c_2} \sum_{i=3}^k \bar{v}_i c_i$$

But $\sum_{i=2}^k \bar{v}_i c_i = 1$; further if $c_i' - c_i$ is small in first order for all i , $\sum_{i=2}^k \bar{v}_i c_i' - 1$ will be small in second order (because $\sum_{i=2}^k c_i d\bar{v}_i = 0$). $\sum_{i=3}^k \bar{v}_i c_i = 1 - \bar{v}_2 c_2$, and to excellent approximation if all $(c_i' - c_i)$ are small, $\sum_{i=3}^k \bar{v}_i c_i' = 1 - \bar{v}_2 c_2'$. Therefore

$$\sum_{i=3}^k n_i^s \bar{v}_i = V \left(\frac{c_2 - c_2'}{c_2} \right)$$

and we have seen previously that if the partial molar volumes also have the values \bar{v} in the interfacial region, this is equal to V^s . For condensed systems $V(c_2 - c_2'/c_2)$ must approximate V^s in any event. If the solution contains only two components, $V(c_2 - c_2'/c_2) = V(\bar{v}_3/\bar{v}_2)(c_3' - c_3/c_2)$. The total surface excess quantities $n_3^s, n_4^s \dots$ hence can be obtained; the surface area of the adsorbent can be measured so the specific surface excess quantities $\Gamma_3, \Gamma_4, \dots$ can be calculated. Suppose $\Gamma_3, \Gamma_4, \dots$ have been evaluated as functions of $T, p, a_3, a_4 \dots$. Thermodynamic information can be obtained most directly from the spreading pressure

$$\phi(T, p, a_3, a_4 \dots) = \gamma_0(T, p) - \gamma(T, p, a_3, a_4 \dots) = \int_{0, 0 \dots}^{a_3, a_4 \dots} \sum_{i=3}^k \Gamma_i RT d \ln a_i \quad (37)$$

where $\gamma_0(T, p)$ is the interfacial tension in the absence of components 3, 4 Then from eq. 29-35

$$s^s = - \left(\frac{\partial \gamma_0}{\partial T} \right)_p + \left(\frac{\partial \phi}{\partial T} \right)_{p, a_i} + \sum_{i=2}^k \Gamma_i (\bar{s}_i^0 - R \ln a_i) \quad (38)$$

$$g^s = \sum_{i=3}^k \Gamma_i (\mu_i^0 + RT \ln a_i) \quad (39)$$

$$f^s = \sum_{i=3}^k \Gamma_i (\mu_i^0 + RT \ln a_i) + \gamma_0 - \phi \quad (40)$$

$$h^s = -T \left(\frac{\partial \gamma_0}{\partial T} \right)_p + T \left(\frac{\partial \phi}{\partial T} \right)_{p, a_i} + \sum_{i=3}^k \Gamma_i \bar{h}_i^0 \quad (41)$$

$$\bar{\mathcal{C}}^s = \gamma_0 - T \left(\frac{\partial \gamma_0}{\partial T} \right) - \phi + T \left(\frac{\partial \phi}{\partial T} \right)_{p, a_i} + \sum_{i=3}^k \Gamma_i \bar{h}_i^0 \quad (42)$$

The quantities $\gamma_0, s_c^s = -(\partial \gamma_0 / \partial T)_p$, and $\bar{\mathcal{C}}_0^s = \gamma_0 - T(\partial \gamma_0 / \partial T)_p$ will not in general be available for solid adsorbents. Alternatively, $(\partial \mathcal{C}^s / \partial n_i^s)_{T, p, A, n_j^s}$ can be obtained by means of eq. 24, and $\bar{\mathcal{C}}^s$ calculated by a modification of eq. 22

$$A \bar{\mathcal{C}}^s = \sum_{i=3}^k n_i^s \left(\frac{\partial \mathcal{C}^s}{\partial n_i^s} \right)_{T, p, A, n_j^s} + A \bar{\mathcal{C}}_0^s - A \left[\phi - T \left(\frac{\partial \phi}{\partial T} \right)_{p, \Gamma_i} \right] \quad (43)$$

Heat of Wetting Experiments.—We shall consider only the wetting of a single-component solid phase by a liquid solution; the solid phase α consists of component 1, the solution phase β of components 2, 3 Component 1 will be assumed insoluble in β , components 2, 3 . . . insoluble in α , and it will be assumed that the wetting process occurs without change in surface area. It is believed that all heat of wetting experiments so far conducted have been intended to conform to this model.

Let $\gamma_0^0, s_0^0 = -d\gamma_0^0/dT, \bar{\mathcal{C}}_0^0 = \gamma_0^0 - T(d\gamma_0^0/dT)$ pertain to the solid-“vacuum” interface, $\gamma_0, s_0^s, \bar{\mathcal{C}}_0^s$ to the interface between solid and pure component 2. The heat absorbed in a constant pressure, constant area process is $\Delta \mathcal{C}$.

Let \bar{h}_1 be the partial molal enthalpy of component 1 in $\alpha, \bar{h}_2', \bar{h}_3' \dots$ the partial molal enthalpies of 2, 3 . . . in β before wetting has occurred, $\bar{h}_2'', \bar{h}_3'' \dots$ corresponding values after wetting has occurred. When the solid is wet by a solution containing $n_2, n_3 \dots$ moles of components 2, 3 . . . (for convenience we shall suppose the total wetting process is isothermal, *i.e.*, initial solid and solution temperatures and final system temperature are all the same) we have

$$\begin{aligned} Q = \Delta \mathcal{C} &= \mathcal{C}_{\text{final}} - \mathcal{C}_{\text{initial}} \\ &= n_1 \bar{h}_1 + \sum_{i=2}^k (n_i - n_i^s) \bar{h}_i'' + \mathcal{C}^s - n_1 \bar{h}_1 - \sum_{i=2}^k n_i \bar{h}_i' - A \bar{\mathcal{C}}_0^0 \\ &= \mathcal{C}^s - \sum_{i=3}^k n_i^s \bar{h}_i'' + \sum_{i=2}^k n_i (\bar{h}_i'' - \bar{h}_i') - A \bar{\mathcal{C}}_0^0 \end{aligned} \quad (44)$$

At constant temperature and pressure $\sum n_i d\bar{h}_i = 0$, hence if bulk concentration changes in β resulting from adsorption are sufficiently small that $\bar{h}_i'' - \bar{h}_i'$ is small in first order for all $i, \sum_{i=2}^k n_i (\bar{h}_i'' - \bar{h}_i')$ will be small in second order and can be neglected. To this approximation

$$Q = \Delta \mathcal{C} = \mathcal{C}^s - \sum_{i=3}^k n_i^s \bar{h}_i'' - A \bar{\mathcal{C}}_0^0 \quad (45)$$

If $Q' = \Delta \mathcal{C}'$ is the heat of wetting of adsorbent by pure component 2 we have also

$$Q - Q' = \Delta\mathcal{H} - \Delta\mathcal{H}' = \mathcal{H}^s - \sum_{i=3}^k n_i^s \bar{H}_i'' - A\mathcal{H}_0^s \quad (46)$$

$$\left(\frac{\partial\Delta\mathcal{H}}{\partial n_i^s}\right)_{T,p,A,n_j^s} = \left(\frac{\partial\mathcal{H}_0^s}{\partial n_i^s}\right)_{T,p,A,n_j^s} - \bar{H}_i'' \quad (47)$$

To obtain $(\partial\mathcal{H}^s/\partial n_i^s)_{T,p,A,n_j^s} - \bar{H}_i^0$ it will in general be necessary to obtain $\bar{H}'' - \bar{H}^0$ from heat of solution measurements.

Comparison of Surface Excess Thermodynamic Functions with Predictions of Statistical Models.—

Statistical models generally will involve actual regions, numbers of molecules, etc., and will predict thermodynamic quantities for these regions, not surface excess quantities. This fact is important when comparing theory with experiment. Statistical treatments based on canonical ensembles will yield $F = E - TS$ as a function of $T, V, A, n_1, n_2 \dots$ with $(\partial F/\partial T)_{V,A,n_1,n_2,\dots} = -S, (\partial F/\partial V)_{T,A,n_1,n_2} = -P, (\partial F/\partial A)_{T,V,n_1,n_2,\dots} = \gamma, (\partial F/\partial n_i)_{T,V,A,n_j} = \mu_i$. Statistical treatments based on grand canonical ensembles will yield the thermodynamic potential $Y = pV - \gamma A$ as a function of $T, V, A, \mu_1, \mu_2 \dots$ with $(\partial Y/\partial T)_{V,A,\mu_i} = S, (\partial Y/\partial V)_{T,A,\mu_i} = P, (\partial Y/\partial A)_{T,V,\mu_i} = -\gamma, (\partial Y/\partial \mu_i)_{T,V,A,\mu_j} = n_i$. Treatments of condensed interfacial regions usually will assume these regions to be nearly incompressible or use approximations equivalent to this assumption.

The method of comparing theory with experiment will be illustrated with a simple statistical model, namely the Langmuir model adapted to adsorption from solution. Consider a solid (phase α , component 1) and a binary solution (phase β , components 2 and 3). Component 1 is insoluble in β , components 2 and 3 insoluble in α . For simplicity we shall suppose molecules of 2 and 3 to be interchangeable in two- and three-dimensional lattices, *i.e.*, to be substantially of the same size. We further suppose that the region of inhomogeneity σ is limited to a monolayer and can be treated as a two-dimensional lattice. We assume that there is no preferential interaction between molecules in σ , or between molecules in σ and molecules in β . The grand partition function treatment of this model parallels closely that given by Fowler and Guggenheim⁶ for perfect mixed crystals. Consider a surface region of area A , volume V at temperature T . μ_2' and μ_3' are the molecular chemical potentials of components 2 and 3, $\psi_2'(T, A/N, V/N)$ and $\psi_3'(T, A/N, V/N)$ the molecular Helmholtz free energies ($E - TS$) of films consisting wholly of 2 and 3, respectively, N_2 and N_3 are the numbers of molecules of 2 and 3 in the lattice, and $N = N_2 + N_3 =$ total molecules in the lattice (not assumed fixed). ψ_2' and ψ_3' are assumed, for fixed N , to be independent of the ratio N_2/N_3 . Let Ξ be the grand partition function for this system, then

$$\Xi = \sum_{N=0}^{\infty} \sum_{N_3=0}^N \frac{N!}{(N-N_3)!N_3!} e^{(N-N_3)(\mu_2' - \psi_2')/kT} e^{N_3(\mu_3' - \psi_3')/kT}$$

$$= \sum_{N=0}^{\infty} \Xi_N \quad (48)$$

defining Ξ_N . If the lattice is nearly incompressible the dependence of ψ_2' and ψ_3' on A/N and V/N will be such that appreciable contributions to Ξ will only be made by terms Ξ_N such that $N \approx N^*$, where N^* is that N for which $\Xi_N = \Xi^*$ is maximum. We therefore replace Ξ with its maximum term Ξ^* ($\psi_2'^*$ and $\psi_3'^*$ are values of ψ_2' and ψ_3' for $N = N^*$) obtaining

$$\Xi = \sum_{N_3=0}^{N^*} \frac{N^*!}{(N^* - N_3)!N_3!} e^{(N^* - N_3)(\mu_2' - \psi_2'^*)/kT} e^{N_3(\mu_3' - \psi_3'^*)/kT} = [e^{(\mu_2' - \psi_2'^*)/kT} + e^{(\mu_3' - \psi_3'^*)/kT}]^{N^*} \quad (49)$$

Where N_0 is Avogadro's number, let $N^* = AN_0 n_m, N_2 = AN_0 n_2, N_3 = AN_0 n_3, \mu_2 = N_0 \mu_2', \mu_3 = N_0 \mu_3', \psi_2 = N_0 \psi_2'^*, \psi_3 = N_0 \psi_3'^*$ to obtain

$$Y = pV - \gamma A = kT \ln \Xi = An_m R T \ln [e^{(\mu_2 - \psi_2)/RT} + e^{(\mu_3 - \psi_3)/RT}] \quad (50)$$

With the assumed equivalence of molal volumes of components 2 and 3 it is convenient to define the functions $\mu_{2a}^0 = \psi_2 + p\bar{V}, \mu_{3a}^0 = \psi_3 + p\bar{V}, \mu_{2a}^0$ and μ_{3a}^0 being supposed functions of T, p and A/N only with $(\partial\mu_{2a}^0/\partial T)_{p,A/N} = -\bar{S}_{2a}^0, \bar{H}_{2a}^0 = \mu_{2a}^0 + T\bar{S}_{2a}^0, \bar{S}_{3a}^0$ and \bar{H}_{3a}^0 being similarly defined. Then

$$-\gamma A = An_m R T \ln [e^{(\mu_2 - \mu_{2a}^0)/RT} + e^{(\mu_3 - \mu_{3a}^0)/RT}] \quad (51)$$

is a thermodynamic potential characteristic of the variables T, p, A, μ_2, μ_3 with

$$n_2 = -\left(\frac{\partial\gamma A}{\partial\mu_2}\right)_{T,p,A,\mu_3} = \frac{n_m e^{(\mu_2 - \mu_{2a}^0)/RT}}{e^{(\mu_2 - \mu_{2a}^0)/RT} + e^{(\mu_3 - \mu_{3a}^0)/RT}} \quad (52a)$$

$$n_3 = -\left(\frac{\partial\gamma A}{\partial\mu_3}\right)_{T,p,A,\mu_2} = \frac{n_m e^{(\mu_3 - \mu_{3a}^0)/RT}}{e^{(\mu_2 - \mu_{2a}^0)/RT} + e^{(\mu_3 - \mu_{3a}^0)/RT}} \quad (52b)$$

From eq. 51, 52a, 52b, we have also

$$\mu_2 = \mu_{2a}^0 + RT \ln \frac{n_2}{n_m} - \frac{\gamma}{n_m} \quad (53a)$$

$$\mu_3 = \mu_{3a}^0 + RT \ln \frac{n_3}{n_m} - \frac{\gamma}{n_m} \quad (53b)$$

Further

$$S = \left(\frac{\partial\gamma A}{\partial T}\right)_{p,A,\mu_2,\mu_3} = An_m R \ln [e^{(\mu_2 - \mu_{2a}^0)/RT} + e^{(\mu_3 - \mu_{3a}^0)/RT}] - \frac{An_m R T}{e^{(\mu_2 - \mu_{2a}^0)/RT} + e^{(\mu_3 - \mu_{3a}^0)/RT}} \times [e^{(\mu_2 - \mu_{2a}^0)/RT} \left(\frac{\mu_2 - \bar{H}_{2a}^0}{RT^2}\right) + e^{(\mu_3 - \mu_{3a}^0)/RT} \left(\frac{\mu_3 - \bar{H}_{3a}^0}{RT^2}\right)] \quad (53c)$$

$$= A \left\{ n_2 \left(\bar{S}_{2a}^0 - R \ln \frac{n_2}{n_m} \right) + n_3 \left(\bar{S}_{3a}^0 - R \ln \frac{n_3}{n_m} \right) \right\} \quad (54)$$

$$F = A(n_2\mu_2 + n_3\mu_3) + \gamma A = A \left\{ n_2 \left(\mu_{2a}^0 + RT \ln \frac{n_2}{n_m} \right) + n_3 \left(\mu_{3a}^0 + RT \ln \frac{n_3}{n_m} \right) \right\} \quad (55)$$

$$\mathcal{H} = F + TS = A \{ n_2 \bar{H}_{2a}^0 + n_3 \bar{H}_{3a}^0 \} \quad (56)$$

Suppose the solution in equilibrium with σ is ideal, and let x = mole fraction component 3, $1 - x$ = mole fraction component 2 in this solution. Then $\mu_3 = \mu_3^0 + RT \ln x, \mu_2 = \mu_2^0 + RT \ln (1 - x),$

(6) R. Fowler and E. A. Guggenheim, "Statistical Thermodynamics," The University Press, Cambridge, 1956, pp. 240-244.

taking pure components as reference states. Using (52a) and (52b) and defining $b = \exp \{(\mu_{2a}^0 - \mu_2^0/RT) - (\mu_{3a}^0 - \mu_3^0)/RT\}$ we obtain

$$\frac{n_2}{n_m} = \frac{1-x}{1+(b-1)x}, \quad \frac{n_3}{n_m} = \frac{bx}{1+(b-1)x} \quad (57)$$

Since (thermodynamic quantity per unit volume/ c_2^0) = [thermodynamic quantity per total mole/(1-x)] we have

$$\Gamma_3 = n_3 - \frac{n_2x}{1-x} = \frac{n_m(b-1)x}{1+(b-1)x} \quad (58)$$

From (51) using (53a) with $\gamma = \gamma_0$ when $\mu_2 = \mu_2^0, n_2 = n_m$ we have

$$\phi = \gamma_0 - \gamma = n_m RT \ln [1 + (b-1)x] \quad (59)$$

from which also

$$\left(\frac{d\phi}{dT}\right)_x = n_m R \ln [1 + (b-1)x] + \frac{n_m RTbx}{1+(b-1)x} \frac{d \ln b}{dT} \quad (60)$$

The form of $\Gamma_3(T,x)$ obtained from isotherms of concentration change or of $\phi(T,x)$ obtained from boundary tension measurements, including temperature dependence, can be readily checked against theoretical values. In case of check, the parameters n_m, b and $d \ln b/dT$ can be determined, and imply $[(\mu_{2a}^0 - \mu_2^0) - (\mu_{3a}^0 - \mu_3^0)], [(\bar{H}_{2a}^0 - \bar{H}_2^0) - (\bar{H}_{3a}^0 - \bar{H}_3^0)],$ and so also $[(\bar{S}_{2a}^0 - \bar{S}_2^0) - (\bar{S}_{3a}^0 - \bar{S}_3^0)].$ These cannot be further resolved unless $\gamma_0 = n_m(\mu_{2a}^0 - \mu_2^0) - d\gamma_0/dT = n_m(\bar{S}_{2a}^0 - \bar{S}_2^0), \gamma_0 - Td\gamma_0/dT = n_m(\bar{H}_{2a}^0 - \bar{H}_2^0)$ are known, in which case $(\mu_{2a}^0 - \mu_2^0), (\mu_{3a}^0 - \mu_3^0), (\bar{H}_{2a}^0 - \bar{H}_2^0), (\bar{H}_{3a}^0 - \bar{H}_3^0), (\bar{S}_{2a}^0 - \bar{S}_2^0), (\bar{S}_{3a}^0 - \bar{S}_3^0)$ can be obtained.

These quantities will include contributions due to the non-uniform environment of surface atoms in α , i.e., the treatment given formally attributes all surface excess free energy, entropy and enthalpy to molecules of components 2 and 3. The contribution to $(\mu_{2a}^0 - \mu_2^0)$ and to $(\mu_{3a}^0 - \mu_3^0)$ from this source, for example, would depend on the method of partitioning interaction energies but by one method could be taken as γ_0^0/n_m for both quantities.

Equations (54-56) present S, F and \mathcal{F} in particularly simple forms. We now consider how these forms might be reached from observations of isotherms of concentration change only. Suppose $\Gamma_3(T,x)$ had been determined, and found to be of the form (58) with n_m temperature independent, b temperature dependent. From

$$\phi = \int_0^x \Gamma_3 RT dx \quad (61)$$

using (58) we obtain (59), and by differentiation we obtain (60). Substitute these expressions for Γ_3, ϕ and $(\partial\phi/\partial T)_x$ in eq. 38, 40 and 42 to obtain

$$s^s = s_0^s + n_m R \ln [1 + (b-1)x] + \frac{n_m RTbx}{1+(b-1)x} \frac{d \ln b}{dT} + \frac{n_m(b-1)x}{1+(b-1)x} (\bar{S}_3^0 - R \ln x) \quad (62)$$

$$f^s = \gamma_0 - n_m RT \ln [1 + (b-1)x] + \frac{n_m(b-1)x}{1+(b-1)x} (\mu_3^0 + RT \ln x) \quad (63)$$

$$\bar{\mathcal{F}}^s = \bar{\mathcal{F}}_0^s + \frac{n_m RT^2 bx}{1+(b-1)x} \frac{d \ln b}{dT} + \frac{n_m(b-1)x}{1+(b-1)x} \bar{h}_3^0 \quad (64)$$

To proceed from these surface excess quantities, directly available from experiment (if s_0^s, γ_0 and $\bar{\mathcal{F}}_0^s$ are unavailable, as generally will be the case if isotherms of concentration change are the only sources of information, $s^s - s_0^s, f^s - \gamma_0$, and $\bar{\mathcal{F}}^s - \bar{\mathcal{F}}_0^s$ should be considered the experimentally available quantities) to thermodynamic quantities for a proposed adsorption region, it always will be necessary to introduce at this point an assumption as to the character of the adsorption region. It is not possible to convert one piece of information (Γ_3) into two pieces of information (n_2 and n_3) otherwise. In the present case we assume

$$n_2 + n_3 = n_m \quad (65)$$

This, together with the definition of Γ_3 (assuming as before no solubility of 2 and 3 in α or of 1 in β)

$$\Gamma_3 = n_3 - \frac{n_2x}{1-x} \quad (66)$$

furnishes two equations in the two unknowns n_2 and n_3 , permitting them to be expressed in terms of n_m, Γ_3 and x . Using the expression (58) for the dependence of Γ_3 on x, n_2 and n_3 are obtained as functions of x and eq. 57 is recovered. We then have

$$\begin{aligned} \frac{S}{A} &= s^s + \frac{n_2}{1-x} [(1-x)\bar{S}_2^0 - R \ln(1-x)] + x(\bar{S}_3^0 - R \ln x) \\ &= s_0^s + n_m R \ln [1 + (b-1)x] + n_2[\bar{S}_2^0 - R \ln(1-x)] + n_3[\bar{S}_3^0 - R \ln x + RT \frac{d \ln b}{dT}] \\ &= s_0^s + n_2 R \left[\bar{S}_2^0 - R \ln \frac{n_2}{n_m} \right] + n_3 R \left[\bar{S}_3^0 - R \ln \frac{n_3}{n_m} \right] + n_3 \frac{d}{dT} (RT \ln b) \quad (67) \end{aligned}$$

This is equivalent to (54) if we identify $d/dT (RT \ln b) = -(\bar{S}_{2a}^0 - \bar{S}_2^0) - (\bar{S}_{3a}^0 - \bar{S}_3^0), s_0^s = n_m(\bar{S}_{2a}^0 - \bar{S}_2^0)$ as before.

$$\begin{aligned} \frac{F}{A} &= f^s + \frac{n_2}{1-x} [(1-x)\mu_2^0 + RT \ln(1-x)] + x(\mu_3^0 + RT \ln x) \\ &= \gamma_0 - n_m RT \ln [1 + (b-1)x] + n_2[\mu_2^0 + RT \ln(1-x)] + n_3[\mu_3^0 + RT \ln x] \\ &= \gamma_0 + n_2 \left(\mu_2^0 + RT \ln \frac{n_2}{n_m} \right) + n_3 \left[\mu_3^0 + RT \ln \frac{n_3}{n_m} - RT \ln b \right] \quad (68) \end{aligned}$$

Identifying γ_0 with $n_m(\mu_{2a}^0 - \mu_2^0)$ and $RT \ln b$ with $(\mu_{2a}^0 - \mu_2^0) - (\mu_{3a}^0 - \mu_3^0)$, we recover (55)

$$\begin{aligned} \frac{\mathcal{F}}{A} &= \bar{\mathcal{F}}^s + \frac{n_2}{1-x} [(1-x)\bar{h}_2^0 + x\bar{h}_3^0] \\ &= \bar{\mathcal{F}}_0^s + n_2 \bar{h}_2^0 + n_3 \left[\bar{h}_3^0 + RT^2 \frac{d \ln b}{dT} \right] \quad (69) \end{aligned}$$

Identifying $\bar{\mathcal{F}}_0^s$ with $n_m(\bar{H}_{2a}^0 - \bar{H}_2^0)$ and $RT^2 d \ln b/dT$ with $-(\bar{H}_{2a}^0 - \bar{H}_2^0) + (\bar{H}_{3a}^0 - \bar{H}_3^0)$, we recover (56).

THE EFFECTS OF REACTOR IRRADIATION UPON THE SUBSEQUENT THERMAL DECOMPOSITION OF LEAD STYPHNATE¹

BY TED B. FLANAGAN²

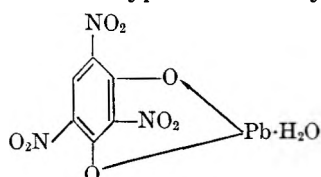
Explosives Research Section, Picatinny Arsenal, Dover, New Jersey, and Brookhaven National Laboratory, Upton, L. I., New York

Received August 21, 1961

The kinetics of the thermal decomposition of lead styphnate have been examined after being subjected to a series of irradiations in the Brookhaven National Laboratory graphite reactor. It was observed that the decomposition rate is enhanced and the activation energy for at least part of the decomposition is significantly decreased by nuclear irradiation. It also was found that it did not make any difference in the subsequent thermal decomposition whether the material was irradiated as the anhydride or as the monohydrate. Possible mechanisms for the decomposition of the irradiated salt are discussed.

Introduction

The dehydration and decomposition of the primary explosive lead styphnate monohydrate³



have been investigated recently.⁴ The detailed kinetics of the dehydration and decomposition of barium styphnate monohydrate also have been examined.⁵ It was observed by Tompkins and Young^{5a} that prior irradiation with ultraviolet light did not affect the subsequent thermal decomposition of the barium salt. With respect to gas evolved during γ -ray irradiation, lead styphnate monohydrate was found to be the most stable of several explosives investigated.⁶ In addition, it was found that γ -ray irradiation (up to 1.8×10^8 r.) had negligible effect upon the subsequent decomposition.^{4b} Thus it appeared that lead styphnate was quite stable toward ionizing radiation. It was of interest to examine how radiation from a nuclear reactor would affect the subsequent decomposition. This was of particular interest because lead styphnate exists as a stable monohydrate and could, therefore, be irradiated either as the monohydrate or as the anhydride.

Experimental

The specimens were irradiated in a water-cooled "hole" (~ 30 – 50°) in the Brookhaven National Laboratory reactor where the approximate neutron fluxes were: 4.5×10^{12} ncm.⁻² sec.⁻¹ (total), 1×10^{12} ncm.⁻² sec.⁻¹ (fast, > 0.6 Mev.), and 2.1×10^{12} ncm.⁻² sec.⁻¹ (thermal). The accompanying γ -ray irradiation was approximately 2.7×10^6 r./hr. Some samples were irradiated at a higher thermal flux (see below). The majority of the samples were irradiated while exposed to the atmosphere. Upon removal of the irradiated samples from the reactor, they were stored

in a desiccator prior to the decomposition studies. The samples were evacuated overnight in a hard vacuum prior to the decomposition runs.

The decomposition apparatus has been described previously^{4b} and the preparation of the well-aged, small, unground styphnate crystals used for the decomposition studies (1–4 mg.) also has been described before.^{4a,b} A few dehydration runs were performed using a quartz helix balance (sensitivity, 1 cm./mg.) purchased from Microchemical Specialties, Berkeley, California.

Results and Discussion

General.—Samples of lead styphnate monohydrate were subjected to a series of reactor irradiations in a water-cooled hole (30 – 50°) of the Brookhaven National Laboratory reactor. Evidence is presented here which strongly supports the view that the samples were irradiated as the monohydrate, *i.e.*, they were not dehydrated during the actual irradiation. Subsequent decomposition studies then were performed in the temperature range 200 – 225° ; dehydration occurs rapidly at these temperatures, *e.g.*, dehydration is complete for unirradiated samples in 1 min. at 197° and less than this for irradiated samples.^{4a} Hence, it is believed that during decomposition runs dehydration is complete before significant decomposition has occurred.

The decomposition of unirradiated lead styphnate has been described elsewhere^{4b} and a decomposition curve (pressure *vs.* time) is shown in Fig. 1 in comparison to curves of reactor-irradiated samples (222.5° , 1 mg.). It can be seen that only after comparatively large doses of radiation is the subsequent decomposition affected.⁷ The decomposition curves shown in Fig. 1 are quite reproducible for samples which have been taken from a batch of irradiated material and also are reasonably reproducible with respect to radiation dose, *i.e.*, a sample irradiated under similar conditions and for the same length of time as those shown in Fig. 1 exhibits a similar decomposition curve. In addition, the irradiated material shows stability towards aging effects, *e.g.*, a heavily irradiated sample stored for 3 years at room temperature exhibited virtually the same decomposition curves as a sample investigated several days after irradiation.

A sample irradiated *in vacuo* (1.1×10^{18} ncm.⁻², curve C) yielded a nearly identical decomposition curve as a sample irradiated in the atmosphere of the reactor (the normal conditions employed). Thus,

(1) This work was performed at Brookhaven National Laboratory and was supported jointly by Picatinny Arsenal and the U. S. Atomic Energy Commission.

(2) Chemistry Department, University of Vermont, Burlington, Vt.

(3) Evidence for an alternative structure is discussed by Zingaro (*J. Am. Chem. Soc.*, **76**, 816 (1954)).

(4) (a) T. B. Flanagan, *Trans. Faraday Soc.*, **55**, 114 (1959); (b) **57**, 797 (1961); (c) F. C. Tompkins and D. A. Young, *J. Chem. Soc.*, 331 (1956).

(5) (a) F. C. Tompkins and D. A. Young, *Trans. Faraday Soc.*, **52**, 1245 (1956); (b) F. C. Tompkins and D. A. Young, *J. Chem. Soc.*, 4281 (1957).

(6) J. V. R. Kaufman, *Proc. Roy. Soc. (London)*, **A246**, 219 (1958).

(7) E. G. Prout, *Nature*, **183**, 884 (1959).

it appears that interaction with the atmosphere during irradiation does not influence the subsequent thermal decomposition. The gas evolved during an average irradiation was negligible, *e.g.*, for sample C less than 0.8% of P_f was found (P_f = final pressure after complete decomposition).

Figure 2 shows the variation of maximum rate of decomposition and the length of the induction period (222.5°) plotted as a function of total neutron dose. It may be seen that the maximum rate of decomposition has increased by a factor of 3 in passing from an unirradiated sample to sample A (the sample irradiated for a given total neutron dose hereafter will be referred to as labeled by the curves shown in Fig. 1). It is of interest that the maximum rate observed for heavily irradiated samples, *e.g.*, A, under conditions where self-heating apparently is not a factor, is greater than that for an unirradiated sample in the vicinity of the latter samples' detonation temperature, *e.g.*, at 225.2° the maximum rate of A is 4.5 $\mu\text{min.}^{-1} \text{mg.}^{-1}$ whereas at 227.9° the corresponding rate for an unirradiated sample is 1.3 $\mu\text{min.}^{-1} \text{mg.}^{-1}$ (at 228.7° self-heating is observed and at temperatures >229° detonation occurs^{4b}). Because of the short acceleratory period the value of the maximum rate is not very accurate and, therefore, two other quantities also have been plotted (Fig. 3), *i.e.*, the rate of the early linear period^{4b} and the pressure evolved after a given time interval. These quantities show a similar dependence upon dose as does the maximum rate (Fig. 2).

The curves A through E shown in Fig. 1 refer to samples irradiated with a flux $4.5 \times 10^{12} \text{ ncm.}^{-2} \text{ sec.}^{-1}$ (total), $1.0 \times 10^{12} \text{ ncm.}^{-2} \text{ sec.}^{-1}$ (fast, >0.6 Mev.), and $2.1 \times 10^{12} \text{ ncm.}^{-2} \text{ sec.}^{-1}$ (thermal). The curves F and G refer to samples irradiated with a flux $1.3 \times 10^{13} \text{ ncm.}^{-2} \text{ sec.}^{-1}$ (total) with approximately the same fast neutron flux as the A through E series. It may be seen from Fig. 2 and 3 that the data of both irradiations fall on approximately the same curves. Thus it appears that the total neutron dose is the important quantity.

Role of the Dehydration Reaction.—Although the samples were irradiated in a water-cooled hole (30–50°), the temperature of the sample may be somewhat higher than its environment due to radiation heating. However, for the small samples and containers (aluminum foil and thin quartz tubing) employed here, the temperature would not be expected to rise more than a few degrees above 50°.

Evidence now will be presented which supports the conclusion that the samples were not dehydrated during irradiation. Previous studies on the dehydration of lead styphnate have been made *in vacuo*.^{4a} It was observed here that the dehydration at 120° in the laboratory atmosphere was approximately 1/3 the rate *in vacuo*. Assuming the same activation energy applies as *in vacuo*, dehydration would be complete in approximately 100 and 40 hr. at 90 and 100°, respectively. In support of these values, it was found that insignificant dehydration occurred after 12 hr. at 87° in an atmosphere of air. Virgin samples exhibit zero order dehydration kinetics with respect to

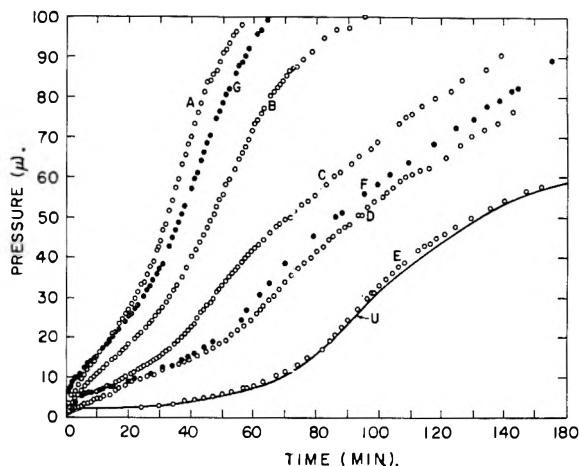


Fig. 1.—The effect of reactor irradiation upon the subsequent thermal decomposition of lead styphnate (222.5°, 1 mg. $P_f = 135 \mu$). A, $2.2 \times 10^{18} \text{ ncm.}^{-2}$; B, $1.6 \times 10^{18} \text{ ncm.}^{-2}$; C, $1.1 \times 10^{18} \text{ ncm.}^{-2}$; D, $5.3 \times 10^{17} \text{ ncm.}^{-2}$; E, $0.7 \times 10^{17} \text{ ncm.}^{-2}$; F, $7.5 \times 10^{17} \text{ ncm.}^{-2}$; G, $1.8 \times 10^{18} \text{ ncm.}^{-2}$; and U, an unirradiated sample. The doses are total neutron doses; samples G and F have been irradiated with a different ratio of thermal to fast neutrons than A–E (see text).

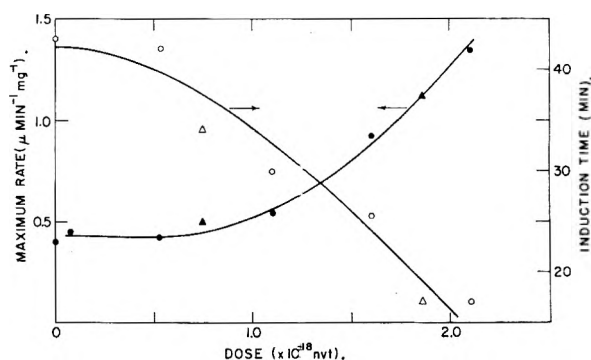


Fig. 2.—The effect of reactor irradiation upon the maximum rate and the induction time of the thermal decomposition of lead styphnate (222.5°, 1 mg., $P_f = 135 \mu$). The approximate neutron fluxes employed for the runs represented by the circles are: $4.5 \times 10^{12} \text{ ncm.}^{-2} \text{ sec.}^{-1}$ (total), $1 \times 10^{12} \text{ ncm.}^{-2} \text{ sec.}^{-1}$ (fast), and $2.1 \times 10^{12} \text{ ncm.}^{-2} \text{ sec.}^{-1}$ (thermal) and for the runs represented by the triangles: $1.3 \times 10^{13} \text{ ncm.}^{-2} \text{ sec.}^{-1}$ (total), $1 \times 10^{12} \text{ ncm.}^{-2} \text{ sec.}^{-1}$ (fast), and $6.5 \times 10^{12} \text{ ncm.}^{-2} \text{ sec.}^{-1}$ (thermal).

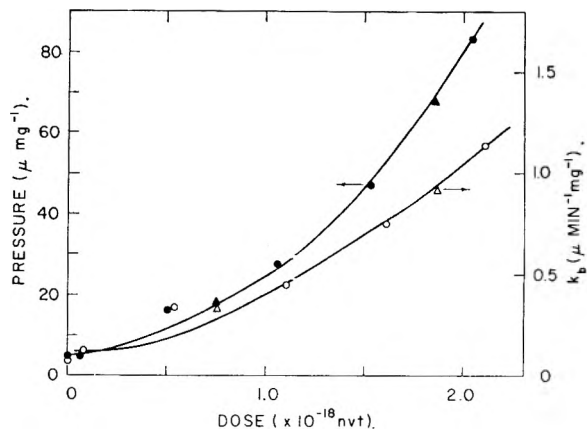


Fig. 3.—The effect of reactor irradiation upon the pressure evolved at the end of an arbitrary time interval (45 min.) and the rate constant of phase (b) of the thermal decomposition of lead styphnate (222.5°, 1 mg., $P_f = 135 \mu$). The symbols have the same meaning as in Fig. 2.

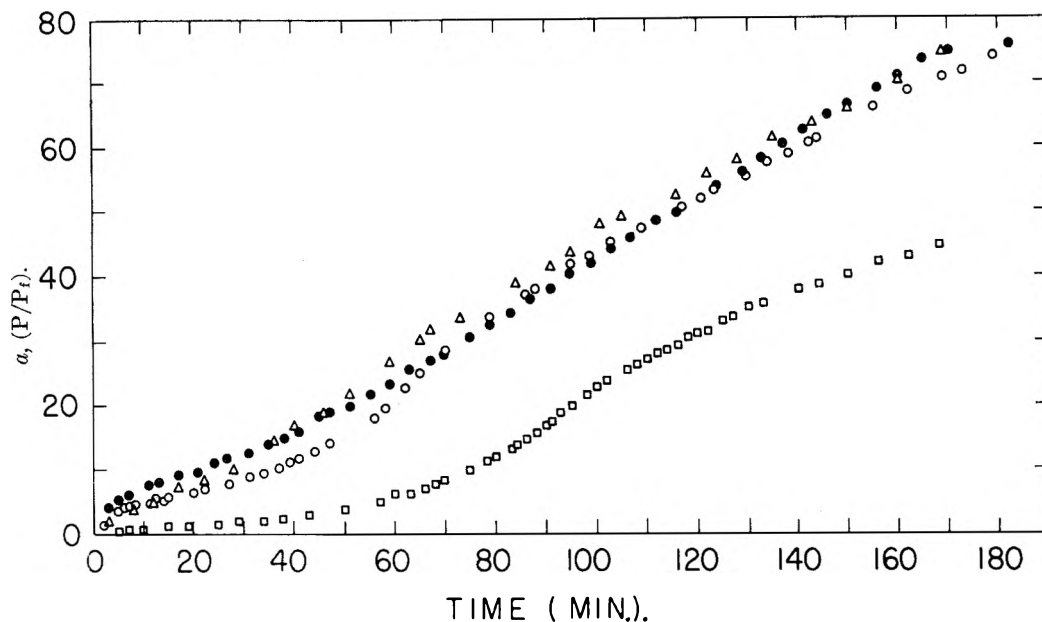


Fig. 4.—The thermal decomposition of lead styphnate (222.5°): O, irradiated as the monohydrate; ●, dehydrated and rehydrated before irradiation; Δ , irradiated as the anhydride; (7.5×10^{17} ncm. $^{-2}$, total); □, unirradiated sample.

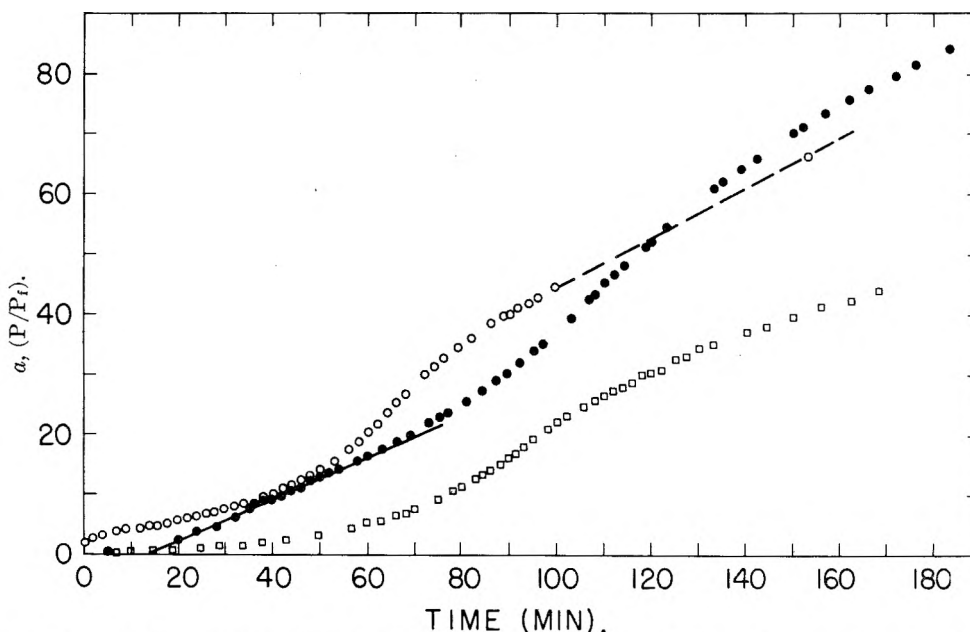


Fig. 5.—The thermal decomposition of reactor irradiated lead styphnate (4.3×10^{17} ncm. $^{-2}$, total). O, dehydrated *in vacuo* prior to decomposition (222.5°); ●, dehydrated in 0.8 mm. of water vapor prior to decomposition (222.5°); □, unirradiated sample (222.5°).

time whereas rehydrated material shows first-order kinetic behavior.^{4a} Two samples were irradiated under similar conditions, one of which had been dehydrated and rehydrated prior to irradiation and the other was irradiated as the virgin monohydrate; the former showed first-order dehydration kinetics and the latter exhibited a linear dehydration rate (enhanced compared to an unirradiated sample). This suggests that the irradiated material was not dehydrated during irradiation. Finally, an X-ray powder pattern of irradiated material more closely resembled virgin rather than dehydrated (or rehydrated) material.

It might be expected that the gross changes introduced into the salt as a result of dehydration would partially mask any effects upon the subsequent thermal decomposition of irradiated material. Although the details of the pressure-time curves differ somewhat, the effect of irradiation (7.5×10^{17} ncm. $^{-2}$ (total)) upon the decomposition of a sample dehydrated and rehydrated before irradiation closely resembled that of a sample irradiated as the virgin monohydrate (Fig. 4). Shown together with these data in Fig. 4 is a decomposition curve of a sample irradiated *in vacuo* as the anhydride; it may be seen that this curve also agrees fairly well

with the other data. This general behavior was reproduced for samples irradiated for a total neutron dose of 1.8×10^{18} nem.^{-2} (total).

It will be recalled from earlier work^{4a,b} that the decomposition of lead styphnate monohydrate dehydrated in 0.8 mm. of water vapor prior to decomposition differed greatly from the decomposition of material dehydrated *in vacuo*; the former decomposition rate was linear, after an induction period, to $\alpha \approx 80\%$ whereas the latter showed the behavior illustrated in Fig. 1 (the unirradiated sample). It was of interest to examine the decomposition of an irradiated sample which had been dehydrated in 0.8 mm. of water vapor *after irradiation*. Figure 5 shows the behavior of an irradiated sample dehydrated in this way as compared to a sample irradiated for the same period and then dehydrated *in vacuo*. It may be seen that the irradiated sample, previously dehydrated in 0.8 mm. of water vapor, shows a closely linear decomposition rate only to about 20% decomposition, at which point an acceleratory period commences. The linear rate is approximately twice that of the unirradiated decomposition; the values of t_0 , the time intercept, for both unirradiated and irradiated samples are comparable. Growth starts from opposite faces in the more perfectly crystallized material resulting from dehydration in 0.8 mm. of water vapor.^{4b} The absence of an early gas evolution shows that the decomposition of internal "irradiation nuclei" has not contributed to the observed pressure in the early stages of reaction. Uni-directional growth, enhanced by the radiation damage as it is uncovered, is an unstable condition when extensive internal nucleation is present, as shown by the onset of an acceleratory period presumably caused by cracking of the crystal either due to escape of internal gas or to extensive internal decomposition.

Nature of the Radiation Damage.—It has been observed previously that aromatic material exhibits greater stability toward nuclear irradiation than does aliphatic material.³ Hence, the relative stability of lead styphnate toward irradiation observed here is not unexpected. γ -Ray irradiation of 1.8×10^8 r. was shown to have an insignificant effect upon the decomposition curves.^{4b} The γ -ray dose accompanying the reactor irradiation slightly exceeded this for sample C and was less than this for sample D. For the purpose of this discussion, the effect of γ -ray irradiation and the resulting ionization will be neglected. Nuclear transformations and atomic displacement can result from neutron capture by N^{14} , *i.e.*, $\text{N}^{14} + \text{n} \rightarrow \text{C}^{14} + \text{p}$; atomic displacement also can result from fast neutron knock-on collisions. For 1 mg. of lead styphnate monohydrate, an irradiation of 2.2×10^{18} nem.^{-2} (total), would result in $\sim 6 \times 10^{12}$ transformations yielding C^{14} atoms with a recoil energy of 45,000 e.v. and a corresponding number of 0.56 Mev. protons. The recoil of the C^{14} would, of course, immediately rupture the original C-N bond in the C- NO_2 linkage and the recoil

carbon subsequently would damage the lattice through elastic collisions after sufficient energy had been lost through inelastic processes. Similarly the ejected protons will produce atomic displacements.

Experimentally, transmutation plus resultant processes and fast neutron damage appear to have similar efficiency (Fig. 2 and 3). A very approximate model predicts fast neutron damage to be more effective; the discrepancy probably is due to some chemical damage caused by inelastic processes resulting from the slowing down of the recoil C^{14} and the ejected proton. In any case, the damaged regions are believed to be homogeneously distributed throughout the material forming "irradiation nuclei." Apparently dehydration does not remove any of these nuclei.

Analysis of the Pressure-Time Relationships.—

The general time sequence of events during the decomposition of irradiated samples, dehydrated *in vacuo*, *e.g.*, Fig. 1, appears to be the same as that of unirradiated material, although the relative importance of each phase is altered progressively with increasing level of radiation, and consequently the appearance of the pressure-time curves has been modified. The general sequence of events is: (a) an initial evolution of gas, (b) a linear period of gas evolution, (c) an acceleratory period, and finally, (d) a deceleratory phase which is linear over a significant time interval for samples C and D, but the linearity disappears as the inflection point comes at greater values of the percentage decomposition. It is of interest to examine separately the influence of radiation upon each of the phases of the decomposition.

In unirradiated material, phase a was describable by a first-order rate law and was attributed to reaction at energetically favorable sites.^{4b} The total gas evolved at the end of phase a was independent of temperature and depended only upon the mass of sample employed.^{4b} This also was true for sample C, whose decomposition was investigated at a series of temperatures. The pressure developed at the end of phase a for a 1-mg. sample is shown as a function of radiation dosage in Table I.

TABLE I
EFFECT OF REACTOR RADIATION ON INITIAL GAS EVOLUTION AND INFLECTION POINT (1 mg., $P_f \cong 135 \mu$, 222.5°)

Sample	Pressure (μ) at end of phase a	Pressure (μ) at end of phase b	Pressure (μ) at inflection point
A	11	23	80
B	9	20	74
C	5-6	14	35
D	2	14	37
E	1.0	2.0	33
U	1.0	2.0	32

An especially large sample of irradiated material (A) was employed to obtain detailed data for the early region of reaction (phases a and b), this is shown corrected to 1 mg. (197.0°) in comparison to an unirradiated run (Fig. 6). Because of the shortened induction period and the enhanced rates of phases a and b, it was difficult to obtain a value of P_f , the pressure at the end of phase a, and hence

(8) F. Seitz and J. Koehler, "Solid State Physics," Ed. F. Seitz and D. Turnbull, Academic Press, Inc., New York, N. Y., 1956, Vol. 2, p. 305.

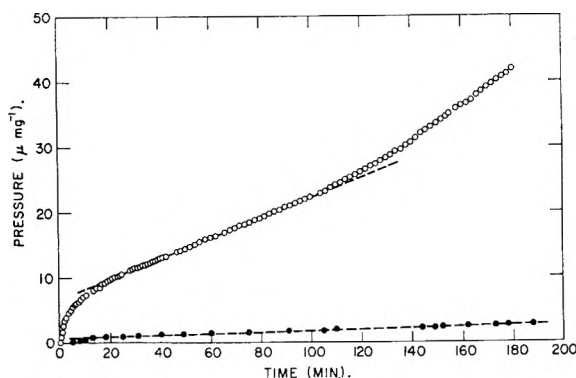


Fig. 6.—Comparison of the initial stages of decomposition of a heavily irradiated sample, (A), and an unirradiated sample (197.0°, 1 mg.): O, irradiated sample, 2.2×10^{18} ncm.⁻² (total) and ●, unirradiated sample.

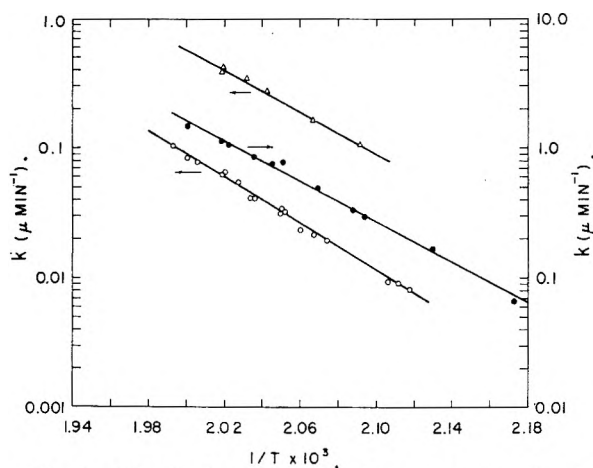


Fig. 7.—The Arrhenius plot of the rate constant for the decomposition of phase (b), (1 mg. sample): O, unirradiated sample; Δ , irradiated sample C, 1.1×10^{18} ncm.⁻²; and ●, irradiated sample A, 2.2×10^{18} ncm.⁻².

to apply a first-order rate law to phase a. Consequently, the method of initial rates was employed to obtain an activation energy of ~ 10 kcal./mole for sample A as compared to 31 kcal./mole for unirradiated samples; the latter value also was determined from initial rates and compares favorably with the value obtained from first-order rate constants.^{4b} As expected from the magnitude of this activation energy, gaseous products were evolved from sample A even at temperatures as low as 100° (4 μ in one hour with reference to the scale in Fig. 1). Since phase a was not eliminated by dehydration, it probably can be attributed to reaction at active sites formed by irradiation and not to desorption of trapped gases. These sites are believed to be the "irradiation nuclei" and are distributed throughout the crystal mass.

Following phase a, a period of constant gas evolution occurs (b); this has an activation energy of 41 kcal./mole for unirradiated material and was ascribed to reaction starting from the surface of dehydrated blocks which comprise the anhydride. Figure 3 shows the dependence of the rate constant, k_b , upon the radiation dosage. After a dose of 2.2×10^{18} ncm.⁻², the k_b for sample A has increased by a factor of ~ 19 (Fig. 3). Activation energies were determined from k_b for samples A and C;

the results are shown in Fig. 7 together with the results for unirradiated material. The activation energies for phase b have decreased with increase of radiation dosage: unirradiated, $\Delta E = 41.0 \pm 0.5$ kcal./mole; C, $\Delta E = 36.1 \pm 1.1$ kcal./mole; A, $\Delta E = 36.2 \pm 0.6$ kcal./mole. The rate constants at 222.5° are 6.3, 42, and $119 \times 10^{-2} \mu \text{ min.}^{-1} \text{ mg.}^{-1}$ for an unirradiated sample, sample C, and sample A, respectively.

In irradiated material it is believed that phase b is no longer confined to the surface of the blocks as in unirradiated material^{4b}; it is suggested that decomposition starts from the "irradiation nuclei" (which decomposed during phase a) producing rod-like nuclei which grow internally in one crystallographic direction with a diameter equal to that of the original damaged region. Evidence has been presented to indicate the anhydride consists of at least partially aligned microcrystallites.^{4b} The porous structure of the anhydride resulting from dehydration *in vacuo* allows the gaseous products to escape during decomposition. Since decomposition during the early, linear phase of the irradiated and unirradiated samples takes place in different regions of the crystal (with different interfacial areas) discussion of the relative values of k_b appears unwarranted.

Phase c represents acceleration from the internal rod-shaped decomposition centers formed during phase b. Detailed analysis of the acceleratory period of heavily irradiated material, e.g., samples A, B, and C, is difficult because of the large and uncertain corrections which must be applied to the observed pressure due to the contributions from the preceding phases of the decomposition. Following a technique suggested by Hill and Welsh,⁹ functions of $d\alpha/dt$ were plotted against α . However, the straight line relationships expected for simple power or exponential rate laws were not found; (the errors due to assigning values of p_0 and t_0 are eliminated in using this approach). This suggests that phase b continues to contribute to the pressure during the acceleratory period and as the fraction of its contribution at various times during phase c is unknown, it seems pointless to try to obtain a fit of the $p-t$ data. In any case, acceleration starts from a larger number of internal sites as the radiation dose increases as evidenced by the location of the inflection point (Table I). This seems compatible with the interesting result that the decomposition rate of heavily irradiated samples considerably exceeds that of unirradiated samples immediately below the detonation temperature of the latter. In unirradiated samples, the acceleratory phase must represent decomposition in much more localized regions of the crystal in order for self-heating and detonation to occur. This suggests that the chain branching mechanism suggested for the decomposition of lead styphnate dehydrated *in vacuo*^{4b} must be localized next to the opposite faces from which branching commenced, or next to internal surfaces formed by cracking due to interfacial strain induced by phase b.

(9) R. A. W. Hill and J. N. Welsh, *Trans. Faraday Soc.*, **56**, 1059 (1960).

Mechanism.—The result that dehydration does not remove any of the radiation damage with respect to the subsequent thermal decomposition is noteworthy. It has been shown that the anhydride and the original monohydrate exhibit different X-ray patterns^{4a} and, therefore, although crystallization occurs following dehydration, it does not remove or significantly alter the regions of radiation damage. This suggests that the significant form of radiation damage is irreversibly altered styphnate units rather than displaced ions and vacancies, *e.g.*, Pb^{++} . This does not seem unreasonable since, in contrast to a metal where the damage due to displaced atoms and vacancies can anneal readily, an atom displaced from the complex styphnate ion would result in a chemically

altered species which could decompose further, rearrange, or perhaps even polymerize in the regions of extensive damage. The very low activation energy for the initial gas evolution, ~ 10 kcal./mole, must represent decomposition of such chemically altered styphnates since it is unlikely that physical changes in the lattice could lower the activation energy to such a small value. The chemically altered styphnates appear to be stabilized in the lattice in some manner because of the stability of the radiation damage and the small quantity of gas evolved during irradiation.

Acknowledgments.—The author thanks Drs. G. J. Dienes and J. Jach for valuable discussions. The interest of Drs. J. V. R. Kaufman and P. W. Levy in this work is greatly appreciated.

THERMAL DECOMPOSITION OF SILVER-COATED α -LEAD AZIDE

BY BRUNO REITZNER, J. V. RICHARD KAUFMAN, AND EUGENE F. BARTELL

Explosives Research Section, Explosives and Propellants Laboratory, Picatinny Arsenal, Dover, New Jersey

Received August 21, 1961

The induction times of the thermolysis reaction $\text{Pb}(\text{N}_3)_2 \rightarrow \text{Pb} + 3\text{N}_2$ can be reduced by coating $\text{Pb}(\text{N}_3)_2$ with metallic silver. This effect is attributed to the catalytic effect of the silver. The induction time of the slow thermolysis in vacuum at 240° is substantially the same with 1.0 and 10.0 atom% Ag. Water incorporated into the lead azide during the coating procedure reverses the effect of the silver causing a poisoning of the autocatalytic reaction. Mass spectrometric analysis shows that the water undergoes a hydrolysis reaction with $\text{Pb}(\text{N}_3)_2$ whereby hydrogen azide is formed. A bridge propagation mechanism is assumed to occur in the later stages of the decomposition in the mass of crystals to explain some anomalies occurring with the silver-coated materials. The sensitization effect of the silver also was found when $\text{Pb}(\text{N}_3)_2$ was ignited in air at higher temperatures, although the presence of air caused some anomalies.

Introduction

The thermal decomposition of α -lead azide is considered to be an autocatalytic process in which the decomposition product—metallic lead—acts as the catalyst.¹ In previous work² it was shown that the autocatalytic reaction was suppressed when the decomposition was carried out in an atmosphere containing water vapor. It was concluded that the water destroyed the lead nuclei which are necessary for the autocatalytic reaction. On this basis it should be possible, therefore, to enhance the autocatalytic reaction by depositing metallic lead on the lead azide surface. This is, however, difficult to achieve. Therefore, the hypothesis was made that the autocatalytic reaction is enhanced not only by lead, but also by any other metal. A confirmation of this hypothesis could be found in the work by Hill and Wittenborn,³ who decomposed lead azide in the presence of zinc powder. A sensitization of the lead azide was obtained which was attributed to the catalytic action of the zinc. Since in mechanical mixtures the contact between the metal and the lead azide is not very good it was decided to use a more intimate mixture. One way of preparing such a mixture is to precipitate a metal on the lead azide by reducing a solution of a salt of this metal. Silver was con-

sidered favorable in this respect since its salts can be reduced easily.

Materials.—The α -lead azide used for this study had an average particle size of about 7μ . The cationic impurities (Na, Cu, Mg, Si, Fe, Ag), as determined by spectral analysis, were less than 0.1%. Silver was deposited on this material according to the following procedure: A suspension of 1.46 g. (0.005 mole) of α -lead azide in 100 cc. of a 9:1 methanol-water mixture⁴ was stirred for 15 min. A measured amount⁵ of 0.1 *N* AgNO_3 solution was added to the suspension. After an additional 10 min. of stirring no silver could be detected in the solution (hydrazine as test reagent). It was assumed that the reaction $\text{Pb}(\text{N}_3)_2 + 2\text{AgNO}_3 \rightarrow 2\text{AgN}_3 + \text{Pb}(\text{NO}_3)_2$ had occurred, and that AgN_3 was deposited on the non-reacted lead azide grains. An excess of hydrazine hydrate (0.3 cc.) then was added to this suspension to reduce the AgN_3 , and stirring was continued for another 30 min. The samples darkened in color to a degree dependent on the amount of silver deposited. To test whether all of the silver azide was reduced, a small portion of the sample was shaken with ammonia, the solution filtered off, and acidified with HCl. The absence of a precipitate indicated complete reduction.

As a control for investigating the effect of hydrazine hydrate alone, a duplicate preparation was made omitting the addition of the silver nitrate.

The silver-coated batches and the batch treated with hydrazine hydrate alone were filtered, washed with 100 cc. of 9:1 methanol-water mixture, and sucked to dryness. The dry batches were stored in a lightproof desiccator over CaCl_2 .

The precipitation of silver caused a reduction in the bulk density of the lead azide. The values as determined by suspending weighed portions of the individual batches in

(1) W. E. Garner, "Chemistry of the Solid State," London, 1955, Ch. 7 and 9.

(2) B. Reitzner, *J. Phys. Chem.*, **65**, 948 (1961).

(3) O. H. Hill and A. F. Wittenborn, Appendix A to Final Report DRL-A-125 under Army Contract DA-44-099-ENG-2566, Univ. of Texas, 1957.

(4) An aqueous suspension of lead azide yielded a product which was not uniformly coated with silver.

(5) The amount of silver nitrate solution was varied depending upon the amount of silver desired in the final batch. For instance, 0.5 cc. was used for the batch containing 10.0 atom% Ag.



Fig. 1.— α -Lead azide coated with 10.0 atom% of silver. (Chromium shadow transfer replica, magnification 40,000.)

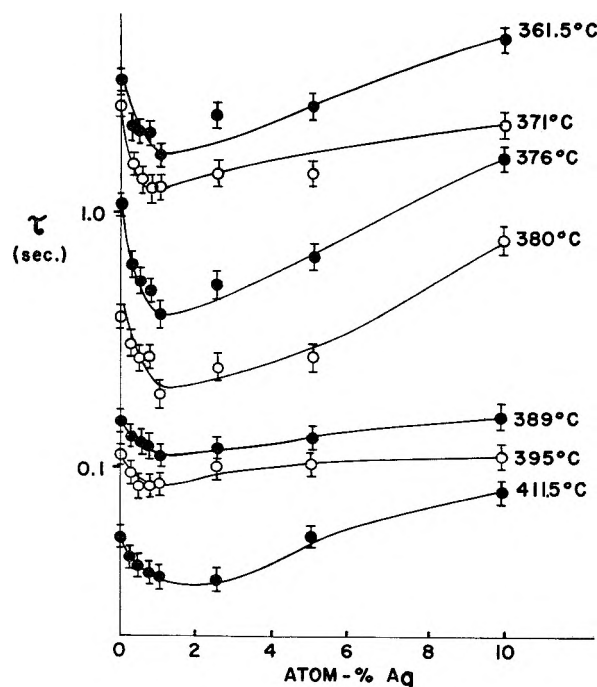


Fig. 2.—Ignition times (τ) vs. atom% silver at various temperatures.

methanol in a graduated centrifuge tube and measuring the volume of the centrifuged precipitate were 1.0 g./cc. for pure lead azide, 0.45 g./cc. for lead azide coated with both 1.0 and 10.0 atom% of Ag, and 0.67 g./cc. for lead azide treated with hydrazine hydrate alone. An explanation for this phenomenon is given later in the discussion.

Microscopic and electron microscopic examination suggest that the silver is precipitated heterogeneously in small dots on the surface of the lead azide grains. An electron micro-

graph of a sample coated with 10.0 atom% of silver is shown in Fig. 1.

Preliminary Experiments.—It was conceived that the effect of a metal on the autocatalytic decomposition of lead azide should be evident not only in slow thermolysis, but also in the relatively fast decomposition associated with its thermal ignition. As a preliminary experiment, therefore, to examine the underlying assumption of the autocatalytic thermal behavior of lead azide, it seemed profitable to explore the ignition behavior of the silver-coated material.

Ignition tests then were carried out in air using a series of lead azide preparations coated with varying amounts of Ag. The apparatus consisted of a hot plate and an electronic timing mechanism. When a sample of lead azide (appr. 3–4 mg.) was dropped on the hot plate, a light beam directed across the hot plate surface was broken. The light fluctuation was detected by a photocell actuating a timing device. The light emitted by the explosion of the sample then was used to stop the timing device. The ignition times (average of 20 shots) vs. percentage of silver at various temperatures are shown in Fig. 2.

It can be seen that the ignition times drop to a minimum value at about 1.0 atom% of Ag and then increase again to values which are equal or higher than those of the untreated material at silver concentrations of 10.0 atom%.

This sensitization effect at the low silver concentrations also is evident in terms of the ignition probability at 351°. The corresponding values are given in Table I for the various silver concentrations used.

TABLE I
IGNITION PROBABILITIES AND TIMES AT 351° FOR VARIOUS SILVER CONCENTRATIONS

Atom % Ag	% Explosion (20 shots)	Ignition time, sec.
0.0	0	∞
.25	10	4.97
.50	40	4.93
.75	100	3.68
1.00	100	2.98
2.5	90	3.40
5.0	40	4.14
10.0	0	∞

Both experiments indicate that silver in small amounts acts as a catalyst in accelerating the reaction leading to explosion. However, at larger concentrations this catalytic activity is hidden by a reverse effect attributed to the heat sink properties of the added silver. In addition, during the increased time required for heating the sample to the hot plate temperature, it is possible that oxygen and moisture of the air react to destroy the lead nuclei necessary for growth of the reaction leading to explosion.

Some attention has been paid to the reactions occurring when lead azide is heated in air at normal humidity below its ignition temperature. Todd⁶ reported the successive formation of two basic lead azides and finally lead oxide at 240°. The two basic lead azides also were reported by Stammer, Abel, and Kaufman⁷ when the decomposition was carried out at 200°. Stammer and Abel⁸ observed the X-ray structure of the second basic lead azide from a lead azide sample which had not exploded after 3 min. in air at 350°. The first basic lead azide also was found when lead azide was decomposed under humid nitrogen at 240°,² indicating that oxygen probably is not the important factor in the conversion of lead azide to the basic lead azide. The first basic lead azide as judged from the analytical values of Todd and the weight loss curves of Stammer, *et al.* is probably $Pb(N_3)_2 \cdot PbO$. An investigation of the formula of the second basic azide presently is underway. Due to the reduced azide content these compounds are less likely to explode at the temperatures used in the present experiments.

The results of ignition tests lent credence to the assumption that the addition of a metal catalyzes the decomposition of

(6) G. Todd, *Chem. & Ind.* (London), 1005 (1958).

(7) M. Stammer, J. E. Abel, and J. V. R. Kaufman, *Nature*, **185**, 456 (1960).

(8) M. Stammer and J. E. Abel, "Advances in X-Ray Analysis," Vol. 4, New York, N. Y., 1960, pp. 130–138.

the lead azide, as evidenced by the reduction of the induction periods. It was felt, however, that more comprehensive results could be obtained if the experiments were carried out at lower temperatures to obtain complete decomposition curves instead of ignition times only. It also was considered necessary to carry out the decomposition in a vacuum to eliminate the effect of the surrounding atmosphere. The criterion for a sensitization of the lead azide by the addition of a metal then would be a reduction of the induction period and an increase in the rate of the reaction.

Thermal Decomposition under Vacuum. Experimental Procedure.—The vacuum system shown in Fig. 3 was used for performing the experiments.

The samples of 6 mg. average weight (each individual sample was weighed accurately to ± 0.02 mg.) were placed in a Pyrex tube which was sealed to the vacuum system. The increase in pressure was detected by a Pirani gage incorporated in a Wheatstone bridge circuit with a millivoltmeter as the measuring instrument. The system was pumped down to better than 5×10^{-6} mm. The final pressure upon completion of the decompositions ranged as high as 2.5×10^{-1} mm. The Pirani gage was calibrated by admitting small known volumes ($v_0 = 0.0446$ cc.) of nitrogen into the system. The volume of the system ($V = 4600 \pm 20$ cc.) was determined by comparing the volume of nitrogen admitted to the system *via* the gas inlet at atmospheric pressure with the pressure measured by the McLeod gage. A trap was provided in order to freeze out the condensable gases evolved during the decomposition. After the sample tube had been sealed to the system, the system was evacuated for 5 hr. and kept overnight with stopcock S closed to determine the rate of leakage. The rate of leakage was equal or less than 10^{-3} cc./hr., corresponding to about 0.07% decomposition (based on a sample weight of 6 mg.). Pumping was continued for 1 hr. the following day, and stopcock S closed. The samples then were heated by means of a liquid metal bath into which the sample tube was immersed. All experiments were carried out at $240 \pm 0.5^\circ$. Toward the end of the decomposition the temperature was increased to 300° in order to obtain the final value α_∞ within a period in which the increase in pressure due to leakage was still negligible. The readings of the millivoltmeter (5 mv. range for the early stages, and 100 mv. for the main reaction) were converted into fractional decomposition α , and plotted against time of decomposition t . The samples investigated consisted of untreated lead azide, lead azide coated with 1.0 and 10.0 atom% Ag, respectively, (these two batches yielded minima and maxima in the ignition tests), and lead azide treated with hydrazine hydrate alone.

Results

The decomposition curves for untreated lead azide are given in Fig. 4.

Curves 1a and 1b were obtained without cooling the trap. Although the controllable parameters were the same, the reproducibility is poor. The decomposition as expressed by curve 2 was carried out by cooling the trap with liquid nitrogen after 5 min. This had the effect that the pressure, which was 1.5×10^{-2} mm. after this short period, went back to about 5×10^{-5} mm. Curve 3 was obtained by cooling from the beginning and then removing the liquid nitrogen dewar after 2 hr., 2 min. The last two samples (curves 2 and 3) exploded at fractional decompositions (α) of 0.25 and 0.47, respectively. Other samples which are not shown behaved in the same way when the trap was cooled with liquid nitrogen. This same explosive effect also could be achieved if the gaseous decomposition products were pumped off in the early stages of the decomposition.

Figures 5, 6, and 7 show the respective decomposition curves obtained with lead azide coated with 1.0 and 10.0 atom% of Ag, and of lead azide treated with hydrazine hydrate alone.

In all cases where hydrazine hydrate had been in

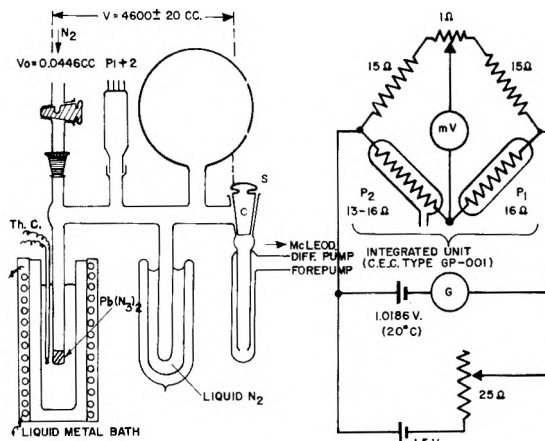


Fig. 3.—Vacuum system and Pirani gage circuit.

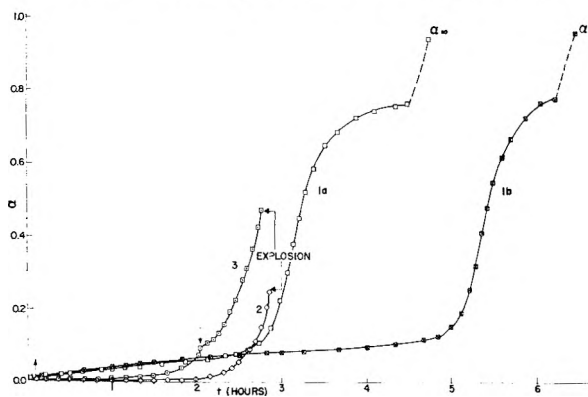


Fig. 4.—Decomposition curves for untreated $Pb(N_3)_2$ ($T = 240^\circ$).

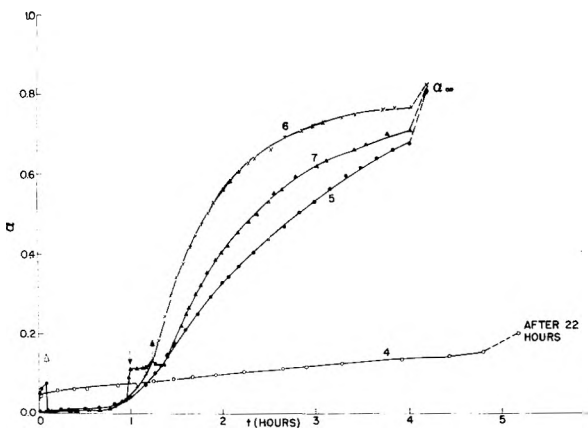


Fig. 5.—Decomposition curves for $Pb(N_3)_2 + 1.0$ atom % Ag ($T = 240^\circ$).

contact with the lead azide, either as a reducing agent for the silver (Fig. 5, 6), or in the blank (Fig. 7) the initial increase in pressure due to the condensable gases is significantly larger than with the untreated material. Five min. after the decomposition had started, the corresponding values, expressed in terms of fractional decomposition, were 0.06–0.08 and 0.007, respectively. Decomposition in the absence of liquid nitrogen cooling, in all those cases (curves 4, 8, 12), did not show an acceleration of the reaction. Furthermore, removal of the liquid nitrogen dewar during the acceleratory period resulted in a reduction of the reaction rate and in a

TABLE II
 PARAMETERS OF DECOMPOSITION CURVES

Curve No.	Material	Treatment	$(d\alpha/dt)_{\max} \times 10^2$ <small>min.⁻¹</small>	t_i	α_∞
1a	Pb(N ₃) ₂	Without liquid nitrogen	1.85	2 hr., 25 min.	0.94
1b	Pb(N ₃) ₂	Without liquid nitrogen	2.08	4 hr., 45 min.	.96
2	Pb(N ₃) ₂	Without liquid N ₂ for 5 min.	2.5 ^a	2 hr., 15 min.	(.27) ^a
3	Pb(N ₃) ₂	Liquid N ₂ on from beginning, removed after 2 hr., 2 min.	2.0 ^a	1 hr., 40 min.	(.47) ^a
4	Pb(N ₃) + 1.0 atom% Ag	Without liquid N ₂	0.0033	>22 hr.	(.20) ^b
5	Pb(N ₃) + 1.0 atom% Ag	Liquid N ₂ on after 5 min.	.56	44 min.	.80
6	Pb(N ₃) + 1.0 atom% Ag	Liquid N ₂ from beginning	1.37	45 min.	.82
7	Pb(N ₃) + 1.0 atom% Ag	Liquid N ₂ on from beginning, removed after 1 hr., 2 min., put on after 1 hr., 15 min.	0.83	37 min.	.81
8	Pb(N ₃) ₂ + 10 atom% Ag	Without liquid N ₂	0.0019	>5 hr.	(.12) ^c
9	Pb(N ₃) ₂ + 10 atom% Ag	Liquid N ₂ on after 5 min.	1.15	38 min.	.83
10	Pb(N ₃) ₂ + 10 atom% Ag	Liquid N ₂ on from beginning	1.17	35 min.	.81
11	Pb(N ₃) ₂ + 10 atom% Ag	Liquid N ₂ on from beginning, removed after 55 min., put on after 1 hr., 20 min.	1.10	43 min.	.81
12	Pb(N ₃) ₂ + N ₂ H ₄ OH	Without liquid N ₂	0.0020	>22 hr.	(.27) ^b
13	Pb(N ₃) ₂ + N ₂ H ₄ OH	Liquid N ₂ on after 5 min.	.76	3 hr., 13 min.	.85
14	Pb(N ₃) ₂ + N ₂ H ₄ OH	Liquid N ₂ on from beginning	.82	4 hr., 15 min.	.89

^a Last value measured before explosion. ^b Interrupted after 22 hr. ^c Interrupted after 5 hr.

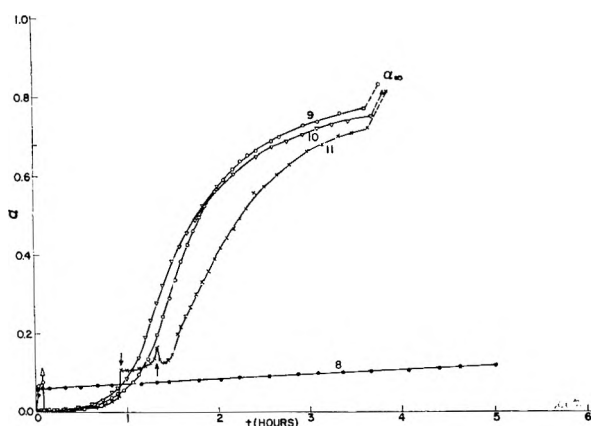


Fig. 6.—Decomposition curves for Pb(N₃)₂ + 10.0 atom % Ag ($T = 240^\circ$).

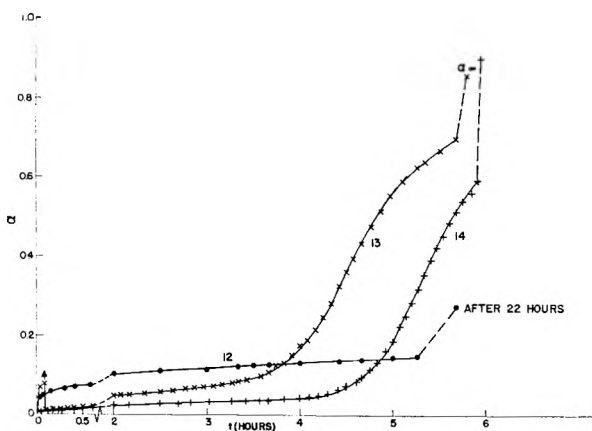


Fig. 7.—Decomposition curves for Pb(N₃)₂ treated with hydrazine hydrate ($T = 240^\circ$).

shifting of the curves (7, 11) towards longer times. Although the induction times t_i for the silver-coated materials are shorter than those for the untreated lead azide, the maximum rates $(d\alpha/dt)_{\max}$ are smaller and comparable to those of the samples

treated with hydrazine hydrate alone. The induction time was arbitrarily defined as the time after which the reaction rate of the acceleratory reaction (not of the outgassing reaction observed in the absence of liquid nitrogen cooling) reached a value of $10^{-3} \text{ min.}^{-1}$. The corresponding values are listed in Table II together with the maximum rates and the final degree of decomposition (α_∞). The figures for α_∞ are lower in all cases where hydrazine hydrate was involved (this of course includes the samples containing silver).

The initial stage of decomposition (up to $\alpha = 0.05$) for the various samples is shown in Fig. 8. (The numbers of the curves correspond to the numbers in Fig. 4-7.)

This figure shows quite clearly that the induction period with the silver-coated materials is considerably reduced, if the initially evolved gases are frozen out. In the initial stage of the decomposition these curves are reproducible, which is not the case for the untreated material (curves 1a, 2, 3) and the material treated with hydrazine hydrate (curves 13, 14).

The condensable gas released shortly after lead azide was heated had the effect of delaying or even suppressing the autocatalytic reaction. It seemed, therefore, advisable to investigate its composition. Previous results² suggested that the gas was a mixture of water and hydrogen azide, the latter being formed in a hydrolysis reaction between lead azide and water trapped originally in the crystals. In order to confirm these earlier observations, 27.7 mg. of lead azide were heated under vacuum at 240° for 4 min., and the gas evolved (appr. 2.7×10^{-2} cc. at s.t.p.) was trapped with liquid nitrogen. When the liquid nitrogen dewar was put in place, the pressure dropped to about 4% of the value before the trap was added. The vial with the condensed gas then was sealed off and analyzed by mass spectrometry, together with a control sample of hydrogen azide obtained by the following procedure: A bulb containing concentrated sulfuric acid

and sodium azide in separate compartments was sealed to the vacuum system and evacuated. The sodium azide then was dumped into the acid and the evolved hydrogen azide was trapped in a second vial by freezing with liquid nitrogen. The results of the mass spectrometric analysis are given in Table III.

TABLE III
RESULTS OF MASS SPECTROMETRIC ANALYSIS
Relative intensities (mass 43 = 1.00)

Mass-charge ratio	Gas from $\text{Pb}(\text{N}_3)_2$	Hydrogen azide
12	0.13	0.02
14	1.34	.80
15	0.71	.75
16	.36	.11
17	.43	.28
18	1.41	.89
28	25.5	10.9
29	0.57	0.41
30	.36	...
42	.10	0.09
43	1.00	1.00
44	1.90	0.26
46	0.02	...

The results indicate that the condensable gas evolved from the lead azide consists mainly of hydrogen azide. The parent molecule (mass 43) is fragmented in the electron beam of the mass spectrometer. Mass 28 ($^{14}\text{N}_2$) is the most frequent fragment; it cannot be attributed to gaseous nitrogen originally present in the gas mixture because the sample contained a condensable gas. The other fragments related to the parent molecule HN_3 are mass 14 (^{14}N), 15 (NH), 29 (HNN and $^{14}\text{N}^{14}\text{N}$), and 42 (N_3). Mass 18 and 17 are attributed to water. They appear in the gas from $\text{Pb}(\text{N}_3)_2$ as well as in the hydrogen azide control sample. It is not quite clear why they are observed in the latter case unless one assumes that there is a finite water vapor pressure over H_2SO_4 or that water is desorbed from the walls of the vacuum system and condensed in the trap. In the first case where we find a greater intensity in mass 18 and 17 the difference may be attributed to the residual water involved in the hydrolysis reaction which will be described later in the discussion.

The remaining peaks of the pattern may be attributed to impurities. CO_2 can account, in decreasing intensity, for mass 44, 16, 28, and 12.⁹ Both lead azide and sodium azide may contain a surface layer of the carbonate of the respective cation, and CO_2 then is formed by the decomposition of the carbonate, either thermally as in the first case (PbCO_3) or by the reaction with H_2SO_4 as in the second case (Na_2CO_3).

The other impurity is most likely NO_2 which, in decreasing intensity, shows the mass numbers 30, 46, 16, 14, 28.¹⁰ It appears only in the gas evolved from $\text{Pb}(\text{N}_3)_2$, and it is most likely that it is the decomposition product of lead nitrate used for the preparation of lead azide.

(9) Am. Petroleum Res. Inst., Mass Spectral Data, Res. Project 44, Ser. No. 157, 1948.

(10) R. A. Friedel, A. G. Sharkey, Jr., J. L. Shultz, and C. R. Humbert, *Anal. Chem.*, **25**, 1314 (1953).

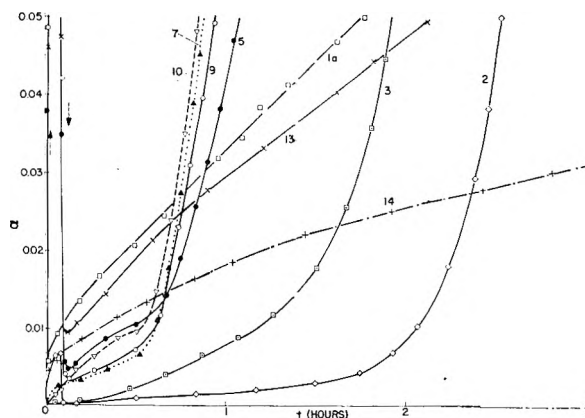
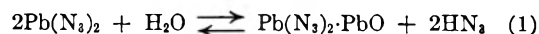


Fig. 8.—Initial stage of decomposition.

Discussion

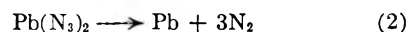
All reactions encountered in the present experiments are characterized by the initial evolution of the condensable gas mixture which consists mainly of hydrogen azide. It is unlikely that hydrogen azide is present in the unheated starting materials. Previously² it has been found that hydrogen azide was formed in a hydrolysis reaction between water and lead azide. The lead azide was converted into a basic lead azide (probably $\text{Pb}(\text{N}_3)_2 \cdot \text{PbO}$)



This reaction could proceed to measurable amounts of basic lead azide, because water was mainly supplied from an external source. A smaller portion could be attributed to water which either was adsorbed on the lead azide crystals or was present in a chemically bound form. Only the latter case need be considered in the present experiments. The presence of chemically bound water was established by Feitknecht and Sahli,¹ who obtained basic lead azides of the general formula $x\text{Pb}(\text{N}_3)_2 \cdot y\text{PbO} \cdot z\text{H}_2\text{O}$ ¹² when they treated $\text{Pb}(\text{N}_3)_2$ with alkaline solutions, and to a smaller extent even with water. The above phenomena are important in explaining the results of the present work. It is assumed that the lead azide used for this work initially was covered with a surface layer of these hydrated basic azides, and that the treatment with hydrazine hydrate, which is a base, further increased the amount of this surface layer.

By heating the samples to 240° both physically adsorbed water and water from the hydrated azide were released in a very short time and reacted with excess lead azide according to the above equation. This gives rise to the outgassing peaks previously discussed, their heights being proportional to the amount of hydrated basic lead azide, which is greater for samples treated with hydrazine hydrate.

Now it has been shown previously² that the autocatalytic reaction



is poisoned in the presence of a hydrogen azide—

(11) W. Feitknecht and M. Sahli, *Helv. Chim. Acta*, **37**, 1423 (1954).

(12) The formula was $\text{Pb}(\text{N}_3)_2 \cdot \text{PbO} \cdot (0.4-0.8)\text{H}_2\text{O}$ when water or small amounts of alkaline solution were used. By increasing the amount of the alkaline solutions, higher $\text{PbO}:\text{Pb}(\text{N}_3)_2$ ratios (up to 9:1) were obtained.

water mixture. Both hydrogen azide and water can react with the lead nuclei which are necessary for the catalytic acceleration of the reaction. This observation is confirmed by the present data. In the case of the untreated lead azide where the initial gas evolution is low ($\alpha = 0.007$) the autocatalytic reaction cannot be stopped completely. However, the induction time becomes longer than in the case where the hydrogen azide-water mixture has been frozen out. In addition, the reaction rate is lower and the sample does not explode. In all cases where the initial gas evolution attributable to the hydrazine hydrate treatment and the ensuing formation of hydrated basic lead azide was high ($\alpha = 0.06-0.08$), a complete poisoning of the autocatalytic reaction was observed if the gasses were not frozen out. This poisoning effect occurs also when the liquid nitrogen is removed at higher conversions, permitting the hydrogen azide-water mixture to exert its influence on the lead azide. We then observe a reduction of the maximum reaction rate and a shift of the curve toward longer times (curve 7, Fig. 5; curve 11, Fig. 6).

The decomposition of all samples where hydrazine hydrate was involved was less complete (α_{∞} around 0.85) than the decomposition of the untreated lead azide (α_{∞} around 0.95). This is attributed to the presence of the basic lead azide which, due to its lower azide content, is less likely to decompose, even at 300°.

When the hydrogen azide-water mixture is removed from the silver-coated samples, the silver shows its catalytic activity. The induction periods become smaller than those of the untreated material. In the initial stages of the reaction the curves are practically identical regardless of whether the amount of silver is 1.0 or 10.0 atom%. This suggests that it is not the amount of the external catalyst that is important, but the contact area between the silver grains and the lead azide, which should be not much different for 1 and 10 atom% of Ag for the following reason: After the first silver

azide has been formed on the lead azide surface, it is more likely that further silver azide is deposited on its own lattice than on new sites on the lead azide surface. This arrangement will not be changed when the silver azide is reduced to metallic silver.

The good reproducibility of the curves for the silver-coated samples in the initial stage of decomposition as well as the sudden rate increase (Fig. 8), which cannot be observed in either the untreated or the hydrazine-treated material, are not inconsistent. Upon completion of the outgassing process there exists a relatively large metal-lead azide interface in the silver-coated samples. In the other cases this interface will have to be formed by the creation and growth of lead nuclei. Obviously the area of the preformed interface with the silver-coated samples is appreciable and permits good reproducibility of the curves and a high rate of reaction in the initial stage.

It must be pointed out that the maximum rate is smaller with the silver-coated samples than with the untreated lead azide, in contrast to the respective behavior in the initial stage as pointed out above. It is assumed that two different propagation mechanisms are operating. In the early stages the reaction front originating from the metallic nuclei is confined to the individual lead azide grains. Later the growing metal specks come into contact with still undecomposed portions of adjacent lead azide grains, and the reaction propagates *via* a bridge mechanism.

Due to the treatment with hydrazine hydrate the silver-coated samples are covered with a surface layer of basic lead azide. Furthermore, the silver grains on the surface separate the individual lead azide crystals, which results in the reduction of the bulk density, as has been found. Both factors reduce the probability of the bridge mechanism occurring. This is not the case for the untreated lead azide, and the bridge mechanism can contribute to the reaction rate so as to result in an explosion.

MONONUCLEAR AND POLYNUCLEAR COMPLEX FORMATION BETWEEN IRON(II) AND 2,3-DIMERCAPTO-1-PROPANOL

BY D. L. LEUSSING¹ AND JERROLD JAYNE

Department of Chemistry, University of Wisconsin, Madison, Wis.

Received August 24, 1961

Iron(II) and 2,3-dimercapto-1-propanol ions react to form intensely colored dark red polynuclear complexes conforming to the series, $\text{DMP}(\text{FeDMP})_n^-$, and a mononuclear complex, $\text{Fe}(\text{DMP})_2^-$, which has a less intense red color. The formation constant for $\text{Fe}(\text{DMP})_2^-$ was found to be about $6 \times 10^{+15}$ in 0.10 M potassium chloride at 30°.

Recent investigations have shown that mercaptide containing ligands form polynuclear complexes with some of the divalent metal ions of the first transition series. These polynuclear complexes can be characterized using the "core plus links" postulate of Sillén.² The bidentate monothiol β -

mercaptoethylamine³ and mercaptoacetate⁴ react with nickel(II) to form complexes belonging to the series $\text{Ni}[\text{Ni}(\text{RS})_2]_n^{2-2n}$ while 2,3-dimercapto-1-propanol (DMP) forms complexes of the type $\text{DMP}(\text{MDMP})_n^-$ where M is zinc(II)⁵ or nickel

(1) To whom inquiries should be addressed at the National Bureau of Standards, Washington, D. C.

(2) L. G. Sillén, *Acta Chem. Scand.*, **8**, 299, 318 (1954).

(3) D. C. Jicha and D. H. Busch, 135th National Meeting of the American Chemical Society, Boston, Mass., April, 1959.

(4) D. L. Leussing, R. E. Laramy, and G. S. Alberts, *J. Am. Chem. Soc.*, **82**, 4826 (1960).

(II).⁶ Mercaptide ions act as bridging groups in these polynuclear complexes and a feature has been postulated to be d,d- π bonding where electrons are donated from the metal ion d orbitals to the vacant sulfur d orbitals.^{5,7} In this respect it is significant that manganese(II) ions with only a half-filled d shell were found not to form polynuclear species under comparable conditions where the nickel(II) and zinc(II) complexes obtain.

We have undertaken the present study of the iron(II)-DMP system to characterize further the properties of the mercaptide complexes with the divalent metal ions of the first transition series; in particular to determine with which of the divalent metal ions in the series Mn to Zn the onset of polynuclear complexes occurs under the conditions used in these studies. The results which we obtained for this highly air-sensitive system were not as precise as those which were obtained for the zinc(II)-DMP system. However, conclusions of a semi-quantitative nature could be drawn.

Experimental

Ferrous chloride stock solutions, approximately 0.1 M, were prepared freshly for each series of experiments by dissolving C.P. iron powder in a slight excess of hydrochloric acid under a nitrogen atmosphere. After completion of the reaction (24 hr. with continual agitation or several days with frequent shaking) aliquots of the solutions were analyzed for iron and chloride. The difference between the chloride as ferrous chloride and the total chloride was taken as the excess of hydrochloric acid concentration.

To study the complexes, the techniques and procedures used were essentially the same as those used earlier.⁵ The titration-pH method was used but each point on the titration curve was the result of a single batch-wise experiment because of the necessity of equilibrating many of the solutions with a solid phase, the high sensitivity of the system to oxygen, and the general sluggishness of DMP systems. Two levels of iron concentration were used, approximately 2.5 or 5 mM. The DMP concentration in each experiment was maintained at a level that was two or three times that of the iron. The required volumes of ferrous chloride, DMP, and standard potassium hydroxide solutions were mixed under air-free conditions with sufficient water and potassium chloride to bring the final volume to 100.0 ml. and be 0.100 M in potassium chloride. After equilibrating at least 36 hr. in a water bath at 30° the pH of each solution was determined.

Values of \bar{n} and (DMP⁻) were calculated using the equations

$$\bar{n} = \text{DMP}_t - \left[1 + \frac{K_{2n}}{a_H} + \frac{K_{1n}K_{2n}}{a_H^2} \right] \frac{2\text{DMP}_t - \text{OH}_t + [\text{OH}^-] - [\text{H}^+]}{2 + \frac{K_{2n}}{a_H}} \quad (1)$$

$$(\text{DMP}^-) = \frac{K_{1n}K_{2n}}{a_H^2} \frac{2\text{DMP}_t - \text{OH}_t + [\text{OH}^-] - [\text{H}^+]}{2 + \frac{K_{2n}}{a_H}} \quad (2)$$

where the subscript t designates the initial analytical concentration of the substance indicated, the quantities in parentheses refer to equilibrium concentration, and a_H refers to the hydrogen ion activity as calculated from the measured pH. The value of OH_t was corrected for the excess acid in the ferrous chloride solutions. The values of K_{1n} and K_{2n} were determined to be 2.03×10^{-9} and 1.91×10^{-11} , respectively, in 0.100 M potassium chloride at 30.0°.

It should be noted that the assumption was made in the derivation of eq. 1 and 2 that both thiol protons of a complexed DMP molecule are replaced. Also the value of \bar{n} so

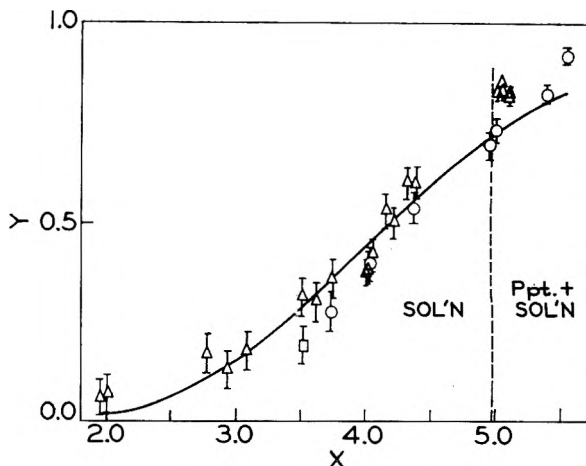


Fig. 1.—Complex formation in the region $\bar{n} > 1.00$: $y = 2 - \bar{n}$; $x = -\log(\text{DMP}^-) + \log \text{Fe}_t$; Δ , $\text{Fe}_t = 1.98 - 2.05 \times 10^{-3} M$; \circ , $\text{Fe}_t = 5.16 \times 10^{-3} M$; \square $\text{Fe}_t = 5.80 \times 10^{-3} M$.

calculated is the average for the solution and solid phases when both are present. The results for $\bar{n} < 1$ are given in Table I and those for $\bar{n} > 1$ are given in Fig. 1 as a plot of y , which equals $2 - \bar{n}$, vs. x , which is $-\log(\text{DMP}^-) + \log[\text{Fe}]_t$.

TABLE I

THE APPARENT VALUES FOR THE SOLUBILITY PRODUCT, $K_{sp} = (\text{Fe}^{++})(\text{DMP}^-) K_{sp} \times 10^{13}$

Fe_t M $\times 10^3$	DMP_t M $\times 10^3$	OH_t M $\times 10^3$	pH	$-\log$ (DMP ⁻)	\bar{n}	Fe_t : DMP ⁻ : 1:1	Fe_t : DMP ⁻ : 1:1.2
2.01	5.77	0.31	5.73	10.20	0.08	1.2	1.1
2.01	3.46	0.31	5.89	10.12	.08	1.4	1.4
4.76	15.00	1.77	5.52	10.22	.17	2.4	2.4
5.80	14.58	2.00	5.62	10.04	.20	4.4	4.5
4.76	15.00	3.67	5.70	9.89	.38	2.6	4.1
2.01	5.77	1.81	6.23	9.26	.45	6.0	6.9
5.16	15.00	5.16	5.78	9.76	.50	4.9	5.2
4.76	15.00	5.57	6.01	9.30	.58	10	12
5.16	15.00	7.15	5.99	9.37	.69	6.8	9.4
4.76	15.00	6.99	6.10	9.15	.73	8.9	13
2.01	5.77	3.30	6.59	8.62	.80	8.3	15
2.01	3.46	3.30	6.82	8.52	.81	12	19
2.04	3.59	3.34	6.76	8.61	.81	9.2	16
4.76	15.00	8.42	6.24	8.90	.88	6.9	16
1.98	3.60	3.62	6.97	8.22	.91	10	28

Results and Discussion

Qualitatively, the following behavior was observed. At the lowest value of \bar{n} (0.08) a small amount of precipitate was obtained and the solution was tinged faintly red. As \bar{n} increased both the amount of precipitate and the color intensity of the supernatant liquid also increased. The solutions were dark red at \bar{n} values around 0.8 and from visual observations no changes in color intensity occurred from this point until \bar{n} attained a value greater than 1.4. Above this value the color intensity decreased with increasing \bar{n} until at \bar{n} equals two the color had changed from a dark red to a light red. No further color change occurred as the solutions were made more basic except in the most alkaline solutions (pH 11), where a slight yellowish tinge was assumed by the red solutions. The precipitate appeared to be absent at \bar{n} equal to 1.2 and greater. As in the case with zinc(II), it is necessary to know this transition point in order to calculate the sta-

(5) D. L. Leussing and T. N. Tischer, *J. Am. Chem. Soc.*, **83**, 65 (1961).

(6) D. L. Leussing, *ibid.*, **80**, 4180 (1958).

(7) J. Chatt and F. A. Hart, *J. Chem. Soc.*, 2807 (1960).

bility constants, but because of the deep color it was not possible to determine visually the point at which the turbidity disappeared. This point was taken as the minimum value of \bar{n} where centrifuging failed to bring down solid material.

The \bar{n} values in Table I and as implied in Fig. 1 are seen to depend on both the (DMP⁻) concentration and the level of iron. This behavior is expected where the solution species are in equilibrium with a solid phase but when the solid phase is absent polynuclear complexes are indicated. Polynuclear complexes also are suggested by the observations described above, since if only mononuclear complexes were formed a progressive color decrease should be noted with increasing values of \bar{n} beginning at 1.00.

The data in the region $\bar{n} > 1$ will be discussed first since their treatment is the most straightforward and the results are similar to those observed with the zinc(II)-DMP system. In Fig. 1 the points which would fall along separate curves in the usual plot of \bar{n} vs. $-\log(\text{DMP}^-)$ are seen to fall approximately along the same curve regardless of the iron level. This is in agreement with the behavior expected for the formation of a "core plus links" series $\text{DMP} \cdot (\text{FeDMP})_n^-$. Employing the curve fitting methods^{2,5} a curve was fitted to the points in Fig. 1 using the relationship $q_n = q_0 q^n$ ⁸ with q_0 equal to 2.0, yielding a value of q equal to 1.3×10^{-4} . The solid line in Fig. 1 represents the curve calculated using these values of q_0 and q . This is the same relationship that was found to describe the behavior of the zinc(II) polynuclear complexes but in this latter case values of q_0 and q equal to 1.5 and 1.4×10^{-6} were obtained. Since the shape of the curve in Fig. 1 depends on q_0 , the nearly identical q values show that for a given degree of complexing the distribution of the various species is about the same in the iron(II) system as with zinc(II). Thus, as was shown with zinc(II), complexes containing a fairly large number of iron(II) ions (up to about eight) are appreciably stable in the solution phase. The absolute stabilities of the iron(II) complexes are, of course, lower than those of zinc(II).

As \bar{n} approaches infinity, the ratio of Fe:DMP in the polynuclear complexes approaches 1:1. This yields a neutral species which most likely comprises the solid phase as was demonstrated with nickel(II)^{6,9} and zinc(II).⁵ On the basis of this assumption values of the solubility product, (Fe⁺⁺)(DMP⁻), were calculated for the two extremes; (a) ferrous and DMP⁻ ions combine in a 1:1 ratio and with regard to the unprecipitated iron the concentrations of polynuclear species are negligible compared to that of free ferrous ions; (b) ferrous and DMP⁻ ions combine in a 1:1.2 ratio¹⁰ and the complexes are in equilibrium with a minute but negligible amount of solid FeDMP. The apparent values of K_{sp} are given in Table I. It is seen that

(8) The quantity q_n is the equilibrium constant for the reaction $(n+1)\text{Fe}(\text{DMP})_2^- \rightleftharpoons \text{DMP} \cdot (\text{FeDMP})_n^- + n \text{DMP}^-$.

(9) P. Zuman and R. Zumanova, *Tetrahedron*, **1**, 289 (1957).

(10) In the presence of solid FeDMP, the equilibria $(n+1)\text{FeDMP}_2 \cdot \text{DMP} \cdot (\text{FeDMP})_n^- + \text{Fe}^{++}$ hold. Therefore, the ratios of the concentrations of the various divalent species are constant as long as solid is present and the average composition of the complexes in solution also remains constant.

for neither case constant values are obtained. In the lowest pH range the "constants" become smaller with decreasing pH. We have not been able to account quantitatively for the drifting "constants" but a reasonable explanation lies in the formation of protonated complexes, which are not taken into account in eq. 1 and 2. This complication does not present a major difficulty because the results indicate that protonated species are absent in the region $\bar{n} > 1$. These species then must disappear as \bar{n} approaches 1 from the low side. Therefore, eq. 1 and 2 should give increasingly more valid results as \bar{n} increases and the true value of K_{sp} should be approached in the limit and bracketed by the apparent values calculated for (a) and (b).

A system in which the over-all value of \bar{n} equaled 0.73 was analyzed and it was found that about one-half the iron had precipitated from solution, presumably as the 1:1 neutral complex. This result indicates that a closer description of the system is given by case (a). Further evidence favoring this conclusion lies in the fact that the K_{sp} values calculated for case (a) appear to lie randomly scattered about a common value in the higher \bar{n} region, while those values calculated for case (b) continue to increase with increasing \bar{n} . Accordingly, we estimate the value of K_{sp} to be about 10×10^{-13} .

The value of Q_2 , the constant for the equilibrium $\text{Fe}^{++} + 2\text{DMP}^- \rightleftharpoons \text{Fe}(\text{DMP})_2^-$, was calculated to be $6 \times 10^{+15}$ using the equation $Q_2 = v_{sol}/qK_{sp}$. The value of v_{sol} was obtained from the data for those solutions where the solid phase just redissolves (\bar{n} equals 1.2). The method of calculation is described in ref. 5. A rough estimate of $5 \times 10^{+16}$ for Q_2 can be made using the results $3 \times 10^{+10}$ and $2 \times 10^{+23}$ for the formation of $\text{Mn}(\text{DMP})_2^-$ and $\text{Zn}(\text{DMP})_2^-$.¹¹ Although the agreement between the two results for Q_2 is only fair, at least some assurance is given that the experimental value of Q_2 is of the correct order of magnitude and therefore the assumptions made in its calculation are valid to a first approximation.

The constant for the reaction $2\text{Fe}^{++} + 3\text{DMP}^- \rightleftharpoons \text{Fe}_2(\text{DMP})_3^-$ is calculated to be about 10^{+28} . That for the formation of $\text{Zn}_2(\text{DMP})_3^-$ is about $4 \times 10^{+40}$. The ratio of the one-fourth root of the constant for $\text{Fe}_2(\text{DMP})_3^-$ to the one-fourth root of that for $\text{Zn}_2(\text{DMP})_3^-$ is about $1:10^{+3}$. For the monomeric bis-DMP complexes of iron(II) and zinc(II) the ratios of the square roots of the formation constants is also about $1:10^{+3}$. From this comparison it appears, at least within the limitations of comparing constants for reactions in which different numbers of particles are involved, that the low result for $\text{Fe}_2(\text{DMP})_3^-$ is due to nothing more than those factors which normally operate to give a lower stability of iron(II) complexes relative to those of zinc(II).

The relatively strong absorption of the polynuclear species relative to the mononuclear suggests that π -bonding also occurs in the iron(II)-DMP system. If so, the parallel decrease in the stabilities of the polynuclear and mononuclear complexes in going from zinc(II) to iron(II) can be

(11) D. L. Leussing, *Talanta*, **4**, 264 (1960).

explained as a manifestation of the "synergistic effect"¹² existing between σ and π bonds.

(12) L. E. Orgel, "An Introduction to Transition Metal Chemistry," John Wiley and Sons, New York, N. Y., 1960.

Acknowledgment.—We wish to thank the National Science Foundation and the Wisconsin Alumni Research Foundation for grants which supported this and related work.

RELATIVE HYDROGEN BONDING OF DEUTERIUM. II. ACID IONIZATION CONSTANTS IN H₂O AND D₂O¹

BY A. O. McDOUGALL AND F. A. LONG

Department of Chemistry, Cornell University, Ithaca, N. Y.

Received August 30, 1961

Studies have been made of the ionization constants of a variety of weak acids in the solvents H₂O and D₂O by glass electrode or by conductometric procedures. Emphasis has been on acids which in either the acid or conjugate base form would be expected to form intramolecular hydrogen bonds. These data, when combined with data of other workers, offer support to the proposal that for weak acids in general ($pK_{DA} - pK_{HA}$) increases with pK_{HA} . However, the data also support the suggestion that the reference line of such a correlation is different for acids of different types. Several of the present results are consistent with earlier studies on maleic acid in that intramolecular hydrogen bonding, relative to bonding to the solvent, appears to be weaker for deuterium than for hydrogen. However, there are enough exceptions to this rule to suggest that a true picture will not be obtained without more explicit consideration of the properties of particular solutes as well as of the solvent differences in the two cases.

Reasons for interest in the relative abilities of hydrogen and deuterium to form hydrogen bonds have been summarized in Part I of this series.² Part I also reported measurements of the ionization constants of acids, one of which involved an intramolecular hydrogen bond; it was found that the ratio of these constants in water and deuterium oxide, for any particular acid, varied according to whether an intramolecular hydrogen bond was concerned in the ionization. The comparison in such a case is of the competition between internal hydrogen bonding and hydrogen bonding with the solvent, and it is not a direct measure of the strength of the intramolecular hydrogen bond involved. The present work extends this comparison to other acids, some of which are hydrogen-bonded, and considers the results on the basis of a general correlation for the dissociation of acids in water and deuterium oxide. Such a relationship first was postulated by Rule and LaMer,³ who found for the small number of acids at that time investigated that $\log(K_{HA}/K_{DA})$ was proportional to $\log K_{HA}$, K_{HA} and K_{DA} being the ionization constants of H- and D- acids in water and deuterium oxide, respectively. This relation has been supported by later workers⁴ but Högfeldt and Bigeleisen⁵ have suggested recently that the type of acid (*e.g.*, phenol, carboxylic acid, etc.) may change the constant of proportionality, *i.e.*, the slope of the line, and this proposal is supported by the present work.

Most of the conventional methods for determination of ionization constants have been applied to studies in deuterium oxide; Dahlgren and Long,² for example, used e.m.f. measurements with a quinhydrone electrode. A much simpler method is suggested by the work of Glasoe and Long⁶ and

others^{7,8} which has established that satisfactory measurements with deuterium oxide solutions can be made with a glass electrode. The determination of hydrogen ion concentration with a glass electrode is by no means as accurate as that with a hydrogen or quinhydrone electrode but it was hoped that satisfactory pK differences could be obtained readily for a series of acids. Studies now have been made for a number of carboxylic acids and phenols, several of which involve intramolecular hydrogen-bonding. In addition some data have been obtained for certain other acids (not hydrogen-bonded species) by conductance measurements, which method of course is considerably more accurate than the glass electrode procedure.

Experimental

Materials.—Reagent grade inorganic chemicals were used throughout. Deuterium oxide was supplied by the Liquid Carbonic Company; it contained at least 99.5% D₂O.

Salicylic acid (m.p. 159–160°), *o*-nitrophenol (m.p. 46°), *p*-nitrophenol (m.p. 112–114°), 2,4-dinitrophenol (m.p. 111°), 2,6-dinitrophenol (m.p. 62–63°), and γ -resorcylic acid (2,6-dihydroxybenzoic acid) (m.p. 167°), were purified by recrystallization from water. Glycolic, oxalic, iodic, and chloroacetic acids were used without further purification except that the oxalic acid first was dehydrated over sulfuric acid. Reagent grade phosphoric acid (containing not less than 85% H₃PO₄) was employed.

Sodium hydroxide solutions were British Drug Houses "Concentrated Volumetric Solutions" diluted appropriately. A stock solution of sodium deuterioxide in deuterium oxide was made up by allowing metallic sodium in toluene to react with boiled-out deuterium oxide in a separatory funnel. This stock solution was diluted according to requirements.

All solutions were made up with boiled-out distilled water or deuterium oxide, and were estimated either by titration against standard base or in the case of certain of the phenols by a bromination procedure or by spectrophotometry.

pH Measurements.—The potential was measured with either a Beckman Model G pH meter or (in some of the later experiments) a Cambridge Instrument Company Research Model Electron-ray pH meter. The electrode assembly, consisting of a Beckman No. 30167 glass electrode and a

(1) Work supported by a grant from the Atomic Energy Commission.

(2) G. Dahlgren, Jr., and F. A. Long, *J. Am. Chem. Soc.*, **82**, 1303 (1960).

(3) C. K. Rule and V. K. LaMer, *ibid.*, **60**, 1974 (1938).

(4) P. Ballinger and F. A. Long, *ibid.*, **82**, 795 (1960).

(5) E. Högfeldt and J. Bigeleisen, *ibid.*, **82**, 15 (1960).

(6) P. K. Glasoe and F. A. Long, *J. Phys. Chem.*, **64**, 188 (1960).

(7) R. Lumry, E. L. Smith, and R. R. Glantz, *J. Am. Chem. Soc.*, **78**, 4330 (1951).

(8) K. Mikkelsen and S. O. Nielsen, *J. Phys. Chem.*, **64**, 632 (1960).

TABLE I
 pK_{HA} AND ΔpK VALUES FROM GLASS ELECTRODE MEASUREMENTS, 25°

	pK_{HA}	pK_{DA}	ΔpK	Previous results
γ -Resorcylic acid	1.87 ± 0.04	2.33 ± 0.04	0.46	$pK_{HA} = 1.22$ at 30° ⁹
Salicylic acid	$2.94 \pm .01$	$3.69 \pm .03$.75	$pK_{HA} = 2.97$; $\Delta pK = 0.61$ ¹⁰
<i>m</i> -Nitrobenzoic acid	$3.62 \pm .04$	$4.12 \pm .02$.50	$pK_{HA} = 3.493$ ¹¹
Glycolic acid	$3.90 \pm .02$	$4.37 \pm .01$.47	$pK_{HA} = 3.821$ ¹² ; 3.80 ¹³
2,6-Dinitrophenol	$3.92 \pm .03$	$4.42 \pm .03$.50	$pK_{HA} = 3.58$; $\Delta pK = 0.45$ at 18° ¹⁴
2,4-Dinitrophenol	$4.12 \pm .02$	$4.82 \pm .02$.70	$pK_{HA} = 4.11$ ¹⁵ ; $pK_{HA} = 4.02$; $\Delta pK = 0.52$ at 18° ¹⁴
Oxalic acid (K_2)	4.30	4.79	.49	$pK_{HA} = 4.266$ ¹⁶ ; 4.29 ¹⁷ ; 4.30 ¹⁸
<i>o</i> -Nitrophenol	$7.19 \pm .02$	$7.94 \pm .02$.75	$pK_{HA} = 7.22$ ¹⁹ ; $pK_{HA} = 7.25$; $\Delta pK = 0.57$ at 18° ¹⁴
<i>p</i> -Nitrophenol	$7.26 \pm .03$	$7.74 \pm .01$.48	$pK_{HA} = 7.15$ ¹⁵ ; $pK_{HA} = 7.24$; $\Delta pK = 0.56$ at 18° ¹⁴

No. 39168 calomel reference electrode, was suspended in a test-tube containing about 5 ml. of the sample solution, which was immersed in an oil-bath maintained at $25.0 \pm 0.05^\circ$. The meter was standardized with either potassium acid phthalate solution (pH 4.005) or a phosphate buffer solution (pH 6.860), according to the range required. The actual measurements were made on appropriate buffer solutions of the acid under investigation; these solutions normally were made up by partial neutralization of the acid solution with sodium hydroxide or deuterioxide and sodium chloride solution was added to make a series of varying ionic strengths—usually between 0.01 and 0.1 *M*. However, in a few cases the solutions were made up directly from the acid and its conjugate base.

The thermodynamic dissociation constant was evaluated from the equation

$$pK = pH + \log \frac{C_{HA} - C_{H^+}}{C_{A^-} + C_{H^+}} - \log y_{\pm}$$

where pH is defined as $-\log [C_{H^+} y_{\pm}]$, C_{HA} and C_{A^-} are the added molar concentrations of free acid and anion, respectively, and y_{\pm} is the mean activity coefficient of the dissociated acid. In the correction term, C_{H^+} was taken as $\text{antilog}(-pH)$. $\log y_{\pm}$ was established from the approximate Debye-Hückel formula

$$-\log y_{\pm} = \frac{0.509\sqrt{I}}{1 + \sqrt{I}}$$

I being the ionic strength of the solution.

The second ionization constant of oxalic acid was established from solutions containing measured amounts of oxalic acid and sodium oxalate (*i.e.*, the disodium salt and the pK calculated from the expression

$$pK = pH + \log \frac{2C_{H_2Ox} - C_{H^+}}{C_{Ox^{2-}} - C_{HOx^-} + C_{H^+}} - 3 \log y_{\pm}$$

where C_{H_2Ox} and $C_{Ox^{2-}}$ are the added molar concentrations of oxalic acid and the disodium salt, respectively, and y_{\pm} is the mean 1:1 activity coefficient. No correction proved to be necessary to take account of the first dissociation since at the pH involved there was essentially no un-ionized oxalic acid present.

The procedure was substantially the same for the deuterium oxide solutions except that the pH meter reading was converted to " pD " by means of the equation

$$pD = pH + 0.40$$

(9) C. T. Abichandari and S. K. K. Jatkari, *J. Indian Inst. Sci.*, **A23** 77 (1941).

(10) S. Korman and V. K. LaMer, *J. Am. Chem. Soc.*, **58**, 1396 (1936).

(11) J. F. J. Dippy and R. H. Lewis, *J. Chem. Soc.*, 1008 (1937).

(12) L. F. Nims, *J. Am. Chem. Soc.*, **58**, 987 (1936).

(13) L. J. Minnick and M. Kilpatrick, *J. Phys. Chem.*, **43**, 259 (1939).

(14) D. C. Martin and J. A. V. Butler, *J. Chem. Soc.*, 1366 (1939).

(15) R. G. Bates and G. Schwarzenbach, *Helv. Chim. Acta*, **37**, 1069 (1954).

(16) G. D. Pinching and R. G. Bates, *J. Research Natl. Bur. Standards*, **40**, 405 (1948).

(17) H. S. Harned and L. D. Fallon, *J. Am. Chem. Soc.*, **61**, 341 (1939).

(18) H. N. Parton and R. C. Gibbons, *Trans. Faraday Soc.*, **35**, 542 (1939).

(19) A. I. Biggs, *ibid.*, **50**, 800 (1954).

established by Glasoe and Long.⁵ All studies in deuterium oxide were with solutions containing 99–99.5% D_2O and the results were not corrected to 100% D_2O .

Some idea of the accuracy of the procedures can be gained from the following typical results for glycolic acid. Separate measurements were made on six different buffer solutions with acid and anion concentrations each about 0.02 *M*, and with values of the ionic strength varying from 0.03 to 0.12. The calculated pK values ranged from 3.75 to 3.82. After activity coefficient corrections, the calculated pK_{HA} values varied from 3.82 to 3.95, with an average value of 3.90 ± 0.02 (standard deviation). A very similar study in deuterium oxide led to $pK_{DA} = 4.37 \pm 0.01$. Hence $\Delta pK = pK_{DA} - pK_{HA} = 0.47 \pm 0.02$. Table I summarizes the pK_{HA} and ΔpK values which were measured by the glass electrode technique and compares the pK_{HA} values with those of other workers.

Conductance Measurements.—The conductivity cell was of a type similar to that described by Baker and LaMer²⁰; the electrodes were lightly platinized and the cell had a capacity of 10 ml. The cell constant was 1.846 cm^{-1} , determined with carefully prepared solutions of potassium chloride. The electrical apparatus comprised a 1-*kc.* oscillator, a Campbell-Shackleton ratio bridge, a Leeds and Northrup precision a.c. resistance box, an amplifier and ear-phones.

Measurements of the conductance of the acid solutions were made at at least two concentrations chosen to provide a compromise between a low ionic concentration (to minimize the activity coefficient correction) and not too high a degree of dissociation (since the method is considerably less accurate for higher α values). In the case of phosphoric acid and, more particularly, oxalic acid it was necessary to use a concentration sufficiently high to minimize the effect of the second dissociation.

The calculation of K_{HA} was carried out essentially by the method of MacInnes and Shedlovsky.²¹ Values of Λ_0 , the equivalent conductivity of the acid at infinite dilution, were obtained from the literature and Λ_i , the equivalent conductivity at the ionic concentration concerned, calculated from the Onsager equation by a successive approximation procedure

$$\Lambda_i = \Lambda_0 - (B_1\Lambda_0 + B_2) \frac{\sqrt{\alpha c}}{1 + B\hat{a}\sqrt{\alpha c}}$$

where B , B_1 and B_2 are known constants, c is the stoichiometric acid concentration (in moles per liter), α is the degree of dissociation and \hat{a} is the ionic size parameter. The values of K , calculated from the relation $\alpha^2c/(1 - \alpha)$, are not unduly sensitive to choice of Λ_0 or of \hat{a} (which was taken as 3.0 Å. unless otherwise mentioned). The activity coefficient term necessary to convert the "concentration" ionization constant to the "thermodynamic" value was evaluated from the modified Debye-Hückel equation

$$\log y_{\pm} = \frac{-A\sqrt{\alpha c}}{1 + B\hat{a}\sqrt{\alpha c}}$$

A being a constant and the other symbols having their usual meanings. For the concentrations involved in these studies the difference between f , the rational activity coefficient (for which this expression is derived) and y , the

(20) W. N. Baker and V. K. LaMer, *J. Chem. Phys.*, **3**, 406 (1935).

(21) D. A. MacInnes and T. Shedlovsky, *J. Am. Chem. Soc.*, **54**, 1429 (1932).

TABLE II
 IONIZATION CONSTANTS FROM CONDUCTANCE MEASUREMENTS, 25°

	<i>d</i>	$\Lambda_0(\text{H}_2\text{O})$	$\Lambda_0(\text{D}_2\text{O})$	pK_{HA}	pK_{DA}	ΔpK	Previous results
Iodic acid	3.0	390.7 ^a	284.2	0.848	1.151	0.303	$pK_{\text{HA}} = 0.772^{26}$
Oxalic acid (K_1)	4.0	390.0 ^b	283.1	1.270	1.666	.396	$pK_{\text{HA}} = 1.62$; $\Delta pK = 0.02^{26}$ $pK_{\text{HA}} = 1.271^{27}$
Phosphoric acid (K_1)	3.0	382.8 ^c	277.6	2.128	2.362	.234	$pK_{\text{HA}} = 2.13^{28}$; 2.148 ²⁹
Chloroacetic acid	3.0	389.6 ^d	282.8	2.851	3.339	.488	$pK_{\text{HA}} = 2.854^{31}$; $pK_{\text{HA}} = 2.76$; $\Delta pK = 0.44^{30}$

^a Ref. 32. ^b Ref. 27. ^c Ref. 33. ^d Ref. 31.

molar activity coefficient, is negligible. Moreover any errors arising from the use of this approximate form of the Debye-Hückel equation probably will not be significant for a situation where the ratio of ionization constants is of greater interest than an accurate value of K_{HA} .

For the deuterium oxide solutions, values of Λ_0 were in most cases not available but the relation²²

$$\left(\frac{\Lambda_0(\text{A}^-)}{\Lambda_0(\text{Cl}^-)}\right)_{\text{H}_2\text{O}} = \left(\frac{\Lambda_0(\text{A}^-)}{\Lambda_0(\text{Cl}^-)}\right)_{\text{D}_2\text{O}}$$

was assumed to be applicable. Since as mentioned above the final value of K is not very sensitive to choice of Λ_0 , errors from the use of this equation probably are not serious. Values of $\Lambda_0(\text{Cl}^-)$ and $\Lambda_0(\text{D}^+)$ in deuterium oxide were obtained from the work of Chittum and LaMer²³ and of Longworth and MacInnes.²⁴ The constants A , B , B_1 and B_2 in the Debye-Hückel and Onsager equations were adjusted to compensate for the changed viscosity and dielectric constant of deuterium oxide. A summary of the results of the conductivity experiments is given in Table II.

Discussion

Table III lists the data for ionization of acids in water and deuterium oxide obtained up to the present time, excluding only some very early figures³⁴; indication is given of the experimental methods used. The temperature is 25° unless otherwise indicated.

(22) J. P. Chittum and V. K. LaMer, *J. Am. Chem. Soc.*, **59**, 2455 (1937).

(23) V. K. LaMer and J. P. Chittum, *ibid.*, **58**, 1642 (1936).

(24) L. C. Longworth and D. A. MacInnes, *ibid.*, **59**, 1666 (1937).

(25) R. M. Fuoss and C. A. Kraus, *ibid.*, **55**, 476 (1933).

(26) J. C. Horne and J. A. V. Butler, *J. Chem. Soc.*, 1361 (1936).

(27) L. S. Darken, *J. Am. Chem. Soc.*, **63**, 1007 (1941).

(28) L. F. Nims, *ibid.*, **56**, 1110 (1934).

(29) R. G. Bates, G. L. Siegel, and S. F. Acree, *J. Research Natl. Bur., Standards*, **30**, 129 (1943).

(30) G. N. Lewis and P. W. Schutz, *J. Am. Chem. Soc.*, **56**, 1913 (1934).

(31) B. Saxton and T. W. Langer, *ibid.*, **55**, 3638 (1933).

(32) E. Bock, *Can. J. Chem.*, **37**, 3888 (1959).

(33) C. M. Mason and J. B. Culvern, *J. Am. Chem. Soc.*, **71**, 2387 (1949).

(34) The recent results of Högfeldt and Bigeleisen,⁴ and Hyman, Kaganove, and Katz³⁵ from indicator experiments have not been included partly because estimation of their probable accuracy is difficult and partly because the acids examined are largely of different charge types (e.g., amino acids) from those we have considered. As a different point, we should note that some additional studies of relative ionization constants by glass electrode procedures have been reported recently.³⁶

(35) H. H. Hyman, A. Kaganove, and J. J. Katz, *J. Phys. Chem.*, **64**, 1653 (1960).

(36) N. C. Li, P. Tang, and R. Mathur, Presented at the 139th National Meeting of the American Chemical Society, St. Louis, April, 1961.

(37) T. Riley and F. A. Long, unpublished work.

(38) C. Drueker, *Trans. Faraday Soc.*, **33**, 660 (1937).

(39) G. Schwarzenbach, A. Epprecht, and H. Erlenmeyer, *Helv. Chim. Acta*, **19**, 1292 (1936).

(39a) D. Bunn, F. S. Dainton, and S. Duckworth, *Trans. Faraday Soc.*, **57**, 1131 (1961).

(40) J. Curry and Z. Z. Hugus, Jr., *J. Am. Chem. Soc.*, **66**, 653 (1944).

(41) T. Riley and F. A. Long, to be published.

TABLE III

IONIZATION CONSTANTS IN WATER AND DEUTERIUM OXIDE,
 $\Delta pK = pK_{\text{DA}} - pK_{\text{HA}}$

Symbols for methods used: C, conductance; H₂, e.m.f.—hydrogen/deuterium electrode; PH, glass electrode; QH, quinhydrone electrode; S, solubility of salts and transfer data; SP, spectrophotometry.

Acid	Method	pK_{HA}	ΔpK	Ref.
Picric	SP	0.38	0.44	37
Iodic	C	0.848	.303	This work
Oxalic (K_1)	C	1.270	.396	This work
Sulfuric (K_2)	C	1.90	.30	38
γ -Resorcylic (K_1)	PH	1.87	.46	This work
Maleic (K_1)	QH	1.91	.62	2
Phosphoric (K_1)	C	2.128	.234	This work
<i>m</i> -Nitroaniline	PH	2.48	.48	6
Chloroacetic	C	2.851	.488	This work
Salicylic (K_1)	PH	2.94	.75	This work
Ethyl hydrogen maleate	QH	3.08	.46	2
Fumaric	QH	3.10	.46	2
Ethyl hydrogen fumarate	QH	3.40	.45	2
<i>m</i> -Nitrobenzoic	PH	3.62	.50	This work
Formic	H ₂	3.75	.40	39
	PH	3.75	.45	6
Glycolic	PH	3.90	.47	This work
2,6-Dinitrophenol	PH	3.92	.50	This work
2,4-Dinitrophenol	PH	4.12	.70	This work
Benzoic	QH	4.21	.50	3
Oxalic (K_2)	PH	4.30	.49	This work
Aniline	PH	4.55	.58	6
Fumaric (K_2)	QH	4.60	.42	2
Hydrazoic (20°)	PH	4.68	.33	39a
Acetic	PH	4.73	.52	6
	QH	4.74	.52	10
	C	4.74	.52	23
Maleic (K_2)	QH	6.33	.38	2
Carbonic (K_1)	H ₂	6.35	.43	40
<i>o</i> -Nitrophenol	PH	7.19	.75	This work
Phosphoric (K_2)	QH	7.19	.56	3
<i>p</i> -Nitrophenol	PH	7.26	.48	This work
Ammonia	H ₂	9.26	.49	39
Methyl acetylacetone	PH	9.35	.40	41
2-Acetylcyclohexanone	PH	9.47	.51	41
Trimethylamine	H ₂	9.90	.59	39
Glycine (KNH_3^+)	H ₂	9.90	.53	39
Carbonic (K_2)	H ₂	10.25	.64 ^a	40
	PH	10.33	.63	6
Hydroquinone	QH	10.58	.62	3
2,2,2-Trifluoroethanol	C	12.37	.65	4
2-Chloroethanol	C	14.31	.70	4
Water	S	15.72	.84	42

^a Recalculated by Glasoe and Long.

(42) R. W. Kingerly and V. K. LaMer, *J. Am. Chem. Soc.*, **63**, 3256 (1941).

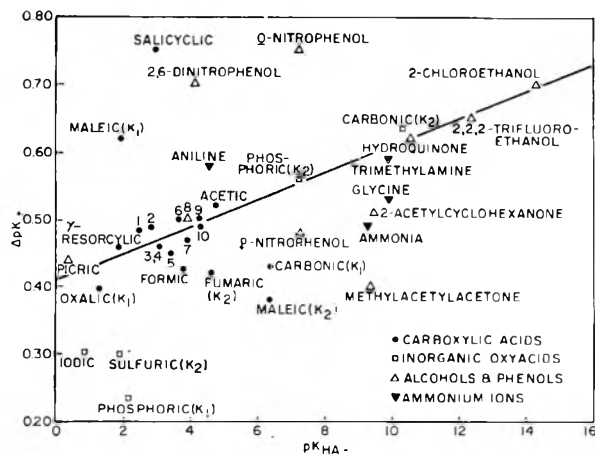


Fig. 1.—Plot of ΔpK against pK_{HA} : 1, *m*-nitroaniline; 2, chloroacetic; 3, ethyl hydrogen maleate; 4, fumaric (K_1); 5, ethyl hydrogen fumarate; 6, *m*-nitrobenzoic; 7, glycolic; 8, 2,6-dinitrophenol; 9, benzoic; 10, oxalic (K_2).

When ΔpK is plotted against the pK_{HA} for all these results (Fig. 1), a graph in the form of an approximate straight line is obtained. The line of Fig. 1 is for the equation

$$\Delta pK = 0.41 + 0.02pK_{HA}$$

as suggested by Bell.⁴³ If the results are grouped according to the structural type of the acid concerned, then straight lines, similar but differing slightly in slope, are obtained for carboxylic acids, inorganic acids, and phenols, although the paucity of results in some of these categories makes the lines uncertain. If the figures of Li, Tang, and Mathur³⁶ for the second and third dissociation constants of citric and tricarballic acids are included in the carboxylic acid plot, and if these are assumed to be "normal" acids, then the slope of the best line is somewhat greater (0.05) than if these results are ignored (0.03) or than if the phenols are plotted on the same diagram (0.02). However, whichever plot is used, some points lie a considerable distance on either side of the line drawn. Since the uncertainty in many of the ΔpK measurements is comparatively large, the significance of a particular point falling away from the drawn line is small unless the discrepancy is striking.

In a number of cases large discrepancies may be rationalized by assumption of internal hydrogen bonding in the acidic or anionic group. The work of Dahlgren and Long² suggests that intramolecular hydrogen-bonding will affect the relation between pK_{HA} and ΔpK in the sense that if the anion of an acid (e.g., maleic acid) contains an internal hydrogen bond then the ΔpK is predicted to fall above the "normal," i.e., above the value which would be expected from consideration of other non-hydrogen-bonded acids. Conversely, if the acid form contains an intramolecular hydrogen bond (e.g., bimaleate ion) the ΔpK should be lower than expected. This implies that the H-anion in its hydrogen bonded form is relatively more stable in water than is the D-anion in D_2O . Consequently the strength of the "deuterium H-bond" relative to intermolecular bonding with the solvent is weaker

(43) R. P. Bell, "The Proton in Chemistry," Cornell University Press, Ithaca, N. Y., 1959, p. 188.

than the "hydrogen H-bond" in similar circumstances. Maleic acid is of course a favorable case for this kind of study since the work of Westheimer and Benfey⁴⁴ already has established that in aqueous solutions the bimaleate ion exists primarily in the internally hydrogen bonded form.

Evidence for the work of other investigators for hydrogen bonding of some of the acids and anions of the present study is considered below. A serious difficulty is that much of the evidence for intramolecular bonding in these compounds comes from studies with crystals or with solutions in non-aqueous solvents of low polarity. Since water as solvent will compete strongly for both donor and acceptor sites for hydrogen bonding, one may expect intramolecular hydrogen bonding to be considerably less in water than in such solvents. Unfortunately for present purposes the central point is whether internal hydrogen bonding exists in aqueous solution.

With the two β -diketone enols, we really do not know the situation for solutions in water. In non-aqueous media, evidence from both infrared and ultraviolet studies points definitely to internal hydrogen bonds.^{45,46} So also does the high enol content found at equilibrium for these ketones in inert solvents.⁴⁷ The enol content is usually sharply lower in aqueous solutions but still large enough to suggest some internal hydrogen bonding of the enols. The size of the pK values for these enols in water is also consistent with considerable intramolecular hydrogen bonding but this argument is rather uncertain. The relatively low ΔpK values of Fig. 1 are, of course, as expected from the proposal that the internal bonding persists into water since from the maleic acid studies the expectation is that the ΔpK for an H-bonded acid will be abnormally low.⁴⁸

Salicylic acid and γ -resorcylic acid are both carboxylic acids with *o*-hydroxy groups and might be expected to behave similarly. Branch and Yabroff⁴⁹ showed by comparison of the dissociation constants of hydroxy- and methoxybenzoic acids that the anion of salicylic acid undoubtedly is hydrogen bonded in aqueous solution. More recently Scheraga and Hermans⁵⁰ have studied salicylic acid in both H_2O and D_2O and interpret their results in terms of extensive intramolecular bonding for the anion. Thus the high position of this acid in Fig. 1 ($\Delta pK = 0.75$) is entirely consistent with the data for maleic acid and suggests a similar explanation. For resorcylic acid on the

(44) F. H. Westheimer and O. T. Benfey, *J. Am. Chem. Soc.*, **78**, 5309 (1956).

(45) R. S. Rasmussen, D. D. Tunnicliff, and R. R. Brattain, *ibid.*, **71**, 1068 (1949).

(46) S. Bratoz, D. Hadzi, and G. Rossmly, *Trans. Faraday Soc.*, **52**, 464 (1956).

(47) For a discussion, see G. S. Hammond in "Steric Effects in Organic Chemistry," edited by M. S. Newman, 1956, John Wiley and Sons, New York, N. Y., Chap. 9.

(48) One further acid which lies well below the line on the ΔpK - pK_{HA} diagram is phosphoric (K_1). No reason can be advanced for this, although it is true that comparatively few inorganic acids have been studied and those that have may not be sufficiently representative to provide a good base line.

(49) G. E. K. Branch and D. L. Yabroff, *J. Am. Chem. Soc.*, **56**, 2568 (1934).

(50) H. A. Scheraga and J. Hermans, unpublished works.

other hand the ΔpK value is very much lower and is in fact close to the line of Fig. 1.

The infrared spectrum of the crystalline potassium salt indicates the existence of two symmetrical internal hydrogen bridges between the carboxylate anion and the hydroxyl groups,⁵¹ and moreover a comparison of the ionization constants of dihydroxybenzoic acids⁵² shows the 2,6-dihydroxy isomer to be by far the most acidic, which strongly suggests hydrogen bonding of the anion in aqueous solution. In view of this evidence the relatively "normal" ΔpK value for resorcylic acid implies that the strengths of the hydrogen and deuterium bonds are about equal. It is not clear, however, why there should be any difference between these two acids which both have a hydroxyl substituent *ortho* to the carboxylic group.

The situation for the nitrophenols is also uncertain. Although the *o*-substituted nitrophenols (*i.e.*, *o*-nitrophenol, 2,4-dinitrophenol, 2,6-dinitrophenol, and picric acid) have infrared spectra in inert solvents which suggest that the undissociated form contains a hydrogen bond,⁵³⁻⁵⁶ the existence of such bonding in water is much less definite. When ionization constants of various nitrophenols are plotted against their Hammett σ -values (obtained from figures quoted by Taft⁵⁷ and Jaffé⁵⁸) and a line of slope $\rho = -2.113$ ⁵⁷ drawn, the *o*-substituted compounds fall below this line, which indicates that they are stronger acids than would have been predicted on the basis of the Hammett equation. Since the phenolate anion cannot be

stabilized by hydrogen bonding, the only effect of such bonding can be to lower the acid strength, and thus it seems quite possible that no intramolecular hydrogen bonding is present in aqueous solutions of nitrophenols. Astle and McConnell⁵⁹ found that the polarographic reduction of *o*-nitrophenol in aqueous solution was much slower than that of the *m*- and *p*-isomers and was dependent on the *pH* of the solution and they suggested that hydrogen-bonding of the acidic form was responsible for this, but steric hindrance is a fairly obvious alternative explanation. It will be seen from Fig. 1 that while *o*-nitrophenol and 2,4-dinitrophenol have relatively high ΔpK values, those for 2,6-dinitrophenol and picric acid are approximately as would have been predicted for normal acids of comparable strength. Thus while there is little support for hydrogen bonding in the acid forms of these phenols in aqueous solution (which would tend to lower the ΔpK) the problem of explaining the observed ΔpK values remains.

There are clearly enough uncertainties in the pK data for these hydrogen bonded systems as to preclude general conclusions about the relative H-bonding of hydrogen and deuterium. Three of the systems do agree with the previous conclusion from the maleic acid work that under the particular competitive situation of H₂O and D₂O as solvents an internal D-bond is weaker than an H-bond. However, the results for resorcylic acid and the nitrophenols point to the existence of complicating factors and suggest that detailed consideration must be given both to the particular species concerned and to changes in solvent effects. Much the same sort of qualified statement applies to the other trends in the values of ΔpK . There is some support for the proposal that ΔpK is an increasing function of pK but here also there is so much evidence for specific effects as to cast doubt on almost any generalization.

(51) H. Musso, *Chem. Ber.*, **88**, 1917 (1955).

(52) W. Baker, *Nature*, **137**, 236 (1936).

(53) O. R. Wulf and U. Liddel, *J. Am. Chem. Soc.*, **57**, 1464 (1935).

(54) G. E. Hilbert, O. R. Wulf, S. B. Hendricks, and U. Liddel, *Nature*, **136**, 147 (1935).

(55) R. J. Francel, *J. Am. Chem. Soc.*, **74**, 1265 (1952).

(56) A. M. Buswell, V. Deitz, and W. N. Rodebush, *J. Chem. Phys.*, **5**, 501 (1937).

(57) R. W. Taft, Jr., in "Steric Effects in Organic Chemistry," edited by M. S. Newman, 1956, John Wiley and Sons, New York, N. Y., Chap. 13.

(58) H. H. Jaffé, *Chem. Revs.*, **53**, 191 (1953).

(59) M. J. Astle and W. V. McConnell, *J. Am. Chem. Soc.*, **65**, 35 (1943).

LATTICE ENERGY AND STABILITY OF CHROMIUM MONOHALIDES

BY LEONIDAS PETRAKIS¹

Department of Chemistry, University of California, Berkeley 4, California

Received August 31, 1961

The lattice energies of the crystalline chromium monohalides are calculated assuming ionic bonding. These energies are combined in the Born-Haber cycle with empirical heats of formation of the ions and with measured and estimated absolute entropies to yield enthalpies and free energies of formation of the crystalline monohalides. The stability of these monohalides is further considered with respect to dissociation and disproportionation.

Introduction

Consideration of the electronic configuration of the elements indicates the possible stability of the plus one (+1) oxidation state for certain transition elements in addition to the groups which ordinarily have stable monovalent compounds. Due to the extra stability associated with half-filled d-shells Cr, Mo and W have a single *ns* electron in addition to the incomplete (*n* - 1)d shell outside the ap-

propriate inert gas configuration [(inert gas)(*n* - 1)d³*ns*, 4 ≤ *n* ≤ 6]. Indeed, claims have been made to have prepared certain such monovalent compounds.² Moreover, Woodbury and co-workers³ recently reported electron spin measurements for

(2) (a) M. J. Udy, "Chromium," Vol. 2, Am. Chem. Soc. Monograph Series, Reinhold Publ. Corp., New York, N. Y., 1956, p. 113; (b) J. W. Mellor, "A Comprehensive Treatise of Inorganic and Theoretical Chemistry," Vol. XI, Longmans, Green and Co., New York, N. Y., 1931, p. 366.

(3) H. H. Woodbury and G. W. Ludwig, *Phys. Rev.*, **117**, 102 (1960).

(1) National Research Council, Ottawa, Canada.

various charge states of several transition metals in silicon, including Cr^+ . They observed that "the resonant species would seem to be Cr^+ , having a half-filled d-shell and no other electrons outside of closed shells. The observed total spin of $5/2$ is in accord with this picture." But Cr^+ samples were unstable over time intervals of days to months, for they diffused even at room temperature and seemed to pair up with the electron acceptor used to dope the host Si crystals. This, along with the inconclusive claims of the preparation of the chromium monovalent compounds, seems to underscore the instability of the plus one state (+1) in chromium.

In this work the possible stability of the chromium plus one state in the chromium halides is examined. Ionic bonding is assumed, and the lattice energies of the crystalline monovalent halides are calculated. The calculated lattice energies along with experimental heats of formation of the ions are used in the Born-Haber cycle to obtain heats of formation of the solid monohalides. These in turn are combined with experimental and calculated absolute entropies to obtain free energies of formation. Finally, the stability of the monohalides is considered with respect to dissociation to the free atoms, and with respect to disproportionation to the stable dihalides and elementary chromium.

Calculation of Lattice Energies.—The lattice energies U are calculated using equation 1

$$U = \frac{N\alpha e^2}{r_0} (1 - \rho/r_0) + \frac{NC}{r_0^6} \left(1 - \frac{6\rho}{r_0}\right) + \frac{ND}{r_0^8} \left(1 - \frac{8\rho}{r}\right) - \frac{9}{4} N h \nu_{\max} \quad (1)$$

This equation is due to Ladd and Lee⁴ who extended the simple Born-Mayer expression for the lattice energy of a crystal to the case where dispersion energy terms are included in addition to ordinary Coulombic and repulsive forces.⁵ Ladd and Lee⁴ used eq. 1 to calculate the lattice energy of various stable monohalides, and they obtained values which are within $\pm 1.5\%$ of the experimentally obtained ones; and Waddington⁶ used it to calculate the energies of CuF and AuF .

In eq. 1 α is the Madelung constant of the crystal; r_0 is the equilibrium internuclear separation of the ions; ρ is a constant calculated by Born and Mayer⁷ equal to 0.345×10^{-8} . The term involving $1/r_0^6$ is the induced dipole-dipole interaction of the ions. C is a function of the polarizabilities of the ions and their corresponding energies. It is equal to $C = S_6' C_{+-} + S_6''(C_{++} + C_{--})/2$, where S_6' and S_6'' are constants characteristic of the crystal structure and they have been computed by Lennard-Jones and Ingham,⁸ (for the NaCl lattice $S_6' = 6.5952$ and $S_6'' = 1.8067$.) Also

$$C_{+-} = \frac{2}{3} \frac{\epsilon_+ \epsilon_-}{\epsilon_+ + \epsilon_-} \alpha_+ \alpha_- \quad \text{and} \quad C_{\pm\pm} = \frac{1}{3} \epsilon_{\pm} \alpha_{\pm}^2$$

where α_+ and α_- are the polarizabilities of the ions and ϵ_+ and ϵ_- their characteristic energies. The term involving $1/r_0^8$ is the induced dipole-quadrupole interaction. It is usually only a few per cent of the induced dipole-dipole interaction and it will be neglected here. Finally, the last term is the zero-point vibrational energy of the lattice, with ν_{\max} being the Debye maximum frequency characteristic of the crystal.

In order to carry out the term by term calculation of the lattice energies the crystal structures are required. On the basis of a hard-sphere model of ionic crystals the range of stability of the NaCl structure is predicted to be $0.414 \leq r_+/r_- \leq 0.732$. For all chromium monohalides, except CrF , this radius ratio is well within these limits; for CrF $r_+/r_- = 0.78$, and therefore a CsCl structure is predicted. However, (i) no fluoride is known with the CsCl structure and (ii) several fluorides (*e.g.*, KF and AgF) are known to crystallize in the NaCl structure in spite of their radius ratios being in excess of 0.732.⁶ For these reasons, the calculation of the lattice energies of all chromium monohalides is based on the assumption that all these halides crystallize in the NaCl structure for which the Madelung constant is 1.757. The ionic radii of the halide ions are those given by Pauling.⁹ They are, respectively, for F^- , Cl^- , Br^- and I^- equal to 1.33, 1.81, 1.96 and 2.20 Å. The radius of Cr^+ is taken as 1.04 Å, and it was obtained by extrapolation of the empirical crystal radii of the other polyvalent chromium ions.⁹

In the calculation of the induced dipole-dipole interaction the polarizabilities and characteristic energies of the negative ions employed by Mayer¹⁰ in the calculation of other stable monohalides were used. The polarizability of Cr^+ was calculated from Pauling's value of the molar refraction using the appropriate refraction screening constant.¹¹ ϵ_+ was taken equal to 90% of the second ionization potential.

For the calculation of the zero-point energy the frequency of the residual rays or "Reststrahlen" may be assigned to ν_{\max} . When this frequency is not available from infrared absorption data, Waddington⁵ has shown that the zero-point energy can be interpolated readily from the zero-point energies of the alkali halides, provided that the absolute entropies of the crystals are known. The S_{abs}^0 of the chromium monohalides have been estimated according to Latimer's rules.¹²

The various terms in the lattice energy expression may be evaluated readily by use of the values indicated here. The results are summarized in Table I.

Stability of the Monohalides.—The calculated lattice energies now can be used in a Born-Haber cycle expression to yield heats of formation of the

(4) M. F. C. Ladd and W. H. Lee, *Trans. Faraday Soc.*, **54**, 34 (1958).

(5) For a brief but excellent discussion of lattice energy calculations see: T. C. Waddington, *Lattice Energies in "Advances in Inorganic Chemistry and Radiochemistry,"* H. J. Emeleus and A. G. Sharpe, Ed., Vol. I, Academic Press, New York, N. Y., 1959.

(6) T. C. Waddington, *Trans. Faraday Soc.*, **55**, 1531 (1959).

(7) M. Born and J. E. Mayer, *Z. Physik*, **75**, 1 (1932).

(8) J. Lennard-Jones and A. E. Ingham, *Proc. Roy. Soc. (London)*, **A107**, 636 (1925).

(9) L. Pauling, "Nature of the Chemical Bond," 3rd Ed., Cornell Univ. Press, Ithaca, N. Y., 1960.

(10) J. E. Mayer, *J. Chem. Phys.*, **1**, 327 (1933).

(11) L. Pauling, *Proc. Roy. Soc. (London)*, **A114**, 181 (1927).

(12) W. M. Latimer, "Oxidation Potentials," Prentice-Hall Book Co., New York, N. Y., 1952, Appendix III.

TABLE I

LATTICE ENERGY OF CHROMIUM MONOHALIDES (NaCl CRYSTAL TYPE)

	$\frac{\alpha e^2}{\tau_0}$, ergs/ molecule	$-\frac{\alpha e^2(\rho/r)}{\tau_0}$, ergs/ molecule	$\frac{c}{\tau_0^2}(1 - \frac{6\rho}{r})$, ergs/ molecule	$-\frac{9}{4}h\nu$, ergs/ molecule	U , kcal./ mole
CrF	17.05	-2.51	0.01	-0.14	209.4
CrCl	14.21	-1.71	.04	-.10	179.1
CrBr	13.50	-1.58	.05	-.07	171.6
CrI	12.50	-1.33	.07	-.05	161.1

solid chromium monohalides. For the calculation equation 2 is used

$$\text{CrX}(r) = \text{Cr}^+(\text{g}) + \text{X}^-(\text{g}) \Delta H = U + 2RT \quad (2)$$

The empirical values of the heats of formation of the ions listed in the U. S. Bureau of Standards Circular 500¹³ are used to yield the $\Delta H_f^0[\text{CrX}(\text{s})]$ listed in Table II.

TABLE II

	$U + 2RT$, kcal./ mole	Calcd. ΔH_f^0 , [CrX- (s)], kcal./ mole	Derived ΔH_f^0 , [CrX- (s)], kcal./ mole	S_{abs}^0 , [CrX- (s)], cal./ deg.- mole	ΔS_f^0 , [CrX- (s)], cal./ deg.- mole	ΔF_f^0 , [CrX- (s)], kcal./ mole
CrF	210.6	-52.7	-89.0	15.7	-14.3	-48.5
CrCl	180.3	-1.2	-46.0	20.2	-12.10	+2.4
CrBr	172.8	+9.3	...	23.2	-11.8	+12.8
CrI	162.3	+24.9	-27.0	24.8	-12.8	+28.7

Of course, there exist no independent, empirical heats of formation with which one could compare the values obtained with the use of the lattice energies. However, one may compare these latter values with derived "experimental" values interpolated from the heats of formation of the di- and trivalent chromium halides. Figure 1 is a graphical display of the empirical heats of formation of the di- and trivalent halides taken from ref. 13. It is evident that the experimental heats of formation of these polyhalides increase smoothly with increasing oxidation number. Assuming that the values of the monovalent compounds would not deviate sharply from the curves determined by the polyvalent compounds, one may derive the relative heats of formation listed in column three of Table II. Figure 1 also shows for comparison the calculated heats of formation. It is interesting to note that the calculated values are less than the derived ones; moreover, the CrF value shows the best agreement and the CrI the poorest. Of course, this trend is expected because any calculations of bond stability on a completely ionic model would be best for the fluoride and poorest for the iodide. Although it is hard to estimate the importance of the contribution of covalent structures to the bonding, it again is expected that such contributions would enhance the stability of the compounds, and thus bring the calculated heats of formation closer to the "derived" values.

The free energies of formation ΔF_f^0 are calculated from the equation $\Delta F_f^0 = \Delta H_f^0 - T\Delta S_f^0$. The absolute entropies of the crystals, estimated according to Latimer's rules, are shown in Table II. These are combined with the experimentally determined S_{abs}^0 of the chromium metal and of the

(13) U. S. National Bureau of Standards Circular No. 500, U. S. Government Printing Office, Washington, D. C., 1952.

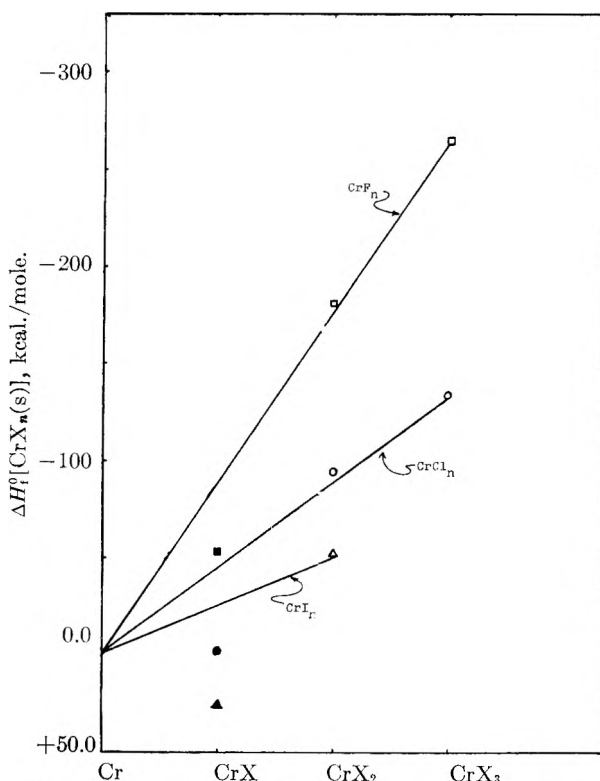
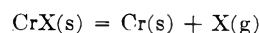


Fig. 1.—Comparison of stabilities of monovalent and polyvalent chromium halides. (Open symbols are empirical values from ref. 13; full symbols are calculated values.)

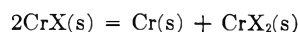
halogens¹³ to yield the ΔS^0 listed. The last column of the same table shows the calculated free energies of formation. It is obvious from Table II that CrF is quite stable with respect to formation from its elements; CrI and CrBr are highly unstable and CrCl slightly unstable with respect to formation from their elements.

However, before any conclusions can be reached about the stability of the monohalides there are two other pertinent reactions that must be considered

(i) dissociation



and (ii) disproportionation to the stable dihalide and metallic chromium



The free energies for these two reactions are calculated by the use of empirical heats of formation and measured entropies,¹³ along with the estimated S_{abs}^0 of $\text{Cr}_2(\text{s})$.¹² The results are shown in Table III. It is seen that all chromium monohalides except CrI(s) are stable to dissociation from 10 up to 63 kcal./mole. However, all of the monohalides including CrF are extremely unstable

TABLE III

FREE ENERGIES OF DISSOCIATION AND DISPROPORTIONATION (AT 298°K.)

	$\Delta F^0_{\text{diss.}}$, kcal./mole	$\Delta F^0_{\text{disprop.}}$, kcal./mole
CrF	62.7	-71.9
CrCl	22.8	-90.0
CrBr	10.1	...
CrI	-5.7	-101.5

to disproportionation. This then may explain the failure of attempts to prepare the chromium monohalides. It is expected that at least the fluoride would be primarily ionic in character and

it is hard to imagine large enough contributions from covalent structures that would stabilize the crystal structure sufficiently and thus prevent the disproportionation reaction.

EFFECT OF SUBSTITUENT GROUPS ON THE IONIZATION POTENTIALS OF BENZENES

BY GEORGE F. CRABLE AND GERARD L. KEARNS*

Gulf Research & Development Company, Pittsburgh, Pennsylvania

Received August 31, 1961

Ionization potentials of a number of substituted benzenes have been measured to determine the changes in ionization potential produced as a function of the properties of the substituent group. In addition to a few alkyl benzenes, measurements were made for a number of benzene compounds having one or two non-hydrocarbon substituent groups. Ionization potentials of monosubstituted benzenes are shown to correlate with σ^+ substituent constants in a linear manner. Changes in ionization potential for the addition of a second substituent group depend on the nature of the original group. Greater changes occur for addition to an original group which is a strong electron acceptor, such as $-\text{NO}_2$. The polarization model for substituent effects is shown to give qualitatively correct predictions. Differences between *ortho* and *para* isomers of disubstituted benzenes are consistent with an explanation of dipole interactions.

Introduction

Although ionization potentials for a number of alkyl substituted benzenes have been reported in the literature,¹ only a few ionization potential values have been reported for benzene compounds with non-hydrocarbon substituents. A collection of such data is of importance to test the results of theoretical calculations of ionization potentials and the effects of substituent groups on chemical activity. Using a limited amount of data, Price² also studied the effects of substituent groups on ionization potentials and Kaufman and Koski³ evaluated substituent effects on radical ionization potentials. The purpose of this work was to determine the changes in ionization potentials resulting from the addition of substituent groups of considerably different properties. Mono- and disubstituted benzenes were studied. The possibility of showing a simple additivity effect on ionization potentials of disubstituted benzenes was examined. Measurements of ionization potentials of *ortho*, *meta* and *para* isomers showed that changes in ionization potentials with position of the substituent groups depends on the nature of the groups. In particular, the electrostatic polarization concept of ionization potential changes⁴ with substituent groups is shown to serve as a semi-quantitative guide to ionization potential changes.

Experimental

Ionization potential data were obtained on a Consolidated Electrodynamics Corporation Model 21-103 mass spectrometer. For all measurements the repeller potential was +1.5 volts, while the anode (or electron catcher) to ion chamber potential was maintained at +40 volts. Although it is desirable to operate the anode at the same potential as the ion chamber to minimize ion formation in this region, adequate electron current control could not always be main-

tained at potentials less than 40 volts. The electron current was maintained at 10 μamp . Gas pressures were maintained at the lowest practical values to minimize the tailing effect resulting from ions produced near the electron collector.⁵⁻⁷ Electron accelerating potentials were measured by means of a potentiometer between the filament and the ion chamber. The accuracy of the potentiometer readings was within ± 0.01 volt. Argon, with an ionization potential of 15.76 e.v., was used as a voltage reference.

A number of techniques have been suggested for measuring ionization potentials with a mass spectrometer having a non-homogeneous electron beam. Of these, a method which combines the use of a semilogarithmic plot of the ionization efficiency curve⁸⁻¹⁰ with a standardization procedure used by Fox and Langer¹¹ and others was chosen for this work. Ion intensities of the compound and the reference were plotted as a function of electron energy in volts. The range of electron energies used was large enough to provide data on both the exponential toe and the initial part of the linear portion of the ionization efficiency curves. The slopes of the linear parts of the curves contain terms representing instrumental sensitivity, cross section for ionization, electron current, and gas pressure or molecules per cm^3 in the ion chamber. Since instrumental factors, including the electron current, were held constant for all measurements, the ratio of the slopes for the reference and measured compounds equals the ratio of the products of respective cross sections and pressures. This ratio then was used to make the ionization efficiency curves equivalent.

Data from the exponential parts of the ionization efficiency curves were plotted as the logarithm of the ion current versus the electron energy in volts. The experimental data for the reference compound, argon, were multiplied by the ratio of the linear slopes before plotting. The voltage difference, ΔV , between the two curves at a given ion intensity was used to calculate the ionization potential of the molecule from the known argon ionization potential. A number of ΔV values were measured over a range of ion intensities to ensure that the two curves were parallel. The measured ΔV 's for a given compound and argon differed by a maximum of 0.1 volt.

As a test of the experimental technique, ionization potentials of several compounds were measured and compared

*W. R. Grace & Company, Washington Research Center, Clarks-ville, Maryland.

(1) F. H. Field and J. L. Franklin, "Electron Impact Phenomena," Academic Press, New York, N. Y., 1957.

(2) W. C. Price, *Chem. Revs.*, **41**, 257 (1947).

(3) J. K. Kaufman and W. S. Koski, *J. Am. Chem. Soc.*, **82**, 3262 (1960).

(4) N. D. Coggeshall, *J. Chem. Phys.*, **32**, 1265 (1960).

(5) R. E. Fox, W. M. Hickam, D. J. Grove and T. Kjeldaa, *Jr., Rev. Sci. Instr.*, **26**, 1101 (1955).

(6) J. D. Morrison, *J. Chem. Phys.*, **19**, 1305 (1951).

(7) G. F. Crable and G. L. Kearns, *ibid.*, **31**, 84 (1962).

(8) R. E. Honig, *ibid.*, **16**, 105 (1948).

(9) F. P. Lossing, A. W. Tickner and W. A. Bryce, *ibid.*, **19**, 1254 (1951).

(10) V. H. Dibeler, R. M. Reese and F. L. Mohler, *ibid.*, **20**, 761 (1952).

(11) R. E. Fox and A. Langer, *ibid.*, **13**, 460 (1950).

with spectroscopically determined ionization potentials. Values of 15.57, 13.77 and 11.36 were determined, in good agreement with spectroscopic values of 15.56, 13.79 and 11.41 for nitrogen, carbon dioxide and acetylene, respectively.¹

Results and Discussion

In Table I the measured ionization potentials of the substituted benzenes obtained in this work are

TABLE I
IONIZATION POTENTIALS OF SUBSTITUTED BENZENES

Compound	This work (e.v.)	Lit. values (e.v.)	
		Electron impact	Photoionization value
Benzene	9.56	9.52 ¹²	9.245 ¹³
Toluene	9.18	9.23 ¹²	8.82 ¹³
<i>o</i> -Xylene	9.04	8.97 ¹²	8.56 ¹³
<i>m</i> -Xylene	9.05	9.02 ¹²	8.56 ¹³
<i>p</i> -Xylene	8.99	8.88 ¹²	8.445 ¹³
1,3,5-Trimethylbenzene	8.74	8.79 ¹²	8.39 ¹³
Styrene	9.00	8.86 ¹⁴	
Aniline	8.32		7.70 ¹³
Nitrobenzene	10.18		
Benzonitrile	10.09	9.95 ¹⁴	
<i>p</i> -Nitrotoluene	9.82		
<i>p</i> -Tolunitrile	9.76		
<i>o</i> -Dichlorobenzene	9.64		
Chlorobenzene	9.60	9.42 ¹⁴	9.07 ¹³
Bromobenzene	9.52	9.41 ¹⁴	8.98 ¹³
<i>p</i> -Nitrophenol	9.52		
<i>o</i> -Chlorophenol	9.28		
<i>p</i> -Chlorophenol	9.07		
<i>p</i> -Bromotoluene	9.22		8.67 ¹³
<i>p</i> -Chlorotoluene	9.21		8.69 ¹³
Phenol	9.16	9.03 ¹⁴	
<i>p</i> -Bromophenol	9.04		
<i>o</i> -Cresol	8.93		
<i>m</i> -Cresol	8.98		
<i>p</i> -Cresol	8.97		
Methoxybenzene	8.83		8.20 ¹³
<i>o</i> -Nitroaniline	8.66		
<i>m</i> -Nitroaniline	8.80		
<i>p</i> -Nitroaniline	8.85		
<i>o</i> -Methylaniline	8.38		
<i>m</i> -Methylaniline	8.27		
<i>p</i> -Methylaniline	8.14		
<i>o</i> -Benzenediamine	8.00		
<i>m</i> -Benzenediamine	7.96		
<i>p</i> -Benzenediamine	7.58		
<i>p</i> -Methoxyaniline	7.82		

given, along with comparative literature values obtained by electron impact methods and by photoionization. The majority of the reported data are the average of from 2 to 5 individual determinations. Although the average deviation between individual runs is approximately 0.03 volt, no remarks can be made concerning the absolute accuracy. The agreement with reported electron impact values, where available, is within 0.1 to 0.2 e.v. As usually is experienced with ionization potentials obtained by electron impact, the experimental values are higher than the photoionization values by approximately 0.3 to 0.6 e.v.

An examination of Table I shows that marked

(12) F. H. Field and J. L. Franklin, *J. Chem. Phys.*, **22**, 1895 (1954).

(13) K. Watanabe, *ibid.*, **26**, 542 (1957).

(14) J. D. Morrison and A. J. C. Nicholson, *ibid.*, **20**, 1021 (1952).

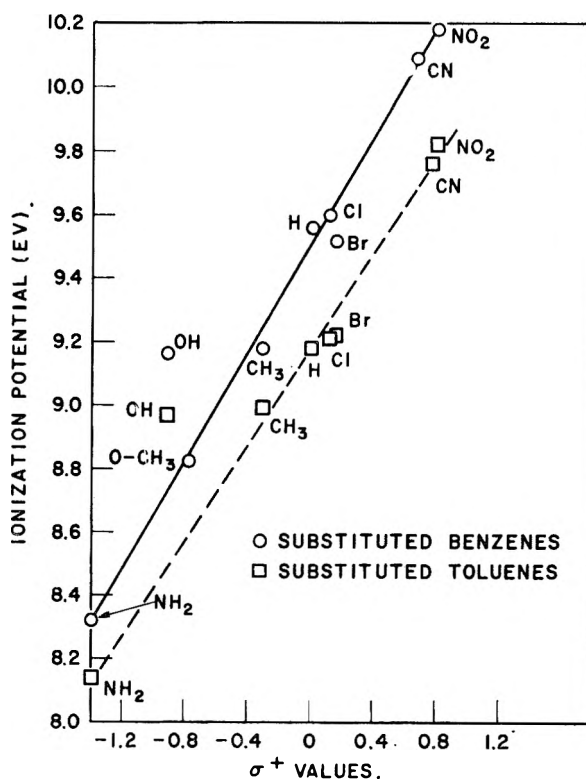


Fig. 1.—Correlation of ionization potentials with Brown's σ^+ -values.

changes occur in the ionization potential of benzene upon the addition of a substituent group. The addition of NH_2 produces a reduction in the benzene ionization potential of 1.24 e.v., while adding an NO_2 group results in an increase of 0.62 e.v. These changes in ionization potential must be related to the properties of the substituent groups. The electron donating property of the substituent group has been related to chemical reactivities of substituted benzenes. To see whether a similar qualitative relationship existed for ionization potentials, the ionization potentials of the mono- and *para*-disubstituted benzenes were arranged in Table II in order of increasing electron accepting properties¹⁵ from left to right and from top to bottom. The monosubstituted data are contained in the row and column indicated by H. Note that all values appear twice in this table. Qualitatively, these results show that electron accepting groups produce an increase in the ionization potential of benzene while the addition of an electron donor group causes a decrease in ionization potential. The effects of the addition of two substituent groups are additive, but not necessarily in a linear manner. For example, a comparison of the $-\text{CH}_3$ and $-\text{H}$ columns gives the effect of adding a methyl group to a series of monosubstituted benzenes. In all cases, the ionization potential is reduced with the addition of the methyl group, while the ionization potential change varies from 0.18 e.v. for aniline to 0.38 e.v. for benzene.

A more quantitative method of expressing the electron donating properties is by means of reaction

(15) C. K. Ingold, "Structure and Mechanism in Organic Chemistry," Cornell University Press, Ithaca, N. Y., 1953, Chapter 6.

TABLE II
 IONIZATION POTENTIALS OF *para*-DISUBSTITUTED BENZENES

Substituent group	Substituent group									
	NH ₂	OCH ₃	OH	CH ₃	H	Cl	Br	CN	NO ₂	
NH ₂	7.58	7.52	..	8.14	8.32	8.85	
OCH ₃	7.52	8.83	
OH	8.97	9.16	9.07	9.04	...	9.52	
CH ₃	8.14	..	8.97	8.99	9.18	9.21	9.22	9.76	9.82	
H	8.32	8.83	9.16	9.18	9.56	9.60	9.52	10.09	10.18	
Cl	9.07	9.21	9.60	
Br	9.04	9.22	9.52	
CN	9.76	10.09	
NO ₂	8.85	..	9.52	9.82	10.18	

rate measurements in terms of Hammett¹⁶ σ -values or more recently the σ^+ -values of Brown.¹⁷ Figure 1 shows, in the solid curve, the ionization potentials of singly substituted benzenes plotted as a function of Brown's σ^+ -values. A reasonably good straight line can be drawn through all points except that of phenol. No explanation is available for this discrepancy. The dashed curve of Fig. 1 was drawn through data for a set of *para*-substituted toluenes. The ionization potentials of the substituted toluenes are plotted as a function of the σ^+ -value of the group added to the toluene. The ionization potential of toluene with H as the substituent group is plotted at a σ^+ -value of 0.0. The dashed curve shows that the effect of the substituent groups on the ionization potential of toluene, except for cresol, is a linear function of σ^+ .

Similar results were obtained for the substituted anilines and nitrobenzenes. Slopes of these curves were 0.70, 0.75, 0.86 and 0.95, respectively, for the anilines, toluenes, benzenes and nitrobenzenes. This result indicates that the effect of an additional substituent group is reduced as the electron accepting power of the original substituent is reduced.

It is of interest to consider the above data in terms of the electrostatic polarization model for predictions of ionization potential changes as proposed by Coggeshall.⁴ This model assumes that the change in ionization potential of a compound upon addition of a substituent group is given approximately by the electrostatic polarization energy of the added group. For purposes of discussion, the process of ionization is considered to proceed stepwise as follows: (1) the lowest lying electron is removed from the unsubstituted basic compound by imparting an energy equal to the ionization potential of this molecule; (2) the substituent group then is placed in its proper position on the molecule; and (3) because of the field of the positive charge and the polarizability of the substituent group, energy, ΔE , is removed from the system. Thus, the difference in energy of ionization of the substituted and original compound equals ΔE . Deviations from linear additivity of substituent effects were predicted⁴ as a result of interactions of the induced dipoles.

The electrostatic polarization model, as discussed above, always results in a lowering of the ionization potential of a molecule by the addition of any sub-

stituent group. This obviously is not true as shown, for example, by the ionization potentials of benzonitrile and nitrobenzene in Table I. If, however, the effect of dipole moment which the substituent group possesses in the neutral molecule is considered, then reasonable results are predicted by the model. The permanent dipole moment can be directed either toward or away from the charge center. The change in ionization potential from the addition of the substituent group now depends on the interaction energies between the induced dipole and the charge center, and between the permanent dipole and the charge center. The sum of these energies now can be either positive or negative, depending on the relative sizes and directions of the two dipoles.

Detailed calculations of ionization potentials are not justified by this procedure for several reasons. Group moments are measures of not only the dipole moment of the substituent group itself, but also of the bonds between the group and the ring carbon in benzenes. In addition, changes in charge distribution in the ring of a substituted benzene would enter into the resulting group moment. The proper selection of the positions of the moments and of the charge center also is relatively arbitrary.

However, the qualitative results, obtainable from a consideration of this model, are useful and reasonable. Polarizability effects from the charge center in the ion will result in an induced dipole of about 1.0 to 1.5 Debye. A comparison of the induced dipole and the group dipole with respect to magnitude and direction for substituted benzenes is necessary for estimations of the effect of a substituent group on the ionization potential of benzene. Substituent groups having group moments in the same direction as the induced moments produce a lowering of the ionization potential. $-\text{CH}_3$ and $-\text{NH}_2$ with respective group moments of 0.36 and 1.48¹⁸ directed toward the ring carbon to which they are attached show $-\Delta E$'s with respect to benzene of 0.38 and 1.24 e.v. Group moments of 1.72 and 1.75 for $-\text{Cl}$ and $-\text{Br}$ are directed away from the ring carbon; *i.e.*, in a direction to produce a positive ΔE . However, the induced dipoles are of approximately the same magnitude but of opposite direction and result in net ΔE 's of only +0.04 and -0.04 e.v., respectively, for the $-\text{Cl}$ and $-\text{Br}$. The $-\text{CN}$ and $-\text{NO}_2$ groups with large group moments directed away from the ring produce relatively large in-

(16) L. P. Hammett, "Physical Organic Chemistry," McGraw-Hill Book Co., New York, N. Y., 1940, Chapter VII.

(17) H. C. Brown and Y. Okamoto, *J. Am. Chem. Soc.*, **80**, 4979 (1958).

(18) A. Weissberger, "Physical Methods of Organic Chemistry," Vol. I, Part II, Interscience Publishers, Inc., New York, N. Y., 1949, p. 1641.

creases in ionization potentials because of the overwhelming effect of the group moment compared to the relatively small induced moments of opposite direction.

In disubstituted benzenes the electrostatic model makes certain predictions on changes in ionization potential with position of the substituent groups. In Table III ionization potentials for the position isomers of a number of disubstituted benzenes are collected along with the maximum differences between isomers. Groups with dipoles in the same direction, regardless of dipole orientation with respect to the ring, should have ionization potentials decreasing in the order: *ortho*, *meta* and *para*. In the *ortho* position the work required to "position" the second substituent is positive because of the repulsion of the two dipoles. In the *para* position the large distance between the dipoles minimizes any interaction energy. Examples of such cases from Table III are the ionization potentials of the toluidines and the benzenediamines which are in good agreement with the predicted changes. Although the xylene series can be included in this group, the small differences observed are not greater than expected experimental error.

TABLE III
IONIZATION POTENTIALS OF DISUBSTITUTED BENZENES IN E.V.

Compound	<i>ortho</i>	<i>meta</i>	<i>para</i>	Maximum Δ
Xylene	9.04	9.05	8.99	0.06
Cresol	8.93	8.98	8.97	.05
Nitroaniline	8.66	8.80	8.85	.19
Chlorophenol	9.28	..	9.07	.21
Toluidine	8.38	8.27	8.14	.24
Benzenediamine	8.00	7.96	7.58	.42

The addition of two substituent groups having opposite dipole moment directions with respect to the ring should result in a minimum ionization potential for the *ortho* position. In this case, a negative amount of work is performed in "positioning" the second group. The nitroaniline data of Table III with an ionization potential of 8.66 e.v. for the *ortho* isomer, compared to 8.85 e.v. for the *para* isomer, is an example of this type of interaction.

Acknowledgment.—The authors are pleased to acknowledge the help obtained from the discussions and comments of Dr. N. D. Coggeshall. Instrumental data were obtained and plotted by Messrs. H. T. Best, J. P. Klems and P. W. Mazak.

THE CONDUCTANCES OF DILUTE AQUEOUS CADMIUM PERCHLORATE SOLUTIONS AT 25°

BY R. A. MATHESON¹

Chemistry Department, The University of New England, Armidale, New South Wales

Received September 6, 1961

Measurements at 25° of the equivalent conductances of aqueous cadmium perchlorate solutions of concentrations from 10^{-3} to 0.1 *N* are reported and values at round concentrations tabulated. The contribution of hydrolysis products to the equivalent conductances of these solutions is assessed. An examination of the concentration dependence of the equivalent conductances reported in this communication provides no evidence for the incomplete dissociation of cadmium perchlorate in dilute aqueous solution.

Introduction

Although the complete dissociation of cadmium perchlorate has been assumed in a number of investigations of ion association in solutions of other cadmium salts, there is no record in the literature of any studies of the properties of cadmium perchlorate solutions designed to test this point. For this reason the following study of the equivalent conductances of cadmium perchlorate solutions was undertaken.

Preparation of Solutions.—Two stock solutions of cadmium perchlorate were prepared from cadmium oxide and perchloric acid. About 20 g. of oxide was agitated in a stoppered vessel with an equivalent amount of perchloric acid solution. A weighed sample of the resulting solution was diluted to about 0.2 *N* and the pH of this dilute solution determined. In each preparation this pH indicated an excess of a few hundredths of a per cent. of acid in the stock solutions. Sufficient oxide to neutralize this excess was added to the stock solution which then was re-agitated. Solutions (0.3 *N*) prepared from the stock solutions then had pH's between 4.8 and 5.0. (According to the figure given by Marcus² for the hydrolysis constant of Cd²⁺, a 0.3 *N* Cd(ClO₄)₂ solution should have a pH of 4.85.) The concen-

tration of the stock solution (equivalents/1000 g.) was determined from the weight of the solution and the number of equivalents of cadmium perchlorate present. The number of equivalents of cadmium perchlorate was taken as the mean of the number of equivalents of oxide and acid used in the preparation of this weight of solution. These two figures differed by 0.04% (solution A) and 0.07% (solution B). Having regard to the estimated uncertainties in the acid analyses ($\pm 0.05\%$) and the possible presence of up to 0.02% impurity in the oxide, it was considered that these differences were not excessive and that the uncertainty in the concentration of either stock solution was unlikely to exceed $\pm 0.05\%$.

Cadmium oxide was prepared from cadmium metal. (Purity stated by the makers to be better than 99.98%). Cadmium metal was dissolved in C.P. nitric acid and the resulting cadmium nitrate solution evaporated to dryness and heated to convert the nitrate to the oxide. After evolution of NO₂ had ceased, the oxide was heated to red heat in a furnace until the weight of the oxide was constant within a few parts in 50,000. This oxide contained less than 0.01% material insoluble in 2 *N* HClO₄.

Perchloric acid solutions were prepared by dilution of A.R. perchloric acid and analyzed by weight titration against A.R. Na₂CO₃ which was dried at 260–270° for half an hour immediately before use.

Four or five titrations were made with each of the perchloric acid solutions used in the cadmium perchlorate preparations. The average deviation from the mean of a series of 4–5 titrations was 0.02 to 0.03%. Two independent

(1) Chemistry Department, Victoria University of Wellington, Wellington, New Zealand.

(2) Y. Marcus, *Acta Chem. Scand.*, **11**, 690 (1957).

checks on the accuracy of this analytical procedure were made. A solution of approximately 2 *M* HCl was prepared and analyzed by weight titration against Na₂CO₃. A second analysis was made by the following method. The HCl was accurately diluted to about 0.05 *N*, and the specific conductivity of this solution was measured and its concentration calculated from the equivalent conductances of Owen and Sweeton³ by successive approximations. The two analyses of the HCl agreed within 0.05%. As a second check, one of the perchloric acid solutions was reanalyzed by weight titration against a sodium hydroxide solution which another worker in this Laboratory had standardized by weight titration against A.R. potassium hydrogen phthalate. These two analyses agreed within 0.03%.

The conductance water, which was prepared by two distillations of tap water in Pyrex stills without any special precautions to exclude carbon dioxide, had a specific conductance of 1.0–1.5 × 10⁻⁶ ohm⁻¹ cm.⁻¹.

Solutions were prepared by weight dilution of the stock solutions with conductance water. For solutions below 0.019 *N*, a known weight of conductivity water was placed in a flask cell, its specific conductance measured, and the more concentrated solution added from a weight pipet. Normalities were calculated from weight concentrations of the solutions *via* a graph of density *vs.* composition prepared from measurements of the densities of some of the solutions in a pycnometer of approximately 10-ml. capacity. Vacuum corrections were applied to all weights.

Measurements.—*pH* measurements were made on a Cambridge *pH* meter. A Leeds and Northrup bridge of Grinnell Jones design was used for the resistance measurements. Two types of conductivity cells were used—for solutions more concentrated than about 0.02 *N*, conventional cells with electrodes coated with platinum black; and for more dilute solutions, a flask cell with bright platinum electrodes. The electrodes in the flask cell were in a separate compartment connected to the main flask by a side tube. Both types of cell were made of Pyrex glass and had widely spaced lead tubes. All resistances were measured at 0.5, 1 and 2 kc./sec., and the resistance at infinite frequency obtained by extrapolation. The change in resistance between 2 and 0.5 kc./sec. was rarely more than 0.1% for the flask cell and 0.01% for the other cells. For the flask cell the resistance at infinite frequency was obtained by linear extrapolation of a plot of *R vs. 1/f* as measurements of the resistance over an extended range of frequencies (0.5 to 20 kc./sec.) showed this method of extrapolation to be preferable to the more conventional linear extrapolation of a plot of *R vs. 1/√f*. An oil thermostat was used to keep cells at 25 ± 0.002°. Cells were calibrated using the 0.1 and 0.01 *D* standards of Jones and Bradshaw.⁴

Correction of Results for Hydrolysis.—The cadmium ion hydrolyzes slightly according to the equation



Because of this, the observed equivalent conductivity of a cadmium perchlorate solution will not be equal to the sum of the equivalent conductivities of the cadmium and perchlorate ions in that solution. To evaluate this difference the equation derived was

$$\Delta\Lambda = \alpha \left(\frac{\lambda_{\text{H}^+}}{2} + \frac{\lambda_{\text{CdOH}^+}}{2} - \lambda_{\text{Cd}^{+2}} \right) + (\beta - \beta^0) \frac{C^1}{C} \left(\frac{\lambda_{\text{H}^+}}{2} + \frac{\lambda_{\text{HCO}_3^-}}{2} \right) \quad (1)$$

where

$$\Delta\Lambda = \Lambda_{\text{obs.}} - (\lambda_{\text{Cd}^{+2}} + \lambda_{\text{ClO}_4^-}), \Lambda_{\text{obs.}} = \frac{1000K_{\text{sp.}}}{2C}$$

C = concn. of cadmium perchlorate in moles/l.

*K*_{sp.} = obsd. specific conductivity of the soln. after the usual solvent correction has been applied

λx = equivalent conductivity of the ion *x* in this soln.

(3) B. B. Owen and F. H. Sweeton, *J. Am. Chem. Soc.*, **63**, 2811 (1941).

(4) G. Jones and B. C. Bradshaw, *ibid.*, **55**, 1780 (1933).

α = degree of hydrolysis of the Cd⁺² ion
*C*¹ = concn. of CO₂ in the conductivity water (moles/l.)
*β*⁰ = degree of ionization of CO₂ in the absence of cadmium perchlorate
β = degree of ionization of CO₂ in the presence of cadmium perchlorate

In the derivation of this equation the conductivity of the solvent is assumed to result partly from the ionization of dissolved CO₂, and partly from the presence of other substances the degrees of ionization of which are unaffected by the addition of cadmium perchlorate. The equivalent conductivities of the ions present in the solvent are assumed to be unaltered by the addition of cadmium perchlorate.

Marcus² has quoted the results of a number of determinations of *K*_h, the equilibrium constant for the hydrolysis of the Cd⁺² ion. From these results it would seem that *K*_h is about 10⁻⁹ mole/l. Using the following figures

*C*¹ = 3 × 10⁻⁶ moles/l.
*K*_h = 10⁻⁹ mole/l.
 1st ionization constant for CO₂ = 4.45 × 10⁻⁷ moles/l.
*λ*_{H⁺} = 350 ohm⁻¹ cm.² g. equiv.⁻¹
*λ*_{Cd⁺²} = 50 ohm⁻¹ cm.² g. equiv.⁻¹
*λ*_{CdOH⁺} = 50 ohm⁻¹ cm.² g. equiv.⁻¹
*λ*_{HCO₃⁻} = 44 ohm⁻¹ cm.² g. equiv.⁻¹

the data in Table I are obtained.

TABLE I

Concn. of Cd(ClO ₄) ₂ (equiv. l. ⁻¹)	ΔΛ (ohm ⁻¹ cm. ² g. equiv. ⁻¹)
10 ⁻³	0.072
4 × 10 ⁻³	.055
10 ⁻²	.043
4 × 10 ⁻²	.027
10 ⁻¹	.018

The value of 3 × 10⁻⁶ for *C*¹, the concentration of CO₂ in the conductivity, was chosen after the following investigations on a number of samples of conductivity water all of which indicated figures between 2 × 10⁻⁶ and 6 × 10⁻⁶: *pH* measurements made by repeatedly rinsing and filling with conductivity water a cell containing glass and calomel electrodes, observations of the decrease in conductivity effected by removing carbon dioxide from the conductivity water, and of the effect upon the specific conductivity of small additions (10⁻⁶ to 10⁻⁵ mole/l.) of perchloric acid and sodium hydroxide.

For the most dilute solutions used (10⁻³ *N*), ΔΛ varies with *C*¹ thus

*C*¹ = 0 ΔΛ = 0.212 ohm⁻¹ cm.² g. equiv.⁻¹
*C*¹ = 10⁻⁶ ΔΛ = 0.119 ohm⁻¹ cm.² g. equiv.⁻¹
*C*¹ = 3 × 10⁻⁶ ΔΛ = 0.072 ohm⁻¹ cm.² g. equiv.⁻¹
*C*¹ = 6 × 10⁻⁶ ΔΛ = 0.053 ohm⁻¹ cm.² g. equiv.⁻¹

These data show that, at worst, errors in the value of ΔΛ resulting from uncertainties as to the true value of *C*¹ will be no more than about ± 0.03 ohm⁻¹ cm.² g. equiv.⁻¹.

Results

The hydrolysis corrections given in Table I have been deducted from all the results recorded below. Data for the more concentrated solutions are given in Table II.

TABLE II
 Λ (Int. ohm⁻¹ cm.² g. equiv.⁻¹)

Concn. (g. equiv. l. ⁻¹)	Λ (Int. ohm ⁻¹ cm. ² g. equiv. ⁻¹)	Stock soln.
0.10101	92.58	B
.10099	92.54	A
.10094	92.53	A
.09662	92.89	B
.09565	92.98	B
.09281	93.16	A
.08923	93.39	A
.07673	94.53	B
.073847	94.77	A
.064691	95.75	B
.063894	95.82	B
.054329	96.86	A
.052714	97.08	A
.049809	97.52	B
.040161	98.93	B
.038439	99.12	A
.033980	100.04	B
.031664	100.47	B
.030399	100.68	A
.024625	101.98	A
.019245	103.45	A
.013807	105.31	A
.013505	105.48	A

The results for solutions less concentrated than 0.01 *N* will not be given in detail as they may be represented within the experimental uncertainty by the equation of Shedlovsky⁵

$$\Lambda'^0 = 120.80 + 370c \quad (2)$$

where

$$\Lambda'^0 = \frac{\Lambda + 111.4\sqrt{c}}{1 - 0.4977\sqrt{c}}$$

c = concn. in equivalents/l.

The mean deviation between Λ'^0 calculated from equation 2 and Λ'^0 obtained from the experimental values of Λ amounts to 0.06 ohm⁻¹ cm.² g. equiv.⁻¹ for 22 solutions having concentrations between 10⁻³ and 10⁻² *N*. In this concentration range the equation of Robinson and Stokes⁶ is almost as

$$\Lambda = \Lambda^0 - \frac{(111.4 + 0.4977 \Lambda^0)\sqrt{c}}{1 + 0.4030\delta\sqrt{c}} \quad (3)$$

satisfactory. The mean deviation between experimental results and equation 3 is 0.08 ohm⁻¹ cm.² g. equiv.⁻¹ with $\delta = 6 \text{ \AA}$. and $\Lambda^0 = 120.87$.

Results for round concentrations are given in Table III. Above 10⁻² *N* these were obtained from a large scale graph of the arbitrary deviation function $\Lambda + 150\sqrt{c} - 150c$ vs. *c*, and below 10⁻² *N* from equation 2. Depending on whether equation 2 or equation 3 is used, figures of 120.80 or 120.87 are obtained for Λ^0 . In the absence of any great evidence for the superiority of one equation over the other it is suggested that Λ^0 be taken as

(5) T. Shedlovsky, *J. Am. Chem. Soc.*, **54**, 1405 (1932).

(6) R. A. Robinson and R. H. Stokes, *ibid.*, **76**, 1991 (1954).

120.84. As $\lambda^0_{\text{ClO}_4^-} = 67.36$ at 25°, $\lambda^0_{\text{Cd}^{2+}} = 53.5$ int. ohm⁻¹ cm.² g. equiv.⁻¹ at 25°. There does not appear to have been a previous determination of $\lambda^0_{\text{Cd}^{2+}}$ at this temperature.

TABLE III

Concn. (g. equiv. l. ⁻¹)	Λ (Int. ohm ⁻¹ cm. ² g. equiv. ⁻¹)	Concn. (g. equiv. l. ⁻¹)	Λ (Int. ohm ⁻¹ cm. ² g. equiv. ⁻¹)
0.1	92.64	0.02	103.30
.08	94.21	.01	107.15
.06	96.22	.005	110.45
.04	98.93	.001	115.74

It is thought that for solutions more concentrated than 0.02 *N* the uncertainties in the experimental values of Λ are not greater than $\pm 0.05\%$, the estimated maximum uncertainty in the concentrations of the stock solutions. Examination of the plot of $\Lambda + 150\sqrt{c} - 150c$ shows that the average deviation of the points from a smooth curve is about 0.03 ohm⁻¹ cm.² g. equiv.⁻¹, and that most of this deviation may be accounted for by assuming a concentration error of $+0.025\%$ for one stock solution and -0.025% for the other. At lower concentrations, random errors (about $\pm 0.03\%$) occur among the results for solutions prepared from a common stock solution. It is, however, considered improbable that the value of Λ^0 obtained above and the values of Λ for solutions below 10⁻² *N* calculated from equation 2 are in error by more than 0.1 ohm⁻¹ cm.² g. equiv.⁻¹.

Discussion

The variation with concentration of the equivalent conductances of cadmium perchlorate is similar to that of other 2:1 electrolytes such as calcium chloride which generally are considered to be completely disassociated in dilute aqueous solutions. Below about 0.01 *N* the equivalent conductivities are represented with moderate accuracy by the equation

$$\Lambda = \Lambda^0 - \frac{(B_1 \Lambda^0 + B_2)\sqrt{c}}{1 + B\delta\sqrt{c}}$$

with the physically reasonable value of 6 \AA . for the δ parameter. At higher concentrations the observed equivalent conductivities become progressively greater than those calculated from this equation using the values of Λ^0 and δ which are satisfactory below 0.01 *N*. Thus the equivalent conductivities of cadmium perchlorate give one no reason to suspect incomplete dissociation in aqueous solutions more dilute than 0.1 *N*.

Acknowledgments—The author is indebted to Professor R. H. Stokes for helpful advice and discussion and to the Electrolytic Zinc Co. of Australia for the gift of the sample of cadmium metal used in this work.

(7) Cf. Appendix 6.2 of "Electrolyte Solutions," R. A. Robinson and R. H. Stokes, Butterworths, London, 1959.

KINETICS OF THE VANADIUM(III)-NEPTUNIUM(V) REACTION IN PERCHLORATE SOLUTIONS¹

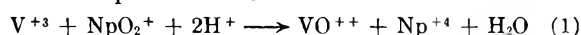
BY E. H. APPELMAN AND J. C. SULLIVAN

The Chemistry Division, Argonne National Laboratory, Argonne, Illinois

Received September 5, 1961

The kinetics of the reaction $V(III) + Np(V) \rightarrow V(IV) + Np(IV)$ were studied in perchloric acid solutions. The empirical form of the rate law is $-d[Np(V)]/dt = [Np(V)][V(III)]\{k_1 + k_2[Np(IV)][V(IV)]^{-1}[H^+]^{-1.6}\}$. At 25°, in $LiClO_4-HClO_4$ solutions 3.0 *M* in total perchlorate, $k_1 = 0.30 M^{-1} sec^{-1}$, and $k_2 = 0.16 M^{0.5} sec^{-1}$. Under these conditions, for the k_1 path $\Delta H^\ddagger = 14.6 \pm 0.8$ kcal./mole and $\Delta S^\ddagger = -12.3 \pm 2.6$ e.u. The second term of the rate law has been interpreted in terms of the rapid equilibrium $Np(IV) + V(III) \rightleftharpoons Np(III) + V(IV)$ followed by the reaction $Np(III) + Np(V) \rightarrow 2Np(IV)$. A comparison has been made between the mechanisms of this and analogous reactions.

The reduction of an MO_2^+ ion entails the disruption of a relatively stable structure, and we might expect the mechanism of such reductions to be rather complex. In this paper we are concerned with the particular reaction



and with its relation to other similar reactions.

Experimental

Preparation of Solutions.—The preparation and standardization of the following stock solutions have been previously described: $Np(IV)$,² $Np(III)$ and (V) ,³ perchloric acid, and sodium, lithium, lanthanum, and thorium perchlorates.⁴ Strontium perchlorate was prepared from reagent grade strontium carbonate, followed by recrystallization. The vanadium(III) and (IV) stock solutions were prepared by dissolving ammonium metavanadate in hot, dilute sodium hydroxide. This solution was centrifuged and the insoluble matter discarded. Hydrated vanadium pentoxide was precipitated by addition of perchloric acid. The oxide was washed with distilled water and suspended in perchloric acid. The suspension was electrolyzed at a platinumized platinum cathode under a nitrogen atmosphere using a potentiostat⁵ to control the cathode potential. The vanadium(III) was further purified by precipitation of the hydroxide under a nitrogen atmosphere, and subsequent dissolution in perchloric acid. Although the vanadium(III) solutions were stored under nitrogen at 5°, there was slow oxidation by perchlorate ion to yield $V(IV)$ and Cl^- .⁶ The vanadium solutions were routinely analyzed using a Cary Model 14 recording spectrophotometer. The extinction coefficients of $V(III)$ and $V(IV)$ were determined at 25° in 1 *M* $HClO_4$ using solutions standardized by titration with ceric sulfate and potassium permanganate, respectively. Both the permanganate and the ceric sulfate were standardized against National Bureau of Standards arsenic trioxide. At 3960 Å. the molar extinction coefficient of $V(III)$ is 8.48 ± 0.04 and at 7650 Å. that of $V(IV)$ is 17.19 ± 0.09 . The absorption at 3960 Å. by $V(IV)$ was determined to be negligible, and on the basis of the results of Furman and Garner⁶ the absorption by $V(III)$ at 7650 Å. also was assumed to be of no significance.

All concentrations were corrected for changes in solution composition with temperature and are reported in terms of moles/l. Unless otherwise indicated all experiments were conducted at 25°, and perchlorate was the only anion present.

Kinetic Experiments.— $Np(V)$ solutions of the appropriate composition were introduced into 2-cm. silica absorption cells and were brought to temperature equilibrium after being deoxygenated by bubbling in nitrogen for about 30

min. The reaction was initiated by the introduction of the $V(III)$ and the progress of the reaction was monitored by use of either the $Np(V)$ band centered at approximately 9800 Å. or the $Np(IV)$ band centered at 9600 Å. The same rate constants were obtained whichever peak was followed. Small corrections were made for interference by other species. Since the extinction coefficients of the $Np(V)$ were particularly sensitive to solution composition, they were evaluated for each experiment. Temperature was controlled to $\pm 0.1^\circ$ in the cell compartment of the spectrophotometer.

Equilibrium Experiments.—Deoxygenated $Np(IV)$ solutions of the appropriate composition were brought to temperature equilibrium in the absorption cells. A known amount of $V(III)$ then was added and the change in the 9600 Å. band of the $Np(IV)$ was measured. Equilibrium appeared to be attained within the time of mixing the solutions and placing them in the spectrophotometer.

Results

Stoichiometry.—Under most conditions the stoichiometry of the reduction of NpO_2^+ by V^{+3} corresponded to reaction 1, which goes to completion. However, if the acidity was less than 0.5 *M*, and only small amounts of VO^{++} were present, measurable quantities of Np^{+3} were produced by the rapid equilibrium



which we have measured directly. Values of the equilibrium constant, K , are given in Table IV. Whenever necessary, the kinetic data have been corrected for the effects of this equilibrium.

Rate Law.—In 3 *M* $HClO_4$ the reaction followed, to more than 90% of completion, the bimolecular rate equation

$$k_{bm}t = (A - B)^{-1} \ln \frac{Ba}{Ab} \quad (3)$$

where A and B are the initial concentrations of the reactants and a and b are their concentrations at time t . Values of k_{bm} were determined graphically. In all of these experiments a small amount of VO^{++} was unavoidably introduced with the V^{+3} . This initial VO^{++} concentration was almost always less than the initial concentrations of the reactants; however the rate was not affected appreciably when much larger quantities of VO^{++} were added. The reaction rate also was unchanged by the presence of 0.01 *M* Cl^- or of 0.001 *M* HSO_4^- . It is most unlikely that chloride or sulfate in excess of these amounts would ever be present as an impurity.

At lower acidities the reaction deviated from equation 3, the slope k_{bm} increasing with time. The deviations became progressively more severe

(1) Based on work performed under the auspices of the U. S. Atomic Energy Commission.

(2) J. C. Sullivan, D. Cohen, and J. C. Hindman, *J. Am. Chem. Soc.*, **76**, 4275 (1954).

(3) J. C. Hindman, J. C. Sullivan, and D. Cohen, *ibid.*, **80**, 1812 (1958).

(4) J. C. Sullivan, A. J. Zielen, and J. C. Hindman, *ibid.*, **82**, 5288 (1960).

(5) P. Wehner and J. C. Hindman, *ibid.*, **72**, 3911 (1950).

(6) S. Furman and C. S. Garner, *ibid.*, **72**, 1785 (1950).

as the acidity decreased, but they were reduced when the VO^{++} concentration was increased. At these acidities addition of $Np(IV)$ markedly accelerated the reaction. The following rate law was postulated

$$\frac{-d[NpO_2^+]}{dt} = [NpO_2^+][V^{+3}] \left\{ k_1 + k_2 \frac{[Np^{+4}]}{[VO^{++}]} \right\} \quad (4)$$

If this law is valid, a plot of $(-d[NpO_2^+]/dt)/[NpO_2^+][V^{+3}]$ vs. $[Np^{+4}]/[VO^{++}]$ should be linear, with intercept k_1 and slope k_2 . This relation for a typical experiment is illustrated in Fig. 1. The values of $-d[NpO_2^+]/dt$ were determined from a plot of $[Np^{+4}]$ vs. time with the aid of a Gerber "Derivimeter" (Gerber Scientific Instrument Co., Hartford, Connecticut).

In some experiments the ratio $[Np^{+4}]/[VO^{++}]$ was held nearly constant throughout the reaction, either by making its initial value equal close to unity or by making the initial Np^{+4} and VO^{++} concentrations so large that they were not greatly altered by the production of these species in the course of the reaction. In such cases the reaction followed equation 3 with k_{bm} replaced by $k_1 + k_2[Np^{+4}]/[VO^{++}]$. Then k_2 was evaluated by combining the slope of a logarithmic plot of equation 3 with the value of k_1 determined in the same medium in the absence of Np^{+4} . When small variation in the $[Np^{+4}]/[VO^{++}]$ ratio during a reaction caused slight deviations from equation 3, the mean slope of the plot at about the first half-time was used.

A similar method was applicable to experiments in which no Np^{+4} and little VO^{++} were present initially. In such experiments the ratio $[Np^{+4}]/[VO^{++}]$ quickly approached a limiting value, and k_2 could be determined from the final limiting slope of a logarithmic plot of equation 3 and an independently measured k_1 .

In experiments in which the second term of equation 4 was not too important, k_1 could be determined most accurately from the initial slope of a logarithmic plot of equation 3. The data on k_1 are summarized in Tables I-III and in Fig. 2. This constant appears to be essentially independent of acidity.

TABLE I

METAL ION DEPENDENCE OF k_1 IN 3.0 M $HClO_4$		
Initial concentration $\times 10^3$ [NpO_2^+]	$[V^{+3}]$	$k_1, (M)^{-1} (sec.)^{-1}$
1.11	1.51	0.333
1.10	7.3	.355
1.10	0.76	.325
1.55	6.8	.362
		Av. 0.344 \pm 0.09

TABLE II

ACID DEPENDENCE OF k_1 AT 3.0 M $[ClO_4^-]$		
Inert salt	$[H^+]$	k_1
....	3.0	0.344
$LiClO_4$	1.0	.265
	0.37	.269
	0.13	.260
$NaClO_4$	1.0	.184
	0.37	.144
	0.13	.112

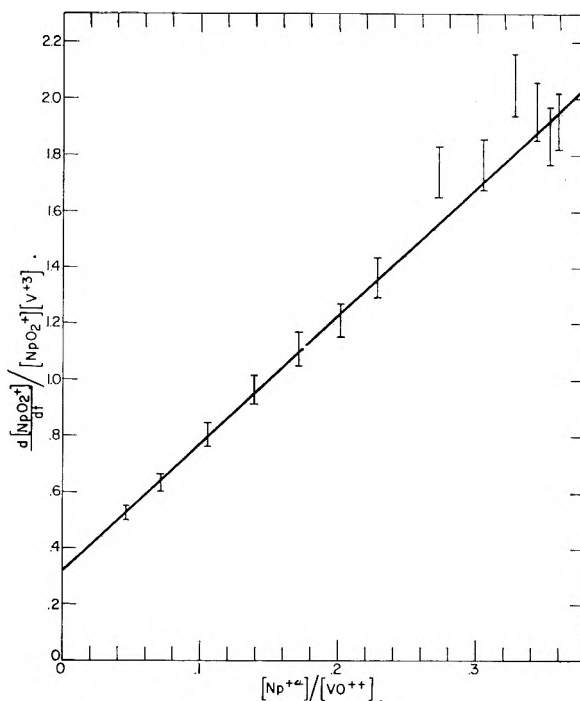


Fig. 1.—Determination of k_1 and k_2 for a typical experiment. Initial concentrations $[H^+] = 0.132 M$; $[NpO_2^+] = 1.63 \times 10^{-3} M$; $[V^{+3}] = 7.54 \times 10^{-3} M$; $[VO^{++}] = 2.43 \times 10^{-3} M$; $[LiClO_4] = 2.9 M$. From the plot $k_1 = 0.315$ and $k_2 = 4.6 (M)^{-1} (sec.)^{-1}$.

TABLE III

TEMPERATURE DEPENDENCE OF k_1 IN 0.37 M $HClO_4$ AND THERMODYNAMIC QUANTITIES OF ACTIVATION ^a					
t	$[LiClO_4]$	k_1	ΔF^*	ΔH^*	ΔS^*
15.05	..	0.0141	19.40 \pm 0.03	15.6 \pm 0.7	-12.6 \pm 2.2
25.00	..	.0377			
34.97	..	.0892			
15.05	2.6	.112	18.23 \pm .03	14.6 \pm .8	-12.3 \pm 2.6
25.00	2.6	.268			
34.97	2.6	.615			

^a ΔH^* and ΔS^* were calculated by least squares analysis of the data. The uncertainties quoted are the 95% confidence level values resulting from the analysis. The uncertainties in ΔF^* were estimated from the experimental scatter.

In Fig. 3 and 4 we have plotted $\log \{-k_1 - (d[NpO_2^+]/dt)/[NpO_2^+][V^{+3}]\}$ vs. $\log \{[Np^{+4}]/[VO^{++}]\}$ for experiments in several media. If our rate law is correct these plots should be linear, with a slope, λ , of unity, and with ordinate equal to k_2 when $\log \{[Np^{+4}]/[VO^{++}]\} = 0$.

The plots have been fitted by a weighted least squares analysis to give the best straight lines. The resulting values of k_2 and λ appear in Table IV. If we set $k_2 = k_2^0[H^+]^h$ we see that $h = -1.6$ in lithium perchlorate and -1.35 in sodium perchlorate. The other entries in Table IV will be discussed subsequently.

Discussion

Equation 4 is consistent with the mechanism

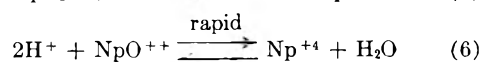
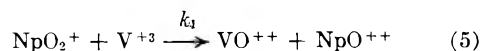


TABLE IV
 LOW ACID REACTION PATH^a

Inert salt	H ⁺	$k_N, (M)^{-1}(\text{sec.})^{-1}$	$K \times 10^4$	λ	$k_2, (M)^{-1}(\text{sec.})^{-1}$		Obsd. ^b	Calcd.
					Obsd.	Calcd.		
LiClO ₄	0.13	0.35 ± 0.04	6.2 ± 0.4	0.88 ± 0.06	3.6 ± 0.3	1.3 ± 0.2	-1.6	-1.65
LiClO ₄	.37	.50 ± .06	6.2 ± .4	1.16 ± .10	0.67 ± .05	0.23 ± .03		
NaClO ₄	.13	.15 ± .02	6.7 ± .6	1.00 ± .04	1.15 ± .06	.59 ± .09	-1.35	-1.5
NaClO ₄	.37	.25 ± .03	6.7 ± .6	1.26 ± .11	0.28 ± .02	.12 ± .02		

^a At 25° and [ClO₄⁻] = 3.0 M. Values of k_N were determined from direct measurements of reaction 7 in solutions $\sim 5 \times 10^{-4}$ M each in Np(III) and Np(V). Values of K , the equilibrium constant of reaction 2, also were measured directly in solutions 0.008–0.017 M in V(III), 0.001–0.002 M in V(IV) and 0.002 M in total neptunium. Between 0.1 and 0.5 M H⁺ the equilibrium displayed the proper hydrogen ion dependence for reaction 2. The uncertainties quoted for λ and k_2 (observed) are the standard deviations determined in the least squares analysis. The other uncertainties are estimated from the experimental scatter.

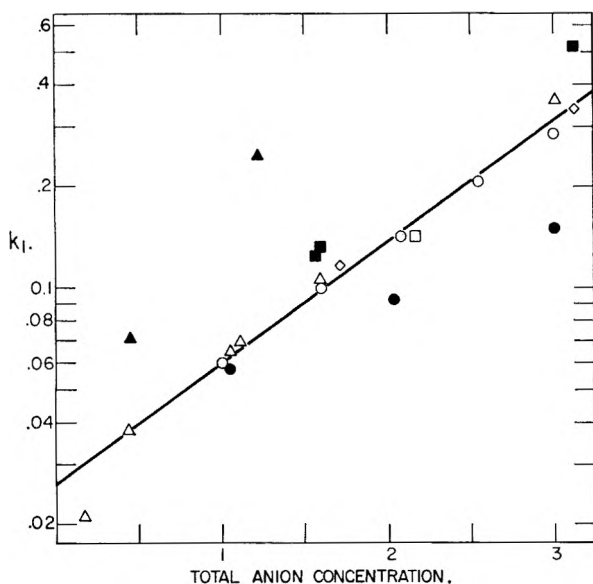
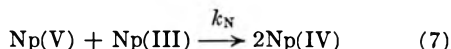
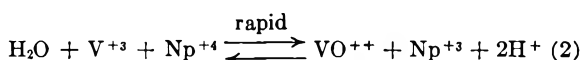


Fig. 2.—Salt dependence of k_1 . Initial concentrations: [NpO₂⁺] = 1.55–1.8 × 10⁻³ M; [V⁺³] = 6.8–8.2 × 10⁻³ M; [VO⁺⁺] = 0.016–0.019 M; [H⁺] = 0.36–0.37 M except when HCl or HClO₄ is the added electrolyte. Added electrolyte: ○, LiClO₄; ●, NaClO₄; △, HClO₄; □, Sr(ClO₄)₂; ◇, La(ClO₄)₃; ■, Th(ClO₄)₄; ▲, HCl.



where k_N is the rate of disappearance of Np(III) in reaction 7. If K is the equilibrium constant for reaction 2, we observe that

$$\frac{-d[\text{NpO}_2^+]}{dt} = [\text{NpO}_2^+][\text{V}^{+3}] \left\{ k_1 + \frac{k_N K [\text{Np}^{+4}]}{[\text{H}^+]^2 [\text{VO}^{++}]} \right\} \quad (8)$$

Hence

$$k_2 = k_N K / [\text{H}^+]^2 \quad (9)$$

We have measured k_N and K directly in these media and have calculated k_2 from them. The measured and calculated k_2 values are compared in Table IV. The measured values can be seen to be consistently some two to three times the calculated ones. The reason for this is not clear. The extensive scatter of our data suggests that catalysis by impurities may be causing trouble.

Both observed and calculated k_2 values show roughly the same H⁺ dependence, corresponding to a direct 0.35–0.65 power dependence of k_N on hydrogen ion. Hindman, *et al.*,³ studied reaction

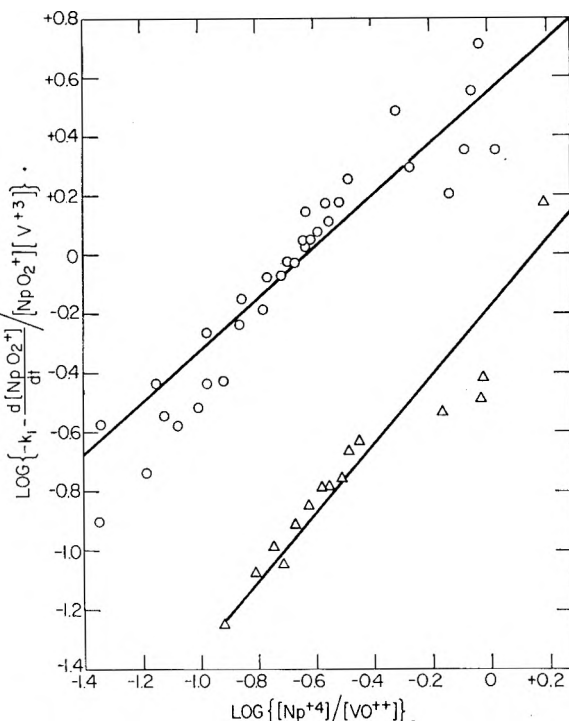
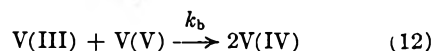
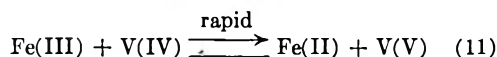
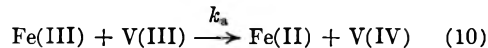


Fig. 3.—Low acid path in LiClO₄ solutions with 3.0 M perchlorate: ○, 0.13 M HClO₄; △, 0.37 M HClO₄.

7 in 2 M perchlorate and found a direct first power hydrogen ion dependence.

The mechanism indicated in equations 5, 6, 2, and 7 is similar to that recently elucidated for the reduction of Fe(III) by V(III),⁷ for which is postulated the reaction sequence



However, these workers were unable to measure directly k_b , the analog of our k_N .

Figure 2 indicates that k_1 is more dependent upon perchlorate ion concentration than upon ionic strength. The straight line in the figure corresponds to the empirical equation

$$\log k_1 = \log(0.026) + 0.36[\text{ClO}_4^-] \quad (13)$$

Equation 13 is not obeyed in thorium or sodium

(7) W. C. E. Higginson, D. R. Rosseinsky, J. B. Stead, and A. G. Sykes, *Discussions Faraday Soc.*, **29**, 49 (1960).

perchlorate solutions over 1 M in perchlorate. In the former k_1 is abnormally high, while in the latter it is abnormally low. Since several different NaClO_4 and $\text{Th}(\text{ClO}_4)_4$ preparations gave similar results, it seems unlikely that impurities were at fault. From Table IV we see that the $\text{Np}(\text{III})$ - $\text{Np}(\text{V})$ reaction is also much slower in sodium than in lithium perchlorate solutions. These observations emphasize the need to consider specific ion effects on reactions studied at high ionic strength.

The marked acceleration of the reaction by chloride seems too great to be attributed to a "medium" effect and probably represents a chloride-dependent reaction path.

Table V summarizes the kinetic data on the reduction of MO_2^+ ions by a number of one-electron reductants. With the exception of the $\text{Np}(\text{III})$ - $\text{Np}(\text{V})$ reaction and the disproportionation of $\text{U}(\text{V})$, each of which has a very large thermodynamic driving force, the reactions proceed relatively slowly. This is not surprising in view of the major structural changes involved.

TABLE V

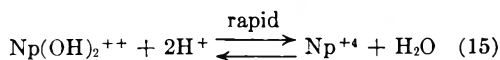
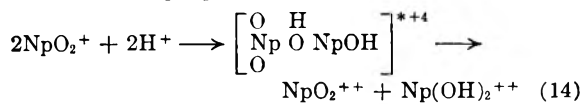
ONE-ELECTRON OXIDATION-REDUCTION REACTIONS INVOLVING DESTRUCTION OF THE MO_2^+ STRUCTURE

Reaction	Rate, ^a M/sec.	Ref.
$\text{Np}(\text{III}) + \text{Np}(\text{V}) \longrightarrow 2\text{Np}(\text{IV})^b$	$40 [\text{NpO}_2^+][\text{Np}^{+3}][\text{H}^+]$	3
$\text{V}(\text{III}) + \text{Np}(\text{V}) \longrightarrow \text{Np}(\text{IV}) + \text{V}(\text{IV})$	$0.06 [\text{NpO}_2^+][\text{V}^{+3}]$	This work
$\text{Fe}(\text{II}) + \text{Np}(\text{V}) \longrightarrow \text{Np}(\text{IV}) + \text{Fe}(\text{III})$	$.08 [\text{NpO}_2^+][\text{Fe}^{+2}][\text{H}^+]$	8
$\text{Pu}(\text{III}) + \text{Pu}(\text{V}) \longrightarrow 2\text{Pu}(\text{IV})$	$.04 [\text{PuO}_2^+][\text{Pu}^{+3}][\text{H}^+]$	9, 10
$\text{Np}(\text{IV})$ - $\text{Np}(\text{V})$ exchange	$10^{-5} [\text{NpO}_2^+]^2[\text{H}^+]$	2
$2\text{Np}(\text{V}) \longrightarrow \text{Np}(\text{IV}) + \text{Np}(\text{VI})$	$10^{-8} [\text{NpO}_2^+]^2[\text{H}^+]^2$	11
$2\text{U}(\text{V}) \longrightarrow \text{U}(\text{IV}) + \text{U}(\text{VI})$	$140 [\text{UO}_2^+]^2[\text{H}^+]$	12
$2\text{Pu}(\text{V}) \longrightarrow \text{Pu}(\text{IV}) + \text{Pu}(\text{VI})$	$0.004 [\text{PuO}_2^+]^2[\text{H}^+]$	13

^a At 25° in perchlorate medium. Unless otherwise specified, $[\text{ClO}_4^-] = 1 M$. ^b $[\text{ClO}_4^-] = 2 M$.

The $\text{V}(\text{III})$ - $\text{Np}(\text{V})$ reaction differs from the other reactions listed in Table V in that the rate law does not exhibit a positive hydrogen ion dependence. This may be understood if we assume the following mechanisms to be typical

For the disproportionation of $\text{Np}(\text{V})$



(8) J. R. Huizenga and L. B. Magnusson, *J. Am. Chem. Soc.*, **73**, 3202 (1951).

(9) S. W. Rabideau, *ibid.*, **75**, 798 (1953).

(10) S. W. Rabideau, *ibid.*, **78**, 2705 (1956).

(11) J. C. Hindman, J. C. Sullivan, and D. Cohen, *ibid.*, **76**, 3278 (1954).

(12) L. J. Heidt, *ibid.*, **76**, 5962 (1954).

(13) S. W. Rabideau, *ibid.*, **79**, 6350 (1957).

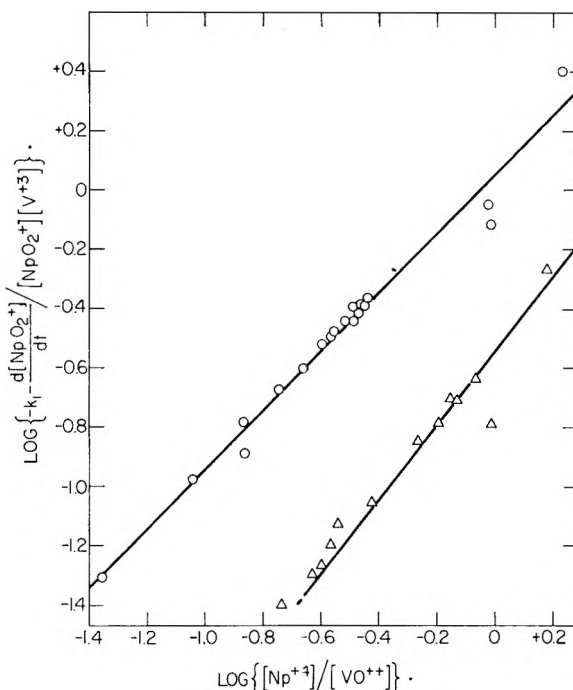
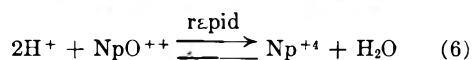
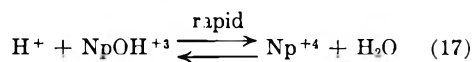
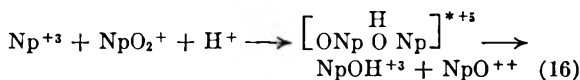
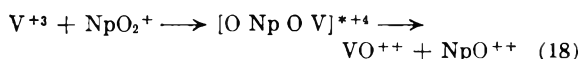


Fig. 4.—Low acid path in NaClO_4 solutions with 3.0 M perchlorate: \odot , 0.13 M HClO_4 ; \triangle , 0.37 M HClO_4 .

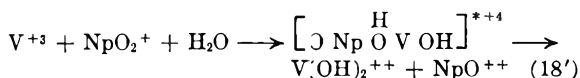
for the reaction between $\text{Np}(\text{III})$ and $\text{Np}(\text{V})$



and for the reaction of $\text{Np}(\text{V})$ with $\text{V}(\text{III})$



or



followed by reaction 6.

Only in the case of reactions 18 and 18' is the bridging group incorporated into a stable product. In the other cases the hydroxo-bridged activated complex leads to intermediate products which are closer to stability than would be those formed from an activated complex containing no hydrogen. The resulting decrease in the activation barrier presumably more than compensates for the coulombic effect of the added charge. In equations 18 or 18', however, addition of a proton to the activated complex would lead to formation of the unstable intermediate VCH^{+3} .

THE RELATION BETWEEN LYOTROPIC AND SPECTROSCOPIC PROPERTIES OF ANIONS IN SOLUTION

BY DAN MEYERSTEIN AND AVNER TREININ

Department of Physical Chemistry, Hebrew University, Jerusalem, Israel

Received September 7, 1961

Anionic effects on the charge-transfer absorption band of I^- were studied in detail. The results indicate that the spectroscopic effects of the added anions depend mainly on their power to desolvate the test ion I^- . Thus a correlation is presented between the spectroscopic and lyotropic series, with the halides forming a separate group. The mechanism of the anionic effect on this type of spectra (C.T.T.S. spectra) is discussed and some evidence is brought in favor of the continuous medium approximation which involves the ionic cavity radius as a variable.

The absorption spectrum of I^- in solution is relatively very sensitive to environmental effects.^{1,2} This property seems to characterize spectra which originate from a charge transfer to the solvent (C.T.T.S.).¹ Through a study of such effects it is possible to derive information on the nature of the electronic transition involved and on the structure of the medium. For this purpose ionic effects seem to be of particular interest. Some work of this kind already was carried out,² indicating specific effects of both cations and anions. This work was limited by the short wave length spectral region studied, where many anions strongly absorb. To overcome this difficulty we investigated the onset of the absorption band of I^- (260–270 $m\mu$), on which we could test the effects of about 15 different anions of various types and valence. The sodium ion thus introduced was shown to have only a small effect,² and thus a scale of anionic effectiveness on C.T.T.S. spectra is established and discussed.

Experimental

Spectrophotometric measurements were carried out with a Hilger Uvispeck spectrophotometer using a thermostated cell compartment. The temperature was kept constant at $20 \pm 0.5^\circ$. One-cm. silica cells were used. Only fresh solutions were taken for the measurements. The absorption at 288 $m\mu$, where I_3^- has its maximum absorption, was checked first to confirm that no autooxidation occurred. Any solution showing an optical density larger than 0.01 at this wave length was discarded.

Solutions of the added electrolytes, the effect of which was to be tested, first were prepared at the appropriate concentrations. To each of these an accurately weighed quantity of KI was added, so as to obtain $5 \times 10^{-2} M$ KI. This procedure brings about only a negligible change in the relatively high concentration of the electrolyte solution, so that another portion of it could serve as a reference solution. Special procedures were used for preparing the concentrated KI solutions and the H^+ containing solutions. To avoid autooxidation in these cases a special vessel was used. This consisted of an all-quartz Thunberg-type tube, the lower branch of which formed the spectrophotometer cell (manufactured by Messrs. Thermal Syndicate Ltd., Wallsend). To obtain the concentrated KI solution, an accurately weighed quantity of KI was introduced into the upper branch of the vessel, which then was weighed, water was introduced into the lower branch, the vessel evacuated using a rotary oil pump, weighed again to determine the exact quantity of water present, and finally the KI was dissolved in it. The spectrophotometer cell had a 9-mm. silica spacer inside so that the effective optical path was only 1 mm. After performing the spectrophotometric measurement the density of the solution was determined, using an ordinary pycnometer. For preparing H^+ containing solutions (e.g., $NaHSO_4$) a simpler procedure was used, since the quantity

of KI then was much smaller. This was essentially similar to the ordinary procedure described at the beginning but the dissolution of KI was carried in the vessel under vacuum. The evaporation of water during evacuation was negligible. In this case no spacer was used and no density measurements determined.

Materials used were of the purest grade available, mostly A.R. The water was redistilled from alkaline permanganate and then from dilute phosphoric acid in an all-glass still.

Results

The Effect of Added Electrolytes.—In the presence of all the added electrolytes studied in this work, the onset of the absorption band of I^- is shifted to the ultraviolet. This is shown for the halides in Fig. 1, the results summarized in Table I. $\Delta\nu$ represents the average shift in wave number corresponding to the same extinction coefficient. When available the shift of the maximum also is recorded. In these cases it is evident that the shift of the maximum is nearly equal to that of the onset and that the height of the band does not alter,² i.e., that the whole band undergoes an almost parallel shift to itself (a small broadening effect is noticed in $NaCl$ and Na_2SO_4 solution). In other cases, when the position of the maximum is unknown, an analytical method was adopted in order to examine the shape of the absorption band. This band already was shown to possess a Gauss error-law shape,³ but its "precision index" was not determined. From our results at 20° we derived the expression

$$\log E = -7.126 + 2 \log (\nu_{\max} - \nu) \quad (1)$$

where $E = \log \epsilon_{\max}/\epsilon$, ϵ and ϵ_{\max} are the molar extinction coefficients at a given frequency ν and at the maximum ν_{\max} , respectively. The values of ϵ_{\max} and ν_{\max} of dilute I^- solution are 1.37×10^4 mole⁻¹ l. cm.⁻¹ and 4.427×10^4 cm.⁻¹, respectively, both these values and the "precision index" being temperature dependent. Equation 1 represents the observed extinction coefficients of the long wave length branch of the band within less than 5%. The other branch is partially overlapped by the second absorption band.

Using this equation we could examine the shape of the absorption band in such solutions where only the onset could be measured. This was done by first assuming that the band shifts parallel to itself, i.e., ϵ_{\max} is not altered and $\Delta\nu$ at the maximum is the same as that observed at the onset. Then we tested whether the observed extinction coefficients could be computed by using eq. 1 with the

(1) M. Smith and M. C. R. Symons, *Trans. Faraday Soc.*, **54**, 338 (1958).

(2) G. Stein and A. Treinin, *ibid.*, **56**, 1393 (1960).

(3) T. R. Griffith and M. C. R. Symons, *ibid.*, **56**, 1125 (1960).

TABLE I
SPECTRAL SHIFT, $\Delta\nu$ (CM.⁻¹ (± 15), AS A RESULT OF ADDING ELECTROLYTES AT DIFFERENT CONCENTRATION (20°)
In parentheses the shift of the maximum is presented²

Electrolyte	0.5 M	1 M	2 M	3 M	4 M	8 M
KF		210	400	635(665)		1600(1530)
NaCl		125(145)	245(285)	315		
NaBr		45	~75	Broadening		
KI		~90				
KOH		165	355		680	
NaOH		165	295		595	
NaClO ₄	105	195	360(370)		725(735)	
NaClO ₃	110	210	365		755	
CH ₃ CO ₂ Na	120	230	445			
HCO ₂ Na	120	230	425			
NaCN		270	475		965	
NaHSO ₄		165	335			
Na ₂ SO ₄	180	310(340)	600(705)			
NaH ₂ PO ₄			400	610		
Na ₂ HPO ₄	165	325	610			
Na ₃ PO ₄	180					
KNa tartrate	185	355				
Na ₃ citrate	220	450				

appropriate ν_{max} . Agreement between calculated and observed data appears to indicate the validity of the assumption. Table II exemplifies the use of this method for the case of 0.5 M sodium citrate.

TABLE II

CALCULATED AND EXPERIMENTAL MOLAR EXTINCTION COEFFICIENTS OF 5×10^{-2} M KI IN 0.5 M Na₃ CITRATE AT 20°

λ , m μ	$(\nu_{max} - \nu) \times 10^3$, cm. ⁻¹	ϵ , l. mole ⁻¹ cm. ⁻¹ Calcd.	ϵ , l. mole ⁻¹ cm. ⁻¹ Expt.
268	7.177	1.93	1.95
267	7.037	2.70	2.75
266	6.896	3.80	3.80
265	6.754	5.29	5.25
264	6.611	7.35	7.20
263	6.467	10.20	10.30
262	6.322	14.07	14.15
261	6.176	19.20	19.40
260	6.028	26.20	25.75

Using this method we confirmed that in most of the solutions studied the shape of the absorption band hardly changes. In concentrated NaBr solution, a distinct broadening was detected, which already could have been observed at the onset.

Spectra of Concentrated Halide Solutions.—

Raising the concentration of KI, KBr, and NaBr solutions results in a non-parallel shift of their own spectra to longer wave lengths, the iodide showing a larger effect. The case of KI is illustrated in Fig. 1. On the other hand under the same treatment the spectrum of Cl⁻ (KCl) suffers a blue shift. These results are in agreement with those of an early work.⁴ Taking into account that raising the concentration of KI results in slightly shifting its own peak to the ultraviolet,⁵ we conclude that the iodides and to a smaller extent the bromides suffer a concentration-broadening effect. In the case of Cl⁻ this effect is probably small and is masked by its own relatively large blue shifting

(4) H. Fromherz and W. Menschick, *Z. physik. Chem.*, **B7**, 439 (1930); H. Diamond and H. Fromherz, *ibid.*, **B9**, 289 (1930).
(5) G. Stein and A. Treinin, unpublished results.

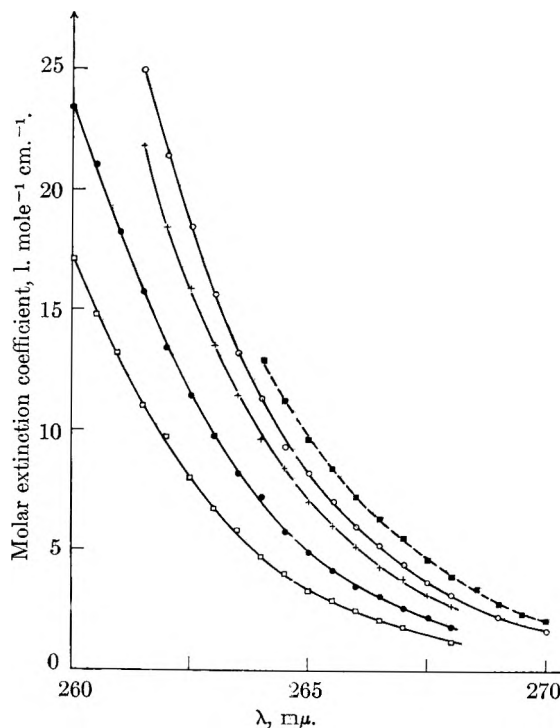


Fig. 1.—The onset of the absorption band of 5×10^{-2} M KI alone, O, and in presence of 2 M of the following salts: NaBr, +; NaCl, ●; KF, □; dashed line, 1 M KI alone.

effect, so that there is a net shift of the whole band to the ultraviolet.

Anionic Specificity.—The effects of the various anions on the spectrum of I⁻ display a pronounced specificity. Thus at the same molarity the effect of citrate is almost ten-fold larger than that of bromide. It will be found convenient to divide the anions into two groups: (a) The halides: their effect is relatively small, the sequence is F⁻ > Cl⁻ > Br⁻ > I⁻. OH⁻, which is isoelectronic with F⁻ and is similar to it in many respects, may be grouped here between F⁻ and Cl⁻. (b) The complex anions: they exert larger effects, the sequence is citrate > tartrate > PO₄⁻⁻⁻ ≥

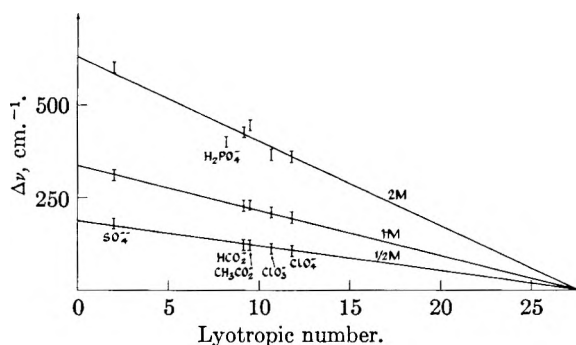
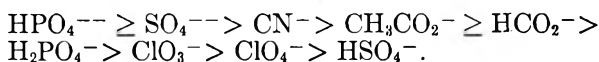


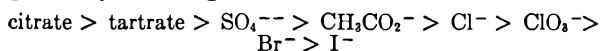
Fig. 2.—Correlation between spectral shifts and lyotropic numbers.



Discussion

Our results generally confirm the conclusion, derived in a previous work,² that the absorption band of I^- retains its shape in the presence of concentrated alkali and alkaline earth salts. The small broadening noticed in some cases probably is a Stark effect caused by the perturbing electrical fields due to the cations in the proximity of the absorbing anion. On the other hand, the relatively large self-broadening effect appears to be mainly a resonance effect, probably originating from dipole-dipole interaction between transitions in similar halide ions, which temporarily manage to approach each other quite closely. This interaction being proportional to the square of the transition moment (*i.e.*, proportional to the intensity of transition) thus should follow the order⁶ $\text{I}^- > \text{Br}^- > \text{Cl}^-$, in agreement with the experimental results. The ion Br^- , which of all other anions most nearly resembles I^- , may derive its broadening effect on the spectrum of I^- from this mechanism.

The Anionic Effect and the Lyotropic Series.—It already was suggested² that the ionic effects on the spectrum of I^- are mainly due to their influence on its solvation properties. The few anions then tested indicated a close relation between their spectroscopic effect and their desolvating or "salting out" properties. The relatively large effect of non-electrolytes as glucose and sucrose also appears to establish this relation. Now it gets further support from the present results. Thus, with some irregularities, the "blue-shifting" effect of the anions run almost parallel to their desolvating power. The order observed is nearly that displayed by the lyotropic (Hoffmeister) series, which generally is arranged in the order



A quantitative expression of the position of the ions in the lyotropic series was provided by the scale of lyotropic numbers (L.N.).⁷⁻⁹ This number is essentially a measure of the power of an ion to

bind water to itself at the expense of hydrated colloids in solution, thus causing their flocculation. But apart from playing a prominent role in colloid chemistry the L.N. have a bearing on many properties of ions in solution, not concerned with colloids.^{8,10} The general features of the phenomena related to the lyotropic series establish its connection with the solvation properties of the ions. This is clearly shown by the linear correlation found between the heat of hydration of the ions and their L.N.⁹

In Fig. 2 the spectroscopic effect is plotted against the L.N. at three different concentrations. Only the ions of group (b) are included, as those of the second group fall much below the straight lines thus obtained. The L.N. of only a few anions are available. The flocculation method when applied to some other ions, in particular those which are of non-neutral character (*e.g.*, HPO_4^{--} and tartrate), gives conflicting results, so that no L.N. were assigned to such ions. Using our spectroscopic data, with the aid of Fig. 2, we are able to estimate these numbers. For example, the lyotropic number estimated for HPO_4^{--} is approximately 1, while the flocculation method gives the values 0.6 (gelatin) and 3.0 (agar).¹¹ The three straight lines in Fig. 2 intersect at a point on the L.N. axis. This point corresponds to an hypothetical sodium salt which does not shift the spectrum of I^- at any concentration. The viscosities of electrolyte solutions behave in a similar way.¹²

These results indicate that it is more proper to state that the halides depart from the general regularity than the contrary, as was done previously,² when besides the halides only ClO_4^- was tested. In the halide-group itself the same law is observed—the smaller the lyotropic number the larger the effect—though the correlation is far from linearity. The reason for this separation into two groups still is obscure, indicating that there is an additional factor which has to be taken into account in the case of spectroscopic effects, probably a structural factor.

The Mechanism of the Anionic Effect.—In a previous work² an expression was derived which relates the transition energy of C.T.T.S. spectra to three variables: the optical and static dielectric constants and the radius of the ionic cavity. If only the macroscopic dielectric constants are taken into account the calculated values of spectral shifts are of the correct sign but appreciably smaller than those observed and—what is more important—they do not reflect the observed ionic specificity (*e.g.*, they predict a reverse order in the halide group). Now it is evident that this specificity is related in some way to the solvation state of the ions. In order to explain this relation it was assumed previously that up to a certain stage the impoverishment of the solvation layer of I^- brings about a contraction of the ionic cavity, and hence a lowering of the energy of the ground state.² No direct experimental evidence was presented for this contraction. To provide such evidence it

(6) The oscillator strength of the first optical transition of the halide ions in water is: I^- , 0.47; Br^- , 0.27; Cl^- , 0.09. See ref. 23.

(7) E. M. Bruins, *Proc. Acad. Sci. Amsterdam*, **35**, 107 (1932).

(8) A. Voet, *Chem. Revs.*, **20**, 169 (1937).

(9) D. F. C. Morris, *J. Inorg. & Nuclear Chem.*, **6**, 295 (1958); *Rec. trav. chim.*, **78**, 150 (1959).

(10) J. W. McBain, "Colloid Science," D. C. Heath Co., Boston, Mass., 1950, Chap. 9.

(11) These values were estimated from Figs. 1 and 2, ref. 8.

(12) J. H. C. Merckel, *Kolloid Z.*, **73**, 67 (1935).

is important to determine the partial molar volumes at infinite dilution (\bar{V}^0) of one electrolyte in the presence of a relatively high concentration of another electrolyte. As far as we know the only available data of this kind was presented by Wirth.¹³ Table III records his results for KCl and KBr in NaCl solution.

TABLE III

PARTIAL MOLAR VOLUMES \bar{V}^0 AT INFINITE DILUTION OF KCl AND KBr IN WATER AND IN NaCl AQUEOUS SOLUTION AT 25°

α and B are the calculated parameters of eq. 2

Medium	KCl	KBr	α	B
H ₂ O	26.74	33.97	1.227	10.99
0.16 <i>N</i> NaCl	27.89	35.03	1.226	9.77
.35 <i>N</i> NaCl	28.46	35.43	1.217	8.48
.62 <i>N</i> NaCl	29.18	36.11	1.214	7.49

The increase of the partial molar volume of KCl and KBr in the presence of NaCl, relative to that in pure water, does not indicate an enlargement of the ionic cavities. One has to consider the effect of added salts on the electrostriction. \bar{V}^0 is the sum of two factors, one representing the actual volume occupied by the ion, while the other is from the electrostriction of the medium. Hepler's equation¹⁴ was modified¹⁵ to give the expression for \bar{V}^0 of a uni-univalent electrolyte

$$\frac{\bar{V}^0}{1/r_c + 1/r_A} = \frac{4}{3} \pi N \alpha^3 \frac{r_c^3 + r_A^3}{1/r_c + 1/r_A} - \frac{B}{\alpha} \quad (2)$$

where r_c and r_A represent the crystallographic radii of the cation and anion, respectively. This expression, which is based on the assumption that at the same conditions α and B are constant for ions both positive and negative (at variance with Hepler's treatment), was shown to be valid for a large group of electrolytes in aqueous solution and also in several organic solvents.¹⁶ This equation can be solved for B and α by inserting the values of \bar{V}^0 for any pair of electrolytes. Assuming its general validity and using the experimental data we thus obtained the values of B and α and included them in Table III. We observe that there is a gradual decrease of both α and B with increase of NaCl concentration. The rather strong decrease of B probably is due partly to the decrease in the compressibility of the solvent which accompanies the solution of an electrolyte.¹⁷ As to the effect on α it is qualitatively in accord with the mechanism suggested for the spectroscopic effect. The ionic cavity radius r_0 is related to the crystallographic radius r by the equation $r_0 = \alpha r$. Using the general expression for $h\nu^2$ we obtained an expression for the variation of $h\nu$ with α

$$\Delta(h\nu) = - \frac{0.77e^2\Delta\alpha}{\alpha^2 r} \quad (3)$$

Inserting the calculated values of α we obtained values of $\Delta(h\nu)$ which though higher than the ex-

perimental values are of the correct order of magnitude. For example in 0.32 *M* NaCl the spectral shift thus calculated is about 350 cm.⁻¹, while the observed shift is about 100 cm.⁻¹.

The above treatment is based on the continuous medium model first presented by Franck and Platzman¹⁸ and modified to include the cavity radius as an additional variable.¹⁹ A satisfactory molecular picture of the excited state of C.T.T.S. spectra has not yet been given. Any model of this kind should take into account the charge distribution in the excited state which is concentrated at relatively small distance from the center of the excited ion (average distance not more than 5–6 Å).² It means that the charge is "smeared" mainly on the first and second hydration layers. This distribution puts a large share of the charge on the protons of the adjacent water molecules. These protons may contribute to the formation of a molecular orbital for the excited electron. A similar model was presented for metal-ammonia solutions.^{20–22} The binding energy of such an orbital should be dependent on the number of the participating protons, being smaller the smaller this number is. Impoverishment of the solvation layer thus will bring about a rise in the energy of the excited state, *i.e.*, an increase in $h\nu$. The main difficulty encountered by this model is the fact that the spectrum of I⁻ in non-protonic solvents (*e.g.*, CH₃CN) does not differ essentially from that in water; both spectra have the same intensities.²³

Conclusion

Though the results indicate a close relation between the state of solvation of the light absorbing ion and the energy of the transitions involved, the exact relation still is obscure. In our opinion the polarization binding energy in the ground state is more strongly affected by changing the environment than the much smaller binding energy in the excited state. The approximations involved in the continuous medium model are too gross for accurately calculating minor effects on the spectra, but this model appears to be helpful for semi-quantitative purposes as was shown in the case of temperature effects²⁴ and even in the calculation of intensities.²³ In order to test the applicability of this model to the present problem we need more experimental data on the partial molar volumes in mixtures of electrolytes. In particular, it is important to check if in concentrated electrolyte solution the contraction of the cavity is a general phenomena and whether this contraction displays the specificity observed spectroscopically. It also is necessary to examine more thoroughly ionic effects on other spectra presumably due to C.T.T.S., *e.g.*, that of Br⁻ and OH⁻, so as to prove that the regularities observed in the case of I⁻ are

(18) R. L. Platzman and J. Franck, "Farkas Memorial Volume," Weizmann Press, Jerusalem, 1952, p. 21; *Z. Physik*, **138**, 411 (1954).

(19) G. Stein and A. Treinin, *Trans. Faraday Soc.*, **55**, 1086 (1959).

(20) J. Kaplan and C. Kittel, *J. Chem. Phys.*, **21**, 1429 (1953).

(21) E. Becker, R. H. Lindquist and B. J. Alder, *ibid.*, **25**, 917 (1956).

(22) G. W. A. Fowlers, W. R. McGregor and M. C. R. Symons, *J. Chem. Soc.*, 3329 (1957).

(23) J. Jortner and A. Treinin, to be published.

(24) G. Stein and A. Treinin, *Trans. Faraday Soc.*, **55**, 1091 (1959).

(13) H. E. Wirth, *J. Am. Chem. Soc.*, **59**, 2549 (1937); **62**, 1128 (1940); **72**, 5292 (1950).

(14) L. G. Hepler, *J. Phys. Chem.*, **61**, 1426 (1957).

(15) J. Jortner, *J. Chem. Phys.*, **30**, 839 (1959).

(16) J. Jortner and A. Treinin, unpublished results.

(17) R. E. Gibson, *J. Am. Chem. Soc.*, **57**, 284 (1935).

indeed characteristic for this type of electronic transition. This also may lead to an unequivocal

criterion for the identification of C.T.T.S. spectra. Such work is being carried out in our Department.

THE MECHANISM OF CHEMISORPTION: CARBON MONOXIDE AND CARBON DIOXIDE ON NICKEL

BY I. E. DEN BESTEN, P. G. FOX, AND P. W. SELWOOD

Chemical Laboratory of Northwestern University, Evanston, Ill.

Received September 11, 1961

Magnetization-volume isotherms on nickel-silica have been obtained for carbon monoxide and carbon dioxide by the low frequency a.c. permeameter method. The mode of bonding of carbon monoxide is dependent on nickel particle size and on surface coverage, in qualitative agreement with the infrared absorption studies by Yates and Garland. The magnetic data suggest linear or bridged bonding at low coverages, depending on nickel particle size, and bridged bonding to nickel atoms already bonded to at least one carbon monoxide molecule at higher coverages. Most of the high-coverage carbon monoxide may be desorbed as such, but the low coverage carbon monoxide may not be desorbed without disproportionation. Carbon dioxide is chemisorbed on nickel. There appear to be rather more than two bonds formed for every molecule adsorbed, but the maximum volume which may be chemisorbed at room temperature is only about one-eighth the volume of hydrogen which may be chemisorbed on the same surface.

Introduction

The purpose of this work was to extend to carbon monoxide and carbon dioxide the method of magnetization-volume isotherms previously applied to hydrogen,¹ ethylene,² oxygen,³ benzene⁴ and other adsorbates. The theory of the method already has been described.⁵

Experimental

All magnetic measurements were made on the low frequency a.c. permeameter previously described.¹ The adsorbent was either Universal Oil Products (UOP) nickel-kieselguhr hydrogenation catalyst containing about 52% nickel, or a coprecipitated nickel-silica containing about 30% nickel and prepared as described by Van Eyk Van Voorthuisjen and Franzen,⁶ and designated by them CLA 5421. Both of these catalysts had been used extensively in this Laboratory in previous investigations. The samples were reduced in flowing purified hydrogen for 15 to 24 hr. at 350–370°, and then were evacuated at the same temperature for 3 to 4 hr., and cooled *in vacuo*. Commercial tank carbon monoxide was purified by passage over hot glass beads and then through a Dry Ice trap. Tank carbon dioxide was found to be sufficiently pure for the purposes of this work and was used without further purification.

Gas analyses were made as required on a Consolidated Electroynamics Model 21-611 mass spectrometer.

Results

Carbon Monoxide.—Magnetization-volume isotherms for carbon monoxide and for hydrogen at –78° are shown in Fig. 1. The corresponding pressure-volume isotherms also are shown. It is well known that a nickel surface will sorb a volume of carbon monoxide considerably greater than the maximum volume of hydrogen which may be taken up by the same surface. This effect and the corresponding magnetic changes at 25° are shown in Fig. 2.

Figure 3 shows a magnetization-volume isotherm for carbon monoxide as compared with that of hydrogen at 24° on the coprecipitated catalyst.

Figure 4 gives similar data for a UOP catalyst sample which had been sintered at 600° for 2 hr. to increase the nickel particle size.

It will be noted that the magnetization-volume isotherms in Fig. 2–4 suffer a rather abrupt change of slope as the volume adsorbed exceeds that corresponding to surface saturation by hydrogen. It will be convenient to refer to that part of the isotherm prior to the change of slope as the "low-coverage" part, and to that beyond the change of slope as the "high-coverage" part.

At low coverage the fraction of carbon monoxide which may be removed by evacuation at room temperature did not exceed 5% of the whole. Removal of this fraction was accompanied by a corresponding slight increase of magnetization. At high coverage the situation was quite different. Evacuation at room temperature removes as such a substantial fraction of the carbon monoxide originally adsorbed beyond the change of slope. Raising the temperature during the evacuation ultimately will remove most of this carbon monoxide, although some of it comes off as carbon dioxide formed, presumably, by disproportionation. An example of these changes is shown in Table I.

TABLE I
VOLUMES DESORBABLE AFTER CHEMISORPTION OF CARBON MONOXIDE ON NICKEL AT 25°

Total volume of CO adsorbed	29.4 cc. per g. Ni
"High-coverage" volume	16.2
Volume desorbed at 25°	5.0 (95–98% CO)
Volume desorbed at 150°	9.5 (92–95% CO) ^a

^a More gas may be removed by raising the temperature to 360° but this is about 90% carbon dioxide.

If the evacuation is continued up to 350° it is possible to remove more carbon in the form of carbon dioxide, together with some hydrogen, and the magnetization as measured at room temperature rises to 90% of its initial value. But the various reactions which occur at elevated temperatures, including disproportionation, carbiding, thermal decomposition of carbide, and reaction with residual water in the silica, are related more to the bulk metal than to its surface.

- (1) P. W. Selwood, *J. Am. Chem. Soc.*, **78**, 3893 (1956).
- (2) P. W. Selwood, *ibid.*, **83**, 2853 (1961).
- (3) R. J. Leak and P. W. Selwood, *J. Phys. Chem.*, **64**, 1114 (1960).
- (4) J. A. Silvent and P. W. Selwood, *J. Am. Chem. Soc.*, **83**, 1033 (1961).
- (5) P. W. Selwood, "Actes du Deuxième Congrès International de Catalyse," Paris, 1960, p. 1795.
- (6) J. J. B. Van Eyk Van Voorthuisjen and P. Franzen, *Rec. trav. chim.*, **70**, 793 (1951).

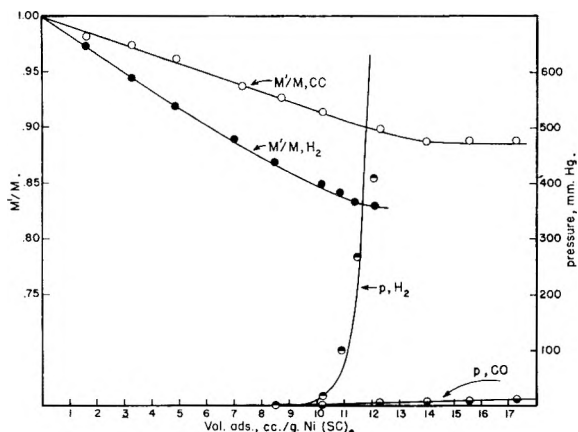


Fig. 1.—Magnetization-volume isotherms for carbon monoxide and for hydrogen at -78° on UOP nickel-kieselguhr. Pressure-volume isotherms also are shown.

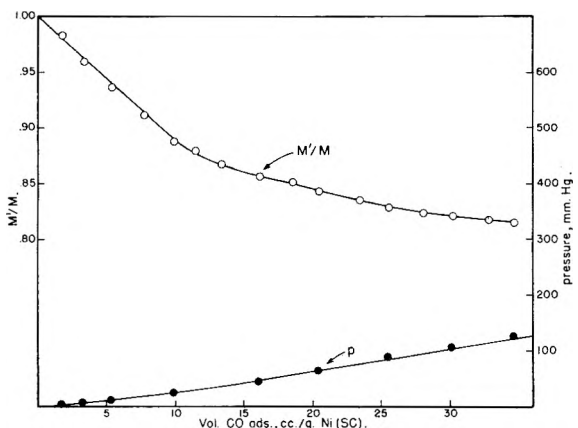


Fig. 2.—Isotherms over a more extended pressure range at 25° .

Carbon Dioxide.—A magnetization-volume isotherm for carbon dioxide on UOP catalyst at 25° is shown in Fig. 5. It may be expected that carbon dioxide would exhibit a fairly large van der Waal's adsorption on a high area ($\sim 175 \text{ m}^2/\text{g.}$, BET N_2) catalyst at room temperature. The magnetic data show that this is the case. If, after the pressure had reached 237 mm. (corresponding to the maximum volume shown in Fig. 5) the sample was evacuated, it was found that about 80% of the carbon dioxide could be desorbed as such without change of magnetization. The final residue was then approximately 2 cc. (sc) of chemisorbed carbon dioxide per g. of Ni and this caused a 6.0% loss of magnetization. This is moderately larger than the fractional loss caused by the same volume of hydrogen. It will be noted that the maximum volume of carbon dioxide which may be chemisorbed on nickel under these conditions is only about one-eighth of the volume of hydrogen which may be chemisorbed.⁷

Discussion of Results

There have been numerous suggestions concerning the mechanism of carbon monoxide chemisorption on nickel. Some of the earlier work is reviewed by Gundry and Tompkins.⁸ The work most nearly

(7) This result is confirmed by heats of adsorption studies made by Trapnell. (Personal communication from B. M. W. Trapnell.)

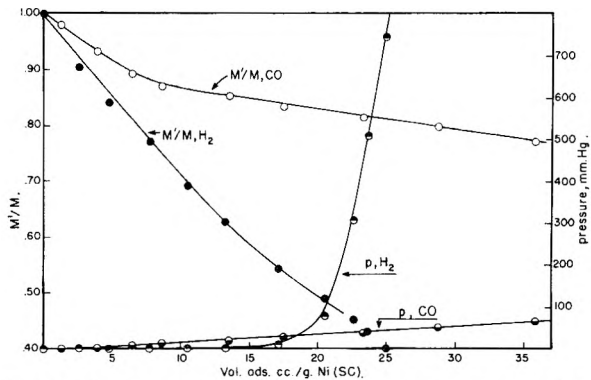


Fig. 3.—Isotherms on a coprecipitated nickel-silica at 24° .

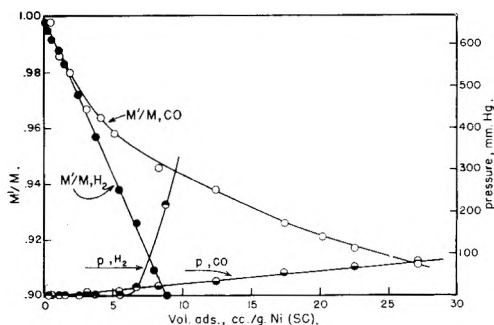


Fig. 4.—Isotherms on a sintered UOP nickel-kieselguhr at 24° .

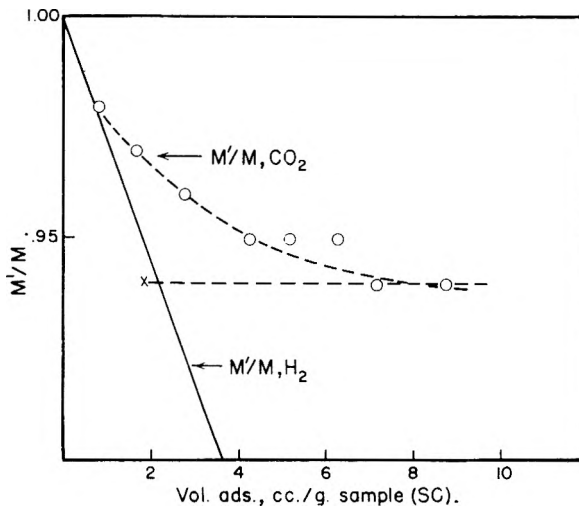
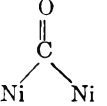
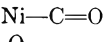
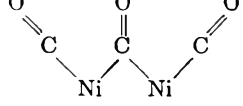


Fig. 5.—Magnetization-volume isotherm for carbon dioxide at 25° on UOP nickel-kieselguhr.

related to that described here is the recent paper of Yates and Garland,⁹ who observed the infrared absorption of carbon monoxide adsorbed on alumina-supported nickel and, in part, on silica-supported nickel. Yates and Garland identified several bands as probably being associated with the structures shown below, and being formed on nickel crystallites of several sizes, the largest being called "crystalline" and estimated by X-ray line width broadening as being 38 Å. in diameter.

Yates and Garland show that adsorption on crystalline sites occurs at very low pressures, adsorption on semi-crystalline and on dispersed sites

(8) P. M. Gundry and F. C. Tompkins, *Quart. Revs.*, **14**, 257 (1960).
 (9) J. T. Yates and C. W. Garland, *J. Phys. Chem.*, **65**, 617 (1961).

Band	Wave number, cm. ⁻¹	Structure	Kind of Ni	Adsorption type
A	1915		cryst.	very strong
C	2035		cryst.	very strong
B	1963		cryst.	very strong
D	2057	Ni—C=O	semi-cryst.	mod. strong
E	2082	Ni—C=O	dispersed	weak

occurs at higher pressures and this carbon monoxide is weakly bonded. The tentative structure assigned to band B is the most interesting for our present purposes. Band B forms on samples containing higher concentrations of nickel, at carbon monoxide pressures of several millimeters, and after bands A and C have been formed. The conclusions then are that the mechanism of chemisorption is dependent on particle size, that the mechanism is pressure-dependent (and hence dependent on surface coverage) and that there is evidence for a bridged mode of adsorption forming between nickel atoms which already are involved in the linear mode (bands C, D or E).

The magnetic data presented in this paper show that the mechanism of chemisorption indeed is dependent on nickel particle size and on surface coverage. On the UOP sample at -78° and on the coprecipitated sample at room temperature (with nickel particle diameters of ~ 42 and ~ 25 Å, respectively)¹⁰ the initial slope of the magnetization-volume isotherm is almost exactly half that shown by molecular hydrogen. This shows that the carbon monoxide molecule is, under these conditions, attached to one, and only one, nickel atom. It appears from this that the mode of adsorption is linear, corresponding to the Yates and Garland band D, or perhaps to C. Over this region the adsorption bond must be fairly strong because little carbon monoxide may be evacuated at room temperature.

If surface coverage is increased the magnetization-volume isotherm changes slope rather abruptly. The slope becomes much more nearly parallel to the volume axis and shows that each carbon monoxide molecule is attached on the average to about one-sixth of a nickel atom. But it will be noted that the formation of a bridged system (band B) on two nickel atoms already involved in a linear mode (bands C, D or E) would cause no further loss of magnetization. A trifling continued linear adsorption on less accessible sites would account for the slope of the isotherm in this region being slightly greater than zero.

A further correlation with the Yates and Garland view is found in Fig. 4. The sintered UOP sample contains nickel particles of about 64 Å. diameter,¹⁰ and while these are at the upper limit of applicability for the low frequency a.c. permeameter method the results apparently show that each carbon monoxide molecule at low coverage is involved with two nickel atoms. This result is

consistent with the Yates and Garland interpretation of bridged molecules (band A) on "crystal-line" nickel at low coverage and linear molecules (band D) at higher coverage.

If in connection with the above considerations we recall that the ease with which carbon monoxide may be desorbed is markedly greater at the higher surface coverages, then it appears that carbon monoxide is most readily desorbed from a nickel atom which is attached to more than one such molecule. On the other hand, desorption from nickel atoms attached to only one carbon monoxide molecule is not only difficult but likely to be attended by disproportionation. It might be thought that the carbon dioxide formed by disproportionation would be chemisorbed and then would contribute to the change of magnetization. While this doubtless is true it may be seen from Fig. 5 that the volume of carbon dioxide chemisorbed is quite small in comparison with the volumes of carbon monoxide with which we are concerned.

The conclusions which may be reached from the magnetic data alone are: (1) The initial stages of carbon monoxide chemisorption may be linear or bridged and this depends to a degree on the nickel particle size. (2) At higher surface coverages there is an abrupt change in the mode of adsorption. This change is consistent with the view that carbon monoxide may be added to nickel atoms which already are involved with at least one carbon monoxide molecule. (3) Desorption of carbon monoxide as such is readily observed at high coverages where, presumably, nickel atoms are attached to two or more molecules. (4) Desorption at low coverages, which involves disproportionation, is presumably from nickel atoms attached to only one carbon monoxide molecule.

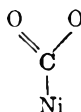
It may be thought that nickel tetracarbonyl formation at the higher pressures of carbon monoxide would be a significant complicating factor, but the rate of formation at room temperature as reported by Yates and Garland seems too low to interfere seriously with the interpretations presented.

The conclusions reached with respect to carbon monoxide are in gratifying qualitative agreement with those of Yates and Garland. It is doubtful if quantitative agreement could be expected for such a complicated system unless magnetic and infrared measurements were made simultaneously on the same sample.

The chemisorption of carbon dioxide has, in contrast to that of carbon monoxide, received

(10) R. E. Dietz and P. W. Selwood, *J. Chem. Phys.*, **35**, 270 (1961).

comparatively little attention. Kokes and Emmett¹¹ have compared the ability of nickel to adsorb carbon dioxide at -78° before and after evacuation at room temperature. The results are interpreted to show that carbon dioxide is chemisorbed at -78° to the extent of 80% of a nitrogen monolayer. Eischens and Pliskin¹² have reported a strong infrared band at 6.4μ and a weaker one at 7.1μ for carbon dioxide adsorbed on nickel-silica at room temperature and a pressure of 1.2 mm. These bands are interpreted as being characteristic of the carboxylate ion, thus

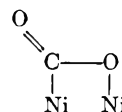


The magnetic data show that the volume of carbon dioxide chemisorbed on nickel-silica at room temperature is quite small, although comparable with the volume of ethane chemisorbed under identical conditions.² The loss of magnetization

(11) R. J. Kokes and P. H. Emmett, *J. Am. Chem. Soc.*, **82**, 1037 (1960).

(12) R. P. Eischens and W. A. Pliskin, *Advances in Catalysis*, **9**, 662 (1957).

is such as to suggest the involvement of at least two (and possibly more) nickel atoms per molecule of carbon dioxide. A possible mode of adsorption is then



although this is not in agreement with the available infrared results, and it does not account for the very low maximum coverage possible. The possibility that some of the magnetization loss could be due to polarization as observed for krypton is quite unlikely. The effect on the magnetization of a molecule of carbon dioxide is at least six times greater than that of a molecule of krypton. The precise mode of adsorption and the reason for the low coverage remain obscure.

Acknowledgment.—It is a pleasure to acknowledge support from the Office of Naval Research, the Petroleum Research Fund of the American Chemical Society, E. I. du Pont de Nemours and Company, and the Abbott Foundation in connection with this work.

FLASH-EXCITATION OF ACRIDINE ORANGE IN ACIDIC AND BASIC SOLVENTS¹

BY G. BLAUER AND H. LINSCHITZ

Department of Chemistry, Brandeis University, Waltham, Mass.

Received September 11, 1961

The flash-excitation of acridine orange in degassed basic (triethylamine) or acidic (acetic acid) solvents at room temperature leads in each case to two types of transient intermediates. The shorter-lived of these is attributed to triplet states on the basis of similarities between the initial flash spectrum and that observed in rigid solvents on cross-illumination. By analogy to previous flash work on fluorescein, the longer-lived products are assumed to be radicals.

The method of flash-excitation is being widely used, at present, to study photochemical processes in aromatic molecules.² In solutions of sensitizing dyes, metastable triplet states and free radicals have been observed, particularly by Lindqvist in his careful and thorough studies on fluorescein.³ In this paper we present absorption spectra of the initial excitation products of acridine orange (AO) in acidic and basic media, as well as evidence for the reversible formation of active intermediates with longer lifetimes. While the small absorbance changes associated with these latter substances limit their detailed study, the initial photo-products are well characterized and the general behavior of the system is shown to be consistent with that of other sensitizing dyes.

Experimental

3,6-Bisdimethyl-aminoacridine (acridine orange, Allied Chemical and Dye Corp.) was purified by precipitating the free base with dilute sodium hydroxide, dissolving in chloroform (A.R.), and chromatographing on alumina.⁴ The

main sharp band was collected, concentrated, and cooled to -20° . The resulting precipitate was filtered and dried in air followed by 2 hr. *in vacuo* at 70° (m.p. $181-182^{\circ}$).

Triethylamine (TEA) (Eastman-Kodak, white label) was fractionated over potassium hydroxide (boiling range 0.2°).

Other reagents were analytical grade.

Method.—The flash-excitation apparatus, general procedure and evaluation of data were similar to those described previously.⁵ It was found that the freezing, thawing, and evaporation operations used in degassing AO solutions resulted in a loss of absorption even when carried out in dim light. The reason for this effect (amounting to several per cent.) could not be ascertained. Accordingly, solutions were prepared by dissolving the dry dye in a side-arm of the sealed-off absorption cell assembly, after all degassing operations had been completed on the pure solvent. Concentrations were determined spectrophotometrically. Beer's law was verified for AO in TEA over the concentration range 1×10^{-3} to $8 \times 10^{-5} M$ (decadic molar extinction coefficient ϵ at $420 m\mu = 2.4 \times 10^4$) and in acetic acid over the range 4×10^{-7} to $2 \times 10^{-6} M$ (ϵ at $493 m\mu = 6.7 \times 10^4$).

Except for minor solvent shifts, the ground state spectrum of AO in acetic acid and in pyridine containing aqueous HCl was of the same type as that given for aqueous solutions of the dye at low pH (main peak in the visible range near $490 m\mu$). Similarly, the spectrum of AO in TEA, in pyridine and toluene containing some TEA, and in ethanol contain-

(1) This work was supported by a grant from the U. S. Atomic Energy Commission to Brandeis University (AT-(30-1)-2003).

(2) J. P. Simons, *Quart. Revs.* (London), **13**, 3 (1959).

(3) L. Lindqvist, *Arkiv Kemi*, **16**, 79 (1960).

(4) V. Zanker, *Z. physik. Chem.*, **199**, 225 (1952).

(5) H. Linschitz and K. Sarkanen, *J. Am. Chem. Soc.*, **80**, 4826 (1958).

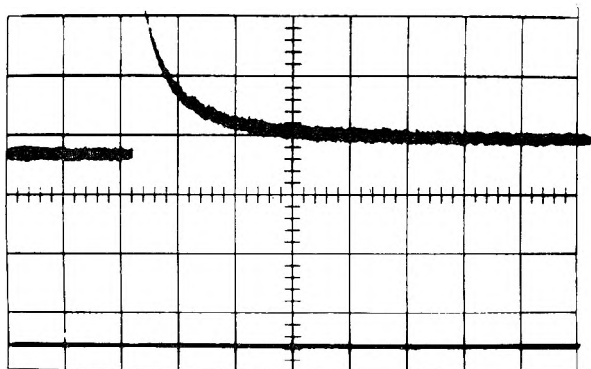


Fig. 1.—Oscillogram showing decay of excited AO in acetic acid: lower trace, base line including scattered light from flash; upper trace, transmission as function of time before and after flash; time scale, 0.5 msec. per grid; concn. = $6.3 \times 10^{-6} M$; $\lambda = 485 m\mu$.

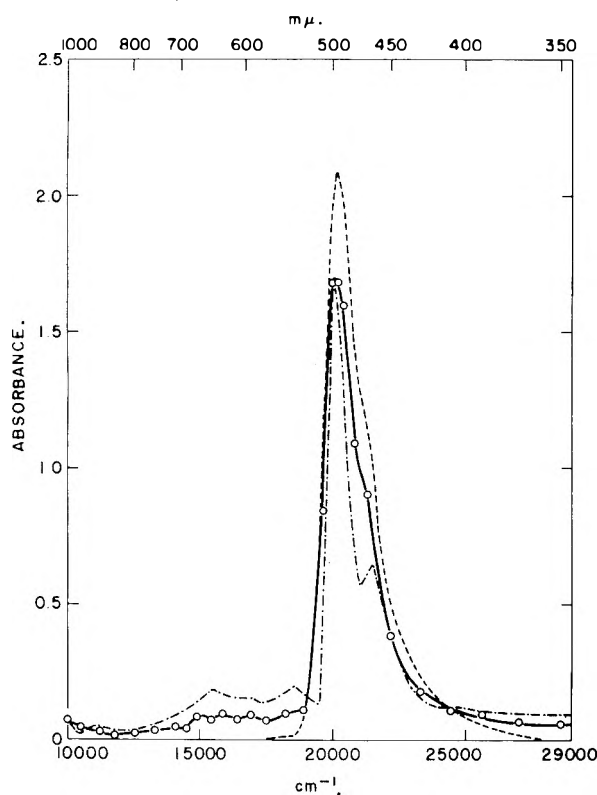


Fig. 2.—Absorption spectra of AO in acetic acid: dashed line, ground state spectrum; solid line, spectrum immediately after flashing; dot-dash line, AO spectrum on strong excitation in ether-alcohol 1:2 at -183° , redrawn to scale for $10^{-5} M$ AO from ref. 7; concn. = $6.3 \times 10^{-6} M$.

ing sodium methylate agreed with that of the neutral base at high pH^4 (main peak near $430 m\mu$).

All measurements reported were carried out at room temperature in cells whose optical path was 5 cm.

The stability of flash-excited AO in various solvents was checked by measurement of the ground state absorption immediately after flashing and also after storage in the dark. In TEA and acetic acid the absorption dropped by about 10% after about 100 excitations, with some recovery after several days. In ethanol and pyridine, however, flashing resulted in considerably larger irreversible changes. When cobaltous acetate hydrate (10^{-3} to $10^{-4} M$) was added to pyridine containing some TEA, the stability on flashing was increased considerably. (As has been reported previously,⁶ the long-lived state could not be observed and the short-lived state was quenched effectively under these conditions.)

(6) G. Blauer and H. Linschitz, *J. Chem. Phys.*, **33**, 937 (1960).

Results and Discussion

Short-Lived and Long-Lived Products.—Figure 1 gives a typical experimental result on AO in acetic acid, at $485 m\mu$, the spectral region where the most marked absorbance changes are found (corresponding to bleaching and recovery of the original dye peak). The oscillogram shows an initially rapid and then a relatively slow recovery of dye. Similar results are obtained in TEA, with the most marked absorbance changes around $410 m\mu$ (increased absorption). In other spectral regions, absorbance changes were much smaller and effects due to the long-lived intermediates could not be separated readily from the short-lived changes. Thus, in acetic acid, the long-lived product could only be observed unambiguously in the bleaching recovery curve near $490 m\mu$ and no clear-cut absorption peak was found for it. In TEA, a broad absorption band of the long-lived material could be detected near $420 m\mu$, in the region of the original dye peak. This is also close to the isosbestic point between the spectra of the short-lived species and original dye (see Fig. 3, below). Thus, in the region between 420 and $440 m\mu$, initial bleaching was observed in TEA, followed by slight increases in absorption and final slow recovery.

The Triplet State Spectra: Initial Products.—The absorption spectra of typical illuminated solutions of AO extrapolated back to the moment of initiation of the flash are given in Fig. 2 (acetic acid) and Fig. 3 (TEA). The interpretation of these spectra evidently depends on whether the long-lived product is formed sequentially from, or simultaneously with, the short-lived one. In the latter case, the relative yields of the two substances must be considered.

In the acetic acid solution, the *initial* recovery half-lives were constant, within experimental error, throughout the spectrum. For later interpretation, it is important to note that the region between 550 and $700 m\mu$, in particular, showed a rapid initial decay and this extrapolated absorption therefore is due primarily to the short-lived product. In this particular example and spectral region, the initial half-life was about $200 \mu\text{sec.}$ and could be distinguished readily from that of the long-lived product (about 7 msec.). Moreover, the amount of long-lived material formed by the flash is relatively small judging from the short- and long-lived bleaching at 493 or $485 m\mu$ (Fig. 1). We conclude, therefore, that this initial flash-spectrum is essentially that of the short-lived substance.

Figure 2 also shows the spectrum of the AO cation under intense cross-illumination, in rigid ether-alcohol solvent at low temperature.⁷ The absorption obtained under these conditions is almost certainly that of the triplet state.⁸ In Fig. 2, the main peak of the unconverted dye in this low-temperature spectrum is normalized to the same height as in the flash spectrum. Taking into account differences in solvent and temperature, the spectra of the two transients agree well in such features as the broad

(7) V. Zanker and E. Miethke, *Z. physik Chem.* (Frankfurt), **12**, 13 (1957).

(8) G. N. Lewis, D. Lipkin and T. T. Magel, *J. Am. Chem. Soc.*, **63**, 3005 (1941).

absorption between 550 and 700 $m\mu$, the isosbestic point at 410 and the minimum at 840 $m\mu$. There thus is little doubt that the short-lived substance of Fig. 1 and 2 is the acid form of the triplet state. It is of particular interest to establish this link between the flash-excitation and rigid solvent studies, in view of the striking discrepancy between flash and low-temperature cross-illumination spectra in the case of fluorescein.³

No low-temperature cross-illumination spectra of the neutral acridine orange base are available. By analogy with the situation in acetic acid it is suggested that the initial spectrum of Fig. 3 is due to the triplet state of the neutral base. While at first glance this spectrum appears to be quite different from that of the protonated dye triplet, particularly with regard to the peak at 410 $m\mu$, it is possible that the acid triplet also has a strong absorption in this region, overlapped by the original dye peak. The extent of dye conversion is uncertain.

Results in Other Solvents.—In pyridine containing TEA (0.007 M) or aqueous HCl (10^{-3} M) results were obtained similar to those in pure TEA or acetic acid, respectively, with regard both to the spectral changes and appearance of short- and long-lived states. Toluene containing TEA (0.01 M) and ethanol containing sodium methylate (0.02 M) acted similarly as basic solvents.

Kinetics.—In previous solution studies, we have found that three rate constants are required to account for the decay of triplet states directly to the ground state.⁵ If the decay occurs *via* further intermediates, additional constants are necessary. The low absorption of the transients makes our present data too incomplete for such analysis, beyond the preliminary rate constants already given.⁶ Further work involving longer cells and higher flash energies is in progress. In particular, it is necessary to establish the spectra of the long-lived products.

However, we wish to stress the general outlines of the phenomena which now appear. Lindqvist's work on fluorescein in aqueous solution has shown that the bimolecular decay processes of triplet

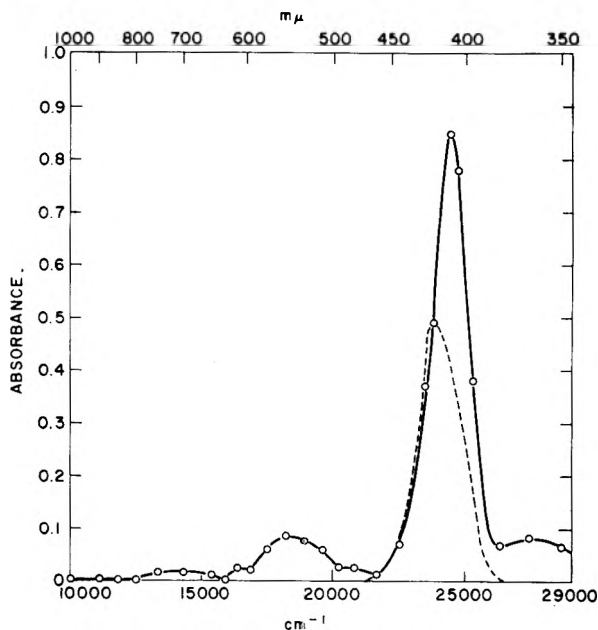


Fig. 3.—Absorption spectra of AO in TEA: dashed line, ground state spectrum; solid line, spectrum immediately after flashing; concn. is 4.2×10^{-6} M .

states may lead either directly to the ground state, or, *via* dismutation, to free radicals. Our results, within the limits imposed by experimental uncertainties, are consistent with this, although the possibility still remains that the long-lived intermediates in the AO case may be formed directly from excited singlets. In organic solvents the further possibility of oxidation-reduction reactions between triplet and solvent must, of course, be considered. However, the similarity within the two groups of reactions of AO in the various acidic and basic solvents suggests that, as in the fluorescein case, the radicals which we now identify with the long-lived products are formed by dismutation processes involving only dye molecules.

The excited molecule does not appear to undergo proton transfer reactions within the range of acidity or basicity covered by the two groups of solvents used here.

OXYGEN QUENCHING OF FLUORESCENCE IN SOLUTION: AN EXPERIMENTAL STUDY OF THE DIFFUSION PROCESS

BY WILLIAM R. WARE

Research Laboratory of Union Carbide Consumer Products Company, Division of Union Carbide Corporation, Parma 30, Ohio
Received September 16, 1961

Unusually large Stern-Volmer constants for the quenching of fluorescence of aromatic hydrocarbons by oxygen in solution are well known. The rate constants for the quenching reaction have been determined by fluorescence lifetime measurements for several hydrocarbons in a series of solvents covering a wide range of viscosities. The diffusion coefficient for oxygen in several solvents also was determined. The rate constants are consistent with a diffusion-controlled reaction when the unusually large diffusion coefficient for oxygen is taken into account.

Introduction

Large Stern-Volmer constants for the fluorescence quenching of polynuclear aromatic hydrocarbons by oxygen have been known for many

years.^{1,2} The Stern-Volmer constant is a product

(1) P. Fringsheim, "Fluorescence and Phosphorescence," Interscience Publishing Co., New York N. Y., 1949, p. 333.

(2) E. J. Bowen, *Trans. Faraday Soc.*, **50**, 97 (1954):

of the second-order rate constant for the quenching reaction and the fluorescence lifetime of the excited state in the absence of the quencher. Recent lifetime studies^{3,4} made with anthracene in benzene permit one to calculate the actual rate constant, and in this case the value is approximately three times as large as one would estimate from theory.⁵⁻⁸ However, such a calculation involves estimating the diffusion coefficient for oxygen in benzene, which makes the comparison very uncertain.

The mechanism for the reaction of oxygen with these hydrocarbons is very complex,^{9,10} but it seems reasonable, in view of the large rate constants, to consider separately the process involving the encounter of an excited molecule with oxygen and the subsequent steps which may include the formation of a moleoxide¹⁰ or a charge transfer complex,¹¹ and which occur probably with almost every encounter. The purpose of this paper is to examine the first of these two aspects of the process.

One would expect the reaction to be diffusion controlled, but the large rate constants raise many questions, since there are several possibilities: (a) the Stokes-Einstein relationship is not suitable for estimating diffusion coefficients from viscosity data; (b) the theory relating the rate constants to the diffusion coefficient may be inadequate; (c) oxygen interacts at a distance and the quenching is thus more efficient than ordinary diffusion-controlled reactions; (d) reasonably stable complexes are formed giving the appearance of large rate constants.

It appeared desirable to determine the rate constants for quenching by a dynamic method and to do this for several hydrocarbons in a series of solvents covering a wide range or properties. The variation of the fluorescence lifetime with quencher concentration is the most direct and satisfactory approach, since if a Stern-Volmer mechanism is followed the rate constant is directly obtained from a slope

$$1/\tau' = 1/\tau + k_q[\text{O}_2] \quad (1)$$

Lifetime studies also can be used in conjunction with fluorescence intensity measurements, since the lifetime of the excited state, which depends upon the solvent, is required to interpret the Stern-Volmer constants.

In addition it was considered desirable to measure the diffusion coefficient for oxygen in several solvents inasmuch as the polarographic studies of Jordan, Ackerman and Berger¹² in water-glycerol mixtures indicated large departures from the Stokes-Einstein relationship for oxygen.

(3) W. S. Metcalf, *J. Chem. Soc.*, 3729 (1960).

(4) W. R. Ware, *J. Am. Chem. Soc.*, **83**, 4374 (1961).

(5) F. C. Collins and G. E. Kimball, *J. Colloid Sci.*, **4**, 425 (1949).

(6) J. Q. Umberger and V. K. LaMer, *J. Am. Chem. Soc.*, **67**, 1099 (1945).

(7) B. Williamson and V. K. LaMer, *ibid.*, **70**, 717 (1948).

(8) A. Weller, *Z. physik. Chem. (Frankfurt)* **13**, 335 (1957).

(9) R. Livingston and S. Rao, *J. Phys. Chem.*, **63**, 794 (1959).

(10) R. Livingston, "Photochemistry in Liquid and Solid States," F. Daniels, Ed., John Wiley and Sons, Inc., New York, N. Y., 1960.

(11) R. S. Mulliken and H. Tsubomura, *J. Am. Chem. Soc.*, **82**, 5966 (1960).

(12) J. Jordan, E. Ackerman and R. L. Berger, *ibid.*, **78**, 2979 (1956).

Experimental

Fluorescence lifetimes were measured with a Rollefson type phase shift instrument. Details of its design and operation have been described elsewhere.^{4,13} This device makes use of the fact that the fluorescence excited by a sinusoidally modulated light source also will be modulated but with a phase shift ϕ such that

$$\tan \phi = 2\pi f / \Sigma(k_i + k_j C_j) \quad (2)$$

where f is the modulation frequency, the k_i 's and k_j 's are first- and second-order rate constants for the disappearance of the excited species, the k_j 's being multiplied by appropriate quencher concentrations C_j . Since low light intensities are used, the C_j 's are constant during a determination. The assumptions involved in this method are discussed elsewhere.^{4,13}

A modulation frequency of 5.2 Mc. was used and the useful range of the instrument started at about 1.8×10^{-9} sec. with an uncertainty of about 20%. At 4×10^{-9} sec. the uncertainty was about 4% and above this value it slowly decreased to 2%. Cells 0.8×0.8 cm.² were used and provision was made to saturate the solutions with either purified helium, dry air, or dry oxygen, and to allow equilibrium to be set up at atmospheric pressure. The lifetime for each hydrocarbon in each solvent was determined after purging with helium and after saturating with oxygen. In some cases air also was used to check the linearity between $1/\tau'$ and $[\text{O}_2]$ and the extrapolation to $1/\tau$. The second-order rate constants for quenching were determined from equation 1. Dilute solutions (10^{-4} to 10^{-5} M) of anthracene, 9,10-dichloroanthracene, 9,10-diphenylanthracene and perylene were used. Oxygen solubilities were determined under identical experimental conditions using a Perkin-Elmer gas chromatograph and probably were accurate to 10%. Agreements with literature values for oxygen solubility¹⁴ were quite good in most cases. Viscosities, where needed, were determined by conventional techniques.

Solvents for these experiments either were reagent grade or were purified by distillation and all were chromatographed on silica gel columns prior to use. Very pure samples of anthracene, perylene and 9,10-dichloroanthracene were available from previous work.⁴ A pure sample of diphenylanthracene was obtained by silica gel chromatography.

The measurement of diffusion coefficients, especially in solutions of low viscosity, is made very difficult by problems of mixing and convection. In addition, diffusion from a source of constant concentration provides one of the few sets of boundary conditions which leads to a simple relationship for linear diffusion. After considerable experimentation, the following apparatus was devised to measure the diffusion coefficient. A hollow vacuum stopcock 8 cm. high was used as the diffusion cell. The straight sidearm was replaced by a capillary having an i.d. of approximately 1.5 mm. which was about 15 cm. long and terminated in a small stopcock. The vacuum stopcock plug was modified by replacing the handle with gas inlet and outlet tubes. At the beginning of an experiment the capillary was filled with an oxygen-free solution containing 9,10-diphenylanthracene (10^{-4} M) as an oxygen indicator. The bulb at the bottom of the stopcock contained a small amount of the same solution saturated with oxygen by a stream of solvent-saturated oxygen slowly passing through. The boundary was set up by turning the stopcock until the hole (normally used to pump out the bulb) was coincident with the capillary and the interface thus exposed to the oxygen-solvent atmosphere of the hollow chamber. The assumption is made that the rate of equilibration at the interface exceeds by a considerable amount the rate of diffusion, and thus essentially at once there is set up a small element of the solution at the interface in the capillary that is saturated. The time required for this to take place is small compared to the diffusion process. Then linear diffusion takes place with the oxygen concentration C given by

$$C = C_0 \exp \left\{ \frac{-x^2}{4Dt} \right\} \quad (3)$$

(13) E. A. Bailey and G. K. Rollefson, *J. Chem. Phys.*, **21**, 1315 (1953).

(14) Gmelins "Handbuch der anorganischen Chemie," 8 Aufl. Verlag Chemie GMBH, 1958.

where x is the distance from the interface, t the time, and D the diffusion coefficient. The oxygen concentration is followed by making use of the fact that oxygen quenches the fluorescence of the added hydrocarbon. Thus

$$C = k_{sv}^{-1} (I_0/I - 1) \quad (4)$$

where k_{sv} is the Stern-Volmer constant and I_0/I the ratio of unquenched to quenched fluorescence intensity. Provision was made to illuminate the capillary with a narrow beam of light and to measure the fluorescence intensity at right angles with a suitable photomultiplier-filter arrangement. The entire stopcock arrangement was mounted with the capillary horizontal on a slider on an optical bench and could be moved past the collimated light beam to vary the distance from the interface at which time dependent data were taken. Compensation was made for variations in light intensity and corrections made for reflections from the capillary. The method was tested by checking the various aspects of equation 3. It is required that $\log (I_0/I - 1)$ vs. $1/t$ plots be linear, that the same value of D be obtained at several distances, and finally that the extrapolation point for the family of curves at various distances agree with the experimental value for the ordinant at infinite time, as determined by letting the oxygen-saturated solution into the capillary. The method was satisfactory and in fact with viscous solutions it even was possible to fill the hollow stopcock completely and obtain fair data, although mixing was a problem. No attempt was made to control the temperature other than to work in an air-conditioned room that was constant to about one degree. The values presented in Table I for a series of solvents at 25 to 26° are considered accurate to within 15%, which was adequate for the purposes of this work.

TABLE I
COMPARISON WITH DIFFUSION THEORY

Solvent	D_h $\times 10^4$ cm. ² sec. ⁻¹	D_0	k_q			
			(eq. 5)	(S-E) ^a	(exp.)	(exp.)
			Anthracene av. ^b $\times 10^{-11} M^{-1} \text{sec.}^{-1}$			
<i>n</i> -Octyl alcohol	0.4	1.6	0.9	0.1	1.7	1.7
Isobutyl alcohol	.7	2.4	1.4	.2	1.8	1.8
Isopropyl alcohol	.9	3.3	1.9	.3	2.2	2.5
Ethyl alcohol	1.4	3.9	2.4	.7	2.5	2.5
Benzene	2.2	5.7	3.5	1.2	3.1	3.0
<i>n</i> -Heptane	3.1	5.6	4.0	1.9	3.5	3.1
Acetone	3.7	9.0	5.7	2.3	3.9	3.9

^a Using Stokes-Einstein equation. ^b Average of anthracene, perylene and 9,10-diphenylanthracene.

Results and Discussion

The results obtained from lifetime measurements are given in Table II. In the case of anthracene the Stern-Volmer constants also were determined using conventional techniques in the solvents listed. Rate constants for the quenching reaction calculated from the Stern-Volmer constant using the measured lifetimes in the absence of quencher were on the average about 7% higher than those obtained directly (equation 1), which is within experimental error but is perhaps significant. This will be discussed below.

The diffusion coefficient for oxygen was measured in seven of the solvents covering the whole viscosity range. The results are given in Table I. Values listed for the diffusion coefficient of the hydrocarbon, D_h , were estimated from the data of Bowen and Metcalf.¹⁵ It can be seen that the diffusion coefficient D_0 is from 2.5 to 4 times greater than D_h and that it falls rather slowly with viscosity. While both the hydrocarbon solutes and oxygen fail to follow the Stokes-Einstein equation, $D = kT/6\pi\eta$, where η is the viscosity, the departures

are much greater in the case of oxygen, both with regard to the magnitude and to the behavior at high viscosity. It is thought that this is due in part to the combined effect of the relative molecular sizes of oxygen and the solvent plus the fact that oxygen has a lower mass than the solvent molecules and a much lower mass than large molecules which obey the Stokes-Einstein equation. It is interesting in this connection that nitrogen, hydrogen and oxygen have quite large diffusion coefficients in water¹⁶ compared to larger solute molecules. Also, the value for carbon dioxide¹⁶ of 3.2×10^{-5} cm.² sec.⁻¹ in ethyl alcohol at 17° compares favorably with our value of 4.0×10^{-5} for oxygen in the same solvent at 25°. Mention already has been made of the large departures from Stokes-Einstein behavior for oxygen in glycerol-water mixtures. Indeed, it would seem unreasonable to expect the Stokes-Einstein equation to hold where the solute molecules are much smaller than those of the solvent since the macroscopic viscosity should become an unsatisfactory parameter under these circumstances.

In Table I there also are listed values for the rate constants calculated from diffusion theory using

$$k_q = 4\pi N(D_h + D_0)(r_h + r_0)/1000 \quad (5)$$

For comparison, values calculated using the Stokes-Einstein equation rather than the measured diffusion coefficients have been included. In both cases a radius of 4 Å. was assumed for the hydrocarbon molecules while 2 Å. was taken for oxygen. A comparison also is given in Table I between the experimental values obtained for anthracene and an average of the values obtained for anthracene, perylene and diphenylanthracene. It is clear from these data that the rate constants and Stern-Volmer constants appeared large because of the gross underestimate of the diffusion coefficients which results from the application of the Stokes-Einstein relationship. In fact, considering the assumptions involved in the derivation of the diffusion equation the agreement between theory and experiment is rather good.

A transient term⁸ $k_q(r_h + r_0)/\sqrt{\tau D}$ frequently is added to equation 5. This term arises from the solution of Fick's equation when steady-state conditions are assumed at low solute concentrations. The lifetimes and diffusion coefficients encountered in this work lead to a correction of about 5 to 10% from this transient term.

A more interesting point concerns the implications of this transient term on the phase shift measurement. This involves introducing a time-dependent term⁸ into the equation

$$\frac{dA^*}{dt} = k \sin \omega t - \left(\frac{1}{\tau} + k_q [O_2] \right) A^* \quad (6)$$

in place of k_q . The solution is very involved, but it appears that to a first approximation the phase shift technique measures only the time-independent part of k_q when the rate constants and diffusion coefficients are of the magnitude found in this work. If this is correct, the fact that the Stern-Volmer

(15) E. J. Bowen and W. S. Metcalf, *Proc. Roy. Soc. (London)*, **206A**, 437 (1951).

(16) "International Critical Tables," McGraw-Hill Book Co., New York, N. Y., 1926.

TABLE II
 RATE CONSTANTS FOR OXYGEN QUENCHING

Solvent	η^{-1} $\times 10^{-4}$, poise ⁻¹	Anthracene		9,10-Dichloro- anthracene		9,10-Diphenyl- anthracene		Perylene		k_q^c av.
		τ^a	k_q^b	τ	k_q	τ	k_q	τ	k_q	
Acetone	3.11	5.7	3.9	7.7	1.6	9.7	3.8	6.1	4.1	3.9
<i>n</i> -Heptane	2.60	5.8	3.5	8.3	2.2	8.9	2.6	5.7	3.1	3.1
Toluene	1.77	4.2	3.1	10.4	1.7	8.1	2.8	5.5	3.4	3.1
Methyl alcohol	1.72	5.7	3.2	8.3	2.2	9.7	3.1	6.2	3.0	3.1
Benzene	1.64	4.2	3.1	1.0	2.4	8.2	2.8	5.2	3.2	3.0
<i>p</i> -Xylene	1.63	4.2	3.0	11.4	2.0	8.3	2.4	5.7	2.6	2.7
Ethyl alcohol	0.905	5.8	2.5	8.7	1.7	9.4	2.3	6.0	2.7	2.5
Dioxane	.835	4.8	2.3	10.6	1.4	8.9	1.9	5.9	2.0	2.1
Isopropyl alcohol	.445	6.0	2.2	8.6	1.6	9.2	2.2	6.1	2.6	2.5
Isobutyl alcohol	.264	5.5	1.8	9.2	1.5	9.0	1.7	6.0	1.9	1.8
<i>n</i> -Octyl alcohol	.130	5.6	1.7	10.1	1.1	8.8	1.6	5.8	1.7	1.7

^a $\times 10^9$ sec. ^b $\times 10^{-10}$ M⁻¹ sec.⁻¹. ^c Average of anthracene, 9,10-diphenylanthracene and perylene.

constant yields a slightly higher rate constant than is obtained with the phase shift technique is understandable, since the former would contain the transient term.

As can be seen from Table II, 9,10-dichloroanthracene gave lower rate constants than the other hydrocarbons. This is probably a manifestation of a lower probability for quenching once an encounter has taken place, compared to the other three hydrocarbons. A slightly lower diffusion coefficient for dichloroanthracene compared to the other hydrocarbons would not produce this effect, since the diffusion coefficient for oxygen is the more important quantity, especially at low viscosity.

The disagreement between the experimental results and eq. 5 at very low and very high viscosities is perhaps the result of a combination of two factors; (a) an incorrect estimate of the radii and (b) failure to take into account separation prior to reaction in the case of very rapid diffusion found in solutions of low viscosity.

Two other possible explanations were given in the Introduction for the apparently large rate constants for oxygen quenching. With regard to interaction at a distance, the essential condition for resonance transfer presumably is not present.¹⁷ Stable non-fluorescent complexes would influence the Stern-Volmer constant measurements but not the lifetime measurements.⁴ Since these agree to within a few per cent., this presumably is not an important factor in determining the magnitude of the rate constant.

Summary.—The rate constants for oxygen quenching of fluorescence of aromatic hydrocarbons in various solvents have been determined. Both the magnitude and the behavior with solvent viscosity are explained in terms of a diffusion-controlled reaction by making use of measured diffusion coefficients to compare theoretical with experimental values.

(17) Th. Förster, *Discussions Faraday Soc.*, **27**, 7 (1959).

PARTICLE-SIZE DISTRIBUTION DETERMINATION BY TURBIDIMETRY

BY R. J. GLEDHILL

Communication No. 2228 from the Kodak Research Laboratories, Eastman Kodak Company, Rochester, N. Y.

Received September 20, 1961

By the application of the Mie theory of light scattering to measurements of the specific turbidity and the dependence of turbidity on wave length, particle-size distributions on a weight basis have been determined for polydispersions of non-absorbing isotropic spheres in the micron to submicron range. The polydispersions studied fit a log-normal type of distribution. A method is described for constructing a graphical calibration grid for a system of known optical constants and known distributional form, from which the weight mean diameter and standard deviation of the distribution corresponding to observed turbidity measurements can be read directly. The particle-size distribution constants obtained by this turbidimetric method agree with those determined from electron-microscopic analysis within an average deviation of 1.3%.

Introduction

The light scattering of most colloidal suspensions of spheres in the micron- to submicron-size range can be treated adequately only on a basis of the general Mie theory. This is especially true where the refractive index of the particle differs significantly from that of the medium of suspension. Such treatments have been applied in the determination of particle size by light-scattering methods,^{1,2}

but these generally have been limited essentially to monodispersed systems. However, more recently Meehan and Beattie³ have used the Mie theory to

(1) R. M. Tabibian, W. Heller, and J. N. Epel, *J. Colloid Sci.*, **11**, 195 (1956).

(2) J. B. Bateman, E. J. Weneck, and D. C. Eshler, *ibid.*, **14**, 308 (1959).

(3) E. J. Meehan and W. H. Beattie, *J. Phys. Chem.*, **64**, 100 (1960).

estimate the dispersity of the particle-size distribution of silver bromide sols.

Our particular interest in particle-size analysis in this range was for the purpose of studying the Kodacolor dispersion. In this material, the photographic dye-forming coupler is suspended as small, colorless, spherical globules of micron to sub-micron sizes. The photographic properties of such systems depend to some extent upon the size of these particles. Since the major part of a system may include particles extending in size over a 3- to 10-fold range, a size distribution on a weight basis is the only adequate description. The refractive index of the particles, which is in the range of 1.50–1.65, differs sufficiently from that of the medium of suspension to necessitate a Mie-theory treatment.

This paper describes a turbidimetric method for determining the particle-size distribution of a polydispersion, applying the Mie theory. From two light-scattering parameters, the specific turbidity and the rate at which turbidity changes with wave length, a two-parameter distribution can be determined if the form of the distribution is known or can be assumed. This method is similar to that used by Meehan and Beattie,³ except that here the slope function of the turbidity-wave length dependence is used directly, and the application is to log-normal distributions on a weight basis.

Theory

Turbidity.—According to familiar definitions in the light-scattering theory of Mie,^{4,5} an expression for the specific turbidity of a dilute suspension of optically isotropic non-absorbing spheres of uniform size is

$$\frac{\tau}{c} = \frac{3\pi n}{100\lambda\alpha^3} \sum_{j=1}^{\infty} \frac{|a_j|^2 + |b_j|^2}{2j+1} \quad (1)$$

where τ is the turbidity of a suspension in which c is the percentage volume occupied by the particles, n is the refractive index of the medium of suspension to incident light of wave length λ (*in vacuo*), and a_j and b_j are complex functions of the size parameter α and the relative refractive index m . The size parameter is defined as

$$\alpha = \frac{\pi nd}{\lambda}$$

where d is the diameter of the particle. The relative refractive index is the ratio of the refractive index of the particle, n_p , to that of the medium

$$m = \frac{n_p}{n}$$

Since the attenuation of a light beam of intensity I by a non-absorbing light-scattering system is

$$-\frac{dI}{I dx} = \tau$$

the turbidity, in terms of the optical specular density D of a suspension of length x cm., is

$$\tau = 2.303 \frac{D}{x} \quad (2)$$

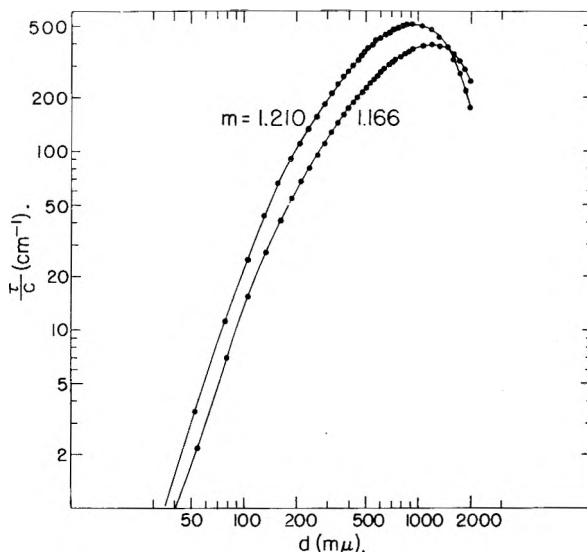


Fig. 1.—Specific turbidity for incident light of 5461 Å. and a medium of water at 25°.

Computed values of the specific turbidity are reported in tabular form for various values of the parameters m and α by Pangonis, Heller, and Jacobsen.^{4,6} These values are for the conditions that the incident light is equivalent to the Hg green line and the dispersing medium is water at 25°. Since the dispersions of this investigation were aqueous suspensions, it was convenient to use the same conditions, so that these computations could be applied directly. Hence, in any subsequent evaluations in this paper it will be assumed that λ is 5461 Å. and the medium is water at 25°. The range of α and m values covered is adequate for the purposes of this work, and the α -value intervals are sufficiently narrow to permit satisfactory interpolation. However, the interval between m values is so large and τ/c as a function of m is so strongly curved that, in order to facilitate interpolation between the tabulated values, recourse must be taken to a logarithmic form of equation 1.^{2,7}

$$\log \frac{\tau}{c} = \log \frac{n}{\lambda} + I_0(\alpha, m) + S_0(\alpha, m) \log(m-1) \quad (3)$$

Heller has shown that this function is fairly linear with $\log(m-1)$, except in the region where the specific turbidity has a maximum value.

Curves for τ/c as a function of particle diameter, d , are plotted in Fig. 1 on logarithmic scales for two interpolated values of the parameter m ($\lambda = 5461$ Å., $n = 1.3340$) which apply to the systems studied.

Turbidity-Wave Length Dependence.—It can be shown that equation 3 is also fairly linear with respect to $\log \lambda$ over the visual spectrum except in the region of maximum τ/c values. It is therefore a better form than equation 1 from which to derive the manner in which τ/c changes with wave length. The negative value of the partial derivative with respect to $\log \lambda$, at a constant value of the diameter d , is the logarithmic slope S (not to be

(4) W. Heller and W. J. Pangonis, *J. Chem. Phys.*, **26**, 498 (1957).

(5) H. C. Van de Hulst, "Light Scattering by Small Particles," John Wiley and Sons, Inc., New York, N. Y., 1957.

(6) W. J. Pangonis, W. Heller, and M. Jacobsen, "Tables of Scattering Functions for Spherical Particles," Wayne State University Press, Detroit, Michigan, 1957.

(7) W. Heller, *J. Chem. Phys.*, **26**, 920, 1258 (1957).

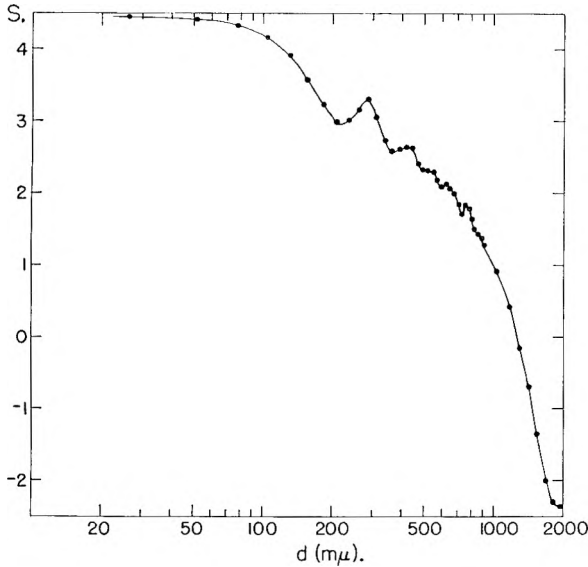


Fig. 2.—The logarithmic slope S for $m = 1.210$ and $d \log (m - 1)/d \log \lambda = -0.217$.

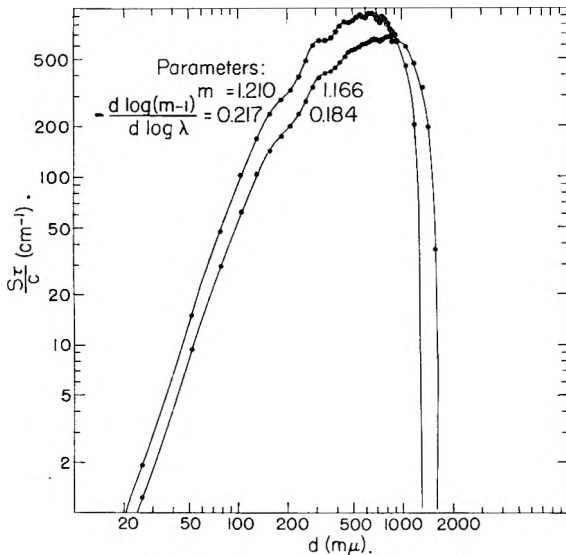


Fig. 3.—The slope function $S\tau/c$.

confused with S_0 of equation 3). Since, in equation 3, the turbidity, at a constant concentration c , is a function of the variables n/λ , α , and m , which are ultimately functions of λ and d for a given system

$$S = - \left(\frac{\partial \log \tau}{\partial \log \lambda} \right)_d = - \left(\frac{\partial \log \tau}{\partial \log n/\lambda} \right)_{\alpha, m} \frac{d \log n/\lambda}{d \log \lambda} - \left(\frac{\partial \log \tau}{\partial \log \alpha} \right)_{m, n/\lambda} \left(\frac{\partial \log \alpha}{\partial \log \lambda} \right)_d - \left(\frac{\partial \log \tau}{\partial \log (m - 1)} \right)_{\alpha, n/\lambda} \frac{d \log (m - 1)}{d \log \lambda}$$

From equation 3

$$\left(\frac{\partial \log \tau}{\partial \log n/\lambda} \right)_{\alpha, m} = 1$$

and, according to the definition of α

$$\left(\frac{\partial \log \alpha}{\partial \log \lambda} \right)_d = \frac{d \log n}{d \log \lambda} - 1$$

and

$$\left(\frac{\partial \log \tau}{\partial \log \alpha} \right)_{m, n/\lambda} = \left(\frac{\partial \log \tau}{\partial \log d} \right)_{m, n/\lambda}$$

Hence, by substitution, the logarithmic slope may be expressed in the form

$$S = \left[1 - \frac{d \log n}{d \log \lambda} \right] \left[1 + \left(\frac{\partial \log \tau}{\partial \log d} \right)_{m, n/\lambda} \right] - \left(\frac{\partial \log \tau}{\partial \log (m - 1)} \right)_{\alpha, n/\lambda} \frac{d \log (m - 1)}{d \log \lambda} \quad (4)$$

Equation 4 includes all the effects of the optical dispersions of the medium and the particles.

For values of the parameter m and the optical dispersion constants, $d \log (m - 1)/d \log \lambda$ and $d \log n/d \log \lambda$, equation 4 can be evaluated using the proper graphical plots of the tabulated values of τ/c to obtain the partial derivatives $\partial \log \tau / \partial \log (m - 1)$ and $\partial \log \tau / \partial \log d$. In Fig. 2, S is plotted as a function of the particle diameter for the optical constants indicated. The contribution of optical dispersion to the slope is evident at small values of the diameter where the slope is substantially greater than the limiting Rayleigh value of 4.

In some instances, a more useful form of the slope is the product of the logarithmic slope and the specific turbidity. Curves of $S\tau/c$ as a function

$$\frac{S\tau}{c} = - \left(\frac{\partial \tau/c}{\partial \ln \lambda} \right)_d$$

of the particle diameter are given in Fig. 3 for the same values of m given in Fig. 1 and the optical dispersion constants indicated. These curves are quite similar in shape to those for the specific turbidity. It is evident that the range over which the diameter is a single-valued function of the slope is greater for the quantity $S\tau/c$ than for S itself. Furthermore, the slope form $S\tau/c$ is more directly involved in the application to polydispersions.

Polydispersions.—So far this development has been for dispersions of uniform particle size. But it can be applied readily to polydispersions in a manner somewhat similar to that of Atherton and Peters.⁸ Their treatment, however, is based on the Debye light-scattering theory and makes use of the difference in weighting of average diameters derived approximately from the specific turbidity and its dependence on wave length. The Mie-theory evaluations of these turbidity functions can be applied more directly.

Since the turbidity of a polydispersion is the sum of all the contributions over the various particle-size classes

$$\tau = \sum c_i \left(\frac{\tau}{c} \right)_i$$

the specific turbidity of the total distribution expressed in integral form is

$$\left(\frac{\tau}{c} \right)_0 = \int_0^\infty \frac{\tau}{c} F(d) d(d)$$

where $F(d)$ is the normalized particle-size distribution function on a weight or volume basis— $F(d) d(d)$ is the mass or volume fraction of particles with diameters within the size range d to $d + d(d)$ —and $(\tau/c)_0$ is the specific turbidity of the total system. The corresponding slope function $(S\tau/c)_0$, obtained by partial differentiation with respect to $\ln \lambda$, is

(8) E. Atherton and R. H. Peters, *Brit. J. Appl. Phys.*, **4**, 344, 366 (1953).

$$\left(\frac{S\tau}{c}\right)_0 = - \int_0^\infty \left(\frac{\partial \tau/c}{\partial \ln \lambda}\right)_d F(d) d(d) = \int_0^\infty \frac{S\tau}{c} F(d) d(d)$$

The turbidity terms under the integral sign are known functions of the particle diameter and measurable optical constants of the system. Hence, these two simultaneous equations define a two-parameter distribution function, the form of which must be established from previous knowledge.

Since it is impractical to attempt a solution by direct integration, the integrals may be approximated by summations. In these equations the *i*th

$$\left(\frac{\tau}{c}\right)_0 = \sum_{i=1}^n \left(\frac{\tau}{c}\right)_i \int_{d_i-\Delta d}^{d_i} F(d) d(d) \quad (5)$$

$$\left(\frac{S\tau}{c}\right)_0 = \sum_{i=1}^n \left(\frac{S\tau}{c}\right)_i \int_{d_i-\Delta d}^{d_i} F(d) d(d) \quad (6)$$

turbidity terms are now average values over the interval Δd for each size-class *i*, in a total of *n* classes. Values for the turbidity terms as functions of diameter can be read directly from curves such as those of Fig. 1 and 3, and the integrals evaluated from appropriate tables. By adjusting the values of the two parameters of the distribution function until the summations agree with the corresponding observed values of $(\tau/c)_0$ and $(S\tau/c)_0$, the solution may be determined. Details of the method of solution for the case of a log-normal distribution will follow.

Experimental

Turbidimetry.—Turbidity measurements were made on a Beckman Model DU spectrophotometer using an attachment between the exit slit and the photometer head. The optics of this attachment are similar to those used by Lewis and Lothian.⁹

The monochromatic light beam diverging from the spectrophotometer exit slit S_1 is collimated by a 10-cm. focal length achromatic lens and, after passing through the sample cell, is focused by a similar lens to form an image of the first slit on the exit slit S_2 , behind which is located the photometer head. Standard Beckman 1-cm. cells are used in a standard cell holder and carriage. Apertures on either side of the cell help reduce stray light. Both slits are masked to a 5-mm. height. Slit S_1 is limited in practice to a maximum width of 0.2 mm., while the exit slit S_2 is fixed at a slightly larger width of 0.35 mm., to allow for slight displacements of the image caused by misalignment of the cell or by non-parallel or wedge-shaped cell windows.

The resolving power of this arrangement to specular transmission may be characterized by the half-angle of scattered light included in the specularly transmitted light beam. This half-angle is 0.11° in a horizontal plane and 2.9° in a vertical plane, equivalent to a solid angle of less than 2×10^{-4} steradians, which, according to Heller and Tabibian,¹⁰ should be sufficiently small to warrant reliable turbidity measurements. The adequacy of this arrangement is indicated by the absence of significant concentration-dependence of the specific turbidity and by the general agreement of the turbidimetric results on particle-size distribution with those obtained by electron microscopy.

The aqueous suspensions, 0.02–0.002% by volume, were adjusted in concentration to give specular densities in a range of 0.2–0.8 over the wave-length region 400–800 mμ. The values of specific turbidity calculated according to equation 2 seldom varied with concentration more than 1%; hence, the extrapolation to zero concentration is assumed to be reliable to 1%. All measurements were made at 25°.

The specific gravity of the particles, which is necessary

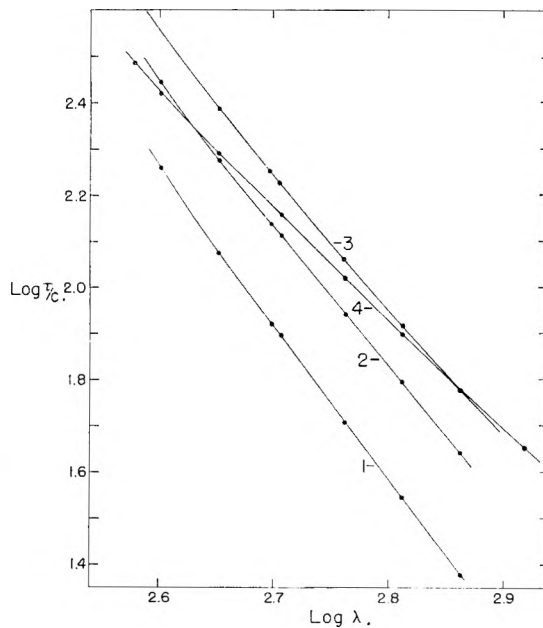


Fig. 4.—Logarithmic plot of specific turbidity vs. wave length for the dispersions of Table I.

for calculating the per cent. volume concentration of the dispersion, was determined on the bulk material by standard pycnometric procedures.

The slope S_0 was calculated from a logarithmic plot of the extrapolated specific turbidities vs. wave length, such as shown in Fig. 4. The slope values are reliable to 0.02 slope unit or about 0.7% for values in the range 2–4.

Optical Constants.—The refractive index and optical dispersion of the particles were determined for the materials in bulk using a hollow-prism spectrophotometer with mercury and hydrogen arc line sources. For the water medium, $d \log n/d \log \lambda = -0.0157$ ($\lambda = 5461 \text{ \AA.}, 25^\circ$).

Electron Microscopy.—As a basis for appraising the turbidimetric method, particle-size distributions also were obtained by electron-microscopic analysis. By usual methods of direct count and size measurement on electron micrographs of 10,000X magnification, weight percentage distributions were determined. Any flattening of the particles on the supporting substrate was detected with well-known metallic shadowing techniques, by sputtering with platinum–palladium at an 18° angle. Where flattening was significant, true diameters of the equivalent undistorted sphere were calculated from a comparison of shadow length with the observed diameter.

Results

The electron-microscopic analyses (see Fig. 6), indicate that a log-normal form on a weight basis fits quite adequately the particle-size distributions of all the systems studied. In this application, equations 5 and 6 assume the form

$$\left(\frac{\tau}{c}\right)_0 = \sum_{i=1}^n f_i \left(\frac{\tau}{c}\right)_i \quad (7)$$

$$\left(\frac{S\tau}{c}\right)_0 = \sum_{i=1}^n f_i \left(\frac{S\tau}{c}\right)_i \quad (8)$$

where

$$f_i = \frac{1}{\sqrt{2\pi}} \int_{d_i-\Delta d}^{d_i} e^{-1/2 t^2} dt$$

$$i = \frac{\log d - \log d_g}{\log \sigma}$$

d_g is the geometric weight mean diameter, and σ is the geometric standard deviation of the distribution.

(9) P. C. Lewis and G. F. Lothian, *Brit. J. Appl. Phys.*, Suppl. No. 3, 71 (1954).

(10) W. Heller and R. M. Tabibian, *J. Colloid Sci.*, 12, 25 (1957).

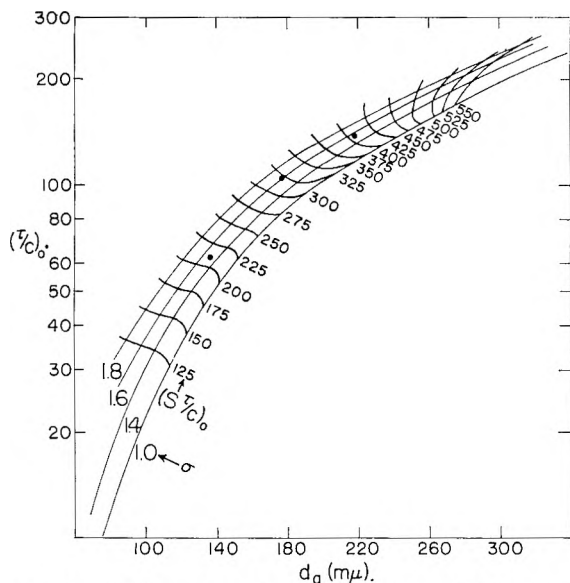


Fig. 5.—Calibration grid for $m = 1.210$ and $d \log(m - 1)/d \log \lambda = -0.217$; points are for dispersions 1-3 of Table I.

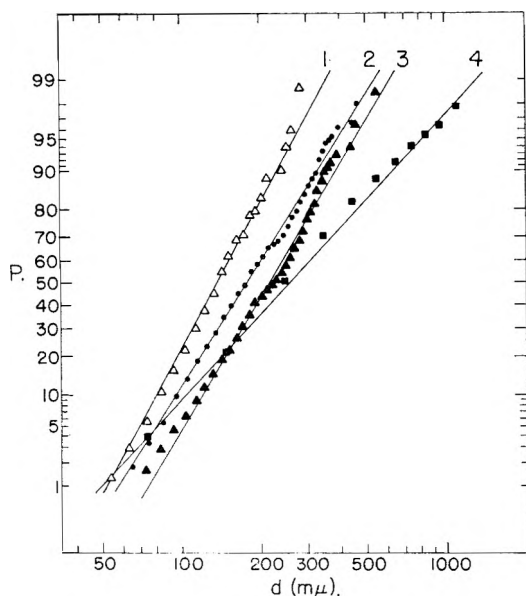


Fig. 6.—Cumulative weight per cent. distributions for dispersions of Table I: points from electron-microscopic analyses; solid lines from turbidimetry.

With the distribution function defined, the solution of these equations for the distribution constants can be approached directly by the following graphical method. For the optical constants of the system involved, $(\tau/c)_0$ is evaluated as a function of d_g for the parameter σ and again for $(S\tau/c)_0$ as a parameter. The two sets of curves are plotted as a network similar to Fig. 5. With the aid of such a calibration grid, approximate values of d_g and σ corresponding to observed values of $(\tau/c)_0$ and $(S\tau/c)_0$ can be read directly.

In Table I the observed turbidity values and optical constants of four dispersions are given. Approximate values of the distribution constants d_g and σ were obtained from the appropriate calibration grid. The points on the grid of Fig. 5 are

for the first three dispersions of the table. These approximate values of the distribution constants then were substituted into equations 7 and 8 and adjusted until the calculated turbidity values agreed precisely with the observed values. This calculation is demonstrated for dispersion No. 3 by the example in Table II. The turbidimetric values of d_g and σ are compared in Table III with those obtained from the electron-microscopic analyses, in which the number of particles sampled ranged over 800-1900. Dispersion No. 2 was a mixture (44.8:55.2 parts by volume) of dispersions 1 and 3. The average difference between the results of the two methods is 1.3%.

TABLE I

TURBIDIMETRIC DATA ON AQUEOUS DISPERSIONS

$t = 25^\circ$; $\lambda = 5461 \text{ \AA.}$; $n = 1.3340$; $d \log n/d \log \lambda = -0.0157$

Disp. no.	$(\tau/c)_0$	$(S)_0$	$(S\tau/c)_0$	n_p	m	$\frac{d \log(m - 1)}{d \log \lambda}$
1	62.4	3.36	210	1.6135	1.210	-0.217
2	105.2	3.06	322	1.6135	1.210	-0.217
3	138.2	2.93	405	1.6135	1.210	-0.217
4	121.5	2.46	299	1.5556	1.166	-0.184

TABLE II

CALCULATION OF $(\tau/c)_0$ AND $(S\tau/c)_0$ FROM SIZE-DISTRIBUTION CONSTANTS

$m = 1.210$; $d \log(m - 1)/d \log \lambda = -0.217$; $d_g = 216.4 \text{ m}\mu$; $\sigma = 1.577$

d_i (m μ) f_i	$f_i \times 10^2$	$(\frac{\tau}{c})_i$	$(\frac{S\tau}{c})_i$	$f_i (\frac{\tau}{c})_i$	$f_i (\frac{S\tau}{c})_i$
70	0.66	6.2	27	0.04	0.2
80	0.78	9.7	42	.08	0.3
90	1.27	14.0	60	.18	0.8
100	1.79	19.0	79	.34	1.4
110	2.36	24.9	103	.59	2.4
125	4.55	33.2	134	1.51	6.1
140	5.54	44.8	173	2.48	9.6
160	8.41	59.4	218	5.00	18.3
180	8.94	76.8	262	6.87	23.4
200	8.82	93.7	295	8.26	26.0
225	10.28	111.7	335	11.48	34.4
250	9.02	132.2	401	11.92	36.2
280	9.00	157.8	503	14.20	45.3
320	9.06	195.0	620	17.67	56.2
360	6.32	234.8	646	14.84	40.8
400	4.33	267.1	694	11.57	30.0
450	3.47	303.4	796	10.53	27.6
500	2.10	342.0	827	7.18	17.4
560	1.46	377.7	872	5.51	12.7
640	0.97	417.2	894	4.05	8.7
700	0.87	461.0	870	4.01	7.6
$\Sigma =$				138.3	405.4

The approximate linearity of the electron-microscopic data, plotted in Fig. 6 as cumulative weight per cent. on logarithmic-probability coordinates, justified the assignment of a log-normal distribution for the dispersions studied. The straight-line cumulative curves, as determined from the turbidimetric observations, are very close to the best linear representation of the microscopic data.

Discussion

It is apparent from Fig. 5 that the curves for the parameter $(S\tau/c)_0$ over the range of values 300-400 have a minimum. This is a consequence of

TABLE III
SIZE-DISTRIBUTION CONSTANTS DETERMINED BY ELECTRON
MICROSCOPY AND TURBIDIMETRY

Disp. no.	$d_g(m\mu)$			σ		
	EM	Turb.	% diff.	EM	Turb.	% diff.
1	138.6	137.2	-1.0	1.479	1.516	2.5
2	177.9	178.1	0.1	1.623	1.621	-0.1
3	217.3	216.4	-0.4	1.559	1.577	-1.2
4	248.7	257.5	3.5	1.982	2.014	1.6

TABLE IV
ESTIMATED ACCURACY OF TURBIDIMETRIC METHOD

Property measured	Reliability of measurement	Av. error in calcd. constants	
		d_g	σ
$\left(\frac{\tau}{c}\right)_0$	1.0%	1.0%	0.6%
$(S)_0$	0.7	1.4	2.6
n_D	0.5	0.4	0.3

the first ripple in the curve for the slope S , Fig. 2. In this region $(\tau/c)_0$ and $(S\tau/c)_0$ do not always uniquely define the system; two solutions may be theoretically possible. However, in practice, there was no ambiguity as to which solution applied. A cursory visual microscopic examination was sufficient to differentiate between two possible σ values. Actually, none of the dispersions examined had a σ value below 1.3. With this limitation the calibration grid is single-valued. The method

could be made more rigorous by including a measure of the rate of change of the slope S with wave length, and so define the system more completely. This, however, was found to be unnecessary in the particle-size range of the dispersions studied.

The accuracy with which the distribution constants can be determined depends upon the region of the calibration grid in which the dispersion falls. In Table IV are listed the average errors which can be expected for the probable reliability of the measurements.

The diameters d_7 and d_8 corresponding to the observed values of $(\tau/c)_0$ and $(S)_0$, as read directly from curves such as in Figs. 1-3, may differ appreciably from the true d_g . Depending upon the magnitude of the dispersity and the region of the size spectrum, this discrepancy may be as large as 20-30%. By inspection of a calibration grid such as Fig. 5, it is obvious that the relative magnitudes of d_g , d_7 and d_8 vary, even with respect to order. Hence, a simple consideration of d_7 and d_8 alone, without regard for the region of the size spectrum involved, can give only an approximate indication of the average diameter and essentially no information about dispersity.

Acknowledgment.—The author wishes to thank Mr. C. F. Oster, of the Eastman Kodak Research Laboratories, for the electron micrographs of the dispersions studied.

OXYGEN DIFFUSION AND REACTION DURING γ -IRRADIATION OF POLYETHYLENE

By R. C. GIBERSON

Nonmetallic Materials Devp. Operation, Hanford Atomic Products Operation, General Electric Co., Richland, Washington

Received September 21, 1961

A model for the diffusion controlled reaction of oxygen with polyethylene in an irradiation environment is presented. Experimental and calculated results on carbonyl formation in thin films (0.0020 to 0.0400 cm.) agree to $\pm 5\%$ for an exposure range of 5 to 100×10^6 r. The effect of dose rate, from 1 to 5×10^6 r./hr., on the rate of carbonyl formation is studied and evaluated in terms of the proposed model.

Introduction

Polyethylene, being one of the simplest of polymers, has been the subject of a large number of investigations. Rugg and co-workers,^{1,2} have conducted infrared studies of the structure and of oxidation of polyethylene. Several workers have reported on the radiation chemistry of polyethylene.³⁻⁶ Matsuo and Dole⁷ have published results on oxidation effects in irradiated polyethylene.

In the present paper a theory is developed based on diffusion kinetics which relates the total oxidation under irradiation to the total dose, the dose rate, and the sample thickness. The theory is compared with experimental observations.

Experimental

The polyethylene used as thin films in this study was Alathon 3, NC-10.⁸ This material is characterized as a high pressure, low density (0.92 g./cm.³) polyethylene with approximate crystallinity of 60%.

To determine the oxidation distribution in thicker pieces, Agilene (0.90 g./cm.³), a polyethylene from American Agilene Corporation, in half-inch thick blocks was used. The physical characteristics of the Agilene were similar to those of the Alathon.

The cobalt-60 irradiation facility used in this work has been described elsewhere.⁵ Dose rates of 1.34×10^6 , 1.49×10^6 , and 4.84×10^6 roentgens/hr. (r./hr.) were available during the course of this work.

The total oxidation occurring in the samples was followed by measuring the increase in carbonyl absorption band (~ 1720 cm.⁻¹) with a Perkin-Elmer Model 112 infrared spectrometer. The thin films were measured by placing them directly in the light path. The solid blocks were

(1) F. M. Rugg, *et al.*, *J. Polymer Sci.*, **11**, 1 (1953).

(2) F. M. Rugg, *et al.*, *ibid.*, **13**, 535 (1954).

(3) M. Dole, *et al.*, *J. Am. Chem. Soc.*, **76**, 430 (1954).

(4) A. A. Miller, *et al.*, *J. Phys. Chem.*, **60**, 599 (1956).

(5) A. Charlesby, *Proc. Roy. Soc. (London)*, **A215**, 187 (1952).

(6) K. H. Sun, *Modern Plastics*, **32**, 141 (1954).

(7) H. Matsuo and M. Dole, *J. Phys. Chem.*, **63**, 837 (1959).

(8) Material supplied by W. W. Spohn of the Polychemicals Department of E. I. du Pont de Nemours and Company, Inc., in sample thicknesses of approximately 2, 7, 15, 25, and 40×10^{-3} cm.

(9) R. Harrington and R. C. Giberson, *Modern Plastics*, **36**, 199 317 (1958).

sliced by a microtome, the individual slices being analyzed for carbonyl.

Results

The experimental results are given in Tables I-III. Table I gives the carbonyl optical density, A , in terms of total exposure and sample thickness for a dose rate of 1.49×10^6 r./hr. Table II presents the optical densities for various sample thicknesses at a total dose of 1×10^8 r. for the three different dose rates used. Table III presents results on sliced samples of oxidized Agilene. A variety of total exposures and dose rates is given.

TABLE I
OPTICAL DENSITIES OF CARBONYL IN ALATHON 3, NC-10 AT
VARIOUS TOTAL EXPOSURES
Dose rate, 1.49×10^6 r./hr.

Total dose, r.	Thickness, cm.	$A =$ optical density at ~ 1720 cm. $^{-1}$
5.7×10^7	0.0020	..
	.0064	0.04
	.0163	.06
	.0234	.07
	.0376	.07
11×10^7	.0020	..
	.0071	.09
	.0173	.14
	.0269	.13
	.0406	.17
57×10^7	.0018	.20
	.0069	.38
	.0142	.72
	.0259	.74
	.0399	.82
113×10^7	.0025	.40
	.0064	.83
	.0147	1.25
	.0198	1.35
	.0394	1.50

TABLE II
OPTICAL DENSITIES OF CARBONYL IN ALATHON 3, NC-10 AT
VARIOUS DOSE RATES
Total dose, 1×10^8 r.

Dose rate, r./hr.	L , cm.	Optical density at ~ 1720 cm. $^{-1}$		% Deviation
		Expt.	Calcd.	
1.34×10^6	0.0020	0.297	0.298	-0.3
	.0074	0.834	0.830	0.5
	.0152	1.175	1.198	-2.0
	.0201	1.344	1.304	3.0
	.0406	1.415	1.434	-1.3
1.49×10^6	.0025	0.358	0.355	0.8
	.0064	0.735	0.729	0.8
	.0147	1.106	1.112	-0.5
	.0198	1.195	1.212	-1.4
	.0394	1.327	1.313	1.1
4.84×10^6	.0023	0.299	0.299	0.0
	.0069	.677	.644	4.9
	.0152	.846	.871	-3.0
	.0269	.915	.937	-2.4
	.0403	.950	.947	0.3

* 1.13×10^8 r. data corrected to a total dose of 1×10^8 .

The general effect of sample thickness and total radiation exposure can be seen in Fig. 1, which

TABLE III
OPTICAL DENSITIES OF CARBONYL IN SLICED SAMPLES OF
IRRADIATED AGILENE

Total dose, r.	Dose rate, r./hr.	Slice no.	Thickness, cm.	Optical density at ~ 1720 cm. $^{-1}$	
1×10^8	7.2×10^6	1	0.0102	0.500	
		2	.0018	.028	
		3	.0051	.050	
		4	.0030	.025	
		5	.0046	.031	
1×10^8	1.49×10^6	1	.0055	.369	
		2	.0023	.168	
		3	.0028	.077	
		4	.0023	.029	
		1	.0147	.719	
	1.32×10^8	1.49×10^6	2	.0074	.086
			3	.0080	.039
			4	.0078	.044
			1	.0131	.623
			2	.0027	.119
3	.0036	.032			
1	.0036	.496			
2	.0017	.146			
3	.0021	.076			
1	.0036	.483			
2	.0017	.221			
3	.0021	.074			

plots the data of Table I in the form A/r vs. sample thickness, L . The general shape of the A/r vs. L curve illustrates the effect of sample thickness on the carbonyl absorption. The observation that a single curve is obtained in Fig. 1, i.e., no consistent variation with total dose, means that carbonyl formation increases linearly with total exposure in the range of thickness investigated. This linear increase is important in the theory to be presented.

The effect of dose rate on the reaction is shown in Fig. 2, which plots A vs. L from Table II. It will be noted that in thin samples the total oxidation occurring is independent of the dose rate whereas in thicker films more oxidation occurs at the lower dose rates.

Figure 3 illustrates the effect of oxygen accessibility to the total oxidation occurring. Again the plot is A vs. L , the top curve being determined from thin samples, the lower curve being obtained by slicing samples from a block of irradiated polyethylene. Total exposure and dose rate were the same for all samples. In the thin samples, for equivalent total thickness, it is observed that more oxidation occurs than in the sample sliced from a block.

Theoretical

A radiation damage model will be developed from which an equation relating carbonyl increase to total dose and sample thickness will be derived. The model will be based on certain observable conditions pertaining to this process, one of the most important being the linear increase in carbonyl concentration with total exposure. The model is intended to describe the process wherein a relatively small fraction of the material is converted

to carbonyl. The ratio of CO groups to CH₂ groups at the highest total exposure ranged from 1:30 to 1:130. Extensions of the theory give the effect of dose rate on the reaction.

Radiation Damage Model.—The following relationship has been found for the oxidation of polyethylene in a radiation field (see Fig. 1)

$$A = gt \tag{1}$$

where

- A = optical density of carbonyl (measured from the infrared absorption peak at ~ 1720 cm.⁻¹)
- g = proportionality constant depending on sample thickness, L, and the dose rate
- t = time of irradiation

Equation 1 can be written in terms of B, the carbonyl groups per square centimeter if Beer's law is obeyed. A test of Beer's law was made in the present work and it was found to hold satisfactorily. Thus

$$B = \frac{AN^*}{KM} = k''t \tag{2}$$

where

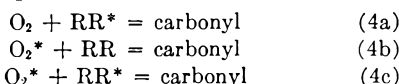
- N* = Avogadro's number
- M = molecular weight of carbonyl
- K = specific adsorption coefficient in cm.²/g.
- k'' = a constant for a given L

We also may write

$$\frac{dB}{dt} = \int_0^L \frac{dc}{dt} dx \tag{3}$$

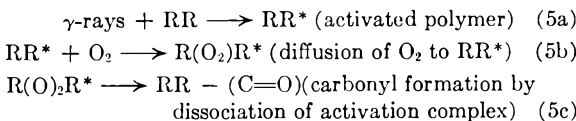
where c is the concentration of carbonyl groups and is a function of x, the distance into the sample. In order to solve (3), dc/dt as a function of x must be determined.

The reaction is a radiation-activated process. Since either the oxygen or polymer, RR, can be activated,¹⁰ the possible reactions become:



where the asterisk denotes an activated species. In the present case, none of the three can be completely ruled out; however, it is easily demonstrated that the following treatment in which the process is assumed to occur by (4a) applies equally well to the other reactions and will produce the same result.

Consider the set of reactions



The following assumptions concerning the reaction mechanism are made: (1) Active sites in the polymer are created by the ionizing radiation. The sites are homogeneously distributed and the number available at any given time during the irradiation is essentially constant. (2) The formation of carbonyl depends on the diffusion-limited reaction of oxygen with an active site in the polymer.¹¹ We thus assume then that (5b) is the slow

(10) RR is the polyethylene polymer. RR* represents those active sites, probably free radicals, which are created in the polymer, where the oxygen can react.

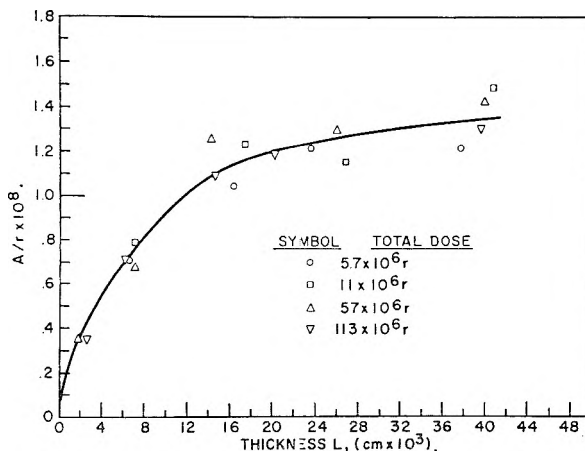


Fig. 1.—A/r vs. L at a dose rate of 1.49×10^6 r./hr.

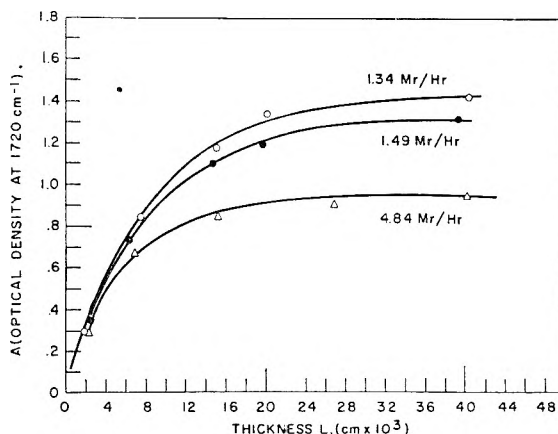


Fig. 2.—Optical density of carbonyl vs. sample thickness effect of dose rate (total dose, 1×10^8 r.); experimental, points; calculated, curves.

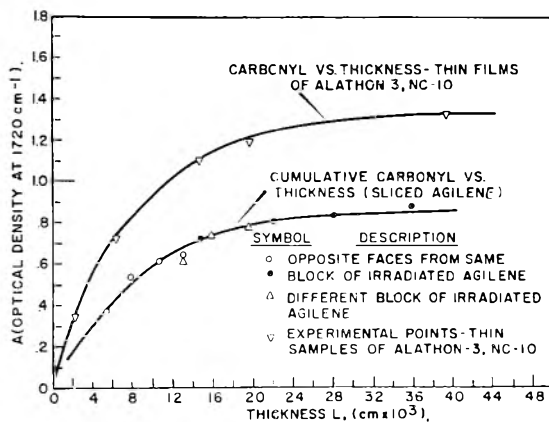


Fig. 3.—Oxidation distribution in agilene (dose rate, 1.49×10^6 r./hr., total dose, 1×10^8 r.).

step in the reaction sequence, and the equation for the rate-determining step is

$$\frac{dB}{dt} = k'(O_2)(RR^*)$$

It has been assumed that RR* was constant for

(11) This is in agreement with statements by Lawton, *et al.*,¹² and Ballentine, *et al.*,¹³ that oxidation of polymers in a radiation field would be diffusion-controlled.

(12) E. J. Lawton, *et al.*, *J. Polymer Sci.*, **32**, 257 (1958).

(13) D. S. Ballentine, *et al.*, *ibid.*, **13**, 410 (1954).

a constant radiation flux. Under conditions that a steady state concentration of oxygen is attained in the polymer, O_2 is also constant, and

$$\frac{dB}{dt} = k''$$

which is identical to the experimental facts illustrated in (1) and (2).

Derivation of Reaction Rate Equation.—Gas diffusion in organic solids is found¹⁴ to obey fairly rigorously the normal diffusion equation¹⁵

$$\frac{dN}{dt} = D \frac{d^2N}{dx^2} \quad (6)$$

where

$$N = \text{concn. of diffusing gas (oxygen)} \\ D = \text{diffusion coefficient, cm.}^2/\text{sec.}$$

If equation 6 is modified to allow for the removal of oxygen in the formation of carbonyl we have

$$\frac{dN}{dt} = D \frac{d^2N}{dx^2} - \alpha N \quad (7a)$$

where α can be defined as the probability per unit time of reaction of oxygen with a site to give carbonyl.

By dividing (7a) by the velocity, v , of the oxygen molecules, the equivalent expression in terms of flux is obtained

$$\frac{1}{v} \frac{d\phi}{dt} = D' \frac{d^2\phi}{dx^2} - \sigma\phi \quad (7b)$$

where $\phi = Nv$, $\sigma = \alpha/v$, and $D' = D/v$.

It is obvious that the change in the concentration of carbonyl groups with time is

$$\frac{dc}{dt} = \alpha N = \sigma\phi \quad (8)$$

From (2) and (3)

$$\frac{d^2B}{dt^2} = \int_0^L \frac{d^2c}{dt^2} dx = 0 \quad (9)$$

There are two ways in which this equation can be satisfied. First

$$\frac{d^2c}{dt^2} = 0$$

Physically this would mean that the concentration in any plane at a distance x into the sample, would increase linearly with time such as the total oxidation has been observed to do. The alternative is that

$$\frac{d^2c}{dt^2} \neq 0$$

Since the integral of d^2c/dt^2 over all x is zero, this would require that an increasing rate at one point be offset by a decreasing rate at another point in the sample. The first case seems physically more reasonable and will be assumed to represent the process.

Therefore, from (8)

$$\frac{d^2c}{dt^2} = \sigma \frac{d\phi}{dt} = 0 \quad (10)$$

(14) R. M. Barrer, "Diffusion in and Through Solids," The University Press, Cambridge, England, 1951.

(15) All of our samples are sufficiently wide to preclude any effect of oxidation from the edges; hence, we consider only the effect of oxidation through the sample thickness—using only a one-dimensional diffusion equation.

It follows that $d\phi/dt = 0$. Therefore, (7b) can be simplified

$$\frac{d^2\phi}{dx^2} - \frac{\sigma\phi}{D'} = 0 \quad (11)$$

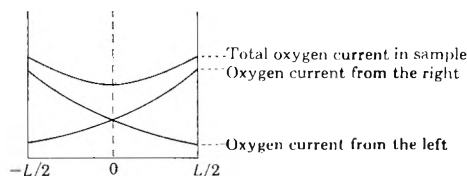
The general solution of (11) is

$$\phi = a \cosh \beta x + b \sinh \beta x \quad (12)$$

where a , b are constants and

$$\beta = \left(\frac{\sigma}{D'}\right)^{1/2} = \left(\frac{\alpha}{D}\right)^{1/2} \quad (13)$$

Consider the following (sketch A) depicting oxygen flux through the sample



Oxygen Current in Polyethylene Sample

From the sample symmetry $b = 0$ in equation 12, the current to the right and left is given by

$$j_+ \text{ (left to right)} = F e^{-\beta(x+L/2)} \quad (14a)$$

$$j_- \text{ (right to left)} = F e^{-\beta(L/2-x)} \quad (14b)$$

and the total current

$$j_T = j_+ + j_- = \phi/2 = F [e^{-\beta(x+L/2)} + e^{-\beta(L/2-x)}] \quad (14c)$$

$$\text{or } \phi(\text{total}) = \frac{2F(1 + e^{-\beta L}) \cosh \beta x}{\cosh \beta L/2} \quad (15)$$

The factor, F , is the current entering the surface of the sample and would be a function of the sample thickness.

Therefore, from (8) and (3)¹⁶

$$\frac{dB}{dt} = \int_{-L/2}^{L/2} \frac{2\sigma F(1 + e^{-\beta L})}{\cosh \beta L/2} \cosh \beta x dx \quad (16)$$

Integrating (16) gives

$$B = t^2 \frac{\sigma}{\beta} 2F(1 + e^{-\beta L}) \tanh \beta L/2 \quad (17)$$

Equation 17 may be simplified

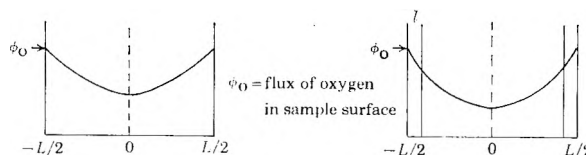
$$A = K'(1 - e^{-\beta L}) \quad (18)$$

where

$$K' = 2 \frac{KM}{N^*} (\sigma D')^{1/2} t 2F' \quad (19)$$

and β is given in (13).

Alternate Solutions of Diffusion Equation.—Two other possibilities for solving (12) are illustrated in sketch B and sketch C. In each case



$b = 0$. The first case (B) assumes the flux dropping off from the surface. In case C a semi-impermeable layer is formed on the surface through which the diffusion coefficient D_{II} operates. The ex-

(16) Note change on integration limits.

pressions equivalent to equation 18 derived for these models are

Case B

$$A = k' \tanh \beta L/2 \quad (20)$$

$$\text{where } k' = 2 \frac{KM}{N^*} (\sigma D')^{1/2} t \phi_0 \quad (21)$$

Case C

$$A = \frac{A_\infty (1 - e^{-\beta L})}{1 + ne^{-\beta L}} \quad (22)$$

$$\text{where } A_\infty = \frac{k'}{1+W} \quad (23a)$$

$$n = \frac{1-W}{1+W} \quad (23b)$$

k' = defined the same as (21)

$$W = \frac{D_1}{D_{11}} l \beta \quad (24)$$

and l is the thickness of the semi-impermeable layer.

A subsequent section will point out the inadequacies of these solutions, as compared to case A, with the experimental results.

Effect of Dose Rate on σ .—A requirement (see equation 1, and definition of l) of the derivation was that the dose rate remain constant during the irradiation time. Significantly, nothing had to be said about the magnitude of the dose rate; thus, if the irradiations were carried out at different dose rates, equation 18 should be applicable if the zero order buildup, equation 1, were observed.

It might be assumed from the definitions and discussion of the model given that

$$\sigma = \rho \delta \quad (25)$$

where ρ is a constant and δ is the dose rate. The following experimental observation will be used in support of (25): At the same total dose carbonyl formation in thin films ($\sim 2 \times 10^{-3}$ cm.) appeared to be the same regardless of dose rate (see Fig. 2).

By definition

$$\delta_1 t_1 = \delta_2 t_2 = \text{total dose}$$

By taking the ratio of equation 18 at different dose rates, and including the definitions cited above

$$\frac{A(\delta_1)}{A(\delta_2)} = \frac{2 \left(\frac{KM}{N^*} \right) (\sigma D')_1^{1/2} t_1 2F(1 - e^{-\beta_1 L})}{2 \left(\frac{KM}{N^*} \right) (\sigma D')_2^{1/2} t_2 2F(1 - e^{-\beta_2 L})} \quad (26)$$

Equation 26 now may be simplified¹⁷

$$\frac{A(\delta_1)}{A(\delta_2)} = \frac{(\sigma D')_1^{1/2} t_1 (1 - e^{-\beta_1 L})}{(\sigma D')_2^{1/2} t_2 (1 - e^{-\beta_2 L})} \quad (27)$$

For small values of βL , $e^{-\beta L}$ may be replaced by $(1 - \beta L)$. Then (27) becomes

$$\left[\frac{A(\delta_1)}{A(\delta_2)} \right]_{\beta L \rightarrow 0} = \frac{\sigma_1 t_1}{\sigma_2 t_2} = (\text{at the same total dose}) \frac{\sigma_1 \delta_2}{\sigma_2 \delta_1}$$

But as cited above for thin films $A(\delta_1) = A(\delta_2)$

$$\therefore \sigma_1 \delta_2 = \sigma_2 \delta_1 \quad (28)$$

Thus

$$\sigma = \rho \delta \quad (25)$$

(17) This assumes that the type of carbonyl being formed (e.g., acid, aldehyde, etc.) does not depend on dose rate; hence, that K is independent of δ .

Effect of Dose Rate on β .—Equation 13 gave the definition of β . Combining this with (25)

$$\beta = \left(\frac{\rho \delta}{D'} \right)^{1/2} \quad (29)$$

If D' were a constant (independent of dose rate) then $\beta \sim (\delta)^{1/2}$. This is not found for any of the evaluations of β (see Table IV). It is to be expected that D' should not be a constant but rather a complex function of the amount of oxidation and other changes occurring in the sample; however, it is reasonable to assume that it would change much less rapidly than the dose rate. Therefore, it can be concluded that β should increase with an increase in dose rate. β also can be shown to increase with an increase in dose rate by considering together: the form of the equation which gives the distribution of carbonyl in a thick sample, and the experimental observation of carbonyl formation further into thick samples at lower dose rates.

Discussion

Evaluation of Constants.—A necessary requirement for (12) to be a general solution of (11) is that the factor β be a constant at a given dose rate. β has been evaluated with the aid of a computer from the experimental data of Table II for each of the cases equations 18, 20, and 22. Typical results are shown in Table IV.

TABLE IV
EVALUATION OF β FROM DATA OF TABLE II

Dose rate, r. $\times 10^6$ /hr.	Values of β , cm.^{-1}		
	Eq. 18	Eq. 20	Eq. 22
1.32	119 \pm 11	209 \pm 50	134 \pm 96
1.49	126 \pm 6	222 \pm 45	119 \pm 59
4.84	165 \pm 25	278 \pm 94	139 \pm 86

^a At 99% confidence limits.

Equation 18 is seen to give values of β with the least scatter, and also to satisfy the criteria that β increases with an increase in dose rate which (22) does not seem to do. It also should be pointed out that equation 20 did not give random scatter to β , but the value depended on the particular thickness ratios at which it was determined, varying from 300 to 147 cm.^{-1} in the case of the 1.49×10^6 r./hr. dose rate—the highest number at the lower thickness. Matsuo and Dole⁷ observed that a solution equivalent to (20) could be made to fit their experimental data; but observed that “It (the calculated curve) rises too steeply at low values of thickness, and then levels off too abruptly at high values of thickness.” The same observation is made here.

After β is evaluated, it is an easy matter to determine K' from (18) and subsequently to evaluate σ and D' from the simultaneous solution of (13) and (19). Actually α , the reaction probability factor and D , the normal diffusion coefficient, have been calculated and listed in Table V instead of σ and D' . The relationship between (7a) and (7b) shows how this is possible.

One parameter of equation 19 that must be evaluated is F . F may be defined as

$$F = \text{current in} = \frac{\eta}{\text{cm.}^2 \text{ sec.}}$$

where n is the number of oxygen molecules entering unit area of surface in one second. From (19) and the definitions given under (7b)

$$K' = \frac{2KM}{N^*} (\alpha D)^{1/2} t \frac{2F}{v} \quad (30)$$

For very thick samples it is noted that

$$\phi = N_S v = 2F$$

Hence
$$\frac{2F}{v} = N_S = \text{constant} \quad (31)$$

N_S is the solubility of oxygen in the polyethylene.¹⁸

TABLE V

EVALUATION OF CONSTANTS AT DIFFERENT DOSE RATES			
Constant	1.34 × 10 ⁶ r./hr.	1.49 × 10 ⁶ r./hr.	4.84 × 10 ⁶ r./hr.
β , cm. ⁻¹	119	126	165
K''	1.45	1.32	0.95
α , sec. ⁻¹	2.4 × 10 ⁻³	2.7 × 10 ⁻³	8.2 × 10 ⁻³
D , cm. ² /sec.	1.75 × 10 ⁻⁷	1.71 × 10 ⁻⁷	3.00 × 10 ⁻⁷
ρ' , r. ⁻¹	6.4 × 10 ⁻⁶	6.5 × 10 ⁻⁶	6.1 × 10 ⁻⁶

^a Evaluated at 1 × 10⁸ r.

It should be pointed out here that the evaluation of α and D assumes a knowledge of K , the specific absorption coefficient. K varies with the type of carbonyl formed.^{2,21} The resolution of our spectrometer was not sufficient to determine accurately the contribution of the various groups. The principal peak appeared to be acidic carbonyl, but aldehyde and ketone groups also contributed.

The specific absorption coefficients for acid, aldehyde, and ketone are 9.47, 2.27, and 6.93 × 10³ cm.²/g., respectively.²¹ In evaluating α and D , the average value of 6.22 × 10³ cm.²/g., was arbitrarily chosen since it was not possible to determine an accurate figure. If all acidic carbonyl had been assumed, the values of α and D would be about two-thirds of that given in Table V.

The Diffusion Coefficient.—Barrer¹⁴ has listed diffusion coefficients for various gases in organic polymers. Near 300°K., typical values were in the range of 2–7 × 10⁻⁷ cm.²/sec. Michaels and Parker²⁰ have given values of oxygen diffusivity in polyethylene in the range 3–6 × 10⁻⁷ cm.²/sec. The values of D in the present work are generally lower than these but of the same order of magnitude.

(18) Estimated value of N_S from data available in ref. 19 and 20.

(19) H. J. Bixler, *et al.*, *J. Polymer Sci.*, in press.

(20) A. S. Michaels and R. B. Parker, *ibid.*, **41**, 53 (1959).

(21) J. A. Anderson and W. D. Seyfried, *Anal. Chem.*, **20**, 998 (1948).

The work of Sobolev, *et al.*,²² on permeability of gases in irradiated polymers showed a decrease in D as a consequence of irradiation.

Reaction Probability Factor.—The factor, α , was introduced into the normal diffusion equation to allow for the removal of diffusing oxygen by reaction to form carbonyl.

Irradiations *in vacuo* and under inert atmosphere have shown no detectable carbonyl increase, thus illustrating that the oxidations occurring in the present work could not result from oxygen originally dissolved in the sample.

The value of α obtained can be shown to be consistent with the assumption that a steady-state concentration of oxygen had been established in the polyethylene.

Comparison with Experiment. Total Oxidation in Thin Films.—Table II shows that at 1 × 10⁸ r. there was less than ±5% variation in the experimental and calculated values of carbonyl optical densities at the three different dose rates.

Total Oxidation in Thick Blocks.—Figure 3 illustrates the effect of oxygen diffusing through a block of polyethylene on the total amount of carbonyl formation. The fact that considerably less carbonyl formation occurred in the sliced samples compared to the thin samples is consistent with the model proposed. Theoretically, for identical materials, the saturation value should be twice as large in the thin samples compared to the sliced samples. The difference noted here can be attributed to difference in materials (Agilene had a density of ~0.90 g./cc. compared to Alathon's 0.921). However, assuming that β is the same in each material and estimating a saturation of $1/2 K' = 0.86$ (A units) the calculated curve for the sliced samples shown in Fig. 3 was made. The fit is quite good.

Effect of Dose Rate.—Table V gives the values of ρ' .²³ The deviation of the values of ρ' from their average is ±4%. Since the dose rates are only known to ±5%, the agreement is satisfactory.

Acknowledgment.—The author wishes to acknowledge the assistance of Dr. H. H. Yoshikawa of the Hanford Laboratories Operation for many helpful discussions and suggestions, especially pertaining to the theoretical section of this work. The review given the paper by Dr. R. E. Nightingale and Dr. D. R. de Halas also is greatly appreciated.

(22) I. Sobolev, *et al.*, *J. Polymer Sci.*, **17**, 417 (1955).

(23) ρ' from $\alpha = \rho' \delta$ similar to equation 25.

AN ISOTOPIC EXCHANGE METHOD FOR MEASURING THE SURFACE AREA OF SUPPORTED TRANSITION METAL SULFIDES

BY H. R. LUKENS, JR., R. G. MEISENHEIMER, AND J. N. WILSON

Shell Development Company, Emeryville, California

Received September 22, 1961

Specific surface areas of supported metal sulfides have been measured by means of the exchange between normal sulfur atoms of the metal sulfides and radioactive sulfur atoms of S^{35} -tagged H_2S . Each determination was carried out in liquid scintillation solution containing a weighed amount of insoluble metal sulfide and a known amount of dissolved H_2S (S^{35}). The disappearance of S^{35} from solution due to exchange with solid was followed by liquid scintillation counting until equilibrium was established.

A constantly reoccurring problem in the field of catalysis is the determination of the fraction of the surface area that is contributed by the various components of a heterogeneous catalyst, particularly in the case of an active agent supported upon an inert base. The desired information is most commonly sought by gas adsorption techniques. In the case of transition metal sulfides supported upon alumina or silica, gas adsorption techniques have yielded no satisfactory method. For this reason an isotopic exchange method was devised in the present work. The method set forth below is, in essence, the establishment of a set of conditions under which a liquid (toluene) containing an element common to only the catalyst component of interest (sulfur as dissolved hydrogen sulfide) reaches exchange equilibrium, for that element, with the surface. Starting with an abnormal isotope distribution in the liquid (rich in S^{35}) and a natural distribution on the solid the equilibrium exchange is a measure of the solid sulfide area available to the solution. Areas obtained by this method appear to be reproducible to $\pm 15\%$. While this is far below the precision possible for total surface area measurements, it still provides useful information concerning the degree of dispersion of the supported metal sulfides.

Experimental

A liquid scintillation system was used for this work, making it possible to place the solid metal sulfide and the tagged H_2S directly in the radioactivity-sensitive medium. Thus the complete study of exchange of sulfur atoms between components could be carried out in a single cell without any further manipulations. The exchange system contained 50–70 mg. of metal sulfide catalyst in 25 ml. of liquid scintillator solution and 10–20 micromoles of tagged H_2S . The liquid scintillator solution contained diphenyloxazole (4 g./l.) and diphenylhexatriene (15 mg./l.) in toluene. A dual-channel coincidence liquid scintillation counter was used to measure the radioactivity.¹

The catalyst, either as a pellet or powder, was added to the scintillator solution at room temperature. Hydrogen sulfide- S^{35} was prepared from alkaline $BaS\cdot S^{35}$ solution (obtained from the Oak Ridge National Laboratory), and freed from possible CO_2 contamination, by the method of Bills and Ronzio.² The tagged H_2S was added by freezing the scintillator with liquid nitrogen, evacuating, and then freezing the H_2S on to the frozen scintillator. The H_2S^{35} was metered in an all-glass system equipped with a glass bourdon gage. Subsequent tests demonstrated that over 98% of the added H_2S dissolved in the toluene; less than 2% remained in the gas phase above the liquid scintillator (checking closely the values expected from the solubility data of Bell for the solubility of H_2S in toluene).³

Other tests were made that demonstrated that the components added to the scintillator during the tests had negligible quenching action on the scintillator, and also that catalyst support materials, such as alumina and silica, did not adsorb appreciable amounts of H_2S from the solution. It also was determined that the S^{35} on the interior surfaces of the pellets as a consequence of exchange did not contribute significantly to the sample count rate. However, this was not true of powder samples, and it was necessary to shield the lower part of the sample cell by means of an aluminum cup in order to avoid counting S^{35} on powder. By this means, only light emitted from the upper portion of the scintillator solution was permitted to enter the photomultiplier tube; the powder settled to the bottom of the cell where light emitted toward the photomultiplier as the result of scintillation was intercepted by the c.p.

Standards of radioactivity were prepared by dissolving measured amounts of the reference H_2S^{35} in scintillator solution in sample cells identical to those used for the exchange experiments. The counting rate of these reference solutions was measured during the exchange experiments in order to provide a reference standard with automatic correction for decay of the S^{35} and for changes in the sensitivity of the counting apparatus. The counting efficiency for the samples was about 65% ($0.01 \mu c. S^{35} = 14,400 \text{ c.p.m.}$) and the background of the measurements was about 70 c.p.m.

Results and Discussion

The primary observables in an experiment are the weight, w , of catalyst used, the number of molecules, M , of hydrogen sulfide charged, the initial counting rate, I_0 of the hydrogen sulfide solution, the final counting rate, I_∞ , and a curve representing the time-dependence of the counting rate between I_0 and I_∞ . These samples always reached an equilibrium, usually within two days, after which there was no further change in the radioactivity level of the solution. A typical time-dependence curve is shown in Fig. 1 (80.0 mg. of MoS_2 in 25 ml. of scintillator, 17.00×10^{-6} mole H_2S^{35}). The primary result derivable from the measurements is the number, N_s , of exchangeable sulfur atoms per g. of catalyst. In the absence of isotope effects on the equilibrium constants, $I_\infty/I_0 = M/(M + N_s w)$ whence $N_s = M(I_0 - I_\infty)/wI_\infty$. It remains to show that N_s is proportional to the total number of atoms in the surface of the sulfide, and to determine the constants of proportionality. This was done experimentally by exchange measurements with unsupported NiS , MoS_2 , WS_2 , and mixed sulfides of various ratios. N_s was determined for many such samples. The surface areas of these samples were measured by the BET method using N_2 or Kr as an adsorbate. With these two pieces of information, it was possible to obtain the area per exchangeable sulfur atom for the various compositions.

(1) V. P. Guinn, "Liquid Scintillation Counting," Pergamon Press, London, 1958, pp. 166–182.

(2) C. W. Bills and A. R. Ronzio, *J. Am. Chem. Soc.*, **72**, 5510 (1950).

(3) R. P. Bell, *J. Chem. Soc.*, 1371 (1931).

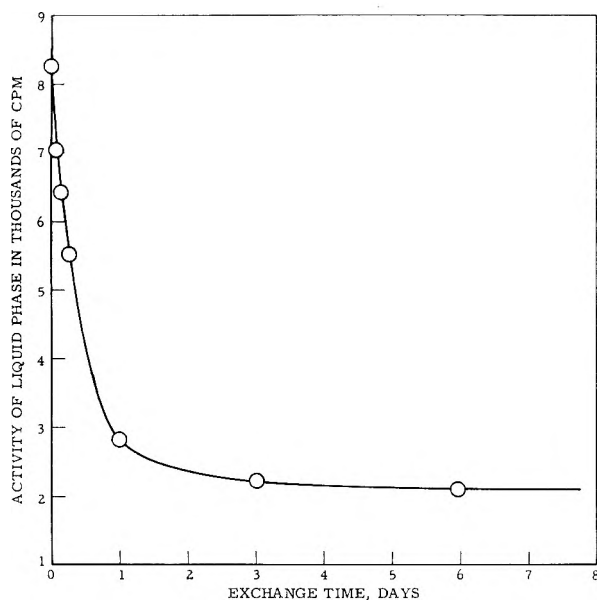


Fig. 1.—Exchange of H_2S (S^{32}) with a metal sulfide.

It was found necessary to take one important precaution when making these measurements. The surface of these sulfides are very non-stoichiometric; under sulfiding conditions the surface may contain excess sulfur, under reducing conditions it may be deficient in sulfur, in the presence of air or oxygen some of the surface sulfur atoms can be replaced by oxygen atoms. For this reason, the catalyst must be subjected to some pre-treatment that results in a reproducible surface condition for a given sulfide. In this work the sample was evacuated to 10^{-4} mm. or better (1–4 hr.) at 275° . It then was swept for 2 hr. with a 10 to 1 volume ratio of hydrogen to hydrogen sulfide at 275° and cooled under vacuum. The degree of variation encountered after such a treatment can be illustrated by the fact that numerous measurements on samples of MoS_2 , NiS, and WS_2 gave values of 5.8 ± 0.4 , 29 ± 2 and $20 \pm 1 \text{ \AA}^2$ per exchangeable sulfur atom. For each substance the precision obtained is about $\pm 8\%$ of the value. This may be contrasted with the values obtained from MoS_2 subsequent to sweeping with pure H_2S , which varied from 5 to 0.03 \AA^2 . The latter value was from a sample possessing a visible coating of sulfur. The area of a mixed sulfide, $NiMo_2WS_x$, was found to be $7.2 \pm 0.5 \text{ \AA}^2/\text{atom}$.

It is of interest to compare the experimental exchange area per sulfur atom with the value expected from considerations of the crystal unit cell dimensions of MoS_2 , NiS, and WS_2 . The unit cell dimensions of all three of these substances result in expected values of about 9 \AA^2 per surface sulfur atom. The exchange values found are both higher than this value (for NiS and WS_2), and lower (for MoS_2). The reason for this discrepancy is not known definitely, but probably is related to the tendencies toward non-stoichiometry, particularly at the crystallite surfaces.

The data on bulk metal sulfides can be used to determine the area of supported sulfides only by assuming the area per exchangeable sulfur atom to be the same in both cases. Metal sulfide crystallite sizes were measured by X-ray diffraction methods on several samples in order to check this assumption. The crystallite sizes so measured were compared with crystallite sizes calculated from the exchange area data. In calculating crystallite sizes from surface area data, cubic crystals of uniform size, with one side masked by the support, were assumed. In Table I, the sizes determined by the two methods are compared.

TABLE I
METAL SULFIDE CRYSTALLITE SIZES

Sulfide	Support	Crystallite sizes	
		Exchange data	X-Ray data ^a
12% NiS	Al_2O_3	26	40
22% WS_2	Al_2O_3	150	100
100% NiMoW/S	Unsupported	350	300–500
20% NiMoW/S	Al_2O_3	46	45
14% NiMoW/S	Al_2O_3	40	45
20% NiMoW/S	SiO_2	48	55

^a X-Ray data kindly supplied by R. M. Curtis and W. F. Sheehan of these Laboratories.

The agreement between the crystallite sizes determined by the two different methods is good enough to give some assurance that the values used for the areas of sulfide ions on the surfaces are not unreasonable.

A typical application of this technique for measuring the specific surface area of a supported metal sulfide is presented below. Three catalysts composed of a mixed NiMoW sulfide on an alumina base showed approximately equal activities for the hydrogenation of α -methyl-naphthalene in spite of both widely varying amounts of the sulfide component and widely varying total surface areas. Examination of the sulfide component by the exchange technique disclosed that all of the catalysts had comparable sulfide areas per gram of catalyst. The pertinent data are listed in Table II.

TABLE II

ALUMINA SUPPORTED MIXED NiMoW SULFIDE		
% Metal sulfide on support	Total areas, $m^2/g.$	Sulfide area $m^2/g.$ of cat.
20	290	35
34	250	27
100	23	23

In conclusion, it may be said that while the isotopic exchange technique described above is not a precise method, as compared with the BET method for measuring total surface areas, nor is it a rapid measurement to perform, it routinely has provided information that is difficult to obtain by other methods, namely, a measure of the available surface area of supported Ni, Mo, W, and mixed sulfides.

The authors wish to thank Miss Edna F. Dean for helpful discussions and assistance in this work.

THE NATURE OF THE REDUCING RADICAL IN WATER RADIOLYSIS¹

BY GIDEON CZAPSKI AND HAROLD A. SCHWARZ

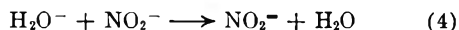
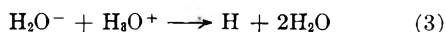
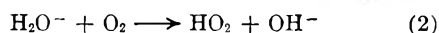
*Department of Chemistry, Brookhaven National Laboratory, Upton, Long Island, New York**Received September 22, 1961*

The kinetic salt effect is utilized to demonstrate that the reducing radical produced in water radiolysis has a unit negative charge and may be considered a solvated electron, designated H_2O^- . The effect of ionic strength on three rate constant ratios among the following four reactions was measured. $\text{H}_2\text{O}^- + \text{H}_2\text{O}_2 \longrightarrow \text{OH} + \text{OH}^- + \text{H}_2\text{O}$ (1), $\text{H}_2\text{O}^- + \text{O}_2 \longrightarrow \text{HO}_2 + \text{OH}^-$ (2), $\text{H}_2\text{O}^- + \text{H}_3\text{O}^+ \longrightarrow \text{H} + 2\text{H}_2\text{O}$ (3), and $\text{H}_2\text{O}^- + \text{NO}_2^- \longrightarrow \text{NO}_2^{\cdot-} + \text{H}_2\text{O}$ (4). The ratio k_2/k_1 is unaffected by ionic strength while k_3/k_1 decreases and k_4/k_1 increases with increasing ionic strength. From the slopes of the ionic strength curves the charge on the reducing radical is determined to be minus one.

The nature of the radicals produced in water radiolysis is not clear, although they generally have been referred to as "H" and "OH." In recent years there has been considerable speculation concerning the reducing radical as it is known to exist in two forms with different kinetic behavior in aqueous solutions.^{2,3} The species produced in water radiolysis is converted into the second species by reaction with acid. Several authors²⁻⁴ have suggested that the species produced in water radiolysis may be some form of a solvated electron. In this paper we will present ionic-strength effect evidence demonstrating that this species does have a unit negative charge. Throughout the rest of the paper we will prejudice our argument by referring to this form as H_2O^- and the acid form as H.

At low salt concentrations, rate constants for reactions between ions of similar charge increase with increasing ionic strength, while rate constants for reactions between ions of opposite charge decrease and rate constants for reactions between ions and neutral molecules do not change. This kinetic salt effect may be used to determine the magnitude and sign of the charge on a species if it reacts with an ion of known charge.

Most of the reactions of the radicals produced in water radiolysis are too rapid to follow directly, so we have measured the effect of ionic strength on rate constant ratios. H_2O^- is known to react readily with H_2O_2 , O_2 , H_3O^+ and NO_2^-



(The products of reactions 2 and 4 may be O_2^- and NO, respectively.) Czapski and Allen⁵ have demonstrated that the rate constant ratio k_2/k_1 can be determined in solutions of O_2 , H_2O_2 and KBr while k_3/k_1 can be determined in the same system upon the addition of acid. Schwarz and Allen⁶ have demonstrated that k_4/k_1 can be measured in solutions of KNO_2 and H_2O_2 .

(1) Research performed under the auspices of the U. S. Atomic Energy Commission.

(2) N. F. Barr and A. O. Allen, *J. Phys. Chem.*, **63**, 928 (1959).

(3) E. Hayon and J. Weiss, *Proc. Second Intern. Conf. Peaceful Uses Atomic Energy*, **29**, 80 (1958).

(4) A. R. Anderson and E. J. Hart, *J. Phys. Chem.*, **65**, 804 (1961); J. T. Allan and G. Scholes, *Nature*, **187**, 218 (1960).

(5) G. Czapski and A. O. Allen, *ibid.*, **66**, 262 (1962).

(6) H. A. Schwarz and A. O. Allen, *J. Am. Chem. Soc.*, **77**, 1324 (1955).

Experimental

All solutions were irradiated in a Co^{60} source at a dose rate of 3.6×10^{20} e.v./l. min. The change in hydrogen peroxide concentration was followed in each system. The earlier studies^{5,6} indicated that analysis for this component was sufficient for following the reactions. The iodide method of analysis developed by Ghormley⁷ was used in the oxygen, peroxide and bromide solutions with and without perchloric acid added. In analyzing solutions of H_2O_2 and KNO_2 for peroxide, the iodide concentration of the reagents was lowered by a factor of five as recommended by Schwarz and Salzman.⁸ The lower iodide concentration eliminated the problem of a time-dependent blank due to the thermal oxidation of iodide by nitrite.

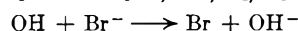
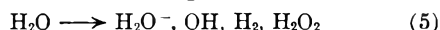
The rate constant ratio k_2/k_1 was determined in air-saturated solutions containing 10^{-4} M KBr and 1.22×10^{-4} M H_2O_2 . The ionic strength was changed by adding two salts, $\text{MgSO}_4 \cdot 7\text{H}_2\text{O}$ and $\text{LiClO}_4 \cdot 3\text{H}_2\text{O}$.

The determination of k_3/k_1 was made in air-saturated solutions containing 10^{-4} M KBr, 10^{-3} M HClO_4 , and varying amounts of H_2O_2 . The ionic strength was varied by the addition of $\text{LiClO}_4 \cdot 3\text{H}_2\text{O}$.

The determination of k_4/k_1 was made in nitrite-peroxide solutions deaerated by nitrogen bubbling. All experiments were performed with a potassium nitrite concentration of 1.02×10^{-3} M. Most of the work was done with a peroxide concentration near 1.5×10^{-4} M, as the data are most sensitive to changes in ionic strength at this concentration. However, two series of experiments were performed with 5.6×10^{-4} M H_2O_2 . Ionic strength was varied by the addition of $\text{LiClO}_4 \cdot 3\text{H}_2\text{O}$, KClO_4 , NaClO_4 , $\text{LaCl}_3 \cdot 6\text{H}_2\text{O}$, $\text{MgSO}_4 \cdot 7\text{H}_2\text{O}$, K_2SO_4 and $\text{Li}_2\text{SO}_4 \cdot \text{H}_2\text{O}$.

Results

Oxygen, Hydrogen Peroxide, Potassium Bromide System.—Czapski and Allen⁵ found that the peroxide yields observed in this system agreed well with a mechanism including reactions 1 and 2 and



Reaction 5 is the production of molecular products and radicals by the absorption of radiation.

The function of the bromide in this system is to convert OH, which oxidizes both H_2 and H_2O_2 , into Br, which reacts on y with H_2O_2 , thus simplifying the kinetics. The equation describing this system is

$$\frac{1}{G_0(\text{H}_2\text{O}_2) - G(\text{H}_2\text{O}_2)} = \frac{1}{2G_{\text{H}_2\text{O}^-}} + \frac{k_2}{2k_1 G_{\text{H}_2\text{O}^-}} \frac{(\text{O}_2)}{(\text{H}_2\text{O}_2)} \quad (I)$$

where $G_{\text{H}_2\text{O}^-}$ is the yield of H_2O^- produced by the radiation (reaction 5) in units of molecules per 100 e.v. absorbed in the solution, $G(\text{H}_2\text{O}_2)$ is the observed yield of hydrogen peroxide and $G_0(\text{H}_2\text{O}_2)$

(7) A. O. Allen, C. J. Hochanadel, J. A. Ghormley and T. W. Davis, *J. Phys. Chem.*, **56**, 575 (1952).

(8) H. A. Schwarz and A. J. Salzman, *Radiation Research*, **9**, 502 (1958).

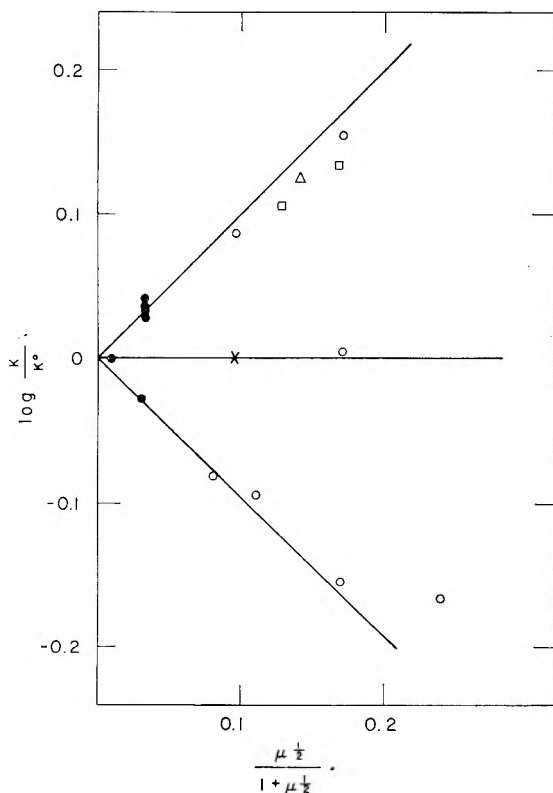


Fig. 1.—The effect of ionic strength on K/K_0 : upper curve, $K = k_4/k_1$, $K_0 = 0.34 = k_4/k_1$ at zero ionic strength; middle curve, $K = k_2/k_1$, $K_0 = 2.0$; lower curve, $K = k_3/k_1$, $K_0 = 1.95$. The ionic strength was varied with LiClO_4 , O ; KClO_4 , \square ; NaClO_4 , Δ ; and MgSO_4 , \times . The closed circles represent no added salt other than the reactants.

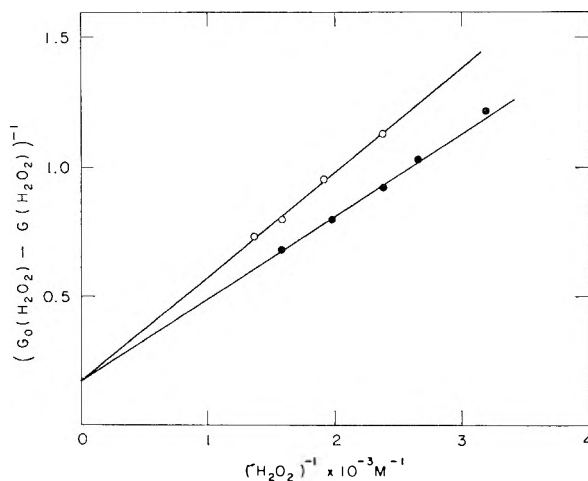


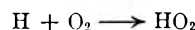
Fig. 2.—The variation of $G(\text{H}_2\text{O}_2)$ with peroxide concentration in air-saturated peroxide solution containing $10^{-3} M \text{HClO}_4$. The data are presented in a form suggested by equation 2: O , $10^{-4} M \text{KBr}$; \bullet , $10^{-4} M \text{KBr}$ and $0.1 M \text{LiClO}_4$ added.

is the initial yield of hydrogen peroxide in solutions containing only air and bromide. $G_0(\text{H}_2\text{O}_2)$ may be seen to be equal to $G_{\text{H}_2\text{O}_2} + \frac{1}{2}(G_{\text{H}_2\text{O}_2} - G_{\text{OH}})$, where $G_{\text{H}_2\text{O}_2}$ is the molecular yield of peroxide and G_{OH} is the yield of OH produced in reaction 5. The value of k_2/k_1 is 2.0, $G_{\text{H}_2\text{O}_2}$ is 2.85 radicals per 100 e.v. and $G_0(\text{H}_2\text{O}_2)$ is 0.86.⁵ Equation I states that the observed yield of peroxide becomes more

negative as $(\text{H}_2\text{O}_2)/(\text{O}_2)$ is increased, which may be seen by inspection of the mechanism.

Air-saturated solutions containing $1.22 \times 10^{-4} M \text{H}_2\text{O}_2$ and $10^{-4} M \text{KBr}$ were irradiated. Three sets of experiments were performed in which no other salt was added, $5 \times 10^{-3} M \text{MgSO}_4$ was added and $4 \times 10^{-2} M \text{LiClO}_4$ was added. $G(\text{H}_2\text{O}_2)$ was 0.099, 0.100 and 0.086, respectively. The values of k_2/k_1 were calculated from these yields and eq. I assuming $G_{\text{H}_2\text{O}_2}$ and $G_0(\text{H}_2\text{O}_2)$ to be unchanged by the addition of the salts. The results, expressed as $\log(k_2/k_1)/(k_2/k_1)_0$, where $(k_2/k_1)_0$ is the extrapolated value of k_2/k_1 at zero ionic strength, are shown in Fig. 1 as the middle set of points. It is seen that varying the ionic strength from $10^{-4} M$ to $4 \times 10^{-2} M$ has no effect on k_2/k_1 .

Oxygen, Hydrogen Peroxide, Potassium Bromide and Perchloric Acid System.—Hydrogen ion competes with peroxide and oxygen for H_2O^- .⁵ The product, H , does not react readily with peroxide. The mechanism used above to describe the system in the absence of acid applies in the presence of acid with the inclusion of reaction 3 followed by



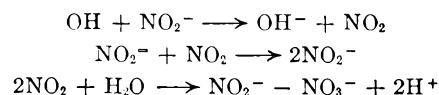
Thus hydrogen ion behaves similarly to O_2 and the kinetic equation describing the mechanism is

$$\{G_0(\text{H}_2\text{O}_2) - G(\text{H}_2\text{O}_2)\}^{-1} = \frac{1}{2G_{\text{H}_2\text{O}_2}} \left\{ 1 + \frac{k_2}{k_1} \frac{(\text{O}_2)}{(\text{H}_2\text{O}_2)} + \frac{k_3}{k_1} \frac{(\text{H}^+)}{(\text{H}_2\text{O}_2)} \right\} \quad (\text{II})$$

The various symbols have the same meaning as before. At an ionic strength of $1.1 \times 10^{-3} M$, k_3/k_1 was found to be 2.0.⁵ $G_0(\text{H}_2\text{O}_2)$, the initial yield of H_2O_2 in peroxide-free solutions, was determined in air-saturated, $10^{-4} M \text{KBr}$ solutions containing $10^{-3} M \text{HClO}_4$. In the presence of $0.4 M \text{LiClO}_4$, $G_0(\text{H}_2\text{O}_2)$ was 0.90. In the absence of added salt it was 0.91, showing that $G_0(\text{H}_2\text{O}_2)$ is independent of ionic strength.

The effect of ionic strength on the peroxide yield is shown in Fig. 2. The reciprocal of $G_0(\text{H}_2\text{O}_2) - G(\text{H}_2\text{O}_2)$ is plotted as a function of the reciprocal of the hydrogen peroxide concentration at the natural ionic strength and at the extreme ionic strength used, $0.1 M \text{LiClO}_4$. $G(\text{H}_2\text{O}_2)$ is considerably more negative in the presence of added salt. Each point in Fig. 2 represents 6 to 10 measurements of the H_2O_2 concentration as a function of the dose. The slopes of Fig. 2 are equal to $1/2G_{\text{H}_2\text{O}_2} \{k_2/k_1 (\text{O}_2) + k_3/k_1 (\text{H}^+)\}$. Since k_2/k_1 is independent of ionic strength, the change in slope is due to a change in k_3/k_1 again assuming $G_{\text{H}_2\text{O}_2}$ to be independent of the ionic strength. The variation of $\log(k_3/k_1)/(k_3/k_1)_0$ with ionic strength is given in the lower curve of Fig. 1 (the constant $(k_3/k_1)_0$ is k_3/k_1 at infinite dilution).

Potassium Nitrite, Hydrogen Peroxide System.—Schwarz and Allen⁶ have studied the radiation induced reaction between nitrite ion and hydrogen peroxide. The data were consistent with the mechanism of reactions 5, 1, 4 and



In further work⁸ it was found that the back re-

action became important as the nitrate concentra-



tion built up during the reaction. The equation describing this mechanism is

$$G(\text{H}_2\text{O}_2) = G_{\text{H}_2\text{O}_2} - \frac{G_{\text{H}_2\text{O}^-}}{1 + \frac{k_4}{k_1} \frac{(\text{NO}_2^-)}{(\text{H}_2\text{O}_2)} + \frac{k_6}{k_1} \frac{(\text{NO}_3^-)}{(\text{H}_2\text{O}_2)}} \quad (III)$$

$G_{\text{H}_2\text{O}_2}$ is the initial yield of H_2O_2 in peroxide-free nitrite solutions and according to the mechanism is equal to the molecular yield of peroxide produced in reaction 5. Equation III suggests that $G(\text{H}_2\text{O}_2)$ will be zero at a certain ratio of reactants and that the measured yields of H_2O_2 will be particularly sensitive to changes in rate constants in the neighborhood of this ratio. In Fig. 3, the upper curve gives the change in peroxide concentration as a function of dose for a solution of KNO_2 and H_2O_2 and the lower curve is the same system with $4 \times 10^{-2} M$ LiClO_4 added. The peroxide yields are small and a large salt effect is observed.

A rearrangement of terms in equation III gives equation IV

$$\frac{k_4}{k_1} = \left\{ \frac{G_{\text{H}_2\text{O}^-}}{G_{\text{H}_2\text{O}_2} - G(\text{H}_2\text{O}_2)_{\text{av}}} - 1 \right\} \left\{ \frac{(\text{H}_2\text{O}_2)_{\text{av}}}{(\text{NO}_2^-)_0 + (k_6/k_4 - 1)(\text{NO}_3^-)_{\text{av}}} \right\} \quad (IV)$$

in which the approximation has been made of equating differential yields and average yields. In this equation, $G(\text{H}_2\text{O}_2)_{\text{av}} = \Delta(\text{H}_2\text{O}_2)/\text{dose}$ and $(\text{H}_2\text{O}_2)_{\text{av}} = (\text{H}_2\text{O}_2)_0 + 1/2\Delta(\text{H}_2\text{O}_2)$. The material balance in this system is given by $(\text{NO}_3^-) + \Delta(\text{H}_2\text{O}_2) = G_{\text{H}_2\text{O}^-}(\text{dose})$ where $G_{\text{H}_2\text{O}^-} = 0.41^4$ and is the molecular hydrogen yield produced in reaction 5, so that $(\text{NO}_3^-)_{\text{av}} = 1/2\{G_{\text{H}_2\text{O}^-}(\text{dose}) - \Delta(\text{H}_2\text{O}_2)\}$.

The rather strong curvature of the curves in Fig. 3 is due primarily to the production of nitrate and its subsequent reaction according to reaction 6. Unfortunately, no independent estimates of k_6/k_4 are available. A value of k_6/k_4 of 1.8 was used as it gave the best fit with curves such as in Fig. 3. The initial yields of H_2O_2 , $G_{\text{H}_2\text{O}_2}$, were determined to be 0.61, 0.61 and 0.59 in solutions containing no added salt, $4 \times 10^{-2} M$ LiClO_4 and $2 \times 10^{-2} M$ K_2SO_4 , respectively, indicating again that the initial yield does not depend on ionic strength. These yields agree well with the value reported earlier for $10^{-3} M$ nitrite solutions,⁸ 0.61. $G_{\text{H}_2\text{O}^-}$ was taken as 2.8.

The values of k_4/k_1 obtained from eq. IV are given in Fig. 1 (upper curve) as $\log(k_4/k_1)/(k_4/k_1)_0$, where $(k_4/k_1)_0$ is the value of k_4/k_1 at infinite dilution. The ionic strength was varied by the addition of several perchlorates. Each point represents the average of five irradiations as a function of dose. The average deviation of the five determinations from the mean was $\pm 1.0\%$. All of the points given in Fig. 1 were obtained with initial (NO_2^-) to (H_2O_2) ratios of about 7. Two series of experiments were performed with a (NO_2^-) to (H_2O_2) ratio of 2 at the natural ionic strength ($1.02 \times 10^{-3} M$) and with $4 \times 10^{-2} M$ LiClO_4 added. k_4/k_1 was found to be 0.44 and 0.63, respectively, compared to values of 0.37 and 0.49 at (NO_2^-) to (H_2O_2) ratios of 7. The relative

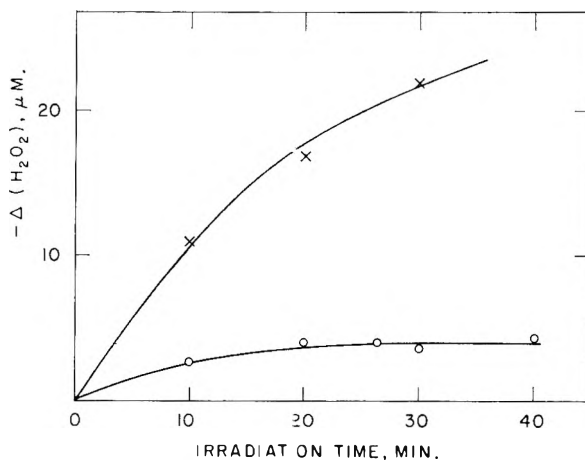


Fig. 3.—The change in hydrogen peroxide concentration with irradiation time in solutions containing $1.02 \times 10^{-3} M$ KNO_2 and $1.51 \times 10^{-4} M$ H_2O_2 : X, no additional salt added; O, $4 \times 10^{-2} M$ LiClO_4 added.

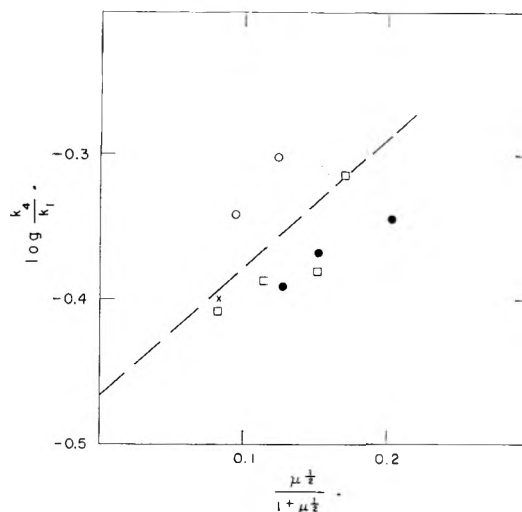


Fig. 4.—The effect on k_4/k_1 of varying the ionic strength with multivalent salts: O, Li_2Cl_2 ; X, MgSO_4 ; ●, K_2SO_4 ; □ Li_2SO_4 . The broken line represents the mean of the data concerning k_4/k_1 from Fig. 1.

effects of ionic strength in the two cases agree well, considering that the error in determining k_4/k_1 is large at the lower (NO_2^-) to (H_2O_2) ratios. There is a discrepancy in the absolute magnitude of k_4/k_1 at the two concentration ratios which undoubtedly reflects errors in the constants used and in the mechanism. Such systematic errors do not affect the relative results at one concentration ratio, and indeed the points of Fig. 1 vary by only ± 0.005 for values of $G_{\text{H}_2\text{O}^-}$ from 2.4 to 3.4 or values of k_6/k_4 from 0 to 4.

Values of $\log k_4/k_1$ obtained by adding LaCl_3 and several sulfates are given in Fig. 4. The broken line represents the mean of the data from Fig. 1.

In calculating the rate constant ratios k_2/k_1 , k_3/k_1 and k_4/k_1 , it was assumed that $G_{\text{H}_2\text{O}^-}$ was independent of ionic strength. This assumption is not subject to simple test in these solutions, as $G_{\text{H}_2\text{O}^-}$ is found as an extrapolated intercept. In all three systems the quantity which is determined with considerable precision, almost independent of $G_{\text{H}_2\text{O}^-}$, is the product of the reciprocal of $G_{\text{H}_2\text{O}^-}$

and the rate constant ratio, for instance $k_3/k_1-G_{\text{H}_2\text{O}^-}$. It is implausible to consider that $G_{\text{H}_2\text{O}^-}$ increases with the square root of the ionic strength in one system, decreases in another and remains unchanged in the third.

Discussion

The usual form of the equation relating rate constants and ionic strength, obtained from the Brønsted model of ionic reactions and the extended Debye theory of ionic solutions, is^{9,10}

$$\log \frac{k}{k_0} = 1.02Z_a Z_b \frac{\mu^{1/2}}{1 + a\mu^{1/2}} \quad (\text{V})$$

where k is the rate constant at ionic strength μ , k_0 is the rate constant at infinite dilution of ions, Z_a and Z_b are the algebraic numbers of charges on the reactants and a is a parameter near unity and taken as such. Thus, the rate constant will increase, decrease, or remain the same with increasing ionic strength, depending on whether the reactants have the same sign, opposite signs or whether one reactant is neutral. All three types of behavior are seen in Fig. 1. The lines drawn are for slopes of +1.02, 0 and -1.02, respectively, corresponding to a unit negative charge on H_2O^- . The agreement with the data is excellent.

Deviations from equation V are observed in Fig. 4, where the ionic strength is varied by the addition of multivalent ions. These deviations are expected and lend support to the interpretation. Rate constants for reactions between ions of the same charge depend more upon the concentration of ions of opposite charge than on ions of similar charge. Hence replacing perchlorate by sulfate does not have much effect on the rate constants, while it increases the ionic strength by a factor of two. Similarly, as lanthanum is a triply charged positive ion, it exhibits an abnormally large effect.

(9) H. A. Schwarz, *J. Am. Chem. Soc.*, **77**, 4960 (1955).

(10) S. E. Benson, "The Foundations of Chemical Kinetics," McGraw-Hill Book Co., New York, N. Y., 1960, p. 525.

The relative effects of perchlorates and sulfates on k_4/k_1 agree quantitatively with the observations of Indelli, Nolan and Amis¹¹ for the alkaline hydrolysis of potassium malonate in which two reactants with unit negative charge are reacting. The enhanced effect of LaCl_3 agrees qualitatively with the observation of Indelli and Prue¹² in their study of the persulfate oxidation of iodide. They observed a larger positive deviation than we observe, which agrees with the higher charge on the activated complex in the I^- , $\text{S}_2\text{O}_8^{2-}$ reaction. Such deviations have been discussed by Scatchard,¹³ who finds them in agreement with predictions based on the Mayer theory of electrolytes.

Two other observations on the nature of H_2O^- may be made on the basis of these data. First, the species is thermal, otherwise the ionic strength effect would not be observed. The derivation of equation V depends upon maintaining a Boltzmann distribution of the concentration of charges around an ion. Secondly, H_2O^- must move slowly enough to maintain its ion atmosphere, *i.e.*, it must be solvated. If it moved rapidly, the charge distribution surrounding the activated complex would resemble that of a univalent ion and the change in the activity coefficient of the activated complex would only be half of that for a divalent ion. One other observation on the nature of H_2O^- , not based on the present data, perhaps is in order. It is known that H_2O^- reacts quantitatively with reagents such as H_2O_2 and O_2 present in low concentrations of the order of several μM without undergoing a first-order reaction to produce a hydrogen atom.^{2,14} This suggests that H_2O^- is quite stable, the rate constant for the reaction $\text{H}_2\text{O}^- \rightarrow \text{H} + \text{OH}^-$ probably being less than 10^4 sec.^{-1} .

(11) A. Indelli, G. Nolan, Jr., and E. S. Amis, *J. Am. Chem. Soc.*, **82**, 3237 (1960).

(12) A. Indelli and J. E. Prue, *J. Chem. Soc.*, 107 (1959).

(13) G. Scatchard, Natl. Bur. Standards Circ. 524, 1953, p. 185.

(14) H. A. Schwarz, *J. Phys. Chem.*, **66**, 255 (1962).

N^{13} -LABELED PRODUCTS FROM $\text{C}^{12}(\text{d},\text{n})$ REACTION IN ALCOHOLS¹

BY W. C. PERKINS AND W. S. KOSKI

Department of Chemistry, The John Hopkins University, Baltimore 18, Maryland

Received September 23, 1961

The N^{13} -labeled compounds produced when gaseous methane, methanol, or ethanol are bombarded with 2 Mev. deuterons have been investigated. HCN^{13} and $\text{CH}_3\text{CN}^{13}$ are the gaseous activities found for CH_4 and CH_3OH . These activities plus $\text{C}_2\text{H}_5\text{CN}^{13}$ were found in ethanol bombardments. Experiments with rare gas additives and Br_2 suggest that cyanogen ion or radical is the B^{13} carrier and that the HCN is formed by reaction with materials on the wall of the vessel, whereas the CH_3CN is formed by reaction with target gas molecules in the gas phase.

Introduction

In a previous investigation² the radioactive N^{13} products, formed when alkyl halide derivatives undergo $\text{C}^{12}(\text{d},\text{n})\text{N}^{13}$ reactions in the gas phase, were identified. Indications were obtained that the radioactive products such as HCN and ClCN

arose from the reactions of N^{13} recoils with the alkyl halide. This could not be determined with certainty because of the possible role of radiation-damage products. In this paper an extension of these studies to methanol and ethanol is described. Through the use of Br_2 as a scavenger, from the effect of rare gas additives on the reaction and from a careful examination of the products obtained from deuteron bombardment of methane and the alcohols, a better insight has been obtained into the nature of these reactions.

(1) Work done under the auspices of the United States Atomic Energy Commission.

(2) H. Schmied and W. S. Koski, *J. Am. Chem. Soc.*, **82**, 4708 (1960).

Experimental

The bombardments were made with 2 Mev. deuterons from an electrostatic generator in our Laboratory. Beam currents and bombardment times were kept as low as possible to minimize complications through radiation damage. Currents as low as 0.03 μ amp. and irradiation times of 2 min. can be taken as the lower limits used for these parameters. The irradiations were made through a 0.0001-inch nickel foil. The irradiation cells were made of brass and of glass and ranged from 2-7 cm. in diameter and were about 16 cm. long. The methyl alcohol used was the Baker analyzed reagent grade product and the absolute ethyl alcohol was a U. S. Industrial product. The methane was Phillips research grade. The gas chromatograph was an all-glass instrument operated from 80-115°. It contained a 12-ft. column of "Celite" coated with silicone oil. Helium was used as a carrier gas and a flow of 40 cc./min. was maintained by a pressure regulator. Detection of macro amounts of material was realized with a thermal-conductivity cell. The radioactive gases were detected with two 2 π methane proportional counters viewing diametrically opposite Mylar windows of a glass cell through which the gas passed on exit from the chromatograph. The responses of the detectors were recorded with a two-pen recorder. Identification of the compounds was made through a comparison of their retention times with those of the reference compounds.

Results and Discussion

Typical radioactive gas chromatograms obtained for deuteron irradiation of methyl and ethyl alcohol in a glass cell are given in Fig. 1. Peak I has been identified as due to N₂ and arises by reaction of N¹³ with residual amounts of nitrogen gas present as an impurity on the walls of the cell or in the target gas. Peak II is due to HCN, III to CH₃CN, and IV to C₂H₅CN. In similar irradiations of CH₄, peaks I, II, and III also appear. No ammonia or amines were detected in spite of a careful search. One can vary the relative intensity of these peaks by changing experimental conditions. For example, addition of 5 mm. of N₂ to 75 mm. of CH₃OH in a brass cell caused the activity of peak I to increase from 370 (no N₂ added) to 7000 c.p.m. Increasing the alcohol pressure resulted in a reduction in absolute amount of N₂ radioactivity. In view of extensive attempts to free the target gas of N₂, it is concluded that the bulk of the radioactive nitrogen, in the case where no N₂ was deliberately added, comes from the reaction of N¹³ with adsorbed N₂ on the walls of the irradiation cell. This exchange reaction apparently also can occur with nitrogen molecules in the gas phase. The idea that the wall plays an important role in the formation of residual nitrogen molecule activity is supported by the following observation. On extensive irradiation, polymeric material from radiation-damage effects can be deposited on the walls of the glass reaction vessel. Under such conditions, the adsorbed nitrogen is covered and subsequent irradiations of methanol give no radioactive N₂. On the other hand, when this polymer coating is removed and an irradiation is made, the radioactive nitrogen again appears even though no N₂ was added to the system. The behavior of the radio-nitrogen yield as a function of target gas pressure also tends to support the view that it results from a wall reaction.

The amount of HCN yield also is considerably influenced by various experimental parameters. The role of metal cells has been mentioned² previously and similar observations have been made with the present system. Use of clean brass cells

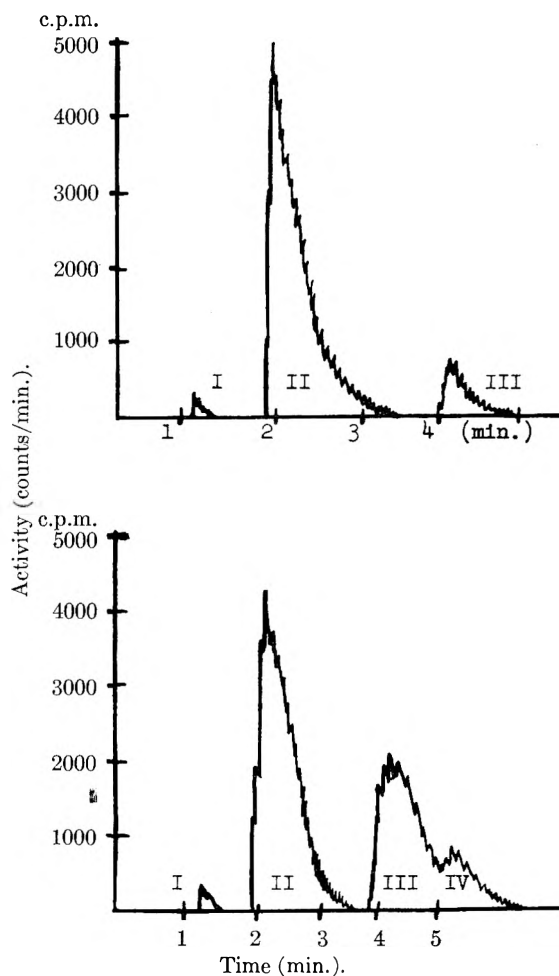


Fig. 1.—Gas chromatograms of N¹³ compounds formed by deuteron bombardment of methanol (upper) and ethanol (lower).

for reaction vessels completely removes the gaseous HCN yield and the activity is found on the wall of the cell. The alcohol system differs in one point from the alkyl halide system previously reported.² In the latter case, it was found possible to condition the metal surface by extensive irradiation of the alkyl halide so that such cells did give a gaseous HCN yield. This presumably arises from the protective polymer coating that is put on the walls of the metal vessel. In the case of the alcohols studied here, such conditioning of the metal surfaces could not be realized and no HCN was detected when brass cells were used.

A second factor that influences drastically the HCN yield is the addition of small amounts of gaseous N₂. The addition of 5 mm. of N₂ to 110 mm. CH₃OH in a glass irradiation cell resulted in a fall in HCN activity from 16,000 to 4500 c.p.m. with a corresponding increase of the radio N₂ activity. There was no discernible effect on the CH₃CN yield.

The cell size also has an influence on radio HCN yield. Increasing the glass cell radius by a factor of three decreased the ratio of HCN/CH₃CN by a factor of five. Such changes favored CH₃CN production and reduced the HCN yield to the extent that now the CH₃CN was the dominant gaseous activity.

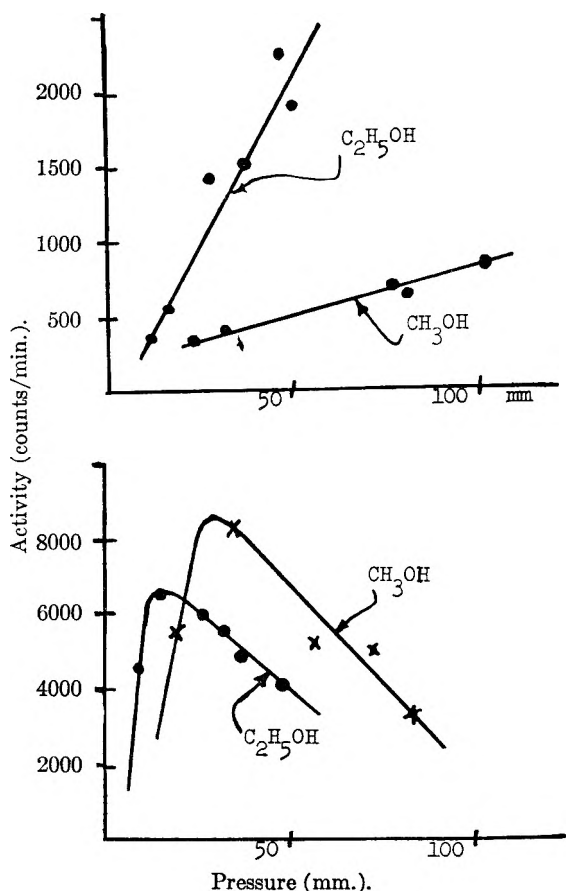


Fig. 2.—Pressure variation of $\text{CH}_3\text{CN}^{13}$ (upper) and HCN^{13} (lower) yield from deuterium bombarded methanol and ethanol, respectively.

The influence of alcohol pressure on the yield of HCN and CH_3CN is shown in Fig. 2. The radio CH_3CN yield increases with alcohol pressure and is approximately linear. The accuracy of the measurements is such that one would not detect a relatively small curvature in the plot. On the other hand, the yield of HCN goes through a definite maximum if one makes measurements at sufficiently low pressures. The general increase of the CH_3CN yield as a function of alcohol pressure is expected if the material is produced in the gas phase since the greater the number of carbon atoms present the greater the N^{13} production and its subsequent products. On the other hand, the HCN yield *vs.* pressure curve could be explained best if the bulk of the HCN production occurs on the walls of the vessel since, with increased pressure, fewer of the N^{13} carriers would get to the walls prior to reacting in the gas phase.

Another parameter that influences the HCN yield is the presence of rare gases. These experiments were performed by adding 15 mm. of alcohol to 5–50 mm. of rare gas and comparing the HCN yield to the case where no additive was present. Examples of typical results obtained are the following. When no rare gas was added to a certain run, the HCN peak was 220 c.p.m.; the addition of 51 mm. of argon gave a peak of 280 c.p.m.; and 51 mm. of Kr gave 570 c.p.m. The corresponding figures for the CH_3CN peak were 250, 170, and 130 c.p.m., respectively. Of the number of experiments

of this type that were run, all indicated this rise in HCN yield and a corresponding fall in CH_3CN yield as one proceeded from no rare gas additive to argon and then to krypton. Rare gases can have several possible effects and two that are probably of pertinent interest here are moderation and charge exchange. Both argon and krypton can act as moderators; *i.e.*, the radioactive carrier, be it N^{13} or CN^{13} in ion or radical form, will undergo collisions with the moderator and be slowed down to thermal energies. There is also the possibility of charge exchange if the ionization potentials are favorable. For example, the first ionization potentials of argon, nitrogen, CN radical,³ and krypton are 15.7, 14.5, 14.5, and 13.9 volts, respectively. Consequently, charge exchange would be expected to occur between krypton and N^+ or CN^+ but not with argon. If moderation and charge exchange are the contributing factors to the variation of the yield of radioactive products, one would conclude that HCN is produced by a thermal reaction involving a neutral reactant since addition of rare gases results in more effective thermalization of the N^{13} carrier. Kr would be expected to be a less efficient thermalizer than Ar; however, the enhancement of the HCN yield realized with Kr can result from a charge transfer process producing more radical carriers, which are presumably one of the reactants. The fall of the CH_3CN yield with rare gas addition can be explained best if the reactant is an ionic N^{13} carrier with greater than thermal energies.

Considerable attention has been given to the possible role that radiation-damage products might play as far as the yield of radioactive products is concerned. Measurements were made with varying beam currents, pressures, and times of irradiation. In these runs, the beam current was as low as 0.03 $\mu\text{amp.}$ and irradiation time as short as 2 min. Under such conditions, less than 1% of the target gas was destroyed. In general, the yield was linear with increasing beam current and time until a large amount (>30%) of the target gas was destroyed. Even under conditions of minimum amount of radiation damage compatible with obtaining a detectable amount of radioactive products, one has a considerable amount of damage along the beam path. Consequently, the N^{13} produced by the nuclear reaction has a high probability of undergoing a number of collisions with ions and free radicals in the beam path. The question then arises whether a significant amount of the final products arise from the reaction of the N^{13} carrier with free radicals or ions resulting from radiation damage, or is the reaction between N^{13} carrier and target gas molecules. An experiment which has some bearing on this question is one in which Br_2 was added to the target gas. Bromine is an efficient scavenger for organic free radicals; consequently, its presence should reduce the radioactive product yield if the radiation-damage fragments were one of the reactants. Experiments in which there was as much as 20 mole % Br_2 in methanol showed that the yield of CH_3CN was not

(3) V. H. Dibeler, R. M. Reese, and J. L. Franklin, *J. Am. Chem. Soc.* **83**, 1813 (1961).

influenced appreciably, whereas the HCN yield was increased by about 30%. This suggests that the reaction between N^{13} carriers to give the final product does not involve the free radicals from radiation-damage but the reaction apparently occurs with the target gas or the materials on the surface of the reaction vessel. The increase in HCN yield in the presence of Br_2 probably results from thermalization and charge-transfer processes.

Although one cannot as a result of this study outline a complete mechanism by which the radioactive products are formed, one can make some pertinent conclusions as to the nature of the mechanism. The fact that CH_4 , CH_3OH , and C_2H_5OH give HCN and CH_3CN , and in addition, the ethanol gives C_2H_5CN , suggests that the cyanogen ion or radical is the N^{13} carrier as far as the observed radio-cyanides are concerned. The fact that neither ammonia nor amines are observed suggests that neither NH nor NH_2 are the N^{13} carriers. The question then arises—how is the C-N bond formed? A possibility is that N^{13} ion can react to form ions such as CH_4N^+ when methane is the target gas, for example, and this ion on decomposition gives

rise to CN^+ . This CN^+ ion can react in the gas phase with methane to give CH_3CN or, on neutralization, it gives the cyanogen radical which can abstract hydrogen mostly from materials deposited on the walls of the vessel to give HCN. It also can replace hydrogen on the wall-adsorbed molecules to form cyanides which remain on the walls of the vessel. Such activity has been found on the walls; however, the material has not been identified as yet.

The fact that a significant amount of N^{13} activity is present in one or more unidentified forms on the walls of the vessel is of some concern since it may have an important influence on the mechanisms of the reactions occurring. It also has prevented the realization of a satisfactory radioactivity balance and this point should be taken into consideration when comparisons are being made between the changes in yields of radioactive products as in Fig. 2. Such comparisons cannot be made in the present data; however, it is expected that this complication will be overcome in future work.

THE EFFECT OF THE EXPONENTIAL DISTRIBUTION FUNCTION ON THE ELECTROPHORETIC CONTRIBUTION TO THE CONDUCTANCE OF 1-1 ELECTROLYTES¹

BY DAVID J. KARL AND JAMES L. DYE

Kedzie Chemical Laboratory, Michigan State University, East Lansing, Michigan

Received September 25, 1961

The use of the exponential ionic distribution function rather than the linear or quadratic expansion of it is demonstrated to have a large effect upon the electrophoretic contribution to conductance. Calculations by digital computer were made for a number of salts in dioxane-water and in ethanol-water mixtures, and it was found that much of the deviation from conductance theory usually attributed to ion-pair formation could arise from neglect of the higher terms in the distribution function.

Introduction

The theoretical calculation of the conductance of electrolytes has attracted attention for many years and has been beset by many problems. Not the least of these has been the calculation of the degree of association of the ions to form ion-pairs. Before one can calculate the association constant, it is necessary to know the proper conductance function for the ionic species. When association is marked, as for a weak acid or a salt in a medium of low dielectric constant, the Onsager limiting law can be used successfully. For cases of slight association, however, the constant is very sensitive to the theoretical conductance function used.

A number of extensions of the limiting law have been proposed²⁻⁴ and Fuoss has used the Fuoss-

Onsager extension to calculate the association constant for ion-pair formation in mixed solvent systems.^{5,6} Since this treatment has been very successful in fitting conductance data and in correlating ion-size parameters, limiting mobilities, and association constants over a wide range of dielectric constants, the basic equations for the conductance of unassociated electrolytes appear to be sound, at least for the case of large ions. This paper shows that terms which were dropped in the treatment of the electrophoretic effect are *not* small for those cases requiring the introduction of an association constant. In fact, simply retaining these terms yields a surprisingly good fit of the data for reasonable and constant ion-size parameters in many cases, without requiring consideration of ion-pair formation. It is suggested that the association constant calculated from conductance data is forced to include ionic interaction effects in addition to effects attributable to the formation of a distinct neutral species.

The Distribution Function.—The terminology

(1) This paper is based in part on a thesis presented by David J. Karl to the School for Advanced Graduate Studies of Michigan State University in partial fulfillment of the requirements for the degree of Doctor of Philosophy, 1960.

(2) E. Pitts, *Proc. Roy. Soc. (London)*, **A217**, 43 (1953).

(3) H. Falkenhagen, M. Leist, and G. Kelbg, *Ann. Physik*, [6] **11**, 51 (1953).

(4) R. M. Fuoss and L. Onsager, *Proc. Natl. Acad. Sci. U. S. A.*, **41**, 274 1010 (1955); *J. Phys. Chem.*, **61**, 668 (1957); **62**, 1339 (1958).

(5) R. M. Fuoss, *J. Am. Chem. Soc.*, **79**, 3301 (1957).

(6) R. M. Fuoss and C. A. Kraus, *ibid.*, **79**, 3304 (1957).

and symbols used in this paper are those of Harned and Owen.⁷ The Onsager limiting law used the distribution function (for the unperturbed distribution)

$$f_{ji}^0 = n_i n_j (1 - e_i \psi_j^0 / kT) \quad (1)$$

obtained by expanding the exponential distribution function

$$f_{ji}^0 = n_i n_j \exp[-e_i \psi_j^0 / kT] \quad (2)$$

in a power series and neglecting higher order terms. Fuoss and Onsager⁴ retained another term in the expansion of (2) as well as other terms from the equations of motion of order c to obtain an expression for the relaxation field. Their distribution function is

$$f_{ji}^0 = n_i n_j \left[1 - \frac{e_i \psi_j^0}{kT} + \frac{1}{2} \left(\frac{e_i \psi_j^0}{kT} \right)^2 \right] \quad (3)$$

In this equation, the second term depends upon $c^{1/2}$ and the third term upon c . All terms of order $c^{3/2}$ and higher were discarded. Since the third term in eq. 3 cancels out of the electrophoretic integral, their results for this effect are the same as were obtained previously for a non-zero ion-size parameter. The functional form of ψ_j^0 was obtained from the solution of the linearized Poisson-Boltzmann equation. Pitts² used the Gronwall-La Mer-Sandved expression for the potential⁸ and the distribution function (3) in his treatment of both the relaxation and the electrophoretic effects. Pitts notes that the approximations made in dropping higher terms limits the applicability of the equations in media of low dielectric constant; for example, to concentrations below about $5 \times 10^{-4} M$ in ethanol ($D = 24.3$). Falkenhagen, Leist, and Kelbg³ used a modification of (1) introduced by Eigen and Wicke⁹ to correct the Boltzmann distribution for the fact that two atmosphere ions cannot simultaneously occupy the same region of space.

It has been pointed out frequently¹⁰⁻¹² that the exponential distribution function (2) is incompatible with the Poisson equation. On the other hand the linear function (1) is certainly incorrect at small values of r because it ignores the exponential dependence of the distribution function upon the interaction energy. Onsager¹³ has shown that the statistically correct expression for the time-average ionic distribution function is

$$f_{ji} = n_i n_j \exp \left[\frac{W_{ji}}{kT} \right] \quad (4)$$

in which W_{ji} is the time-average interaction energy. At close distances of approach the most important contribution to W_{ji} is the pair-wise coulombic interaction of the two ions, and screening effects are

(7) H. S. Harned and B. B. Owen, "The Physical Chemistry of Electrolytic Solutions," Third Edition, Reinhold Publishing Corporation, New York, N. Y., 1958.

(8) T. H. Gronwall, V. K. La Mer, and K. Sandved, *Physik. Z.*, **29**, 358 (1928).

(9) M. Eigen and E. Wicke, *Naturwissenschaften*, **38**, 453 (1951).

(10) R. H. Fowler, "Statistical Mechanics," Cambridge University Press, New York, N. Y., 1929, Chap. XIII.

(11) R. H. Fowler and E. A. Guggenheim, "Statistical Thermodynamics," Cambridge University Press, New York, N. Y., 1952, Chap. IX.

(12) R. A. Robinson and R. H. Stokes, "Electrolytic Solutions," Butterworths Scientific Publications, London, 1955, pp. 76, 128, 142.

(13) L. Onsager, *J. Chem. Phys.*, **2**, 599 (1934).

of secondary importance.¹⁴ The distribution function of Bjerrum¹⁵ for $r < q = [e_1 e_j] / 2DkT$ includes only this pair-wise interaction. At large values of r , $e_i \psi_j^0 / kT \ll 1$ and the exponential function and the linear function are essentially the same.

The differences among the various distribution functions can be examined qualitatively by utilizing a graph of the radial charge distribution about an ion. Such a graph is shown in Fig. 1 for a representative case using $D = 25$, $T = 298$, $\kappa a = 0.100$, $a = 4 \times 10^{-8}$ cm., $|Z_+| = |Z_-| = 1$. For these conditions it can be seen that when $r > 4a$, the linear function and the exponential function give nearly the same charge distribution, and that most of the atmosphere is outside of this distance. The diagram also shows that the form of the charge distribution curve obtained using the potential function of Gronwall, La Mer, and Sandved and the exponential distribution function is similar to that obtained using the Debye-Hückel potential function. It is to be noted that because of a cancellation of terms, the distribution function (3) gives the same charge density as the linear function (1).

Recently, Fuoss and Onsager¹⁶ have proposed a new distribution function which includes the pair-wise interactions at close distances and merges into an extension of the Debye function at the Bjerrum distance q . While this approach still involves the linear-superposition approximation, and the somewhat arbitrary choice of q as the matching distance, it has the advantage of being normalized to unit charge in the atmosphere. It would be of interest to use this new distribution function in the electrophoretic integral.

We have chosen to examine the effect of the higher terms in the distribution function on the electrophoretic contribution to conductance by calculating the equivalent conductance for various salts over a range of dielectric constants and viscosities using the exponential distribution function (2). It is not our intention to claim validity of the distribution function, but rather to show that the effects are appreciable and in such a direction that the true association constants are probably much smaller than generally has been thought.

The assumptions inherent in the model and treatment used in this paper are: 1. The Debye-Hückel potential function is used; 2. The treatment of the relaxation effect derived by Fuoss and Onsager⁴ is used. This involves the distribution function (3) and drops all terms in the relaxation field of order $c^{3/2}$ and larger; 3. The exponential distribution function (2) is used in deriving the expression for the electrophoretic effect¹⁷; 4. Stoke's law for the movement of a sphere through a viscous medium is used in deriving the expression for the electrophoretic effect, although this is not expected to be valid at distances less than about 7Å .¹⁸ This assumption is expected to yield values

(14) J. G. Kirkwood, *ibid.*, **2**, 767 (1934).

(15) N. Bjerrum, *Kgl. Danske Videnskab. Selskab., Mat.-fys. Medd.*, **7**, No. 9 (1926).

(16) R. M. Fuoss and L. Onsager, *Proc. Natl. Acad. Sci. U. S. A.*, **47**, 818 (1961).

(17) J. L. Dye and F. H. Spedding, *J. Am. Chem. Soc.*, **76**, 888 (1954).

(18) Reference 12, p. 118.

of \hat{a} which are too small; 5. The ions are considered to be hard, non-polarizable spheres, not subject to association effects. Breakdown of this assumption would tend to yield values of \hat{a} which are too small.

In comparing the calculations with experiment, two parameters, \hat{a} and Λ^0 were adjusted to minimize the deviations. When fitting the data to include ion-pairing, Fuoss and co-workers^{5,6,19} utilize three adjustable parameters, Λ^0 , \hat{a} , and the association constant A . In the case of large ions, both methods involve in addition a hydrodynamic radius parameter, R .

Method of Calculation. —The calculations were programmed for the MISTIC digital electronic computer in two parts. The first was the calculation of the electrophoretic contribution to conductance, $\Delta\Lambda_e$, using

$$\Delta\Lambda_e = \Lambda\lambda_+ + \Delta\lambda_- \quad (5)$$

in which

$$\Delta\lambda_+ = \frac{96,493 DkT}{1800\pi\eta\epsilon(|Z_+| + |Z_-|)} \int_x^\infty \rho \left\{ \exp \left[\frac{-Z_+^2 P e^{-\rho}}{\rho} \right] - \exp \left[\frac{Z_+ Z_- P e^{-\rho}}{\rho} \right] \right\} d\rho \quad (6)$$

For symmetrical electrolytes, $\Delta\Lambda_e = 2\Delta\lambda_+$. The program also can be used for unsymmetrical electrolytes, in which case $\Delta\lambda_-$ is calculated separately. In equation 6, $P = \kappa e^z / DkT(1+x)$ and $x = \kappa a$. Integration was performed numerically with the aid of the Newton-Cotes quadrature formula.²⁰ For small values of ρ , the integrand is very large and changes very rapidly with ρ . In order to assure proper integration of the function, the integral was re-evaluated with successively smaller increments until $|(\Delta\lambda_+)_{n+1}| - |(\Delta\lambda_+)_n| < \epsilon = 2 \times 10^{-3}$. This gives a precision to the calculation of $\Delta\Lambda_e$ of ± 0.004 conductance units. Input for this program included DT , η , \hat{a} , and \sqrt{c} .

The equivalent conductance then was calculated using the expression

$$\Lambda = \frac{(\Lambda^0 - \Delta\Lambda_e) \left(1 + \frac{\Delta X}{X} + \frac{\Delta P}{X} \right)}{1 + \frac{5}{2} Fc} \quad (7)$$

in which the relaxation field term, $\Delta X/X$, the kinetic term, $\Delta P/X$, and the Einstein viscosity term, $5/2 Fc$, are obtained from the equations of Fuoss and Onsager^{4,19} as

$$-\frac{\Delta X}{X} = \alpha c^{1/2} (1 - \Delta_1 + \Delta_2) + \beta c^{1/2} \Delta_3' / \Lambda^0 \quad (8)$$

$$\frac{\Delta P}{X} = \frac{\kappa^2 a^2 (b - 1)}{12b} \quad (9)$$

$$F = \frac{4}{3} \frac{\pi R^3 N}{1000} \quad (10)$$

The program computed Λ at the experimental concentrations for various values of Λ^0 and \hat{a} .

Results

The conventional expression for the electrophoretic contribution to conductance obtained from the linear distribution function for finite-sized ions is

(19) R. M. Fuoss and F. Accascina, "Electrolytic Conductance," Interscience Publishers, Inc., New York, N. Y., 1959.

(20) K. S. Kunz, "Numerical Analysis," McGraw-Hill Book Company, Inc., New York, N. Y., 1957. p. 145.

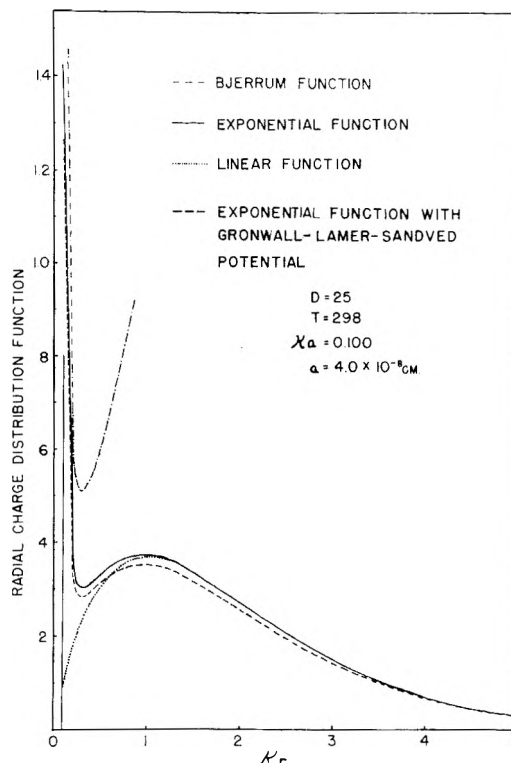


Fig. 1.—Charge distribution in the ionic atmosphere according to various distribution functions.

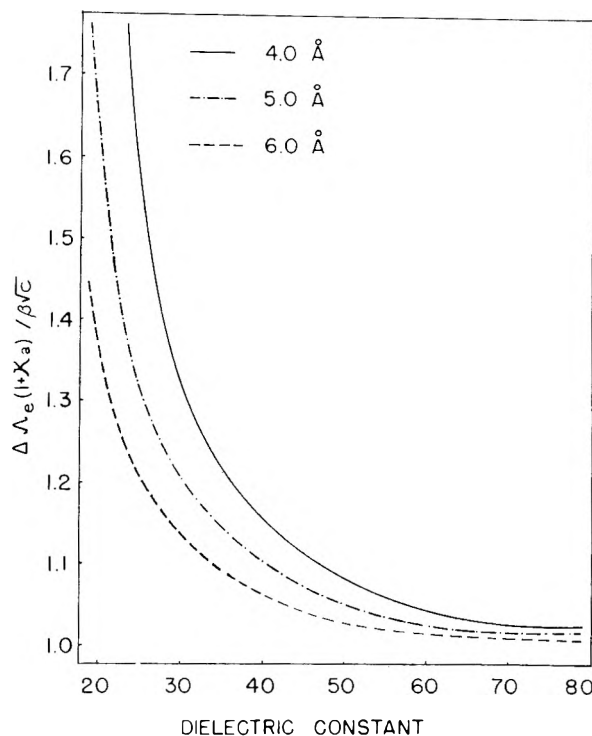


Fig. 2.—The ratio of the complete to the linear electrophoretic contribution to conductance vs. dielectric constant for 1-1 salts in dioxane-water mixtures at 25° for the case $\sqrt{c} = 0.07$.

$$(\Delta\Lambda_e)_{\text{linear}} = \frac{-\beta\sqrt{c}}{1 + \kappa a} \quad (11)$$

That the effect of higher terms is large is illustrated by Fig. 2 in which the ratio of the complete to the

linear electrophoretic contribution is plotted *vs.* dielectric constant for a particular concentration of solute in dioxane-water mixtures.

Calculations were performed for a number of salts in dioxane-water mixtures, including both large ions for which a viscosity correction was necessary, and small ions for which R was set equal to zero. Data of Martel and Kraus²¹ on the conductance of tetraisoamylammonium nitrate in mixtures up to 50% dioxane were fit using an ion-size parameter of 4.5 Å. and a hydrodynamic radius parameter of 7.5 Å. for all mixtures. These data are given in Table I.²² While an approach distance of 4.5 Å. seems incompatible with a hydrodynamic radius of 7.5 Å., molecular models (Stuart-Briegleb type) indicate an outer radius for the cation of about 7.3 Å., and also show that a shorter anion-cation distance of about 3.6 Å. is possible.

TABLE I

COMPARISON OF CALCULATED AND OBSERVED CONDUCTANCES OF TETRAISOAMYLAMMONIUM NITRATE IN DIOXANE-WATER MIXTURES AT 25°C^a USING $\bar{d} = 4.5$ Å., $R = 7.5$ Å.

10% ϵ	Λ	10 ² $\Delta\Lambda$	10% ϵ	Λ	10 ² $\Delta\Lambda$
0%, $D = 78.54$ $\Lambda^0 = 89.30$			30%, $D = 53.28$ $\Lambda^0 = 53.99$		
1	88.45	-2	1	53.34	+1
4	87.60	-2	4	52.65	+1
16	85.79	-6	16	51.24	-1
49	82.95	-9	49	49.07	-4
10%, $D = 70.33$ $\Lambda^0 = 74.55$			50%, $D = 35.85$ $\Lambda^0 = 42.55$		
1	74.12	+2	1	41.77	0
4	73.31	-1	4	40.96	+2
16	71.69	-4	16	39.30	+3
49	69.09	-16	49	36.94	+3

^a Data of Martel and Kraus.²¹

Data of Mercier and Kraus²³ on the conductance of tetra-*n*-butylammonium bromide in 0% to 70% dioxane-water mixtures were compared with calculated values. The results are given in Table II and show that the conductances can be fit over the entire range of dielectric constants using $\bar{d} = 5.0$ Å., $R = 7.0$ Å. Models indicate a minimum approach distance of 3.7 Å. and an outer radius of 6.7 Å. for the tetra-*n*-butylammonium ion.

Tetra-*n*-butylammonium iodide conductance data of Martel and Kraus²¹ also could be fit, but required too low an \bar{d} value (3.5 Å. for $R = 8.0$ Å.).

It was desired to examine the conductance of small ions for which no hydrodynamic correction would be required. Data for sodium bromate²¹ were used and the results are given in Table III for the "best" \bar{d} value for each solvent mixture. The average value of \bar{d} is 3.55 Å. and varies from 3.48 to 3.65 Å.

Recent data of Lind and Fuoss²⁴ on the conduct-

(21) R. W. Martel and C. A. Kraus, *Proc. Natl. Acad. Sci. U. S.*, **41**, 9 (1955).

(22) Values listed for Λ in Tables I and II were taken from large graphs of the data. For the other systems, calculations were performed for the experimental concentrations. In all cases, $\Delta\Lambda$ refers to $\Lambda_{\text{obsd.}} - \Lambda_{\text{calcd.}}$

(23) P. L. Mercier and C. A. Kraus, *Proc. Natl. Acad. Sci. U. S.*, **41**, 1033 (1955).

(24) J. E. Lind, Jr., and R. M. Fuoss, *J. Phys. Chem.*, **65**, 999 (1961).

TABLE II

COMPARISON OF CALCULATED AND OBSERVED CONDUCTANCES OF TETRA-*n*-BUTYLAMMONIUM IODIDE IN DIOXANE-WATER MIXTURES AT 25°C^a USING $\bar{d} = 3.7$ Å., $R = 6.7$ Å.

10% ϵ	Λ	10 ² $\Delta\Lambda$	10% ϵ	Λ	10 ² $\Delta\Lambda$
0%, $D = 78.54$ $\Lambda^0 = 97.45$			55%, $D = 31.53$ $\Lambda^0 = 41.56$		
1	96.64	+3	1	40.71	+2
4	95.75	0	4	39.77	-1
16	93.97	-3	16	37.98	0
49	91.30	-1	49	35.60	+1
10%, $D = 70.33$ $\Lambda^0 = 80.85$			60%, $D = 27.21$ $\Lambda^0 = 39.75$		
1	80.09	1	1	38.75	0
4	79.29	-2	4	37.65	-1
16	77.68	-6	16	35.54	0
49	75.40	+5	49	32.65	-17
30%, $D = 53.28$ $\Lambda^0 = 57.25$			65%, $D = 23.14$ $\Lambda^0 = 38.30$		
1	56.57	0	1	37.05	-2
4	55.88	0	4	35.69	+5
16	54.51	1	16	33.03	-5
49	52.50	1	49	29.70	-4
50%, $D = 35.85$ $\Lambda^0 = 43.70$			70%, $D = 19.07$ $\Lambda^0 = 37.05$		
1	42.90	-2	1	35.43	0
4	42.10	0	4	33.48	-7
16	40.48	-2	16	29.97	0
49	38.30	-1	49	25.90	-4

^a Data of Mercier and Kraus.²³

TABLE III

COMPARISON OF CALCULATED AND OBSERVED CONDUCTANCES OF SODIUM BROMATE IN DIOXANE-WATER MIXTURES AT 25°C^a

10% ϵ	Λ	10 ² $\Delta\Lambda$	10% ϵ	Λ	10 ² $\Delta\Lambda$
0%, $D = 78.54$ $\Lambda^0 = 105.778, \bar{d} = 3.50$			50%, $D = 35.85$ $\Lambda^0 = 50.735, \bar{d} = 3.48$		
2.60004	104.465	+46	5.89543	48.555	+9
5.20539	103.840	-16	11.8047	47.566	-10
10.4396	103.071	-2	23.5952	46.228	-22
20.8887	101.989	-18	35.4006	45.259	-1
41.8148	100.508	-22	47.2113	44.486	+25
83.6224	98.566	+15			
10%, $D = 70.33$ $\Lambda^0 = 90.360, \bar{d} = 3.60$			55%, $D = 31.53$ $\Lambda^0 = 47.825, \bar{d} = 3.65$		
5.76328	88.525	-58	5.93793	45.397	+51
11.4833	87.796	+33	11.8609	44.247	-3
22.8762	86.764	+31	23.6794	42.710	-25
45.6798	85.332	-2	35.5217	41.609	-25
91.2034	83.466	-2	47.3833	40.736	+5
			94.9003	38.329	-5
30%, $D = 53.28$ $\Lambda^0 = 66.290, \bar{d} = 3.50$					
5.82789	64.710	-5			
11.6555	63.986	+7			
23.3262	62.976	-1			
46.6973	61.594	-1			
93.3465	60.793	0			

^a Data of Martel and Kraus.²¹

ance of KCl in dioxane-water mixtures were examined and the results are given in Table IV. It is

seen that the data through 56.69% dioxane agree with calculated values with a variation of \bar{a} from 3.4 to 3.8 Å. Above this dioxane content the deviations become larger, but even for 69.88% dioxane an ion-size parameter of 3.7 Å. would leave only about 0.2 conductance unit at the highest con-

TABLE IV

COMPARISON OF CALCULATED AND OBSERVED CONDUCTANCES OF POTASSIUM CHLORIDE IN DIOXANE-WATER MIXTURES AT 25°^a

10 ³ c	Λ	10 ³ ΔΛ	10 ³ c	Λ	10 ³ ΔΛ
0%, D = 78.54			56.69%, D = 30.26		
Λ ⁰ = 149.898, \bar{a} = 3.78			Λ ⁰ = 56.272, \bar{a} = 3.43		
19.368	145.813	+1	8.514	52.706	+18
40.166	144.141	+1	15.362	51.319	+2
58.689	143.060	+1	22.559	50.207	-30
78.577	142.117	-3	29.624	49.333	+10
99.697	141.275	+2	36.749	48.573	0
22.2%, D = 60.16			61.74%, D = 25.84		
Λ ⁰ = 100.738, \bar{a} = 3.82			Λ ⁰ = 52.082, \bar{a} = 3.60		
14.966	97.589	+5	6.756	48.237	+54
43.004	95.566	-15	13.239	46.430	-23
56.758	94.852	+9	19.479	45.154	-32
71.619	94.237	-1	25.964	44.086	-19
			32.813	43.157	+21
43.65%, D = 41.46			69.88%, D = 19.32		
Λ ⁰ = 69.142, \bar{a} = 3.65			Λ ⁰ = 45.650, \bar{a} = 4.00		
11.671	66.031	0	4.830	40.501	-20
22.430	64.815	-8	9.455	37.981	+90
33.716	63.890	+2	14.217	36.186	+80
45.892	63.079	+10	18.875	34.838	-10
55.446	62.524	+2	23.476	33.770	-140

^a Data of Lind and Fuoss.²⁴

centration to be accounted for by other effects. It is of interest to note that the residual deviations are systematic but in a direction *opposite* to that which would be caused by ion-pair formation. Data of Lind and Fuoss²⁵ for CsI in dioxane-water mixtures also were treated, and the results are given in Table V. Inexplicably, the calculations for the aqueous solution give a very low value of \bar{a} (3.49 Å) compared to those for dioxane-water mixtures up to 70.7% dioxane which fit with \bar{a} values averaging 4.4 Å. and varying from 4.25 to 4.55 Å. Even for 70.7% dioxane, with \bar{a} = 4.55 Å., the deviations, while systematic, stay within ±0.06 conductance unit. Again the deviations are not in the direction expected for ion-pair formation.

Data of Hawes and Kay²⁶ on potassium chloride in ethanol-water mixtures were used and the results are given in Table VI. An ion-size parameter of average value 3.45 Å. results in a good fit of the data. The variation of \bar{a} with dielectric constant and the deviations are systematic rather than random.

Cesium chloride in ethanol water mixtures [data of Hawes and Kay²⁶] appears to be more associated than the other salts examined. The data can be fit only by using very low and variable values for \bar{a} (2.5 to 3.1 Å.).

(25) J. E. Lind, Jr., and R. M. Fuoss, *J. Phys. Chem.*, **65**, 1414 (1961).

(26) J. Hawes and R. L. Kay, Brown University, Providence, R. I., private communication, data to be published.

TABLE V

COMPARISON OF CALCULATED AND OBSERVED CONDUCTANCES OF CESIUM IODIDE IN DIOXANE-WATER MIXTURES AT 25°^a

10 ³ c	Λ	10 ³ ΔΛ	10 ³ c	Λ	10 ³ ΔΛ
0%, D = 78.54			57.1%, D = 29.79		
Λ ⁰ = 154.109, \bar{a} = 3.49			Λ ⁰ = 56.502, \bar{a} = 4.32		
19.933	149.905	+21	9.294	52.923	+3
37.919	148.368	+6	16.741	51.694	-2
55.585	147.211	-19	24.306	50.762	0
76.474	146.095	-29	32.302	49.966	0
94.416	145.329	+21	41.508	49.199	-2
22.1%, D = 60.18			63.7%, D = 24.44		
Λ ⁰ = 99.477, \bar{a} = 4.40			Λ ⁰ = 52.203, \bar{a} = 4.25		
15.445	96.326	-2	6.590	48.282	-11
30.294	95.158	+1	12.368	46.719	-6
44.480	94.350	-7	19.172	45.396	+4
58.272	93.741	+20	24.447	44.583	-9
73.736	93.115	-10	30.929	43.741	+17
44.6%, D = 40.57			70.7%, D = 18.68		
Λ ⁰ = 66.911, \bar{a} = 4.50			Λ ⁰ = 47.825, \bar{a} = 4.55		
9.909	64.154	0	5.492	42.482	+58
19.788	63.063	-3	9.839	40.408	-50
29.285	62.308	+4	14.616	38.790	-47
38.799	61.692	+2	19.379	37.549	0
49.652	61.105	-5	24.646	36.440	+38

^a Data of Lind and Fuoss.²⁴

TABLE VI

COMPARISON OF CALCULATED AND OBSERVED CONDUCTANCES OF POTASSIUM CHLORIDE IN ETHANOL-WATER MIXTURES AT 25°^a

10 ³ c	Λ	10 ³ ΔΛ	10 ³ c	Λ	10 ³ ΔΛ
38%, D = 55.5			79%, D = 33.1		
Λ ⁰ = 57.873, \bar{a} = 3.68			Λ ⁰ = 44.024, \bar{a} = 3.28		
13.918	55.937	+4	15.643	39.952	+6
33.004	54.902	-3	25.226	38.767	-4
65.339	53.780	-3	45.546	36.962	-11
98.849	52.936	+2	67.130	35.578	+6
			91.853	34.344	+1
40%, D = 55.1			88%, D = 29.0		
Λ ⁰ = 56.708, \bar{a} = 3.63			Λ ⁰ = 44.564, \bar{a} = 3.45		
11.465	54.952	+2	13.088	39.633	+11
26.392	54.047	0	20.203	38.346	-9
57.379	52.850	+5	28.457	37.165	-19
90.101	51.952	-3	37.421	36.119	+6
123.48	51.237	-4	45.376	35.332	+26
60%, D = 43.3			88%, D = 29.0		
Λ ⁰ = 46.785, \bar{a} = 3.23			Λ ⁰ = 44.564, \bar{a} = 3.45		
12.619	44.456	+11	54.810	34.523	+16
22.922	43.608	-3	65.150	33.753	-32
48.560	42.149	-21			
70.644	41.252	-9			
105.032	40.170	+22			

^a Data of Hawes and Kay.²⁵

Conclusions

It is quite surprising that the extended terms of the electrophoretic effect are not only large, but can in many cases account for the conductance behavior usually attributed to ion-pair formation. Since the conductance curves are smooth, monotonic functions of concentration, a good fit of the data does not necessarily mean validity of the fit-

ting function. Simply keeping higher terms in the electrophoretic effect admittedly does not give a theoretically correct result, but certainly neglecting these terms does not either. It would be of interest to examine transference numbers in mixed solvent systems since this property is independent of the relaxation effect.

Acknowledgments.—The authors wish to acknowledge a grant from the National Science Foundation in support of this work. Our thanks go also to Professor R. L. Kay and Mr. J. Hawes for permitting the use of their conductance data on KCl and CsCl in ethanol–water mixtures prior to its publication.

THE ADSORPTION OF XENON AND HYDROGEN ON EVAPORATED FILMS OF TUNGSTEN AND NICKEL

BY J. R. ANDERSON AND B. G. BAKER

Chemistry Department, University of Melbourne, Melbourne, Australia

Received September 25, 1961

Surface areas of evaporated films of nickel and tungsten have been measured by chemisorption of hydrogen and by physical adsorption of xenon and krypton; these methods give results which are in substantial agreement. Xenon adsorption has been used to study the sintering of tungsten and nickel films: it was found that tungsten films did not sinter at 510°K., while the presence of hydrogen markedly reduced the rate of sintering of nickel at 468°K. although the ultimate areas for vacuum sintered and hydrogen sintered nickel films were the same and equal to about four times the apparent geometric area. A model is suggested to account for the effect of chemisorbed hydrogen on the rate of sintering. The effect of sintering on the electrical resistance of nickel films has been measured and the surface structure studied by electron-microscopic examination; the implications of these observations for the sintering process are discussed.

While krypton often has been used for the estimation of surface areas of evaporated metal films by the B.E.T. method,¹⁻⁴ xenon has been largely neglected despite its obvious advantage that, with a higher heat of adsorption and low saturation vapor pressure, measurements will be made at lower equilibrium pressures and dead-space corrections will be smaller. This feature was of particular importance in the present instance since it was desired to assess the importance of film sintering under conditions similar to those used in catalytic experiments and a considerable dead-space was unavoidable. Accordingly, the adsorption of xenon on evaporated films of tungsten and nickel has been investigated together, for comparison, with measurements with krypton and hydrogen. The use of these measurements for surface area estimation has been examined and the technique applied to a study of the sintering of nickel films. Structural changes in nickel films on sintering have been studied by electron microscopic examination.

Experimental

(i) **Apparatus and Technique.**—The apparatus was similar to that used by Beeck⁵ and by Kemball.⁶ The adsorption vessel onto the inside walls of which films were deposited was cylindrical with internal diameter 73 mm. and length 100 mm. and was attached by a water-cooled ground glass joint with Apiezon L grease.

Throughout adsorption measurements films were protected from mercury vapor by an adjacent cold trap, liquid air being used for hydrogen and a Dry Ice–acetone slurry for xenon and krypton.

Pressures were measured using McLeod gages, one covering the range 10^{-6} to 4×10^{-2} mm., the other 10^{-3} to 4 mm.,

except for xenon on tungsten at 80°K. when the low pressures necessitated the use of an ionization gage (C.V.C. inc. type G.I.C. 011). The latter was calibrated using xenon against the McLeod gage in the range 10^{-4} to 10^{-3} mm. Cylinder hydrogen was purified by diffusion through a heated palladium thimble and through liquid air traps. Xenon and krypton were used directly from glass bulbs supplied by the British Oxygen Company; the only significant impurities were 0.5% krypton in the xenon and 0.5% xenon in the krypton. Doses of gas were measured in the McLeod gage and expanded into the reaction vessel. Equilibrium pressures were measured after 10 min. for xenon and krypton and after five min. for hydrogen except for xenon at 80°K., when 15 min. were required to establish equilibrium. Pressure readings were corrected for thermomolecular flow using the method of Porter.⁷ The total dead-space was about 1200 cm.³. The volumes of the different parts of the apparatus were calibrated by sharing experiments using the McLeod bulb as a standard volume. Low temperatures were measured using an oxygen vapor pressure thermometer.

(ii) **Film Preparation.**—Films were prepared by direct evaporation from hair-pin filaments situated on the axis of the adsorption vessel. Nickel wire, diameter 0.5 mm., was Johnson and Matthey spectroscopically standardized, with the following metallic impurities in parts per million: Fe, 5; Si, 3; Ca, 2; Cu, 1; Mn + Mg + Na + Li < 1. Tungsten wire (diameter 0.2 mm.) was Johnson and Matthey pure grade. Tungsten filaments were held in small molybdenum spring clips. Tungsten films were deposited at 273°K. after the adsorption vessel had been baked at 720°K. under vacuum for 15 hr., during the last hour of which the filament was outgassed at 5.2 amp. The rate of evaporation was about 20 mg. hr.⁻¹ at 6.3 amp. Only one film was obtained from each tungsten filament and a clean adsorption vessel was used for each film. Nickel films were deposited at 273°K. at 6.2 amp. at rates in the range 15–45 mg. hr.⁻¹ after the adsorption vessel had been baked at 720°K. for 15 hr., during the whole of which time the filament was outgassed at 4.1 amp. Before use, nickel filaments were purified by the evaporation of one film and for this two alternative techniques were used: technique A—a film was deposited at the usual rate after baking at 720°K. either (i) for 2 hr. and outgassing at 4.7 amp. for 0.5 hr. or (ii) for 15 hr. and outgassing at 4.1 amp. for 15 hr. (in neither (i) nor (ii) did appreciable evaporation occur); technique B—during a 15-hr. baking period the filament was heated at 4.7 amp., during which time a film of about 10 mg. deposited.

(1) O. Beeck, *Advances in Catalysis*, **2**, 151 (1950).

(2) R. A. Pierotti and G. D. Halsey, *J. Phys. Chem.*, **63**, 680 (1959).

(3) D. F. Klemperer and F. S. Stone, *Proc. Roy. Soc. (London)*, **A243**, 375 (1957).

(4) M. W. Roberts, *Trans. Faraday Soc.*, **56**, 128 (1960).

(5) O. Beeck, A. Smith, and A. Wheeler, *Proc. Roy. Soc. (London)*, **A177**, 62 (1940).

(6) C. Kemball, *ibid.*, **A207**, 539 (1951).

(7) A. S. Porter, *Discussions Faraday Soc.*, **8**, 358 (1950).

In each case the preliminary film was discarded and a clean reaction vessel used for each subsequent film.

The pressure in the reaction vessel at the completion of baking and outgassing of a filament prepared by technique B was within the range 2 to 5×10^{-7} mm., as measured by the ionization gage attached at the head of the vessel, and remained unchanged when the filament was raised to evaporation temperature.

Results

(i) **Adsorption on Tungsten Films.**—Adsorption of hydrogen was measured on films in the range 12–14 mg. at 90°K. (films W1, W2) and at 273°K. (films W2, W3, W5). With film W2 the isotherm first was measured at 273°K. and then continued at 90°K. Data are summarized in Table I and a typical isotherm is contained in Fig. 1. At 273°K. hydrogen adsorption isotherms were sensibly horizontal at pressures in the region of 10^{-3} mm. Adsorption of xenon was studied at 90°K. on bare tungsten (W4) and on films (W1, W2, W3) onto which hydrogen had been preadsorbed up to an equilibrium pressure of about 10^{-3} mm., followed by pumping at 293°K. to $< 10^{-6}$ mm. Films thus pretreated subsequently are referred to as "hydrogen covered." Xenon adsorption also was studied on films W1, W2, W3 after subsequent heating in 15 mm. of hydrogen for 16.5 hr. at 510°K. followed by pumping at 293°K. to better than 10^{-6} mm. An estimate of the ease of reversibility of xenon adsorption was made by repeating the xenon adsorption on films W3 and W4 after pumping at 293°K. for 2 hr., after which the pressure above the isolated specimen did not rise above 5×10^{-6} mm. in 0.5 hr. A typical xenon adsorption isotherm on "hydrogen covered" tungsten is shown in Fig. 2 together with these results plotted according to the B.E.T. equation.⁸ Similar results for xenon on bare tungsten at 80°K. are shown in Fig. 2 and isotherms of xenon on bare and "hydrogen covered" tungsten at 90°K. are compared in Fig. 3.

TABLE I
ADSORPTION OF HYDROGEN ON TUNGSTEN FILMS

Film	Weight, mg.	T, °K.	N_{H_2} no. of hydrogen molecules adsorbed $\times 10^{-16}$ ^a	Film area, ^b cm. ²
W1	12.0	90	3.27	
W2	14.0	273 90	2.95	4850
			3.70	
W3	12.6	273	2.27	3740
W5	13.8	273	2.67	4400

^a At 1×10^{-3} mm. ^b Assuming a monolayer of hydrogen atoms at 273°K. and 1×10^{-3} mm. and number of sites 1.215×10^{16} cm.⁻².

(ii) **Adsorption on Nickel Films.**—Film weights were in the range 6 to 40 mg. In series ON films were prepared by a technique essentially similar to that used by Kembal⁶: that is, a virgin filament was purified by technique A (*cf.* Experimental). Films ON1, ON2, ON3 and films ON4, ON5 were, within each set, prepared consecutively by evaporation from one filament and on each of these films the adsorption of hydrogen at 90°K. followed by the adsorption of xenon at 90°K. was measured.

(8) S. Brunauer, P. H. Emmett, and E. Teller, *J. Am. Chem. Soc.*, **60**, 309 (1938).

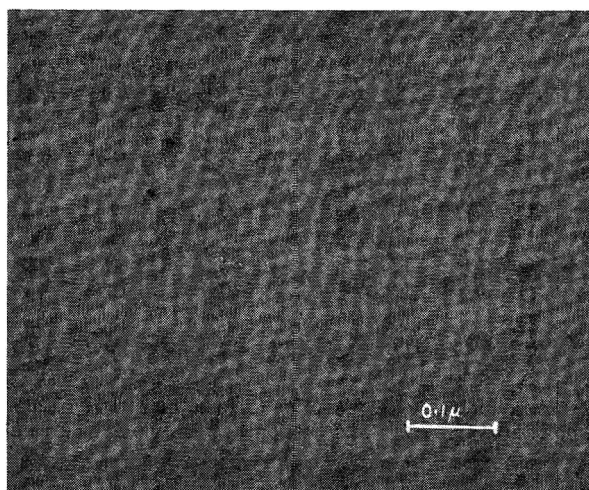


Plate 1.—Electron micrograph of nickel films; for details see text.

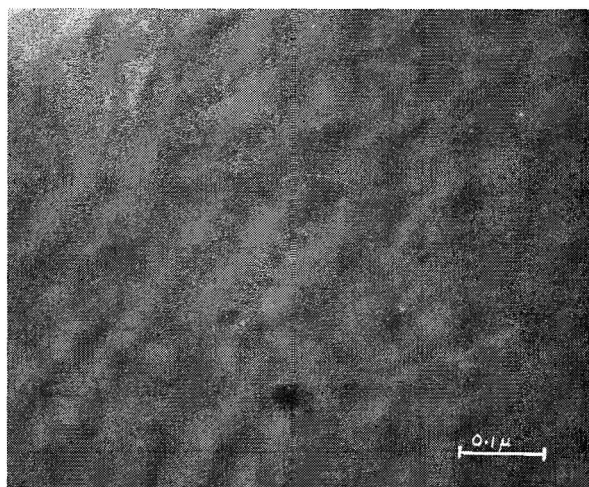


Plate 2.—Electron micrograph of nickel films; for details see text.

The filament was exposed to the air between each experiment, while the adsorption vessel was changed, but was subjected to the out-gassing procedure described previously before each subsequent film deposition. Between the hydrogen adsorption and xenon adsorption the vessel was pumped to $< 10^{-6}$ mm. at 273°K. Films thus

TABLE II
ADSORPTION OF XENON ON TUNGSTEN FILMS AT 90°K.
Films W1, W2, W3 hydrogen covered; film W4 bare tungsten

Film	N_m (mole $\times 10^{-16}$) ^c	Film area, ^a cm. ²	—Film deposited at 273°K.—		Film deposited at 273°K. and then heated in hydrogen ^b
			$2^\circ N_m$ after pumping, mole $\times 10^{-16}$	% of surface cleaned by pumping at 293°K. for 2 hr.	
W1	1.41	3240	1.45 3330
W2	1.88	4320	1.68 3860
W3	1.63	3750	0.917	56
W4	1.87	4300	0.382	20

^a Assuming Xe area 23.0 \AA^2 [*cf.* Discussion]. ^b Heated in 15 mm. of hydrogen for 16.5 hr. at 510°K. ^c Monolayer adsorption, obtained from B. E. T. plots.

TABLE III
COMPARATIVE ADSORPTION OF XENON, HYDROGEN, AND KRYPTON ON NICKEL FILMS

Film	Hydrogen adsorption at 90°K.			Xenon adsorption at 90°K.		Krypton adsorption at 77°K.	
	Weight, mg.	N_{H_2} at 1×10^{-3} mm. (mole $\times 10^{-18}$)	Film area, cm. ² ^a	N_m (mole $\times 10^{-18}$)	Film area, cm. ² ^b	N_m (mole $\times 10^{-18}$)	Film area, cm. ² ^c
ON1	11.4	0.157	204	0.392	765
ON2	9.7	0.230	300	.349	680
ON3	20.1	1.01	1310	.676	1320
ON4	12.2	0.684	890	.756	1475
ON5	14.9	0.940	1220	.782	1525
NN1	14.0	1.02	1330	.671	1310
NN2	11.0	0.893	1160	.521	1020
NN9	39.3	0.951 (80°K.)	1860	1.063 (77°K.)	1900

^a Assuming a monolayer of hydrogen atoms at 90°K. and 1×10^{-3} mm. and number of sites 1.54×10^{16} cm.⁻². ^b Assuming Xe area 19.5 \AA^2 [cf. Discussion]. ^c Assuming Kr area 17.9 \AA^2 [cf. Discussion].

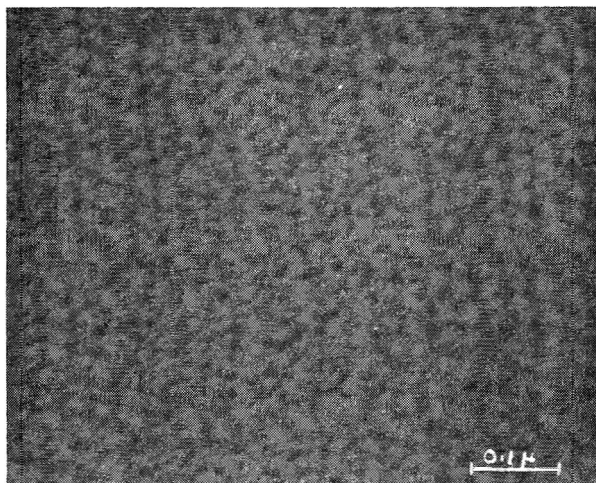


Plate 3.—Electron micrograph of nickel films; for details see text.

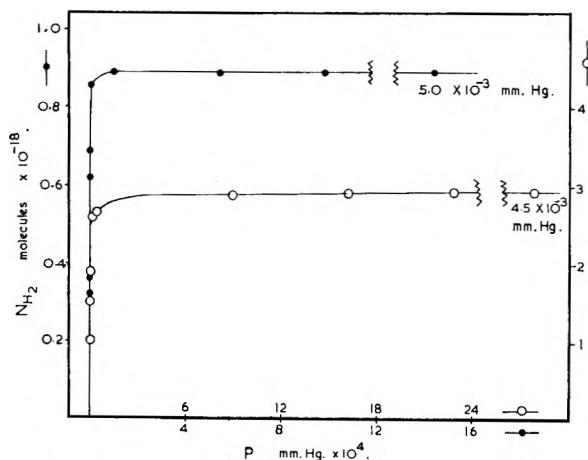


Fig. 1.—Adsorption of hydrogen: ●, on nickel (film NN2) 90°K.; ○, on tungsten (film W2) 273°K.

pretreated are subsequently referred to as “hydrogen covered.”

Results for these films (Table III) show that the ratio A_{Xe}/A_H of surface area by xenon adsorption (A_{Xe}) to that by hydrogen adsorption (A_H) had values ON1 3.75; ON2 2.27; ON3 1.02; and ON4 1.66; ON5 1.25. The fall in this ratio with consecutive evaporation from a given filament clearly showed that this filament purification technique was inadequate and therefore in series NN filaments

were purified by technique B. Adsorption measurements similar to those on films ON1-ON5 were made on films NN1 and NN2 for which A_{Xe}/A_H was 1.01 and 0.90, respectively (cf. Table III), thus showing the efficacy of the modified filament purification technique. A typical hydrogen adsorption isotherm at 90°K. is included in Fig. 1. At 90°K. hydrogen adsorption isotherms on nickel were substantially horizontal at pressures above 10^{-4} mm. A typical isotherm and the corresponding B.E.T. plot for the adsorption of xenon at 90°K. is included in Fig. 2. Isotherm data from a number of experiments for xenon adsorption at 90°K. on bare nickel and on “hydrogen-covered” nickel are collected into Fig. 4, for which values of N_m were obtained from B.E.T. plots on the individual isotherms. Data for xenon adsorption at 80°K. on bare nickel (NN4) and on “hydrogen-covered” nickel (NN9) also are collected in Fig. 4 for measurements in the range $0 < p/p_0 < 0.04$. The values of p_0 , the saturation vapor pressure of xenon, were measured by the McLeod gage and, after correction for thermomolecular flow, were 6.3×10^{-2} mm. at 90°K. and 4.6×10^{-3} mm. at 80°K., in both cases in equilibrium with solid xenon.

An estimate of the ease of reversibility of xenon adsorption on nickel films was made with films NN2, NN3, NN4 using the same method as described for tungsten films. On “hydrogen-covered” nickel (NN2) and on bare nickel (NN3, NN4) the fraction of surface cleaned by pumping was about 90%.

The adsorption of krypton on nickel was studied at 77°K. Since p_0 for krypton, measured as for xenon, was found to be 1.75 mm. at 77°K. (in agreement with Kington and Holmes⁹) dead space corrections limited measurements to $p/p_0 < 0.009$. Typical data are shown in Fig. 5 and comparative surface areas obtained from B.E.T. plots are listed in Table III. Since repeated krypton isotherms showed that adsorbed krypton could be completely removed by the pumping procedures previously described, the krypton isotherm was taken before xenon.

(iii) **Xenon Isotherms on Nickel at Higher Pressures.**—Isotherms for the adsorption of xenon on nickel at 90 and 80°K. taken to the maximum value of p/p_0 consistent with accurate dead-space

(9) G. L. Kington and J. M. Holmes, *Trans. Faraday Soc.*, **49**, 417 (1953).

corrections are collected into Fig. 6 for which values of N_m were obtained from B.E.T. plots of the individual isotherms in the low pressure region, $p/p_0 < 0.04$. Figure 6 also includes B.E.T.-type plots. The full line in the figure is an extrapolation of that which fits the data for both temperatures in the region $p/p_0 < 0.04$: this line also approximately fits the data for 90°K. in the range $0.04 < p/p_0 < 0.21$. The data for 80°K. fit a B.E.T.-type plot in the range $0.04 < p/p_0 < 0.33$, but this is not colinear with that from the same isotherm in the region $p/p_0 < 0.04$.

(iv) **Sintering of Nickel Films.**—The rate of sintering of nickel films was studied at 468°K. (a) in the presence of 15 mm. of hydrogen and (b) *in vacuo*, for periods in the range 20 min. to 17 hr. The results are contained in Fig. 7. Each point on the graph represents a separate experiment with a fresh film and surface areas were measured by xenon adsorption at 90°K. Initial areas were in the region of 1300 cm.² for all specimens.

To obtain information about the nature of the sintering process, particularly with lighter films, electrical resistances of films were measured during vacuum sintering at 703°K. and an electron microscopic examination was made of film surfaces before and after sintering. Resistance measurements were made between Pt-foil contacts, using a shunted Wheatstone bridge. Data are recorded in Table IV.

TABLE IV

RESISTANCE CHANGES ON SINTERING OF NICKEL FILMS	3.8 mg. film	1.0 mg. film
Resistance (R_1) before sintering (ohms)	6.1	82
Resistance (R_2) after heating <i>in vacuo</i> for 1 hr. at 703°K. (ohms)	4.9	72
100 ($R_1 - R_2$)/ R_2	24.5	13.9

Both films showed the normal positive temperature coefficient of resistance characteristic of metallic nickel. Specimens for electron microscope examination were obtained by smashing the glass vessels onto the inside walls of which films had been deposited. The insertion of glass specimen slides into the vessel was rejected because of the impossibility of temperature control during evaporation. Specimens were shadowed by carbon-platinum evaporation (20° incident angle) and replicas recovered by solution of the nickel in hydrochloric acid. Plates 1-3 show, respectively: (1) 8.6 mg. Ni film deposited at 273°K. and warmed only to 293°K.; (2) 3.4 mg. Ni film deposited at 273°K. and heated to 703°K. for 1 hr. *in vacuo*, specimen taken from the densest part of the film; (3) same as 2, but specimen taken from near the edge of the film. As judged by visual comparison of the transparencies, the thickness of specimen 3 was roughly the same as that of a 0.5-1 mg. film.

Discussion

(i) **Adsorption Measurements.**—The data in Table I show that on tungsten films at about 10⁻³ mm. the ratio of hydrogen adsorbed at 90°K. to that adsorbed at 723°K. is 1.28, in substantial agreement with Trapnell,¹⁰ who found a corresponding ratio

(10) B. M. W. Trapnell, *Proc. Roy. Soc. (London)*, **A206**, 39 (1951).

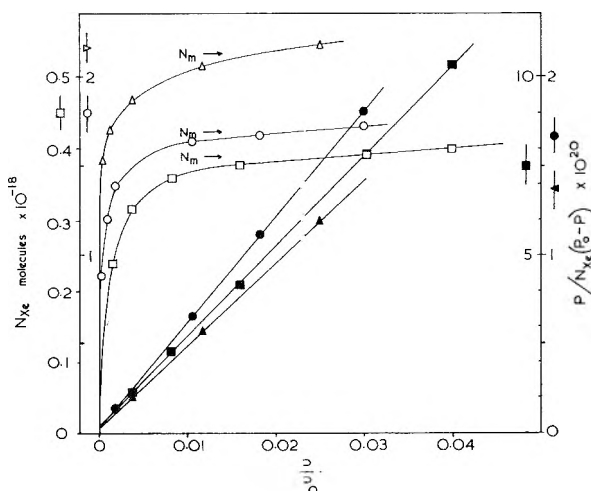


Fig. 2.—Adsorption of xenon: Δ, on bare tungsten (W8 13.1 mg.) 80°K.; O, on hydrogen covered tungsten (W3) 90°K.; □, on hydrogen covered nickel (ON3 11.4 mg.) 90°K. B.E.T. plots are shown by corresponding closed symbols.

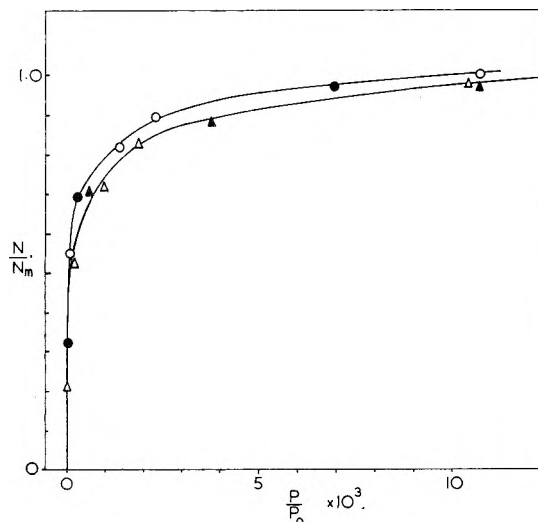


Fig. 3.—Adsorption of xenon at 90°K.: bare tungsten: O, (W6 20.0 mg.) and ● (W8 13.1 mg.); hydrogen covered tungsten Δ (W3) and ▲ (W6)

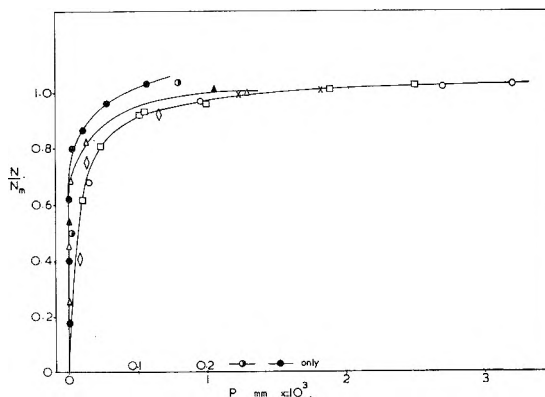


Fig. 4.—Adsorption of xenon on nickel and hydrogen covered nickel: ●, (NN4 19.6 mg.) nickel at 80°K.; Δ, (NN3 7.3 mg.) and ▲, (NN6 9.4 mg.) nickel at 90°K.; ○, (NN9 39.3 mg.) hydrogen covered nickel at 80°K.; O, (NN2 11.0 mg.), □, (ON3 11.4 mg.), ×, (ON2 9.7 mg.), and ◇, (ON5 14.9 mg.) hydrogen covered nickel at 90°K.

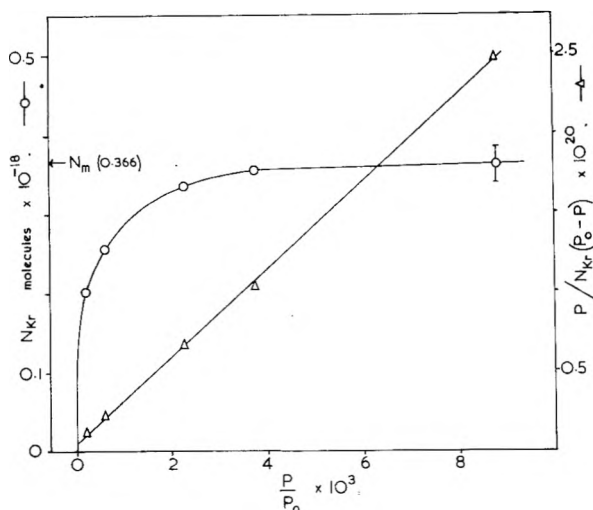


Fig. 5.—Adsorption of krypton on nickel at 77°K. (Film NN5 6.4 mg.).

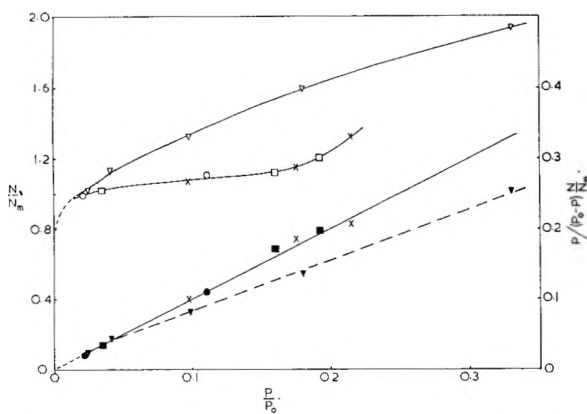


Fig. 6.—Adsorption of xenon on nickel at higher pressures: 80°K. ∇ (NN4); 90°K. \circ (NN3), \times (NN7), \square (NN8 7.3 mg.). Corresponding B.E.T. plot shown by closed symbols. (For significance of the line see text.)

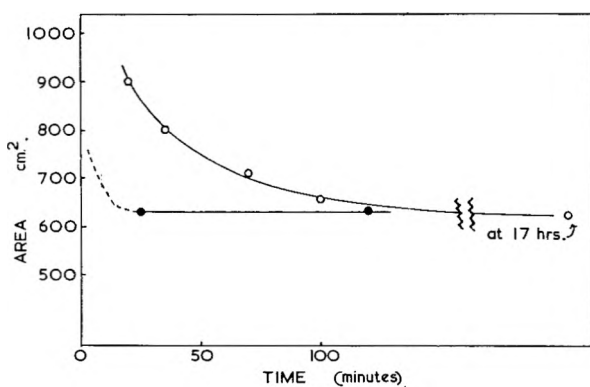


Fig. 7.—Sintering of nickel films at 468°K.: \circ , in the presence of hydrogen; \bullet , in vacuo.

of 1.21. Mignolet¹¹ has suggested that hydrogen may be adsorbed as molecules but the recent flash-filament experiments of Eisinger¹² and Hickmott¹³ have shown that the molecular form exists only at low temperatures: isotherms measured by Hick-

mott¹³ indicate that a monolayer of adsorbed hydrogen atoms exists at 273°K. and about 10^{-4} mm. Accordingly, we have adopted, as a criterion of monolayer coverage by hydrogen atoms on tungsten, adsorption at 273°K. to a pressure in the range $2 \times 10^{-4} - 10^{-3}$ mm., where the isotherm is substantially horizontal. In calculating surface areas it has been assumed that there are, on the average, 1.215×10^{15} sites cm^{-2} , a figure calculated on the assumption that the film exposes the (100) and (110) planes since this was shown by Johnson¹⁴ to be true for tungsten filaments and, in the absence of more conclusive evidence, has been taken to apply to films.

On nickel films at 90°K. hydrogen adsorption isotherms were substantially flat in the region $10^{-4} - 10^{-3}$ mm. and this again has been taken as the criterion of monolayer coverage by hydrogen atoms. In calculating surface areas it has been assumed that there are, on the average, 1.54×10^{15} sites cm^{-2} , a figure calculated on the assumption that the (100), (110) and (111) planes are equally exposed. The difficulty experienced in outgassing nickel filaments so that evaporated films were clean to chemisorption lends emphasis to the recent remarks of Hume-Rothery¹⁵ that, although the metallic impurity limits usually quoted for spectroscopically standardized metals may indicate a high degree of purity, in fact gaseous impurity may be considerable. Indeed, analysis of the present grade of virgin nickel wire for dissolved non-metals¹⁶ gave the following result: O_2 , 0.48% (w./w.), H_2 , 0.013%; N_2 , 0.004%; C, 0.02%; S, 0.001% — a situation which was not suspected when the investigation was commenced! For comparison, this wire after purification technique B (followed by standing in air at room temperature for some weeks) gave the analytical results¹⁷: O_2 , 0.0025% (w./w.); N_2 , 0.002%; H_2 , 0.0002%. It is clear that such nickel filaments cannot be satisfactorily purified in a reasonable period by heating to any temperature below the evaporation temperature, and that outgassing procedures previously recommended may not be adequate.

On both tungsten and nickel xenon adsorption isotherms at 90°K. showed a comparatively sharp "knee" in the very low pressure region of $p/p_0 \sim 0.005$. The isotherms accurately obeyed B.E.T. plots in the range generally investigated, $p/p_0 < 0.04$ (cf. Fig. 2). The reproducibility is shown by the substantial concordance achieved between a number of separate experiments collected into Fig. 3, 4, and 6.

In the adsorption of carbon dioxide at 195°K.⁸ and of krypton at 77°K.,^{18,19} values of p_0 extrapolated for the supercooled liquid have been used in calculating areas by the B.E.T. method. However, present measurements with xenon were so far below its melting point (m.p. 161°K.) that we have preferred to use p_0 for solid xenon. We have

(14) R. P. Johnson, *Phys. Rev.*, **54**, 459 (1938).

(15) W. Hume-Rothery, *Nature*, **184**, 1794 (1959).

(16) By courtesy of Johnson and Matthey Ltd.

(17) By courtesy of Defence Standards Laboratory, Melbourne.

(18) R. A. Beebe, J. B. Beckwith and J. M. Honig, *J. Am. Chem. Soc.*, **67**, 1554 (1945).

(19) R. T. Davis, T. W. DeWitt, and P. H. Emmett, *J. Phys. & Colloid Chem.*, **51**, 1232 (1947).

(11) J. C. P. Mignolet, "Chemisorption," Ed. Garner, Butterworths, London, 1956, p. 169.

(12) J. Eisinger, *J. Chem. Phys.*, **29**, 1154 (1958).

(13) T. W. Hickmott, *ibid.*, **32**, 810 (1960).

similarly used p_0 for solid krypton (m.p. 116°K.), following the usage of some (but not all) recent workers.^{2,4,9} In the present low pressure range the use of the alternative values for p_0 alters the calculated surface areas by less than 5%.

Effective areas per adsorbed xenon atom have been adduced from the following considerations. On some non-metallic adsorbents areas for adsorbed krypton¹⁸ and xenon¹⁹ have been obtained by comparative B.E.T. measurements using nitrogen as a standard: it was established that the effective rare gas areas were in excess of the values which would correspond to close-packed monolayers. It therefore was pointed out¹⁸ that the effective krypton area may be dependent on the arrangement of adsorption sites in the surface. For instance, the effective areas on anatase were 19.5 Å.² for krypton¹⁸ and 27.4 Å.² for xenon²⁰ compared to expected (solid) close-packed areas of 14.0 and 16.5 Å.², respectively. To examine more specifically the case of xenon where the effect is greatest, it may be noted that in anatase the dense (001) plane probably is predominately exposed at the surface, particularly since this is a natural cleavage plane: the oxide ions of the (001) plane do not, in fact, lie exactly in the plane since half lie slightly above and half are depressed slightly below. Examination of a model suggests that the most likely site for adsorption of a xenon atom is immediately above a "depressed" oxide ion and in contact, or near contact, with two titanium ions and with four oxide ions which lie above the plane. Due to the size of xenon, adjacent sites cannot be occupied and the adsorbed xenon atoms form an array with coördinates $(ha, ka, 0)$, $h + k$ even; where h and k are integers and a is the lattice constant of anatase. On this basis the effective area per adsorbed xenon is 28.3 Å.², calculated using $a = 3.77$ Å., a value obtained from an X-ray examination of the original sample.²¹ However, as shown by Beeck²² for nickel and iron, comparative B.E.T. measurements using nitrogen are invalid for metal surfaces which chemisorb nitrogen. Therefore, in the absence of such comparative data we adopt the model that the xenon "monolayer" measured for the low pressure isotherms in the region $p/p_0 < 0.04$ (cf. Fig. 2 and 3) consists of xenon atoms which are adsorbed at crystallographic surface sites. We shall refer to this as a "lattice-packed" monolayer. That such a model is not unreasonable is further suggested by the data of Ehrlich and Hudda,²³ who have shown that the activation energy for surface migration of xenon on a sparsely covered tungsten surface is ~ 3 kcal. mole⁻¹, which is large compared to RT at 90°K. (0.18 kcal. mole⁻¹). Such a high value for the energy difference between a crystallographic adsorption site and a position on the surface between such sites suggests that crystallographic adsorption sites will be preferred. Using the diameters of xenon and krypton calculated

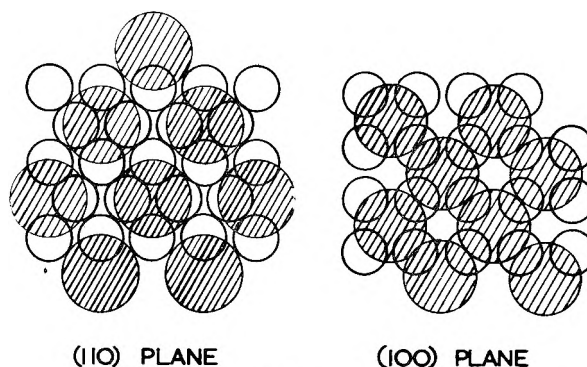


Fig. 8.—Xenon adsorbed on tungsten.

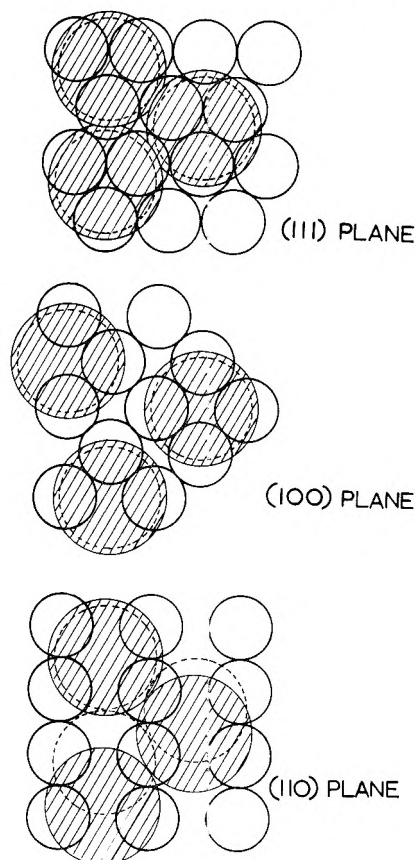


Fig. 9.—Xenon and krypton adsorbed on nickel. (Xe shaded, Kr broken circle.)

from the lattice constants of the solids, 4.36 and 3.94 Å., respectively (cf. Moelwyn-Hughes²⁴), lattice-packing is shown to scale in Fig. 8 for tungsten and Fig. 9 for nickel. On this basis the average effective area occupied by a xenon atom is 23.0 and 19.5 Å.² on polycrystalline tungsten and nickel films, respectively, while for krypton on nickel the corresponding figure is 17.9 Å.².

B.E.T. plots of xenon adsorption data in the region $p/p_0 < 0.04$ show that a monolayer, which we assume to be lattice-packed, is reached at $p/p_0 \approx 0.02$ on tungsten and ≈ 0.03 on nickel. As shown in Fig. 6, the extension of the xenon isotherm on nickel at 80°K. into the region $0.04 < p/p_0 < 0.33$ leads to a B.E.T. plot for this region with a slope

(24) E. A. Moelwyn-Hughes, "Physical Chemistry," Pergamon Press, London, 1957, p. 25.

(20) J. H. Singleton and G. D. Halsey, *J. Phys. Chem.*, **58**, 330 (1954).

(21) W. D. Harkins and G. Jura, *J. Am. Chem. Soc.*, **66**, 919 (1944).

(22) O. Beeck, *Discussions Faraday Soc.*, **8**, 159 (1950).

(23) G. Ehrlich and F. G. Hudda, *J. Chem. Phys.*, **30**, 493 (1959).

different from that from the same isotherm in the range $p/p_0 < 0.04$. The ratio of the low pressure B.E.T. slope to the high pressure B.E.T. slope is 0.78, while if it were assumed that in the high pressure region the adsorbed xenon atoms could close-pack the expected ratio is 0.85. We therefore suggest that at 80°K. on nickel a type of phase transition occurs in the vicinity of $p/p_0 \approx 0.05$ in which further adsorption into a lattice-packed monolayer leads to approximate close packing.

Because of the much higher absolute pressures involved, krypton measurements could not be made with high accuracy above $p/p_0 \approx 0.005$. Nevertheless it is clear from Fig. 5 that at 77°K. on nickel the "knee" of the isotherm is well defined in the region $p/p_0 \approx 0.002 - 0.003$ and a monolayer, which we assume to be lattice-packed, is approached at $p/p_0 \approx 0.01$. Very similar behavior has been found by Roberts⁴ in the adsorption of krypton on iron films at 77°K.

The present agreement between film areas measured by hydrogen and by rare-gas adsorption is contrary to the conclusion reached by Klemperer and Stone³ that on nickel films the area available for krypton adsorption at 77°K. is 2.5 times that for hydrogen adsorption. It should be noted, however, that Klemperer and Stone's B.E.T. areas were obtained under rather different conditions to the present work in that they (a) measured krypton isotherms over a higher pressure range, $p/p_0 > 0.01$ (taking as p_0 1.75 mm.), (b) used for p_0 in the B.E.T. plots an extrapolated value for liquid krypton (about 4.3 mm.) instead of p_0 for solid krypton as adopted in the present work, and (c) used 20 Å.² for the effective area of adsorbed krypton.

In the preparation of "hydrogen covered" films both for tungsten and nickel, the pumping procedure undoubtedly removes some hydrogen from the surface. However, from the hydrogen adsorption isotherms this would not amount to more than about 10% when pumped to an equilibrium pressure of 10^{-6} mm. It is apparent from Fig. 3 and 4 that on both nickel and tungsten the heat of adsorption of xenon on a "hydrogen covered" surface is lower than on a bare surface: if we define

$$\Delta(\Delta H) = \Delta H_{\text{bare}} - \Delta H_{\text{H cov}}$$

it is easily shown that, provided the entropy of adsorption depends on N/N_m only

$$\Delta(\Delta H) = 2.303RT \log p_{\text{bare}}/p_{\text{H cov}}$$

when the ratio of xenon equilibrium pressures $p_{\text{bare}}/p_{\text{H cov}}$ is taken at constant coverage and constant temperature T . With nickel at coverages 0.7, 0.8 and 0.9 the values of $\Delta(\Delta H_{\text{Xe}})$ are -300, -150 and -80 cal. mole⁻¹, respectively, while with tungsten the corresponding values are -150, -70 and -90 cal. mole⁻¹. A similar analysis of a pair of krypton isotherms on nickel gave values of $\Delta(\Delta H_{\text{Kr}})$ of -170 and -70 cal. mole⁻¹ at coverages of 0.3 and 0.5, respectively.

In Table V are listed for various systems values of the B.E.T. parameter C obtained by fitting calculated and experimental isotherms in the region

$0.4 < N/N_m < 0.9$. Using the expression for C from B.E.T. theory (cf. Cassie²⁵)

$$C = j_s/j_c \exp[(\Delta H - \Delta H_1)RT]$$

where j_s is the partition function for the internal degrees of freedom of the adsorbed molecule and j_c is the partition function of the molecule in the condensed phase, together with the values for ΔH_c , the heat of condensation of the adsorbate, of -3.30 and -2.68 kcal. mole⁻¹ for xenon and krypton, respectively,²⁶ values of ΔH_1 , the (average) heat of adsorption in the first layer, were obtained and are recorded in Table V. It was assumed that $j_s/j_c = 2$ for immobile adsorption (cf. Hill²⁷).

TABLE V
DATA FROM B.E.T. ANALYSIS

System, °K.	C	ΔH_1 (kcal. mole ⁻¹)
Xe/Ni, 90	2300	-4.56
Xe/Ni, H ₂ 90 ^a	1000	-4.41
Xe/W, 90	4000	-4.66
Xe/W, H ₂ 90 ^a	2500	-4.57
Kr/Ni, 77	2300	-3.76
Kr/Ni, H ₂ 77 ^a	1000	-3.63

^a Hydrogen-covered surfaces.

In view of the assumptions involved, the data in Table V are mainly significant in a relative sense: taken with the values obtained above for $\Delta(\Delta H)$ it seems clear that the heat of adsorption of xenon on hydrogen-covered nickel and tungsten is lower than on the bare metal by ~ 300 and ~ 150 cal. mole⁻¹, respectively, at $N/N_m \sim 0.7$, and for krypton on nickel at $N/N_m \sim 0.5$ the corresponding figure is ~ 100 cal. mole⁻¹. The comparatively small magnitude of these differences in ΔH presumably means that there can be no major change in the rare gas-metal distance, thus supporting the idea that the chemisorbed hydrogens are effectively buried in the surface.

(ii) **Sintering of Films.**—Tungsten film areas measured after heating in hydrogen at 510°K. (cf. Table II) show that no significant sintering has occurred, in agreement with Pierotti and Halsey,² who found that tungsten films did not sinter on heating to 720°K. *in vacuo*. However, using hydrogen chemisorption for area measurement, Campbell, Moss, and Kembal²⁸ have reported an area reduction of 31% for tungsten films heated to 573°K. for 10 min. *in vacuo*. We emphasize however that, in general, chemisorption is unsuitable for measuring the extent of high temperature sintering because of the difficulty of avoiding film contamination by gas evolved from the heated glass.²⁹

From the results in Fig. 7 it is clear that the presence of chemisorbed hydrogen markedly reduces the rate of sintering of nickel films. This conclusion also has been inferred indirectly from the internal self-consistency of kinetic data from catalytic experiments using nickel films.³⁰ The

(25) A. B. D. Cassie, *Trans. Faraday Soc.*, **41**, 450 (1945).

(26) Evaluated from vapor pressure data in Landolt-Bornstein.

(27) T. L. Hill, *J. Chem. Phys.*, **16**, 181 (1948).

(28) J. S. Campbell, R. L. Moss, and C. Kembal, *Trans. Faraday Soc.*, **56**, 1481 (1960).

(29) J. R. Anderson, to be published.

(30) C. Kembal, *Proc. Roy. Soc. (London)*, **A214**, 413 (1952).

results of Roberts⁴ show that iron films behave in a similar manner.

It seems reasonable to propose that chemisorbed hydrogen acts in this way by reducing the surface mobility of nickel and iron atoms: this is readily understood if a hydrogen atom is held at the surface not by a single bond from an individual surface metal atom but by a multicentered orbital involving those metal atoms which are nearest neighbors to the hydrogen, a suggestion previously made by Takaishi.³¹ This would effectively link together surface metal atoms by bonds which are not formed in the absence of such a chemisorbed atom. We tentatively suggest that the metal orbitals used in this way are the same as those proposed by Altmann, Coulson and Hume-Rothery³² to be the major bonding orbitals directed between nearest neighbors and determining the structure of the metallic crystal; that is, p^3d^3 hybrids for face-centered cubic nickel and $sd^3 + d^3$ hybrids for body-centered cubic tungsten and iron: we suggest that at the surface the residual parts of these orbitals project into space and a multi-centered orbital is formed by overlap with the hydrogen $1s$ orbital.

A consequence of this proposal is that on the (100) face of a body-centered cubic metal such as tungsten there is also the possibility of bonding between the hydrogen atom and a tungsten atom in the layer immediately below the surface layer, since this atom is only $b/\sqrt{3}$ below the surface layer (where b is the nearest neighbor distance). For this we suggest the use of a tungsten d^3 hybrid orbital³²; this orbital would be normal to the surface. A hydrogen atom in such a site is thus bonded with five tungsten atoms, which is more than reasonably can be expected at any other surface site: we believe that this would be a major contributing factor to the variation in binding energy found by Hickmott¹³ for hydrogen atoms chemisorbed on a polycrystalline tungsten filament.

The ultimate area from sintering at 468°K.—about 600 cm.²—is independent of the presence or absence of hydrogen and is about four times the apparent geometric film area.

Nickel films with weights as low as 1 mg. showed the normal temperature coefficient of resistance of nickel, thus showing that one of the alternative

suggestions of Logan and Kemball³³ that such light films consist of discrete non-touching crystallites cannot be correct; furthermore, the absolute value of the measured resistance is much too small to agree with such a suggestion, unless the gaps are so small that easy electron tunnelling occurs. The relative resistance change on sintering a 1 mg. film was much smaller than that for a film of weight 3.8 mg. (cf. Table IV), indicating that the lighter film had sintered relatively less extensively. This is in agreement with the electron-microscopic evidence in plates 1-3, which show that very light nickel films retain after sintering a rough surface with asperities about 200 Å. across, whereas heavy films sinter to yield a surface which, at this resolution, shows no marked deviation from flatness. This is in agreement with the conclusion which Logan and Kemball inferred from catalytic kinetic data with nickel films of varying weight. It is clear that under the present conditions nickel films are continuous at least down to 1 mg.

Heavy films deposited in a cylindrical vessel always will possess a very thin region; on this basis alone one thus would not expect the actual area of a sintered nickel film to equal the geometric area. However, the contribution of the rough very thin region cannot nearly account for the overall factor of four found. On the assumption that the asperities are close-packed hemispheres and that the very thin region occupies 20% of the apparent geometric area, the calculated ratio is only about 1.2. There seem three possible explanations: (a) fissures (perhaps at grain boundaries) which are beyond the present electron-microscopic resolution, run from the surface into the metal and so the sintered film retains some internal surface; (b) the sintered surface retains some roughness on an atomic scale due to terraces and steps; (c) "adsorbed" atoms penetrate extensively into the lattice. The latter seems most improbable in view of the large size of the xenon atom and the agreement between areas measured by xenon and hydrogen adsorption. Extensive solution of hydrogen at higher temperatures is of course well known.

Acknowledgments.—The authors are grateful to the Shell Co. (Aust.) Ltd. for a grant toward the cost of materials and to Drs. J. Sanders and J. Nicholas of the Division of Tribophysics, C.S.-I.R.O., for taking the electron micrographs and for helpful discussion, respectively.

(31) T. Takaishi, *Z. physik. Chem. (Frankfurt)*, **14**, 164 (1958).

(32) S. L. Altmann, C. A. Coulson, and W. Hume-Rothery, *Proc. Roy. Soc. (London)*, **A240**, 145 (1957).

(33) S. R. Logan and C. Kemball, *Trans. Faraday Soc.*, **56**, 144 (1960).

THE RHODIUM-CHLORINE SYSTEM AT HIGH TEMPERATURE¹

BY WAYNE E. BELL, M. TAGAMI, AND ULRICH MERTEN

John Jay Hopkins Laboratory for Pure and Applied Science, General Atomic Division of General Dynamics Corporation, San Diego, California

Received September 25, 1961

The rhodium-chlorine system has been studied over the temperature range 700 to 1500° and over the chlorine-pressure range 0.01 to 1.0 atm. Results show that solid RhCl₃ is the only stable condensed chloride under the conditions studied. The dissociation pressure of the chloride reaches 1 atm. at 970°. Chlorine-pressure-dependence data indicate that RhCl₂ and RhCl₃ are the important gaseous species. At 1504° and 1 atm. chlorine pressure, $p_{\text{RhCl}_2} = 6.5 \times 10^{-3}$ atm. and $p_{\text{RhCl}_3} = 15 \times 10^{-3}$ atm. Below 970°, where RhCl₃(s) is the condensed phase, the vapor pressures fall off rapidly with decreasing temperature, and at 802°, $p_{\text{RhCl}_2} = 4 \times 10^{-7}$ atm. and $p_{\text{RhCl}_3} = 1.7 \times 10^{-5}$ atm.

Introduction

The rhodium-chlorine system has been studied in the temperature range 700 to 1500° and the chlorine-pressure range 0.01 to 1.0 atm. This work was undertaken to identify condensed phases and vapor species, obtain dissociation pressure and vapor pressure data, and calculate thermodynamic values for the various reactions and species involved.

In previous investigations of the rhodium-chlorine system at high temperature, Wöhler and Müller² measured dissociation pressures and studied condensed chloride phases, and Puche³ measured dissociation pressures.

Experimental

Dissociation Pressure Studies.—Dissociation pressures were measured by both the static and the transpiration methods as described in detail in a previous paper.⁴ In the transpiration method, gas flow rates were around 2 ml. STP/min., which is in the range where measured pressures were found to be independent of flow rate.

Vapor Pressure Studies.—Vapor pressures were determined by the transpiration method. Except for the use of a radioactive-tracer method of analysis, techniques were essentially the same as those used in previous work.⁵ Mullite reaction tubes were used. Chlorine served as the carrier gas and was collected in KI solution and determined volumetrically. The vapor was collected in a condensing region at the edge of the furnace.

Slight chlorine corrosion of the mullite occurred at the highest temperatures used. At 1500°, the mullite radiation shield (which weighed about 2.5 g.) lost about 10 mg. during an experiment, whereas at 1000° the loss in weight was negligible.

Flow rates ranged from 0.01 to 0.1 mmole Cl₂/min., depending on temperature and pressure conditions. The results of flow-rate studies given in Table I show that these flow rates were in the range where the mole ratio (moles Rh:mole Cl₂) was independent of flow rate.

The rhodium metal used was irradiated in an electron linear accelerator by means of bremsstrahlung emitted from a platinum converter under bombardment by 25-Mev. electrons. The radionuclides 220-d Rh¹⁰² and 4.5-d Rh¹⁰¹ were produced by (γ, n) and ($\gamma, 2n$) reactions, respectively. Initially, the activity of the Rh¹⁰¹ was about three times that of the Rh¹⁰²; however, when the counting was done at the end of the experimental work, the Rh¹⁰¹ activity was negligible. Two different metal samples were used having activities of about 400 and 1500 c.p.m./mg., respectively, under our counting conditions. As a check on the analytical technique, each of the active metal samples was used in a vapor pressure measurement at 1102°; the

TABLE I

EFFECT OF FLOW RATE ON MOLE RATIO

Temp., °C.	System pressure, atm.	Flow rate [mmoles (Cl ₂ + Rh)/min.]	Rh:Cl ₂ mole ratio ($\times 10^3$)
852	0.497	0.016	0.167
852	.492	.038	.190
852	.500	.044	.174
902	.496	.050	.82
902	.495	.118	.88
1301	.977	.029	11.0
1301	.977	.092	10.8
1301	.978	.098	11.6
1301	.975	.33	11.5

two vapor pressure values obtained were found to agree. γ -Ray spectra of the samples agreed with spectra reported for Rh¹⁰² and Rh¹⁰¹.

To determine the quantity of rhodium condensed, the mullite condensing region (see Fig. 1 of ref. 5 for diagram of reaction tube) was crushed, placed in a plastic vial, and counted utilizing a NaI well-counter and a single-channel analyzer. Optimum counting conditions were obtained by counting integrally above 0.38 Mev. (The main γ -energy peak of Rh¹⁰² is 0.46 Mev.) Statistical counting errors were less than 2% standard deviation. For standards, samples of the radioactive metal were weighed out, mixed with crushed mullite, and counted in the same manner as the unknowns. Activities of the unknowns ranged from about 50 to 6000 c.p.m. The background stabilized at about 85 c.p.m.

At the beginning of the present work, attempts were made to develop a chemical method of analysis; however, no convenient means was found for dissolving the condensate.

General.—The materials used were rhodium sponge (Johnson Matthey, 99.995% purity); RhCl₃·3H₂O (Fisher, 99.9% rhodium purity); chlorine gas (Matheson, 99.85% minimum purity); and argon gas (Liquid Carbonic, 99.9% minimum purity). The gases were dried and purified as described in an earlier paper.⁵

Tube furnaces and Pt, Pt-10% Rh thermocouples were used as described previously.⁵ Temperature uncertainties are believed to range from $\pm 2^\circ$ at 800° to $\pm 4^\circ$ at 1500°.

Results and Discussion

Condensed Phase Studies.—Crystals made by reacting rhodium sponge and chlorine gas directly at 800° for three days showed a chlorine content of 49.68% by weight as determined gravimetrically by hydrogen reduction. Dehydration of commercial RhCl₃·3H₂O in a chlorine stream at 600° yielded an anhydrous product which analysis showed to contain 50.43% chlorine. Gavis and Sienko,⁶ by prolonged chlorination at 800°, obtained a product which contained 50.60% chlorine. On comparing these values with the 50.83% theoretical value for RhCl₃, it is apparent that the chloride formed was RhCl₃(s).

(1) This work was supported in part by the U. S. Atomic Energy Commission under Contract AT(04-3)-164.

(2) L. Wöhler and W. Müller, *Z. anorg. u. allgem. Chem.*, **149**, 125 (1925).

(3) F. Puche, *Ann. Chem.*, **9**, 233 (1938).

(4) W. E. Bell, M. C. Garrison, and U. Merten, *J. Phys. Chem.*, **64**, 145 (1960).

(5) W. E. Bell, U. Merten, and M. Tagami, *ibid.*, **65**, 510 (1961).

(6) J. Gavis and M. J. Sienko, *J. Am. Chem. Soc.*, **77**, 4983 (1955).

X-Ray powder patterns of samples of $\text{RhCl}_3(\text{s})$ formed at 800° showed the compound to be isomorphous with the black form of $\text{RuCl}_3(\text{s})$ and the violet form of $\text{CrCl}_3(\text{s})$. The latter two compounds previously were shown to be isomorphous by Stroganov and Ovchinnikov.⁷

To test for lower chlorides, a mixture was made in which rhodium and chlorine were in the atom ratio 1 to 1. This mixture was sealed in an evacuated quartz tube, annealed overnight at 800° , quenched, and then examined by X-ray techniques. Diffraction lines only for $\text{RhCl}_3(\text{s})$ and $\text{Rh}(\text{s})$ were found.

As a further test for lower chlorides, the chlorine content of the samples used in the dissociation-pressure work (discussed below) was varied over a wide range. There was no apparent effect on the dissociation pressure data.

On the basis of these results, we conclude that the stable condensed chloride is solid RhCl_3 and that no other stable condensed chlorides exist within the temperature and chlorine-pressure ranges studied.

Wöhler and Müller,² on the basis of gravimetric analyses of chloride fractions separated by flotation methods, claimed the existence of $\text{RhCl}_3(\text{s})$, $\text{RhCl}_2(\text{s})$, and $\text{RhCl}(\text{s})$ under conditions similar to ours. However, since they did not demonstrate homogeneity of the phases separated, and in light of the present results, their conclusions regarding $\text{RhCl}_2(\text{s})$ and $\text{RhCl}(\text{s})$ would appear to be in error.

Dissociation Pressures.—The dissociation pressure data, measured over the range 722 to 963° by two different methods, are plotted in Fig. 1. The data show a linear relationship between $\log p$ and $1/T$ within experimental error. Extrapolation of the line shows the dissociation pressure to be 1 atm. at 970° .

The chlorine content of the samples used in the static method gradated from 50.4%, essentially the content of RhCl_3 , to less than one chlorine atom per rhodium atom. Transpiration experiments at 800 and at 843° were continued to complete decomposition of the chloride, and in each case only one pressure plateau was observed. These results show that the degree of chlorination had no apparent effect on the dissociation-pressure data and suggest that RhCl_3 was the only solid chloride involved.

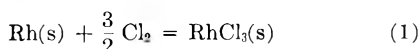
From the slope of the line in Fig. 1, we calculate, at the mean temperature of the measurements (1100°K .)

$$\Delta H_{1100}^0 = -67.8 \pm 2.0 \text{ kcal./mole}$$

and from this

$$\Delta S_{1100}^0 = \frac{\Delta H^0}{T} - \frac{3}{2} R \ln p = -54.5 \pm 2.0 \text{ e.u.}$$

for the reaction



From a rough rule given by Kubaschewski and Evans,⁸ we estimate ΔC_p for reaction 1 to be 4.5

(7) E. V. Stroganov and K. V. Ovchinnikov, *Vestnik Leningrad Univ.*, **12**, No. 22, Ser. Fiz. i Khim., No. 4, 152 (1957).

(8) O. Kubaschewski and E. L. Evans, "Metallurgical Thermochemistry," 3d ed., Pergamon Press, New York, N. Y., 1958.

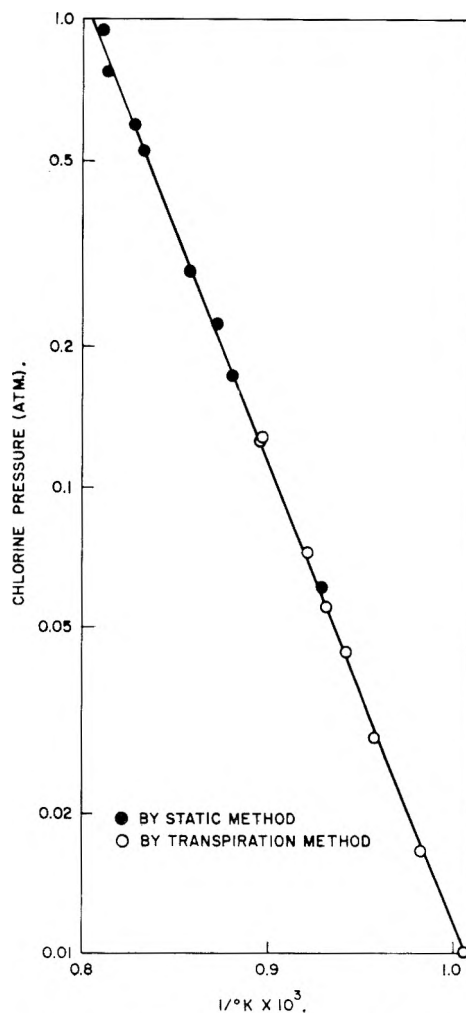


Fig. 1.—Dissociation pressure of $\text{RhCl}_3(\text{s})$.

± 1.0 cal./mole $^\circ\text{K}$., and assuming it to be constant over the range 298 to 1100°K ., we calculate

$$\Delta H_{298}^0 = -71.5 \pm 3.0 \text{ kcal./mole}$$

$$\Delta S_{298}^0 = -60.4 \pm 3.0 \text{ e.u.}$$

$$\log p_{\text{Cl}_2} = -\frac{10,620}{T} - 1.510 \log T + 13.20$$

Combining ΔS_{298}^0 with standard entropies S_{298}^0 $\text{Rh} = 7.53 \pm 0.05$ e.u. and $S_{298}^0 \text{Cl}_2 = 53.29 \pm 0.01$ e.u. given by Kelley and King,⁹ we obtain $S_{298}^0 \text{RhCl}_3(\text{s}) = 27.1 \pm 3.0$ e.u. This value may be compared with the experimental values $S_{295}^0 \text{RuCl}_3(\text{s}) = 30.5 \pm 2.5$ e.u., obtained by Bell, Garrison and Merten,⁴ and $S_{298}^0 \text{CrCl}_3(\text{s}) = 29.4 \pm 0.2$ e.u., reported by Kelley and King⁹ and based on low temperature heat capacity data. The value for $S_{298}^0 \text{RhCl}_3(\text{s})$ also may be compared with 38.0 ± 6.0 e.u., estimated by Brewer, *et al.*,¹⁰ and with 33.2 e.u., estimated by Latimer's rules.¹¹

Wöhler and Müller² reported dissociation-pressure data for RhCl_3 , RhCl_2 , and RhCl (as mentioned above, we find no evidence for the lower chlorides),

(9) K. K. Kelley and E. G. King, U. S. Bur. Mines Bull. 592, 1961.

(10) L. Brewer, *et al.*, in "The Chemistry and Metallurgy of Miscellaneous Materials: Thermodynamics," National Nuclear Energy Series, Div. IV, Vol. 19B, McGraw-Hill Book Co., Inc., New York, N. Y., 1950.

(11) W. M. Latimer, *J. Am. Chem. Soc.*, **73**, 1480 (1951).

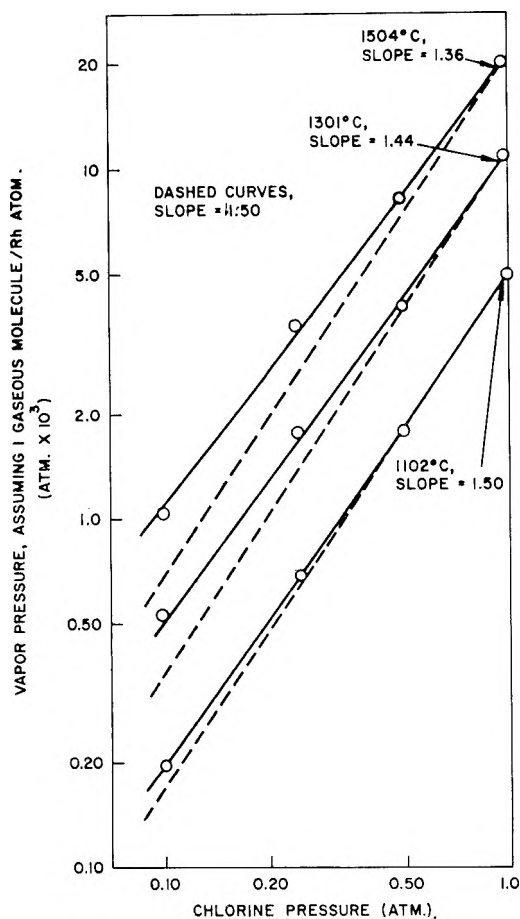
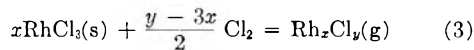
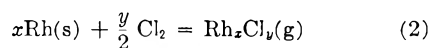


Fig. 2.—Effect of chlorine pressure on vapor pressure at 1102, 1301 and 1504°.

and Puche³ reported data for RhCl_3 and RhCl_2 . The data which Wöhler and Müller report for RhCl fall fairly well on our curve in Fig. 1; however, the data which they and Puche report for RhCl_3 and RhCl_2 fall above our curve.

Identification of Vapor Species.—Since $\text{Rh}(s)$ and $\text{RhCl}_3(s)$ are the stable condensed phases in the temperature range and the chlorine-pressure range studied, the solid-vapor equilibria to be considered are



From the equilibrium constant for eq. 2, we obtain

$$\log p_{\text{Rh}_x\text{Cl}_y} = \frac{y}{2} \log p_{\text{Cl}_2} + \log K$$

A similar expression is obtained for eq. 3, and we evaluate $y/2$ and $(y-3x)/2$ by studying the effect of chlorine pressure on vapor pressure.

Figures 2 and 3 show the isotherms obtained. The break in the 902° isotherm at 0.35 atm. fixes the equilibrium dissociation pressure of $\text{RhCl}_3(s)$ and agrees with the dissociation-pressure data in Fig. 1. The points in Fig. 2 and 3 represent the results of individual experiments with the following exceptions. The point at 1301° and 0.98 atm. chlorine pressure is the average of the vapor-

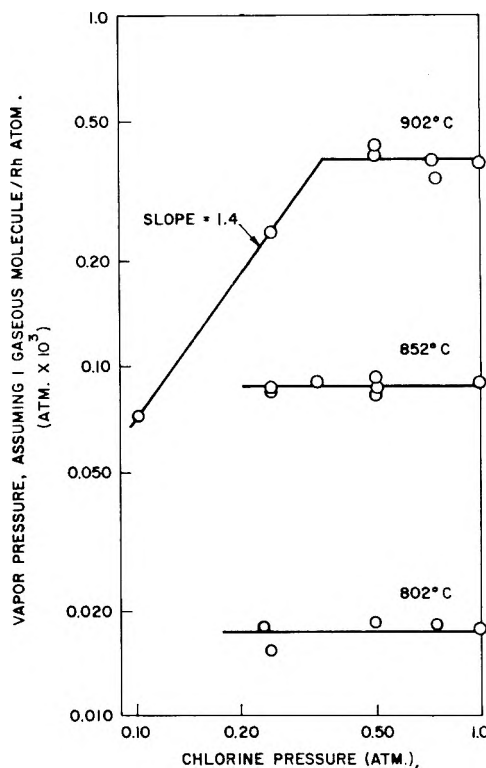


Fig. 3.—Effect of chlorine pressure on vapor pressure at 802, 852 and 902°.

pressure values $10.8, 10.6, 11.4,$ and 11.2×10^{-3} atm. obtained in flow rate studies (see Table I). The point at 1102° and 0.99 atm. chlorine pressure is the average of the values 4.98 and 4.96×10^{-3} atm. obtained using metal samples of different specific radioactivity. The uncertainty of the individual points is about $\pm 5\%$ at the higher temperatures and 1 atm. chlorine pressure and increases to about $\pm 15\%$ as the temperature and chlorine pressure are lowered. The curves of Fig. 2 were drawn to be consistent not only with the experimental points, but also with each other.

In Fig. 2, the slopes of the isotherms taken at 1 atm. chlorine pressure are 1.36 (1504°), 1.44 (1301°), and 1.50 (1102°). Those of Fig. 3 are 1.4 (902°) and zero (902, 852, and 802°). Thus, $y/2 \cong 1.5$ and $(y-3x)/2 \cong 0$; $y = 3$ and $x = 1$. It therefore is apparent that the principal vapor species is RhCl_3 .

Comparison of the experimentally determined (solid) curves and the dashed curves (drawn with a slope of 1.5) in Fig. 2 shows that the experimental curves decrease in slope with increasing temperature and decreasing chlorine pressure. The effect apparently is the result of a contribution from a lower chloride. This means that the experimental curves are actually the sum of linear pressure-dependence curves representing RhCl_3 and at least one unknown lower chloride.

By successive approximations, we were able to resolve each of the experimental curves into two linear curves having slopes of 1.5 and 1.0, respectively. From the latter value, we find that $y/2 \cong 1.0$ and $y = 2$; thus, the lower chloride species

appears to be RhCl_2 (in this case, we assume that $x = 1$).

Table II gives individual partial-pressure values for RhCl_3 and RhCl_2 taken from the resolved linear curves at 1 atm. chlorine pressure and at pressures corresponding to those used in the experimental work. To show how the data correlate, the sums of the individual partial pressures are compared with experimentally determined total vapor-pressure values. The agreement appears satisfactory.

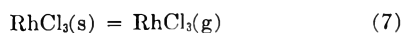
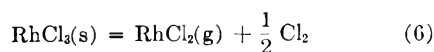
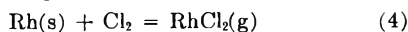
TABLE II
COMPARISON OF EXPERIMENTAL AND
RESOLVED VAPOR PRESSURES

p_{Cl_2} (atm.)	Resolved vapor pressures, atm. $\times 10^3$			Exptl. vapor pressures, ^b atm. $\times 10^3$
	p_{RhCl_2} ^a	p_{RhCl_3} ^a	$p_{\text{RhCl}_2} +$ p_{RhCl_3}	
	1504°			
0.100	0.63	0.465	1.10	1.04
.243	1.53	1.80	3.33	3.56
.485	3.03	5.1	8.1	8.3
.972	6.1	14.5	20.6	20.3
1.00	6.3	15.2
	1301°			
0.099	0.238	0.275	0.51	0.53
.246	0.59	1.08	1.67	1.76
.490	1.17	3.08	4.25	4.02
.98	2.35	8.8	11.2	11.0
1.00	2.40	9.0
	1102°			
0.100	0.056	0.138	0.194	0.197
.246	.137	0.54	0.68	0.69
.492	.273	1.55	1.82	1.78
.99	.55	4.45	5.00	4.98
1.00	.56	4.50

^a Taken from resolved linear curves at the appropriate chlorine pressures. ^b Experimental vapor pressures, assuming one vapor molecule per rhodium atom condensed.

Although the results correlate very nicely if $\text{RhCl}_2(\text{g})$ is taken to be the lower-chloride gaseous species, we cannot entirely eliminate the possibility that the deviations from a 1.5 slope of the experimental curves of Fig. 2 may have resulted from a rhodium-bearing species formed from chlorine corrosion of the mullite. The species $\text{RhCl}(\text{g})$ appears to be eliminated by the fact that the curves of Fig. 2, because of their large radius of curvature, do not resolve into two linear curves having slopes of 1.5 and 0.5, respectively.

Temperature Dependence of Vapor Pressures.—Since RhCl_2 and RhCl_3 appear to be the important vapor species under our experimental conditions, the solid-vapor equilibria to be considered are



When $\text{Rh}(\text{s})$ is the stable condensed phase, the observed vapor pressure must be the sum of contributions from reactions 4 and 5; and when $\text{RhCl}_3(\text{s})$ is the stable condensed phase, the observed pressures must be the sum of contributions from

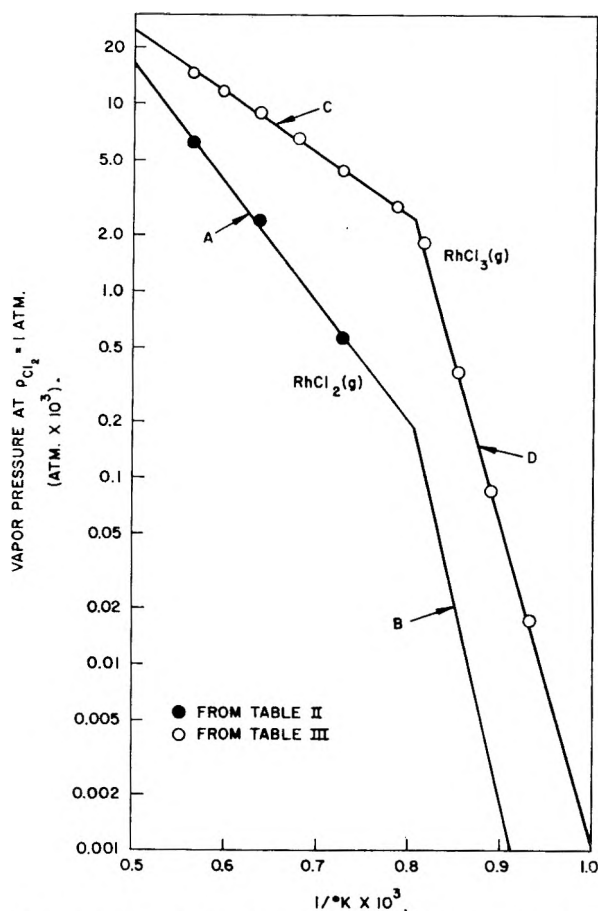


Fig. 4.—Individual partial pressures of RhCl_2 and RhCl_3 .

reactions 6 and 7. Reaction 4 is related to (6) and reaction 5 is related to (7) by reaction 1.

Figure 4 shows the individual partial pressures of RhCl_2 and RhCl_3 as a function of $1/T$. Curves A and C represent vapor pressures of the two species in equilibrium with $\text{Rh}(\text{s})$ at 1 atm. chlorine pressure (reactions 4 and 5), and curves B and D represent the pressure data for $\text{RhCl}_3(\text{s})$ at 1 atm. chlorine pressure (reactions 6 and 7). These curves were arrived at in the following manner.

The three RhCl_2 pressure values at 1 atm. chlorine pressure, obtained as described above and included in Table II, were plotted and curve A was drawn through the points. Curve B was drawn to intercept curve A at $1/T = 0.804$ (970° , the dissociation temperature of the solid chloride at 1 atm. chlorine pressure) so that the slope changes by -67.2 kcal./mole, the heat of reaction 1 at 970° . Partial pressure values for RhCl_2 , shown in Table III, were taken from curves A and B at the appropriate $1/T$ values and were subtracted from the experimentally observed vapor pressures to obtain the partial pressure values for RhCl_3 shown in Table III. These were plotted in Fig. 4 and curves C and D were drawn through the points. The curves were drawn as straight lines, since the data are not considered sufficiently accurate to warrant taking into account heat capacity effects over the short range of temperature involved.

Thermodynamic values for reactions 4 through 7 are summarized in Table IV. The ΔH_{1243}^0 and

ΔS^0_{1243} values for reaction 4 were obtained from curve A. These values were combined with the ΔH^0_{1243} and ΔS^0_{1243} values for reaction 1 to obtain ΔH^0_{1243} and ΔS^0_{1243} values for reaction 6. The latter values are represented by curve B. The ΔH^0_{1243} and ΔS^0_{1243} values for reactions 5 and 7 were obtained from curves C and D. The ΔC_p values of Table IV were obtained from C_p values estimated from values for similar halides given by Kelley,¹² and the ΔH^0_{298} and ΔS^0_{298} values were calculated by assuming ΔC_p to be constant over the temperature range involved.

TABLE III

OBSERVED TOTAL VAPOR PRESSURES RESOLVED INTO INDIVIDUAL PARTIAL PRESSURES OF RhCl_2 AND RhCl_3 AT 1 ATM. CHLORINE PRESSURE

Temp., °C.	Obsd. total pressures, ^a atm. $\times 10^3$	Resolved individual pressures, atm. $\times 10^3$	
		p_{RhCl_2} ^b	p_{RhCl_3} ^c
802	0.0175	0.0004	0.0171
852	.088	.003	.085
902	.394	.018	.376
956	1.95	.11	1.84
1003	3.10	.25	2.85
1102	5.00	.57	4.43
1202	7.8	1.20	6.6
1301	11.4	2.3	9.1
1401	15.8	3.9	11.9
1504	21.3	6.5	14.8

^a Experimental vapor pressures, assuming one vapor molecule per rhodium atom condensed. The 956° value is the average of three experimental values—1.90, 1.96, and 1.99×10^{-3} atm. The 1003, 1202, and 1401° values are from individual experiments. A slight correction was required to bring these values to 1 atm. chlorine pressure. The remaining values were taken from Figs. 2 and 3. ^b From the RhCl_2 curve of Fig. 4. ^c Column 2 minus column 3.

By combining the ΔH^0_{1243} and ΔS^0_{1243} values for reaction 5 with the respective ΔH^0_{1243} and ΔS^0_{1243} values for reaction 7, we obtain $\Delta H^0_{1243} = -64.6 \pm 3$ kcal./mole and $\Delta S^0_{1243} = -51.7 \pm 3.0$ e.u. for reaction 1. These values agree, within the uncertainty of the data, with the values $\Delta H^0_{1243} =$

(12) K. K. Kelley, U. S. Bur. Mines Bull. 584, 1960.

TABLE IV

THERMODYNAMIC DATA FOR VAPORIZATION REACTIONS	
$\text{Rh(s)} + \text{Cl}_2 = \text{RhCl}_2(\text{g})$	$\text{Rh(s)} + 3/2\text{Cl}_2 = \text{RhCl}_3(\text{g})$
$\Delta H^0_{1243} = +29.2 \pm 2.0$ kcal./mole	$\Delta H^0_{1243} = +14.9 \pm 1.0$ kcal./mole
$\Delta S^0_{1243} = +6.4 \pm 2.0$ e.u.	$\Delta S^0_{1243} = +0.2 \pm 1.0$ e.u.
$\Delta C_p = -1.2$ cal./mole °K. (estimated)	$\Delta C_p = -1.1$ cal./mole °K. (estimated)
$\Delta H^0_{298} = +30.3 \pm 3.0$ kcal./mole	$\Delta H^0_{298} = +16.0 \pm 2.0$ kcal./mole
$\Delta S^0_{298} = +8.1 \pm 3.0$ e.u.	$\Delta S^0_{298} = +1.8 \pm 2.0$ e.u.
$\text{RhCl}_3(\text{s}) = \text{RhCl}_2(\text{g}) + 1/2\text{Cl}_2$	$\text{RhCl}_3(\text{s}) = \text{RhCl}_3(\text{g})$
$\Delta H^0_{1243} = +96.4 \pm 4.0$ kcal./mole	$\Delta H^0_{1243} = +79.5 \pm 2.0$ kcal./mole
$\Delta S^0_{1243} = +60.5 \pm 4.0$ e.u.	$\Delta S^0_{1243} = +51.9 \pm 2.0$ e.u.
$\Delta C_p = -5.7$ cal./mole °K. (estimated)	$\Delta C_p = -5.6$ cal./mole °K. (estimated)
$\Delta H^0_{298} = +101.8 \pm 5.0$ kcal./mole	$\Delta H^0_{298} = +84.7 \pm 3.0$ kcal./mole
$\Delta S^0_{298} = +68.6 \pm 5.0$ e.u.	$\Delta S^0_{298} = +59.8 \pm 3.0$ e.u.

-67.2 ± 2.0 kcal./mole and $\Delta S^0_{1243} = -54.0 \pm 2.0$ e.u. obtained from the dissociation pressure measurements.

Combining ΔS^0_{298} values for reactions 4 and 5 with standard entropies S^0_{298} $\text{Rh(s)} = 7.53 \pm 0.05$ e.u. and S^0_{298} $\text{Cl}_2 = 53.29 \pm 0.01$ e.u. given by Kelley and King,⁹ we obtain S^0_{298} $\text{RhCl}_2(\text{g}) = 68.9 \pm 4.0$ e.u. and S^0_{298} $\text{RhCl}_3(\text{g}) = 89.3 \pm 4.0$ e.u. These values may be compared, respectively, with the estimated values of 79.4 and 83.1 e.u. calculated from an empirical equation given by Kubaschewski and Evans.⁸ They also may be compared with the following experimental values for analogous gaseous species: S^0_{298} $\text{CrCl}_2(\text{g}) = 76.0$ e.u. and S^0_{298} $\text{CrCl}_3(\text{g}) = 86.1$ e.u. (found by Doerner¹³), and S^0_{298} $\text{RuCl}_3(\text{g}) = 95.1$ e.u. (found by Bell, Garrison, and Merten¹⁴).

Acknowledgments.—The authors are indebted to R. E. Inyard for performing part of the experimental work and to J. M. Dixon for performing the X-ray analyses.

(13) H. A. Doerner, U. S. Bur. Mines Tech. Paper 577, 1937.

(14) W. E. Bell, M. C. Garrison, and U. Merten, *J. Phys. Chem.* **65**, 517 (1961).

EFFECTS OF ELECTROLYTES ON ROTATORY DISPERSION OF AQUEOUS TARTRATE SOLUTIONS¹

BY LEONARD I. KATZIN AND ELSIE GULYAS

The Chemistry Division, Argonne National Laboratory, Argonne, Illinois

Received September 27, 1961

Rotatory dispersion data over the range 6500–2650 Å., for aqueous tartaric acid systems containing HCl and chlorides of sodium, lithium, calcium, praseodymium, or thorium, and for alkaline tartrate, are fitted to a two-term Drude equation. The wave length parameters obtained are found to be in fair agreement with the absorption spectra. The data are compatible with the hypothesis of direct interaction between the cations and the OH groups of the un-ionized tartaric acid.

One of the facts that continually has to be kept in mind in working with solutions of salts in water is that the ions formed interact with the water.

(1) Based on work performed under the auspices of the U. S. Atomic Energy Commission. Presented in part at American Chemical Society National Meeting, Chicago, September 3–8, 1961.

The type of interaction of most significance with regard to magnitude of energy effects, and influence on chemical behavior, is that of cations with the non-bonding electrons of the water OH groups. Such interaction may give a coordinate bond of varying degrees of strength. This mode is, in

aqueous medium, often the dominant one. Frequently one deals with a donor which is not water but in which the electron-donating groups likewise may be OH groups. It is most useful, therefore, if one can follow the effects of the cation on specific hydroxyl groups, unperturbed by the over 55 moles per liter of aqueous hydroxyls which are not involved in the interaction.

The device used in the work to be reported here is to label the hydroxyl groups of interest with optical activity. That is, use is made of hydroxylic optically-active materials, in which the hydroxyl group is attached to an asymmetric center. A cation influencing this hydroxyl group might be expected to perturb the optical rotation of the substance as a whole. Scattered prior observations of the effects of cationic complexing on the optical rotation of active substances support the feasibility of the approach. We ourselves have made similar studies.² There is also an older literature dealing with salt effects on specific rotatory materials, such as tartrate, which is too voluminous to cite. There is, indeed, no logical restriction to hydroxylic reagents: the method can be extended to amino compounds, or to any substance containing donor atoms.

To be maximally useful, such studies must relate in some reasonable, quantitative way to concepts and quantities of theoretical significance. In our case, this linkage is furnished through the optical rotatory dispersion, and the Drude relation.³⁻⁵ This relation gives the optical rotation of a substance as the sum of a series of terms

$$R\lambda = \sum I_n/(\lambda^2 - \lambda_n^2)$$

The constants λ_n in the denominators, with the dimensions of wave length, refer to energy level differences in the molecule and, therefore, to part of its absorption spectrum. Not all absorption peaks are optically active, and maximal optical activity may be associated with a rather weak absorption peak. In the form given, the equation is valid at a distance from an optically active absorption peak. The region of the peak itself constitutes a singular point in the mathematical description.

In this paper we shall show that a two-term Drude equation is adequate to describe the results of a precise determination of the rotatory dispersion of tartrate ion and of undissociated tartaric acid in various chloride salt solutions. The wave length range is 650-265 μ . As 4 parameters are required, two for each Drude term, maximum precision and widest possible spectral range (without intruding into the region of the absorption band) are required to yield significant values of the parameters. In the case of the tartaric acid system above, agreement is found with the absorption spectrum.

Experimental

Computations.—The experimental data were fitted to a two-term Drude equation, containing 4 parameters, with the aid of the IBM 704 computer. After trials of numerous

procedures, a generalized least-squares program due to Dr. James E. Monahan of this Laboratory was used. This involves refinement of preliminary guesses of the values of the parameters. The nature of the equation is such that the usual least squares approach, in which preliminary values of the parameters need not be specified, is not practical. Six significant figures in the parameters give the calculated rotation to about 0.01° for most of the spectral range, but at the shortest wave lengths one more significant figure may be needed. The parameters therefore are given to 7 figures.

As the dispersion curve is a smooth one, with a single broad maximum, more than one set of values of the parameters might be expected to reproduce the same calculated rotations to the second decimal place. We therefore must analyze the computations more closely to appraise the significance of the particular parameters which result.

The two-term Drude equation in the form appropriate to the tartrate specific rotation

$$[\alpha] = A/(\lambda^2 - B) - C/(\lambda^2 - D) \quad (1)$$

can be written in the equivalent form

$$[\alpha] = ((A - C)\lambda^2 - (AD - BC))/(\lambda^4 - (B + D)\lambda^2 + BD) \quad (2)$$

as has been noted also by Lowry and Cutter.⁶ It is seen that the direct parameters are now the complex ones, $(A - C)$, $(AD - BC)$, $(B + D)$ and BD . One may make the further substitutions, $B = L - \Delta$, $D = L + \Delta$ (i.e., $2L = (B + D)$), and rearrange (2) to the form

$$[\alpha] = [1/\lambda^2((1 - L/\lambda^2)^2 - (\Delta/\lambda^2)^2)][(A - C) - (A - C)L/\lambda^2 - (A + C)\Delta/\lambda^2] \quad (3)$$

As can be seen from the equation,⁷ at very long wave lengths the relation reduces essentially to $(A - C)/\lambda^2$, Biot's relation, and the parameter $(A - C)$ therefore should be obtainable readily with good precision. Let us now assume that $L \gg \Delta$, as will be seen to fit the tartrate situation. As one moves to somewhat shorter wave lengths, the parameter L should become determinable with fair precision. The parameter $((A - C)L + (A + C)\Delta)$ may be obtained with comparable ease, depending on the exact numerical relations for the given system. The parameter Δ will require a further extension toward the shorter wave length region, and rather more precise data, to be obtained with reliability. This means that the absolute magnitudes of the Drude parameters A and C will be even less reliable: they are obtained from the compound parameter above after first subtracting the product $(A - C)L$, with its precision probably limited by that of L , and then dividing the residual by the less precise factor Δ . The $(A + C)\Delta$ value may be expected to be much more accurately determined than any of its components. These considerations will be illustrated in the following.

Dispersion data were obtained in the standard way for an alkaline (pH 7) solution of commercial sodium tartrate, not specially purified. In alkaline solution, the rotation is still highly positive even at 265 μ ; acid solutions show large negative rotation at this wave length. Two different computations with the same data gave the respective equations

$$[\alpha] = 651.9583/(\lambda^2 - 0.03921965) - 637.2467/(\lambda^2 - 0.03979033), \text{ and}$$

$$[\alpha] = 395.4362/(\lambda^2 - 0.03902818) - 381.6248/(\lambda^2 - 0.03997448)$$

The rotations computed from the two equations for each of the 38 experimental wave lengths differ from each other by more than 0.01° only for the extreme point at 265 μ . The differences in A and in C between the two equations are obvious, and the respective Δ values are 0.000285 and 0.000473, yet the $(A + C)\Delta$ values are 0.3676 and 0.3677, respectively. This agreement is fortuitously close, as the L values differ by 1 part per 1000, but the principle is illustrated. It also should be pointed out that even with this large percentage uncertainty in Δ , the difference between the B values for the two equations amounts to that between 1980.4 and 1975.6 Å. for the absorption peak, and for D , between 1994.7 and 1999.4 Å. In general the computer

(2) L. I. Katzin and E. Gulyas, *J. Phys. Chem.*, **64**, 1347 (1960).

(3) P. Drude, *Göttinger Nachrichten* (1892).

(4) E. U. Condon, *Rev. Mod. Phys.*, **9**, 432 (1937).

(5) W. Moffitt and A. Moscovitz, *J. Chem. Phys.*, **30**, 648 (1959).

(6) T. M. Lowry and J. O. Cutter, *J. Chem. Soc.*, **127**, 604 (1925).

(7) Analogous relations, in increasing numbers of parameters, can be obtained with more than two Drude terms.

would throw up parameters differing in this way only when one or two very bad points would give a local minimum in the least squares sums. When this occurred, the rotations computed by the two equations would not agree as well as in the case used for illustration, and choice between them could readily be made by observing the error distribution pattern. One of the two generally had a non-Gaussian error distribution, all points in essence being equally poorly fitted, to compensate for improved fit at the one or two very bad points.

We are indebted to Dr. Gordon Goodman for stimulating discussions on some of these points.

Polarimetry.—The rotatory dispersion measurements were made with a Rudolph photoelectric spectropolarimeter, Model 200S, and a xenon compact arc lamp. The 100 mm. polarimeter tube was jacketed, and had quartz end plates. Temperature was controlled by circulating water at $25 \pm 0.1^\circ$ through the jacket. Optical rotations were measured at 10 $m\mu$ intervals in the wave length region 650 to 300 $m\mu$, and at 5 $m\mu$ intervals at wave lengths below 300 $m\mu$. With PrCl_3 solutions, interference from absorption peaks at some points in the visible necessitated variations in this program. At each wave length, a minimum of four instrument settings were read and averaged to give the rotation. The average deviation of the readings was 0.002–0.003° in the wave length region 650–300 $m\mu$, and 0.006–0.04° below 300 $m\mu$. A good over-all average in this latter region is about $\pm 0.01^\circ$. For our tartaric acid solutions (0.2 *M*) a measured 0.003° corresponds to 0.1° in $[\alpha]$. As a blank reading must be subtracted, the statistical expectation is about $\pm 0.15^\circ$.

pH Measurement.—A Beckman Model G pH meter giving a precision of ± 0.02 pH unit was used to determine the pH values of the solutions.

Purification of Materials.—The analyzed reagent grade of *d*-tartaric acid (2–5 p.p.m. iron) shows a small absorption peak at about 265 $m\mu$. The acid was purified twice by ether extraction of the solid by the Soxhlet procedure. The 265 $m\mu$ absorption was no longer present in the repurified acid, and with it disappeared a marked irregularity in the rotatory dispersion below 300 $m\mu$.

Sodium chloride was recrystallized by prolonged boiling of excess salt with 6 *N* HCl, to remove any iron. The crystals were washed with ethyl alcohol and dried at about 100° . An approximately 4 *M* solution of the purified salt showed no absorption at wave lengths greater than 215 $m\mu$.

$\text{PrCl}_3 \cdot x\text{H}_2\text{O}$ obtained from Lindsay Light and Chemical Co. showed a small foreign absorption peak around 270 $m\mu$, in aqueous solution. A 1 *M* solution of the salt in 6 *N* HCl was passed through a Dowex-1 anion exchange column. After the anion-exchange process was repeated, the eluate was reduced in volume to about one-half the original in a vacuum desiccator. A solution of the product crystals showed no ultraviolet absorption down to 235 $m\mu$.

A 2 *M* solution of ThCl_4 in 3 *N* HCl was twice passed through a Dowex-1 anion resin column. Crystals obtained by partial evaporation of the eluate were filtered off, washed with ether, and stored in a desiccator over sulfuric acid to dry. A broad absorption peak centering at about 290 $m\mu$ in the starting material was reduced to a small absorption at approximately 255 $m\mu$.

Lithium chloride and calcium chloride dihydrate, analyzed reagent grade, were not further purified.

We are indebted to Miss Gail Norman for technical assistance in the purifications.

Preparation of Solutions.—All solutions contained 0.2000 mole per liter of *d*-tartaric acid (H_2T). On the basis of previous data,⁸ pH 0.3 was chosen as a suitable compromise between an acidity at which the ionization of H_2T is less than 0.1%, and one in which the HCl concentration might be so high as to introduce complications. In general, solutions were made from a stock solution 0.4000 *M* in H_2T by dissolving the salt to be tested in a small volume of 0.8 *N* HCl, adding the appropriate amount of the tartaric acid stock, and making up to volume with 0.8 *N* HCl. Higher-valent salts (CaCl_2 , PrCl_3 , and ThCl_4) gave a slightly lower final pH, as noted in the data. In some instances, the pH was altered deliberately through the addition of an appropriate amount of HCl. The alkaline tartrate solution was prepared by the addition of 10 *M* NaOH to the H_2T .

Absorption spectra were obtained through 0.1-mm. path lengths with the Cary spectrophotometer.

Results

The full data are given as two-term Drude equations, together with plots of the deviations of the experimental values of the rotation from the rotation calculated by the equation given (open circles). At several wave lengths, for orientation, the experimental rotation is written in. (Fig. 1–6). Many of the error plots show systematic drifts suggesting lack of optimum match of the equation with the data, owing to difficulties at the short wave lengths. Since the data below 300 $m\mu$ already were considered less reliable than the rest, the computation was repeated using only the data through 300 $m\mu$. Rotations were computed from the parameters so derived for the wave lengths below 300 $m\mu$. The deviation plots for these equations also are included in the figures as solid circles. The root mean square deviations for the 36 out of 40–43 original points retained were considerably improved, often by about a factor of 2, to a modal value of *ca.* $\pm 0.25^\circ$. (If one used only the data through 350 $m\mu$, the error function was ± 0.1 – 0.2° , verifying that the experimental precision in the measurements was about that stated earlier.)

The compound parameters discussed above were taken from the Drude equation constants for the data through 300 $m\mu$, and are listed in Table I. The parameters having to do with peak wave lengths (L , $L + \Delta (\equiv \lambda_2^2)$ and $2\Delta (\equiv \lambda_2^2 - \lambda_1^2)$) are essentially indistinguishable for the pH 0.29 HCl, and the solutions with 0.5 *M* LiCl and 0.5 *M* NaCl. The two more dilute CaCl_2 solutions, and the PrCl_3 solution, show essentially the same values for 2Δ , but the CaCl_2 solutions show a consistent though small change in L , and the PrCl_3 solution a larger change in this parameter. The two ThCl_4 solutions are consistent with each other, but show both L and 2Δ sharply altered from the standard pH 0.29 solution. The 1 *M* CaCl_2 parameters indicate some marked alteration in the solution, possibly formation of a complex between the cation and bitartrate ion. Alkaline tartrate ion, in addition to the marked shift of L to shorter wave lengths, has a smaller value for 2Δ , though this parameter is larger than the corresponding one for the solutions containing thorium.

The absorption spectrum of the aqueous tartaric acid at pH 0.29 shows a broad peak (width at half-maximum *ca.* 300 Å.), with extinction about 225 at its maximum (*ca.* 2116 Å.), set on the slope of a much more intense peak whose maximum lies below 1950 Å. (Hereafter these will be designated P and S, respectively.) The spectrum is not changed significantly in the presence of 0.5 *M* LiCl, 0.5 *M* NaCl, or 0.2 *M* CaCl_2 , though the first seems to give perhaps 3% lower, and the last, 3% higher absorption at the P maximum.

The solution 1.0 *M* in CaCl_2 shows a definite shift of the S absorption to longer wave lengths, so that the P absorption becomes a shoulder on it, essentially flat from 2065 to 2110 Å., with the same height as the 2116 Å. peak of the 0.2 *M* CaCl_2 solution. The 6 *N* HCl solution also shows a displacement of the S absorption to longer wave

(8) L. I. Katzin and E. Gulyas, *J. Phys. Chem.*, **64**, 1739 (1960).

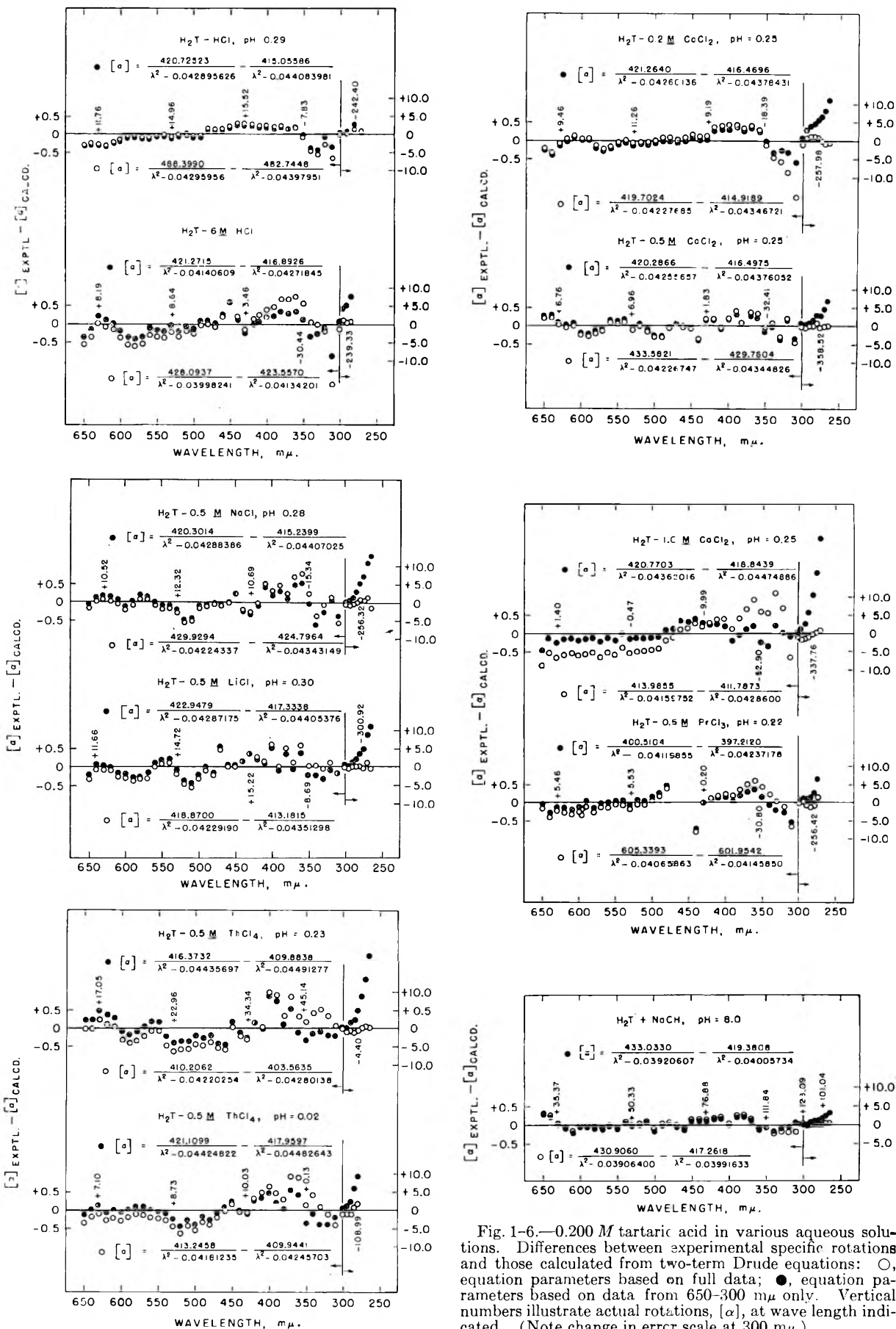


Fig. 1-6.—0.200 M tartaric acid in various aqueous solutions. Differences between experimental specific rotations and those calculated from two-term Drude equations: ○, equation parameters based on full data; ●, equation parameters based on data from 650–300 mμ only. Vertical numbers illustrate actual rotations, [α], at wave length indicated. (Note change in error scale at 300 mμ.)

TABLE I
COMPARATIVE FUNCTIONS OF DRUDE EQUATION PARAMETERS FOR TARTRATE DATA THROUGH 300 $m\mu$

System	I_1^a	$I_1 + I_2$	L^b	λ_2^2	$\lambda_2^2 - \lambda_1^2$
HCl, pH 0.29	420.7252	5.669	0.0434898	0.04408398	0.001188
6 M HCl	421.2715	4.379	.0420622	.04271845	.001312
0.5 M LiCl, pH 0.30	422.9479	5.614	.0434628	.04405376	.001182
.5 M NaCl, pH 0.28	420.3014	5.061	.0434770	.04407025	.001186
.2 M CaCl ₂ , pH 0.25	421.2641	4.794	.0431923	.04378431	.001183
.5 M CaCl ₂ , pH 0.25	420.2866	3.789	.0431585	.04376052	.001204
1.0 M CaCl ₂ , pH 0.25	420.7703	1.926	.0441845	.04474886	.001129
0.5 M PrCl ₃ , pH 0.22	400.5104	3.298	.0417851	.04237178	.001173
.5 M ThCl ₄ , pH 0.23	416.3732	6.489	.0446349	.04491277	.000556
.5 M ThCl ₄ , pH 0.02	421.1099	3.150	.0445373	.04482643	.000578
NaOH, pH 8	433.0330	13.652	.0396317	.04005734	.0008513

$$^a [\alpha] = \frac{I_1}{\lambda^2 - \lambda_1^2} + \frac{I_2}{\lambda^2 - \lambda_2^2} \equiv \frac{A}{\lambda^2 - B} - \frac{C}{\lambda^2 - D}, \quad ^b L = \frac{1}{2}(B + D); \quad \Delta = \frac{1}{2}|B - D|.$$

length, slightly less marked than for the 1.0 M CaCl₂. A similar alteration is seen for the pH 0.02 solution containing 0.5 M ThCl₄, but accompanying it is a definite movement of the P absorption to shorter wave lengths. At pH 0.23 the P shift seems the same, but the S contribution at *ca.* 2100 Å. is more marked. In spite of interference from the 2135 Å. peak of Pr⁺³ (*cf.* Stewart and Kato⁹), which is of comparable intensity, the absorption above 2225–2250 Å. is decreased from the standard, indicating a probable shift to shorter wave length in the P absorption. In the alkaline tartrate, finally, although the S absorption completely obscures the P absorption to 2160 Å., from 2175 Å. the absorption falls well below that expected for the P absorption, which would be consistent with a strong movement of the P absorption to shorter wave lengths.

Discussion

From the above it is seen that a two-term Drude equation can fit the data quite well. With readings from 6500 to 3000 Å. the differences between experimental rotations and calculated approach the reproducibility of the experimental rotations. With data down to 2650 Å. included, Drude constants are modified somewhat, and the root mean square deviation may double. Less homogeneity and reproducibility of the data are indicated. A number of factors contribute to this: decreased precision in the data, effects of minor impurities, possible contributions of more than the two absorption peaks implied, and possible deviations from the Drude relation itself as one gets nearer to the absorption wave length, and into the Cotton effect region.

A significant datum is the difference between the rotations calculated for the 3000–2650 Å. wave length region *via* the parameters deduced from the data for the 6500–3000 Å. span, and the experimental rotations. In all cases, the computed rotation is increasingly more negative in the shorter wave length region than is the corresponding experimental value. This difference ranges from 2° or so for the pH 0.29 HCl at 2700 Å. (rotation, –380.70°) to 20° for the pH 0.23 ThCl₄ solution at 2650 Å. (rotation, –77.14°) and 26° at 2700 Å. for the 1 M CaCl₂ solution (rotation, –481.60°).

Possible error in calibration of the instrumental rotation scale or wave length setting inaccuracies where the rotation may be changing by as much as 100–120° in 50 Å. cannot explain the behavior. There is, as might be anticipated, some correlation with the statistical fit to the points above 3000 Å. The pH 0.29 HCl, and the alkaline tartrate, for which the root mean square deviations in the 6500–3000 Å. region most closely approach the experimental precision, deviate only some 3° or so from the experimental points at 2650 Å. The two solutions indicated above as having large deviations show relatively large values of the root mean square deviation even above 3000 Å., and the distribution of deviations in the 6500–3000 Å. region is non-Gaussian. The implication is strong that the factors involved are related to some (probably minor) species for which at least one more Drude term would be involved. The deviation from the Drude relation due to the Cotton effect region would seem to be much less significant, inasmuch as the alkaline tartrate for which the absorption wave length is more remote than for the acid solutions also shows the effect.

All the dispersion curves show positive rotation at the longest wave lengths, which passes through a maximum as the wave length decreases. Below some wave length the rotation is negative. Alkaline tartrate has a rotation maximum of 130.76° at about 3050 Å., and the rotation is still +61.76° at 2650 Å. Thorium chloride at pH 0.23 gives the maximum tartrate rotation of 45.70° at 3400 Å., and shows negative rotations below 2830 Å. The more acid ThCl₄ solution shows a maximum rotation of 10.43° at 4500 Å., the sign becomes inverted below 3500 Å., and at 2800 Å. the rotation is –109°. Tartrate in HCl at pH 0.29 has its rotation maximum of 16.26° between 4600 and 4700 Å., and turns negative between 3600 and 3700 Å. The rotation is –380.7° at 2700 Å. The extreme of the solutions seen is that 1.0 M in CaCl₂, with the maximum positive rotation of 1.60° at 6400 Å., sign inversion at 5400 Å., and a rotation of –481.6° at 2700 Å. This rather marked difference in gross features, as indicated in the figures and in Table I, involves relatively small alterations in the Drude parameters.

The most marked gross characteristic of the dispersion curves, the rapidity with which the rota-

(9) D. C. Stewart and D. Kato, *Anal. Chem.*, **30**, 164 (1958).

tion turns negative with decreasing wave length, correlates obviously with ($A - C$) of Table I. This parameter is largest for alkaline tartrate, smaller for the pH 0.23 ThCl_4 , still smaller for the pH 0.29 HCl, and finally least for the 1.0 M CaCl_2 solution. The L and Δ parameters in this system appear primarily to modify the detailed shapes of the curves, but in terms of energy levels in the tartrate group and correlation to these levels as they are revealed by other sorts of spectra, they are of great significance.

The P absorption maximum, 2116 Å., is 15–16 Å. longer than the wave length corresponding to λ_2^2 for pH 0.29 HCl solution of tartaric acid (see Table I), and about that for the solutions containing ThCl_4 . This suggests that λ_2^2 is related to the P absorption. For both the alkaline tartrate solution and the tartaric acid solution containing PrCl_3 there is a marked movement of λ_2 to shorter wave lengths, and in both instances the P absorption apparently has done likewise. The S absorption of the alkaline tartrate has moved decidedly in the opposite direction. The implied movements of the 1.0 M CaCl_2 and the ThCl_4 solutions' λ_2 peaks some 15–18 Å. to longer wave lengths than for the standard solution is of uncertain meaning, as the parameters for the full data through 2650 Å. (see figures) indicate them to be at perhaps shorter wave length than the standard. There is no certain movement of the P absorption for the CaCl_2 solution, though the S absorption has moved to longer wave length. In the case of the ThCl_4 solutions, a definite movement of the P absorption to shorter wave length is apparent. It is of interest that the Δ parameter for the ThCl_4 solutions is markedly smaller than for the other systems, suggesting that this apparent movement of the P absorption also could be a sharpening due to relative movement of the two absorptions suggested by the Drude relation.

The intensity of the P absorption is half-maximum at about 2265 Å. Assuming it to be symmetrical, in wave length measure, the second half-maximum point would be at about 1966 Å., and the respective λ^2 terms would be 0.05130 and 0.03865. The difference, 0.01265, is over 10 times the 2Δ for most of the solutions in Table I. With the agreement in this parameter for most of the solutions, and the characteristic and marked deviations of the ThCl_4 and alkaline tartrate solutions toward smaller values, it seems unreasonable to assume that the values listed in Table I are too small by a factor of 10 or more. But such an assumption is necessary if one is to deny that the two Drude absorptions fall within the half-maximum width of the P absorption. This means that either the P absorption is "complex" in this sense, or that the λ_1 peak may be associated with one of the (probably) several components of the S absorption, and the λ_2 peak with the P absorption. In this latter case it is necessary to make the supporting assumption that when the S absorption moves to longer wave lengths in the several tartrate systems, only in certain instances (such as the ThCl_4 solutions) is it the optically-active component which has moved. From the failure of the Table I pa-

rameters to match satisfactorily the observed rotations below 3000 Å., one might justify the contention that the small value of Δ for the ThCl_4 solutions is a consequence of squeezing into the two-term Drude form a third rotation related to the S absorptions. This would imply again the point of view that the "normal" rotations involve two P absorption peaks.

The equivalent of the P absorption seems characteristic of carboxylic acids. It generally is referred to as a carbonyl absorption, presumably because OH absorption comes at rather shorter wave lengths. But true carbonyl absorption comes at notably longer wave lengths, *ca.* 2800 Å. The carboxyl absorption may reasonably be considered as resulting from interaction of carbonyl and hydroxyl oxygens present on the same carbon. A "complex" nature in the above sense therefore should not be surprising.

Some comparisons have been made in the older literature of Drude constants and absorption peaks.¹⁰ Generally, however, neither rotatory parameters nor absorption spectra were too well known—*e.g.*, the absorption of tartaric acid was not known at short enough wave lengths to demonstrate the P absorption peak. Furthermore, for the tartrates specifically, calculations were based on measurements at relatively few wave lengths, well above 3500 Å. This factor alone would give λ_2^2 values of longer wave lengths, as we can demonstrate with our own data. More importantly, parameters were fixed arbitrarily, taking advantage of the adjustability of the four-parameter computation. Thus, in their work with ethyl tartrate,^{10b} Lowry and Cutter arbitrarily set λ_1^2 at 0.03, reducing the fitting problem to one in three parameters. Their λ_2^2 value of 0.056 therefore is not necessarily related to the absorption peak. The ethyl tartrate rotations are small,^{10b} and the precision is low, particularly in the critical region 4600–3860 Å., the lowest wave lengths recorded. The Lowry–Cutter equation, $[\alpha] = 25.005/(\lambda^2 - 0.03) - 20.678/(\lambda^2 - 0.056)$ seems to give a good fit. We have recomputed the rotations with this equation, and find a root mean square deviation of $\pm 0.11^\circ$. On putting the Lowry–Cutter data through the computer least-squares procedure, however, one obtains the equation

$$[\alpha] = 388.9684/(\lambda^2 - 0.044416) - 384.7171/(\lambda^2 - 0.0458956)$$

with a root mean square deviation of $\pm 0.07^\circ$. Both equations actually fit the data better than its probable precision, but the correspondence of the improved fit parameters for these data to our own for the tartaric acid systems is obvious. The Lowry–Cutter ($A - C$) is 4.33, ours is 4.25, and $L = 0.086$ *vs.* 0.090, in accord with the considerations discussed above.

One advantage of electronic computation over hand computation is that the computer does not get bored, and will not be satisfied with a fit that "looks good." This may be illustrated with the

(10) (a) T. M. Lowry and J. O. Cutter, *J. Chem. Soc.*, **127**, 604 (1925); T. M. Lowry, "Optical Rotatory Power," Longmans, Green and Co., 1935; (b) T. M. Lowry and J. O. Cutter, *J. Chem. Soc.*, **121** 532 (1922).

Lowry and Cutter^{10a} data on camphor in benzene. Their equation is

$$[\alpha] = 29.384/(\lambda^2 - 0.08720) - 20.138/(\lambda^2 - 0.05428)$$

The computer-derived equation

$$[\alpha] = 19.0834/(\lambda^2 - 0.092746) - 10.14135/(\lambda^2 - 0.017626)$$

gives obviously improved fit in 29 of 41 points. The λ_1^2 parameter 0.0927, and the relatively low value of λ_2^2 , explain why three-parameter fits to rotatory data for camphor and its derivatives^{10a,11,12} in which λ_2^2 is set at 0, give λ_1^2 values 0.09–0.11.

It seems to be the general practice, when using a three-parameter approximation for the Drude relation, to use the form $[\alpha] = A/(\lambda^2 - B) + C/\lambda^2$. From the analysis given above of the two-term relation, it is seen that this is equivalent to setting $2\Delta = \lambda_1^2$. This is not only arbitrary, but also not in accord with the accepted origin of the rotations, and probably will not give the best fit. For three-parameter fittings it would be advisable to use $(A + C)$, $L (= (\lambda_1^2 + \lambda_2^2)/2)$ and $(A - C)\Delta$. One may then choose a Δ value such that $(L + \Delta)$ bears some reasonable relationship to the absorption of known chromophores in the molecule, and expect improved fit from the two-term Drude relation. To fix arbitrarily the values for both λ_1^2 and λ_2^2 , and from the data for a relatively few wave lengths to draw conclusions as to chemical species from the resulting values for A and C ,¹³ appears highly questionable. In addition, when one has a series of "plain" dispersion curves,¹⁴ similar to those described above for the tartrates, it may be tempting to postulate that the differences are due to additional Drude terms of opposite sign,¹⁴ but as we have seen above, alterations in the intensity parameters of the two-term equation can reproduce the effects.

(11) G. Owen, *Trans. Faraday Soc.*, **26**, 423 (1930).

(12) J. O. Cutter, H. Burgess, and T. M. Lowry, *J. Chem. Soc.*, **127**, 1262 (1925).

(13) M. K. Hargreaves and P. J. Richardson, *ibid.*, 2260 (1957).

(14) A. E. Lippman, E. A. Foltz, and C. Djerassi, *J. Am. Chem. Soc.*, **77**, 4364 (1955).

The concentrations of salts used in our experiments are in the lower range of those producing "salting-out" effects of the conventional sort, and the increased effects on the rotatory parameters with increased cationic charge are parallel to the salting-out effects. We have had evidence in previous work⁸ that the activity coefficients of tartaric acid are affected by salt in agreement with expectation. It is reasonable to conclude that the rotatory dispersion results and the associated spectral changes we report reflect the effects on the internal energy relations of the tartaric acid molecule of the phenomena which manifest themselves as changes in "activity." The abundant literature concerning salt effects on optical rotation¹⁵ indicates this to be a general relationship. The assumption outlined at the beginning of this paper was that the changes expected would be manifestations of interactions of the salt cations with electron-donor groups of the optically active material. It perhaps might be argued that the primary interaction is between the optically active material and the solvent, and that the effect of the salts is an indirect one, *via* action on the solvent properties. This alternative cannot be ruled out completely at this stage, but it seems significant that the total pattern of action of a given cation, as revealed by the Drude parameters, is distinctive, and apparently different from that of other cations. This would not be consistent with the solute-solvent interaction picture, and gives support to the original assumption.

Some of the sensitivity to impurity found in working with these tartaric acid systems suggests that optical rotatory dispersion measurements may present a sensitive means of detecting small amounts of metal ion compounds for analytical purposes.

(15) *E. g.*, G. W. Clough, *J. Chem. Soc.*, **105**, 49 (1914); **107**, 96, 1509 (1915); **113**, 526 (1918); P. A. Levene and A. Rothen, *J. Phys. Chem.*, **34**, 2565 (1930); E. Darmois, *Trans. Faraday Soc.*, **26**, 384 (1930); J. Liquier-Milward, *ibid.*, 390 (1930); G. Bruhat, *ibid.*, 400 (1930); Y. K. Heng, *Bull. soc. chim. France* [5], **3**, 1004 (1936).

STUDIES OF THE FISCHER-TROPSCH SYNTHESIS. PREPOISONING OF IRON CATALYSTS BY SULFUR COMPOUNDS

By J. F. SHULTZ,¹ L. J. E. HOFER,¹ F. S. KARN,¹ AND R. B. ANDERSON¹

Coal Research Center, Bureau of Mines, Pittsburgh, Pa.

Received September 27, 1961

The poisoning of iron catalysts by sulfur compounds in the Fischer-Tropsch synthesis was investigated, since synthesis gas obtained by the gasification of coal contains H₂S and other sulfur compounds. The pretreated catalysts were prepoisoned by immersion in a solution of the sulfur compound in heptane prior to synthesis. Sulfur dioxide was the most severe poison, and hydrogen sulfide and ethyl mercaptan were nearly as effective. Results of tests of reduced catalysts poisoned by carbonyl sulfide and carbon disulfide, as well as a nitrated catalyst poisoned by hydrogen sulfide, were erratic. However, for all sulfur compounds tested the activity of a reduced fused iron catalyst was decreased to less than 2% of the value for the fresh sample by the addition of about 10 mg. S per g. Fe or 0.7 mg. S per m.² of surface. Activated steel turnings were more susceptible to sulfur poisoning than the reduced fused iron oxide catalyst. Sulfur poisoning decreased the average molecular weight of the synthesis products and increased the H₂:CO usage ratio. These changes in selectivity suggest that the poison may in part react with the alkali promoter.

Introduction

Sulfur poisoning of iron catalysts in the ammonia synthesis was observed about 50 years ago.² Fischer³ in 1935 cited a practical upper limit for sulfur concentration of 1 to 2 mg./m.³ for synthesis gas for the Fischer-Tropsch synthesis, and most commercial applications of this process have used synthesis gas containing smaller concentrations of sulfur than this limit.

A survey of the literature to 1956⁴ showed only a few important contributions to the problem of sulfur poisoning of iron catalysts in either the Fischer-Tropsch or ammonia synthesis. Brill⁵ found that the resistance of fused catalysts to sulfur poisoning in the ammonia synthesis at atmospheric pressure increases in the following order: pure iron, Fe-K₂O, Fe-Al₂O₃-K₂O, Fe-Al₂O₃-CaO-K₂O. Frear, Shultz and Elmore⁶ found that about 20 mg. of hydrogen sulfide per gram of catalyst was required to decrease the activity to very low values in the ammonia synthesis at 100 atm. on doubly promoted catalysts. Sulfur dioxide was found to be a temporary poison similar to oxides of carbon and water vapor. More recently Bulstuiikova, Apel'baum, and Temkin⁷ investigated the poisoning of iron catalysts by hydrogen sulfide in the ammonia synthesis at atmospheric pressure. Potassium oxide, either alone or in the presence of alumina, increased the resistance of the catalysts to poisoning. Activity for ammonia synthesis decreased to zero when the concentration of sulfur was 0.4, 0.9, and 2.5 mg. S/m.² for Fe-Al₂O₃, Fe-Al₂O₃-K₂O, and Fe-K₂O catalysts, respectively. The amount of sulfur required to inactivate the catalysts were 1.7, 3.2, and 8.1 mg. S/g. catalyst for Fe-K₂O, Fe-Al₂O₃, and Fe-Al₂O₃-K₂O, respectively.

Rapoport and Muzovskaya⁸ investigated the poisoning of precipitated iron oxide-copper oxide catalysts by organic sulfur compounds in the Fischer-Tropsch synthesis. Catalysts that were reduced only to Fe₃O₄ or not at all were remarkably resistant to sulfur poisoning, and the synthesis could be continued at moderate to high yields until the sulfur content of the catalyst was increased to about 10 weight %. On the other hand, a similar catalyst completely reduced in hydrogen at 500° was reported to be inactive at a sulfur content of only 0.9 weight %.

British workers investigated the sulfur poisoning of reduced iron catalysts prepared from mill scale in the Fischer-Tropsch synthesis.⁹ Prepoisoning by hydrogen sulfide introduced into an evacuated bulb containing the catalyst was more effective than poisoning by sulfur compounds in the synthesis gas. Methane production was increased by sulfur poisoning.

In the present investigation iron catalysts were prepoisoned by immersing the pretreated catalyst in a solution of the sulfur compound in heptane before testing in the Fischer-Tropsch synthesis. Thus, the amount of poison may be referred to the surface area of the fresh catalysts, and interpretation is not complicated by structural and chemical changes of the catalyst that accompany synthesis. This procedure also avoids concentration gradients of poison along the length of the bed that lead to severe problems in the interpretation of results.¹⁰ Concentration gradients of poison often are produced when the feed gas contains the poison. Poisoned catalysts usually were tested in the temperature range 240-300°, but in some cases temperatures were increased to as high as 390° in attempts to obtain moderate conversions.

In the present paper catalyst activity is expressed as cubic centimeters (S.T.P.) of synthesis gas consumed per hr.-g. of iron at 240°, when 65% of H₂+CO is reacting. The activity was corrected to these conditions using the empirical rate equation¹¹ $-\ln(1-x) = (A/S) \exp(-E/RT)$,

(1) Supervisory Physical Chemist, Bureau of Mines, Coal Research Center, Pittsburgh, Pa.

(2) A. Mittasch, *Advances in Catalysis*, **2**, 90 (1950).

(3) F. Fischer, *Brennstoff-Chem.*, **16**, 1 (1935).

(4) R. B. Anderson, "Catalysis," Vol. IV, ed. P. H. Emmett, Reinhold Publ. Corp., New York, N. Y., 1956, p. 242.

(5) R. F. Brill, captured documents, TOM Reel 300, FIAT Reel R-19, frames 7088-7104, 1941.

(6) G. L. Frear, J. F. Shultz, and K. Elmore, Tennessee Valley Authority Internal Report R545.

(7) Yu. I. Bulstuiikova, L. O. Apel'baum, and M. I. Temkin, *Zhur. Fiz. Khim.*, **32**, 2717 (1958).

(8) I. B. Rapoport and O. A. M. Muzovskaya, *Khim. i Tekhnol. Topliva*, No. 2, 18 and No. 5, 19 (1957).

(9) Fuel Research, Report of the Fuel Research Board, 1955, p. 20; 1956, p. 22.

(10) R. B. Anderson and A. M. Whitehouse, *Ind. Eng. Chem.*, **53**, 1011 (1961).

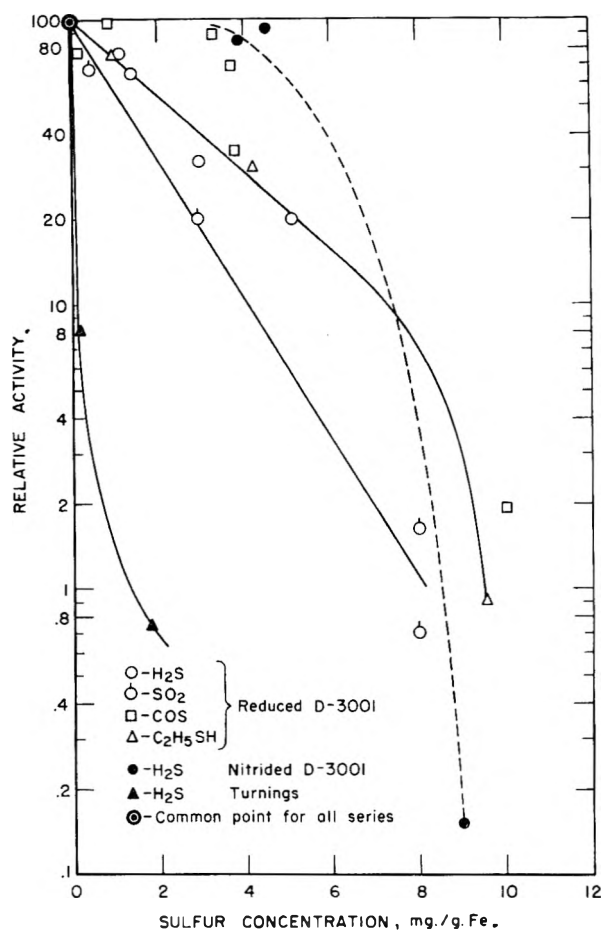


Fig. 1.—Relative activities of prepoisoned iron catalyst (log scale) as a function of sulfur concentration.

where x is the fraction of $H_2 + CO$ reacted, S hourly space velocity, A is a constant, and the activation energy E has a value of 19 kcal./mole. In this paper hourly space velocity is defined as volumes of synthesis gas (S.T.P.) introduced per hr. per vol. of catalyst space. Although this equation may not be accurate for some of the present experiments, especially those at higher temperatures, the computed activities in every case are in the correct order in any group of experiments.

Experimental

Catalysts used were: (a) 6–8 mesh fused iron oxide catalyst D-3001, containing in the raw state, Fe 67.4 weight %, Mg 4.61, Cr 0.65, and K_2O 0.57; and (b) activated SAF 1018 steel lathe turnings L-2201, approximate dimensions $8 \times 3 \times 0.4$ mm., oxidized with steam at 700° to convert 24.6% of the iron to magnetite, and impregnated with K_2CO_3 to give a concentration of 0.13 weight % K_2O .

Catalyst D-3001 was reduced in hydrogen at an hourly space velocity of 2500 and 450° for 40 hr. to give a weight loss of about 24% corresponding to 90% reduction of the oxides of iron. The surface area of reduced catalyst was 14.8 $m^2/g.$ Fe. In some tests this catalyst subsequently was treated with gaseous ammonia at an hourly space velocity of 1000, atmospheric pressure, and 350° for 8 hr. to convert the iron essentially to $\epsilon-Fe_2N$.

Catalyst L-2201 was reduced in hydrogen at an hourly space velocity of 1000 and 450° for 8 hr. to give a loss in weight of about 6.5%, corresponding to about 98 weight %

reduction of the oxidized zone. The surface area of the reduced catalyst was 0.83 $m^2/g.$ Fe.

In an attempt to poison all the particles uniformly, the pretreated catalyst was immersed in a 1% solution of the sulfur compound in *n*-heptane for 24 hr. at room temperature under conditions that prevented exposure of the pretreated catalyst to atmospheric oxygen. Only part of the sulfur compound introduced was adsorbed by the catalyst, but with H_2S , SO_2 , COS , and CS_2 , concentrations of 1 to 10 mg. S/g. Fe were attained easily. With ethyl mercaptan only small amounts of sulfur were adsorbed in the room temperature treatment, and the poisoning was accomplished by heating the catalyst immersed in ethyl mercaptan–heptane solution in a stainless steel autoclave at 250° for 4 hr. Samples of the catalysts were analyzed for iron and sulfur after the poisoning step, after synthesis at 250 – 300° , and after synthesis at higher temperatures (if this step was included in the testing sequence).

Catalysts were tested at 21.4 atm. in stainless steel reactors similar in design to the reactors that have been described previously.¹² Before each test an experiment of 24 hr. duration was made on a standard catalyst to demonstrate that sulfur from the previous experiment was not transferred to the catalyst in the new test by the wall of the reactor. All of these experiments showed that the wall of the reactor was inert. Synthesis gas containing 50% H_2 and 50% CO was used in all the tests. This gas, containing less than 1 mg. S/ m^3 , was passed through a large bed of activated charcoal at 21.4 atm. to remove traces of sulfur compounds before entering the testing unit. Tests were started at 200° and an hourly space velocity of synthesis gas of 300. The temperature was increased slowly over a period of 48 hr. until an apparent CO_2 -free contraction of 65% or a temperature of 300° was attained. In the first 2 to 3 weeks of synthesis the temperature did not exceed 300° . For active catalysts the temperature was adjusted to maintain the apparent CO_2 -free contraction between 63 and 65%. For inactive catalysts the temperature was held at 300° , and the hourly space velocity was decreased to 100 to maintain the contraction at a measurable level.

The initial period of synthesis, in which the temperature was less than 300° , extended for 6 weeks for active catalysts and only 2 to 3 weeks for inactive samples. During this time, the activity of the prepoisoned catalyst changed more rapidly than that of the unpoisoned catalyst. The activity increased in some tests and decreased in others. The average (absolute) change in activity from the second to fifth week was about 25%.

After the initial period of synthesis at temperatures at or below 300° , the catalyst was removed from the reactor, sampled for analysis, and in some cases returned to the reactor for further testing. For severely poisoned catalysts the temperature in this second period was increased progressively to as high as 390° to determine if: (a) moderate conversion of synthesis gas could be obtained, and (b) if any of the sulfur was removed by synthesis at higher temperatures.

Experimental Results

Activity data for tests of prepoisoned catalysts are given in Fig. 1. Here the logarithm of relative activity is plotted as a function of sulfur content of the pretreated catalyst. Relative activity is defined as the activity of the poisoned catalyst divided by the activity of a corresponding unpoisoned catalyst times 100. The activities given are averages for the first 3 weeks of the test. For H_2S , C_2H_5SH , and SO_2 on reduced D-3001 these plots are approximately linear in the range of relative activity from 100 to 20%.

For COS on reduced and H_2S on nitrided D-3001, the data were erratic, and high relative activities were obtained for some samples containing moderate concentrations of sulfur. However, the relative activities decreased to less than 2% in the

(11) R. B. Anderson, B. Seligman, J. F. Shultz, R. Kelly, and M. A. Elliott *Ind. Eng. Chem.*, **44**, 391 (1952).

(12) (a) R. B. Anderson, A. Krieg, B. Seligman, and W. E. O'Neill, *ibid.*, **39**, 1548 (1947); (b) J. F. Shultz, L. J. E. Hofer, E. M. Cohn, K. C. Stein, and R. B. Anderson, Bureau of Mines Bulletin 578, 1959, 139 pp.

Test number	X843	X818	X809	Z8	X800
Sulfur concentration mg. S/g. Fe	0	1.1	1.5	3.0	12.9
Temperature, °C	260	269	278	300	380
Contraction (CO ₂ -free), %	64	64	63	58	61

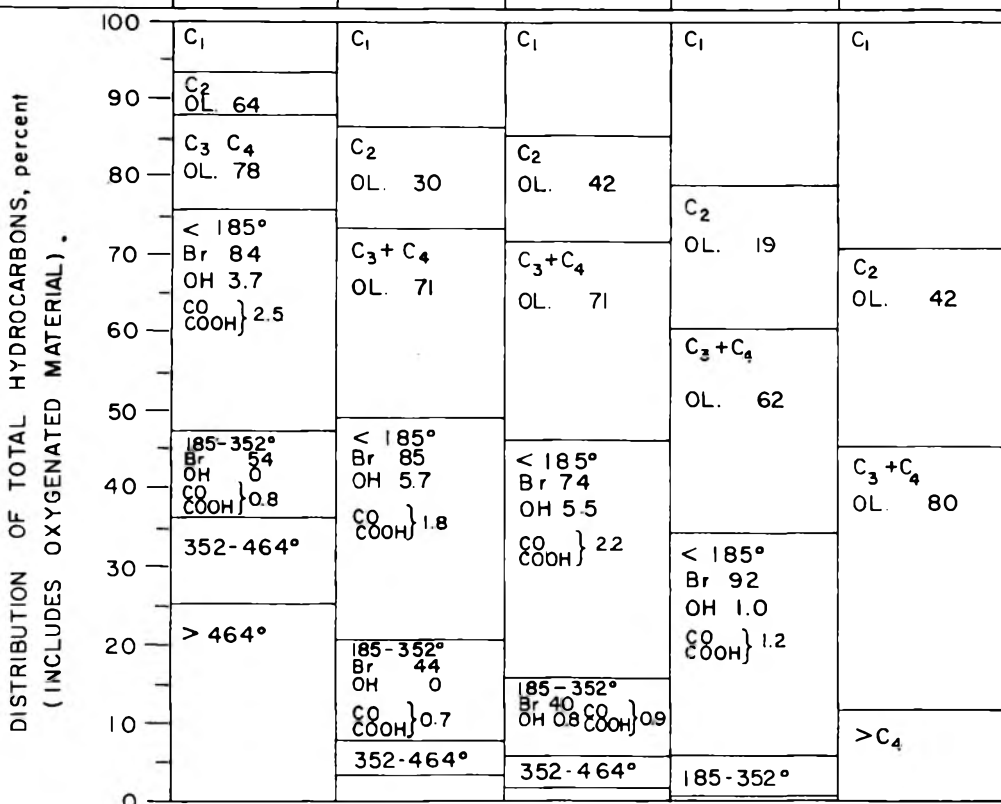


Fig. 2.—Selectivity of catalyst D-3001 prepoisoned with H₂S. 1H₂ + 1CO gas at 21.4 atm. and hourly space velocity of 300. Symbols in histograms have the following meaning: OL., % olefin; Br, bromine number, OH and $\left. \begin{matrix} \text{CO} \\ \text{COOH} \end{matrix} \right\}$, the weight % hydroxyl group, and weight % carbonyl group, respectively.

range 8 to 10 mg. S/g. Fe for H₂S, COS, and C₂H₅SH on reduced and H₂S on nitrated D-3001. Poisoning by SO₂ was more severe than for other sulfur compounds at concentrations less than 7 mg. S/g. Fe.

For activated steel turnings, L-2201, poisoning by 0.18 mg. S/g. Fe as H₂S decreased the relative activity to 8.1%, compared with 7.8 mg. S/g. Fe required for catalyst D-3001. Sulfur concentrations in mg. S/m.² of surface required to decrease the relative activity to 8.1% were 0.22 and 0.58 for turnings and reduced D-3001, respectively.

For reduced catalyst D-3001 prepoisoned with CS₂ and nitrated D-3001 with H₂S, the relative activities were erratic, and the catalyst particles in many of these tests disintegrated sufficiently

to cause the pressure drop in the bed to increase appreciably even in the initial period at temperatures less than 300°. In several tests catalysts prepoisoned with CS₂ at concentrations less than 3 mg. S/g. Fe were more active than fresh catalysts. Catalyst disintegration observed in these tests probably results from carbon deposition, as these catalysts contained moderately high concentration of carbon although their temperature of operation had not exceeded 270°. An increase in activity often accompanies catalyst disintegration by carbon deposition, because the activity increases with decreasing particle size. Carbon deposition generally was not increased by the presence of sulfur in the catalyst, and severely poisoned catalysts often could be operated at

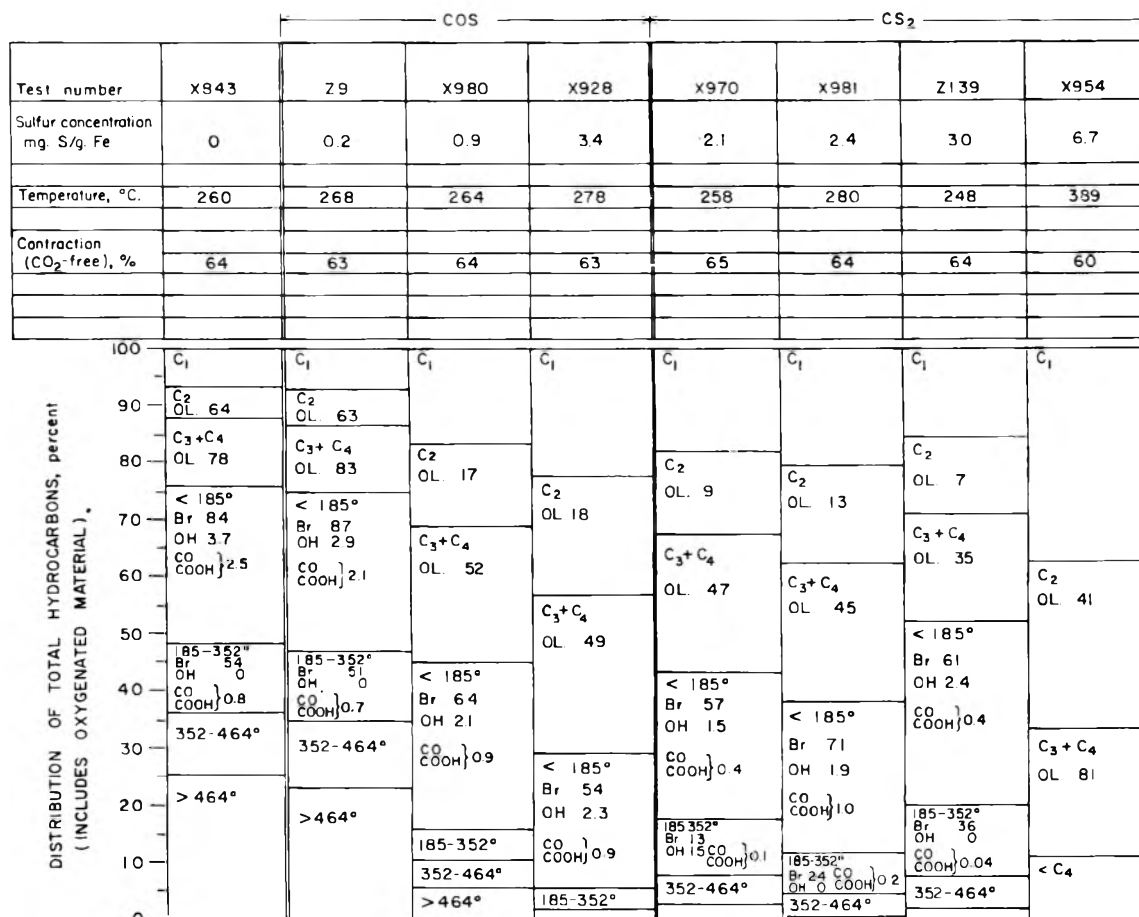


Fig. 3.—Selectivity of prepoisoned catalyst D-3001. $\text{H}_2 + \text{1CO}$ gas at 21.4 atm. and hourly space velocity of 300. Symbols in histograms are defined in Fig. 2.

temperatures in excess of 350° without encountering exceptional difficulties.

In the present poisoning studies the yield of products of low molecular weight increased with increasing concentration of sulfur, as shown for reduced catalyst D-3001 in Figs. 2 and 3. The histograms present the distribution of total hydrocarbons, including oxygenated molecules dissolved in condensed hydrocarbons. Water-soluble oxygenated molecules are not shown. Numbers preceded by "OL" indicate percentages of olefins; "Br" is bromine number; "OH" weight % hydroxyl group; and "CO" weight % carbonyl group as aldehydes, ketones and acids. The results in Fig. 2 for poisoning by H_2S are complicated by the increase in temperature required to compensate for decreased activity, which would be expected to change the selectivity in the same direction. However, as shown in Fig. 3 for CS_2 -poisoning, for which the activity data were erratic, a similar increase of products of low molecular weight with increasing concentration of sulfur was observed for tests Z-139 and X-970, where the poisoned catalysts were operated at a lower temperature than the unpoisoned. Figure 3 also shows selectivity data for catalysts poisoned by COS. For tests X-980 and Z-9 the average molecular weight of the products also decreased with sulfur content of the catalyst, although the syn-

thesis temperatures were only 4 and 8° greater than in control test X-843.

Sulfur poisoning increased the $\text{H}_2:\text{CO}$ usage ratio (moles H_2 consumed/moles CO consumed) by a small amount. Since the usage ratio varies widely with conversion, only data for which the apparent CO_2 -free contraction was between 60 and 65% were compared. Under these conditions for reduced catalyst D-3001 the usage ratios for the fresh catalyst averaged 0.70, compared with averages of 0.75, 0.74, 0.80, 0.76, and 0.81 for catalysts poisoned with H_2S , COS, SO_2 , $\text{C}_2\text{H}_5\text{SH}$, and CS_2 , respectively.

Chemical analyses of catalysts before and after synthesis indicated that in all cases little if any sulfur was removed during synthesis.

In addition to the tests of prepoisoned catalysts, 4 samples of reduced D-3001 were used in the synthesis for 400–800 hr., removed from the reactor and extracted with heptane in a Soxhlet apparatus to remove most of the adsorbed wax, immersed in a solution of H_2S in heptane, and tested in the synthesis with $\text{1H}_2 + \text{1CO}$ gas at 21.4 atm. When compared at equal amounts of sulfur per g. of iron, the relative activities of the poisoned catalysts in the initial period of synthesis were only about 20% of that of the prepoisoned catalyst. However, the surface area of the extracted used catalyst was about 0.75 m.²/g.

Fe compared with 14.8 for the reduced catalyst.¹³ The activity data for poisoning by the two methods at low sulfur concentrations may be brought into reasonable agreement if the sulfur concentration is expressed per unit surface area as shown below

Test	Sulfur concn., mg. S/m. ²	Relative activity of poisoned- used catalyst	Relative activity of prepoisoned cata- lyst at same concn. of sulfur per m. ²
Z-50	0.24	0.28	0.36
Z-114	0.60	.12	.10
Z-177	2.79	.09	<.01
Z-87	3.90	.05	<.01

The activity of the poisoned-used catalysts, except for test Z-87, increased more than 2-fold during synthesis. Activity changes of this magnitude were not observed with any of the prepoisoned catalysts.

Discussion

The present experiments with prepoisoned catalysts show that 10 mg. S/g. Fe will decrease the relative activity of reduced D-3001 to less than 2%. At smaller concentrations SO₂ is a more effective poison than H₂S, C₂H₅SH and COS.

Several estimates were made of the quantity of sulfur necessary to cover the iron surface with a monolayer and to react with the alkali present as a promoter. It was assumed that sulfur atoms adsorb at specific sites, such as directly on top of iron atoms or in interstices between them. According to Pauling¹⁴ the radii of the covalent sulfur (S⁰) and sulfide ion (S⁼) are 1.04 and 1.84 Å., respectively. Covalent sulfur is small enough to adsorb on each iron atom on the surface, but the sulfide ion can adsorb on only half of the iron atoms. Table I presents estimates of the amounts of each type of sulfur required to cover a surface composed entirely of iron or ε-Fe₂N. Estimates were made for γ-Fe and ε-Fe₂N to include the possibilities of iron being present in more closely packed structures on the surface or as nitrides, carbonitrides or carbides. Values for sulfide ion seem too low to account for our results without assuming the formation of multilayers or bulk sulfides. For calculations we have used the value for covalent sulfur on bcc-111, 0.74 mg. S/m.². For reduced D-3001 and turnings L-2201 the surface areas were 14.8 and 0.83 m.²/g. Fe, and the calculated sulfur monolayers were 10.95 and 0.61 mg. S/g. Fe, respectively, assuming the surface is entirely covered with iron atoms.

Sulfur compounds also may react with the alkali promoter. On the basis of a stoichiometric reaction with all of the alkali, the amount of sulfur required for D-3001 is 5.8 and 2.9 mg. S/g. Fe, if adsorbed as SH⁻ or HSO₃⁻, and S⁼ or SO₃⁼, respectively. Corresponding values for turnings L-2201 are 0.93 and 0.47 mg. S/g. Fe.

Adsorption studies^{15,16} suggest that the surface

(13) K. C. Stein, G. P. Thompson, and R. B. Anderson, *J. Phys. Chem.*, **61**, 928 (1957).

(14) L. Pauling, "The Nature of the Chemical Bond and the Structure of Molecules and Crystals," 2d Ed., Cornell Univ. Press, Ithaca, N. Y., 1944, p. 450.

(15) S. Brunauer and P. H. Emmett, *J. Am. Chem. Soc.*, **62**, 1732 (1940).

TABLE I

SULFUR REQUIRED TO COVER AN IRON SURFACE

Structure and face	S ⁰ (1.04 Å.) mg. S/m. ²	S ⁼ (1.84 Å.) mg. S/m. ²
bcc 100 and 110	0.65	0.325
111	as in α-Fe	.74
	γ-Fe	
fcc 111	.98	.49
100		
hcp 001	as in ε-Fe ₂ N	.79

of doubly promoted iron catalysts contains metallic iron, alkali promoter, and structural promoter. Chemisorption of carbon monoxide on reduced D-3001 at -195° suggests that about 45% of the surface is covered by iron atoms. On this basis, for example, if covalent sulfur is adsorbed on a 111 face of bcc iron and all of the alkali reacts to form KHS, the sulfur required is (10.95 × .45) + 5.8 = 10.7 mg. S/g. Fe. A variety of other combinations can be chosen, and these usually lead to a lower concentration of sulfur for surface coverage. In studies of the ammonia synthesis, Temkin⁷ used a value of 0.5 mg. S/m.², on the assumption that the entire surface was covered by FeS. Based on this value for surface coverage, Temkin calculated the number of monolayers required to cover the active surface as about 0.8, 1.8 and 5.0 for Fe-Al₂O₃, Fe-Al₂O₃-K₂O, and Fe-K₂O, respectively. For the Fe-Al₂O₃-K₂O catalyst, the activity decreased to zero at 0.9 mg. S/m.², which compares favorably with our value for the Fischer-Tropsch synthesis on D-3001 of 0.75.

The equal effectiveness of H₂S and ethyl mercaptan is not unexpected as ethyl mercaptan should decompose cleanly to ethylene, ethane and adsorbed sulfur at the temperatures of poisoning and synthesis. Two explanations may be offered for SO₂ being the most effective poison tested: (a) the chemisorbed SO₂ may be larger than S⁰ or S⁼, and (b) SO₂ may react with alkali to form SO₃⁼, whereas H₂S and other compounds may form SH⁻.

Adsorption studies in this Laboratory have demonstrated that the amount of CO₂ chemisorbed at -78° on iron catalysts decreases more rapidly than the amount of CO chemisorbed at -195° when the catalyst is prepoisoned with increasing amounts of H₂S. For reduced D-3001 the addition of 7 mg. S/g. Fe as H₂S decreased CO₂ chemisorption by 91% and CO by 43%. These data suggest that the sulfur compounds are preferentially adsorbed on the alkali. In the present synthesis tests poisoned catalysts yield a product of lower average molecular weight and have a higher usage ratio than fresh catalysts, and the selectivity of iron catalysts varies in this direction as the alkali content is decreased substantially.

The amount of sulfur required to poison the catalyst to a given degree seems to be approximately proportional to the surface area at the time

(16) W. K. Hall, W. H. Tarn, and R. B. Anderson, *ibid.*, **72**, 5426 (1950).

of poisoning, as shown by comparison of poisoning of fresh and used catalyst D-3001 or prepoisoned turnings. Similarly in poisoning tests of used catalysts by synthesis gas containing trace amounts of sulfur compounds, now in progress, the quantities of sulfur for rather complete poisoning are of about the same magnitude as those reported here for the prepoisoned used catalyst.

In tests of reduced catalyst D-3001 prepoisoned by CS_2 and COS and nitrided D-3001 prepoisoned with H_2S , the activity was higher than expected, at times exceeding the activity of the unpoisoned catalyst, and disintegration of the catalyst often occurred at lower temperatures than observed in other experiments. The higher activities probably

are related to disintegration of the catalyst by excessive carbon deposition, which was not observed for reduced catalysts poisoned with other sulfur compounds. Nevertheless, nitrided catalysts poisoned with sulfur compounds in the synthesis gas also show greater resistance to poisoning.

Bashkirov and Barabanov¹⁷ observed that CS_2 decomposed on reduced iron at 200° to produce carbon and COS to CO and carbon. Ethyl mercaptan was less reactive and decomposed to ethylene and ethane. These results seem consistent with our observations.

(17) A. N. Bashkirov and N. L. Barabanov, *Doklady Akad. Nauk S.S.S.R.*, **104**, 854 (1955).

ACTIVITY COEFFICIENTS OF MANNITOL AND POTASSIUM CHLORIDE IN MIXED AQUEOUS SOLUTIONS AT 25°

BY R. A. ROBINSON¹ AND R. H. STOKES

The Department of Chemistry of the University of New England, Armidale, N.S.W., Australia

Received September 27, 1961

From isopiestic vapor pressure data, equations are derived for the activity coefficients of both solutes in mixed solutions of mannitol and potassium chloride at 25°. The mutual salting-in is of similar magnitude to that for the system mannitol-sodium chloride-water.

In a previous paper,² the isopiestic vapor pressure method was applied to the ternary system mannitol-sodium chloride-water at 25°. The present note reports similar data for the system mannitol-potassium chloride-water. The materials and experimental technique were the same, except that in most of the measurements the reference solution was potassium chloride. The results are given in Table I, and analysis of these by the

m_{ref}	m_B	m_C	$-\Delta/m_B m_C$	% diff.					
0.7066	0.1605	0.6177	0.0182	-0.03	3.0169	0.3124	2.8746	.0269	- .02
	.4092	.4792	.0230	+ .03		.5497	2.7630	.0257	- .04
	.6479	.3441	.0242	+ .05		.8551	2.6157	.0241	- .06
	1.1414	.0618	.0113	- .04		1.0233	2.5355	.0257	+ .04
0.8760	0.2194	0.7565	.0307	+ .10	3.4415	0.2733	3.3214	.0262	- .06
	.4045	.6535	.0242	+ .04		.5592	3.1947	.0275	- .04
	.8018	.4290	.0218	+ .05		.8459	3.0617	.0257	- .07
	1.2279	.1821	.0094	- .05		1.1077	2.9367	.0243	- .09
1.5791	0.3110	1.4161	.0211	- .04	4.3687	0.3983	4.2142	.0350	- .02
	.4965	1.3174	.0225	- .01		.5742	4.1411	.0318	- .04
	.7072	1.2041	.0233	+ .06		.8673	4.0223	.0327	+ .04
	.9345	1.0783	.0226	+ .07		1.1916	3.8824	.0308	+ .03
2.1999	0.4000	2.0010	.0231	- .03	4.5078	0.3042	4.3879	.0283	- .10
	.5876	1.9055	.0227	- .03		0.5924	4.2782	.0339	.00
	.7640	1.8136	.0210	- .07		1.1167	4.0626	.0332	+ .07
	1.0410	1.6679	.0211	- .03		1.3906	3.9376	.0290	- .04
2.5315	0.7473	2.1665	.0233	- .02	4.6509	0.3004	4.5328	0.0278	+ .13
	0.9978	2.0379	.0224	- .03		.6118	4.4182	.0356	+ .03
						1.1536	4.1973	.0332	+ .08
						1.4379	4.0715	.0306	+ .03
3.0169	0.3110	1.4161	.0211	- .04	4.7198	0.3610	4.5879	.0397	+ .06
	.4965	1.3174	.0225	- .01		.5191	4.5261	.0375	+ .05
	.7072	1.2041	.0233	+ .06		.6748	4.4658	.0367	+ .07
	.9345	1.0783	.0226	+ .07		1.1056	4.2921	.0348	+ .13
4.5125*	1.2993	4.7271	.0360	+ .11					
Mean $\pm 0.05\%$									

(1) National Bureau of Standards, Washington 25, D. C.

(2) F. J. Kelly, R. A. Robinson, and R. H. Stokes, *J. Phys. Chem.*, **65**, 1958 (1961).

* Reference-electrolyte potassium chloride except in run marked *, where it was sodium chloride. $\Delta = 2\varphi_{ref}m_{ref} - m_B\varphi_B^0 - 2m_C\varphi_C^0$. φ = molal osmotic coefficient; φ_B^0 = molal osmotic coefficient of B at molality m_B in absence of C; φ_C^0 = molal osmotic coefficient of C at molality m_C in absence of B. "Difference" column gives the percentage accuracy with which the molality of the reference solution can be computed by equation 1.

same methods as previously² leads to the equations

$$-\left(\frac{\partial \ln \gamma_B}{\partial m_C}\right)_{m_B} = -2\left(\frac{\partial \ln \gamma_C}{\partial m_B}\right)_{m_C} = -\Delta/(m_B m_C) = 0.0216 + 0.0016m_C + 0.00042m_C^2 - 0.0031m_B \quad (1)$$

$$\log \gamma_B = 0.00295m_B + 0.00274m_B^2 - 0.00940m_C - 0.00035m_C^2 - 0.000061m_C^3 + 0.00135m_B m_C \quad (2)$$

$$\log \gamma_C = \log \gamma_C^0 - 0.0047m_B + 0.00034m_B^2 - 0.00035m_B m_C - 0.00009m_B m_C^2 \quad (3)$$

In these equations: m_B = molality of mannitol; m_C = molality of potassium chloride; γ_B, γ_C are the respective activity coefficients in the mixture; γ_C^0 is the activity coefficient of potassium chloride at molality m_C in the absence of mannitol; and Δ is defined in Table I.

Calculations of the solubility of each solute in the presence of the other were made by the same method as in the previous paper,² the calculated solubilities being given in Table II. Table III gives activity coefficients of both solutes at round concentrations. The salting-in of mannitol by potassium chloride is similar in magnitude to that by sodium chloride,

TABLE II

CALCULATED SOLUBILITY RELATIONS IN THE SYSTEM MANNITOL (B)-POTASSIUM CHLORIDE (C)-WATER AT 25°

(a) Solutions saturated to mannitol

m_C	0	1	2	3	4	4.919 ^a
$m_{B(sat)}$	1.185	1.207	1.232	1.262	1.297	1.335

(b) Solutions saturated to potassium chloride $m_{C(sat)} =$

$$4.810 + 0.082m_B$$

^a Saturated to both components.

TABLE III

ACTIVITY COEFFICIENTS OF MANNITOL (B) AND POTASSIUM CHLORIDE (C) IN MIXED AQUEOUS SOLUTION AT 25°

m_B	m_C	0	1	2	3	4	4.8
0	γ_B	1.000	0.978	0.953	0.927	0.897	0.871
	γ_C	1.000	.6038	.5728	.5689	.5768	.5879
0.3	γ_B	1.003	.981	.958	.932	.903	.877
	γ_C	0.9967	.6016	.5705	.5663	.5738	.5846
0.7	γ_B	1.008	.987	.965	.940	.912	.887
	γ_C	0.9928	.5991	.5677	.5631	.5701	.5801
1.0	γ_B	1.013	.994	.972	.948	.920	.896
	γ_C	0.9900	.5972	.5656	.5607	.5673	.5769
1.2	γ_B	1.018	.998	.977	.954	.927	.902
	γ_C	0.9882	.5960	.5644	.5593	.5656	.5749

though its concentration-dependence is somewhat different.

So far, the solution has been considered as one containing two solutes, potassium chloride and mannitol, in water. It could equally well be considered as a solution of potassium chloride in the mixed solvent, water-mannitol. The data for γ_C in the column $m_C = 0$ of Table III are the activity coefficients of potassium chloride at zero salt concentration in various water-mannitol mixtures. They all are relative to unity in pure water. By the usual transform, they can be expressed as activity coefficients on the mole fraction scale. Thus $f_C = 0.0034$ in 1 M mannitol at $m_C = 0$ and this is what Owen³ calls the primary medium effect. The quantity represents the increment

$$2 RT \lim_{m_C \rightarrow 0} \ln f_C$$

in chemical potential when a mole of potassium chloride is transferred from a given mole fraction in water to the same mole fraction in the water-mannitol mixture, the transfer in this case being at the limit, $m_C = 0$. Similar increments in chemical potential for the transfer of hydrochloric acid from water to a mixed solvent can be calculated from the standard potential of the cell: $H_2|HCl|AgCl, Ag$. It is of interest to look at the magnitude of some of these energies of transfer. The following have been calculated

Solute	Medium	Cal. mole ⁻¹
KCl ⁴	Ethylene glycol	5,600
NaCl ⁴	Methanol	1,380
HCl ⁵	20% Dioxane	242
HCl ⁶	10% Methanol	100
HCl ⁷	10% Fructose	57.2
HCl ⁸	20% Sorbitol	45
NaCl ²	15.41% Mannitol ^a	13.6
KCl	15.41% Mannitol	9.3
HCl ⁸	5% Sorbitol	-19.4

^a A 1 M solution contains 15.41 g. of mannitol/100 g. solution.

(3) B. B. Owen, *J. Am. Chem. Soc.*, **54**, 1758 (1932).

(4) J. K. Gladden and J. C. Faaming, *J. Phys. Chem.*, **65**, 76 (1961).

(5) H. S. Harned, *J. Am. Chem. Soc.*, **60**, 336 (1938).

(6) H. S. Harned and H. C. Thomas, *ibid.*, **57**, 1666 (1935).

(7) H. D. Crockford and A. A. Szekhnovsky, *ibid.*, **73**, 4177 (1951).

(8) H. D. Crockford, B. J. Aley, and C. S. Patterson, *J. Elisha Mitchell Sci. Soc.*, **73**, 284 (1957).

THE CALCULATION OF ACTIVITY COEFFICIENTS FROM OSMOTIC COEFFICIENT DATA¹

BY M. H. LIETZKE AND R. W. STOUGHTON

Chemistry Division, Oak Ridge National Laboratory, Oak Ridge, Tennessee

Received September 28, 1961

A non-linear least squares method of fitting osmotic coefficient data in order to calculate activity coefficients is described. With this technique, the osmotic and activity coefficients of electrolytes can be expressed within the precision of the measurements over wide ranges of concentration. The method is greatly to be preferred over graphical integration if a high speed computer is available to perform the calculations.

Several different semi-empirical equations have been considered for representing the logarithm of an activity coefficient over a wide range of concentration. Each equation involves a one parameter Debye-Hückel term plus two or three higher terms, each of which is the product of a parameter and a simple function of the ionic strength I . When any one of the activity coefficient equations is substituted into the Gibbs-Duhem relation and integrated analytically, a corresponding equation may be obtained for the osmotic coefficient in which each of the parameters retains its identity. Thus the parameters may be evaluated using a non-linear least squares method from osmotic coefficient data and used to calculate activity coefficients *vs.* concentration, or *vice versa*. Since it is relatively difficult to get accurate osmotic coefficient data at low concentrations and since an integration from zero concentration is required to evaluate activity coefficients therefrom, the possibility of obviating some of the difficulty usually encountered in such graphical integrations has been investigated by the use of analytical methods using an IBM 7090 computer.

When a single-parameter Debye-Hückel expression for the activity coefficient of an electrolyte

$$\ln \gamma_{\pm} = - \frac{s\sqrt{I}}{1 + A\sqrt{I}} \quad (1)$$

is differentiated and substituted into

$$\phi = 1 + \frac{1}{m} \int_0^m m \, d \ln \gamma_{\pm} \quad (2)$$

and the integration performed analytically, then the following expression for the osmotic coefficient ϕ is obtained

$$\phi = 1 - \frac{s}{A^3 I} \left[(1 + AI^{1/2}) - 2 \ln (1 + AI^{1/2}) - \frac{1}{1 + AI^{1/2}} \right] \quad (3)$$

For use at higher concentrations linear, quadratic and cubic terms may be added as

$$\phi = 1 - \frac{s}{A^3 I} \left[(1 + AI^{1/2}) - 2 \ln (1 + AI^{1/2}) - \frac{1}{1 + AI^{1/2}} \right] + BI + CI^2 + DI^3 \quad (4)$$

The corresponding equation for the activity coefficient then becomes

$$\ln \gamma_{\pm} = - \frac{s\sqrt{I}}{1 + A\sqrt{I}} + (2B)I + (3/2C)I^2 + (4/3D)I^3 \quad (5)$$

In equation 4 the parameters A , B , C and D for any particular electrolyte may be evaluated by the method of least squares² and the corresponding activity coefficients may be computed immediately using equation 5.

In order to determine how many parameters were needed to give a good fit with equation 4, the osmotic coefficients of NaCl (as listed by Robinson and Stokes³) were fitted both with and without a cubic term. At both 25 and 100° the inclusion of the cubic term produced a significantly better fit: the variance of the fit at 25° was 3.1×10^{-6} without the cubic term and 1.2×10^{-7} with the cubic term; at 100° the variance of the fit was 1.2×10^{-6} without the cubic term and 7.3×10^{-7} with the cubic term. Hence all the calculations presented in this paper were performed with equation 4 as written.

In Table I are given the parameters describing the concentration dependence of the osmotic coefficients of a variety of electrolytes as well as the variances of fit. Most of the data were taken from Robinson and Stokes.³ However, the values for LiCl,⁴ LiBr,⁵ LiI,⁴ KCl,⁴ KBr,⁵ RbCl,⁴ BeSO₄,⁶ and UO₂SO₄,⁶ were computed from the original isopiestic molalities, while the values at 99.6° were computed from the isopiestic molalities reported by Patterson, Gilpatrick and Soldano.⁷ In all cases the value of s (the Debye-Hückel limiting slope) was taken as 1.17202 at 25°, 1.4107 at 99.6°, and 1.4122 at 100° for a 1:1 electrolyte.

When the coefficients obtained by fitting osmotic coefficient data with equation 4 are used in equation 5 it is not necessary to normalize any of the activity coefficients to a particular value at 0.1 m since the integration of equation 2 was performed analytically from $m = 0$. Thus the activity coefficients reflect better the differences between various salts (particularly the 2:2 sulfates). Calculations with 25° data and equations 4 and 5 have shown that osmotic coefficients in the range 1–3 m can be used to calculate values of both osmotic and activity

(2) H. Margenau and G. Murphy, "The Mathematics of Physics and Chemistry," D. Van Nostrand Co., Inc., New York, N. Y., 1956.

(3) R. A. Robinson and R. W. Stokes, "Electrolyte Solutions," Academic Press, Inc., New York, N. Y., 1955.

(4) R. A. Robinson and D. A. Sinclair, *J. Am. Chem. Soc.*, **56**, 1830 (1934).

(5) R. A. Robinson, *ibid.*, **57**, 1161 (1935).

(6) R. A. Robinson, *J. Chem. Soc.*, 4543 (1952).

(7) C. S. Patterson, L. O. Gilpatrick and B. A. Soldano, *ibid.*, 2730 (1960).

(1) This document is based on work performed for the U. S. Atomic Energy Commission at the Oak Ridge National Laboratory, Oak Ridge, Tennessee, operated by Union Carbide Corporation.

TABLE I
PARAMETERS DESCRIBING THE CONCENTRATION DEPENDENCE OF THE OSMOTIC COEFFICIENTS OF A VARIETY OF ELECTROLYTES

Electrolyte	A	B × 10 ³	C × 10 ³ 25°	D × 10 ⁴	σ _{fit} ² × 10 ⁶ ^a	Range, ^b m
NaCl	1.45397	2.23565	9.30838	- 5.36209	0.12	0.006-6.0 m
LiCl	1.48996	10.2909	6.04782	5.40012	5.91	.111-3.159
LiBr	1.24741	14.7940	- 0.61962	12.8635	6.09	.166-3.325
LiI	2.12556	13.8683	- 0.261474	40.7768	19.39	.120-3.152
KCl	1.30752	- 0.359188	7.17091	- 5.67500	1.46	.106-4.810
KBr	1.29231	0.994831	4.34095	- 3.50742	0.24	.100-5.000
RbCl	1.30240	- 2.05431	13.9445	-15.6796	74.82	.423-4.962
CaCl ₂	1.61291	4.56577	8.57310	- 2.73800	4.03	.002-6.00
MgCl ₂	1.60067	6.63253	9.00272	- 2.54526	15.01	.100-5.00
BaCl ₂	1.59925	1.23161	8.81121	- 6.92099	0.84	.100-1.80
BaBr ₂	1.62543	3.81918	8.02100	- 5.19535	1.90	.100-2.00
Na ₂ SO ₄	1.24072	- 6.58044	7.26282	- 1.94540	4.41	.100-4.00
BeSO ₄	1.23250	- 1.54261	5.10411	- 0.945238	37.08	.102-4.286
UO ₂ SO ₄	0.998119	0.399490	2.27077	- 0.563181	11.14	.113-6.371
MgSO ₄	1.37486	- 5.42492	8.42636	- 1.89929	3.84	.100-3.00
MnSO ₄	1.28920	- 5.47447	7.36518	- 1.56926	17.58	.100-4.00
NiSO ₄	1.31677	- 7.20761	10.2081	- 2.45406	3.34	.100-2.50
CuSO ₄	1.14652	- 2.25375	- 1.13297	6.24346	3.42	.100-1.40
ZnSO ₄	1.27839	- 5.56227	7.60615	- 1.25189	5.67	.100-3.50
CdSO ₄	1.20516	- 5.08061	7.00382	- 1.69009	4.52	.100-3.50
99.6°						
LiCl	1.36704	4.62413	20.9758	-25.0075	8.03	0.950-3.845
KCl	1.87392	- 2.83699	19.5070	-21.7686	6.64	0.993-4.742
CsCl	1.40727	- 1.45738	10.1090	- 8.77824	18.53	1.018-4.924
BaCl ₂	1.17244	6.81811	- 7.60404	5.47538	17.97	0.714-2.199
Na ₂ SO ₄	2.18824	-11.0123	15.2961	- 7.04151	0.55	0.891-3.178
MgSO ₄	1.58747	- 6.80762	6.51886	- 1.15772	10.90	1.901-4.753
UO ₂ SO ₄	1.11309	- 2.11182	2.52142	- 0.580834	40.99	2.083-5.041
100°						
NaCl	1.55510	3.64784	6.43661	- 7.13179	0.73	0.05-4.0

^a Variance of fit. ^b Range of concentrations used in making the fit.

coefficients at lower concentrations with good accuracy. Thus activity coefficients may readily be calculated over a wide range of concentrations from relatively few osmotic coefficient data. Moreover, the use of equations 4 and 5 is greatly to be preferred over graphical integration if a high-speed computer is available to perform the non-linear least squares fits. Care should be exercised, however, in using the equations (particularly if a cubic term is included) for extrapolation to concentrations higher than those used in making the fit since fictitious points of inflection may be encountered in this region. The method also will fail if an electrolyte exhibits sufficient ion association so that values of the osmotic coefficients fall below the limiting slope at low concentrations.

The method of computation described in this paper represents a considerable extension over the method recently described by Guggenheim and Stokes.⁸ In their paper Guggenheim and Stokes demonstrated that a two-parameter equation was valid for CaCl₂ solutions to $m = 0.4$. They then assumed that the two-parameter expressions were valid for other typical 2:1 and 1:2 electrolytes and chose the two parameters in each case to give the best fit of the isopiestic values at molalities

0.1, 0.2, 0.3 and 0.4. With the coefficients so obtained the activity coefficient of each salt was computed at 0.1 m . In the present work the osmotic coefficients are fitted with equation 4 and those parameters are immediately chosen for any electrolyte which satisfy the statistical criterion that $\sum_i (\phi_{\text{obs}} - \phi_c)^2$ be minimized. It is interesting to compare the values of the activity coefficients at 0.1 m computed in the present work with those reported by Guggenheim and Stokes for several electrolytes. These values are presented in Table II.

TABLE II
VALUES OF THE ACTIVITY COEFFICIENT OF SEVERAL ELECTROLYTES AT 0.1 m

	γ (old) ⁸	γ (G. and S.) ⁸	γ (present calcd.)
MgCl ₂	0.529	0.528	0.525
CaCl ₂	.518	.518	.520
BaCl ₂	.500	.508	.509
BaBr ₂	.513	.517	.519
Na ₂ SO ₄	.445	.452	.448

Acknowledgments.—The authors wish to express their appreciation to Drs. George Scatchard and G. E. Boyd for helpful suggestions and encouragement.

(8) E. A. Guggenheim and R. H. Stokes, *Trans. Faraday Soc.*, **54**, 1646 (1958).

ACTIVATION OF METAL HYDROGENATION CATALYSTS BY IRRADIATION

BY DONALD GRAHAM

*Contribution No. 289—Jackson Laboratory, Organic Chemicals Department, E. I. du Pont de Nemours and Company, Wilmington, Delaware**Received October 2, 1961*

The catalytic activities of supported metal hydrogenation catalysts (nickel, palladium, and platinum) have been increased by high energy irradiation. The improvement sometimes exceeded 20%. Active centers appeared to be both created and destroyed by irradiation, the latter effect possibly involving an annealing process. In general, the energy required for forming new active centers and also the stability of these centers vary directly with the temperature required for diffusion of the atoms in the surface of the catalyst metals, which temperature is a function of their melting points.

Introduction

Lattice defects long have been considered to be possible sites of catalytic activity in solid surfaces. The creation of such active centers by high energy irradiation was proposed over 25 years ago.¹ The introduction of defects into metals such as silver and copper by irradiation has been studied widely,² usually by measuring accompanying changes in the low temperature physical properties of the metals. The defects resulting from radiation tended to be annealed out as room temperature was approached.

Due possibly to their higher annealing temperatures, the first catalysts successfully activated by irradiation were oxides. In 1955, the irradiation of silica gel with fast neutrons was reported to increase its activity in catalysis of double bond isomerization in hexene.³

Thermal neutrons produced a variety of effects on oxide catalysts for the decomposition of nitrous oxide.⁴ The activity of nickel oxide was slightly reduced. That of alumina was increased or decreased depending on whether B₂O₃ or Li₂O was added and that of stannic oxide showed a marked increase.

Some progress also has been made in the radiation activation of metal catalysts. Three developments seem particularly pertinent.

Deuteron irradiation of copper catalysts for the decomposition of formic acid (zero order) altered both the frequency factor and the energy of activation of the reaction.⁵

Argon ion bombardment of single crystal silver catalysts for the same reaction also changed both frequency factor and activation energy. The radiation effects differed with the energy of the radiation and with the crystal face bombarded (111, 110 and 100) and a compensation effect was observed.⁶

The activity, for hydrogenation of ethylene, of a nickel surface cleaned by heating to 800° followed by positive ion bombardment was much greater immediately after bombardment than that of a similar sample cleaned by heating alone. However, this enhanced activity was short lived; and, after annealing at 600° for 1 minute, the activity approached zero.⁷

It was hoped, in undertaking this investigation, that the higher melting points of nickel, palladium and platinum and the accompanying greater resistance to surface diffusion would result in improved stability of active centers generated by radiation.

Experimental

(A) **Catalysts.**—Three different catalysts were employed in this investigation, nickel (30%) on Filter-Cel, platinum (1%) on an active carbon (Darco G-60), and palladium (5%) on a carbon black (Shawinigan Acetylene Black). The nickel catalyst was prepared by precipitation of the basic carbonate on Filter-Cel followed by reduction with hydrogen.^{8,9} The palladium and platinum catalysts were prepared by precipitation of the noble metal on the substrate as the hydroxide followed by reduction to the active metallic form with formaldehyde.¹⁰

(B) **Radiation.**— β -Radiation at 2 mev. and 10 watts/cm.² and also at 3 mev. and 15 watts/cm.² was obtained from the Van de Graaff generators of the Du Pont Central Research Department through the courtesy of Dr. R. D. Souffie.

1–2 mev. X-radiation also was obtained from a Van de Graaff generator by allowing the e⁻ beam to impinge on a 2 mm. gold target. Dosage was estimated (from measurements on comparable samples) at 700 rad/sec.

Deuteron radiation at 15 mev. and 20 μ a. was obtained from the cyclotron in the Radiation Laboratory of the University of Pittsburgh, Professor A. J. Allen, Director.

Irradiation with neutrons at a flux of 10¹² n/ μ amp./cm.²/sec. and a current of 10 μ amp. was carried out in the same cyclotron using a beryllium target.

Measurement of Catalyst Activity.—The activity of the nickel catalysts before and after irradiation was determined from the rate of hydrogenation of nitrobenzene in isopropyl alcohol at 100° and 500–400 p.s.i.g. H₂ in stainless steel equipment. The first drop and the last few drops were disregarded to eliminate effects of the initial induction period and the nitrobenzene concentration fall-off at the end. In other words, only those drops were used which showed a constant time for the 100 p.s.i. drop.

Activities of the palladium and platinum catalysts were determined from the rates of hydrogenation of *p*-nitrotoluene in glacial acetic acid. Again, only that part of the reaction period was used which showed a constant rate of hydrogen uptake.

Results

The experimental results are presented in Table I.

Nickel Catalyst (30% Ni on Filter-Cel).—The activity of the nickel catalyst was appreciably improved by a very brief β -irradiation and then decreased with continued exposure. The active centers produced by irradiation were unstable. The activity of the sample decreased rapidly, until after one week all of the gain plus some of the

(1) P. Günther, *Ergeb. tech. Roentgenkunde*, **4**, 100 (1934); *Chem. Abstr.*, **30**, 4093⁷ (1936).

(2) J. W. Glen, *Advances in Phys.*, **4**, 381 (1955).

(3) P. B. Weisz and E. W. Swegler, *J. Chem. Phys.*, **23**, 1567 (1955).

(4) Y. Sailo, Y. Yoneda, and S. Makishima, *Nature*, **183**, 388 (1959).

(5) C. C. Roberts, A. Spilners, and R. Smoluchowski, *Bull. Am. Phys. Soc.*, Series 2, **3**, 116 (1958).

(6) H. M. C. Sosnovsky, *J. Phys. and Chem. Solids*, **10**, 304 (1959).

(7) R. F. Woodcock and H. E. Farnsworth, *Phys. Rev.*, **98**, 1152 (1955).

(8) L. W. Covert, R. Connor, and H. Adkins, *J. Am. Chem. Soc.*, **54**, 1651 (1932).

(9) H. Adkins, "Reactions of Hydrogen with Organic Compounds over Copper-Chromium Oxide and Nickel Catalysts," The University of Wisconsin Press, 1937, p. 19.

(10) J. M. Hamilton, U. S. 2,857,337 (October 21, 1958).

TABLE I
EFFECTS OF RADIATION UPON CATALYST ACTIVITY

Radiation	Exposure, sec.	% Change in activity—		
		Nickel	Palladium	Platinum
2 mev. β at 10 watts/cm. ²	1.1	+ 31		
	5.5	+ 14		
	11.0	- 14		
	55.0		+ 2	
	110	- 25		+ 1
	275		+ 6	
	660		+10	
	730	-100		
	1025		+13	
	1100	-100		-11
3 mev. β at 15 watts/cm. ²	600			+13
	660		+ 2	+16
1 to 2 mev. X-rays (dose approx. 700 rad/sec.)	600	+ 26	+ 7	+ 2
	6000	+ 5	+ 3	+ 3
Neutrons at 10 ¹³ n/cm. ² per sec.	600		-11	
	1800		+16	
Deuterons at 15 mev. and 20 μ amp.	30		+ 3	
	60		+ 2	

original activity had been lost. Irradiation thus produced centers of catalytic activity in the nickel lattice and at the same time destroyed other active centers.

Qualitatively, comparable results were obtained with X-radiation, possibly involving the action of secondary electrons.

Palladium Catalyst (5% Pd on Carbon Black).—2 Mev. β -radiation increased the activity of palladium catalysts with increasing dosage up to a maximum increase of 13%. This consistency was not obtained with other kinds of irradiation, the gain varying between 2 and 16% (plus one loss of 11%).

Palladium responded to irradiation more slowly than did nickel but the resulting activity lasted longer. Palladium catalyst which had been subjected to the most extended irradiation lost activity on storage at an initial rate of about 10% per month. In some cases, as with nickel, the activity eventually dropped to a level below that of the unirradiated standard, indicating again that some original active centers were destroyed by irradiation while new, and to some degree less stable, centers were being formed.

Platinum Catalyst (1% Pt on Active Carbon).— β - and X-radiation at the 2 mev. level had negligible effect on the activity of the platinum catalyst. However, 3 mev. β -radiation produced a significant gain in activity. Furthermore, the increase in activity was more stable than that of the irradiated palladium catalysts. The initial rate of decay of the activity of these irradiated platinum catalysts was only about 2% per month.

Stability of Activity and Ease of Surface Diffusion.—It has been reported that diffusion in the surfaces of solids becomes appreciable at temperatures above $0.23T_m$, in which T_m is the absolute melting point.¹¹ In nickel, palladium and platinum, the values of $0.23T_m$ are 400, 420 and 470°K. The energy required for generating or augmenting catalytic activity in these metals by irradiation and the subsequent stability of the radiation induced activity both follow this same sequence. It therefore seems probable that the generation of active centers involves the creation of lattice defects and that the decay of this activity is due to annihilation of these defects by surface diffusion or annealing.

(11) G. F. Hüttig, "Metal Treatment," 1938; see also T. J. Gray, "The Defect Solid State," Interscience Publishers, New York, N. Y., 1957, p. 77.

HEATS OF IMMERSION. II. SILICA-BENZENE AND SILICA-CYCLOHEXANE

BY JAMES W. WHALEN

Socony Mobil Oil Company, Inc., Field Research Laboratory, Dallas, Texas

Received October 18, 1961

Immersion heats (ΔH_i) are given for three silica gels and a particulate amorphous silica in benzene and cyclohexane. Contrary to previous reports, ΔH_i values are not comparable for all silica gel samples. Values of ΔH_i ranging from 75 to 160 ergs/cm.² are encountered in dry benzene. For each material there is a characteristic immersion heat dependence on surface hydration determined by the nature of the bound water and by its disposition. ΔH_i values in benzene can increase or decrease with decreasing surface hydration depending on the relative contribution of coulombic and dispersion forces. Given favorable hydroxyl site distribution, coulombic interaction energies obtained from the immersion data are in agreement with calculated values for the OH group- π electron interaction. The influence of trace quantities of water in benzene is shown to depend on the rehydration characteristics of the silica surface. Immersion heats in cyclohexane show little dependence on surface hydration but are not independent of individual surface character. ΔH_i values range from 30 to 85 ergs/cm.² in dry cyclohexane.

Introduction

The surface structure of silica is quite complex. Infrared absorption studies on amorphous silica have indicated the presence of molecular water, widely spaced, non-interacting hydroxyl groups, and closely spaced hydroxyl groups with interactions between such groups.¹ The condensation

of these latter hydroxyl groups at elevated temperatures, producing oxide sites, is widely recognized.² Brunauer, Kantro, and Weise³ have determined

(1) R. S. McDonald, *J. Phys. Chem.*, **62**, 1168 (1958).

(2) R. K. Iler, "The Colloid Chemistry of Silica and Silicates," Cornell Univ. Press, Ithaca, N. Y., 1955, p. 242.

(3) S. Brunauer, D. L. Kantro, and C. H. Weise, *Can. J. Chem.*, **34**, 1483 (1956).

the average energy required for such surface dehydration from heat of solution measurements. Recent work from this Laboratory⁴ has shown that heats of immersion in water reflect the rehydration properties of oxide sites and the hydrogen bond interaction between adsorbed water and surface hydroxyl sites. Rehydration energies, obtained from the variation in immersion heat with hydroxyl content, confirm the average values reported,² but also reflect the differences in disposition and stability of hydroxyl and bound water sites. In addition, immersion heats in water demonstrate the partial stabilization of oxide sites due to strain relief during outgassing at elevated temperatures. Incomplete rehydration of such stabilized sites negates the application of aqueous immersion heat data to the detailed characterization of surface structure. Immersion fluids specific to the functional surface groups and their disposition but incapable of extensive surface structure modification must be utilized.

Kiselev⁵ has shown that heats of adsorption for benzene on silica gel decrease with decreasing silanol surface content and has suggested that the adsorption of benzene on the silica surface is specific, involving the interaction of π electrons of the benzene molecule with surface hydroxyl groups. Gregg and Wheatley⁶ have determined the heat of adsorption of benzene on alumina, reaching the conclusion that maximum interaction energies are encountered for surfaces of intermediate hydration state. The alumina surface is considered to consist of oxide and hydroxyl sites analogous to the silica surface.

Although the results of Kiselev and those of Gregg and Wheatley are in apparent contradiction, the interactions of benzene on oxide-hydroxyl surfaces is of considerable interest since, from immersion heat data, the variation of thermodynamic functions with coverage for adsorbed molecules can be obtained on stable surfaces of varying hydroxyl content. Prior to undertaking such studies the interaction of benzene on oxide-hydroxide surfaces should be clarified. Immersion heats in benzene have been obtained as a function of surface hydration state for three amorphous silicas and for Cabosil, a flame hydrolyzed particulate silica of low surface hydroxyl content. All of these materials have been the subject of surface study by other techniques^{1,3,4} and are becoming increasingly well characterized.

Immersion heats in cyclohexane are of interest in confirming the non-specific interaction of a saturated ring with surface hydroxyls.

Experimental

The calorimeter used in these studies has been described in detail.⁷ It was modified for hydrocarbon studies only by the substitution of Teflon "O" rings for the neoprene rings used in the lid seals and by the addition of a container for drying agent. Immersion fluids were Eastman spectro-

scopic grade benzene and cyclohexane used without further purification other than the removal of trace quantities of water. Initial drying was accomplished by filling the reaction calorimeter with fluid passed through a Linde 5A Molecular Sieve column. After insertion of the sample for immersion a small wire basket (1 cm. diameter by 3 cm. long) filled with activated 5A sieves was positioned in the sample holder below the sample. The calorimeter system was stirred until drying was complete, as indicated by the absence of heat evolution associated with the drying process. With an initial filling of the calorimeter it often was necessary to replace the Molecular Sieves with a freshly activated charge and repeat the drying process. Once dried the immersion fluid was used for a series of experiments, replacing the Molecular Sieves with freshly activated material for each immersion sample. Activation of the sieves was accomplished by heating in a stream of dry nitrogen at 300°.

The amorphous silicas used in this work have been described previously⁴ with one exception. Previous designations, silica SB (353 m.²/g.), silica SL (665 m.²/g.), silica FS (746 m.²/g.) are retained in this paper. In addition to these materials, Cabosil (188 m.²/g.) supplied by Godfrey L. Cabot Company was used without further treatment other than thermal outgassing. Thermal outgassing and surface dehydration was accomplished by evacuation under selected thermal conditions between 110 and 400° until a residual pressure of 10⁻⁶ mm. was attained. Surface areas were obtained over the 110-400° thermal pretreatment range by BET treatment of nitrogen adsorption data. No evidence of sintering at these temperatures was encountered except for a decrease in the indicated surface area of silica SL from 665 to 650 m.²/g. at approximately 200°. Further decreases at 300 and 400° were not encountered. Slightly higher surface areas for silica SL and silica SB reported by Brunauer, Kantrou, and Weise,³ together with an indication of slight sintering (an approximate 10% decrease in surface area) at 200° may be due to slightly different characteristics between batches. In view of the over-all accuracy of the surface area determination, the hydration state of the silica surface, and the immersion heat determination, the noted variation in silica SL surface area was considered to be insignificant.

Results and Discussion

The immersion heats for the four amorphous silicas studied are shown as a function of sample pretreatment temperature in Fig. 1. The immersion heat values show a wide variation, ranging from 80 to 160 ergs/cm.² for the several materials in their original surface states following 110° outgassing. Only fragmentary data are available for comparison. Harkins and Boyd⁸ report 150 ergs/cm.² for the immersion heat of quartz in dry benzene. Quartz is believed^{4,9} to present a predominately hydroxyl surface, analogous to the silica gel surface, to the immersion fluid. Bartell and Suggitt¹⁰ report 97 and 100 ergs/cm.² for Linde silica powder and a "commercial silica gel." Our data do not support the conclusion drawn by Bartell and Suggitt regarding the single valued nature of benzene immersion heats on silica. The state of surface hydration, in OH groups per 100 Å.², is indicated at each experimental point for the three materials (silicas SB, SL, and SF) previously characterized. The bound water loss for these materials was obtained gravimetrically. Total bound surface water initially present on silica SB, indicated as equivalent hydroxyl sites in Fig. 1, was shown⁴ to consist of 2.2 water molecules and 7 hydroxyl sites per 100 Å.². In view

(4) J. W. Whalen, "Solid Surfaces and the Solid Gas Interface," *Advances in Chemistry* No. 33, 1961, p. 281.

(5) A. V. Kiselev, "Colston Papers 10," Butterworths Publ. Ltd., London, 1958, p. 195.

(6) S. J. Gregg and K. H. Wheatley, "Proc. Sec. Intern. Congr. on Surface Activity 11," Butterworths Sci. Publ., London, 1957, p. 102.

(7) J. W. Whalen, *J. Phys. Chem.*, **65**, 1676 (1961).

(8) W. D. Harkins and G. E. Boyd, *J. Am. Chem. Soc.*, **64**, 1195 (1942).

(9) A. C. Makrides and N. Hackerman, *J. Phys. Chem.*, **63**, 594 (1959).

(10) F. E. Bartell and R. M. Suggitt, *ibid.*, **58**, 36 (1953).

of the complex nature of the Cabosil surface,¹ including the possible presence of organic contamination, and the very low condition of surface hydration, the gravimetric procedure is not regarded as reliable for this material. Infrared absorption studies¹¹ have shown that low hydroxyl concentrations, anticipated on the basis of the preparation procedure (flame hydrolysis), do prevail. Other workers^{12,13} have found hydroxyl concentrations ranging from 1 to 3 OH groups per 100 Å.² on this and similar flame hydrolyzed silicas.

The Fig. 1 immersion heat data are characterized by a region of decreasing immersion heats accompanying a decrease in surface hydroxyl content. The regions of decreasing immersion heat do not correlate with specific surface hydroxyl content or with the sample pretreatment temperature, although the general correspondence is better with pretreatment temperature. These observations are in general agreement with conclusions reached as a result of the immersion heat studies in water, where interaction energies involving hydroxyl groups were shown to be related to the disposition of surface hydroxyls, and thus to the ease with which condensation can be accomplished. The immersion heat data for Cabosil will be discussed outside the framework under which the gels are discussed in view of the low surface hydroxyl content and the probable presence of functional groups other than hydroxyl.

The entropy values calculated by Gregg and Wheatley⁶ from their adsorption heat data on alumina correspond to those for a model suggested by Kemball,¹⁴ in which the benzene molecule has two degrees of translational freedom and an additional degree of rotational freedom in the plane parallel to the surface. The decline in heats of adsorption on hydroxyl depleted silica surfaces, as compared to the calculated coulombic energy of interaction between a hydroxyl group and the π electrons of a benzene molecule, has led Kiselev to suggest a model in which a benzene molecule lies flat on the surface, situated over a hydroxyl group. The value calculated by Kiselev¹⁵ for this interaction, 4–6 kcal./mole, is in reasonable agreement, 2–3 kcal./mole, with that obtained from adsorption heat data.

For the three gels, declining immersion heats in regions of decreasing silanol content confirm Kiselev's suggestion that the OH group- π electron bond is a major interaction source. For silica SB the decline in immersion heats occurs over the range 2.2 to 0 water molecules per 100 Å.², for silica SL the range over which immersion heats decrease is 3.1 to 1.7 hydroxyl groups per 100 Å.², and for silica SF, 4.8 to 2 hydroxyl groups per 100 Å.². Over these regions the immersion heats decline as an approximately linear function of the hydroxyl content. Excess interaction energies associated with the hydroxyl nature of the site

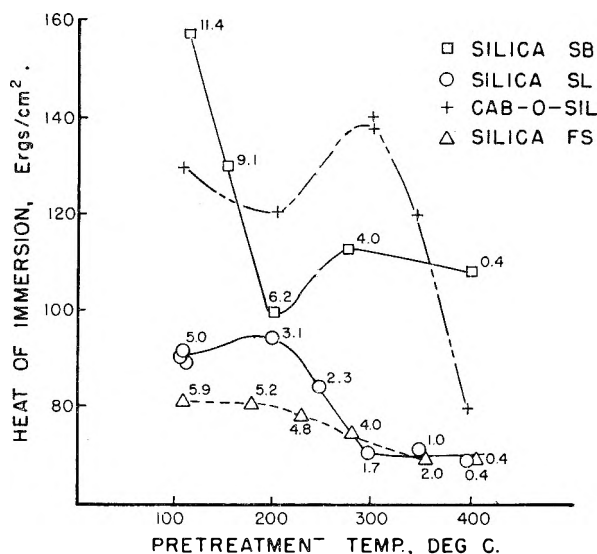


Fig. 1.—Immersion heats of amorphous silica materials in dry benzene. Total bound surface water content, OH groups per 100 Å.² (ref. 4), indicated for each point.

(as opposed to sites remaining on removal of bound water or condensation of hydroxyl groups) are obtained from the slope of the linear curve. These values are 2.6×10^{-13} , 1.7×10^{-13} , and 0.4×10^{-13} ergs per site for silicas SB, SL, and SF, respectively. Kiselev's calculated value for the coulombic interaction energy of a single hydroxyl site with a benzene molecule (4–6 kcal./mole) is equivalent to approximately 3.5×10^{-13} ergs per site. Kiselev's model is quite crude, as is required in the face of the complexity involved in considering all interactions and does not consider, except in discussion, the effects of increasing dispersion forces on interaction energies as the coulombic interaction decreases.

Among the surfaces investigated only silica SB and silica SL yield values in general agreement with those predicted by the Kiselev-Poshkus model. For one-to-one correspondence between benzene molecules and active surface sites (bound water molecules or hydroxyl groups) the density of such sites should not exceed the equivalent of 3 OH groups per 100 Å.². Both silica SB and silica SL fall within this range, silica SB having 2.2 to 0 water molecules and silica SL having 3.1 to 1.7 hydroxyl groups per 100 Å.². The hydroxyl content of silica SF (4.8 to 2 OH groups per 100 Å.²) exceeds the geometrically required value over much of the range of decreasing immersion heat. Non-compliance with the one-to-one correspondence required by the Kiselev-Poshkus model, whether due to a high site density or to non-uniform site distribution, would result in interaction energy values in disagreement with those predicted by the model.

The extremely high interaction energy of benzene with the Cabosil surface is unexpected in view of the low surface hydroxyl content. The sharp decline in immersion heat following outgassing in the 300–400° temperature range, together with reported infrared studies, suggest that the interaction is due to the presence of organic contamination on the surface. The removal of at least a

(11) G. J. Young and T. P. Brush, *J. Colloid Sci.*, **15**, 361 (1960).

(12) W. H. Wade, R. L. Every, and N. Hackerman, *J. Phys. Chem.*, **64**, 355 (1960).

(13) G. J. Young, *J. Colloid Sci.*, **13**, 67 (1958).

(14) C. Kemball, *Proc. Roy. Soc. (London)*, **A187**, 73 (1946).

(15) A. V. Kiselev and D. P. Poshkus, *Doklady Akad. Nauk, S.S.S.R.*, **120**, 834 (1958).

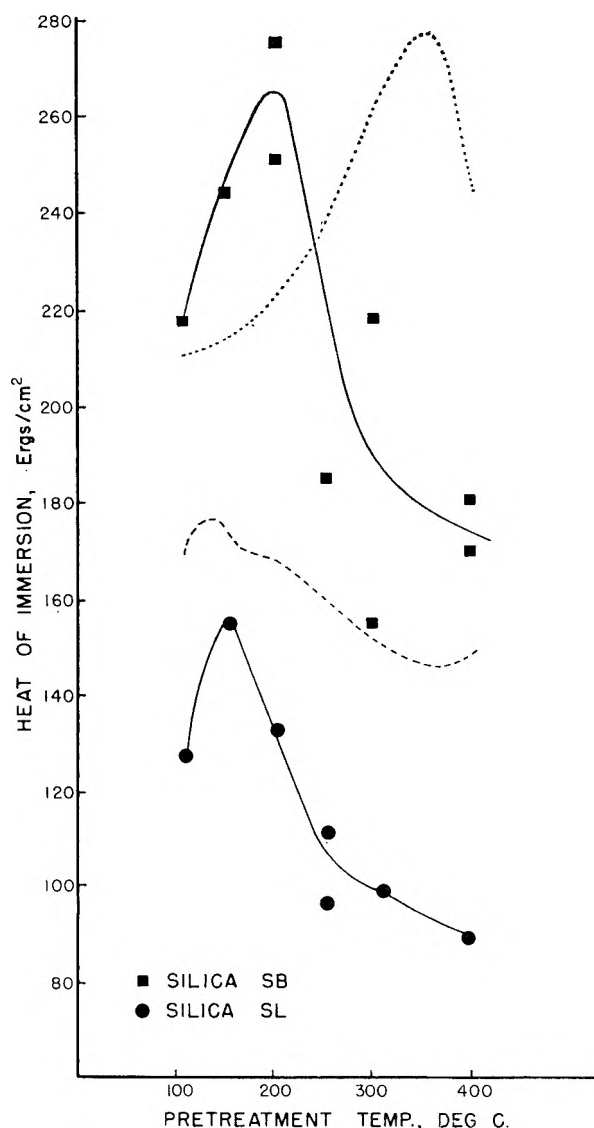


Fig. 2.—Heats of immersion of silica SB and silica SL in benzene dried by silica gel. Immersion heats, silica SB . . . , and silica SL - - - , in water (ref. 4) are shown for comparison.

portion of this material during high temperature outgassing procedures has been observed¹ and would appear to be confirmed by the close approach of the immersion heat for Cabosil outgassed at 400° to that obtained for silicas SL and SF under the same thermal treatment conditions. Hydroxyl contents of all silicas are believed to be quite low, less than 0.5 OH group per 100 Å.², under these conditions. The presence of adsorbed water tightly enough bound to withstand thermal outgassing is indicated by the immersion heat values over the 110–200° range. In this respect the Cabosil surface resembles that of silica SB.

In addition to the regions of hydroxyl or bound water content over which the interaction energy decreases with decreasing OH content there is, for silica SB, silica SL, and Cabosil, a region over which the heat of immersion increases with decreasing hydroxyl content. There is not complete correspondence between the immersion heat increase and the total bound water content, although

for silicas SL and SB the region corresponds roughly, *i.e.*, from 6.2 to 4 OH groups per 100 Å.² for silica SB and from 5 to 3.1 OH groups per 100 Å.² for silica SL. However, as previously noted, Cabosil contains no more than two and probably only one OH group per 100 Å.² over this region. The behavior, best defined for silica SB, seems rather to be related to increasing interactions which occur during the initial stages of surface dehydration following the removal of bound water molecules. The silicon-oxygen sites exposed by the dehydration process now offer new interaction sites to benzene molecules, but sites which apparently do not allow the molecule to assume a minimum distance of approach because of surrounding hydroxyl sites and interacting benzene molecules. Following the initial hydroxyl group condensation, however, these sites are enlarged to the point where maximum dispersion interaction is accommodated, with significant increases in total interaction energy. Again the actual disposition of hydroxyl groups would be controlling in this process rather than the total number.

The above considerations may well explain the apparent contradiction which exists between the previously mentioned studies of Gregg and Wheatley⁶ and those of Kiselev.⁵ Gregg and Wheatley report that maximum interaction between benzene and alumina is encountered for alumina surfaces which are only partially hydroxylated. Kiselev reports continuously decreasing interaction as the hydroxyl content of silica surfaces is decreased. Rather than demonstration of a basic difference in interaction mechanism, the data reported herein suggest that the experiments of Gregg and Wheatley may have been obtained over a hydration region in which the dispersion forces between benzene and the alumina structure were just becoming of importance.

Figure 2 demonstrates the importance of working with dry immersion fluids. Some previous workers have dried non-aqueous immersion fluids with silica gel.^{10,16} Other elaborate drying procedures also have been used^{8,17} but there has been little effort to ensure dryness of the fluid from the time of assembly to the time of breaking the sample.

In preliminary studies with benzene and other non-aqueous immersion fluids, immersion heats higher than those anticipated and with point scatter entirely outside our experience suggested that the drying technique being used was unsatisfactory. The technique, recommended by Bartell and Suggitt,¹⁰ consisted of placing a large quantity of dried silica, in the same surface state as the immersion sample, into the calorimeter just prior to assembly. Although the immersion fluid initially was dry, the amount of atmospheric water vapor diffusing into the system prior to and during the run apparently was sufficient to saturate the drying agent. This problem was solved, very satisfactorily, by continuous drying using Molecular Sieves.

(16) C. M. Hollabaugh and J. J. Chessick, *J. Phys. Chem.*, **65**, 169 (1961).

(17) F. H. Healey, J. J. Chessick, A. C. Zettlemoyer, and G. J. Young, *ibid.*, **68**, 887 (1954).

The Fig. 2 data were obtained during the studies described above. They are most striking from the standpoint that immersion heats higher than those encountered in either water or dry benzene were obtained for silica SB. Harkins and Boyd⁸ report that immersion heats in benzene containing trace quantities of water approach those in water. Our data show this to be true only for silica SB at the point of complete surface hydration. Silica SL, which has a reasonably small rehydration tendency, does not show significant point scatter and yields immersion heat values intermediate between those in water and in dry benzene. Immersion heats in wet benzene for silica SB reach a maximum at approximate correspondence to the removal of bound water molecules. The affinity of the silica surface for water in this form is obviously quite high. Although the quantity of water in the benzene was uncontrolled, the partial drying by silica gel should have maintained a sufficiently low water content to ensure incomplete hydration of the surface. This was demonstrated by a single immersion run using benzene saturated with water. Immersion heats in excess of 300 ergs per cm.² were obtained, confirming the low water content present in previous runs. As such experiments are not subject to close control the work was not extended. The data suggest that immersion heats in organic fluids containing water represent the sums of energy changes associated with rehydration, water molecule-hydroxyl group hydrogen bond interactions, and benzene-adsorbed water interactions.

Figure 3 presents immersion heats of the four amorphous silicas in cyclohexane. Here the absence of any unsaturation in the cyclohexane molecule, particularly of the aromatic character, does not offer coulombic interaction possibilities such as were encountered with benzene. Dispersion forces are the effective mechanism for adsorption over the entire surface and only insignificant effects would be anticipated on decrease of the degree of surface hydration. These expectations are confirmed with immersion heats ranging from 27 to 45 ergs per cm.². Only silica SB indicates significant dependence of immersion heat on hydroxyl content. The influence of hydroxyl content on the cyclohexane interaction energy is confined to the region for which hydroxyl group condensation occurs. The immersion heat of Cabosil in cyclohexane is essentially constant over the pretreatment temperature investigated except for an initial decrease from 83 to 75 ergs per cm.² in the region 110-200°, where the removal of strongly adsorbed water is probable. The immersion heats are approximately double those for the silica gel samples. Although this may be a reflection of the presence of organic functional groups on the Cabosil surface as observed by McDonald,¹ the immersion heat

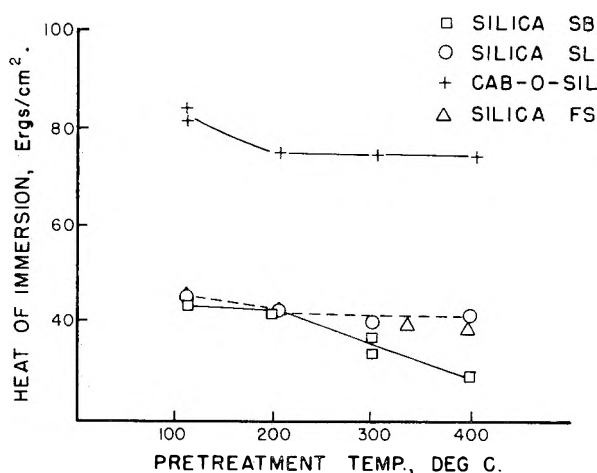


Fig. 3.—Immersion heats of amorphous silica materials in dry cyclohexane.

data in benzene indicate removal of such surface impurity at high outgassing temperatures. Immersion heats for Cabosil in cyclohexane show no tendency to approach the values obtained for the remaining silicas following 400° outgassing.

Conclusions

1. Heats of immersion of amorphous silica surfaces in dry benzene are found to range from 70 to 160 ergs per sq. cm. depending on the surface silanol content and on the disposition of silanol groups.
2. Although the general tendency is toward a decrease in immersion heats with decreasing hydroxyl content, there are limited regions of decreasing surface hydration over which slight increases in immersion heats are observed with some materials.
3. The coulombic interaction energy for a benzene molecule and a surface hydration site may be obtained from the variation in immersion heat with surface bound water content. These values range from 2.6×10^{-13} to 0.4×10^{-13} ergs per site depending on the nature of the surface hydration.
4. Immersion heats of dehydrated silica samples in benzene containing trace quantities of water may exceed the heats observed in pure water.
5. Immersion heats in cyclohexane are essentially constant over wide ranges of surface hydration.
6. From the standpoint of immersion heats the Cabosil surface is anomalous. High immersion heats in both benzene and cyclohexane for Cabosil may result from the presence of functional surface groups other than hydroxyl groups.

Acknowledgment.—The author expresses appreciation to L. R. Bedell for assistance in the experimental work and to Socony Mobil Oil Company, Inc., for permission to publish the results of this study.

SPECTROPHOTOMETRIC EVALUATION OF ACTIVITY COEFFICIENTS IN AQUEOUS SOLUTIONS OF SULFUR DIOXIDE

BY DAVID A. RATKOWSKY AND JOSEPH L. MCCARTHY

The Department of Chemical Engineering, University of Washington, Seattle, Washington

Received October 16, 1961

Ultraviolet absorption spectrophotometry was used for the evaluation of mean molar ionic activity coefficients for aqueous solutions of sulfur dioxide. Although the chemical constitution of such solutions is not yet completely elucidated, the best evidence available in the literature from ultraviolet and infrared spectral studies indicates that the simple model $\text{SO}_2, \text{H}_2\text{O} \rightleftharpoons \text{H}^+ + \text{HSO}_3^-$, appears to be the most likely. From this model and experimental data acquired by ultraviolet spectrophotometric measurements on aqueous sulfur dioxide solutions of concentration range 3.27×10^{-3} to $12.6 \times 10^{-3} M$, mean molar ionic activity coefficients have been obtained for the hydrogen and bisulfite ions. These activity coefficients, to a precision estimated at 1%, are successfully correlated by a semi-theoretical equation for weak electrolytes.

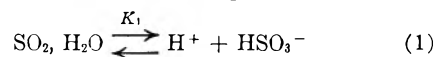
Introduction

Early investigations¹⁻⁵ of the ultraviolet absorption spectra of solutions of various sulfites showed that whereas aqueous solutions of sulfur dioxide exhibited a well-defined absorption band in the vicinity of 276μ , solutions of the acid sulfite NaHSO_3 and the neutral salt Na_2SO_3 were essentially transparent in this region. The absorbent in aqueous solutions of sulfur dioxide at 276μ was thought to be either a hydrate of sulfur dioxide or the postulated compound H_2SO_3 , the so-called sulfurous acid.

Falk and Giguere,⁶ in 1958, employed infrared spectrometry to try to detect the presence of a stable H_2SO_3 molecule. In addition to aqueous solutions of sulfur dioxide, they also studied the sulfur dioxide-water mixtures in the solid state, wherein the formation of the compound H_2SO_3 might be favored. Their attempt to detect molecular H_2SO_3 proved negative. However, their studies of aqueous solutions of sulfur dioxide showed that the infrared spectrum contained three bands due to the fundamental vibrations of the dissolved SO_2 molecules in addition to four absorption bands attributed to liquid water. The sulfur dioxide bands were only slightly removed from the corresponding frequencies in pure liquid sulfur dioxide. For solid mixtures of SO_2 and H_2O , it also was found that the observed spectrum was essentially a superposition of the spectra of the pure components with no new absorption bands appearing and no change in frequency, appearance or intensity for the usual bands. Falk and Giguere concluded that sulfur dioxide molecules are not strongly hydrated in aqueous solution and that the component H_2SO_3 is not formed. Jones and McLaren,⁷ in an independent infrared study, drew substantially the same conclusions.

These results provide support for the mechanism advanced by Ley and König⁸ in 1938, who studied the ultraviolet absorption spectra of aqueous solutions of sulfur dioxide. They assumed that the compound H_2SO_3 did not exist, and that undissociated sulfur dioxide was present

only in the form of dissolved sulfur dioxide $\text{SO}_2, \text{H}_2\text{O}$. Because of the small value of the secondary ionization constant, K_2 , the dissociation of the bisulfite ion, HSO_3^- , was neglected. On this basis Ley and König considered the equilibrium



with

$$K_1 = \frac{C_i^2}{C_u} \quad (2)$$

where C_u and C_i represented the concentration in moles per liter of the dissolved sulfur dioxide and the bisulfite ion, respectively. Activity coefficients were considered to be unity. The total concentration of the sulfur containing components, C_T , was taken to be the sum of the concentration of the dissolved sulfur dioxide and the bisulfite ion.

$$C_T = C_i + C_u \quad (3)$$

By combining eq. 3 with eq. 2 and rearranging, they obtained eq. 4 for the undissociated specie

$$C_u = C_T + K_1/2 - \sqrt{K_1 C_T + K_1^2/4} \quad (4)$$

Ley and König noted that the Beer-Lambert law⁹ was not applicable when total concentration was used, *i.e.*, the absorptivity, a , was not constant in the expression

$$A = aC_T l \quad (5)$$

where

A = absorbance
 l = path length, cm.

but that the law did apply when the concentration of the undissociated specie was employed, a' being the absorptivity based upon the concentration of the dissolved sulfur dioxide in the expression

$$A = a' C_u l \quad (6)$$

However, there was a considerable scatter in the experimental data points, and the authors suggested that it would be advantageous to repeat the experiments using a spectrophotometer instead of the photographic instrument and technique available at that time.

The situation did not change substantially until 1957, when De Maine¹⁰ obtained the spectra of aqueous solutions of sulfur dioxide using a Beckman Model DU spectrophotometer. Calculating

(1) R. Wright, *J. Chem. Soc.*, **105**, 669 (1914).

(2) C. S. Garrett, *ibid.*, **107**, 1324 (1915).

(3) K. Shaeffer and W. Koehler, *Z. anorg. u. allgem. Chem.*, **104**, 212 (1918).

(4) E. C. C. Baly and R. A. Bailey, *J. Chem. Soc.*, **121**, 1813 (1922).

(5) F. H. Getman, *J. Phys. Chem.*, **30**, 266 (1926).

(6) M. Falk and P. A. Giguère, *Can. J. Chem.*, **36**, 1121 (1958).

(7) L. H. Jones and E. McLaren, *J. Chem. Phys.*, **28**, 995 (1958).

(8) H. Ley and E. König, *Z. physik. Chem.*, **B41**, 365 (1938).

(9) G. F. Lother, "Absorption Spectrophotometry," 2nd Ed., Hilger and Watts, Ltd., London, 1958.

(10) P. A. D. De Maine, *J. Chem. Phys.*, **26**, 1049 (1957).

the concentration of the dissolved sulfur dioxide C_u , and the absorptivity, a' , by employing eq. 4 and 6, respectively, he found that a' decreased with increasing concentration rather than remaining constant as suggested by Ley and König. Also, DeMaine studied the spectra at six different temperatures, 1, 10, 20, 25, 30 and 35° and found that the absorbance increased with increasing temperature. Ley and König made their measurements only at 25°.

It appears that the observed decrease of a' is attributable to the assumption of unity for the activity coefficients in the definition of K_1 in eq. 2. However, if K_1 is to be the thermodynamic ionization constant, then the appropriate definition is

$$K_1 = \frac{a_{H^+} a_{HSO_3^-}}{a_{SO_2, H_2O}} = \frac{y_{\pm}^2 C_i^2}{y_u C_u} = \frac{y_{\pm}^2 (C_T - C_u)^2}{y_u C_u} \quad (7)$$

where y_{\pm} is the mean molar activity coefficient for the hydrogen and bisulfite ions, and y_u is the molar activity coefficient of the dissolved sulfur dioxide SO_2, H_2O .

For weak electrolytes, based upon the work of MacInnes and Shedlovsky¹¹ and also of Owen,¹² it is believed to be permissible to make the following modification of the Debye-Hückel theory to account for the "medium effect" of the undissociated molecules upon the activity of the ions

$$\log (y_{\pm}^2 / y_u) = -1.0112 \sqrt{C_i} + \beta C_u \quad (8)$$

In eq. 8 it is assumed that this effect is proportional to the concentration of the undissociated species, C_u , i.e., the dissolved sulfur dioxide in the case of aqueous solutions of sulfur dioxide. At infinite dilution, the limiting slope of eq. 8 is in exact numerical agreement with the limiting slope predicted by the Debye-Hückel theory for aqueous solutions at 25°. The present experiments and calculations are directed toward the evaluation of the constant of proportionality, β , from ultraviolet spectrophotometric measurements of aqueous solutions of sulfur dioxide.

Experiments and Calculations

Aqueous solutions of sulfur dioxide were prepared by bubbling sulfur dioxide (C.P., The Matheson Co.) gas into distilled water which had been deoxygenated by passing nitrogen through the water for a minimum of 15 min. Great care had to be taken in working with these solutions to prevent air from re-entering and possibly causing oxidation of the sulfur dioxide. The solution was placed in one cell of a matched pair of fused silica absorption cells of path length 1 cm., each cell being fitted with a ground glass stopper. Distilled water was placed in the second cell of the pair. The instrument used for measuring the absorbance of these solutions was a hand-operated Beckman Model DU spectrophotometer.

The total sulfur concentration, C_T , was determined by iodometry. A known volume of aqueous sulfur dioxide solution was pipetted into an excess of standardized 0.1 *N* iodine and the remaining iodine titrated with standard 0.1 *N* sodium thiosulfate to a starch end-point. Fifteen solutions were prepared, all at 25°, ranging in concentration from $C_T = 3.27 \times 10^{-2} M$ to $C_T = 12.6 \times 10^{-2} M$.

Absorbance readings were taken at millimicron intervals from 230 to 310 $m\mu$. These readings are shown in Table I. The dotted entries represent absorbance values so high that they could not be accurately read.

To calculate activity coefficients, it is necessary to determine which fraction of the total concentration is in the ionic

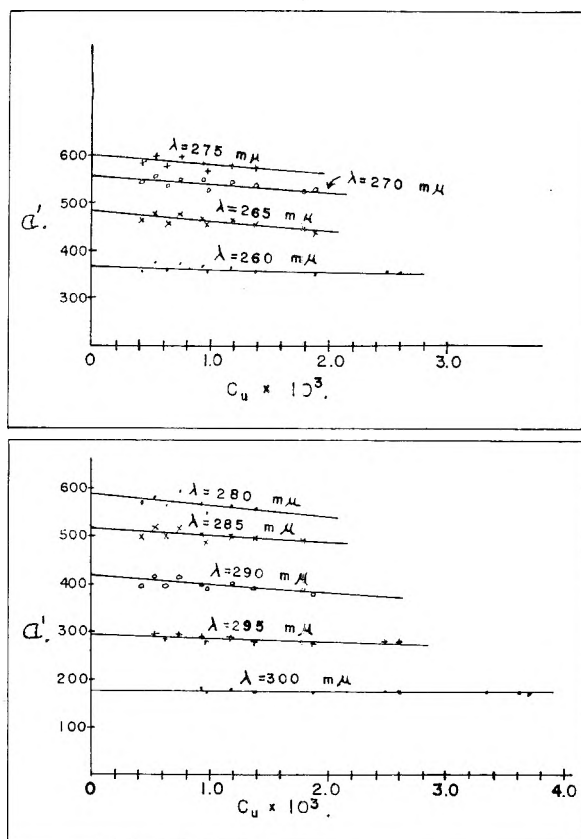


Fig. 1.—Apparent absorptivity at several wave lengths vs. concentration of dissolved sulfur dioxide in solution.

form and which fraction is in the dissolved form. In the vicinity of 276 $m\mu$, it is presumed that only the dissolved sulfur dioxide absorbs ultraviolet radiation, with the bisulfite ion not absorbing any appreciable radiation above a wave length of 240 $m\mu$. Therefore, in this region, eq. 6 should apply and the absorptivity, a' , must be estimated for each wave length.

Neglecting momentarily the "medium effect" term of eq. 8, and combining eq. 7 with eq. 8, gives

$$\log (K_1 C_u / C_i^2) = -1.0112 \sqrt{C_i} \quad (9)$$

Employing Tartar and Garretson's¹³ value of the ionization constant at 25°, $K_1 = 0.0172$, obtained from e.m.f. measurements and apparently the best available, then for each total concentration, C_T , values of C_u and C_i which satisfy eq. 9 and eq. 3 simultaneously were computed. Having C_u , eq. 6 was employed to calculate a' . Since eq. 9 is valid at infinite dilution, extrapolation of a plot of a' vs. C_u to infinite dilution should give the true value of the absorptivity.

Not all of the absorbance values listed in Table I were used in the calculations. Lottian⁹ shows, with accompanying calculations, that the greatest accuracy in absorption measurements may be obtained when the absorbance is 0.4343, but that absorbances between 0.2 and 0.8 may be used without any major loss of accuracy. In the present calculations, all absorbance values between 0.15 and 1.0 were used and the others were discarded. The wave lengths employed ranged from 260 to 300 $m\mu$.

Values of a' and C_u calculated by the method described above are plotted in Fig. 1, and the extrapolation to infinite dilution is shown. The extrapolation was made, for each wave length, by fitting the best straight line by the method of least squares as described by Bennett and Franklin.¹⁴ All nine straight line fits were statistically significant at either the 0.10 level or levels of lower probability, suggesting that a straight-line extrapolation may be justified.

(13) H. V. Tartar and H. H. Garretson, *ibid.*, **63**, 808 (1941).

(11) D. A. MacInnes and T. Shedlovsky, *J. Am. Chem. Soc.*, **54**, 1429 (1932).

(12) B. B. Owen, *ibid.*, **54**, 1758 (1932).

(14) C. A. Bennett and N. L. Franklin, "Statistical Analysis in Chemistry and the Chemical Industry," John Wiley and Sons, Inc., New York, N. Y., 1954.

TABLE I
SPECTROPHOTOMETRIC READINGS OF ABSORBANCE *vs.* WAVE LENGTH, READINGS AT FIXED CONCENTRATION, SULFUR DIOXIDE-WATER

λ , $m\mu$	Total concentration, moles/liter														
	0.0126 A	0.0124 A	0.0118 A	0.0100 A	0.0097 A	0.00808 A	0.00788 A	0.00668 A	0.00606 A	0.00538 A	0.00524 A	0.00458 A	0.00417 A	0.00376 A	0.00327 A
230	0.335	0.338	0.314	0.246	0.236	0.176	0.170	0.135	0.120	0.140	0.103	0.085	0.077	0.057	0.042
235	.205	.207	.194	.151	.145	.108	.104	.085	.075	.088	.064	.054	.047	.034	.026
240	.259	.260	.239	.186	.179	.135	.127	.103	.090	.085	.074	.060	.050	.040	.030
245	.403	.403	.371	.292	.280	.209	.200	.157	.137	.113	.110	.090	.072	.061	.046
250	.642	.641	.581	.458	.439	.326	.314	.244	.211	.170	.168	.137	.111	.097	.075
255	.927	.925	.855	.678	.641	.480	.460	.359	.312	.248	.250	.202	.165	.143	.110
260	1.301	1.275	1.184	.930	.890	.660	.631	.493	.430	.342	.340	.278	.228	.198	.151
265	1.638	...	1.509	1.272	1.141	.821	.805	.630	.550	.438	.432	.354	.289	.254	.195
270	1.900995	.940	.741	.640	.511	.510	.407	.340	.296	.230
275	1.074	1.019	.790	.682	.550	.542	.441	.363	.317	.246
280	1.880	1.400	1.009	0.990	.769	.667	.532	.530	.440	.354	.309	.240
285	1.750	...	1.579	1.271	1.200	0.883	.876	.680	.590	.472	.467	.379	.315	.274	.210
290	1.393	1.379	1.294	1.011	0.960	.708	.691	.540	.469	.376	.371	.304	.250	.219	.167
295	0.993	0.998	0.918	0.722	.692	.510	.497	.384	.332	.270	.268	.216	.179	.155	.120
300	.629	.621	.578	.450	.431	.320	.311	.241	.210	.169	.166	.135	.110	.096	.074
305	.350	.349	.323	.253	.242	.180	.171	.135	.116	.094	.095	.075	.061	.054	.040
310	.169	.166	.155	.121	.116	.090	.082	.064	.057	.045	.045	.036	.029	.025	.018

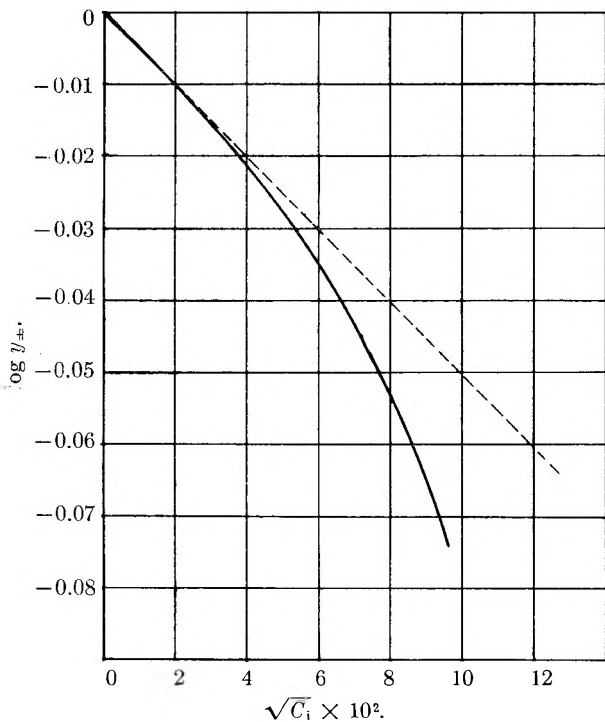


Fig. 2.—Activity coefficients *vs.* ionic concentration, 25°, showing Debye-Hückel limiting slope.

With the extrapolated values at infinite dilution, $a'_{c_T=0}$, it is possible to use statistical methods to evaluate the constant, β , in eq. 8. Thus by substituting eq. 7 and eq. 3 into eq. 8 and transposing, eq. 10 is obtained.

$$\log [K_1 C_u / (C_T - C_u)^2] + 1.0112 \sqrt{C_T - C_u} = \beta C_u \quad (10)$$

Further, by substitution of eq. 6 into eq. 10, one obtains

$$\log \frac{K_1 \frac{A}{a'_{c_T=0}}}{\left(C_T - \frac{A}{a'_{c_T=0}} \right)} + 1.0112 \sqrt{C_T - \frac{A}{a'_{c_T=0}}} = \beta \frac{A}{a'_{c_T=0}} \quad (11)$$

Thus, at a fixed wave length, λ , it is possible to use the values of the absorbance as a function of concentration to obtain the best estimate of β by the least squares method. Rather than obtain an estimate for β from each wave length, however, it seems best, from a statistical point of view, to use the data from all wave lengths simultaneously to obtain the best estimate of β . Representing the left-hand

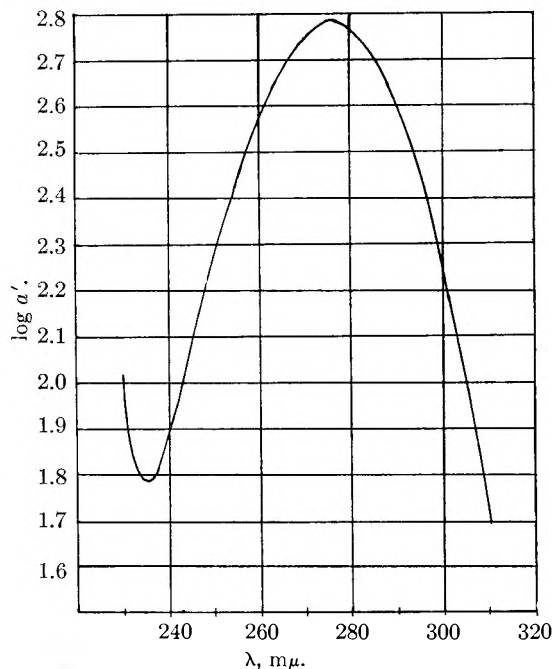


Fig. 3.—Logarithm of absorptivities a' *vs.* wave length λ sulfur dioxide in water, 25°.

side of eq. 10 by the symbol, L , then the best estimate¹⁴ of β is

$$\hat{\beta} = \frac{\sum_{\lambda=1}^9 \left[\sum_{j=1}^{n\lambda} (L_j C_{uj}) \lambda \right]}{\sum_{\lambda=1}^9 \left[\sum_{j=1}^{n\lambda} (C_{uj}) \lambda^2 \right]} \quad (12)$$

where $n\lambda$ is the number of data points available for wave length λ .

The value of $\hat{\beta}$ determined by use of eq. 12, utilizing the 90 data points available from measurements at nine wave lengths, was -15.02 , with the 99% confidence limits being -12.22 and -17.82 . Equation 8 thus becomes

$$\log (y_{\pm}^2 / y_u) = -1.0112 \sqrt{C_i} - 15.02 C_u \quad (8a)$$

Assuming y_u to be unity this relation was used with eq. 3 and 7 to compute values of y_{\pm} , C_i and C_u . Figure 2 is a graph of $\log y_{\pm}$ *vs.* $\sqrt{C_i}$ and indicates a reasonable, if not typical, dependence of the ion activity coefficient on the ion concentration.

If the error criterion is based upon the 99% confidence limits for β , the maximum error in y_{\pm} is about 1%. How-

ever it should be noted that the values of y_{\pm} depend upon the choice of the value of the ionization constant, K_1 , and the assumption $y_{\pm} = 1$.

Using the estimated best values of the dissolved sulfur dioxide concentration, C_u , eq. 6 was employed to obtain final best estimates for the absorptivities a' . These estimates were made for six wave lengths below 260 $m\mu$ and the two wave lengths above 300 $m\mu$ as well as for the nine wave lengths used to estimate β in eq. 8. The logarithms of these absorptivities are plotted *vs.* wave length in Fig. 3.

The ionization constant, K_1 , for aqueous solutions of sulfur dioxide decreases with increasing temperature.¹⁵ Hence, for a fixed total sulfur concentration, C_T , the concentration of the dissolved portion, C_u , and hence the absorbance, A , by eq. 6, must increase with increasing temperature. This increase in absorbance with increasing temperature is in accordance with the observations of DeMaine¹⁰ at temperatures other than 25°.

(15) A. E. Rabe, Ph.D. Thesis, University of Wisconsin, 1958.

It should be mentioned that Simon and Waldmann,¹⁶ working with Raman spectra and aqueous solutions of sulfur dioxide of concentration greater than 1 M , detected lines attributable to $S_2O_5^{2-}$, suggesting that another ionic equilibrium exists in this system, namely



As the concentration of sulfur dioxide is reduced, however, the equilibrium shifts sharply to the left and for the dilute solutions employed in the present study (0.00327–0.0126 M), the number of $S_2O_5^{2-}$ ions probably is negligible, just as the secondary ionization of the bisulfite ion



can be safely neglected. Evidence in the present study that the quantity of $S_2O_5^{2-}$ ions is negligible is the absence of any selective absorption at 257 $m\mu$, the wave length characteristic of the $S_2O_5^{2-}$ ion.

(16) A. Simon and K. Waldmann, *Z. anorg. u. allgem. Chem.*, **283**, 359 (1956).

THE STANDARD ENTHALPY OF FORMATION OF COMPLEX SULFATE IONS IN WATER. I. HSO_4^- , $LiSO_4^-$, $NaSO_4^-$

By J. M. AUSTIN AND A. D. MAIR

Department of Chemistry, University of Canterbury, Christchurch, New Zealand

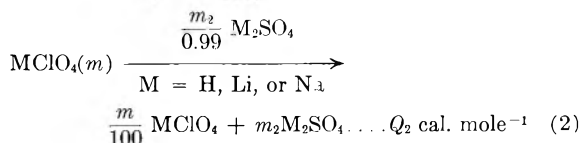
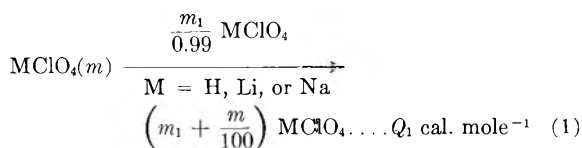
Received October 17, 1961

The heat of dilution of perchloric acid, lithium perchlorate, and sodium perchlorate solutions in perchloric acid, lithium perchlorate, and sodium perchlorate solutions, respectively, has been compared with similar dilution in dilute solutions of sulfuric acid, lithium sulfate, and sodium sulfate, respectively. The differences between the observed heat effects have been used to calculate the standard heats of formation of the ions HSO_4^- , $LiSO_4^-$, and $NaSO_4^-$.

The thermodynamic functions associated with complex-ion formation may be found either from temperature coefficient studies of the free energy of formation or by direct calorimetric measurement at 25° of the enthalpy change on forming that amount of complex determined by its free energy of formation at 25°. Whereas there have been several investigations^{1–4} of the heat of formation of the HSO_4^- ion by temperature coefficient methods in solutions of low ionic strength, the calorimetric data available has been obtained in solutions of high ionic strength. These observations involved measurement of the heat of dilution of concentrated solutions of sodium sulfate in the presence of hydrochloric acid⁵ or perchloric acid⁶ at ionic strengths of one and two, respectively. A value for the standard heat of formation calculated from these observations can be in error as the result of heat effects associated with the reduced amount of $NaSO_4^-$ present after dilution or by the inadequacies of activity coefficient expressions used to correct heat effects observed at such high ionic strengths.

As the $NaSO_4^-$ and $LiSO_4^-$ ions have been characterized only by their association constants determined from conductance data at a single temperature the heats of formation of these ions are not known.

As part of a general calorimetric investigation of the heats of formation of complexes formed by the sulfate ion we report here a calorimetric re-investigation of the heat of formation of the HSO_4^- ion along with an investigation of the heats of formation of $NaSO_4^-$ and $LiSO_4^-$. Observations have been made of the heat effects produced by the one hundred-fold dilution of the perchlorate $MClO_4$ ($M = H, Li, \text{ or } Na$) with: (1) a solution of the same perchlorate and (2) a solution of the corresponding sulfate. The molalities of the perchlorate (m_1) and sulfate (m_2) solutions were chosen so that the ionic strengths of the resultant solutions in (1) and (2) always were equal. These two dilution processes may be represented as



As in an earlier investigation⁷ of the heats of formation of the lead halide complex ions PbX^+ ($X = Cl^-, Br^-, I^-$), it has been considered that the difference between Q_2 and Q_1 the heat of dilution per mole of $MClO_4$, results from the formation of extra

(1) V. S. K. Nair and G. H. Nancollas, *J. Chem. Soc.*, 4144 (1958).

(2) C. W. Davies, H. W. Jones, and C. B. Monk, *Trans. Faraday Soc.*, **48**, 921 (1952).

(3) W. J. Hamer, *J. Am. Chem. Soc.*, **56**, 860 (1934).

(4) C. R. Singleterry, I. M. Klotz, Theses, University of Chicago (1940), see R. A. Robinson and R. H. Stokes "Electrolyte Solutions," Butterworths Scientific Publications, London, 1955, p. 374.

(5) K. S. Pitzer, *J. Am. Chem. Soc.*, **59**, 2365 (1937).

(6) A. J. Zielen, *ibid.*, **81**, 5022 (1959).

(7) J. M. Austin, R. A. Matheson, and H. N. Parton, "The Structure of Electrolyte Solutions," John Wiley and Sons, Inc., New York, N. Y., 1959, p. 365.

MSO_4^- ions. If $\Delta[\text{MSO}_4^-]$ represents the number of moles of complex ion formed for each mole of MClO_4 diluted and ΔH_A represents the molal enthalpy of formation of the complex ion at the particular ionic strength of the solution, ΔH_A has been found from eq. 3.

$$\Delta Q = Q_2 - Q_1 = \Delta H_A \cdot \Delta[\text{MSO}_4^-] \quad (3)$$

The amount of complex ion formed $\Delta[\text{MSO}_4^-]$ has been calculated by successive approximations from the known association constants and the concentration of the ions concerned.

Experimental

Apparatus.—The dilution experiments were performed in the same calorimeter as used by one of us to investigate the heats of formation of the lead halide complex ions. The apparatus, similar in design to that of Gucker, Pickard, and Planck,⁸ consisted of a pair of identical 500-ml. calorimeters supported by bakelite shafts in an air-bath immersed in a thermostat regulated at $25.00 \pm 0.001^\circ$. The bakelite shafts carried leads to 70 ohm manganin wire heaters for electrical calibration of the calorimeters, stirrer shafts, and a spring-loaded mechanism to allow a stirrer blade to fracture a thin walled glass vessel of about 5 ml. capacity within the calorimeters. The ends of an 80 junction copper-constantan thermel 10 cm. long were embedded in the calorimeters and the shielded thermel leads were connected through oil-thermostated switches to a Paschen galvanometer. The thermel and galvanometer usually were operated at such a sensitivity that 1-mm. galvanometer scale deflection represented a difference of 0.001 cal. between the heat content of the two calorimeters, *i.e.*, a difference of 2×10^{-6} in the temperature of the two calorimeters.

When heat effects larger than 0.1 cal. were observed electrical energy was supplied in an endeavor to balance the energy change on dilution. The actual heat of dilution then was found from the electrical energy supplied and the resultant galvanometer deflection and its electrical calibration. Heat effects of less than 0.1 cal. were found directly from the resultant galvanometer deflection and its electrical calibration. The heating current for energy compensation or matching of heat effect and galvanometer calibration was measured with the aid of a potentiometer and standard resistance. The heating period of from 2–8 min. was measured with a 0.1-sec. stop-watch. The calorimeters were checked by measuring the heat of solution of potassium chloride. The mean value of 4.145 kcal. mole⁻¹ at 25° compares well with other determinations.

Materials. Perchloric Acid.—Analar acid was used without further purification and diluted stock solutions were standardized against recrystallized Analar borax.

Sulfuric Acid.—Constant boiling acid was prepared from Analar acid.

Sodium Sulfate.—Analar material dried at 300° was used without further purification to prepare stock solutions.

Lithium Sulfate.—Analar lithium sulfate monohydrate was dehydrated at 700° to constant weight and used to prepare stock solutions.

Sodium Perchlorate.—A solution of sodium perchlorate was prepared by neutralizing carbonate-free sodium hydroxide solution with some of the above perchloric acid. The solution was analyzed by evaporating an aliquot to dryness and drying at 160° to constant weight.

Lithium Perchlorate.—A solution of lithium perchlorate was prepared by neutralizing some perchloric acid with lithium carbonate thrice recrystallized from hot water to remove sulfate impurity. The solution was analyzed by evaporating an aliquot to dryness with sulfuric acid, heating to 700°, and weighing to constant weight as anhydrous lithium sulfate.

The concentrations of all stock sulfate solutions were checked by gravimetric analysis as barium sulfate. All stock solutions were prepared and diluted by weight with vacuum corrections being applied.

Results

The results of the dilution experiments represented

(8) F. T. Gucker, H. B. Pickard, and R. W. Planck, *J. Am. Chem. Soc.*, **61**, 459 (1939).

by eq. 1 are shown in Table I and those represented by eq. 2 are shown in Table II.

TABLE I

(a)	$m \text{MClO}_4 = 0.5219 m \text{HClO}_4$ $m_1 \text{MClO}_4 = 0.01478 m \text{HClO}_4$	$I = 0.02$
	Moles of $\text{MClO}_4 \times 10^3$	ΔH , cal. (measured)
	2.0502	0.0763
	2.2616	.0829
	2.0806	.0807
		Mean $Q_1 = 37.5$
(b)	$m \text{MClO}_4 = 1 m \text{LiClO}_4$ $m_1 \text{MClO}_4 = 0.015 m \text{LiClO}_4$	$I = 0.025$
	4.1778	-0.6946
	4.1188	-.7097
	4.0698	-.6681
	4.0775	-.6708
		Mean $Q_1 = -166.8$
(c)	$m \text{MClO}_4 = 1 m \text{NaClO}_4$ $m_1 \text{MClO}_4 = 0.015 m \text{NaClO}_4$	$I = 0.025$
	4.1176	1.667
	4.1465	1.674
		Mean $Q_1 = 404.3$

TABLE II

(a)	$m \text{MClO}_4 = 0.5219 m \text{HClO}_4$ $m_2 \text{M}_2\text{SO}_4 = 0.007077 m \text{H}_2\text{SO}_4$	$I = 0.02$
	Moles of $\text{MClO}_4 \times 10^3$	Q_2 , cal. mole ⁻¹
	2.0650	1.157
	2.2208	1.244
	2.1150	1.181
	2.1155	1.179
		Mean $Q_2 = 559.1$
(b)	$m \text{MClO}_4 = 1 m \text{LiClO}_4$ $m_2 \text{M}_2\text{SO}_4 = 0.005161 m \text{Li}_2\text{SO}_4$	$I = 0.025$
	4.1559	-0.6960
	4.1630	-.7003
	4.1809	-.6853
		Mean $Q_2 = -166.3$
(c)	$m \text{MClO}_4 = 1 m \text{NaClO}_4$ $m_2 \text{M}_2\text{SO}_4 = 0.005186 m \text{Na}_2\text{SO}_4$	$I = 0.025$
	4.1688	1.7414
	4.2082	1.7574
	4.0646	1.6748
	3.8653	1.5969
		Mean $Q_2 = 413.1$

$\Delta[\text{MSO}_4^-]$, the number of moles of complex ion formed in the resulting solutions for each mole of MClO_4 , was calculated from the activity coefficient expressions and association constants listed in the literature^{9,10} for HSO_4^- , LiSO_4^- , and NaSO_4^- , respectively. The value of ΔH_A obtained from eq. 3 at the ionic strength given in Tables I and II was corrected to zero ionic strength using the expression

(9) E. C. Righellato and C. W. Davies, *Trans. Faraday Soc.*, **26**, 592 (1930).

(10) I. L. Jenkins and C. B. Monk, *J. Am. Chem. Soc.*, **72**, 2695 (1950).

$$\Delta H_A^0 = \Delta H_A + \frac{3}{2} RT^2 \left(\frac{1}{D} \cdot \frac{\partial D}{\partial T} + \frac{1}{T} \right) \ln \gamma_{\text{HSO}_4^-}$$

The value of $1/D \cdot \partial D / \partial T$ where D is the dielectric constant of the solvent at 25° was obtained from the data of Malmberg and Maryott.¹¹ The results of these calculations are summarized in Table III.

TABLE III

Species	I	ΔQ cal. mole ⁻¹	$\Delta[\text{MSO}_4^-]$ mole	ΔH_A cal. mole ⁻¹	ΔH_A^0 cal. mole ⁻¹
HSO ₄ ⁻	0.020	522.2 ± 4	0.0939	5560	5740 ± 200
LiSO ₄ ⁻	.025	(0.3) ± 4	.0100
NaSO ₄ ⁻	.025	10.8 ± 4	.0115	940	1120 ± 800

Since the amount of HSO₄⁻ formed in these measurements was found from the results of Nair and

(11) C. G. Malmberg and A. A. Maryott, *J. Research Natl. Bur. Standards*, **56**, 1 (1956).

Nancollas,¹ the observed value of $\Delta H_A^0 = 5.74$ kcal. is directly comparable with and in excellent agreement with their result, $\Delta H_A^0 = 5.60$ kcal. The agreement with the calorimetric result found by Pitzer,⁵ $\Delta H_A^0 = 5.2 \pm 0.5$ kcal, is only fair. However, since we have found that ΔH_A^0 for NaSO₄⁻ is +1.1 kcal. mole⁻¹ an allowance for the dissociation of NaSO₄⁻ in the 90-fold dilution of 0.79 m Na₂SO₄ in his experiments would increase his results for ΔH_A^0 of HSO₄⁻. The results for the LiSO₄⁻ complex indicate that the heat of formation of the LiSO₄⁻ complex is zero or that there is no complex ion formation between the lithium and sulfate ions.

The results presented here are being used to extend our knowledge of the heats of formation of complexes formed by the sulfate ion with cations of higher valence.

A STUDY OF THE PHOTOLYSIS OF CYCLOHEXANE AND ACETONE. I. SOME REACTIONS OF THE CYCLOHEXYL RADICAL

BY ALVIN S. GORDON AND S. RUVEN SMITH

Research Department, U. S. Naval Ordnance Test Station, China Lake, California

Received October 19, 1961

The E_{act} for abstracting an H atom from cyclohexane by a methyl radical is 9.7 kcal./mole and the pre-exponential factor relative to the pre-exponential factor for a methyl radical abstracting a D atom from acetone- d_6 is 2.5. For the abstraction reaction from cycloheptane the $E_{\text{act}} = 9.1$ and the ratio of pre-exponential factors = 2.6. Cyclohexyl radicals, formed by the reaction of methyl radicals with cyclohexane, have been studied over the temperature range from 150 to 480°. The reactions fall into two categories, a low temperature region (150–375°) and a high temperature region (above 375°). In the low temperature region there is no evidence that the cyclohexyl radical cleaves to smaller fragments. The high temperature region is characterized by products resulting from the cleavage of the cyclohexyl radical. Starting at 300° and increasing with temperature, molecular hydrogen is eliminated from the free radicals present in the mix. Our previous work indicates that this is a general reaction of alkyl hydrocarbon radicals where there are methylene groups α and β to the carbon atom with the free electron.¹ As would be predicted by the radical isomerization mechanism presented by Gordon and McNesby,² there is no ethylene produced in the thermal reactions of the cyclohexyl radicals even at 440°. The reactions of cycloheptyl radicals have not been investigated in much detail. The study indicates that the reactions parallel those for the cyclohexyl radical.

Introduction

The reactions of cyclohexyl radicals are of interest since its pyrolytic reaction results in a large linear radical which permits the study of competitive processes involving C–C bond breaking and intraradical abstraction.

Recent work of Arai, Sato, and Shida³ on cyclohexyl radicals formed from the mercury sensitized photolysis of cyclohexane at 400° shows a number of the compounds which have been identified in the present work. One outstanding exception is that they report ethylene in the products and we see no evidence of this compound over the extended temperature range of our studies.

Apparatus and Materials

Cyclohexane from the National Bureau of Standards was shown to be free of impurity when analyzed by gas chromatography. Acetone- d_6 was purchased from Merck and Company, Canada. Its D/D+H content is 0.995.

The cyclohexane–acetone- d_6 mixes were photolyzed in a quartz reaction cell set in an aluminum block furnace. Unfiltered radiation from a medium pressure quartz mercury arc was used to irradiate the mix. The products were

analyzed by gas chromatography and mass spectrometry. For the gas chromatography a 1.5% squalane on Pelletex column and a 1-methyl-5-(2-methoxyethyl)-tetrazole on C-22 brick⁴ column were used. There was provision for trapping any fraction for subsequent mass spectrometer identification.

TABLE I

ENERGIES OF ACTIVATION AND PRE-EXponential FACTOR RATIOS FOR THE REACTION OF $\dot{\text{C}}\text{D}_3$ RADICALS WITH CYCLO-

ALKANES	E_{act} for H abstraction	$\frac{A_{\text{Cycloalkane}}}{A_{\text{Acetone}}}$	$\frac{A_{\text{C}}}{A_{\text{A}}}$ predicted
Cyclopropane	13.1	0.9	1.3
Cyclobutane	10.5	1.5	1.6
Cyclopentane	9.5	1.5	2.1
Cyclohexane	9.7	2.5	2.5
Cycloheptane	9.1	2.6	2.9

Results

The CD₃H/CD₄ ratios are determined by the reactions




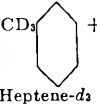
(1) A. S. Gordon and S. R. Smith, *J. Chem. Phys.*, **34**, 331 (1961).

(2) A. S. Gordon and J. R. McNesby, *ibid.*, **31**, 833 (1959).

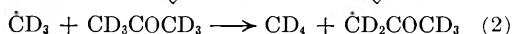
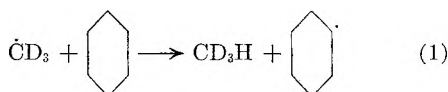
(3) S. Arai, S. Sato, and S. Shida, *ibid.*, **33**, 1277 (1960).

(4) W. G. Finnegan and S. R. Smith, *J. Chromatography*, **5**, 461 (1961).

TABLE II^a
 PRODUCT ANALYSIS OF CYCLOHEXANE-ACETONE-*d*₆

<i>T</i> , °C.	Total methanes	CD ₃ H + CH ₄	Ethanes	Propylenes	Butenes	1,3- Butadiene		 + Heptene- <i>d</i> ₃	Methyl cyclo- pentanes (<i>d</i> ₀ + <i>d</i> ₁)	Hexadiene + cyclo- hexane
154	228	202	641	0	0	0	0	185	0	0
213	540	476	290	0	0	0	0	337	0	0
250	739	641	181	0	0	0	0	405	0	0
298	1095	934	86	0	0	0	0	348	95	285
337	1351	1127	190	0	0	0	39	191	305	340
381	1586	1318	95	209	50	0	10	110	315	360
440	1507	1218	314	490	85	285	143	137	0	615

^a The values in the table are approximately moles × 10⁹.



Only 1–2% of the reaction mix is consumed and the rate equations may be integrated since the ratio of the parent molecules remains almost constant.

$$\frac{\text{CD}_3\text{H}}{\text{CD}_4} = \frac{k_1 \left(\text{C}_6\text{H}_{10} \right)}{(\text{Ad}_6)}$$

From the best least squares fit of the methane ratios in Table III to an Arrhenius equation, $E_2 - E_1$ is calculated to be 1.6 kcal./mole and A_1/A_2 , the ratio of the pre-exponential factors, is 2.5. Since E_2 has been established independently⁵ as 11.3 kcal./mole, $E_1 = 9.7$ kcal./mole. E_1 and A_1/A_2 may be compared with the values for the other cyclic hydrocarbons in Table I. The energy of activation is slightly greater than for cyclopentane, and probably reflects a slightly stronger C–H bond in the C₆ ring over the C₅ ring. The E_{act} for abstraction of H from cyclopentane is the same as that from a linear methylene hydrogen. If the pre-exponential factors for the cyclo-alkane are normalized on the basis of their average velocities, the factors are proportional to the number of H atoms/molecule within experimental error.

The product distribution (Table II) indicates that there is a low temperature reaction region from 150 to 375° and a high temperature region from 375 upwards. In the low temperature region there is no evidence that the C₆ radicals are fragmented, the major cyclohexyl radical products being the C₆ radicals are fragmented, the major cyclohexyl radical products being methylcyclohexane and methylcyclopentane. In the high temperature region the radicals break down and form CH₃ and C₂H₅ (see Table III for markings of methane and Table IV for marking of ethane as a function of temperature) radicals and C₃ and C₄ unsaturates. Of especial interest is that no ethylene is found in the products, contrary to the results of Arai and co-workers,³ from the mercury photosensitized reaction of cyclohexane.

Reference to Table III shows that the H₂/HD ratios are over three times the CD₃H/CD₄ ratio in the temperature range above 300°. Below 300°

there is so little hydrogen in the products that the determination of the H₂/HD ratio is subject to considerable error. In addition, photolyses at room temperature show that some of the hydrogen is formed *via* excited molecules. The presence of HD shows that an H atom mechanism is operative. If the H₂ and HD are formed exclusively by an H atom mechanism the relative rates for H abstracting H and D must be considerably different than the analogous rates for methyl radical abstracting the same atoms. We compared the H atom and CD₃ radical abstraction by the high temperature photolysis and pyrolysis of mixtures of acetone-*d*₆ and ethane.⁶ The ethyl radical formed in the reaction of CD₃ with ethane pyrolyzes rapidly over 420° and injects H atoms into the mix; in this manner the abstraction reactions of H atoms and methyl radicals may be studied in the same system. The results show that there is a pre-exponential factor of less than two in favor of an H atom abstracting an H atom over abstracting a D atom relative to the same reactions of a methyl radical. The H₂/HD ratios generated in the photolysis of cyclohexane-acetone-*d*₆ mixes are over three times the corresponding methyl ratios (Table III) and the H₂ must be partly formed *via* a molecular elimination of H₂ from the cycloalkyl radical in addition to the atom mechanism. The cycloheptyl radical also appears to eliminate molecular hydrogen in addition to a hydrogen atom above 300°.

 TABLE III
 PERCENTAGE OF VARIOUS HYDROGENS AND METHANES
 IN THE PRODUCTS FROM CYCLOHEXANE-ACETONE-*d*₆

<i>T</i> , °C.	H ₂	HD	Ratio H ₂ / HD	CD ₃ H	CD ₄	Ratio CD ₃ H/ CD ₄	CH ₄	CH ₃ D
254	0.25	0.03	8.3	86.2	13.5	6.4		
288	.62	.08	7.8	84.7	14.6	5.8		
293	.35	.05	7.0	84.5	15.0	5.6		
318	2.50	.13	19.2	81.6	15.8	5.2		
344	6.7	.34	19.7	76.9	16.0	4.8		
419	20.7	1.36	14.8	60.2	13.3	4.5	4.5	
438	24.7	1.69	14.5	60.4	14.4	4.2	6.9	3.26
445	21.2	1.53	14.1	55.4	13.1	4.2	7.4	1.41
460	25.5	1.87	13.4	51.1	12.2	4.2	8.5	0.91
481	22.9	1.85	12.1	47.6	11.9	4.0	11.7	3.96

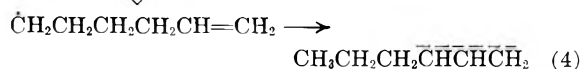
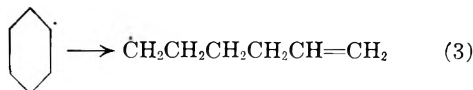
The butenes are primarily *d*₃ (Table IV). The propylene is mostly light, the *d*₀/*d*₁ ratio ≈ 40.

(5) M. H. J. Wijnen, *J. Chem. Phys.*, **22**, 1075 (1954).

(6) A. S. Gordon and S. R. Smith, to be published.

Discussion

Cyclohexyl radicals formed *via* reaction 1 are remarkably stable against reactions which result in the formation of smaller fragments. This suggests that the cyclohexyl radical can be converted into a resonance stabilized radical *via* some easy reaction path. A likely sequence is

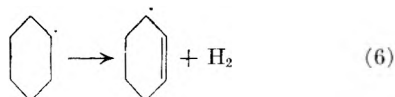


Reaction 4 is an easy intraradical abstraction since the "reaction complex" is an unstrained 5-atom ring and the abstraction of a secondary allyl hydrogen atom should require about 5-6 kcal./mole energy of activation (neglecting the unknown value for any partial eclipsing of the ring hydrogens in the activated complex). The estimate of the energy of activation is based on the value of 7.7 ± 0.5 kcal./mole obtained by Trotman-Dickenson and Steacie⁷ for abstraction of H from propylene. Since reaction 4 is an abstraction of a secondary hydrogen α to a double bond, it is about 2 kcal./mole less than for abstraction from propylene. The resonance stabilized hexenyl radical formed in reaction 4 would be very stable against pyrolysis. At temperatures below those at which it pyrolyzes, it would disappear by methyl radical addition to its two canonical forms. At least one heptene has been identified in the same chromatogram peak containing methylcyclohexane.

Arai and co-workers³ studied the mercury sensitized decomposition of cyclohexane at 400° and found many of the same products that we find. The outstanding exception, as previously noted, is that they found ethylene in the products. Ethylene presumably would form by the reaction

$$\dot{\text{C}}\text{H}_2\text{CH}_2\text{CH}_2\text{CH}_2\text{CH}=\text{CH}_2 \rightarrow \text{C}_2\text{H}_4 + \dot{\text{C}}\text{H}_2\text{CH}_2\text{CH}=\text{CH}_2 \quad (5)$$

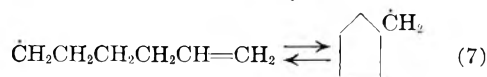
It does not appear because the competitive intraradical isomerization (reaction 4) is much more rapid. Arai and co-workers³ may have found ethylene because of a reaction of excited mercury atoms with cyclohexane which gives a reaction path which is not present in our system. The H_2/HD ratios relative to the corresponding $\text{CD}_3\text{H}/\text{CD}_4$ ratios suggest that molecular H_2 is eliminated from the hydrocarbon radical. One possible reaction is



The methyl adduct of the cyclohexenyl radical Cyclohexene-CD_3 is found in the products at higher temperatures.

Methylcyclopentanes, $\text{Cyclopentane-CH}_2\text{D}$ and Cyclopentane-CH_3 , are found in the reaction products (Table II) disap-

pearing at temperatures over 420° . It could be formed by reaction 3 followed by



Arai and co-workers³ found methylcyclopentane in their products at 400° and postulated its formation *via* reactions 3 and 7. They did not carry out experiments above 430° so that they did not notice its disappearance due to the reverse of reaction 7. Reaction 7 is an intraradical addition to the non-terminal position of the double bond. It may be estimated to have an E_{act} of 12 ± 2 kcal./mole, on the basis that a terminal addition has an $E_{\text{act}} = 8$ kcal./mole. Since there is no evidence of non-terminal addition to a double bond relative to terminal addition at temperatures up to 100° , the non-terminal energy of activation for addition is probably 4 kcal./mole or more higher than the energy of activation for the terminal addition.⁸ As previously noted, reaction 4 has an $E_{\text{act}} \approx 5-6$ kcal./mole. Both E_4 and E_7 have been estimated without considering eclipsing of H atoms in the activated complex, but any eclipsing of H atoms in the activated complex would affect both reactions almost equally. Thus reaction 7 could compete with reaction 4 only in the unlikely event that its pre-exponential factor was over 100 times as favorable as that for reaction 4. An

alternative mechanism is that the $\text{Cycloheptyl radical}$ radical

forms from $\text{Cyclohexyl radical}$ without the $\dot{\text{C}}\text{H}_2\text{CH}_2\text{CH}_2\text{CH}_2\text{CH}=\text{CH}_2$ radical forming as an intermediary.

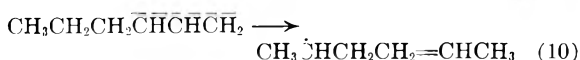
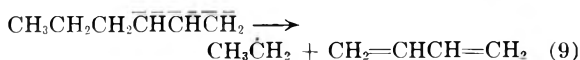
A product corresponding to the formula of methylcyclopentene also is found in the products at higher temperatures. Since this product is

light it is probably Cyclopentene-CH_2 formed from the

$\text{Cycloheptyl radical}$ radical by the loss of a hydrogen atom.

The cycloheptyl radical similarly forms methylcyclohexane and methylcyclohexene in this temperature range. Cyclopentyl radical does not yield methylcyclobutane, nor does the cyclobutyl radical form methylcyclopropane.⁹ In the latter radical the great strain in the 3-membered ring must prevent its formation. In the former radical the competitive reaction to form ethylene and an allyl radical in addition to any strain in the 4-membered ring would swamp the reaction to form the 4-membered ring.

The resonance stabilized hexenyl radical reacts at temperatures over 375° and accounts for the



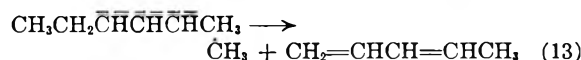
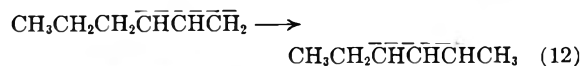
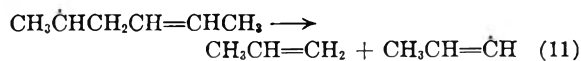
(7) A. F. Trotman-Dickenson and E. W. R. Steacie, *J. Chem. Phys.*, **19**, 169 (1951).

(8) R. K. Brinton, *ibid.*, **29**, 781 (1958).

(9) A. S. Gordon, S. R. Smith, and C. M. Drew, *ibid.*, in press.

TABLE IV
% DEUTERATION OF ETHANE AND BUTENE IN PRODUCTS OF PHOTOLYSIS OF CYCLOHEXANE-ACETONE-*d*₆

T, °C.	Ethane						Butene						
	<i>d</i> ₀	<i>d</i> ₁	<i>d</i> ₂	<i>d</i> ₃	<i>d</i> ₄	<i>d</i> ₅	<i>d</i> ₀	<i>d</i> ₁	<i>d</i> ₂	<i>d</i> ₃	<i>d</i> ₄	<i>d</i> ₅	
276						100							
376	46.5	26.0		4.8		22.5							
424	62.2	29.0	1.3	2.5		4.9							
475	66.1	27.4	2.7	1.6	0.3	0.2	1.6	35.9	1.3	6.3	55.0	1.1	0.6



CH₃ and C₂H₅ radical found in the high temperature region. At low temperatures all the ethane results from the addition reaction of two CD₃ radicals. The propylene formed in reaction 11 is only light. The further reactions of the CH₃-

CH=CH radical generate C₃H₆ and C₃H₅D by abstraction. It also reacts in part with CD₃ to give the preponderance of butene-*d*₃ found in the high temperature region. The only other butene of significance, butene-*d*₀, could form by the addition reaction of a CH₃ radical with a CH₃-CH=CH radical.

Acknowledgments.—We wish to acknowledge the assistance of Mr. Joseph H. Johnson who helped with the mass spectrometer and gas chromatography analyses, and of Mrs. Helen R. Young who aided with the reduction of the analytical data.

HEAT CAPACITIES AND THERMODYNAMIC PROPERTIES OF GLOBULAR MOLECULES. III. TWO METHYL-SUBSTITUTED POLYTHIAADAMANTANES¹

BY SHU-SING CHANG AND EDGAR F. WESTRUM, JR.

Department of Chemistry, University of Michigan, Ann Arbor, Michigan

Received October 25, 1961

Heat capacities of 1,3,5,7-tetramethyl-2,4,6,8,9,10-hexathiaadamantane and 1,3,5,7-tetramethyl-2,4,6,8-tetrathiaadamantane have been determined from 5 to 350°K. by adiabatic calorimetry. Derived thermodynamic functions were calculated from these data. No thermal anomaly has been found for either substance within the temperature range investigated. The molal values of heat capacity at constant pressure; the entropy; and the free energy function for the two compounds are 67.74, 65.71; 70.63, 65.93; and -34.39, -31.84 cal. mole⁻¹ °K.⁻¹, respectively, at 273.15°K.

Introduction

In continuation of the study of the thermal behavior of globular molecules with an adamantane-like structure,^{2,3} two methyl-substituted polythiaadamantanes have been studied. Both of them were known long before the discovery of adamantane and were characterized as the dimers of dithioacetylacetone⁴ and of dithioacetic anhydride.⁵ More recently, the structures of these molecules have been reinterpreted by Fredga^{6,7} as that of cage molecules similar in structure to adamantane. Spectral data⁸ also favor the new structural formulas. Therefore, these two compounds could be designated, according to the nomenclature proposed by Stetter,⁹ as 1,3,5,7-tetramethyl-2,4,6,8-tetrathiaadamantane and

1,3,5,7-tetramethyl-2,4,6,8,9,10-hexathiaadamantane, respectively. The former molecule possesses four co-planar methylene groups of an adamantane molecule and the latter all six replaced by corresponding numbers of sulfur atoms. In addition, one methyl group is attached to each of the four bridge-head carbon atoms in both molecules.

Experimental

Preparation of 1,3,5,7-Tetramethyl-2,4,6,8-tetrathiaadamantane.—The calorimetric sample of this compound was prepared in accordance with a method described by Fredga and Brändström.⁷ About 50 ml. of acetylacetone was introduced into 200 ml. of absolute alcohol saturated with anhydrous hydrogen chloride gas at 0°. The solution was chilled in a Dry Ice-alcohol-bath. Into this a steady stream of hydrogen sulfide gas was passed until in excess beyond saturation. The mixture then was allowed to warm slowly to room temperature. The solid material was collected and washed with concentrated hydrochloric acid. The remaining yellowish tint which could not be removed by recrystallization was removed by refluxing the compound in an alcoholic solution with a quantity of active carbon (Norit). The substance was further recrystallized twice from absolute methanol. The final crystalline sample was composed of long prismatic needles with a melting point of 168°. Microanalysis indicated the following composition for this sample: 45.56% C, 6.05% H, and 48.21% S (calcd.: 45.41% C, 6.10% H, and 48.49% S for C₁₆H₁₆S₄).

1,3,5,7-Tetramethyl-2,4,6,8,9,10-hexathiaadamantane.—This compound was prepared by the method described for

(1) From the dissertation of S. S. Chang submitted in partial fulfillment of the requirements of the Doctor of Philosophy Degree at the University of Michigan. This work was supported in part by the Division of Research of the U. S. Atomic Energy Commission.

(2) S. S. Chang and E. F. Westrum, Jr., *J. Phys. Chem.*, **64**, 1547 (1960).

(3) S. S. Chang and E. F. Westrum, Jr., *ibid.*, **64**, 1551 (1960).

(4) F. Leteur, *Compt. rend.*, **133**, 48 (1901).

(5) J. Bongartz, *Ber.*, **19**, 2182 (1886).

(6) A. Fredga, *Arkiv Kemi, Mineral. Geol.*, **25B**, No. 8, 1 (1948).

(7) A. Fredga and A. Brändström, *ibid.*, **26B**, No. 4, 1 (1948).

(8) R. Mecke and H. Spiesscke, *Chem. Ber.*, **88**, 1997 (1955).

(9) H. Stetter and K. H. Steinacker, *ibid.*, **85**, 451 (1952).

tetraethenyl hexasulfide.¹⁰ Thiolacetic acid was refluxed overnight with one-third of its weight of crushed, fused zinc chloride. The crystalline product from the reaction mixture was washed with dilute hydrochloric acid and water to dissolve away zinc compounds. It then was recrystallized twice from absolute methanol. The crystals melted at 232° with slight decomposition. Microanalytical results indicated the composition: 31.94% C, 4.14% H, and 64.17% S (calcd.: 31.94% C, 4.02% H, and 64.01% S for C₈H₁₂S₆).

Cryogenic Technique.—The Mark I cryostat, a gold-plated copper calorimeter (laboratory designation W-9), and a calibrated platinum resistance thermometer (laboratory designation A-3) were used in measuring the heat capacities of both samples. These instruments and the general operating technique have been described in the previous papers of this series.^{2,3} Samples weighing (*in vacuo*) 49.912 g. of tetramethyltetrathiaadamantane and 45.383 g. of tetramethylhexathiaadamantane were used. After evacuation of the loaded calorimeter, helium gas at pressures of 6.0 and 10.5 cm., respectively, was sealed in at 300°K. in order to provide thermal contact between the sample and the calorimeter. The heat capacity of the heater-thermometer-calorimeter assembly (without sample) was determined in a separate series of measurements. This heat capacity represents a contribution increasing from 10% at 10°K. to a maximum of 58% at 70°K. and gradually decreasing to less than 40% at 350°K.

Results

The experimentally determined heat capacities of both compounds are presented in Table I in

TABLE I
HEAT CAPACITIES OF 1,3,5,7-TETRAMETHYL-2,4,6,8,9,10-HEXATHIAADAMANTANE AND 1,3,5,7-TETRAMETHYL-2,4,6,8-TETRATHIAADAMANTANE

Units: cal. mole⁻¹ °K.⁻¹

T, °K.	C _p	T, °K.	C _p	T, °K.	C _p
1,3,5,7-Tetramethyl-2,4,6,8,9,10-hexathiaadamantane (C ₈ H ₁₂ S ₆ ; 1 mole = 300.572 g.)					
Series I	233.80	60.06	14.77	3.592	
	242.98	61.89	16.27	4.188	
69.54	18.07	251.84	63.63	18.01	4.858
74.91	19.71	260.63	65.30	20.01	5.566
82.00	22.10	269.53	67.13	22.22	6.272
89.41	24.55	278.57	68.60	24.64	6.972
96.73	26.85	287.71	70.42	27.30	7.641
104.45	29.16	296.88	72.05	30.27	8.326
		306.29	73.10	33.53	9.010
Series II	315.81	74.91			
		324.55	76.06		
114.68	32.21	332.03	77.38	Series VII	
123.31	34.76	339.62	78.58		32.86
131.88	37.15	346.93	79.98		36.52
140.47	39.50				40.49
149.14	41.88				44.62
		Series V			49.14
					54.23
Series III	4.94	0.164	54.23	13.618	59.83
	5.50	0.233	59.83	15.167	65.72
166.71	45.95		65.72	16.939	
175.74	47.93	Series VI	72.00	18.798	
184.82	50.05				
194.01	52.02	5.14	0.185	Series VIII	
203.45	54.07	6.29	.392		
212.94	56.05	7.33	.662	151.87	42.77
		8.42	1.023	161.37	44.78
Series IV	9.54	1.423			
	10.71	1.890	Series IX		
215.55	56.51	11.99	2.419		
224.50	58.27	13.35	2.988	291.48	71.05

1,3,5,7-Tetramethyl-2,4,6,8-tetrathiaadamantane (C₁₄H₁₆S₄; 1 mole = 264.492 g.)

Series I	28.25	7.460	162.20	42.26	
	31.15	8.111			
4.85	0.136	34.28	8.750	Series V	
5.38	.203	37.71	9.410		
6.13	.321	41.50	10.097	167.74	43.16
7.09	.503	45.72	10.899	176.38	45.10
7.97	.741			185.00	47.08
8.87	1.003	Series III		193.81	49.01
9.86	1.325			202.71	50.84
10.82	1.664	46.48	11.06	211.60	52.74
11.75	1.984	51.56	12.11	220.61	54.73
		56.75	13.28	229.78	56.60
Series II	62.55	14.71		Series VI	
6.31	0.337	Series IV		235.14	57.63
7.23	.545			244.41	59.61
8.11	.794	64.89	15.36	253.66	61.60
9.07	1.064	70.92	16.93	262.70	63.44
10.13	1.420	77.78	18.87	271.53	65.33
11.26	1.839	85.34	21.18	280.34	67.14
12.48	2.266	93.59	23.56	289.28	69.09
13.74	2.755	101.97	25.93	298.33	70.80
15.04	3.276	110.07	28.27	307.47	72.44
16.47	3.826	118.33	30.32	316.86	74.22
18.06	4.423	126.80	32.89	326.43	76.12
19.82	5.039	135.42	35.18	336.00	78.09
21.85	5.716	144.25	37.46	345.56	80.00
24.14	6.399	153.29	39.88		
25.47	6.769				

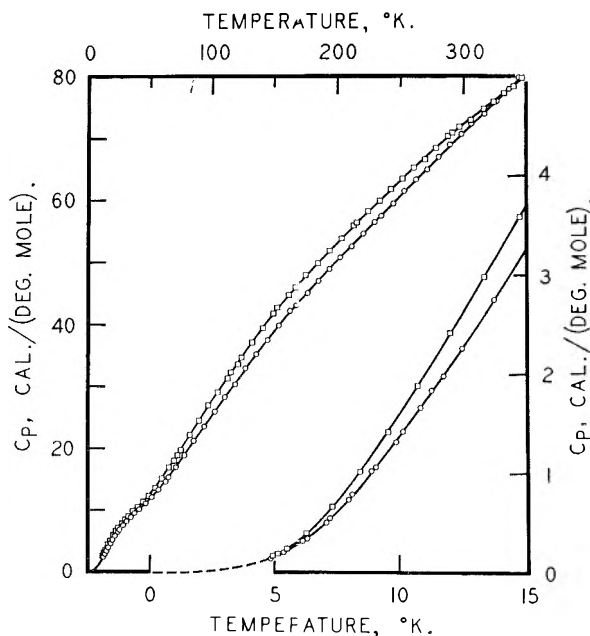


Fig. 1.—Heat capacities of tetramethyltetrathiaadamantane \circ and tetramethylhexathiaadamantane \square .

chronological order to permit the estimation of the approximate temperature increments of the individual runs from the adjacent mean temperatures. The data are stated in terms of the defined thermochemical calorie equal to 4.1840 j., an ice point of 273.15°K., and the gram molecular weight of tetramethyltetrathiaadamantane and tetramethylhexathiaadamantane taken as 264.492 and 300.572

(10) E. Fromm and G. Mangler, *Ber.*, **34**, 204 (1901).

g., respectively. An analytically determined curvature correction, amounting to less than 0.1%, has been applied to the observed $\Delta H/\Delta T$ values.

The molal values of heat capacities at constant pressure, the entropy and enthalpy increments, and the free energy functions are listed at selected temperatures for both compounds in Table II. These values were obtained by integration of a least-square-fit polynomial through the data points by means of a high-speed digital computer. Below 5°K. the data were extrapolated by means of the Debye limiting law. Nuclear spin and isotope mixing contributions have not been included in the entropies and the free energy functions. The probable error of the reported heat capacity values is considered to be less than 0.1% at temperatures above 25°K., 1% at 10°K., and about 5%

TABLE II
THERMODYNAMIC PROPERTIES OF 1,3,5,7-TETRAMETHYL-
2,4,6,8,9,10-HEXATHIAADAMANTANE AND
1,3,5,7-TETRAMETHYL-2,4,6,8-TETRATHIAADAMANTANE
Units: cal., mole, °K.

$T, ^\circ\text{K.}$	C_p	S°	$H^\circ - H^\circ_0$	$-(F^\circ - H^\circ_0)T^{-1}$
1,3,5,7-Tetramethyl-2,4,6,8,9,10-hexathiaadamantane ($\text{C}_8\text{H}_{16}\text{S}_6$, 1 mole = 300.572 g.)				
5	0.168	0.056	0.209	0.014
10	1.605	0.533	4.065	.127
15	3.681	1.574	17.26	.424
20	5.563	2.900	40.52	.874
25	7.065	4.309	72.24	1.420
30	8.269	5.709	110.7	2.018
35	9.300	7.062	154.7	2.643
40	10.31	8.369	203.7	3.277
45	11.39	9.645	257.9	3.914
50	12.56	10.905	317.7	4.550
60	15.22	13.424	456.3	5.819
70	18.22	15.992	623.3	7.088
80	21.41	18.632	821.4	8.365
90	24.63	21.340	1051.6	9.656
100	27.82	24.101	1313.9	10.962
110	30.90	26.898	1607.6	12.283
120	33.87	29.715	1931.5	13.619
130	36.70	32.538	2284.5	14.965
140	39.41	35.358	2665.2	16.321
150	41.99	38.166	3072.3	17.684
160	44.45	40.955	3504.6	19.051
170	46.80	43.721	3960.9	20.421
180	49.05	46.460	4440.3	21.792
190	51.22	49.171	4941.7	23.162
200	53.31	51.851	5464.3	24.529
210	55.35	54.502	6007.7	25.894
220	57.36	57.123	6571.3	27.254
230	59.35	59.717	7154.8	28.609
240	61.32	62.284	7758.2	29.959
250	63.29	64.828	8381.3	31.303
260	65.24	67.348	9023.9	32.641
270	67.15	69.846	9685.9	33.972
280	68.99	72.321	10366.6	35.298
290	70.74	74.773	11065.4	36.617
300	72.39	77.200	11781.1	37.929
350	80.58	88.945	15596.0	44.385
273.15	67.74	70.63	9898	34.39
298.15	72.09	76.75	11648	37.69

1,3,5,7-Tetramethyl-2,4,6,8-tetrathiaadamantane
($\text{C}_{14}\text{H}_{16}\text{S}_4$, 1 mole = 264.502 g.)

5	0.154	0.052	0.194	0.013
10	1.374	0.464	3.515	0.112
15	3.252	1.368	14.98	.369
20	5.107	2.563	35.98	.764
25	6.639	3.874	65.49	1.254
30	7.864	5.199	101.9	1.802
35	8.865	6.488	143.8	2.380
40	9.803	7.733	190.5	2.971
45	10.76	8.943	241.9	3.568
50	11.79	10.129	298.2	4.165
60	14.10	12.478	427.4	5.355
70	16.72	14.845	581.3	6.541
80	19.53	17.259	762.4	7.729
90	22.43	19.927	972.2	8.925
100	25.34	22.241	1211.1	10.130
110	28.22	24.792	1478.9	11.347
120	31.02	27.368	1775.2	12.575
130	33.75	29.959	2099.1	13.812
140	36.40	32.558	2450.0	15.058
150	38.95	35.157	2826.8	16.312
160	41.41	37.750	3228.7	17.571
170	43.77	40.332	3654.7	18.834
180	46.04	42.898	4103.8	20.099
190	48.22	45.446	4575.2	21.366
200	50.35	47.974	5068.1	22.634
210	52.43	50.481	5582.0	23.900
220	54.50	52.968	6116.6	25.165
230	56.57	55.436	6671.9	26.427
240	58.67	57.888	7248.1	27.687
250	60.79	60.326	7845.4	28.944
260	62.93	62.752	8464.1	30.198
270	65.05	65.167	9104.0	31.448
280	67.13	67.570	9765.0	32.695
290	69.14	69.961	10446.4	33.939
300	71.06	72.338	11147.4	35.180
350	80.74	84.018	14942.3	41.326
273.15	65.71	65.93	9310	31.84
298.15	70.71	71.90	11016	34.95

at 5°K. The estimated probable error in the thermodynamic functions is less than 0.1% above 100°K.

Discussion

No thermal anomaly has been observed in the heat capacity measurements for either compound between 5 and 350°K. Simple differential thermal analysis measurements establish the absence of such anomalies over the entire solid range. Failure to find transitions similar to that of adamantane² is not an unexpected result for these substances. The heat capacity *vs.* temperature curves for these two compounds are very similar in shape to each other, but they are distinctively different from that of adamantane and hexamethylenetetramine which form another pair. The sulfur atoms present in the skeletal structure of the cage of these two molecules may have increased the intermolecular force and hence the potential barrier for the re-orientation of the molecules into other equivalent positions. Moreover, it is likely that the four methyl groups extant in both molecules prevent the rotation of molecules through simple steric

hindrances. These molecules deviate considerably from sphericity and appear to have molecular envelopes in the shape of a large tetrahedron. However, although tetrahedrally-shaped molecules often show the onset of the plastically crystalline phase, this phenomenon does not appear to be present in either of the two methyl-substituted polythiaadamantanes studied.

It is of interest to note that the hexathia compound has been reported to exist in a crystal lattice of rather low symmetry.¹¹ The monoclinic

space group $C_{2h}^2-P2_1/c$ is said to characterize the lattice and the molecules do not appear to possess any element of crystallographic symmetry.

Acknowledgment.—The authors acknowledge with gratitude the assistance of Elfreda Chang and H. Gary Carlson in the experimental measurements, and the financial support of the Division of Research of the United States Atomic Energy Commission in the performance of these studies.

(11) G. Hägg and B. Nygardh, reported by A. Fredga, ref. 6.

ACID-BASE EQUILIBRIA OF METHYL RED

BY RICHARD W. RAMETTE, EDWARD A. DRATZ, AND PRESTON W. KELLY

Leighton Hall of Chemistry, Carleton College, Northfield, Minnesota

Received October 30, 1961

The cation of methyl red, or *o*-(*p*-dimethylaminophenylazo)-benzoic acid, has an acid dissociation constant $K_1 = 0.0040$ according to spectrophotometric measurements as well as solubility studies in HCl-KCl buffers in which $S = 6.0 \times 10^{-6} + 1.54 \times 10^{-3}[\text{H}_3\text{O}^+]$. Distribution studies using these buffers with carbon tetrachloride show that the aqueous/ CCl_4 concentration ratio for methyl red follows the relationship $E = 0.00295 + 0.585[\text{H}_3\text{O}^+]$, indicating the higher value for K_1 of 0.0050, perhaps because of the dissolved CCl_4 . Spectrophotometric studies and solubility measurements in acetate buffers, in which $S = 6.0 \times 10^{-6} + 8.9 \times 10^{-11}/[\text{H}_3\text{O}^+]$, show that the dissociation constant for the zwitterion $K_2 = 1.50 \times 10^{-3}$. The intrinsic solubility of the zwitterion is thus 6.0×10^{-6} according to both solubility studies. These values refer to a temperature of 25° and are calculated for zero ionic strength, but the work was carried out at ionic strength equal to 0.020.

Introduction

Methyl red, or *o*-(*p*-dimethylaminophenylazo)-benzoic acid, has been the subject of ionization constant studies for half a century.¹⁻⁷ The collected results refer to several temperatures, the effects of ionic strength often were not considered, and some of the experimental approaches were inherently inaccurate. The purpose of the present work has been to use refined spectrophotometric techniques for the determination of accurate ionization constant values, and to examine the usefulness of immiscible solvent extraction and solubility studies for the same purpose.

In aqueous solution methyl red exists in three forms: a cation, H_2M^+ , which is intensely red, a species HM which is undoubtedly a zwitterion because of the similarity of its absorption spectrum to that of H_2M^+ (see Fig. 1), and a yellow anion, M^- . The familiar use of methyl red as an acid-base indicator is based on the equilibrium between M^- and HM. In neutral solvents such as benzene and carbon tetrachloride HM is yellow, indicating that the zwitterion reverts to the non-ionic structure: $(\text{CH}_3)_2\text{NC}_6\text{H}_4\text{N}=\text{NC}_6\text{H}_4\text{COOH}(o)$.

The cation may be regarded as a diprotic acid, and two equilibrium quotients (in terms of molarities) may be defined in the usual way

$$Q_1 = [\text{H}_3\text{O}^+][\text{HM}]/[\text{H}_2\text{M}^+] \quad Q_2 = [\text{H}_3\text{O}^+][\text{M}^-]/[\text{HM}]$$

The corresponding equilibrium constants, K_1 and K_2 may be calculated from the experimentally

determined Q values if the values of the activity coefficients can be estimated reliably.

Experimental

Reagents.—Methyl red (Eastman 431) was purified by slow recrystallization from redistilled toluene, resulting in large crystals. For the spectrophotometric work ethanolic stock solutions were prepared by weighing the calculated quantity and diluting to make the molarity equal to 1.00×10^{-3} . The carbon tetrachloride was redistilled, solutions were standardized by conventional methods, and all reagents were of high quality.

Apparatus.—Photometric measurements were made with a Beckman Model B instrument using both 1-cm. rectangular and 5-cm. cylindrical Pyrex cells. The 5-cm. cells were calibrated "to contain" and were glass-stoppered. A calibrated Gilmont ultramicroburet, 0.1-ml. size, was used to make additions directly to the solution in the cell. In the solubility studies the temperature was controlled by a thermostated air-bath mechanical rotator. A special apparatus facilitated the combined techniques of equilibration and sampling (see Fig. 2).

Spectrophotometric Procedure.—For the determination of Q_2 the 5-cm. cell was filled (14.50 ml.) with 0.0220 M sodium acetate solution containing $1.0 \times 10^{-6} M$ methyl red. Under these conditions ($p\text{H} \approx 8$) the dye is quantitatively in the yellow form and the absorbance was taken as the value for A_m (see Discussion). The ultramicroburet was used to make successive 0.100-ml. additions of 5.178 M acetic acid until a total of 0.1 ml. had been added. The solution was mixed and the absorbance was measured at 420, 405, and 390 $m\mu$, (in separate runs) after each addition. Since the volume change was so small the ionic strength remained effectively constant and only minor corrections in absorbance were required to take account of dilution.

In the determination of Q_1 the 5-cm. cell was filled with $8 \times 10^{-6} M$ methyl red in water, and increments of 0.2017 M hydrochloric acid were added until 0.2 ml. was present. Then the ultramicroburet was filled with 4.034 M hydrochloric acid and increments up to a total of 0.1 ml. were added. After each addition the absorbance was measured at 560 $m\mu$. In the spectrophotometric work the ambient room temperature was approximately 25°.

Solubility Procedure.—A large excess of crystalline methyl red (HM form) was added to the various buffer solutions in borosilicate bottles which were rotated at 25° for several days. The glass frit in the special sampling apparatus

- H. T. Tizard, *J. Chem. Soc.*, **97**, 2477 (1910).
- A. Thiel, F. Wulfsen, and A. Dassler, *Z. anorg. u. allgem. Chem.*, **136**, 393 (1924).
- I. M. Kolthoff, *Rec. trav. chim.*, **43**, 144 (1924); **44**, 75 (1925).
- A. Meretoja, *Ann. Acad. Sci. Fennicae Sec. A, II, Chemica*, No. **12**, 7 (1944).
- F. A. F. Vermast, *Indonesian J. Nat. Sci.*, **109**, 57 (1953).
- S. W. Tobey, *J. Chem. Educ.*, **35**, 514 (1958).
- C. N. Reilly and E. M. Smith, *Anal. Chem.*, **32**, 1233 (1960).

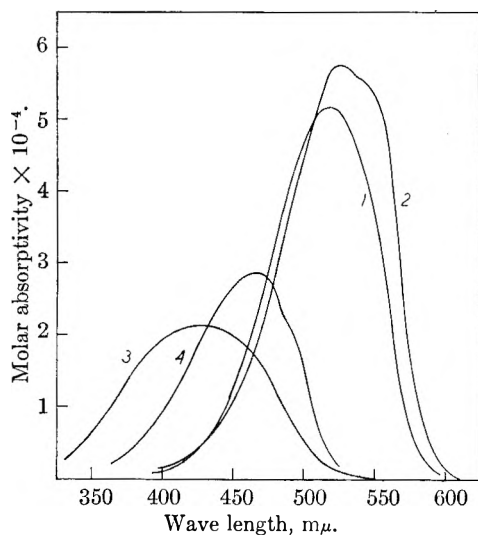


Fig. 1.—Absorption spectra of methyl red. Curve 1 is the spectrum of the cation measured in 0.5 *M* HCl. Curve 2 is the calculated spectrum for the zwitterion in 2.5×10^{-4} *M* HCl (isoelectric point) obtained by using the determined values of Q_1 and Q_2 to correct the composite spectrum measured at this *pH*. Curve 3 is the spectrum of the anion measured in 0.01 *M* NaOH. Curve 4 is the spectrum of methyl red dissolved in carbon tetrachloride, obtained with a 4.2×10^{-6} *M* solution in a 5-cm. cell. The aqueous spectra were obtained with 1.00×10^{-5} *M* solutions in 1-cm. cells.

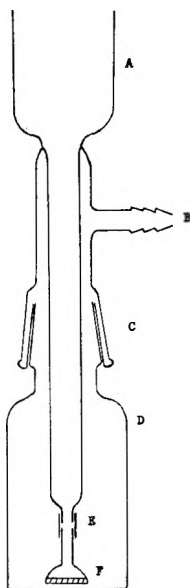


Fig. 2.—Equilibration and sampling apparatus: A, sample well for pipetting; B, air pressure inlet; C, $\text{F } 19/22$ joint; D, Corning 1560 bottle, used with external cap for equilibration; E, Tygon tubing; F, Corning 39535 fine porosity filter disk.

adsorbed methyl red from solution so the first filtered portions were rejected. Five-ml. samples were pipetted into 10-ml. volumetric flasks and dilution to the mark was made with the inclusion of enough sodium hydroxide to insure complete conversion to the yellow form. The absorbances of the resulting solutions were measured at 425 $m\mu$ and were compared with the values obtained for a series of solutions of known concentration in the same cells. Beer's law was followed closely and the molar absorptivity was calculated to be 2.07×10^4 l./mole cm.

Solvent Extraction Procedure.—Ten-ml. portions of 2.11×10^{-3} *M* stock solution of methyl red in carbon tetrachloride were equilibrated with equal volumes of the various

buffer solutions in borosilicate glass-stoppered tubes. These were kept in a constant temperature water-bath at 25° with removal for vigorous shaking eight times in a one-hour period. The phases were separated by centrifuging and were sampled by pipet. One-ml. portions of the carbon tetrachloride layers were allowed to evaporate and the residue was taken up in sodium hydroxide, diluted to known volume, and the absorbance was measured at 425 $m\mu$. Seven-ml. aliquots of the aqueous layers were made basic with sodium hydroxide, diluted to 10 ml. in volumetric flasks, and were measured similarly.

Calculations.—In all parts of this study the data were interpreted with the aid of an IBM 610 digital computer which applied the method of least squares and calculated the limits in the equilibrium quotients corresponding to 90% confidence.⁸ In the spectrophotometric work corrections, no matter how small, were applied for the dilution inherent in the use of the ultramicroburet, and in all of the interpretations the mutual existence of all three forms of methyl red was recognized even though one would be present to an almost negligible extent.

In the spectrophotometric determination of Q_2 the ionic strength was 0.022, and the *pH* values for the acetate buffers were calculated using 2.33×10^{-5} for the dissociation quotient of acetic acid at 25°. The acetate buffers used in the solubility study had an ionic strength of 0.020, and Q_a for acetic acid was taken as 2.31×10^{-6} . The *pH* values for the hydrochloric acid solutions were simply calculated by molarity-volume relationships recognizing complete ionization.

Discussion and Results

Spectrophotometric Studies.—In the standard spectrophotometric determination of equilibrium quotients relating conjugate pairs one chooses a wave length at which the molar absorptivities of the two forms differ as greatly as possible, prepares a series of solutions having the same total concentration of colored material but varying *pH*, and determines the effect of *pH* on the absorbance, *A*. At one end of the series is a solution sufficiently acidic to cause quantitative formation of the "acid species" while at the other end is a basic solution which contains only the "alkaline species" in significant concentration. The intermediate solutions have *pH* values such that appreciable amounts of both colored species are present, and under these ideal conditions the equilibrium quotient may be calculated from the equation

$$Q = [\text{H}_3\text{O}^+] \frac{A - A_{\text{acid}}}{A_{\text{basic}} - A} \quad (1)$$

where $[\text{H}_3\text{O}^+]$ is the acidity (moles per liter) of the intermediate solution having the absorbance *A*, and the other absorbances refer to the two extreme solutions in the series.

With methyl red it is not possible to make a direct determination of the molar absorptivity of the zwitterion, HM, because the quotients Q_1 and Q_2 differ only by a factor of about 250, and even at the isoelectric point (*pH* \approx 3.6) only about 90% of the dye exists as the zwitterion. For the determination of Q_2 equation 1 may be rearranged as

$$A = Q_2 \frac{A_m - A}{[\text{H}_3\text{O}^+]} + A_{\text{bm}} \quad (2)$$

where A_m is the absorbance of the basic solution containing only the yellow form, M^- , A_{bm} is the non-measurable absorbance of a hypothetical

(8) F. S. Acton, "Analysis of Straight-Line Data," John Wiley and Sons, New York, N. Y., 1959.

(9) H. S. Harned and B. B. Owen, "The Physical Chemistry of Electrolytic Solutions," 3rd edition, Reinhold Publ. Corp., New York, N. Y., 1958, p. 676.

solution containing only the zwitterion, and A is corrected for dilution and for the presence of a small amount of H_2M^+ . Although A_{hm} is unknown it is presumed to be constant for a given run, and therefore equation 2 predicts that a plot of the absorbance, A , vs. the quantity $(A_m - A)/[H_3O^+]$ should be linear with an intercept equal to the value of A_{hm} (of incidental interest) and a slope of Q_2 . Thus, the unknown quantity is not needed. This approach was used in separate runs at three wave lengths, yielding the data and calculated quantities shown in Table I. The linear relationships illustrated in Fig. 3 were interpreted to give the values and confidence limits of Q_2 as summarized in Table II. On the assumption that the activity coefficient of the zwitterion is unity at the ionic strength of 0.022 and using 0.86 as the value of the activity coefficient of a singly-charged ion¹⁰ we calculate the thermodynamic value of the equilibrium constant, K_2 , to be $1.11 \pm 0.01 \times 10^{-5}$. However, this confidence limit does not include the uncertainty in the activity coefficients.

TABLE I

DATA FOR SPECTROPHOTOMETRIC DETERMINATION OF Q_2						
$[H_3O^+]$ $\times 10^5$	Obsd. Absorbance			$10^{-4} \times (A_m - A)/[H_3O^+]$		
	420 m μ	405 m μ	390 m μ	420 m μ	405 m μ	390 m μ
3×10^{-4}	1.049	0.980	0.848
1.135	0.666	.598	.513	3.358	3.351	2.939
1.513	.603	.533	.457	2.932	2.940	2.571
1.891	.554	.478	.411	2.602	2.641	2.299
2.269	.514	.442	.378	2.343	2.358	2.060
2.647	.482	.409	.349	2.128	2.144	1.874
3.026	.455	.384	.324	1.950	1.958	1.722
3.404	.432	.360	.306	1.800	1.810	1.583
3.782	.413	.342	.289	1.670	1.676	1.469

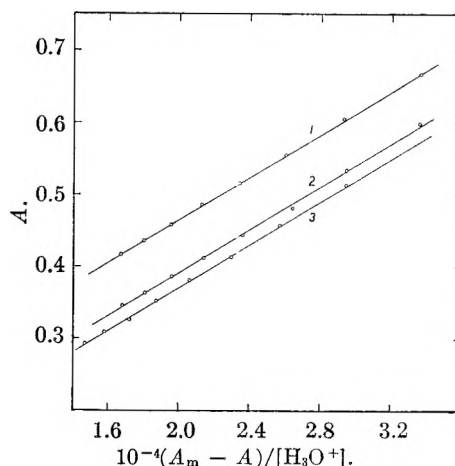
TABLE II

SPECTROPHOTOMETRIC RESULTS FOR Q_2			
Wave length, m μ	$Q_2 \times 10^5$	Confidence (90%) $\times 10$	
420	1.488	\pm	0.006
405	1.509	\pm	.051
390	1.515	\pm	.027
	av. 1.504	\pm	.013

In the determination of Q_1 the situation is still further from the ideal because the absorption spectra of the two red forms are so similar. The maximum difference is at about 560 m μ on the steeply rising side of the peaks. In this case the extreme "basic" solution would be the one containing only zwitterion and as discussed above such a solution cannot be prepared. Nevertheless, equation 1 may be rearranged differently to give

$$[H_3O^+](A - A_{hm}) = -Q_1 A + Q_1 A_{hm} \quad (3)$$

Again it becomes unnecessary to know the value of A_{hm} because this equation predicts that a plot of the quantity on the left side vs. the negative of the corresponding absorbance values would be a straight line with a slope equal to Q_1 . However, it clearly is necessary to know the value of A_{hm} and one would expect to determine this quantity by adding strong acid to the solution until the absorbance at 560 m μ stopped decreasing and became constant, showing quantitative conversion to the red cation species. When this was tried the absorbance did not become constant but

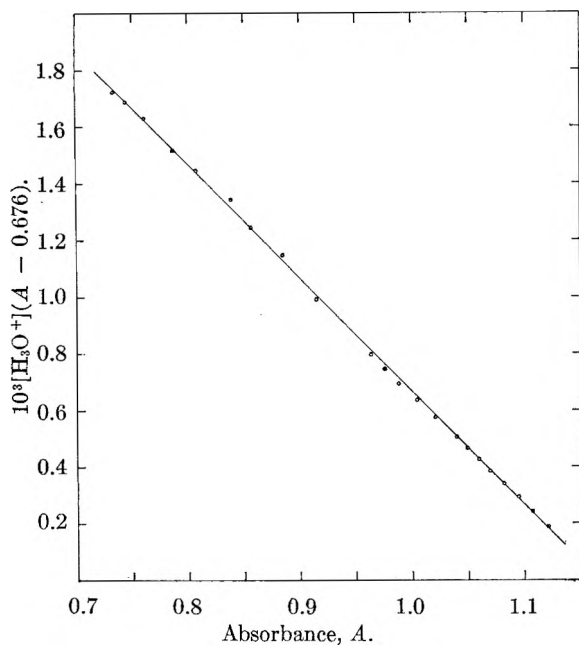
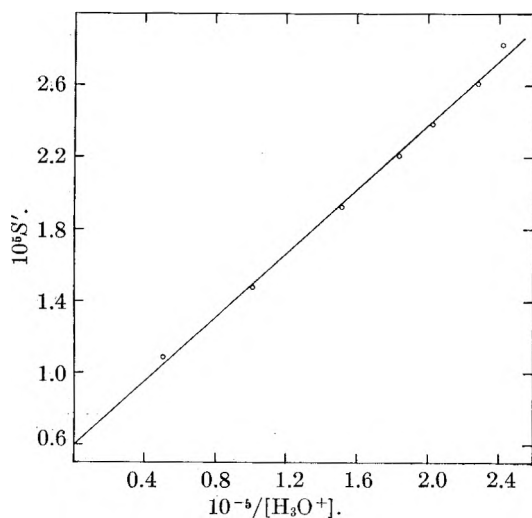
Fig. 3.—Spectrophotometric determination of Q_2 , at 420 (1), 405 (2), and 390 (3) m μ .

went through a minimum and began increasing at acidities too low (less than 0.4 M) to cause quantitative conversion to H_2M^+ . This indicates that another proton is adding to the methyl red cation causing a change in the spectrum, or else that the spectrum shifts slightly as the ionic strength becomes large. In any case it becomes impossible to make a direct determination of the value of A_{hm} . Equation 3 indicates that the use of too large a value for A_{hm} would cause negative deviations from linearity as the absorbance, A , approached similar values in the more acid solutions. Positive deviations would be caused at the "acid end" of the plot in case too small a value were used for A_{hm} . These observations suggested the use of a series of values for this quantity. In each case the computer was used to calculate the slope of the line and the sum of the squares of the deviations. The values of A were corrected for dilution and for the presence of small amounts of M^- . The value of 0.676 thus was found to result in the best linear fit of the data, and slight variations from this value caused obvious curvature at the "acidic end" of the graph. The data necessary for the determination of Q_1 are in Table III, and Fig. 4 shows the linear plot suggested by equation 3. The least-squares slope gives a value of 0.00401 ± 0.00003 for Q_1 .

TABLE III

SPECTROPHOTOMETRIC DATA FOR DETERMINATION OF Q_1					
$[H_3O^+]$ $\times 10^2$	A_{560}	$[H_3O^+]$ ($A - 0.676$) $\times 10^2$		$[H_3O^+]$ ($A - 0.676$) $\times 10^2$	
0.4193	1.091	0.1864	2.490	0.961	0.747
.5587	1.084	.2407	2.763	.948	.795
.6979	1.075	.2918	4.143	.901	.991
.8369	1.065	.3396	5.522	.870	1.146
.9757	1.054	.3838	6.900	.843	1.243
1.114	1.045	.4274	8.278	.825	1.341
1.254	1.035	.4677	11.03	.794	1.445
1.391	1.026	.5059	13.78	.773	1.517
1.667	1.007	.5744	19.26	.747	1.630
1.942	.990	.6366	24.73	.730	1.688
2.217	.974	.692	30.19	.718	1.722

In the determination of Q_2 the ultramicroburet was used to add acetic acid, which did not change the ionic strength of the solution. However, in the study of Q_1 hydrochloric acid was added and

Fig. 4.—Spectrophotometric determination of Q_1 .Fig. 5.—Determination of Q_2 through solubility in acetate buffers.

the ionic strength changed gradually from zero to a highest value of 0.03, so that activity coefficients were not constant during the run. However, since the expression for Q_1 involves the ratio of concentrations of two singly-charged ions it is a fair approximation to state that the value of Q_1 does not vary in the range of low ionic strengths used. Therefore we conclude that the above-mentioned value of 0.00401 also serves as the thermodynamic value, K_1 .

An interesting approach to the spectrophotometric determination of Q_1 and Q_2 has been described by Reilly and Smith,⁷ who used the principles of complementary tristimulus colorimetry in various applications including the determination of indicator pK values. Their method did not require direct measurement of the spectrum of the zwitterion, but made use of the intersection of two straight lines relating the tristimulus chromaticity coordinates derived with the help of an analog

computer from the absorption spectra obtained as a function of pH . They obtained 5×10^{-3} for Q_1 and 1.05×10^{-5} for Q_2 but do not specify ionic strength, temperature or confidence limits, presumably because methyl red was chosen merely as an illustrative example of this new approach.

Solubility Studies.—A saturated solution of methyl red will contain all three forms of the dye in equilibrium with solid HM. The molar solubility, S , is given by

$$S = [H_2M^+] + [HM]_s + [M^-] \quad (4)$$

where the subscript s indicates that the molarity of the zwitterion is the "intrinsic solubility" of the uncharged species. For simplicity we call this quantity Q_0 , and in view of the definitions of Q_1 and Q_2 equation 4 becomes

$$S = \frac{Q_0[H_3O^+]}{Q_1} + Q_0 + \frac{Q_0Q_2}{[H_3O^+]} \quad (5)$$

Simple differentiation shows that the solubility goes through a minimum when $[H_3O^+]$ becomes equal to $(Q_1Q_2)^{1/2}$, *i.e.*, at the isoelectric point. The solubility study is conveniently divided into two parts, one dealing with buffer solutions well above the isoelectric pH and the other in more strongly acid solutions.

In the determination of Q_2 , using acetate buffers of ionic strength 0.0200, the dye was present almost entirely as HM and M^- and a more useful version of equation 5 is

$$S - \frac{Q_0[H_3O^+]}{Q_1} = S' = Q_0 + \frac{Q_0Q_2}{[H_3O^+]} \quad (6)$$

where S' is the solubility corrected for the presence of a slight (less than 0.5%) amount of H_2M^+ . Equation 6 predicts that a plot of S' vs. $1/[H_3O^+]$ should be linear with an intercept equal to Q_0 and a slope equal to Q_0Q_2 . Thus, the slope/intercept ratio would yield a value for Q_2 . The data are in Table IV and Fig. 5 shows the linear plot. The least-squares analysis gives $0.597 \times 10^{-5} M$ for the intrinsic solubility and $1.50 \pm 0.24 \times 10^{-5}$ for the value of Q_2 , in startling agreement with the spectrophotometric result but with lower precision.

TABLE IV

SOLUBILITY DATA FOR DETERMINATION OF Q_2 USING BUFFERS CONTAINING 0.0200M NaOAc		
[HOAc] $\times 10^2$	$10^{-3}/[H_3O^+]$	$S \times 10^5$
3.58	2.418	2.829
3.80	2.278	2.609
4.28	2.023	2.388
4.72	1.834	2.208
5.72	1.514	1.929
8.575	1.010	1.480
17.15	0.505	1.090

In the second part of the solubility study a series of hydrochloric acid, potassium chloride buffers were used which had ionic strengths of 0.0200. In these solutions only a very small amount of M^- was present, and equation 5 takes the form

$$S - \frac{Q_0Q_2}{[H_3O^+]} = S' = Q_0 + \frac{Q_0[H_3O^+]}{Q_1} \quad (7)$$

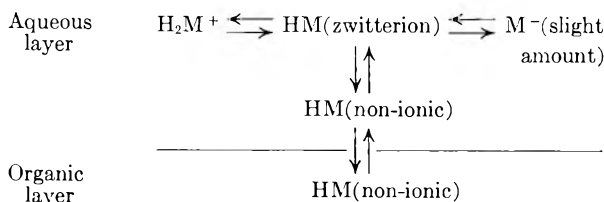
According to this equation a plot of S' vs. $[H_3O^+]$

should be a straight line with an intercept equal to Q_0 and an intercept/slope ratio equal to Q_1 . The data are in Table V and the linear plot is shown in Fig. 6. The least-squares treatment yields $0.602 \times 10^{-5} M$ for Q_0 in excellent agreement with the value obtained using the acetate buffers. The average of the two 90% confidence limits on Q_0 is $\pm 0.07 \times 10^{-5} M$. The intercept/slope ratio gives 0.0039 ± 0.0003 as the value of Q_1 , in very good agreement with the spectrophotometric value but less precise.

TABLE V
SOLUBILITY AND EXTRACTION COEFFICIENT RESULTS IN
HCl-KCl BUFFERS OF $\mu = 0.0200$

$[H_3O^+] \times 10^3$	$S \times 10^5$	$E \times 10^3$
1	0.783	3.521
4	1.208	5.405
7	...	6.993
10	2.106	8.888
13	2.647	10.48
16	3.082	12.40
20	3.681	14.65

Solvent Extraction Study.—In principle the solvent extraction approach is very similar to the solubility method. In both cases an aqueous buffer is equilibrated with an "inexhaustible reservoir" of HM, and the transfer of methyl red to the buffer goes through a minimum at the isoelectric point. However, we have not attempted an extraction study at the higher pH values because of the complications which would be introduced by the distribution and dimerization of acetic acid. The hydrochloric acid, potassium chloride buffers of ionic strength 0.0200 were used and a diagram of the equilibrium system may be shown as



The distribution of HM between the two phases has been indicated in two steps, (1) the "true" distribution of the non-ionic form which would have a distribution coefficient K_d , and (2) the zwitterion formation which is presumably a process having an equilibrium constant K_z . In practice it is not possible to observe the presence of the non-ionic form in the aqueous phase and we resort to writing a combined distribution coefficient, $D = [HM]_{w1}/[HM]_{org}$, which includes both K_d and K_z .

Following Sandell¹¹ we define an extraction coefficient, E , to be the ratio of the total aqueous methyl red concentration to the total organic layer concentration. When the quotients Q_1 , Q_2 , and D are algebraically combined we find that

$$E = \frac{D[H_3O^+]}{Q_1} + D + \frac{DQ_2}{[H_3O^+]} \quad (8)$$

The right-hand term of equation 8 is due to the

(11) E. B. Sandell, "Colorimetric Determination of Traces of Metals," 3rd edition, Interscience Publishers, New York, N. Y., 1959, p. 55.

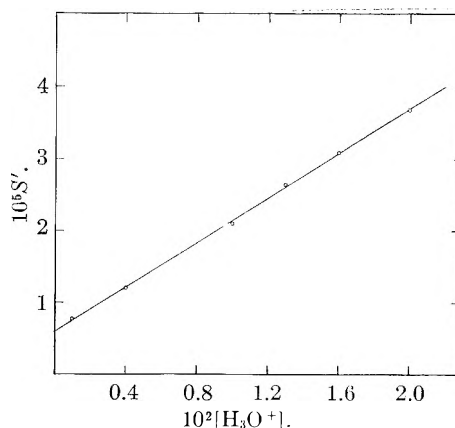


Fig. 6.—Determination of Q_1 through solubility in HCl-KCl buffers.

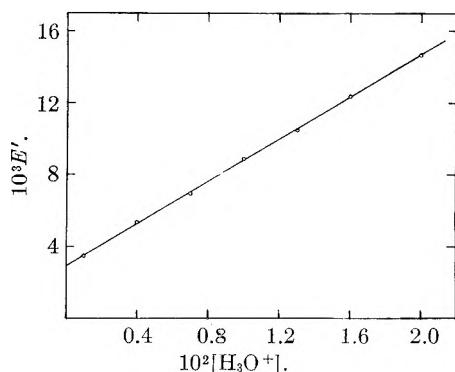


Fig. 7.—Determination of Q_1 through distribution of methyl red between carbon tetrachloride and HCl-KCl buffers.

presence of a slight amount of M^- in the series of solutions. This term can be evaluated with ample accuracy because Q_2 is known from the other studies and D can be determined by successive approximations. In any case, the term is very small compared to the others and we write

$$E' = D + \frac{D[H_3O^+]}{Q_1} \quad (9)$$

which suggests that a plot of E' vs. $[H_3O^+]$ (analogous to the solubility study at higher acidity) would be linear with an intercept equal to D and an intercept/slope ratio equal to Q_1 . The data are in Table V and Fig. 7 shows the straight-line plot. The least-squares calculations give a value of 0.00295 ± 0.00013 for the distribution coefficient. The results are fairly precise and yet the value for Q_1 (0.0050 ± 0.0002) is significantly higher than those obtained in the spectrophotometric and solubility studies. A possible explanation for this difference is that the HM form of methyl red tends to associate with the carbon tetrachloride which has dissolved in the aqueous phase. This would shift the aqueous equilibrium somewhat in favor of HM, or in other words would make H_2M^+ appear to be a bit stronger as an acid.

It might be asked whether methyl red undergoes polymerization in the carbon tetrachloride solutions. Attempts to study this were inconclusive and this aspect was not pursued because in the extraction study so little dye was transferred from the organic layer that the effect of dimerization

would be constant, and would mean only that D as reported here was not a true monomer distribution coefficient.

Acknowledgment.—We are grateful to the Re-

search Corporation for a Cottrell Grant, and to E. I. du Pont de Nemours & Company for departmental grants which were used partially for support of this work.

TUNNELLING CORRECTIONS FOR UNSYMMETRICAL ECKART POTENTIAL ENERGY BARRIERS

BY HAROLD S. JOHNSTON AND JULIAN HEICKLEN

Department of Chemistry, University of California, Berkeley 4, California

Received October 30, 1961

Tunnelling corrections have been evaluated for the unsymmetrical Eckart potential for ranges of parameters expected for ordinary chemical reactions at ordinary temperatures.

In computing chemical reaction rates using activated complex theory, one must include a correction for quantum mechanical barrier penetration and non-classical reflection, the effects referred to as "tunnelling." For small degrees of tunnelling, a correction was derived by Wigner.¹ Bell² worked out the tunnelling problem for a truncated parabola and a Boltzmann distribution of incident systems. Shavitt³ and Johnston and Rapp⁴ computed tunnelling corrections for symmetrical Eckart⁵ functions for chemically interesting values of the parameters involved. The present article presents similar calculations for the unsymmetrical Eckart function.

Eckart's one-dimensional potential energy function is

$$V = -\frac{Ay}{1-y} - \frac{By}{(1-y)^2} \quad (1)$$

$$y = -\exp(2\pi x/L) \quad (2)$$

where x is the variable dimension and L is a characteristic length. For the symmetrical function, A is zero. Both a symmetrical and an unsym-

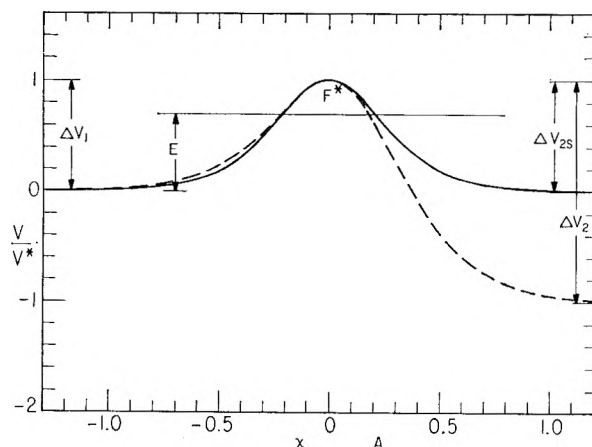


Fig. 1.—Symmetrical and unsymmetrical Eckart function. E is one example of the variable energy considered in eq. 13. V^* is the same as ΔV_1 . F^* is d^2V/dx^2 evaluated at the maximum.

- (1) E. Wigner, *Z. physik. Chem. (Leipzig)*, **B19**, 203 (1932).
- (2) R. P. Bell, *Trans. Faraday Soc.*, **55**, 1 (1959).
- (3) I. Shavitt, Theoretical Chemistry Laboratory, University of Wisconsin, Madison, Wisconsin, Report AEC-23, Series 2, 3 (1959).
- (4) H. S. Johnston and D. Rapp, *J. Am. Chem. Soc.*, **83**, 1 (1961).
- (5) C. Eckart, *Phys. Rev.*, **35**, 1303 (1930).

metrical Eckart function are given by Fig. 1. It is seen to be flat at both $-\infty$ and $+\infty$. The maximum value is ΔV_1 above the value at $-\infty$ and ΔV_2 above the value at $+\infty$. F^* is the second derivative of the potential energy function evaluated at its maximum. The parameters A , B , and L in eq. 1 and 2 are related to ΔV_1 , ΔV_2 , and F^* of Fig. 1 by

$$A = \Delta V_1 - \Delta V_2 \quad (3)$$

$$B = [(\Delta V_2)^{1/2} + (\Delta V_1)^{1/2}]^2 \quad (4)$$

$$\frac{L}{2\pi} = \left(-\frac{2}{F^*}\right)^{1/2} \left[\frac{1}{(\Delta V_2)^{1/2}} + \frac{1}{(\Delta V_1)^{1/2}}\right]^{-1} \quad (5)$$

The inverse relations are

$$\Delta V_1 = (A + B)^2/4B \quad (6)$$

$$\Delta V_2 = (A - B)^2/4B \quad (7)$$

$$-F^* = \pi^2(A^2 - B^2)/2L^2B^3 \quad (8)$$

A particle of mass m and energy E approaching the barrier is characterized by the parameters u^* , α_1 and α_2

$$u^* = h\nu^*/kT \quad (9)$$

$$\nu^* = (1/2\pi)(-F^*/m)^{1/2} \quad (10)$$

$$\alpha_1 = 2\pi\Delta V_1/h\nu^* \quad (11)$$

$$\alpha_2 = 2\pi\Delta V_2/h\nu^* \quad (12)$$

In these variables, the probability $\kappa(E)$ that a particle starting toward the barrier with energy E at $-\infty$ will pass the barrier and appear later at $+\infty$ with energy E is found by solving Schrodinger's equation for the Eckart function, and the transmission probability is⁵

$$\kappa(E) = 1 - \frac{\cosh 2\pi(a-b) + \cosh 2\pi d}{\cosh 2\pi(a+b) + \cosh 2\pi d} \quad (13)$$

where

$$2\pi a = 2[\alpha_1\xi]^{1/2}(\alpha_1^{-1/2} + \alpha_2^{-1/2})^{-1} \quad (14)$$

$$2\pi b = 2[(1+\xi)\alpha_1 - \alpha_2]^{1/2}(\alpha_1^{-1/2} + \alpha_2^{-1/2})^{-1} \quad (15)$$

$$2\pi d = 2[\alpha_1\alpha_2 - 4\pi^2/16]^{1/2} \quad (16)$$

$$\xi = E/\Delta V_1 \quad (17)$$

When d is imaginary, the function $\cosh 2\pi d$ in eq. 13 becomes $\cos 2\pi|d|$.

The tunnelling correction factor Γ^* is interpreted as

$$\Gamma^* = \frac{\text{quantum mechanical rate}}{\text{classical mechanical rate}}$$

With a Boltzmann distribution of incident particles

TABLE I
COMPUTED BARRIER PENETRATION QUANTUM CORRECTIONS Γ^* FROM UNSYMMETRICAL ECKART BARRIERS AS A FUNCTION OF $\alpha_1, \alpha_2,$ AND u^*

α_1	α_2	2	3	4	5	6	8	10	12	16
0.5	0.5	1.16	1.25	1.34	1.44	1.55	1.80	2.09	2.42	3.26
	1	1.13	1.21	1.29	1.38	1.47	1.68	1.93	2.22	2.94
	2	1.09	1.14	1.20	1.27	1.34	1.51	1.71	1.94	2.53
	4	1.04	1.07	1.11	1.16	1.22	1.35	1.50	1.69	2.16
	8	0.99	1.00	1.03	1.06	1.11	1.21	1.34	1.49	1.88
	12	0.96	0.97	0.99	1.02	1.06	1.15	1.26	1.40	1.76
	16	0.94	0.95	0.97	0.99	1.02	1.11	1.22	1.35	1.68
1	20	0.93	0.94	0.95	0.97	1.00	1.08	1.19	1.31	1.64
	1	1.27	1.43	1.62	1.83	2.09	2.72	3.56	4.68	8.19
	2	1.21	1.35	1.51	1.71	1.93	2.50	3.26	4.28	7.48
	4	1.14	1.24	1.37	1.53	1.71	2.16	2.78	3.60	6.16
	8	1.08	1.16	1.26	1.39	1.54	1.92	2.43	3.12	5.25
	12	1.06	1.12	1.21	1.33	1.46	1.81	2.28	2.91	4.88
	16	1.04	1.10	1.18	1.29	1.42	1.75	2.20	2.80	4.66
2	20	1.03	1.08	1.16	1.26	1.39	1.70	2.14	2.72	4.52
	2	1.32	1.58	1.91	2.34	2.90	4.55	7.34	12.1	34.0
	4	1.26	1.47	1.77	2.16	2.66	4.20	6.85	11.4	33.4
	8	1.19	1.36	1.61	1.93	2.36	3.65	5.87	9.69	28.0
	12	1.16	1.32	1.54	1.84	2.23	3.41	5.44	8.94	25.6
	16	1.14	1.29	1.50	1.78	2.15	3.27	5.20	8.51	24.2
	20	1.12	1.27	1.47	1.74	2.10	3.18	5.03	8.22	23.3
4	4	1.30	1.58	2.02	2.69	3.69	7.60	17.3	42.4	304
	8	1.25	1.51	1.93	2.56	3.56	7.57	18.0	46.7	376
	12	1.22	1.47	1.86	2.46	3.39	7.16	17.0	44.0	354
	16	1.20	1.44	1.81	2.39	3.28	6.88	16.2	41.9	335
	20	1.19	1.42	1.78	2.34	3.20	6.68	15.7	40.3	321
8	8	1.24	1.56	2.04	2.94	4.54	13.8	57.0	307	..
	12	1.22	1.54	2.04	2.96	4.68	15.4	71.7	445	..
	16	1.21	1.53	2.02	2.93	4.65	15.6	74.4	473	..
	20	1.20	1.51	2.00	2.90	4.61	15.5	74.2	474	..
12	12	1.2	1.5	2.1	3.1	5.2	22	162	1970	..
	16	1.2	1.5	2.1	3.1	5.4	25	220	3300	..
	20	1.2	1.5	2.1	3.1	5.4	26	246	3920	..
16	16	1.2	1.5	2.1	3.2	5.7	32	437
	20	1.2	1.5	2.1	3.2	5.9	37	616
20	20	1.2	1.5	2.1	3.2	6.1	46	1150

at $-\infty$ in Fig. 1, the correction factor can be expressed as

$$\Gamma^* = e^{\Delta V_1/kT} \int_0^\infty e^{-E/kT} \kappa(E)_d(E/kT) \quad (18)$$

With the transmission function given by eq. 13, we have numerically integrated eq. 18 by means of the IBM 704 computer at the Berkeley Computing Center. The results can be expressed in terms of α_1, α_2 and u^* , eq. 9-12. For chemically interesting values of these parameters, the quantum correction factors are listed in Table I. It can be seen that for a given α_1 and u^* , the tunnelling correction is moderately sensitive to the value of α_2 . One would make a fairly large error, in most cases, if one used the symmetrical Eckart correction^{3,4} for an unsymmetrical case. It should be further noted⁶

that if α_1 and α_2 are interchanged, the value of Γ^* is unaffected.

In ref. 4 and 6, it was emphasized that for chemical reactions, ΔV_1 is *not* the activation energy. The one-dimensional reaction coordinate does not extend from the activated complex to the products or reactants. The reaction normal mode, when extended beyond the quadratic region near the saddlepoint, soon encounters "side-wall-repulsions" on the two-dimensional potential energy surface. In fitting an Eckart potential to a potential energy surface for a chemical reaction, $-\infty$ is not at reactants and $+\infty$ is not at products; rather in terms of the potential energy surface, $-\infty$ is a cirque immediately adjacent to the col and $+\infty$ is a similar cirque on the other side of the col.

(6) H. S. Johnston, *Advances in Chem. Phys.*, **3**, 131 (1961).

IONIZATION CONSTANT OF 2,2'-DIHYDROXYBIPHENYL IN LIGHT AND HEAVY WATER

BY JOHN E. GORDON AND S. L. JOHNSON

Mellon Institute, Pittsburgh 13, Pennsylvania

Received November 8, 1961

The first ionization constant of 2,2'-dihydroxybiphenyl has been measured in light and heavy water at 25°, giving the values of $pK_1^H = 7.56$ and $K_1^H/K_1^D = 6.34$. K_1^H/K_2^H is estimated to be 10^6 or greater. This large isotope effect on pK_1 and the large separation between pK_1^H and pK_2^H reflect the formation of a strong hydrogen bridge in the monoanion.

In comparison with the acid salts of carboxylic acids, $(RCO_2)_2H^-$, M^+ , little is known about hydrogen bonding in the acid salts of phenols, although a number of these have been known in the solid state for many years.¹ Zollinger and Büchler² report pK values from potentiometric titrations of dihydroxynaphthalenesulfonic acids, and identify the wide separation of the first and second dissociations of the 1,8-dihydroxy compounds with formation of a strong hydrogen bridge in the monoanion. Mahler³ gives approximate pK values for chloro derivatives of bis-(2-hydroxyphenyl)-methane which appear to show the same effect.

This article reports precise measurements of the thermodynamic first dissociation constant of 2,2'-dihydroxybiphenyl, one of the simplest dihydric phenols geometrically well disposed for formation of a hydrogen-bridged monoanion.

Experimental

Materials.—Aldrich Chemical Co. 2,2'-dihydroxybiphenyl was crystallized five times from toluene and sublimed at 60° and 10^{-4} mm. shortly before use, m.p. 108.5–109.5° (lit.⁴ m.p. 108°); equiv. wt. calcd., 186.2; found, 186.6. Distillation Products white label *p*-nitrophenol was crystallized four times from water and sublimed as above, m.p. 112.5–113.5° (lit.⁶ m.p. 113.8°). Disodium hydrogen phosphate, A. R. grade, was crystallized twice from water and was air-dried before oven-drying. Potassium dihydrogen phosphate, A. R. grade, was crystallized twice from water, once from 50% ethanol, and once again from water. Fisher certified sodium chloride was precipitated twice from saturated aqueous solution with ethanol. The preceding salts were dried overnight at 126° before use. Water deionized with a mixed-bed ion exchanger and possessing a specific resistance $\sim 5 \times 10^6$ ohm/cc. was used throughout. The deuterium oxide (Stuart Oxygen) had a deuterium fraction >0.995 . For preparation of the buffer solutions, both water samples were boiled and cooled in a nitrogen atmosphere.

Equilibrium Measurements.—Absorbance values of solutions of the phenols in appropriate buffer solutions and in 0.01 *m* sodium hydroxide and 0.01 *m* hydrochloric acid were determined on a Beckman DU spectrophotometer equipped with an efficiently thermostated cell compartment in which the temperature of the solutions was held at $25.00 \pm 0.01^\circ$; the data are given in Tables I–III. Absorbance values were corrected for absorbance of the pure buffer. The 0.01 *m* NaOD (carbonate-free) was prepared from sodium and the above deuterium oxide; the 0.01 *m* DCl was prepared from Merck 38% DCl with deuterium fraction >0.94 .

Preliminary measurements showed that the second ionization of 2,2'-dihydroxybiphenyl cannot be detected

even in 0.1 *N* alkali (Fig. 1); hence the material can be treated as a monobasic acid in measuring pK_1 near pH 7.

Three types of experiment were performed. In method a pK_1 was computed from equation 1 and the measured de-

$$pK = pH - \log \frac{\alpha}{1 - \alpha} - \log \gamma_{A^+O^-} \quad (1)$$

grees of dissociation obtained from $\alpha = (E_{\text{buffer}} - E_{\text{HCl}}) / (E_{\text{NaOH}} - E_{\text{HCl}})$. The pH of the buffer was obtained from the accurate e.m.f. data of Bates and Acree⁵ (using their equation 24). Values of pH for the deuterium oxide solutions were computed using the K_2^H/K_2^D value (3.62) for phosphoric acid determined by Rule and LaMer⁷ and the expression of Bates and Acree⁵ for the activity coefficients, thus introducing the assumption that the activity coefficient quotient is the same in light and heavy water. Davies⁸ equation, $-\log \gamma_- = 0.509 \sqrt{\mu} / (1 + \sqrt{\mu}) - 0.1 \mu$ was used to compute $\gamma_{A^+O^-}$, and a small correction (ΔpH in Table I) for the effect of the substrate on the pH of the buffer was computed from the formula of Robinson and Kiang.⁹

In method b the pH of the buffer was obtained by measuring the degree of dissociation of *p*-nitrophenol in a separate portion of the buffer and employing the carefully measured value (7.149) of Robinson and Biggs¹⁰ for the pK of this indicator. Assuming that $\log \gamma_{A^+O^-}$ is the same for the substrate and indicator anions, and letting α^I and E^I represent the degree of dissociation and the optical density for the indicator, equation 1 can be transformed to

$$pK = pK^I + \log \frac{\alpha^I(1 - \alpha)}{\alpha(1 - \alpha^I)} \quad (2)$$

which was used to obtain the results in Table II.^{11,12} The agreement with method a is good.

Method c is an improved version of that used by Martin and Butler,¹³ in which measurement of the degree of dissociation of the substrate in identical buffers made up in light and heavy water yields K^H/K^D by use of

$$\log (K^H/K^D) = \log (K^H/K^D)_{\text{buffer}} + \log (\alpha/(1 - \alpha))^H / (\alpha/(1 - \alpha))^D \quad (3)$$

This involves the same assumption as method a; the value

(6) R. G. Bates and S. F. Acree, *J. Research Natl. Bur. Standards*, **30**, 129 (1943).

(7) C. K. Rule and V. K. LaMer, *J. Am. Chem. Soc.*, **60**, 1974 (1938).

(8) C. W. Davies, *J. Chem. Soc.*, 2093 (1938). This gave a better extrapolation to zero ionic strength than did use of 0.2 as coefficient of the linear ionic strength term, which was found to be superior for a number of phenols by Robinson [in Hamor, "The Structure of Electrolytic Solutions," John Wiley and Sons, Inc., New York, N. Y., 1959, p. 253].

(9) R. A. Robinson and A. K. Kiang, *Trans. Faraday Soc.*, **51**, 1398 (1955).

(10) R. A. Robinson and A. I. Biggs, *ibid.*, **51**, 901 (1955).

(11) Equation 2 is strictly accurate only if the pK values and concentrations of substrate and indicator are closely enough matched that the corrections ΔpH are equal for the two, as is the case in the present system; otherwise, a correction is readily applied.

(12) Since it requires no knowledge of the pH of the buffer used, method b seems ideally suited to measurements in pH ranges where no buffers of accurately known pH are available (especially in deuterium oxide where the choice of buffer is greatly restricted) or where the buffer systems of accurately known pH interact chemically (*e.g.*, borate) with, or absorb light in the same wave length range as the substrate.

(13) D. C. Martin and J. A. V. Butler, *J. Chem. Soc.*, 1366 (1939).

(1) (a) J. Fritzsche, *Ann.*, **110**, 150 (1859); (b) G. J. van Meurs, *Z. physik. Chem.*, **91**, 313 (1916).

(2) H. Zollinger and W. Büchler, *Helv. Chim. Acta*, **34**, 591 (1951).

(3) W. Mahler, *J. Am. Chem. Soc.*, **76**, 3920 (1954); the use of borate buffers makes these measurements difficult to interpret, as it is known that boric acid forms stable complexes with dihydric phenols [*e.g.*, H. Schäfer, *Z. anorg. u. allgem. Chem.*, **250**, 127 (1942)].

(4) W. R. Spencer and F. R. Duke, *Anal. Chem.*, **26**, 919 (1954).

(5) N. V. Sidgwick, W. J. Spurrell, and T. E. Davies, *J. Chem. Soc.*, 1202 (1916).

TABLE I
IONIZATION OF 2,2'-DIHYDROXYBIPHENYL IN PHOSPHATE BUFFERS AT 25.00° BY METHOD a

χ^a	μ	pH	E_{buffer}^b	A. H ₂ O			
				$-\log \alpha/(1-\alpha)$	$-\log \gamma_{\text{A}^+ \text{O}^-}$	$-\Delta p\text{H}$	pK_1
0.01528	0.10067	7.035	0.1875	0.4115	0.113	0.001	7.559
.007599	.05005	7.115	.204	.3575	.088	.002	7.559
.003797	.02501	7.180	.217	.317	.067	.004	7.560
.001898	.01250	7.232	.225	.2925	.050	.009	7.566
							av. = 7.561
χ^c	μ	pD	E_{buffer}^b	B. D ₂ O			
				$-\log \alpha/(1-\alpha)$	$-\log \gamma_{\text{A}^+ \text{O}^-}$	$-\Delta p\text{H}$	pK_1
0.01134	0.09085	7.723	0.208	0.535	0.109	0.001	8.366
.005589	.04479	7.802	.233	.469	.085	.002	8.354
.002985	.02392	7.860	.239	.454	.066	.005	8.375
.001389	.01113	7.915	.258	.407	.048	.012	8.358
							av. = 8.363

^a $m_{\text{KH}_2\text{PO}_4} = \chi$, $m_{\text{NaCl}} = 1.0001 \chi$, $m_{\text{Na}_2\text{HPO}_4} = 1.5289 \chi$. ^b Optical density at 308 m μ ; substrate concentration = 7.70×10^{-5} m; $E_{\text{NaOH}} = 0.6505$, $E_{\text{HCl}} = 0.008$, both measured at 0.01 m. ^c $m_{\text{KH}_2\text{PO}_4} = \chi$, $m_{\text{NaCl}} = 1.008 \chi$, $m_{\text{Na}_2\text{HPO}_4} = 2.0018 \chi$. ^d Optical density at 309 m μ ; substrate concentration = 1.09×10^{-4} m; $E_{\text{NaOH}} = 0.907$, $E_{\text{HCl}} = 0.004$. Measurements at two other wave lengths gave identical degrees of dissociation.

TABLE II
IONIZATION OF 2,2'-DIHYDROXYBIPHENYL IN PHOSPHATE BUFFERS AT 25.00° BY METHOD b

χ^a	μ	E^b	α	E^{1c}	α^1	$\log \frac{\alpha^1(1-\alpha)}{\alpha(1-\alpha^1)}$	pK_1
0.01213	0.0848	0.230	0.3455	0.548	0.574	0.407	7.556
0.006048	0.0423	0.246	0.370	0.5775	0.605	0.416	7.565
							av. = 7.560

^a $m_{\text{KH}_2\text{PO}_4} = \chi$, $m_{\text{Na}_2\text{HPO}_4} = 1.998 \chi$. ^b Optical density at 308 m μ ; substrate concentration = 7.70×10^{-5} m; $E_{\text{NaOH}} = 0.6505$, $E_{\text{HCl}} = 0.008$. ^c Optical density at 406 m μ ; substrate concentration = 5.45×10^{-6} m; $E_{\text{NaOH}} = 0.952$, $E_{\text{HCl}} = 0.003$.

TABLE III
ISOTOPE EFFECT ON 2,2'-DIHYDROXYBIPHENYL IONIZATION AT 25.00°

	E_{buffer}^a	E_{NaOH}	E_{HCl}	$\alpha/(1-\alpha)$	$\log \frac{\alpha/(1-\alpha)_{\text{H}_2\text{O}}}{\alpha/(1-\alpha)_{\text{D}_2\text{O}}}$	$\log(K_{\text{H}}/K_{\text{D}})$
H ₂ O	0.278	0.777	0.040	0.470		
D ₂ O	0.181	0.740	0.037	0.2575	0.261	0.820

^a Optical density at 309 m μ in phosphate buffer: $m_{\text{Na}_2\text{HPO}_4} = 0.02734$, $m_{\text{KH}_2\text{PO}_4} = 0.01532$.

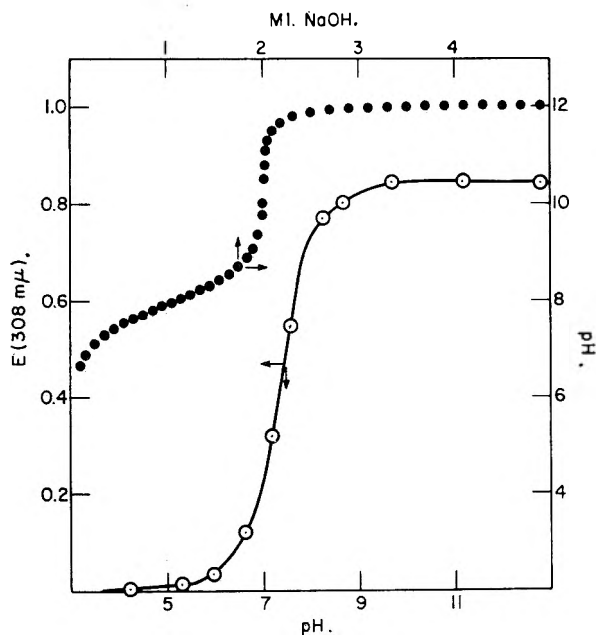


Fig. 1.—Ionization of 2,2'-dihydroxybiphenyl: ●, potentiometric titration of 0.3789 g. of phenol in 5 ml. of 50% methanol with N NaOH; ○, optical density at 308 m μ as a function of pH, determined in buffers of ionic strength ca. 0.01 m and containing 1% methanol.

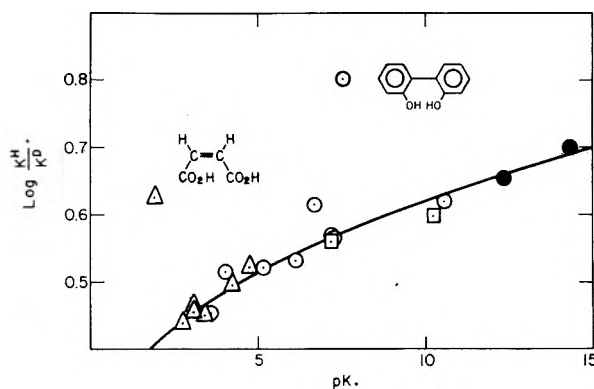


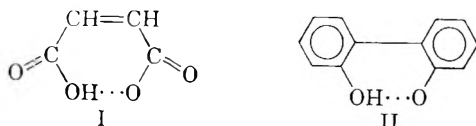
Fig. 2.—Deuterium oxide solvent isotope effects on acid ionization constants vs. acidity: ○, phenols; Δ, carboxylic acids; ●, alcohols; □, HCO₃⁻ and H₂PO₄⁻. Taken from ref. 14 and from R. P. Bell, "The Proton in Chemistry," Cornell University Press, Ithaca, N. Y., 1959, p. 188.

obtained for $\log K^{\text{H}}/K^{\text{D}} = 0.82$ (Table III) checks that from Table I (0.80).

Discussion

The results in Table I lead to a deuterium oxide solvent isotope effect for the thermodynamic first dissociation constant of 2,2'-dihydroxybiphenyl, $K^{\text{H}}/K^{\text{D}} = 6.34$. This is a very large effect, as may be judged from Fig. 2, where it is seen that the

vertical displacement from the curve on which "normal" acids fall fairly precisely is about the same as for maleic acid.¹⁴ These two acids have much larger isotope effects than "normal" acids because of the additional hydrogen frequency lowering in the respective anions, I and II, due to the



formation of a strong intramolecular hydrogen bond. "Normal" acid anions hydrogen bond only weakly with a water molecule (hence, a higher stretching frequency prevails in the hydrogen bond formed) leading to a smaller total OH frequency lowering in going from the acid to the anion, and therefore leading to a smaller isotope effect. In bimalate ion the OH stretching frequency falls near 1650 cm^{-1} , a region characteristic¹⁵ of hy-

(14) G. Dablgren, Jr., and F. A. Long, *J. Am. Chem. Soc.*, **82**, 1303 (1960).

drogen bonds of the single, symmetric minimum variety. In agreement with the observed isotope effect, the OH stretching vibration in II also is found¹⁶ in the neighborhood of 1650 cm^{-1} . Another criterion supporting the conclusion that a strong hydrogen bond exists in II is that K_2 , although it could not be directly measured, can be estimated (Fig. 1) to be a factor of 10^6 smaller than K_1 . Hydroquinone is a good model for comparison since electrostatic effects in the dianions should be similar in the two compounds, the distance between oxygens being nearly the same in hydroquinone as in the *trans* conformation of the dihydroxybiphenyl; hydroquinone can form no intramolecular hydrogen bond in the monoanion, however, and the observed¹⁷ value of K_1/K_2 is 45. This large stabilization of the monoanion II may be compared with the situation in maleic ($K_1/K_2 = 26,000$) vs. fumaric ($K_1/K_2 = 32$) acid.¹⁴

(15) R. Blinc, D. Hadži, and A. Novak, *Z. Elektrochem.*, **64**, 567 (1960).

(16) D. Hadži, private communication.

(17) H. Staude and M. Teupel, *Z. Elektrochem.*, **61**, 181 (1957).

VISCOELASTIC PROPERTIES OF DILUTE POLYSTYRENE SOLUTIONS AND VERIFICATION OF THE ZIMM THEORY¹

BY RICHARD B. DE MALLIE, JR., MEYER H. BIRNBOIM, J. E. FREDERICK, N. W. TSCHOEGL, AND JOHN D. FERRY

Department of Chemistry, University of Wisconsin, Madison, Wisconsin

Received November 9, 1961

Storage (G') and loss (G'') shear moduli have been measured over a wide frequency range with the apparatus of Birnboim and Ferry for dilute solutions of a polystyrene with sharp molecular weight distribution, $M_w = 267,000$, in a chlorinated diphenyl. The high viscosity of the solvent (2.2 poises at 25°) ensured that the viscoelastic dispersion fell within the experimental frequency region. The concentration range was 0.5 to 4% and the temperature range from 0 to 40°. The results are in close accord with the theory of Zimm, as follows: (a) the ratio $(G'' - \omega\eta_s)/G'$, where ω is circular frequency and η_s solvent viscosity, agrees with the theoretical value of 1.73 at higher frequencies; (b) $G'' - \omega\eta_s$ and G' are proportional to $\omega^{2/3}$ in this region, though some deviation appears at higher concentrations; (c) the experimentally determined terminal relaxation times agree with those calculated from the solution viscosity within experimental error; (d) the molecular weights calculated from the Zimm theory are correct at low concentrations, though somewhat too high at the higher concentrations; (e) the local effective viscosities calculated from the terminal relaxation times, at low concentrations, are close to the solvent viscosity. The sharp molecular weight distribution and the high solvent viscosity, which should minimize effects of internal viscosity of the polymer chain, probably are important in achieving the good agreement with the theory.

Introduction

The Rouse theory² for viscoelastic properties has been applied rather successfully to a variety of experimental data on concentrated polymeric systems. However, it would not be expected to give quantitative agreement with data on dilute solutions, since it neglects hydrodynamic interaction between different segments of the same molecule and it reduces to an unsatisfactory expression for the intrinsic viscosity at zero frequency. As Cerf³ has pointed out, it is surprising that some measurements on dilute solutions appear to fit the Rouse theory quite well. Nevertheless, the available data are sparse and rather widely spaced on the frequency scale, especially at high

frequencies.⁴ More measurements are needed to make critical comparison of the Rouse theory with that of Zimm,⁵ which takes hydrodynamic interaction into account. (Neither theory accounts for internal viscosity of the polymer chain, which may be important in solvents of low viscosity.³)

An essential difference between the predictions of the two theories is illustrated in Fig. 1, where the dimensionless reduced shear modulus components are plotted against a dimensionless frequency $\omega_R = \omega\tau_1$. Here $G'_R = G'M/cRT$ and $G''_R = (G'' - \omega\eta_s)M/cRT$; G' and G'' are the storage and loss shear moduli, M the molecular weight (assumed homogeneous), c the polymer concentration in g./ml., ω the circular frequency, and η_s the solvent viscosity; τ_1 is the terminal or longest relaxation time in each theory.⁶ At high fre-

(1) Part XXXVIII of a series on Mechanical Properties of Substances of High Molecular Weight. Presented at the Society of Rheology, Oct. 30, 1961.

(2) P. E. Rouse, *J. Chem. Phys.*, **21**, 1272 (1953).

(3) R. Cerf, *Advances in Polymer Sci.*, **1**, 382 (1959).

(4) W. P. Mason, "Handb. d. Physik," Edited by S. Flügge, Vol. XI/1, p. 361, Springer-Verlag, Berlin, 1961.

(5) B. H. Zimm, *J. Chem. Phys.*, **24**, 269 (1956).

quencies according to the Rouse theory, $G'_R = G''_R$ and both are proportional to $\omega^{1/2}$; according to the Zimm theory, the ratio G''_R/G'_R is not 1 but 1.73, and both quantities are proportional to $\omega^{2/3}$.

For an adequate experimental test, it is desirable to measure the shear moduli G' and G'' at many rather closely spaced frequencies through a range of about two decades on each side of $\omega = 1/\tau_1$, and to employ a polymer with the sharp molecular weight distribution which is assumed in the theories. Dilute solutions can be measured over a continuous frequency range from 0.01 to 400 c.p.s. in the apparatus of Birnboim and Ferry,⁸ and the desired region near $\omega\tau_1 = 1$ can be encompassed by using a highly viscous solvent in which the terminal relaxation time is 10^2 to 10^3 longer than in ordinary organic liquids. The high viscosity probably has another advantage in that the frictional resistance to configurational changes provided by the environment of the polymer molecules is much higher than any intramolecular hindrance (internal viscosity) which might be present but is ignored in the theories.

The present paper describes some measurements on a sample of polystyrene with a sharp molecular weight distribution, dissolved in a chlorinated diphenyl, in a concentration range from 0.5 to 4% polymer by weight.

Materials.—The polystyrene, S-108, was generously provided by Dr. H. W. McCormick of Dow Chemical Company. It had been prepared by anionic polymerization followed by terminating the chains with water.⁹ Its weight-average molecular weight was 267,000 and the ratio of weight to number average was 1.08.

The chlorinated diphenyl, Aroclor 1248, was donated by the Monsanto Chemical Company through the kindness of Mr. C. M. Williams. Its viscosity at 25° was 2.2 poises, determined by the falling sphere method with spheres of synthetic ruby, and its density was 1.442 g./ml. Viscosities (η_s) determined at other temperatures between 1 and 25° followed the empirical equation $\log \eta_s = 2.63 - 5.89t/(39.2 + t)$, where t is Centigrade temperature. This equation was used to obtain values of η_s for subsequent calculations.

The intrinsic viscosity of the polymer in this solvent also was determined by the falling sphere method to be 0.85 dl./g. at 25°. This value is quite close to the predicted intrinsic viscosity of a polystyrene of this molecular weight in *o*-dichlorobenzene, a more conventional solvent of similar chemical nature—namely, 0.86 dl./g. The latter value is estimated from the data of Streeter and Boyer¹⁰ and established viscosity-molecular weight relationships¹¹ in benzene.

Method.—A few measurements were made with the apparatus of Birnboim and Ferry as originally described,⁸ but unless otherwise identified the data reported here were obtained after two important changes in procedure.

A flexible yoke was attached to the lower pole piece in such a way that by raising it the driving coil mounting could be forced up against the central pole piece and immobilized. A long threaded rod, projecting outside the brass case and the thermostat bath, is used to raise and lower the yoke while the apparatus is in operation. Thus, for operation in the impedance mode, the components of

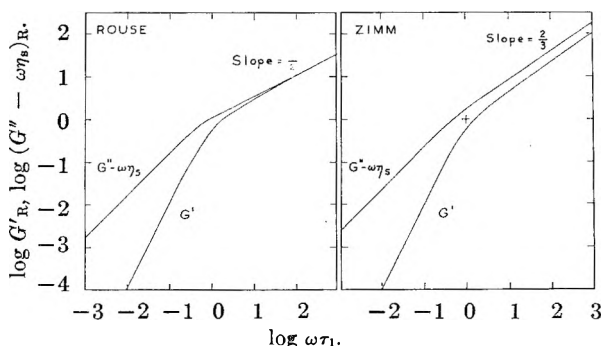


Fig. 1.—Logarithmic plots for the contributions of a polymer solute to the components of the complex shear modulus, as predicted by the theories of Rouse and Zimm.

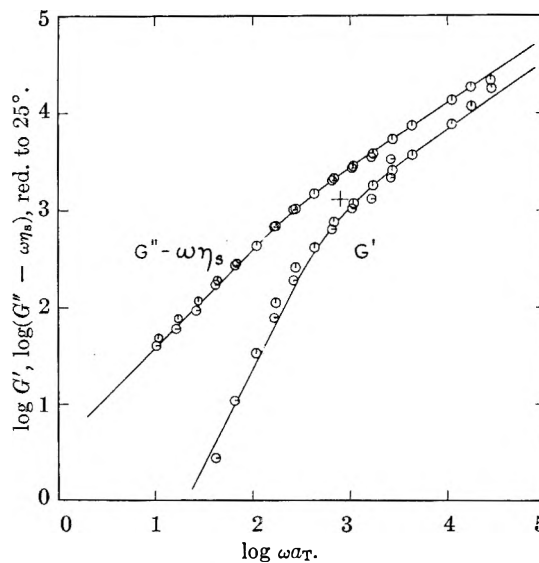


Fig. 2.—Logarithmic plots of G' and $G'' - \omega\eta_s$ for 1% polystyrene S-108 in Aroclor 1248, referred to 25°: pip up, measured at 9.4°; pip right, measured at 24.8°. Curves represent the Zimm theory with the coordinates adjusted so the cross corresponds to the origin of the reduced plot in Fig. 1.

the clamped impedance, R_0 and X_0 , can be determined at every frequency immediately before or after the impedance in motion, R and X . The estimation of R_0 and X_0 at various frequencies and temperatures from empirical power series based on earlier calibration measurements thereby is eliminated. Smaller values of $R - R_0$ and $X - X_0$ (corresponding to samples with higher viscosity and/or rigidity) now can be determined with adequate precision.

The method for determining the coefficient C in the phase meter mode also has been modified so that frequent calibrations can be made while a sample is in the cell. When the sample is a viscoelastic liquid, the forces arising from displacement of the moving system to a new fixed position all will relax eventually, except for that due to the spring stiffness S_M . Under such conditions equation 11 of reference 8 reduces to

$$C = \varepsilon_M R_4 d_1 / d_2 \quad (1)$$

where d_1 and d_2 are maximum recorder trace heights for the displacement and force signals, respectively, and R_4 is the variable resistance in series with the driving coil. To determine C , the coil is energized with a square wave of frequency 0.01 c.p.s. from the 202A oscillator, and the appropriate measurements are made. For most samples, relaxation is complete within the half period. For longer relaxation times, a constant voltage of 20 v. from dry cells can be substituted for the square wave input. (This method is not applicable to gelatinous samples, however, for which there is a non-relaxing force contribution from the sample.)

(6) The numerical evaluations were made by Dr. S. E. Lovell⁷ of the Theoretical Chemistry Laboratory. Tables of values may be obtained upon request.

(7) S. E. Lovell and J. D. Ferry, *J. Phys. Chem.*, **65**, 2274 (1961).

(8) M. H. Birnboim and J. D. Ferry, *J. Appl. Phys.*, **32**, 2305 (1961).

(9) H. W. McCormick, F. M. Brower, and L. Kim, *J. Polymer Sci.*, **39**, 87 (1959).

(10) D. J. Streeter and R. F. Boyer, *Ind. Eng. Chem.*, **43**, 1790 (1951).

(11) P. J. Flory, "Principles of Polymer Chemistry," Cornell University Press, Ithaca, N. Y., 1953.

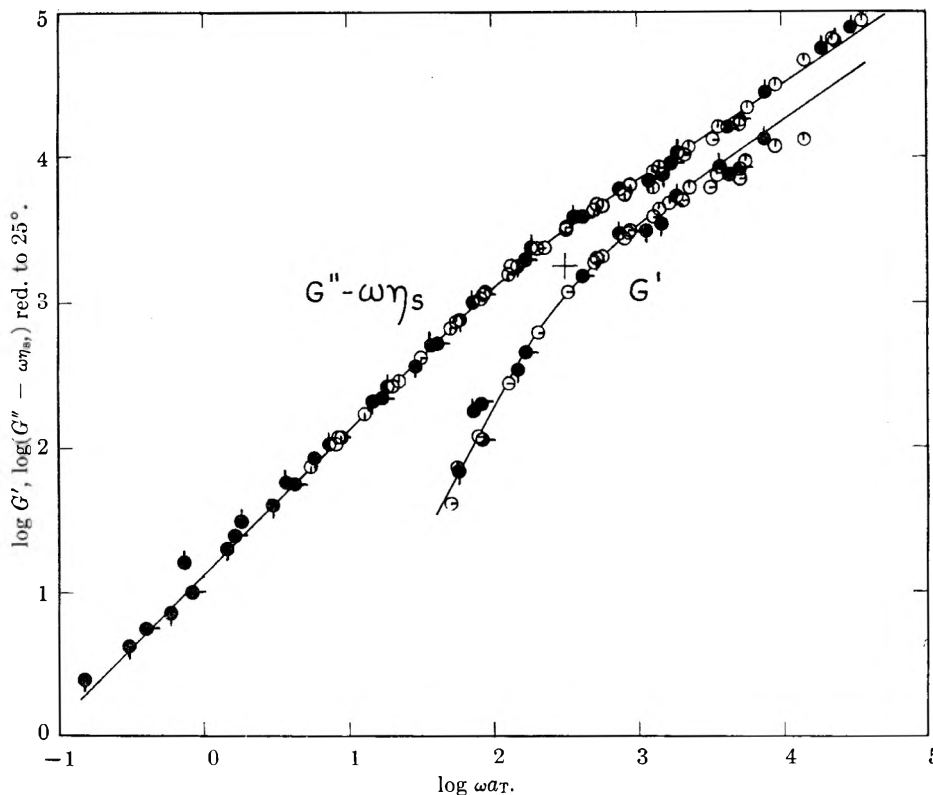


Fig. 3.—Logarithmic plots of G' and $G'' - \omega\eta_s$ for 2% polystyrene S-108 in Aroclor 1248, referred to 25°. Black circles, measurements before apparatus improvements: pip up, 10.2°; pip right, 18.1°; pip down, 25.1°. Open circles, measurements after improvements: pip up, 10.0°; pip right, 20.0°; pip down, 30.0°.

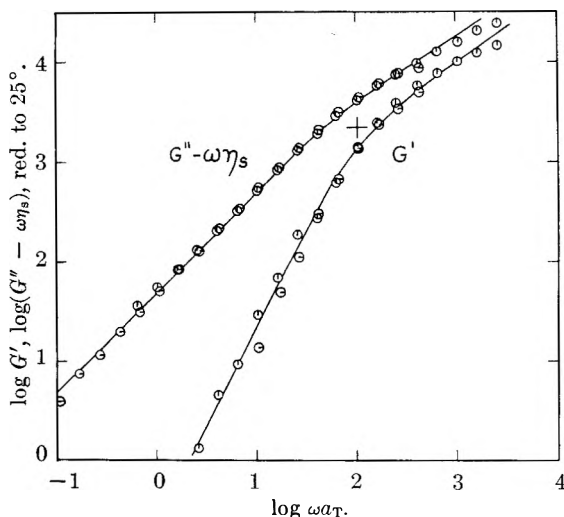


Fig. 4.—Logarithmic plots of G' and $G'' - \omega\eta_s$ for 4% polystyrene S-108 in Aroclor 1248, referred to 25°: pip up, measured at 24.8; pip right, measured at 40.0°.

Results

Each solution was studied at two or more temperatures, and the results were reduced to 25.0° by the method of reduced variables, plotting $G'T_0\rho_0/T\rho$ and $(G'' - \omega\eta_s)T_0\rho_0/T\rho$ against ωa_T . Here ρ_0 and ρ are the solution densities at the reference temperature T_0 and the temperature of measurement T . The shift factor a_T was determined from the contribution of the polymer to the steady-flow viscosity, $\eta - \eta_s$, which is the limiting value of $G''/\omega - \eta_s$ at low frequencies¹²

$$a_T = (\eta - \eta_s)T_0\rho_0/(\eta - \eta_s)_0T\rho \quad (2)$$

where the subscript 0 again refers to the reference temperature. The temperature dependence of $\eta - \eta_s$ was nearly the same as that of η_s .

Logarithmic plots of G' and $G'' - \omega\eta_s$ reduced in this manner for solutions of 1.0, 2.0 and 4.0% polymer by weight are shown in Fig. 2-4. At each concentration, the measurements at different temperatures superpose extremely well to provide composite reduced curves. Moreover, the data of 2% taken before and after the improvements in apparatus and procedure agree very well, though the latter are expected to be more reliable.

Similar plots at concentrations of 0.5% (measurements at 0.1 and 25.0°) and 3% (measurements at 25.0 and 40.2°), not shown, gave comparable superposition, though the data at 0.5% were more scattered and it evidently was not practical to attempt measurements at still lower concentrations.

The separation between G' and $G'' - \omega\eta_s$ at higher frequencies in Fig. 2-4 shows at once that the results conform to the Zimm theory rather than that of Rouse. In fact, the data fit the Zimm theory, which is represented by the solid lines in these figures, with remarkable precision. The theoretical curves are drawn by matching the right side of Fig. 1 to the experimental points, with suitable horizontal and vertical shifts. The cross in each of Fig. 2-4 corresponds to the origin in the dimensionless plot of Fig. 1; its position on the abscissa scale is $-\log \tau_1$ and its position on the ordi-

(12) J. D. Ferry, "Viscoelastic Properties of Polymers," John Wiley and Sons, New York, N. Y., 1961, pp. 159, 204.

nate scale is $\log cRT/M$. The values of the $\log M$ and $\log \tau_1$ thus determined are listed in Table I, together with some other derived quantities. The values of these parameters also serve to verify the Zimm theory, as described below.

TABLE I
PARAMETERS OBTAINED FROM ZIMM THEORY AND DERIVED CALCULATIONS
Reference temp., 25°

poly- mer	c , g./ml.	\log $\eta - \eta_s$	\log M obsd. ^b	\log τ_1 obsd. ^c	\log τ_1 calcd. ^d	\log η_z	\log $\frac{\eta - \eta_s}{[\eta]c}$
0.5	0.0072	0.31	5.44	-2.89	-2.87	0.37	0.52
1.0 ^a	.0144	0.64	5.46	-2.83	-2.82	.36	.55
1.0	.0144	0.58	5.44	-2.90	-2.90	.41	.49
2.0	.0286	1.10	5.60	-2.50	-2.52	.53	.71
3.0	.0430	1.42	5.61	-2.38	-2.37	.64	.86
4.0	.0568	1.69	5.81	-2.01	-2.02	.71	1.01

^a Measurements made before apparatus improvements. ^b From position of cross on ordinate scale. ^c From position of cross on abscissa scale. ^d From equation 3, using M from column 4.

Discussion

Frequency Dependence of G' and G'' .—While the experimentally determined frequency dependence follows the theoretical curves very closely over most of the range, a systematic deviation does appear at higher frequencies in the 4% solution, where both G' and G'' increase somewhat less rapidly with frequency than predicted. Since the theory treats the polymer molecules as independent of each other, it is natural that there should be some deviations at concentrations where overlapping of the polymer coil domains becomes substantial. The transition from dilute to concentrated solutions will require further study, however.

Molecular Weight from Viscoelastic Measurements.—Since $\log M_w$ from ultracentrifuge measurements at Dow Chemical Company is 5.43, it is clear that the values derived from application of the Zimm theory at concentrations of 1% and below are in excellent agreement. At higher concentrations, the molecular weights obtained in this manner become progressively too large. This deviation again no doubt reflects the overlapping of the polymer coils, though it is not clear why this should affect the apparent molecular weight in the manner observed.

Terminal Relaxation Times.—The terminal relaxation time of the Zimm theory can be expressed in terms of the polymer contribution to viscosity as follows,¹³ noting that the coefficient λ'_1 is 4.04

$$\tau_1 = 0.422(\eta - \eta_s)M/cRT \quad (3)$$

Values calculated in this manner, using the *apparent* values of M , also are given in Table I. For this calculation, $\eta - \eta_s$ is obtained as the limiting value

(13) Reference 12, p. 159, equation 18.

of $(G'' - \omega\eta_s)/\omega$ at low frequencies. The agreement between observed and calculated values of τ_1 is quite precise, reflecting the close fit of the experimental data to the Zimm functions in each case. (Of course, if the true value of M is used in this calculation, the observed and calculated values of $\log \tau_1$ will differ by the error in the observed $\log M$ in column 4.)

Local Effective Viscosity.—The terminal relaxation time of Zimm also can be expressed⁵ as

$$\tau_1 = 0.200 \eta_z a^2 Z^{3/2} / kT \quad (4)$$

Here η_z is the effective local viscosity opposing motion of a chain segment, taken in the Zimm theory to be identical with η_s but distinguished here so its numerical value can be calculated separately; a^2 is the mean square molecular length per monomer unit, and Z the degree of polymerization. The characteristic length a for polystyrene in the Aroclor is calculated from the intrinsic viscosity¹⁴ to be 9.3 Å. (about 26% higher than in a θ -solvent). Values of $\log \eta_s$ obtained from equation 4 are included in Table I. Since $\log \eta_s = 0.34$, the local effective viscosity at lower polymer concentrations is indeed very close to the solvent viscosity as inherent in the Zimm theory. At higher concentrations, it is somewhat higher (2.5-fold at 4%), but it remains far smaller than the solution viscosity.

Calculation of η_z provides somewhat the same sort of information as comparing the contribution of polymer to the steady-flow viscosity, $\eta - \eta_s$, with that expected on the basis of direct proportionality to the intrinsic viscosity, $[\eta]\eta_s c$. Peterlin¹⁵ has defined an effective local viscosity in this sense as $(\eta - \eta_s)/[\eta]c$. Logarithms of the latter quantity are given in the last column of Table I. The effective viscosity of Peterlin is somewhat larger than η_z ; it increases in a similar manner, though somewhat faster, with increasing concentration.

Applications of the Zimm theory to viscoelastic properties of polymers of different molecular weights and molecular weight distribution, as well as the effects of solvents of different viscosities, will be reported subsequently.

Acknowledgments.—This work was supported in part by the Office of Naval Research under Contract N7onr-28509, and in part by the Research Committee of the Graduate School of the University of Wisconsin from funds supplied by the Wisconsin Alumni Research Foundation. We are indebted to Professor Bruno H. Zimm for his comments.

(14) Reference 11, p. 618.

(15) A. Peterlin, "Proc. 2nd Int. Congr. Rheology," Butterworths, London, 1954, p. 343.

A PROTON MAGNETIC RESONANCE STUDY OF HINDERED INTERNAL ROTATION IN SOME SUBSTITUTED N,N-DIMETHYLAMIDES¹

BY MAX T. ROGERS AND JAMES C. WOODBREY²

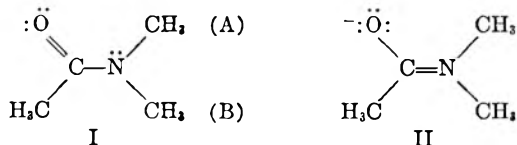
Kedzie Chemical Laboratory, Michigan State University, East Lansing, Michigan

Received November 20, 1961

Several studies of hindered internal rotation about the C-N bond in amides have been made by high-resolution proton magnetic resonance (p.m.r.) spectroscopy. Various methods have been reported for obtaining the activation energies E_a and frequency factors A for internal rotation from the temperature dependence of the p.m.r. spectrum. Recent methods make it possible to reduce the rather large experimental errors associated with these parameters in the earlier studies. We therefore have made a redetermination of the energy barrier and frequency factor for internal rotation about the central C-N bond of N,N-dimethylacetamide (DMA). The same experimental techniques and methods of calculation then were applied for the measurements of the barrier heights for internal rotation in a series of substituted N,N-dimethylamides, none of which had been studied previously. A detailed treatment of the errors in the present method leads to the conclusion that the probable error in E_a has been reduced to less than ± 0.8 kcal./mole. The effect of structure on E_a therefore may be discussed with some assurance that differences among different substituted amides are significant.

Introduction

The p.m.r. spectrum of DMA at $\nu_0 = 60$ Mc. and room temperature shows a single line for the C-methyl protons but a chemical shift doublet for the protons of the N-methyl groups (A, B of I). Gutowsky and Holm³ observed that the separation



between the lines of the doublet decreased upon heating the sample until at a sufficiently high temperature, termed the *coalescence temperature*, a single line remained. They found an energy barrier $E_a = 12 \pm 2$ kcal./mole and a frequency factor $A = 10^7$ to 10^{10} sec.⁻¹ for DMA and $E_a = 7 \pm 3$ kcal./mole and $A = 10^3$ to 10^7 sec.⁻¹ for N,N-dimethylformamide (DMF) from a series of measurements of apparent chemical shift at a spectrometer frequency $\nu_0 = 17.735$ Mc. Several other studies have been made on formamide, DMF, and DMA.^{4,5} The earlier work and theory have been reviewed.⁶ Piette and Anderson⁷ have shown that the mean lifetime τ of exchangeable nuclei at chemical sites (as A or B of I) may be related to the changes in the resonance line widths which accompany the exchange averaging. Grunwald, Loewenstein, and Meiboom⁸ and Loewenstein and Meiboom⁹ noted that the mean lifetime τ of exchangeable nuclei at a chemical site may be

related to r , the ratio of maximum to central minimum ν -mode intensities, and to the coupling constant when τ is very large, for symmetrical spin-spin multiplets. The mean lifetime 2τ of a methyl group at one of the chemical sites (A or B of I) is similarly related to r , the ratio of maximum to central minimum ν -mode intensities, and to $\delta\nu = \nu_A - \nu_B$, the chemical-shift difference under conditions where there is no rotational averaging. We have found for the compounds studied here that the use of these latter line-shape parameters leads to much more precise values of τ than does either of the earlier methods^{3,7} which also were tried. The errors in the barrier heights, which were obtained from the temperature dependence of τ , are ± 0.3 to ± 0.8 kcal./mole for the compounds studied if the limits of 90% confidence are computed statistically. The standard deviations are smaller but we have preferred the more severe criterion of error. Since comparisons of barrier heights in different compounds become more significant as errors are reduced, we have used a ratio method similar to that of Loewenstein and Meiboom⁹ for the analyses of the p.m.r. spectra of a series of substituted N,N-dimethylamides over a range of temperature. The effects of substituents on the barrier heights and frequency factors have been discussed.

Experimental

Spectrometer.—The spectra were obtained by use of a Varian Associates high-resolution nuclear magnetic resonance (n.m.r.) spectrometer with Model V-4311 RF probe for operation at $\nu_0 = 60.000$ Mc. and Model V-4310 RF probe for operation at $\nu_0 = 40.000$ Mc. A Model V-4320 spin decoupler allowed fluorine-proton spin-spin interactions to be decoupled while observing proton spectra at $\nu_0 = 60.000$ Mc. Ambient room temperature was regulated to $\pm 2^\circ$. All accessory components and the spectrometer console were supplied from an a.c. line regulated by a Sorensen Model 1000 S voltage regulator. Radofrequencies were measured with a calibrated Collins 51J-M4 communications receiver.

A vacuum-jacketed variable-temperature receiver-coil insert¹ was employed to provide sample temperatures from -100 to 220° . The design was somewhat similar to earlier models.^{10,11} Sample temperature could be controlled to better than $\pm 0.1^\circ$ in the region 0 to 100° and to better than $\pm 0.5^\circ$ through the extreme high and low regions.

Electrical shim coils constructed in this Laboratory were employed to provide high-resolution fluorine spectra at a spectrometer frequency $\nu_0 = 60.000$ Mc. Sample tubes were precision drawn,¹² thin-wall Pyrex tubes, 0.192 ± 0.002 in.

(1) Presented before the Division of Physical Chemistry at the 138th National Meeting of the American Chemical Society, New York, N. Y., Sept., 1960. Abstracted in part from a thesis submitted by J. C. Woodbrey in partial fulfillment of the requirements for the Ph.D. degree, June, 1960. Supported by grants from the National Science Foundation and from the Atomic Energy Commission.

(2) Union Carbide Research Fellow, 1958-1959.

(3) H. S. Gutowsky and C. H. Holm, *J. Chem. Phys.*, **25**, 1228 (1956).

(4) B. Sunners, L. H. Piette, and W. G. Schneider, *Can. J. Chem.*, **38**, 681 (1960).

(5) C. Franconi and G. Fraenkel, *J. Am. Chem. Soc.*, **82**, 4478 (1960).

(6) J. A. Pople, W. G. Schneider, and H. J. Bernstein, "High-resolution Nuclear Magnetic Resonance," McGraw-Hill Book Co., Inc., New York, N. Y., 1959.

(7) L. H. Piette and W. A. Anderson, *J. Chem. Phys.*, **30**, 899 (1959).

(8) E. Grunwald, A. Loewenstein, and S. Meiboom, *J. Chem. Phys.*, **27**, 630 (1957).

(9) A. Loewenstein and S. Meiboom, *ibid.*, **27**, 1067 (1957).

(10) J. N. Shoolery and J. D. Roberts, *Rev. Sci. Instr.*, **28**, 61 (1957).

(11) C. Franconi and G. Fraenkel, *ibid.*, **31**, 657 (1960).

TABLE I
CHEMICAL SHIFTS^a IN THE N.M.R. SPECTRA OF SOME N,N-DISUBSTITUTED AMIDES OF THE TYPE R'CONR₂
($\nu_0 = 60,000$ Mc.)

Amides	$t, ^\circ\text{C.}$	-NR ₂ Group		R' Group	ν_D	Magnitudes of coupling constants, ^b c.p.s.
		ν_B	ν_A	ν_C		
Proton spectra						
-N(CH ₃) ₂ Group						
HCON(CH ₃) ₂	25	232.3 ^d	241.7 ^d	-71.4 ^e		$J_{AC} = 2J_{BC} = 0.50$
CH ₃ CON(CH ₃) ₂	-27.6	205.7	216.3	261.5		$J_{AC}, J_{BC} < 0.2$
CH ₃ CH ₂ CON(CH ₃) ₂	-27.5	225.2	234.4	261.7(CH ₂) ^f	341.1(CH ₃) ^g	(J_{AC}, J_{BC}) 0.2, $J_{CD} = 7.2$
CCl ₃ CON(CH ₃) ₂	-26.8	132.9	150.5			
CF ₃ CON(CH ₃) ₂	25	217.3 ^f	224.7 ^f			$2J_{AC} = J_{BC} = 1.4$
CH ₂ =CHCON(CH ₃) ₂	4.3	215.3	224.8	"vinyl" spectrum ^h		$J_{AC} = J_{BC} = 0.0$
C ₆ H ₅ CON(CH ₃) ₂ ^c	-26.6	202.9	212.1	-60.7 (C ₆ H ₅)		$J_{AC} = J_{BC} = 0.0$
CICON(CH ₃) ₂	-24.2	209.8	216.3			
CH ₃ CH ₂ OCON(CH ₃) ₂	25	229.5		158.2(CH ₂) ^f	332.7(CH ₃) ^g	$J_{AC} = J_{BC} = 0.0, J_{CD} = 6.8$
CH ₃ OCON(CH ₃) ₂	25			170.9		$J_{AC} = J_{BC} = 0.0$
Fluorine spectra						
-N(CH ₃) ₂ Group						
CH ₃ CON(CF ₃) ₂	25	-315.2 ^f	701.8 ⁱ			$J_{AC} = J_{BC} = 5.6$
CH ₃ OCON(CF ₃) ₂	25	-315.6				$J_{AC} = J_{BC} = 0.0$
CH ₃ CON(CH ₃) ₂	25		462.7 ^j			$2J_{AC} = J_{BC} = 1.4$

^a Chemical shifts in c.p.s. (increasing with the applied field) for protons are relative to the ring protons of toluene as external reference and are relative to 1,2-dibromo-1,1,2,2-tetrafluoroethane as external reference for fluorine. Reference tubes were 1-mm. Pyrex capillaries concentric to sample tubes. ^b All $J_{AB} = 0.0$ c.p.s. ^c A 36.34 mole % amide solution in dibromomethane. ^d Center of a resolved 1:1 doublet. ^e Center of a poorly resolved 1:3:6:10:12:12:10:6:3:1 multiplet. ^f Center of a resolved 1:3:3:1 quartet. ^g Center of a resolved 1:2:1 triplet. ^h Thirteen of the 15 theoretical lines of the ABC "vinyl" spectrum were observed; the intensities of two of the three combination lines were apparently too small for observation. ⁱ Center of a resolved 1:6:15:20:15:6:1 septet. ^j Center of a resolved 1:3:6:10:12:12:10:6:3:1 multiplet.

o.d., straight to within 0.003 in. over an 8 in. length, and with hemispherical bottoms. Samples were thoroughly degassed and sealed *in vacuo*.

Materials.—The materials employed were purified by fractional distillation *in vacuo* or by repeated recrystallization. Some were commercial products and some were prepared in this Laboratory. Methyl-N,N-bis-(trifluoromethyl)-carbamate and perfluoro-N,N-dimethylacetamide were the gift of Profs. R. Dresdner and J. A. Young, University of Florida. Experimental and literature values for physical constants agreed for all the materials used except N,N-dimethyltrichloroacetamide, for which no literature values were found. This material, prepared in this Laboratory, had b.p. 85.2° (5 mm.). Calcd. for C₄H₆ONCl₃: C, 25.22; H, 3.18; N, 7.36; Cl, 55.85. Found: C, 25.43; H, 3.25; N, 7.52; Cl, 55.66.

Experimental Method.—High-resolution n.m.r. spectra for the amides were obtained at a series of temperatures. A linear sweep rate of ~0.012 p.p.m./sec. was used. Internal frequency separations were measured by the audio-sideband technique and counted with a calibrated electronic frequency counter (Hewlett-Packard Model 521 A). The chemical-shift difference $\delta\nu$ between lines of the resolved -N(CH₃)₂ doublet was taken as the largest measurable value which was the limiting maximum value at the lower temperatures. The ratio of the average of the intensity maxima of the two components of the doublet to the central minimum was taken from the spectrum as recorded on a Varian Associates modified Model G-10 recorder. The average of the base lines on either side of the doublet was the zero of intensity. All spectra were recorded at the same value of the applied RF field H_1 which was always much below the lowest value giving noticeable RF saturation and at the maximum time-constant setting of the frequency response control of the spectrometer. From eight to twelve spectra were obtained at each temperature, half being recorded with increasing and half with decreasing linear sweep fields. The probe was moved slightly between each pair of observations to search for increasing field homogeneity. Field homogeneity was repeatedly checked by observing the beating and/or decay of "wiggles" on rapid-passage for standard samples of acetaldehyde and/or pentachloroethane, respectively.

Results

Chemical shifts ($\nu - \nu_{ref}$), in c.p.s., for the principal lines in the n.m.r. spectra of the substances studied are listed in Table I. All lines were measured at a spectrometer frequency $\nu_0 = 60,000$ Mc. Proton chemical shifts are relative to the ring

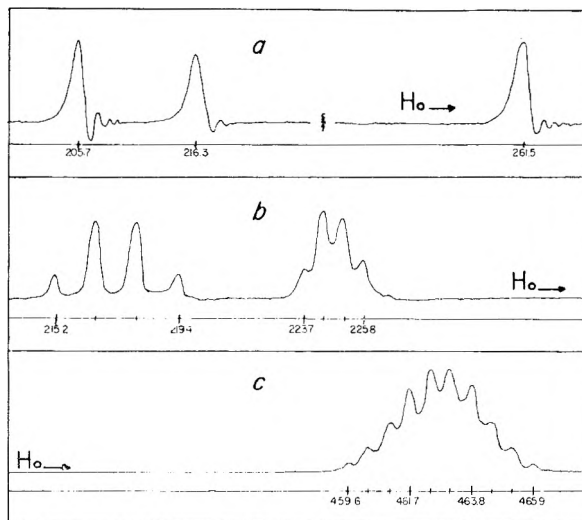


Fig. 1.—The 60,000 Mc. n.m.r. spectra of N,N-dimethylacetamide (DMA) and N,N-dimethyltrifluoroacetamide (DM-TFA); (a) proton resonance of DMA, (b) proton resonance of DM-TFA, and (c) fluorine resonance of DM-TFA.

protons of toluene as an external reference and fluorine chemical shifts are relative to 1,2-dibromo-1,1,2,2-tetrafluoroethane as an external reference. Where two values are quoted for an -NR₂ group, they represent the limiting maximum separation observed for the doublet at the temperature shown.

The p.m.r. spectrum of DMA is shown in Fig. 1a. The high-field line at 261.5 c.p.s. arises from the C-methyl protons and the doublet at 205.7 and 216.3 c.p.s. is due to the protons of the two non-equivalent N-methyl groups. Very weak non-equivalent spin-spin coupling of the C-methyl protons with the protons of each N-methyl group causes the effective natural line width for the high-field N-methyl group to be broader than that for the low-field N-methyl group. These spin-spin couplings could not be resolved. A similar, but much smaller, difference in line width is observed

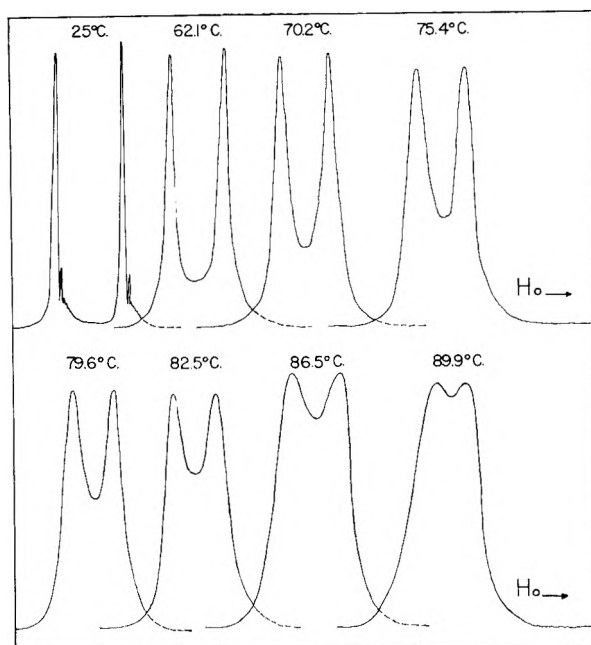


Fig. 2.—The p.m.r. spectrum of *N,N*-dimethyltrifluoroacetamide at various temperatures under conditions of double irradiation; $\nu_0 = 60.000$ Mc., $\nu_1 = 56.452$ Mc. The linear sweep rate and recorder gain were not exactly the same for all the doublets shown.

for the two *N*-methyl resonances in *N,N*-dimethylpropionamide (DMP) but was not noticeable for *N,N*-dimethylacrylamide and *N,N*-dimethylbenzamide (DMB).

The p.m.r. spectrum of *N,N*-dimethyltrifluoroacetamide is shown in Fig. 1b and the fluorine resonance spectrum is shown in Fig. 1c. Non-equivalent spin-spin coupling of the protons of the two non-equivalent *N*-methyl groups with the fluorine nuclei of the *C*-trifluoromethyl group produces the two p.m.r. quartets. These two quartets are simplified to a single doublet by decoupling the proton-fluorine spin-spin interactions by irradiating the sample with a strong 56.452 Mc. fluorine-resonance RF field in addition to the weak 60.000 Mc. proton-resonance RF field. The doublet resulting from the double irradiation of *N,N*-dimethyltrifluoroacetamide at various temperatures is shown in Fig. 2. The similarity of the line widths for the components of each doublet is a good indication of the completeness of the fluorine-proton decoupling. These doublets are representative of those observed for many of the other amides studied without double irradiation.

The mean lifetime of protons at sites A and B (as in I), τ_A and τ_B , respectively, must be equal and the quantity $\tau = [\tau_A\tau_B/\tau_A + \tau_B]$ may be related to the ratio r of maximum to central minimum ν -mode intensities for the $-N(CH_3)_2$ doublet by the equation

$$\tau\delta\nu = \pm \frac{1}{\pi\sqrt{2}} \cdot \sqrt{r \pm (r^2 - r)^{1/2}} \quad (1)$$

for $\pi\sqrt{2}\tau\delta\nu > 1$

where $\delta\nu$ is the chemical-shift difference between the two *N*-methyl resonances A and B in the absence of rotational averaging. Equation 1 implies that the effect of overlap of the components of the

doublet is negligible [$1/\tau_{2A} \ll \langle\delta\nu\rangle > 1/T_{2B}$, where $2/T_{2A}$ and $2/T_{2B}$ are the line widths at one-half maximum intensity of the components A and B, respectively, in radians per second (r.p.s.), and in the absence of rotational averaging]. It also assumes that the fraction of protons is the same at each site ($P_A = P_B$, $\tau_A = \tau_B = 2\tau$), that RF saturation is negligible, and that "slow-passage" conditions are maintained. Equation 1 is easily derived from equation A1 in the Appendix by imposing the first and second restrictions just mentioned and by defining $r = (\nu_{\max.}/\nu_{\min.}) = [\nu(2\Delta\omega = \delta\omega_e)/\gamma(\Delta\omega = 0)]$, where $\delta\omega_e$ is given by equation 6 of ref. 3. Negligible RF saturation and "slow-passage" conditions already are implied by equation A1. The assumption that the overlap effect is negligible is not valid for all the amides studied. The method used for correcting for the effect of overlap for these amides is discussed in the Appendix.

The experimental activation energy E_a , here identified with the barrier height restricting internal rotation about the central C-N bond of the amide, is obtained from the measurements of the rate of internal rotation ($1/2\tau$) at a series of temperatures by fitting the data to the Arrhenius equation

$$\log(1/2\tau) = \log A - E_a/2.3026RT \quad (2)$$

Values of E_a and the frequency factor A were derived from linear plots of $\log(1/2\tau)$ vs. $10^3/2.3026RT$ by the method of least squares. To illustrate the precision of the present measurements the Arrhenius plots for the compounds studied are shown in Fig. 3.

The activation energies and frequency factors obtained from these plots are shown in Table II along with the free energies of activation ΔF^* based on the absolute reaction rate theory. Coalescence temperatures T_c also are given. The free energies of activation are computed from the relationship

$$\Delta F_T^* = 2.3026RT \log \left(\frac{2\tau\kappa kT}{h} \right) \quad (3)$$

where τ is taken from the Arrhenius plot as the least-squared value at the temperature T . Transmission coefficients κ are assumed to be unity. Each coalescence temperature is taken from the least-squared Arrhenius plot as the lowest temperature for which r is unity.

The precision obtained by use of this method is satisfactory for most of the substituted *N,N*-dimethylamides studied because values of $\delta\nu$ were large enough that overlap of the doublet components could be neglected (*i.e.*, $1/T_{2A} \ll \langle\delta\nu\rangle > 1/T_{2B}$), the ratio r could be measured quite precisely, and the changes in r are more pronounced than changes in line widths or changes in apparent chemical-shift differences. The chief disadvantage was the limited temperature range (about 25°) which could be used. The data of Table III, from which the Arrhenius plot for *N,N*-dimethyltrifluoroacetamide in Fig. 3 was drawn, illustrate the magnitude of the average deviations in r and in $\log(1/2\tau)$ in a typical case. The limits of E_a and $\log A$ were computed for each compound for 90% confidence using conventional statistical

TABLE II

VALUES OF E_a , $\log A$, $\Delta F^*_{298.2}$ AND T_c FOR HINDERED INTERNAL ROTATION ABOUT THE CENTRAL C-N BOND OF SOME SUBSTITUTED N,N-DIMETHYLAMIDES AS DETERMINED BY PROTON MAGNETIC RESONANCE SPECTROSCOPY^{a,b} ($\nu_0 = 60,000$ Mc.)

Amide	E_a , kcal./mole	$\log A$	$\Delta F^*_{298.2}$, kcal./mole	T_c , °K.
N,N-Dimethylformamide	18.3 ± 0.7	10.8 ± 0.4	21.0	421.6
N,N-Dimethylacetamide	10.6 ± .4	7.8 ± .2	17.4	360.3
N,N-Dimethylpropionamide	9.2 ± .7	7.3 ± .5	16.7	334.4
N,N-Dimethyltrifluoroacetamide	9.3 ± .6	6.8 ± .4	17.6	367.9
N,N-Dimethyltrichloroacetamide	9.9 ± .2	9.1 ± .2	14.9	287.1
N,N-Dimethylacrylamide	6.8 ± .7	6.0 ± .5	16.1	
N,N-Dimethylbenzamide ^c	7.7 ± .5	7.2 ± .4	15.3	284.9
N,N-Dimethylcarbamyl chloride	7.3 ± .5	6.1 ± .3	16.5	326.0

^a These results are all derived from equations 1, 2, and 3 without corrections for the effect of overlap of the components of the chemical-shift doublets. ^b The values and errors given include the limits of 90% confidence. ^c A 36.34 mole % amide solution in CH_2Br_2 .

methods. For N,N-dimethyltrifluoroacetamide these limits (Table II) are 9.3 ± 0.6 kcal./mole in E_a and 6.8 ± 0.4 in $\log A$.

TABLE III

TEMPERATURE DEPENDENCE OF THE RATE OF INTERNAL ROTATION ABOUT THE CENTRAL C-N BOND OF N,N-DIMETHYLTRIFLUOROACETAMIDE^a

$\nu_0 = 60,000$ Mc., $\delta\nu = 7.48 \pm 0.30$ c.p.s. at 21.4°

t , °C.	$10^3/2.3026RT$, mole/kcal.	τ	$\log(1/2\tau)^b$
89.87 ± 0.11	0.6020 ± 0.0002	1.066 ± 0.008	1.1584 ± 0.0040
86.48 ± .06	.6077 ± .0001	1.221 ± .014	1.1002 ± .0041
82.54 ± .07	.6144 ± .0001	1.527 ± .023	1.0283 ± .0044
79.62 ± .07	.6195 ± .0001	1.843 ± .011	0.9756 ± .0016
76.47 ± .04	.6251 ± .0001	2.324 ± .012	0.9153 ± .0013
75.40 ± .04	.6270 ± .0001	2.426 ± .031	0.9045 ± .0042
70.21 ± .15	.6365 ± .0003	3.513 ± .069	0.8146 ± .0004
62.07 ± .11	.6519 ± .0002	5.822 ± .185	0.6975 ± .0701

^a The errors given are the average deviations from the average of five or more measurements. ^b These values were calculated from equation 1.

The slope $b = -E_a$ and the intercept $a = \log A$ of the linear plot of $y = \log(1/2\tau)$ vs. $x = 10^3/2.3026 RT$ were found by the method of least squares. The limits of 90% confidence in E_a are given by¹³

$$-b \pm t\sigma / \left(\sum_i |x_i - \bar{x}|^2 \right)^{1/2} \quad (4)$$

where \bar{x} is the average of the n values of x_i and

$$\sigma^2 = \left[\sum_i y_i^2 - a \sum_i y_i - b \sum_i x_i y_i \right] / (n - 2) \quad (5)$$

t depends on the number of degrees of freedom ($n - 2$) and the confidence limits and converts the standard error to the confidence limits desired. The limits of 90% confidence in $\log A$ were computed from

$$a \pm t\sigma \left[\sum_i x_i^2 / n - \sum_i |x_i - \bar{x}|^2 \right]^{1/2} \quad (6)$$

Attempts to measure E_a by other methods did not yield satisfactory results for the compounds studied here. The method of Piette and Ander-

(13) J. F. Kenney and E. S. Keeping, "Mathematics of Statistics," part two, 2nd ed., D. Van Nostrand Co., Inc., New York, N. Y., 1951, pp. 207-211, 416-417.

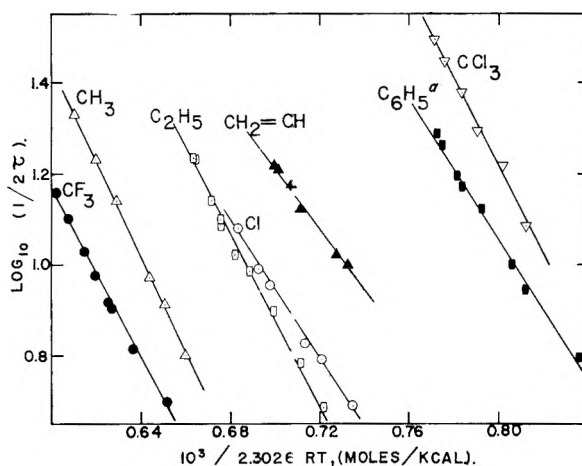


Fig. 3.—Arrhenius plots for the process of internal rotation about the central C-N bond of amides of the type $\text{RCON}(\text{CH}_3)_2$. Each curve is designated with the appropriate functional group R. ^a A 36.34 mole % amide solution in CH_2Br_2 .

son⁷ did not yield a reliable value for E_a in DMP since the range of line widths that could be used was small (0.3 to 3.0 c.p.s.) and the errors in measurement of the widths large (± 0.3 c.p.s.). The method of Gutowsky and Holm³ was applied to DMF but the limits of 90% confidence in E_a were 14.3 ± 3 kcal./mole. In the region of slow rotational rates $\delta\nu_{\text{obsd}}$ can be obtained precisely but it is very insensitive to τ . Near coalescence, $\delta\nu_{\text{obsd}}$ becomes quite sensitive to τ but the former cannot be measured precisely because of the line broadening which accompanies the averaging process.

Neglecting the effect of overlap of the components of the N-methyl doublet we find $E_a = 10.6 \pm 0.4$ kcal./mole and $\log A = 7.8 \pm 0.2$ in DMA (Table II). When the overlap corrections are made, as discussed in the Appendix, the values $E_a = 11.6 \pm 0.8$ kcal./mole and $\log A = 8.4 \pm 0.6$ are obtained. For DMF, each component of the N-methyl chemical-shift doublet consists of a resolvable spin-spin doublet (Table I). Neglecting the effect of overlap of these components we find $E_a = 18.3 \pm 0.7$ kcal./mole and $\log A = 10.8 \pm 0.4$ in DMF. The appropriate corrections⁵ for the effect of overlap would increase the uncorrected values we find for E_a and A in DMF. Overlap corrections for all the other amides studied are estimated to be smaller than the normal experimental errors given in Table II.

Discussion

The energy barrier hindering internal rotation about the central C-N bond of DMA is 11.6 ± 0.8 kcal./mole, in agreement with the value 12 ± 2 kcal./mole reported earlier by Gutowsky and Holm.³ Without making the appropriate corrections⁵ for the spin-spin splitting and the overlap of the chemical-shift doublet we find $E_a = 18.3 \pm 0.7$ kcal./mole for the barrier hindering rotation in DMF. This value is at variance with two values, 7 ± 3 kcal./mole³ and 3.6 ± 1.5 kcal./mole⁵ reported earlier. We cannot offer an explanation for these large discrepancies. Our data for DMF,

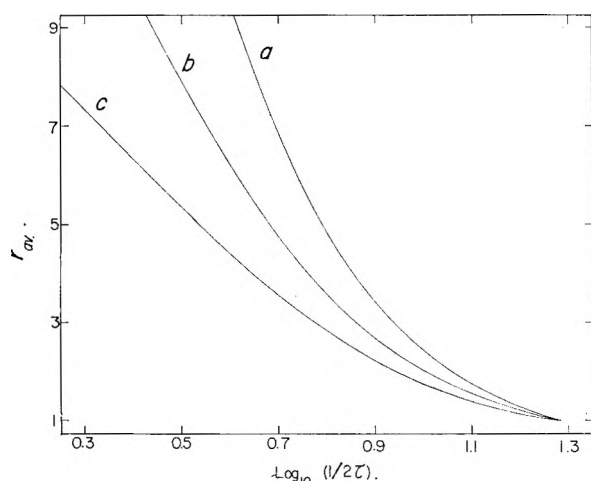
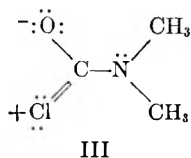


Fig. 4.—Plots of $r_{av.}$ vs. $\log(1/2\tau)$ for $P_A = P_B = 1/2$, $\delta\omega = 66.288$ r.p.s., and (a) $1/T_{2A} = 2.20$ r.p.s., $1/T_{2B} = 1.90$ r.p.s., (b) $1/T_{2A} = 4.30$ r.p.s., $1/T_{2B} = 3.80$ r.p.s., (c) $1/T_{2A} = 6.46$ r.p.s., $1/T_{2B} = 5.70$ r.p.s.

with the appropriate corrections for the spin-spin couplings and the effect of overlap of the chemical-shift doublet, would give a value for E_a greater than 18.3 kcal./mole. These corrections are estimated to be of the order of +1 to +2 kcal./mole. Our uncorrected value is in agreement with an earlier value of about 18 kcal./mole¹⁴ for the barrier height in DMF. These high barriers are the same as the value 18 ± 3 kcal./mole reported⁴ for the barrier height restricting internal rotation about the C-N bond in formamide.

The values of E_a for DMP (9.2 ± 0.3 kcal./mole), N,N-dimethyltrichloroacetamide (9.9 ± 0.3 kcal./mole) and N,N-dimethyltrifluoroacetamide (9.3 ± 0.6 kcal./mole) are smaller than for DMA but the differences are not very large compared to the errors involved. Since the $-\text{CF}_3$, $-\text{CCl}_3$, $-\text{C}_2\text{H}_5$, and $-\text{CH}_3$ groups differ greatly in ability to withdraw electrons, in ability to participate in hyperconjugation, and in size it does not appear that these factors influence the barrier heights very strongly.

The barrier height is significantly smaller in N,N-dimethylacrylamide, $E_a = 6.8 \pm 0.7$ kcal./mole, and in N,N-dimethylcarbonyl chloride (DMCC), $E_a = 7.3 \pm 0.3$ kcal./mole. In these compounds cross-conjugation as represented by structure III (for example) may tend to reduce the double bond character of the central C-N by competing with the resonance form to which the major portion of the energy barrier is attributed (structures analogous to II). The lower barrier in DMB (7.7

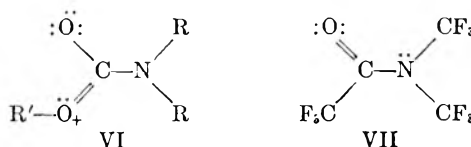


± 0.5 kcal./mole) could similarly result from cross-conjugation. The latter value was measured in a 36.3 mole % solution of DMB in dibromomethane so it is not directly comparable with the other

(14) Technical Information Bulletin from the Radio-frequency Spectroscopy Laboratory of Varian Associates, Instruments Division, Vol. 2 of Series A, No. 28, Palo Alto, California, 1957.

values. However, it should be comparable with the value for DMP in a 36.3 mole % solution in dibromomethane and with the value for DMCC in a 36.3 mole % solution in dibromomethane, which are estimated to be 9.7 ± 0.7 and 8.5 ± 0.6 kcal./mole, respectively.^{15,16}

A number of N,N-disubstituted amides failed to show the expected doublet for the $-\text{NR}_2$ resonance, even at the lowest temperatures at which we were able to make observations. Thus ethyl N,N-dimethylcarbamate, $\text{R} = \text{CH}_3$ and $\text{R}' = \text{C}_2\text{H}_5$ in VI, and methyl N,N-bis-(trifluoromethyl)-carbamate, $\text{R} = \text{CF}_3$ and $\text{R}' = \text{CH}_3$ in VII, show a single sharp resonance line for the $-\text{NR}_2$ group down to their respective freezing points. The spectrum of perfluoro-N,N-dimethylacetamide (VII) consists of a single 1:3:3:1 spin-spin quartet for the $\text{N}(\text{CF}_3)_2$ group at temperatures down to the freezing point. One cannot say whether in these cases the chemical-shift differences between the $-\text{NR}_2$ groups are zero or whether the exchange rates ($1/2\tau$) between the



sites remain rapid down to the freezing points. For the carbamates cross-conjugation involving important structures such as VI would tend to make the two C-O bonds more similar. Since the chemical-shift difference $\nu_A - \nu_B$ depends¹⁷ extensively on the magnetic anisotropies of these bonds, it seems likely that the similarity of the two C-O bonds results in a small chemical-shift difference. To the extent that structures such as VI contribute to the ground state the barrier restricting internal rotation about the central C-N bond would, of course, be correspondingly lower. Both effects may operate simultaneously.

The failure to detect a chemical-shift difference between the N-trifluoromethyl groups in VII is quite unexpected since the barrier height might be expected to be about the same as that for N,N-dimethyltrifluoroacetamide (9.3 ± 0.6 kcal./mole). Possibly the chemical-shift difference between the N-trifluoromethyl groups of perfluoro-N,N-dimethylacetamide is very small even under conditions of no rotational averaging about the central C-N bond. The strongly electron-withdrawing trifluoromethyl groups bonded directly to nitrogen may, however, suppress the double-bond character of the central C-N bond. This latter effect would suppress the energy barrier and, to the extent it is important in VII, it also would be operative in methyl-N,N-bis-(trifluoromethyl)-carbamate.

(15) J. C. Woodbrey and M. T. Rogers, *J. Am. Chem. Soc.*, **84**, 13 (1962).

(16) It has been pointed out by a referee that the differences among barrier heights in the different pure materials may be, at least in part, solvent effects, since each is measured in a different solvent—namely itself. One might expect that these disubstituted amides would be rather similar as solvents so that at least the large differences among the barriers should be significant. However, until measurements of a variety of these compounds are made in a single solvent this point will not be settled.

(17) P. T. Narasimhan and M. T. Rogers, *J. Phys. Chem.*, **63**, 1388 (1959).

The experimental frequency factors A (Table II) obtained from the Arrhenius equation vary between 10^6 and 10^{10} sec.⁻¹. These are much lower than kT/h and suggest that the transmission coefficients κ of the Eyring rate expression are low for these internal rotations if Laidler's suggestion¹⁸ that internal rotations have low entropies of activation is true. As a consequence of the low frequency factors the free energies of activation, as calculated from equation 3 with $\kappa = 1$, are much larger than the energy values E_a determined from the Arrhenius equation.

It should be noted that in DMF the N-methyl protons resonating at higher field are coupled *stronger* to the aldehydic proton than are the N-methyl protons resonating at lower field; see Fig. 1 and Table I. A similar but much less pronounced effect is observed in DMA and DMP. These latter interactions are rare examples of H-H coupling through five bonds. In these amides the *trans* coupling presumably exceeds the *cis* coupling as in the case of ethylenic-type fragments.¹⁹ Here the interpretation requires that the N-methyl protons *cis* to oxygen resonate at higher field than those *trans* to oxygen, a reasonable assumption in view of the high magnetic anisotropy of the C=O bond¹⁷ and the high electron density surrounding the oxygen atom. In contrast, in N,N-dimethyltrifluoroacetamide the protons resonating at higher field are coupled more weakly to the fluorine nuclei than are the protons resonating at lower field. Providing the protons *cis* to oxygen in this amide resonate at the higher field, so that $|J_{cis\ H-F}| = 2|J_{trans\ H-F}|$, then the *cis* H-F coupling observed here must involve a mechanism strikingly different from that for H-H coupling. The above interpretation of the *cis-trans* relationships suggests that a through-space electron-coupling mechanism, rather than a through-bond mechanism, may dominate for H-F coupling in cases where the proton and fluorine nuclei are very proximate but not directly bonded to each other. It has been suggested²⁰ that such a through-space mechanism may be responsible for a rare H-F coupling of nuclei separated by five bonds. The interactions in N,N-dimethyltrifluoroacetamide are other rare examples of H-F coupling of nuclei separated by five bonds. In particular, the *trans* coupling in this amide, probably with $|J_{HF}| = 0.7$ c.p.s., is a very rare case of H-F coupling *through* five bonds; it is unlikely that this *trans* coupling could involve any through-space mechanism.

Appendix

To correct for the effect of overlap of the -N(CH₃)₂ chemical-shift doublet the lines arising from the spin-spin couplings of the N-methyl protons with other nuclei are not treated individually. Rather, only the effect of such interactions on the apparent natural line width of each N-methyl resonance is considered. This restriction leads to no serious limitations in the amides studied, except

(18) K. J. Laidler, "Chemical Kinetics," McGraw-Hill Book Co., Inc., New York, N.Y., 1950, pp. 105-108, 382-387.

(19) M. Karplus, *J. Chem. Phys.*, **30**, 11 (1959).

(20) D. R. Davis, R. P. Lutz, and J. D. Roberts, *J. Am. Chem. Soc.*, **83**, 246 (1960).

in DMF⁵ where the formyl-methyl proton-proton couplings can be resolved; see Table I.

The non-equivalent couplings of the protons of each N-methyl group of DMA with the C-methyl protons are the cause of the different apparent natural line widths for the two N-methyl resonances. Each N-methyl proton resonance line actually consists of an envelope resulting from an unresolved 1:3:3:1 spin-spin quartet. Because the widths of these envelopes are different, the resulting -N(CH₃)₂ doublet has considerable asymmetry. The numerical solutions²¹ for the exchange averaging of a symmetrical spin-spin doublet therefore are not valid for the -N(CH₃)₂ doublet of DMA. To account for the asymmetry we have solved the appropriate equations numerically.

Following Gutowsky and Holm,³ for the more general case of a completely asymmetrical doublet, their equation 3 may be rewritten as

$$v = \frac{-\omega_1 M_0 \left\{ P \left[1 + \tau \left(\frac{P_E}{T_{2A}} + \frac{P_A}{T_{2B}} \right) \right] + QR \right\}}{P^2 + R^2} \quad (\text{A } 1)$$

where

$$P \equiv \tau \left[\frac{1}{T_{2A}T_{2B}} - \Delta\omega^2 + \left(\frac{\delta\omega}{2} \right)^2 \right] + \frac{P_B}{T_{2B}} + \frac{P_A}{T_{2A}} \equiv S - \tau\Delta\omega^2$$

$$Q \equiv \tau \left[\Delta\omega - \frac{\delta\omega}{2} (P_A - P_B) \right]$$

$$R \equiv \Delta\omega \left[1 + \tau \left(\frac{1}{T_{2A}} + \frac{1}{T_{2B}} \right) \right] + \frac{\delta\omega}{2} \left(\frac{1}{T_{2B}} - \frac{1}{T_{2A}} \right) + \frac{\delta\omega}{2} (P_A - P_B)$$

Similarly, for the more general case, their equation 5 becomes

$$2\tau^2 A \Delta\omega^5 + 3\tau^2 B \Delta\omega^4 + 4\tau^2 C \Delta\omega^3 + (BD - AE)\Delta\omega^2 + 2(CD - AF)\Delta\omega + (CE - BF) = 0 \quad (\text{A } 2)$$

where

$$A \equiv \tau^2 \left(\frac{P_A}{T_{2A}} + \frac{P_B}{T_{2B}} \right), \quad B \equiv \tau^2 \delta\omega \left(\frac{P_B}{T_{2B}} - \frac{P_A}{T_{2A}} \right),$$

$$C \equiv \tau \left(\frac{\delta\omega}{2} \right)^2 \left[1 - (P_A - P_B)^2 + \frac{A}{\tau} \right] + \frac{\tau}{T_{2A}T_{2B}} \left[1 + P_A^2 + P_B^2 + \tau \left(\frac{P_A + P_B}{T_{2A}T_{2B}} \right) \right] + \tau P_A P_B \left(\frac{1}{T_{2A}^2} + \frac{1}{T_{2B}^2} \right) + \frac{A}{\tau^2}$$

$$D \equiv \left[1 + \tau \left(\frac{1}{T_{2A}} + \frac{1}{T_{2B}} \right) \right]^2 - 2\tau S$$

$$E \equiv \delta\omega \left[1 + \tau \left(\frac{1}{T_{2A}} + \frac{1}{T_{2B}} \right) \right]$$

$$\left[P_A - P_B + \tau \left(\frac{1}{T_{2B}} - \frac{1}{T_{2A}} \right) \right]$$

$$F \equiv S^2 + \left(\frac{\delta\omega}{2} \right)^2 \left[P_A - P_B + \tau \left(\frac{1}{T_{2B}} - \frac{1}{T_{2A}} \right) \right]^2$$

The effect of overlap on the apparent separation $\delta\omega_\infty$ of the two A and B resonance lines in the absence of exchange is obtained by letting $\Delta\omega \rightarrow \Delta\omega_\infty$ as $\tau \rightarrow \infty$ in equation A2. The resulting equation, fifth order in $\delta\omega$, may be used to correct for the effect of overlap on the apparent separation of any two Lorentzian line shapes.

(21) "Tables of Exchange Broadened Multiplets," Technical Note No. 2, Contract AF 61 (052)-03, The Weizmann Institute of Science, Rehovot, Israel, 1958.

Equations A1 and A2 were programmed to a Bendix G-15 digital computer. This program allows one to calculate from equation A2 the set of positions of the maxima and of the central minimum in the shape function ν corresponding to a set of values for the rate of internal rotation ($1/2\tau$). Then, in the same program, the set of intensities of ν_{\max} and ν_{\min} corresponding to the same set ($1/2\tau$) are computed from equation A1. These programs²² allow one to obtain by direct computations the apparent line separations and the relative values of the maxima and central minimum intensities for any Lorentzian doublet as a function of the rate of averaging between the two sites. In addition, the programs may be used for the direct computation of the line position and of relative intensities ν_{\max} for the *coalesced* doublet²³ as a function of the rate of averaging.

For each amide studied the fraction of protons P_A and P_B at each site A and B, respectively, must always be the same; *i.e.*, $P_A = P_B = 1/2$. The apparent natural line widths, $1/\pi T_{2A}$ and $1/\pi T_{2B}$

(22) Copies of the programs may be obtained from J. C. W.

(23) M. Takeda and E. O. Stejskal, *J. Am. Chem. Soc.*, **81**, 62 (1959).

in c.p.s. were the limiting minimum values measured directly from the p.m.r. spectra at the lower temperatures. The effect of overlap on the apparent separation of the two $-\text{N}(\text{CH}_3)_2$ resonance lines was negligible in the absence of internal rotation for each amide studied; *i.e.*, $\delta\omega \simeq \delta\omega_m$.

When obtaining the rates of internal rotation from the ratios of intensities (except for DMF) the only one of the amides studied for which the apparent natural line widths could not be neglected was DMA. Changes in the apparent natural line widths for DMA due to changes in the applied field homogeneity were determined from the width of the C-methyl resonance line at each temperature. The ratio of the average of the maxima to central minimum intensities r_{av} was computed from equations A1 and A2 for the appropriate values of $1/T_{2A}$ and $1/T_{2B}$ and for different values of τ . Typical plots of r_{av} vs. $\log(1/2\tau)$ for representative values of $1/T_{2A}$ and $1/T_{2B}$ are shown in Fig. 4. From such plots, the value of $\log(1/2\tau)$ for DMA was obtained from the observed values of the natural line widths and of r_{av} at each temperature.

NOTES

THERMODYNAMICS OF H-BONDING PYRROLE-PYRIDINES

BY HAROLD J. WIMETTE¹ AND ROBERT H. LINNELL¹

Department of Chemistry, University of Vermont, Burlington, Vt.

Received June 13, 1961

Introduction

H-Bonding equilibrium in the system pyrrole-pyridine has been investigated by several workers. Vinogradov and Linnell² reported a 1:1 H-bonded complex with pyrrole-pyridine in CCl_4 and $K = 2.56$ l. mole⁻¹ (from infrared)³ at room temperature; the heat of formation was determined calorimetrically using pure pyrrole and pyridine (no CCl_4 solvent) to be 3.8 kcal./mole. Fuson and co-workers have reported a number of investigations on pyrrole: an infrared study of solvent effects on the N-H of pyrrole,⁴ and later work⁵ which yielded $K = 2.7 \pm 0.3$ l. mole⁻¹ for the pyrrole-pyridine equilibrium at room temperature in CCl_4 . Halleux⁶ has used infrared to study H-bonding equilibria between various pyridines or anilines and phenol in CCl_4 . None of these workers has made a thermodynamic study. When the present work was almost finished, Happe's⁷ double resonance nuclear magnetic res-

onance study of pyrrole-pyridine association was published, including thermodynamic work.

We were interested in studying the pyrrole-pyridine association with several pyridines and at several temperatures so as to obtain thermodynamic data useful in understanding basicity and steric and solvent clustering effects in acid-base equilibrium.

Experimental

All infrared measurements were made on a Perkin-Elmer Model 112 instrument equipped with a LiF prism. The entire light path was continuously swept with dry air. The source and sample compartment was equipped with a thermostat air-bath consisting of electric heaters, refrigerator coils, air circulating fan, and a thermoregulator-relay, maintaining temperatures to $\pm 0.2^\circ$. A 5-mm. NaCl cavity cell was used for all measurements. Three thermocouples were inserted into holes bored in the cavity cell and temperatures were read on a L. and N. type K-2 potentiometer. A special clamp arrangement held the Teflon plug in the cavity cell and prevented solvent evaporation. Spectra were run after all three thermocouples came to within 0.5° of the same temperature; this thermal equilibrium required from 30-45 min. for each sample. Spectral slit widths of 5-8 cm.^{-1} were used.

Eastman sulfur-free CCl_4 , dried over silica gel, was used as a solvent. The pyridines, obtained from Reilly Tar and Chemical Company, were dried over NaOH pellets and purified by distillation in an all-Pyrex Todd column at high reflux ratio, then stored over NaOH pellets under pre-purified N_2 in the dark. The boiling points of the cuts were found to be: pyridine, 115° ; 2-methylpyridine, 128° ; 2,6-dimethylpyridine, 142° . Pyrrole was given to us by E. I. du Pont de Nemours & Company and was purified by distillation under prepurified N_2 at atmospheric pressure in the Todd column at high reflux. The pyrrole sample had a b.p. of 128° , and was stored under N_2 at -10° . Pyrrole- CCl_4 solutions in contact with air, at room temperature,

(1) Scott Research Laboratories, Inc., Perkasie, Pa.

(2) S. N. Vinogradov and R. H. Linnell, *J. Chem. Phys.*, **23**, 93 (1955).

(3) Recalculated from ref. 2. Original value in mole fraction units.

(4) M. L. Josien and N. Fuson, *J. Chem. Phys.*, **22**, 1169 (1954).

(5) N. Fuson, P. Pineau, and M. L. Josien, *J. chim. phys.*, **55**, 454 (1958).

(6) A. Halleux, *Bull. soc. chim. Belges*, **68**, 381 (1959).

(7) J. A. Happe, *J. Phys. Chem.*, **65**, 72 (1961).

TABLE I

PYRROLE-PYRIDINES H-BONDING EQUILIBRIA^{a,b}

C_x^0, M	C_y^0	C_x	C_y	C_{xy}	$K, l./mole$
A. Pyrrole-Pyridine					
47°					
0.00667	0.0835	0.00600	0.0828	0.00067	1.38
.00667	.125	.00566	.124	.00101	1.47
.00667	.167	.00547	.166	.00120	1.35
.00667	.209	.00512	.207	.00155	1.49
					Av. = 1.42
40°					
0.00675	0.0787	0.00583	0.0778	0.00092	2.05
.00675	.0984	.00552	.0972	.00123	2.35
.00675	.148	.00506	.146	.00169	2.35
.00675	.197	.00485	.195	.00190	2.06
.00675	.246	.00440	.244	.00235	2.25
					Av. = 2.21
33°					
0.00645	0.0426	0.00593	0.0420	0.00057	2.32
.00645	.0532	.00575	.0525	.00075	2.51
.00645	.0798	.00555	.0789	.00095	2.20
.00645	.133	.00505	.132	.00145	2.18
					Av. = 2.30
.00678	.0813	.00565	.0802	.00113	2.53
.00678	.102	.00546	.101	.00132	2.43
.00678	.153	.00498	.151	.00180	2.42
.00678	.203	.00467	.201	.00211	2.28
.00678	.254	.00424	.251	.00254	2.42
					Av. = 2.42
20°					
0.00672	0.0813	0.00554	0.08012	0.00118	2.67
.00672	.102	.00527	.101	.00145	2.74
.00672	.153	.00477	.151	.00195	2.72
.00672	.203	.00435	.201	.00237	2.72
.00672	.254	.00401	.251	.00271	2.69
					Av. = 2.71
12°					
0.00677	0.0632	0.00565	0.0621	0.00112	3.16
.00677	.0790	.00536	.0776	.00141	3.35
.00677	.119	.00493	.117	.00184	3.21
.00677	.158	.00457	.155	.00220	3.05
.00677	.197	.00424	.194	.00253	3.03
					Av. = 3.16
B. Pyrrole-2-Methylpyridine					
47°					
0.00642	0.0628	0.00582	0.0622	0.00066	1.71
.00642	.126	.00522	.124	.00120	1.96
.00642	.189	.00503	.187	.00139	1.52
.00642	.226	.00474	.224	.00168	1.63
.00642	.251	.00459	.249	.00183	1.65
					Av. = 1.69
20°					
0.00609	0.0634	0.00499	0.0622	0.00110	3.55
.00609	.127	.00441	.125	.00168	3.03
.00609	.190	.00383	.186	.00226	3.17
.00609	.228	.00365	.226	.00244	2.97
.00609	.254	.00348	.251	.00261	2.99
					Av. (not including 1st value) = 3.04

12°

0.00609	0.0634	0.00481	0.0621	0.00128	4.24
.00609	.127	.00424	.125	.00185	3.46
.00609	.190	.00370	.188	.00239	3.40
.00609	.228	.00342	.226	.00267	3.44
.00609	.254	.00330	.251	.00279	3.34

Av. (not including 1st value) = 3.41

C. Pyrrole-2,6-Dimethylpyridine

47°

0.00616	0.0554	0.00560	0.0548	0.00056	1.87
.00616	.111	.00510	.110	.00106	1.95
.00616	.166	.00450	.165	.00166	2.30
.00616	.222	.00416	.220	.00200	2.25
.00616	.277	.00385	.275	.00231	2.33

Av. = 2.14

18°

0.00616	0.0554	0.00520	0.0544	0.00096	3.39
.00616	.111	.00427	.109	.00189	4.06
.00616	.166	.00372	.164	.00244	4.00
.00616	.222	.00345	.219	.00271	3.59
.00616	.277	.00310	.274	.00306	3.60

Av. = 3.73

11°

0.00616	0.0554	0.00500	0.0542	0.00116	4.23
.00616	.111	.00430	.109	.00186	3.93
.00616	.166	.00375	.164	.00241	4.89
.00616	.222	.00325	.219	.00291	4.05
.00616	.277	.00292	.274	.00324	4.01

Av. = 4.02

^a Each K represents an average of three separate experimental determinations on the same solution. ^b All concentrations are expressed as M at 20°. For each temperature other than 20° a concentration correction was made by a ratio of densities of the CCl_4 , using density data from the International Critical Tables, Vol. III, p. 28.

slowly deposit a dark brown polymer. In this work, all measurements were made on fresh solutions that showed no visible decomposition.

Since pyrrole associates with itself, solutions sufficiently dilute to avoid this association were used. Experimentally we found no evidence of association below 0.01 M . The recently published equilibrium constant for pyrrole dimerization,⁷ 4.3 mole fraction⁻¹, indicates that about 1% of the pyrrole is dimerized in a 0.01 M solution. As shown in Fig. 1 of the paper by Fuson, Pineau, and Josien⁵ a small shoulder on the long wave length side of the "free" N-H is observed. We measured the absorbancy at 3498 ± 3 cm^{-1} (Fuson, *et al.*, use 3495 cm^{-1}) as a measure of free pyrrole. The shoulder is found at 3480 cm^{-1} . Integrated absorbancy measurements were made on the 3498 - 3480 cm^{-1} bands with pyrrole- CCl_4 solutions from 5×10^{-4} to 4×10^{-3} M (NaCl cells 50-12 and 5 mm.) but attempts made to fit the data to a monomer-dimer equilibrium were unsuccessful. We do not believe the 3480 cm^{-1} shoulder is due to pyrrole association. The explanation for this shoulder remains unclear.

A series of pyrrole- CCl_4 solutions from 2 - 8×10^{-3} mole l^{-1} were made and the peak absorbancy at 3498 cm^{-1} measured at each temperature used in this study. Good straight lines resulted in plotting absorbancy *vs.* concentration for each temperature. Even after temperature-volume corrections the absorbancy decreases as the temperature increases. Figure 1 shows this effect. These curves then were used to determine the concentration of free pyrrole in the pyrrole-pyridine mixtures.

Results and Discussion

The equilibrium constants for pyrrole-pyridine

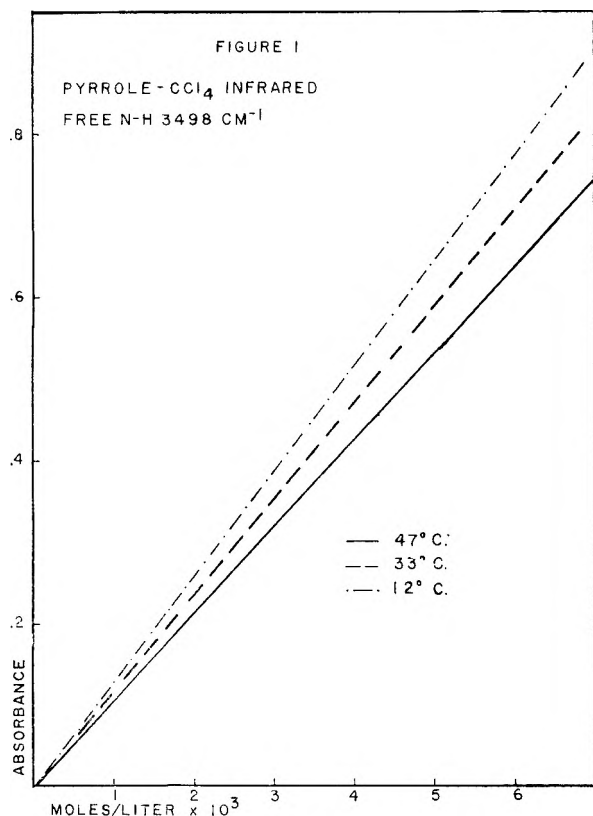


Fig. 1.

association were computed from the equation

$$x + y \rightleftharpoons xy \quad K = \frac{C_{xy}}{C_x \cdot C_y}$$

- x = pyrrole
- y = pyridine or substituted pyridine
- xy = pyrrole-pyridine complex
- C_x^0 = initial pyrrole concentration
- C_y^0 = initial pyridine concentration
- C_x = equilibrium pyrrole concentration
- C_y = equilibrium pyridine concentration
- C_{xy} = equilibrium complex concentration

All of the data are given in Table I. Because of experimental limitations, a large number of determinations were made to minimize errors.

Table II gives the thermodynamic data computed by least squares from $\log K$ vs. $1/T$ plots of the data in Table I. Our solutions are sufficiently dilute to assume ideal behavior.

TABLE II^a

Pyridines	THERMODYNAMIC VALUES FOR PYRROLE-PYRIDINES ALL VALUES IN KCAL. PER MOLE		
	ΔH_{298}^0	ΔF_{298}^0	ΔS_{298}^0
Pyridine	-3.2 (-5.70)	-0.54 (-7.12)	-8.9 (+4.76)
2-Methylpyridine	-3.8 (-6.95)	-.58 (-8.13)	-10.8 (+3.95)
2,6-Dimethylpyridine	-3.4 (-6.15)	-.68 (-9.17)	-9.2 (+10.11)

^a Values in parentheses are for aqueous solutions, $B + H_3O^+ \rightleftharpoons BH^+ + H_2O$, by Mortimer and Laidler.⁸

It is interesting to compare our values with other literature data. Happe⁷ gives $\Delta H^0 = -4.3$ kcal./mole and $\Delta S^0 = -8.0$ for pyrrole-pyridine in cyclohexane solvent. We would not expect such a large difference from our values due simply to

(8) C. T. Mortimer and K. J. Laidler, *Trans. Faraday Soc.*, **55**, 1731 (1959).

solvent effect with our CCl_4 . Comparing with the data of Mortimer and Laidler,⁸ which also are given in Table II, we see that the ΔH^0 values follow the same trend. Adding a methyl group increases the basicity of the pyridine and makes ΔH^0 , ΔF^0 , and ΔS^0 all more negative. In our study, with CCl_4 solvent, it is difficult to imagine any solvent clustering effects and we therefore interpret the less negative ΔH^0 and ΔS^0 of 2,6-dimethylpyridine as due entirely to a steric effect which overshadows the inductive effect of the added methyl group. This interpretation supports the ideas of Mortimer and Laidler.⁸ In their aqueous solutions it is noted that ΔS^0 is very much larger for 2,6-dimethylpyridine; in aqueous solution, ΔS^0 is positive since S^0 of H_3O^+ is very small compared to S^0 for BH^+ . Solvent clustering is greatly decreased in the dimethyl compound, thus giving it an abnormally high entropy and enthalpy. The predicted ΔH^0 for the dimethyl compound, if no steric or solvent effects were operating, would be: (a) aqueous, $-2(6.95-5.70)-5.70 = -8.20$ (observed is -6.15 or 75% of the predicted value); (b) CCl_4 with pyrrole, $-2(3.8-3.2)-3.2 = -4.4$ (observed is -3.4 or 89% of the predicted value). We therefore can conclude that our values for the 2,6-dimethylpyridine reflect a steric effect, only, and that the work of Mortimer and Laidler for aqueous pyridines depends on solvent exclusion.

Acknowledgment.—The authors appreciate helpful discussions with Dr. R. G. Inskeep. Financial assistance from the Research Corporation is gratefully acknowledged.

SOLUBILITIES OF SOME STRONG ELECTROLYTES IN THE HYDROGEN PEROXIDE-WATER SYSTEM. II. RUBIDIUM AND CESIUM NITRATES¹

BY MARTIN E. EVERHARD² AND PAUL M. GROSS, JR.³

Cobb Chemical Laboratory of the University of Virginia, Charlottesville, Va., and the Department of Chemistry of Wake Forest College, Winston-Salem, N. C.

Received July 19, 1961

The solubilities of the smaller alkali metal nitrates in the mixed solvent hydrogen peroxide-water have been reported by Floyd and Gross.⁴ They found that for $LiNO_3$, $NaNO_3$, and KNO_3 that the solubilities in water-rich solutions decreased with increasing cation size and that in the hydrogen peroxide rich solutions, the solubilities increased with increasing cation size. In addition $LiNO_3$ showed a discontinuity in the curve of mole fraction hydrogen peroxide in the solvent vs. molal solubility at low hydrogen peroxide concentrations while the KNO_3 solubility curve showed a discontinuity in the hydrogen peroxide-rich solutions.

(1) This work received support from the Office of Ordnance Research, U. S. Army. The experimental work presented in this paper was carried out at the University of Virginia as a part of the thesis submitted by Martin E. Everhard in partial fulfillment of the requirements for the degree of Doctor of Philosophy in the Graduate School of the University of Virginia, June, 1960.

(2) Philip Francis du Pont Fellow.

(3) To whom inquiries should be directed at Wake Forest College.

(4) J. D. Floyd and P. M. Gross, Jr., *J. Am. Chem. Soc.*, **77**, 1435 (1955).

Subsequent data obtained as a part of this series of studies showed that these discontinuities corresponded to the changes in phase $\text{LiNO}_3 \cdot 3\text{H}_2\text{O}$ - LiNO_3 and $\text{KNO}_3 \cdot 2\text{KNO}_3 \cdot \text{H}_2\text{O}_2$.⁵ This behavior indicated that cation size was an important factor in the solubility relations with varying hydrogen peroxide concentration.

To examine further this possible role of the cation size, the solubilities of RbNO_3 and CsNO_3 were examined as well as the nature of the solid phases in equilibrium with these systems.

Experimental

The hydrogen peroxide⁶ used was 95-98% by weight except the most concentrated solutions, which were obtained by distillation using the method of Gross and Taylor.⁷ The RbNO_3 was prepared from Rb_2CO_3 by a modification of the method of Puschin and Radoicic.⁸ The final material was repurified to the constant melting point of 313° (cor.) of Haigh.⁹ The solubility in water agreed with Jones.¹⁰ Recrystallized C. p. grade CsNO_3 was used.

The solubilities were determined by the method of Floyd and Gross.⁴ Castor and Basolo's¹¹ procedure, as modified by Turner,⁵ was used to analyze the solid phases.

Results

Figures 1 and 2 show the relation of the molal solubilities of RbNO_3 and CsNO_3 to the mole fraction H_2O_2 in the solvent. The discontinuities in the RbNO_3 curves correspond to the changes in phase $\text{RbNO}_3 \cdot 7\text{RbNO}_3 \cdot 3\text{H}_2\text{O}_2$ and $7\text{RbNO}_3 \cdot 3\text{H}_2\text{O}_2 \cdot 2\text{RbNO}_3 \cdot \text{H}_2\text{O}_2$ as determined by analysis of the solid phases on each side of the discontinuities.

The formation of the above hydroperoxidates and the increase in solubility of the salts with larger cations in hydrogen peroxide-rich solutions indicate preferential solvation of these ions by H_2O_2 rather than by H_2O . Conversely, the formation of hydrates and lower solubility in hydrogen peroxide-rich solutions of the smaller cation salts indicate preferential solvation of these ions by water. The deviation of the molal solubility, M' , of the alkali nitrates in H_2O_2 from that in H_2O ($M_{\text{H}_2\text{O}_2}$ minus $M_{\text{H}_2\text{O}}$) at 25° was found to follow the straight line $M' = 33.5r - 39.7 (\pm 0.03 \text{ in } M')$, where r is the radius of the cation. CsNO_3 , however, did not fall on the line, which probably is due to the lower charge density of the cesium ion. The cesium ion would have an effective radius of 1.53 \AA . if it would lie on the above line.

These solubility results cannot be explained in terms of the dielectric constant, ϵ , of these two solvents since $\epsilon_{\text{H}_2\text{O}_2}$ is about 10% lower than $\epsilon_{\text{H}_2\text{O}}$ at the temperature of this work. However, it is possible that the smaller ions depress $\epsilon_{\text{H}_2\text{O}_2}$ more than the larger ions, resulting in a lower solubility of these ions as first suggested by Åkerlöf and Turck.¹² Undoubtedly changes in the activity coefficients occur. These changes will be quite

(5) J. W. Turner, Ph.D. Thesis, University of Virginia, Charlottesville, 1957.

(6) Donated by the Becco Division of the F. M. C. Corporation.

(7) P. M. Gross, Jr., and R. C. Taylor, *J. Am. Chem. Soc.*, **72**, 2075 (1950).

(8) N. A. Puschin and M. Radoicic, *Z. anorg. u. allgem. Chem.*, **42**, 233 (1937).

(9) F. L. Haigh, *J. Am. Chem. Soc.*, **34**, 1144 (1912).

(10) B. M. Jones, *J. Chem. Soc.*, **93**, 1743 (1908).

(11) W. S. Castor, Jr., and F. Basolo, *J. Am. Chem. Soc.*, **75**, 4808 (1953).

(12) G. Åkerlöf and H. E. Turck, *ibid.*, **57**, 1746 (1935).

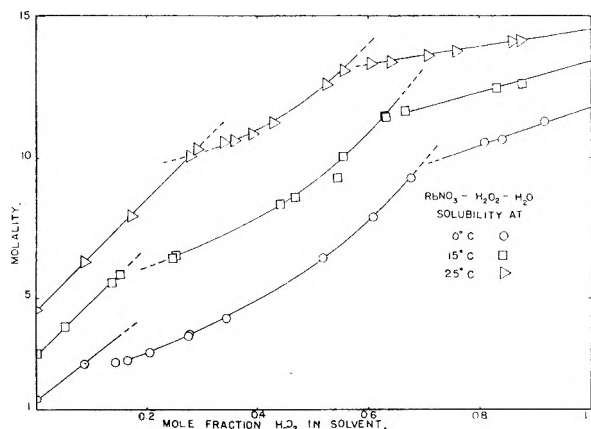


Fig. 1.

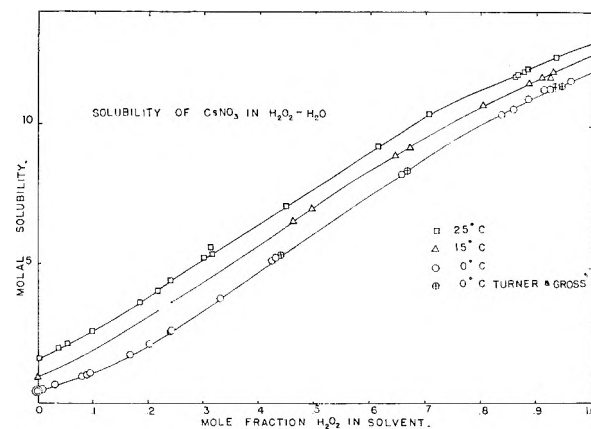


Fig. 2.

significant especially with the formation of new species as occurs in the LiNO_3 , KNO_3 , and RbNO_3 systems. However, since the activity coefficient and the dielectric constant changes of these solutions have not been measured, it is difficult to assess these effects properly.

To determine the extent and the nature of the solvation in these solutions, the vapor pressure, vapor composition, and liquid composition of these solutions have been measured over the full range of H_2O_2 concentrations. These results will be reported in a later paper. They support the contention that the smaller ions are preferentially solvated by the water molecules and the larger ions by hydrogen peroxide molecules.

It is interesting to note that the solubilities of the alkali metal salts in the nitrogen analogs of H_2O and H_2O_2 , ammonia and hydrazine, show decreasing solubility with increasing ion size in both N_2H_4 and NH_3 .¹³⁻¹⁶ Since the N-N distance in hydrazine is about the same as the O-O distance in H_2O_2 , one might expect to observe the same solubility trends in the N_2H_4 - NH_3 system as in the H_2O_2 - H_2O system. The observed difference could be due to the weaker ion-dipole interactions of the nitrogen compounds as compared to those that occur in the oxygen solvents.

(13) H. Hunt and L. Boneyk, *ibid.*, **56**, 3528 (1933).

(14) H. Hunt, *ibid.*, **54**, 3509 (1932).

(15) L. de Bruyn, *Rec. trav. chim.*, **15**, 174 (1896).

(16) T. W. B. Welsh and H. J. Broderick, *J. Am. Chem. Soc.*, **37**, 816 (1915).

THE TRANSFERENCE NUMBER AND
ACTIVITY COEFFICIENT OF
TRIS-(ETHYLENEDIAMINE)-COBALT(III)
CHLORIDE IN WATER AT 25°

BY DAVID J. KARL AND JAMES L. DYE

*Kedzie Chemical Laboratory, Michigan State University, East Lansing,
Michigan*

Received August 21, 1961

In connection with studies of high-charge type electrolytes in this Laboratory, we have measured the transference number and the e.m.f. of cells with transference of solutions of tris-(ethylenediamine)-cobalt(III) chloride $[\text{Co}(\text{en})_3\text{Cl}_3]$ in water as a function of concentration. These data were used to calculate mean activity coefficients for this salt.

Experimental

Materials.— $\text{Co}(\text{en})_3\text{Cl}_3$ was prepared by the method of Work.¹ The crude product was recrystallized three times from ethanol and then a four-step fractional crystallization from 50% ethanol-water was performed. Solutions of constant molality were prepared at each step and the conductivity measured. Constant specific conductance was obtained for the third and fourth fractions. Chloride analysis gave 30.79%; calcd., 30.78%. Solutions were made by weight dilution of a stock solution.

Potassium chloride, lithium chloride and conductivity water (used to prepare all solutions) were purified as described elsewhere.² Traces of bromide in the potassium chloride used for electrode preparation were removed by the method of Pinching and Bates.³

Apparatus.—The transference and conductance apparatus has been described previously.² The cells for e.m.f. studies are of the same type as those used by Spedding, Porter and Wright.⁴ A Leeds and Northrup type K-2 potentiometer and type R galvanometer were used for the e.m.f. measurements. Average readings obtained by switching electrodes and replacing the solutions were reproducible to about ± 0.01 mv.

Results

Transference Numbers.—The transference numbers obtained for $\text{Co}(\text{en})_3\text{Cl}_3$ with lithium chloride as an indicating electrolyte are given in Table I. Volume corrections were made with the aid of solution densities measured with a 50-ml. calibrated pycnometer. Within experimental error, the densities followed the equation

$$\rho = 0.99707 + 0.155m$$

Solvent corrections were made using measured conductances which furnished a smooth extension of the conductance data of Jenkins and Monk.⁵ Conductance data also are given in Table I.

Activity Coefficients.—The cell with transference employed in this work may be represented by



The e.m.f. data and calculated mean molar activity coefficients, γ_{\pm} , are given in Table I. The calculations were made in standard fashion⁶ using the transference data of Table I. Uncertainties

(1) J. B. Work, "Inorganic Syntheses," Vol. II, ed. by W. C. Fernelius, McGraw-Hill Book Co., Inc., New York, N. Y., 1945, p. 221.

(2) J. L. Dye, M. P. Faber and D. J. Karl, *J. Am. Chem. Soc.*, **82**, 314 (1960).

(3) G. D. Pinching and R. G. Bates, *J. Research Natl. Bur. Standards*, **37**, 311 (1946).

(4) F. H. Spedding, P. E. Porter and J. M. Wright, *J. Am. Chem. Soc.*, **74**, 2781 (1952).

(5) I. L. Jenkins and C. B. Monk, *J. Chem. Soc.*, 68 (1951).

TABLE I

EXPERIMENTAL TRANSFERENCE NUMBERS, CONDUCTANCES AND E.M.F. VALUES, AND CALCULATED MEAN MOLAR ACTIVITY COEFFICIENTS OF $\text{Co}(\text{en})_3\text{Cl}_3$

Concn. (moles/l.) $\times 10^3$	T_+ (cor.)	Λ	E.m.f. (mv.)	γ_{\pm}
0.6790	22.83	0.804
1.3805	12.48	.733
1.9718	0.4872	125.0	7.43	.695
3.3735 ^a	0.000	.634
4.668	.4850	114.3	-4.25	.592
7.733	.4836	107.1	-10.73	.528
	.4835			
15.337	.4824	96.7	-18.87	.435
	.4821			
23.651	.4811	90.4	-23.79	.381

^a Used as a reference solution for e.m.f. measurements.

in extrapolation could give rise to a maximum error of $\pm 1\%$ in the absolute values, but the relative values are accurate to at least $\pm 0.2\%$.

TABLE II

SMOOTHED VALUES OF THE MEAN MOLAL ACTIVITY COEFFICIENT OF $\text{Co}(\text{en})_3\text{Cl}_3$

m	γ_{\pm}	m	γ_{\pm}
0.0010	0.766	0.10	0.221
.0025	.669	.25	.148
.005	.583	.50	.101
.010	.495	.75	.0805
.025	.374	1.00	.0691
.05	.296	1.11 ^a	.0659

^a Saturated solution.

Conclusions

The transference numbers form a smooth curve when graphed vs. \sqrt{C} . The extrapolation to $T_+^0 = 0.4945$ as given by the conductance of the $\text{Co}(\text{en})_3^{+++}$ ion⁵ forms a reasonable extension of the experimental curve. The graphical use of the extended Debye-Hückel equation⁷ in an attempt to evaluate the ion-size parameter \bar{a} yielded a curve rather than a straight line, and the value of \bar{a} obtained from the slope of any part of the curve was less than 3.5 Å. This indicates that the activity coefficients lie below the predictions of the Debye-Hückel theory for any reasonable value of \bar{a} . This is in the direction to be expected if ion-association occurs.

The data fit in well with the activity coefficient data of Brubaker⁸ determined by the isopiestic method at higher concentrations, except that his values for $m = 0.01$ and $m = 0.025$ (extrapolated below the experimental range) appear to be high by about 2.7%. The data of Brubaker at higher concentrations fall on a smooth extension of our curve. Table II gives smoothed values of the mean molal activity coefficient, γ_{\pm} , of this salt up to the saturation point.

Acknowledgment.—This work was supported in part by a grant from the National Science Foundation.

(6) D. A. MacInnes and T. Shedlovsky, *J. Am. Chem. Soc.*, **61**, 200 (1939); T. Shedlovsky, *ibid.*, **72**, 3680 (1950).

(7) See for example, F. H. Spedding and J. L. Dye, *ibid.*, **76**, 879 (1954), Fig. 2.

(8) C. H. Brubaker, Jr., *ibid.*, **79**, 4274 (1957).

THERMOLUMINESCENCE OF GOLDEN SAPPHIRE AND FUSED BORAX SEEDED WITH Ni, Mg, AND UO₃

By H. A. WOODBURY, H. EYRING, AND A. F. GABRYSH

Department of Chemistry, University of Utah, Salt Lake City, Utah

Received September 1, 1961

Several investigators¹⁻⁴ have studied absorption and emission properties of α -Al₂O₃ and a number of glasses. Levy and Dienes⁵ have reported on the effects of Co⁶⁰ γ -rays on the light transmission properties of corundum. Gabrysh, *et al.*,⁶ reported on the effects of oxygenation and solarization of synthetic sapphire. Rieke and Daniels⁷ have studied thermoluminescence of various crystal phases of polycrystalline aluminum oxide in the 5 to 425° region. Rieke⁸ also has reported on the thermoluminescence of inorganic crystals and glasses. The object of this study was the influence of impurities and single-crystal structure on thermoluminescence glow curves for samples irradiated at liquid nitrogen temperatures.

Thermoluminescence of golden sapphire (Al₂O₃ containing nickel and magnesium impurities) is first compared to a sample of soda boron oxide glass containing a small amount of nickel, then to a sample containing magnesium, and finally to a sample containing both nickel and magnesium. A comparison also is made of glow curves for various wt. % of UO₃ as the network modifier in the glass structure.

Experimental

Specimens were held in an aluminum holder which was submerged in liquid nitrogen during exposure to a high intensity Co⁶⁰ γ -source. The intensity of the field was determined by standard⁹ ceric sulfate dosimetry as 1.4×10^5 rad/hr. After irradiation the samples immediately were transferred from the liquid nitrogen into a measuring apparatus described elsewhere.¹⁰ The temperature was monitored by an iron-constantan thermocouple placed into a hole which was drilled into the holder next to the sample. Thermoluminescence intensity and specimen temperature (glow curve) were automatically and simultaneously plotted as a function of time by an X-Y recorder.

Four boron oxide glass samples were made by fusing, in a platinum crucible, the following reagents with 5.0-gram portions of Na₂B₄O₇·10H₂O: Sample 1 was a "blank" for background study, sample 2 contained 0.1 g. of NiO, sample 3 contained 0.1 g. of MgO and sample 4 contained 0.1 g. of NiO + 0.1 g. of MgO. Fusion of these mixtures was carried out at $\sim 1000^\circ$ after which thin-rod samples were drawn from the melt. The diameter of the one-inch long glass specimens used in this study was about 0.7 mm. The sliver-like golden sapphire (Al₂O₃ with Ni and Mg impurities) specimen was 4.0 mm. long and had sides of 1 and 2 mm.

(1) R. A. Hunt and R. H. Schuler, *Phys. Rev.*, **89**, 664 (1953).

(2) R. W. Kehler, "Optical Properties of Synthetic Sapphire," F-8727, Linde Air Products Company, Indianapolis, Ind.

(3) R. Bauple, A. Gilles, J. Ramand, and B. Vodar, *J. Opt. Soc. Am.*, **40**, 788 (1950).

(4) G. E. Rindone, Report; Reprinted from the Travaux du IV Congress International du Verre, Paris, 1956.

(5) P. W. Levy and G. J. Dienes, "Report of the Conference of Defects in Crystalline Solids," H. G. Wells Physical Laboratory, University of Bristol, Physical Society, London, 1954, pp. 256-260; *Phys. Rev.*, **94**, 1409 (1954).

(6) A. F. Gabrysh, H. Eyring, and Taikyue Ree, *J. Phys. Chem.*, **65**, 1547 (1961).

(7) J. K. Rieke and F. Daniels, *ibid.*, **61**, 629 (1957).

(8) J. K. Rieke, *ibid.*, **61**, 633 (1957).

(9) J. Weiss, *Nucleonics*, **10**, 28 (1952).

(10) A. F. Gabrysh, V. LeFebvre, M. Evans, and H. Eyring, " γ -Ray Induced Thermoluminescence in α -Al₂O₃," in preparation for publication.

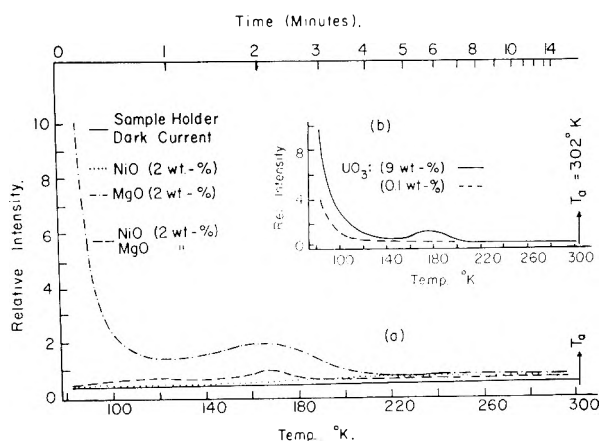


Fig. 1.—(a) Fused borax glow-curve intensity as a function of time and temperature (T_a = ambient room temperature); (b) glow curves for uranium as the network modifier.

Results

Thermoluminescence glow curves are produced after irradiation with γ -rays for samples of fused borax glass seeded with nickel, magnesium, and uranium. All of the thermoluminescence peaks, Fig. 1, are reproducible after successive irradiations and are found to lie in one of three ranges; $\sim 80^\circ\text{K}$., $168 \pm 5^\circ\text{K}$., and $228 \pm 5^\circ\text{K}$.. The quantity of light emitted generally remains the same in the specimens seeded with Mg and Mg + Ni for successive irradiations of equal exposure periods. However, after many irradiations at liquid nitrogen temperatures and annealing to room temperature, the sample containing only Ni as the network modifier showed an increase in the intensity for the 228°K . peak. Perhaps the increase is due to permanent capture of an electron by Ni⁺⁺⁺ atoms, thus decreasing the number of these "poison" Ni⁺⁺⁺ atoms. (A microscopic examination of newly broken ends of the samples showed green and olive spots together with many brown-black spots. There is little agreement¹¹ on the existence of either Ni⁺⁺⁺ or Ni⁺⁺ or Ni⁺⁺⁺⁺; however, it is theorized, on the basis of evidence given by Sidgwick,¹² that the brown-black color results when Ni⁺⁺⁺ ions are present.)

Figure 1b gives the glow curves for UO₃ as the network modifier in the host borax lattice. A sample containing 0.1 wt. % exhibits a curve typical of the host network with nothing added. Successive increases of the amount of UO₃ in the host lattice resulted in a growth of the glow peak at 180°K . The peak began to appear at about 2 wt. %.

The glow curves for single crystalline golden sapphire (Al₂O₃ containing Ni and Mg), Fig. 2a, show characteristics different from the Ni and Mg seeded glass samples. Here the intensity of light and the temperatures at which the maxima occur vary somewhat. The thermoluminescence peaks, unlike those of the fused glass specimens, generally show a decrease with cumulative and succes-

(11) J. W. Mellor, "A Comprehensive Treatise on Inorganic and Theoretical Chemistry," Longmans Green and Co., London, Vol. 15, 1936, p. 393.

(12) N. V. Sidgwick, "The Chemical Elements and their Compounds," Oxford Univ. Press, London, 1950, pp. 1449-1450.

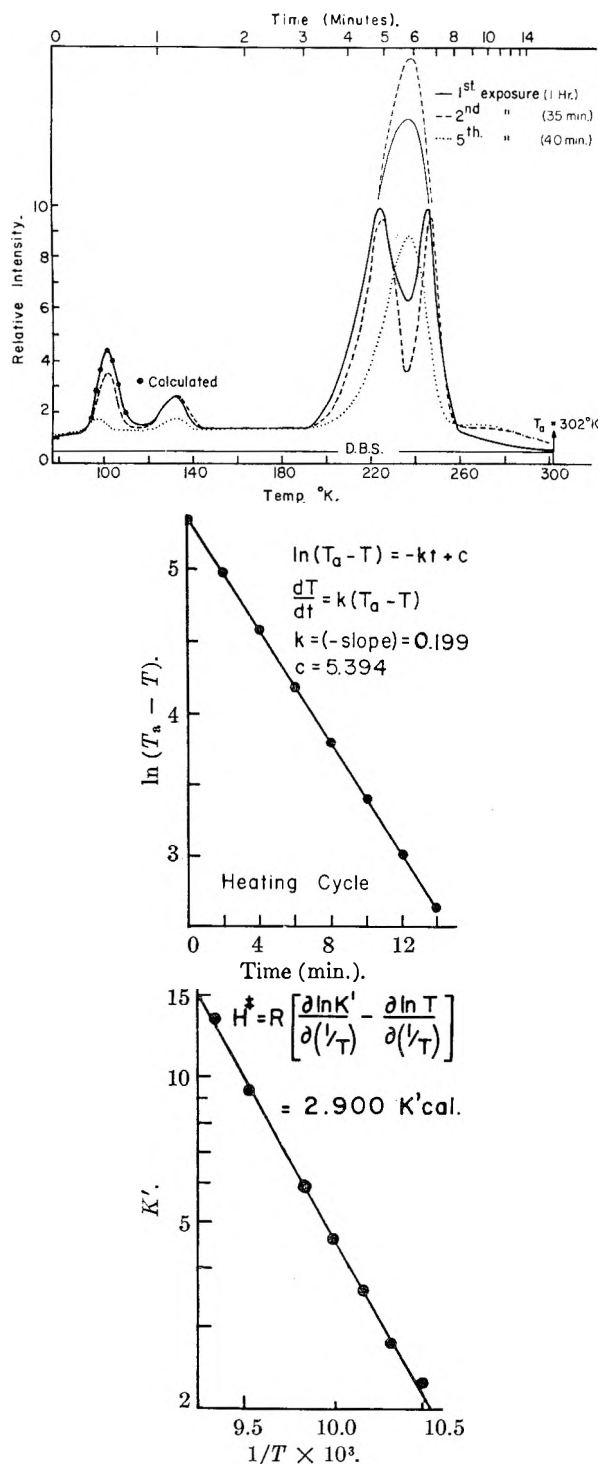


Fig. 2.—(a) Glow curves for golden sapphire. Curves (DBS) coincide for dark current, background for non-irradiated sample, and sample-holder background after irradiation; (b) heating cycle where T_a is the ambient room temperature; (c) heat of activation.

sive 30-min. irradiations. Also, the peaks occur at slightly increased temperatures. Thermoluminescence did not occur without previous exposure to γ -radiation in either the glass specimens or the sapphire. After exposure to γ -radiation, only the golden sapphire showed light-induced thermoluminescence even weeks after the initial exposure to γ -rays. Heating the sapphire to about 400° an-

nealed out the γ -ray induced defects and there was no subsequent light-induced thermoluminescence.

In golden sapphire three (possibly 4—the apparent resolution of peaks at $\sim 236^\circ\text{K}$. is not presently understood) dominant absorption bands are noted with maxima at $100 \pm 5^\circ\text{K}$., 133, and 236°K ., with an additional weak band appearing in the region around 273°K . for a sample irradiated and annealed to room temperature many times. For all bands the temperatures at which the peaks occur appear to be similar, while the intensities vary greatly. At 236° the band from a new specimen, irradiated for 1 hr., appears to be resolved (solid curve—Fig. 2) into two peaks, ~ 225 and 245° . The sample immediately was returned to liquid nitrogen and irradiated for 35 min. The resulting (dashed) glow curve shows even greater resolution with the peaks slightly shifted to higher temperature. A similar resolution was observed¹⁰ in several samples of white sapphire; however the resolution was slight and the trough dropped only about 2–5% of the peak intensity. The above curves show a drop of 30 (solid curve) and 60% (dashed curve) after the first and second irradiations, respectively. A week later subsequent irradiations of the same sample resulted in a glow band similar to that shown for the fifth irradiation (dotted curve). Successive irradiations of other samples for 5, 10, 20, 30, and 40 min. effected thermoluminescence of increasing intensity; e.g., the constructed light dashed curve of Fig. 2. Longer irradiation periods of 60, 80, 100, and 120 min. resulted in a gradual decrease of the intensity peak; e.g., the constructed light solid curve of Fig. 2. In some samples resolution of the 236°K . peaks with varied trough intensity occurred after a 40–60 min. exposure to the γ -rays.¹³

Discussion

The glow curves of Fig. 1 and 2a indicate that thermoluminescence is induced by Co^{60} γ -irradiation. The locations of the maxima for the fused boron matrix specimens do not vary but the areas under the maxima vary markedly with the type of impurity.

In order to contrast the luminescence of boron glass seeded with the same impurities, Ni and Mg, which are present in the single-crystal hexagonal close-packed structure of golden sapphire, it might be well to inquire into the structure of the boron matrix. Because different metal oxides have various miscibilities with the boron oxide (p. 382 of ref. 12) the exact compositions of the samples cannot be predicted. In the process of heating, the composition $\text{Na}_2\text{B}_4\text{O}_7 \cdot 10\text{H}_2\text{O}$ is reduced to $\text{Na}_2\text{B}_4\text{O}_7 \cdot 8\text{H}_2\text{O}$ at 75° , to $\text{Na}_2\text{B}_4\text{O}_7 \cdot 5\text{H}_2\text{O}$ at 120° and to Na_2

(13) The parameters effecting a resolution of the 236°K . peak are not yet determined due to the loss of access to an irradiation facility. Irradiating time and heating rate appear to play a prominent part in the resolution. Phenomena similar to that observed in golden sapphire were observed in white (Al_2O_3) sapphire, pink ($\text{Al}_2\text{O}_3 + \text{Cr}_2\text{O}_3$) sapphire, blue ($\text{Al}_2\text{O}_3 + \text{Fe}_2\text{O}_3 + \text{FeTiO}_3 + \text{LiO}$) sapphire, garnet, and spinel. Also, using a resonant-bar technique with quartz¹⁴ as the piezoelectric resonator, a preliminary study showed an appreciable change in resonant frequency for a composite Al_2O_3 -quartz resonator when the previously γ -irradiated Al_2O_3 was exposed to a light beam. Non-irradiated specimens did not exhibit this phenomenon. These studies will be resumed when a new γ -source becomes available.

(14) J. Marx, *Rev. Sci. Instr.*, **22**, 503 (1951).

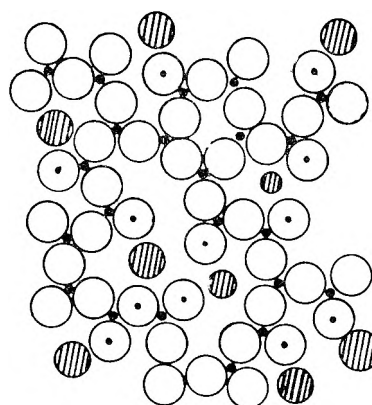
B_4O_7 at 741° . When the $Na_2B_4O_7$ is heated to 966° , the metaborate, $NaBO_2$, is obtained; e.g., $Na_2B_4O_7 = NaBO_2 + B_2O_3$. If NiO or MgO is present, the balanced equations probably will be¹⁵ $NiO + Na_2B_4O_7 = Ni(BO_2)_2 + 2NaBO_2$ or $MgO + Na_2B_4O_7 = Mg(BO_2)_2 + 2NaBO_2$. Although these formulas balance, the resulting compounds of $NaBO_2$, $Ni(BO_2)_2$, $Mg(BO_2)_2$, and B_2O_3 do not exist as separate, discrete molecules, but probably are combined in a polymer or a crystal lattice of random arrangement, as originally proposed by Zachariasen.¹⁶

Figure 3 shows a proposed schematic, somewhat different from models of other investigators,¹⁶⁻¹⁸ for the structure of the soda-boron oxide glass. The radii of the atoms are approximately proportional to their actual ionic radii.¹⁹ The impurity atoms are shown as the network modifiers.

According to the conjectural model in Fig. 4 luminescence emission does not occur after γ -irradiation, with Ni^{+++} (or Ni^{++++}) as a network modifier because Ni^{+++} traps incorporated locally (Fig. 4a) in the conduction region permanently hold electrons ($Ni^{+++} + e \rightarrow Ni^{++}$) preventing their radiative transition to lower energy states (dotted curve of Fig. 1a). The radiationless loss of energy by these electrons includes collapse of exciton states by small increments corresponding to phonon energies. With Mg as the modifier, Fig. 4b, an electron makes a radiative transition from levels near the lower edge of the conduction band. The energy is emitted as a photon, resulting in a glow peak at $165^\circ K$. (dot-dash curve of Fig. 1a). The initial "tail" at $90^\circ K$. is characteristic of the host lattice, which showed a curve like the dashed curve of Fig. 1b. When both Ni and Mg are present in the host network, the glow curve (dashed curve of Fig. 1a) exhibits an emission process that is a composite (Fig. 4c) of strong electron capture by Ni, resulting in general intensity decrease and radiative transition in Mg, which effects a weak glow peak at $165^\circ K$.

The model of Fig. 4c shows energy states in the golden sapphire lattice. In this model, the γ -rays induce traps of the Ni and Mg type, plus trap and metastable states characteristic of the Al_2O_3 lattice (hexagonal close-packed). Two types of Al_2O_3 -traps corresponding to 100 and $133^\circ K$. are of lower energy than the Ni trap but higher than the Mg trap ($168^\circ K$). A third type is lower ($236^\circ K$.) than the Mg trap. Metastable states correspond to electrons in γ -ray induced levels from which radiative transitions to lower unoccupied levels are not possible. However, the metastable-state electrons can be raised to higher levels from which radiative transition (the light induced luminescence observed after the crystal was annealed to room temperature) to lower levels is allowed.

(15) J. R. Partington, "General and Inorganic Chemistry," The Macmillan Co., Ltd., London, 1958.
 (16) W. H. Zachariasen, *J. Am. Chem. Soc.*, **54**, 3841 (1932).
 (17) B. E. Warren, *J. Appl. Phys.*, **8**, 645 (1937).
 (18) J. M. Stevels, "Non-Crystalline Solids," John Wiley and Sons Inc., New York, N. Y., 1960, p. 412, Edited by V. D. Frechette.
 (19) J. Kleinberg, W. J. Argersinger, and E. Griswold, "Inorganic Chemistry," D. C. Heath and Co., Boston, Mass., 1960, p. 75.



- Network Former - B^{+++}
- ◐ Network Modifier - Na, Mg and Ni.
- Bridging Oxygen
- ◑ Non-Bridging Oxygen

Fig. 3.—Schematic representation of random atom arrangements for soda boron oxide glass.

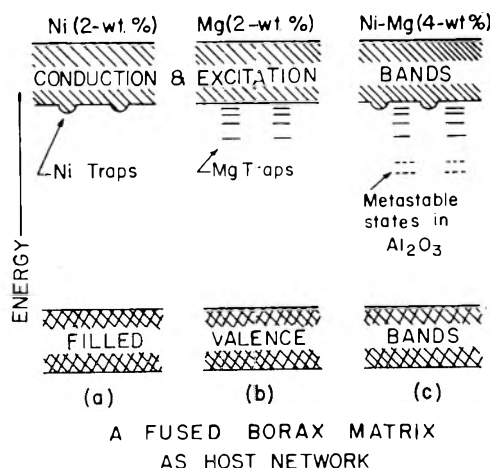


Fig. 4.—Energy-band model for luminescent characteristics of the host matrix and impurities; (a) Ni, (b) Mg, and (c) Ni + Mg.

Williams and Eyring²⁰ have successfully treated the luminescence of solids in terms of spontaneous and metastable recombinations of electron traps. In terms of a model where metastable states of equal depth empty with a single rate determining step to produce luminescence, one can write for the emission intensity I

$$I = \alpha cN/dt = \alpha Nk' \quad (1)$$

where α is a constant correlating emission intensity and the rate of decrease of trapped electrons. If N and N_0 are the number of electrons in the metastable state at times t and t_0 and k' is the specific rate constant for crossing the potential barrier of the metastable and emitting states, the rate of decrease of trapped electrons is then

$$N = N_0 \exp\left(-\int_{t_0}^t k' dt\right) \quad (2)$$

(20) F. E. Williams and H. Eyring, *J. Chem. Phys.*, **15**, 289 (1947).

For a heating rate dT/dt , I becomes

$$I = \alpha N_0 k' \exp\left(-\frac{1}{dT/dt} \int_{T_0}^T k' dT\right) \quad (3)$$

Solving and expanding (3) with the heating rate one gets

$$\int_{T_0}^T K' dT = \frac{dT}{dt} \ln \left[1 - \left(\frac{N_0 - N}{N_0} \right) \right] = \frac{dT}{dt} \left[\sum_{n=1}^{\infty} \frac{1}{n} \left(\frac{N_0 - N}{N_0} \right)^n \right] \quad (4)$$

If the number of trapped electrons undergoing radiationless recombination is negligible, N_0 and N can be expressed in terms of the integrals of the emission intensities and the number of radiating electrons so that the specific rate constant, from (4), becomes

$$K' = \frac{d}{dT} \left\{ \frac{dT}{dt} \left[\sum_{n=1}^{\infty} \frac{1}{n} \left(\frac{\int_{T_0}^T I dT}{\int_{T_0}^{\infty} I dT} \right)^n \right] \right\} \quad (5)$$

Equations 1 to 5 may be used to analyze the data as illustrated below, using the experimental curve at 100°K. of Fig. 2. By measuring the area under the glow peak a total light sum from a particular energy state is obtained. Areas up to specific temperatures also are measured to obtain that part of the total light sum that is a function of the number of photons emitted before reaching the specific temperature. The light sums are inserted in (5) and a rate constant is obtained by graphic estimation of the slope. The integral of the rate constant over the temperature, plotted as a function of the absolute temperature, gives a curve whose slope is the specific rate constant.²¹ The values of A and E in the specific rate constant expression, $k' = AT \exp(-E/kT)$, may be estimated from a plot against $1/T$ of the logarithms of the slopes of a plot of $\int_{T_1}^{T_2} k' dT$ vs. T_1 as done in Fig. 2c. The heat of activation, 2900 cal. per mole, is obtained from the slope of the line and the frequency coefficient, 1.02×10^5 , from the intercepts. The explicit form of the rate constant, $k' = 1.02 \times 10^5 T \exp(-2900/RT)$, is substituted in (3) along with the value $\alpha N_0 = 1.5$, obtained from a graphical integration of

$$\alpha N_0 = \frac{1}{dT/dt} \int_{T_0}^{\infty} I dT$$

Calculated points (solid dots) for the curve at 100°K. are compared with the experimental curve (solid line) in Fig. 2a.

Acknowledgment.—One of us (H.A.W.) is grateful for the privilege of taking part in an Undergraduate Research Participation program sponsored by the National Science Foundation and for its support. Appreciation is extended to I. Cutler and J. M. Sugihara for their encouragement and interest in the program. It was a pleasure to participate in this project, which is being continued by V. LeFebvre, M. Evans, and F. Wanlass.

The authors thank Miss Nola McKee for preparing the drawings and the manuscript.

(21) S. Glasstone, K. J. Laidler, and H. Eyring, "The Theory of Rate Processes," McGraw-Hill Book Co., Inc., New York, N. Y., 1941.

TRANSLATIONAL ENERGY ACCOMMODATION IN THE NICKEL-CHLORINE SURFACE REACTION¹

By J. D. MCKINLEY

National Bureau of Standards, Washington, D. C.

Received September 11, 1961

A method of measuring the transfer of translational energy in gas-surface collisions is described. The experiments are part of an experimental investigation of the kinetics of the high temperature surface reaction between chlorine and nickel.² Mass spectrometric measurements were made of a collimated beam of unreacted chlorine reflected from the nickel surface at surface temperatures between 1100 and 1600°K. By a simple modification of the mass spectrometer ion source it was possible to measure the flux and density of this beam. The latter equals the flux divided by the average velocity of the beam molecules, and the ratio of the two quantities gives the average beam velocity. The accommodation coefficient of the beam gas on the reflecting surface can be computed from this velocity together with the temperature of the beam before reflection and the surface temperature.³ In the chlorine-nickel reaction it was found that from 20 to 40% of the chlorine reacts on the surface to form NiCl or NiCl₂, while the remaining chlorine is reflected without reacting and without a measurable gain in translational energy. The experimental method has fairly general application to measurements of translational energy accommodation, and should be especially useful when a chemical reaction occurs between the gas and the surface as is the case here. The method together with some results for the nickel-chlorine reaction is described below.

Experimental

Experiments were carried out in a stainless steel vacuum system consisting of three separately pumped chambers connected in series by collimating slits, 0.005×0.5 in. Chlorine from an effusion source in the first chamber passes as a collimated beam into the second chamber where it strikes a nickel target mounted with its long axis 45° to the beam direction. A beam of evaporated reaction products and reflected chlorine collimated at right angles to the incident beam passes into the third chamber containing the ion source of a pulsed beam time-of-flight mass spectrometer.⁴ By means of a quartz liner, the ion source is completely enclosed except for the electron beam ports, ion exit grid, sample beam inlet, and sample beam outlet. The latter may be closed by a stainless steel door controlled magnetically from outside the vacuum. With this door open, the reflected chlorine beam passes once through the ion source and is condensed on a liquid nitrogen cooled surface above the ion source. With the door closed the beam gas accumulates in the ion source to a pressure determined by the escape area of the ion source, the size of the inlet slit, and the beam flux. The escape area of the closed ion source is about 1/20 of the interior surface area, and the density of the scattered gas is about 60% of the density of the beam at 300°K.

The nickel target was a strip of high purity polycrystalline nickel 3 mm. wide and 5 cm. long mounted on 1/4 in. diam.

(1) This research was supported by the U. S. Atomic Energy Commission.

(2) J. D. McKinley and K. E. Shuler, *J. Chem. Phys.*, **28**, 1207 (1958).

(3) For a discussion of the important features of the measurements by J. K. Roberts and the pertinent references see A. R. Miller, "The Adsorption of Gases on Solids," Cambridge University Press, Cambridge, 1949.

(4) W. C. Wiley and I. H. McLaren, *Rev. Sci. Instr.*, **26**, 1150 (1955).

copper rods, which served as electrical leads. The nickel was pretreated by heating to 1000°K. for at least 12 hr. while hydrogen from the effusion source flowed over it at pressures of about 10⁻⁵ mm. By extensive baking and outgassing the background pressure in the target chamber was reduced to less than 10⁻⁷ mm. The problem of surface contamination of the nickel is minimized to some extent by the high efficiency of the reaction with chlorine and by the use of intense beams; fluxes of chlorine at the surface were 10¹⁵ to 10¹⁶ molecules cm.⁻² sec.⁻¹. The first-order pressure dependence of the reaction both in these beam experiments and at chlorine pressures up to 0.5 mm.² indicates that the surface is effectively free of chlorine. Chlorine obtained from a commercial cylinder was subjected to several bulb-to-bulb distillations and stored in a 5-liter Pyrex reservoir at about 1 atmosphere. It flowed to the effusion cell through copper tubes and monel valves. It contained no impurities detectable as such in the mass spectrometer.

With liquid nitrogen cooled traps connected to each chamber and separate traps within the second and third chambers, background chlorine from the target chamber is not detectable above the hydrocarbon background, which is less than 5% of the total signal. Background chlorine in the ion source chamber was not measured directly; the positions of slits and traps, and the results in Table I below indicate that it must be very small.

Measurements were made of the ⁷⁰Cl₂⁺ ion current with the door open and closed under the various conditions described below. In order to minimize uncertainties in the ion current due to inevitable fluctuations in the various factors affecting the instrumental sensitivity, argon was admitted to the mass spectrometer through a controlled leak 15 cm. from the ion source. It flowed continually past the ion source at a low constant pressure (less than 10⁻⁸ mm.). The chlorine ion currents reported below are ratios of ⁷⁰Cl₂⁺ ion current to ⁴⁰Ar⁺ ion current. The two ion currents are measured concurrently in a two channel gated pulse counter. The ratio, $I(\text{Cl}_2^+)/I(\text{Ar}^+)$, is independent of fluctuations in instrumental sensitivity. The argon current is not affected by the door position as is to be expected since argon can enter the ion source from all directions. In these experiments the sample density is either (door open) the density of the reflected chlorine beam, f/\bar{v}_b

$$I_0 = Sf/\bar{v}_b = SK_b f/(T_b)^{1/2} \quad (1)$$

TABLE I

CHLORINE ION CURRENT ⁷⁰ Cl ₂ ⁺ ;		CHLORINE BEAM DIRECTLY FROM EFFUSION FURNACE				
<i>T_b</i> , °K.	<i>I₀</i> ^b	<i>I₀</i>	<i>R</i> - 1	$\frac{R-1}{(T_b)^{1/2}} \times 10^2$	<i>T_{outd.}</i> , °K.	
1	339	1045	1720	0.65	3.53	301
2 ^a	355	3400	5750	.69	3.66	345
3 ^a	368	3450	6000	.74	3.85	397
4 ^a	557	2670	5080	.90	3.81	586
5 ^a	613	2450	4770	.95	3.84	647
6	680	540	1050	.95	3.64	647

^a At same Cl₂ flow, approximately 10¹¹ molecules sec.⁻¹ into ion source. ^b Arbitrary units, the ion currents are in the range 10-100 ions sec.⁻¹.

or (door closed) the sum of the beam density and the density of the scattered gas in the ion source, $f/\bar{v}_s + 4a/A$

$$I_e = S[K_b f/(T_b)^{1/2} + K_s f 4a/(T_s)^{1/2} A] \quad (2)$$

f = reflected beam flux, molecules cm.⁻² sec.⁻¹

\bar{v}_b = av. velocity of beam molecules = $(11.1RT/M)^{1/2} = (T_b)^{1/2}/K_b$

\bar{v}_s = av. velocity of molecules in equilibrium with ion source walls $(8RT/M)^{1/2} = (T_s)^{1/2}/K_s$

T_b = temp. of gas in reflected beam

T_s = temp. of gas in equilibrium with ion source

I₀, *I_e* = chlorine ion currents with door open and closed

S = instrumental sensitivity, a function of ionization cross section, ionizing electron current, attenuation of ion beam in flight tube, detector efficiency

a = cross sectional area of beam inlet slit

A = total escape area of closed ion source

The ratio of the ion currents with the door closed and open is related to the beam temperature by

$$I_c/I_0 = R = 1 + C(T_b)^{1/2}, [C = (4a/A)(T_s)^{1/2}K_s/K_b] \quad (3)$$

In using equation 3 the assumption is made that reflected chlorine that strikes the closed door comes quickly to equilibrium with the ion source walls. A scattered molecule makes on the average 20 wall collisions before leaving the ion source. If the chlorine is at room temperature after reflection the question of equilibration with the ion source is immaterial. If it were at a significantly higher temperature after reflection but did not equilibrate with the ion source, the ratio, *R*, would be independent of *T_b*. This seems unlikely, however, because of the results in Table I, and also because it implies substantial energy transfer on the nickel surface during one collision, but none on the ion source walls during several collisions.

The technique was tested by replacing the nickel target with a Pyrex effusion furnace from which chlorine effused directly into the ion source. The temperature of the effusing chlorine was measured with a thermocouple inside the furnace. Ion currents measured at several furnace temperatures are shown in Table I. Since *A* is not known accurately, the applicability of the method is demonstrated by the constancy of $(R-1)/(T_b)^{1/2}$, (*C* in equation 3). From equation 3 and the mean value of *C* from the six measurements, the temperatures in column 6 were obtained.

The results of experiments in which chlorine was reflected from nickel at room temperature and at temperatures between 1100 and 1600°K. are shown in Table II. The beam temperature is calculated with equation 3 using the \bar{C} from three measurements with the nickel target unheated (300°K.). The range of the three values of *T_b* with the

TABLE II

CHLORINE ION CURRENT;		CHLORINE BEAM REFLECTED FROM NICKEL SURFACE		
Nickel temp. ^a	<i>I₀</i> ^b	<i>I₀</i> ^b	<i>R</i> - 1	<i>T_b</i>
Unheated	915	1485	0.62	342
Unheated	385	625	.62	342
Unheated	305	459	.50	223
1107	140	240	.71	450
1190	850	1350	.59	311
1256	125	200	.60	321
1325	825	1255	.52	236
1430	335	510	.52	236
1525	260	420	.61	332

^a Determined with optical pyrometer. ^b Arbitrary units.

nickel unheated is 40% of the mean. The instabilities in the counter circuitry seem to be a main factor affecting the precision of these determinations. The remaining values of *T_b* in Table II exhibit considerable scatter (range of 210°, mean 330°) but show no trend with surface temperature when the latter is increased by 1200°. The values of (*R*-1) corresponding to complete accommodation would be 1.03 at 1100°K., 1.25 at 1500°K.; the observed values range from 0.50 to 0.71. Using this range as a measure of the uncertainty, an upper limit of 0.15 can be placed on the accommodation coefficient for unreacted chlorine.

Discussion

The results in Table II indicate that very little translational energy is transferred during the one collision that the chlorine molecule makes with the reacting surface. Such poor accommodation is surprising since a large fraction of the incident chlorine reacts with the same surface. There are very few direct measurements of accommodation coefficients on clean metals. The early experiments of Roberts which were performed with He and Ne on carefully cleaned W with temperature differences of about 20° probably are the most reliable, and under these conditions accommodation coefficients in the vicinity of 0.05-0.06 were obtained.³ Since

the reaction with nickel most probably involves an initial dissociation of chlorine on the surface, the low accommodation coefficient of the unreacted gas indicates that little or no energy transfer occurs except in those surface collisions favorable for chlorine dissociation.

Acknowledgments.—Thanks are due to Mr. J. H. McAuley for designing and building much of the apparatus and for assistance with the experiments.

KINETICS OF EXCITED MOLECULES.

III. PHOTOOXIDATION OF ACETONE¹

BY ALEXANDER D. KIRK AND GERALD B. PORTER

Department of Chemistry, University of British Columbia, Vancouver, Canada

Received September 11, 1961

Although the photooxidation of acetone has been studied in detail in the temperature range above 100°,^{2,3} the only information available about the reactions at or near room temperature is that of Marcotte and Noyes.² At the high temperatures, it usually is assumed that acetone dissociates with unit quantum yield, however, it has been established that the primary yield is less than one at 25°.⁴ Biacetyl, like oxygen, quenches the phosphorescence of acetone and at the same time reduces the primary quantum yield. Hence, it is of considerable interest to investigate the photooxidation at room temperature to determine the nature of the interaction of oxygen with excited molecules.

Experimental

Photolyses were carried out in a cylindrical reaction vessel of about 170-ml. volume. In most runs, a mixture of oxygen and nitrogen (78.7% O₂) was added from a doser, but it also was possible to add pure oxygen from a second storage system. Nitrogen, which cannot affect the reaction in the small concentrations used, served as an internal standard for gas chromatographic analyses. Acetone was purified by standard procedures.

The light source used throughout was a B.T.H. 250-watt medium pressure mercury arc. Monochromatic light at about 2800 Å. was obtained with a Bausch and Lomb grating monochromator. For 3130 Å., a filter consisting of 3 mm. of Corning 9863 glass, 10 mm. of potassium chromate solution (0.014 g./100 ml.) and 10 mm. of potassium hydrogen phthalate (0.2 g./100 ml.) was used.⁵ Transmitted light intensities were measured by potassium ferrioxalate actinometry.⁶ For convenience in the measurement of the extinction coefficients of acetone, the ratio of transmitted and incident intensities was determined with an RCA 935 photocell and recorder. Beer's law was obeyed under all conditions of the experiments. Absorbed intensities were calculated from the transmitted intensity, integrated by the actinometer, the acetone pressure and the extinction coefficients. Corrections were applied for window reflections and absorptions. These procedures were checked by photolyzing acetone at 128° and measuring the quantum yield of carbon monoxide. The average values obtained, 0.90 at

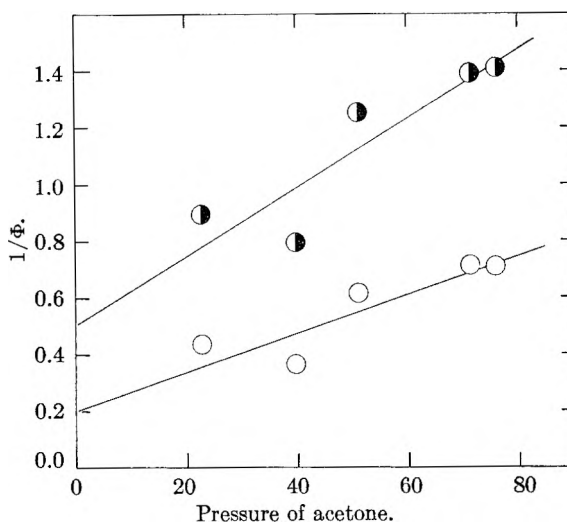


Fig. 1.—Plot of $1/\phi$ versus pressure of acetone (mm.) at 2800 Å. and 25°: ●, CO₂; ○, O₂.

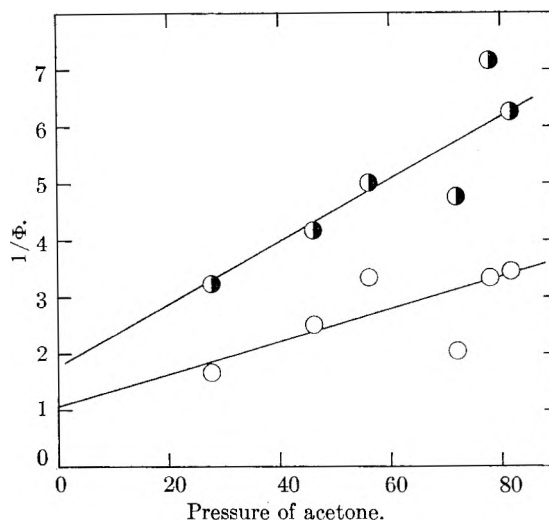


Fig. 2.—Plot of $1/\phi$ versus pressure of acetone (mm.) at 3130 Å. and 25°: ●, CO₂; ○, O₂.

2800 Å. and 1.05 at 3130 Å., are in reasonable agreement with the expected value of unity.

Analysis of the oxidation products was limited to methane, ethane, carbon monoxide, carbon dioxide, nitrogen (as a standard) and unreacted oxygen. This mixture was separated into non-condensable and condensable fractions at -196°. The carbon dioxide fraction was distilled off at the temperature of a petroleum ether slurry (about -140°) thus excluding other oxidation products as well as unreacted acetone. These fractions were measured in a gas buret and analyzed by gas chromatography using a Molecular Sieve column for the non-condensable fraction and silica gel for the condensable. The practical maximum oxygen pressure which could usefully be employed was set by the limited capacity, 10 μmole, of the analysis system.

Results

The experimental results are summarized in Table I. Several features may be noted: 1. The quantum yield of carbon dioxide and the quantum uptake of oxygen are independent of oxygen pressure but vary with acetone pressure as shown in Fig. 1 and 2. The small yields of carbon monoxide and the resulting scatter in the analyses preclude any firm conclusion; however, a similar trend appears. 2. The quantum yields are larger at 2800

(1) This research was supported in part by a grant from the Petroleum Research Fund administered by the American Chemical Society and in part by a grant from the National Research Council of Canada. Grateful acknowledgment is hereby made for this support.

(2) F. B. Marcotte and W. A. Noyes, Jr., *Discussions Faraday Soc.*, **10**, 236 (1951); *J. Am. Chem. Soc.*, **74**, 783 (1952).

(3) D. E. Hoare, *Trans. Faraday Soc.*, **49**, 1292 (1953).

(4) J. Heicklen and W. A. Noyes, Jr., *J. Am. Chem. Soc.*, **81**, 3858 (1959).

(5) M. Kasha, *J. Opt. Soc. Am.*, **38**, 929 (1948).

(6) C. G. Hatchard and C. A. Parker, *Proc. Roy. Soc. (London)*, **A235**, 518 (1956).

Å. than at 3130 Å. by a factor of about four. 3. The ratio of the quantum uptake of oxygen to the quantum yield of carbon dioxide is close to two under all conditions studied. 4. No significant amounts of either methane or ethane were detected.

TABLE I
PHOTOOXIDATION OF ACETONE

Acetone pressure, mm.	I_a , quanta/sec. $\times 10^{-13}$	t , sec.	Φ_{CO}	Φ_{CO_2}	$-\Phi_O$
3130 Å., 25°					
27.7	5.3	7200	0.055	0.31	0.60
46.2	5.5	7800	.023	.24	.40
56.2	12.6	3600	.016	.20	.30
71.9	11.0	8200	.037	.21	.49
77.9	4.5	7200	.011	.14	.30
81.6	35.9	3100	.037	.16	.29
3130 Å., 45°					
56.1	28.7	11100	0.070	0.23	0.47
55.9 ^a	21.9	11400	.079	.20	.54
55.4	21.3	4400	.056	.26	.55
52.0	19.6	3500	.058	.31	.69
50.2	15.4	6400	.060	.27	.59
2800 Å., 25°					
22.7	3.5	7600	0.29	1.12	2.30
39.9	4.7	7900	.34	1.26	2.74
51.1 ^b	6.7	5400	.14	0.80	1.62
71.4	4.0	5400	.14	.72	1.40
76.0	7.9	6200	.13	.71	1.41
2800 Å., 45°					
50.0	5.1	7200	0.10	0.79	1.64
57.0	3.1	7300	.18	1.32	2.57
58.0	2.9	8000	.16	1.21	2.03
79.0 ^b	2.7	6300	.16	1.68	3.60

^a O₂ pressure = 0.85 mm. ^b O₂ pressure = 0.56 mm.

Discussion

Although the detailed radical mechanism for the photooxidation of acetone has not been firmly established, the constancy of the ratio $-\Phi_{O_2}/\Phi_{CO_2}$, as well as of the ratios of the quantum yields at the two wave lengths clearly demonstrates that the variations in the quantum yields observed in this work are not due to any change in mechanism. Instead they must be caused by changes in the primary quantum yield with, on the one hand, acetone pressure and, on the other, wave length absorbed. The primary quantum yield, ϕ , cannot be calculated directly from the data, but it is possible to establish maximum values. At 2800 Å., the carbon dioxide quantum yield is about 1.2 at the lowest acetone pressure studied, while the value obtained by extrapolation to zero pressure (Fig. 1) is about two. Since the primary quantum yield cannot exceed unity, the ratio ϕ/Φ_{CO_2} cannot exceed 0.8 or, based on the extrapolation, 0.5. When these figures are carried over to the longer wave length, it is found that at 50 mm. of acetone, for example, ϕ must certainly be less than 0.16, and possibly as small as 0.1. Heicklen and Noyes⁵ estimate ϕ in the photolysis of acetone under the same conditions to be about 0.65. Hence oxygen decreases ϕ by at least a factor of 0.65/0.16 or about four.

The behavior of the primary quantum yield, which is proportional to either Φ_{CO_2} or $-\Phi_{O_2}$, is simi-

lar to that found in other systems.⁷ It can be interpreted as a competition between dissociation of an excited singlet molecule and its collisional degradation. At the shorter wave length, the excited molecules have considerable vibrational energy and decompose rapidly, while at the longer wave length, dissociation is slower and a relatively larger proportion of the excited molecules is deactivated by collision to the near vibrationless states. This mechanism predicts the linear relationship between $1/\phi$ and pressure shown in Fig. 1 and 2.

Although collisional deactivation is occurring, a change of oxygen pressure over wide limits has no effect on the quantum yields. However, oxygen does lower the primary quantum yield significantly at 3130 Å. The deactivation described above leads, by intersystem crossing, to a long-lived triplet state, which is known, by quenching of the phosphorescence, to be degraded by oxygen.⁸ In the absence of oxygen even at room temperature, triplet state molecules must be able to dissociate thermally and it is this reaction which makes up the major part of the primary quantum yield in the photolysis.

Biacetyl also removes triplet state excitation by energy transfer and reduces the primary quantum yield to a limiting value of 0.2 at 3130 Å. at 0.1 mm. of biacetyl.⁴ Further, under these conditions, Φ_{CO} is reduced to about 0.04, essentially the same as found here in the presence of oxygen. Thus the effect of oxygen with regard to its effect on the primary processes in acetone photolysis is completely analogous to that of biacetyl, both of which efficiently degrade triplet state acetone molecules without chemical reaction.

(7) G. B. Porter and B. T. Connelly, *J. Chem. Phys.*, **33**, 81 (1960).
(8) G. W. Luckey and W. A. Noyes, Jr., *ibid.*, **19**, 227 (1951).

IONIC TRANSPORT AND THE CRYSTALLOGRAPHIC TRANSITION IN CESIUM CHLORIDE

BY I. M. HOODLESS AND J. A. MORRISON

Department of Chemistry, The University, Glasgow, W. 2, Scotland and Division of Pure Chemistry, National Research Council, Ottawa 2, Canada

Received September 15, 1961

It is well known that CsCl undergoes a crystallographic transition from a bcc form to an fcc form. Values reported for the transition temperature vary, because there appears to be some hysteresis in the transition, but a recent careful investigation¹ places the transition in the region of 465–472°.

The transition from a solid to a liquid is accompanied by a rapid increase in the concentration of vacancies in the lattice as the melting point is approached.² Menary, Ubbelohde and Woodward³ have made X-ray measurements on CsCl in the region of the crystallographic transition and their results indicate that a similar excess

(1) L. J. Wood, W. Secunda and C. H. McBride, *J. Am. Chem. Soc.*, **80**, 307 (1958).

(2) See for example, A. B. Lidiard, "Handbuch der Physik," Vol. 20, part 2, 1957, p. 246.

(3) J. W. Menary, A. R. Ubbelohde and I. Woodward, *Proc. Roy. Soc. (London)*, **A208**, 158 (1951)

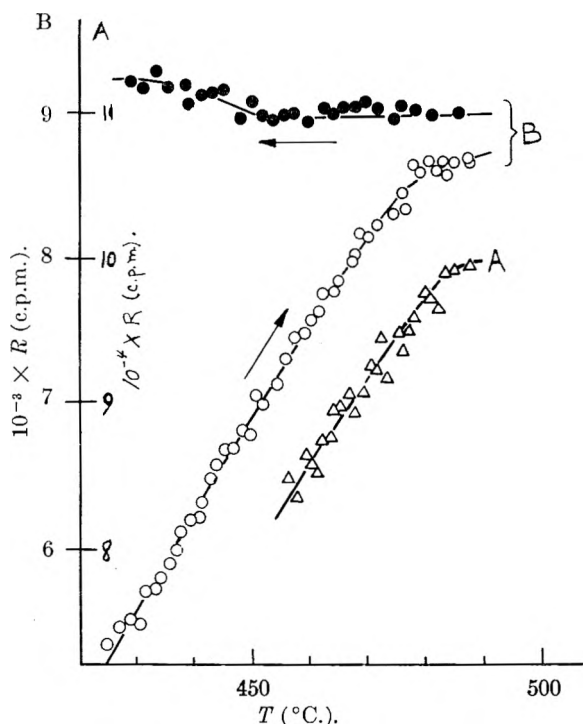


Fig. 1.—The counting rate, R , as a function of temperature: Δ , specimen A—heating; O , specimen B—heating; \bullet , specimen B—cooling.

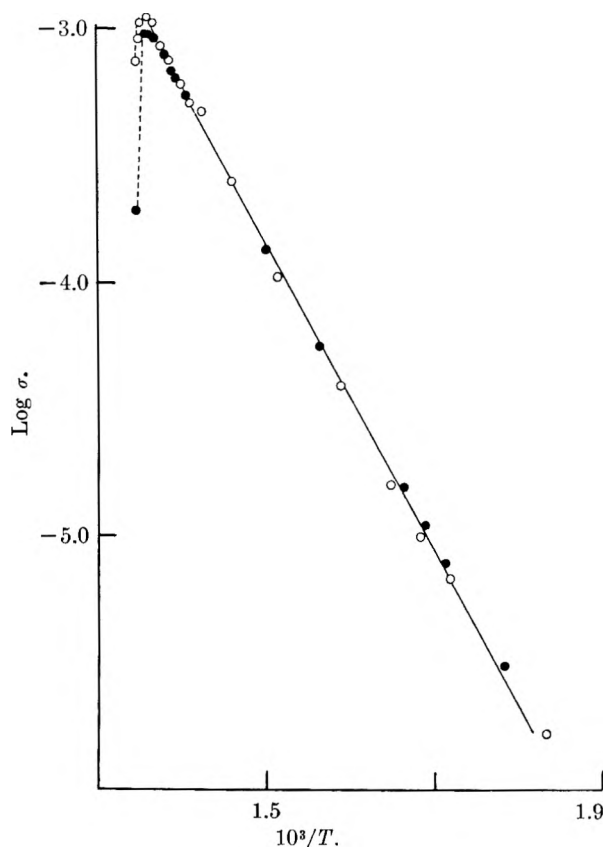


Fig. 2.—Variation of conductivity with temperature for the single crystal of CsCl.

concentration of vacancies is formed. However, conductivity measurements^{4,5} designed to test this gave somewhat ambiguous results; there was evi-

dence that the conduction was mainly electronic in nature and so significant changes in the ionic conductivity were unlikely to be observed experimentally. In other work, Lantelme and Pauly⁶ have shown that, when crystals of CsCl were irradiated with neutrons at room temperature and subsequently heated, an enhanced release of ³⁵S from the lattice occurred at approximately 480°. This observation might be interpreted as indicating the presence of a high concentration of lattice vacancies at the transition point.

We now have investigated ionic motion in the transition region directly by measuring self-diffusion of the chloride ion in CsCl and by measuring the conductivity of a single crystal. The results show that the transition occurs without the formation of an excess concentration of lattice vacancies.

Experimental

Diffusion.—The apparatus and technique of measurement of chloride ion diffusion by isotopic exchange have been described previously.^{7,8} The radioactive chlorine, ³⁶Cl, was obtained in the form of Cs³⁶Cl with a specific activity of 20 $\mu\text{c./g.}$ Crystals (1 to 2 mm. in length) were grown slowly from a concentrated solution of CsCl at 60°, filtered under an atmosphere of dry nitrogen and dried *in vacuo*. An X-ray examination of the crystals did not reveal any of the fcc form. Two crystal specimens were used; specimen A was a sample of the undiluted Cs³⁶Cl while specimen B was diluted with "Specpure" CsCl to give a final specific activity of 4 $\mu\text{c./g.}$

Conductivity.—A single crystal of CsCl, large enough (5 × 5 × 2 mm.) for conductance measurements, was grown slowly from a concentrated solution of CsCl in water containing a small quantity of urea.⁹ Carbon electrodes were painted on a polished slice of the crystal which then was clamped between platinum electrodes. The crystal was maintained in a dry nitrogen atmosphere. The resistance of the specimen was measured over the temperature range 280–470° with a Philips PR 9500 a.c. conductivity bridge. The temperature of the specimen was measured by a Pt—Pt + 13% Rh thermocouple.

Results

Diffusion.—Diffusion rates were measured for both specimens at four temperatures between 260 and 430°. Plots of R^2 (R = counting rate in the gas phase) against time were accurately linear, showing that the kinetics of simple bulk diffusion were being obeyed. However, plots of the logarithm of the diffusion rate against the reciprocal of the absolute temperature were slightly curved, indicating a variation in the apparent activation energy from 1.3 e.v. at 270° to 1.0 e.v. at 400°. The magnitude of these activation energies is closely similar to that found in other measurements on the cesium halides (Cl^- in polycrystalline CsCl,¹⁰ Br^- in CsBr and I^- in CsI).¹¹

The temperature of the specimens then was increased to 487° at a uniform rate of 25°/hr. and the count rate in the gas phase recorded at 3 min.

(4) W. W. Harpur, R. L. Moss and A. R. Ubbelohde, *Proc. Roy. Soc. (London)*, **A232**, 196 (1955).

(5) W. W. Harpur and A. R. Ubbelohde, *ibid.*, **A232**, 310 (1955).

(6) F. Lantelme and J. Pauly, *Compt. rend.*, **249**, 677 (1959).

(7) D. Patterson, G. S. Rose and J. A. Morrison, *Phil. Mag.*, **1**, 393 (1956).

(8) L. G. Harrison, J. A. Morrison and R. Rudham, *Trans. Faraday Soc.*, **54**, 106 (1958).

(9) P. Avakian and A. Smakula, *J. Appl. Phys.*, **31**, 1720 (1960).

(10) J. P. Laurent and J. Bénard, *J. Phys. and Chem. Solids*, **3**, 7 (1957).

(11) D. W. Lynch, *Phys. Rev.*, **118**, 468 (1960).

intervals. The results are shown in Fig. 1. Above 470° the rate of change of the counting rate with temperature decreases steadily, which is consistent with a smooth change to the lower diffusion rate in the fcc form.¹⁰ The curves indicate that the transformation is complete at 480°, but this is necessarily an overestimate because the time for complete mixing of the gas in the apparatus was about 10 min.⁸

Some further measurements were made of the count rate during the cooling of sample B. The specimen had been maintained at approximately 545° for 1 hr. and then was cooled at the rate of 40°/hr. The counting rate in the gas phase was recorded at 3-min. intervals over the temperature range 480 to 430°. These results also are shown in Fig. 1; there is a small but significant increase in the count rate in the region of 440°. Since the specimen had been at a higher temperature for an appreciable time, the increase in R upon cooling cannot be accounted for by diffusion. The probable cause is an increase in the surface area of the specimen brought about by some fragmentation of the crystals during the transformation from the fcc to the bcc form.

Conductivity.—The results of the two conductivity runs on the single crystal of CsCl are shown graphically in Fig. 2 as a plot of $\log \sigma$ against $1/T$ (for the sake of clarity some of the results have been omitted from this graph). The $\log \sigma$ vs. $1/T$ plot is linear up to 467° in one case and to 462° in the other. Above these temperatures $\log \sigma$ decreases smoothly. The apparent activation energy, obtained from the linear portion of the graph, is 1.22 e.v. and the conductivity in this region can be represented by

$$\sigma = 2.3 \times 10^4 \exp(-1.22/kT)$$

Discussion

The magnitude of the conductivity of the single crystal of CsCl is very close to the values reported for the conductivity of CsBr and CsI¹¹ (Table I).

TABLE I
CONDUCTANCE PARAMETERS FOR CsCl, CsBr AND CsI

Material	Temp. range, °C.	σ_0 , ohm ⁻¹ cm. ⁻¹	E , e.v.
CsBr ¹¹	Impurity region—475	2.51×10^4	1.285
CsI ¹¹	Impurity region—480	1.38×10^4	1.25
CsCl	280–470	2.3×10^4	1.22

Lynch¹¹ already has shown, from a comparison of the self-diffusion and the conductivity in CsBr and CsI, that these salts are essentially ionic conductors, the anion being the more mobile species. The magnitude of the conductivity of CsCl compared to that of CsBr and CsI and the agreement between our values for the activation energies for conduction and for chloride ion diffusion would indicate that CsCl is also predominantly an ionic conductor.

The absence of any enhanced diffusion in the pretransition region shows clearly that the transition from the bcc form to the fcc form occurs without the formation of a large excess of lattice vacancies. It seems probable, therefore, that the transformation does not involve an extensive disruption

of the lattice but rather a simple change such as dilatation, as has been suggested by Buerger.¹² This being so, the observation of Lantelme and Pauly⁶ has to be attributed to some other cause, possibly to the release of radiation damage.

Acknowledgment.—We wish to thank Dr. J. Trotter for the X-ray analysis.

(12) M. J. Buerger, "Phase Transformations in Solids," John Wiley and Sons, Inc., New York, N. Y., 1951, p. 183.

INFRARED SPECTRA OF SOME PHOTOGRAPHIC STABILIZERS ADSORBED ON SILVER BROMIDE

BY MIKIO TAMURA, HIROSHI HADA, JUNPEI NOGUCHI, AND SOICHI HAYASHI

Department of Industrial Chemistry and Institute for Chemical Research, Kyoto University, Yoshida, Kyoto, Japan

Received September 18, 1961

There is no convincing explanation for the mechanism of the stabilizing or antifoggant action of organic stabilizers on photographic emulsion.¹⁻³ Matthies and Wendt suggest that the compounds which form soluble silver salts in the same range as or less than silver halide have stabilizing action. Carroll and Hubbard suggest that the stabilization is caused by the adsorption of stabilizers on silver halide.

In this work, the authors have studied the adsorption state of some photographic stabilizers on silver bromide by comparing the infrared spectra of stabilizers adsorbed on silver bromide with those of the stabilizers, the silver salts of the stabilizers, and the sodium salts of the stabilizers in an aqueous solution, and it was found that the adsorption state of the stabilizers on silver bromide was the same as or similar to that of the silver salt of the stabilizers.

The stabilizers used were 2-mercaptobenzothiazole (I), 2-mercaptobenzoxazole (II), 1-phenyl-5-mercaptotetrazole (III), benzotriazole (IV) and 5-methyl-7-hydroxy-2,3,4,7-tetrazaindene (V).

The infrared spectra of the stabilizer and those of the silver salts, which were precipitated from solutions of silver nitrate and the stabilizers without controlling the pH, were measured as an AgBr disk; those of the aqueous solution of the sodium salts of the stabilizers were measured between two KRS-5 plates; and those of the stabilizers adsorbed on silver bromide were measured as a disk with silver bromide adsorbent at several points on the adsorption isotherm curve determined previously. The adsorption isotherms of the stabilizers on silver bromide were obtained from colorimetric measurements⁴ using ultraviolet absorption of the stabilizers at pH 5. The solutions of stabilizers employed for adsorption measurements contained several per cent. methanol or ethanol, and 10^{-3} M potassium bromide, which decreases the solubility of silver bromide adsorbent. The solutions did not contain

(1) C. E. K. Mees, "The Theory of the Photographic Process," Rev. Ed., The Macmillan Co., New York, N. Y., 1954, p. 667.

(2) S. Kikuchi, R. Nishimura, S. Fukushima and S. Fujisawa, "Kagaku Shashin Binran," Vol. II Maruzen, Tokyo, 1959, p. 42.

(3) E. J. Birr, *Z. wiss. Phot.*, **48**, 103 (1953); **49**, [I] 261 (1954); **50**, [I] 107, 124 (1955).

(4) Cf. e.g., Y. Koseki, *Bull. So. Sci. Phot. Japan*, **6**, 1 (1956).

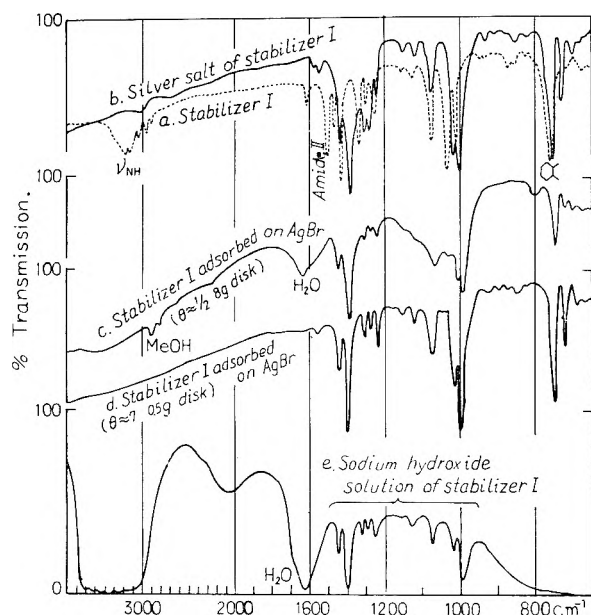


Fig. 1.—Infrared spectra of 2-mercaptobenzothiazole (stabilizer I) in various states.

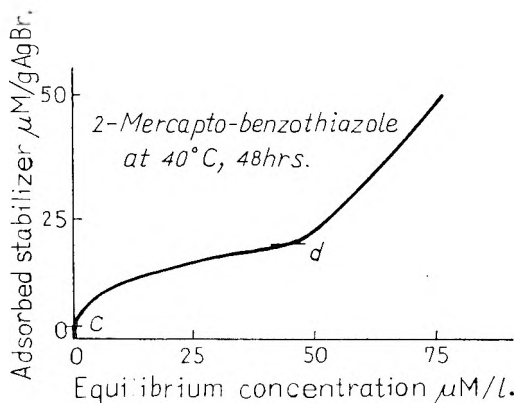


Fig. 2.—Adsorption isotherm of 2-mercaptobenzothiazole on silver bromide.

buffer solution for adjustment of the pH. The noticeable change in the ultraviolet absorption of the stabilizers before and after adsorption was not observed. The specific surface of the silver bromide adsorbent was determined by using 3,3'-diethyl-9-methyl-thiocarbocyanine dye. The adsorption ratio, θ , was calculated from the dimension of the stabilizer molecules and the specific surface of the silver bromide adsorbent. There was no difference between the infrared spectrum of the dye adsorbed on silver bromide and that of the dye (as a silver bromide disk). This fact shows that the force of the adsorption between cyanine dye and silver bromide is not of the nature of the covalent bond

The curves a, b, c, d and e in Fig. 1 show the infrared spectra of stabilizer I in various states. Figure 2 shows the adsorption isotherm of stabilizer I on silver bromide. The curves of c and d in Fig. 1 are the infrared spectra of the adsorbed stabilizer at c and d on the adsorption isotherm in Fig. 2.

Making a comparison between a and b spectra in Fig. 1, we see marked differences between the infrared spectrum of stabilizer I and that of the silver salt of stabilizer I. The ν_{NH} and amide II

bands, etc., of the stabilizer disappear and some characteristic bands of silver salt are observed at 1393, 1280, 1000 cm^{-1} , etc. It is seen from the b, c, d and e spectra in Fig. 1 that the spectrum of the silver salt is equal to that of the stabilizer in the adsorption state and that of an aqueous solution of the sodium salt of the stabilizer (negative ion of stabilizer). It is very interesting that the spectrum of adsorbed stabilizer I at $\theta \approx 1/2$ is the same as that at $\theta \approx 7$.

From the above experimental results, it may be concluded that stabilizer I is adsorbed on silver bromide as a silver salt in both low and high adsorption ratios and that the state of the adsorbed stabilizer is the same as that of the negative ion of the stabilizer. These results suggest that the silver salt of stabilizer I is in an ionic crystal state and that stabilizer I reacts with silver bromide crystals and forms a silver salt ionic crystal on the surface of the silver bromide. The band at 2902 cm^{-1} is assigned to methanol adsorbed on silver bromide. This band cannot be found in higher adsorption ratios (Fig. 1d). This fact indicates that the stabilizer is adsorbed more firmly than methanol in silver bromide.

Though the situation of stabilizer I described above also was observed for stabilizers II and III, the infrared spectra of stabilizers IV and V adsorbed on silver bromide were somewhat different from those of the silver salts or aqueous solutions of the sodium salts. As the difference is minor, it may be stated that these photographic stabilizers exist on silver bromide as silver salts of the stabilizers, although these stabilizers were not adsorbed more than $\theta = 1$.

On the mechanism of the stabilizing action of stabilizers on photographic emulsion, we consider for the present that the negative ion of the stabilizer adsorbed in incomplete regions on the silver bromide surface by exchange reaction with bromide ion exerts a stabilizing, or antifoggant action by retarding the growth of fog nuclei or reducing the rate of development.

PROTON N.M.R. SPECTROSCOPY. XIV. ACCURATE MEASUREMENT OF THE SPECTRAL POSITION OF THE FORMYL PEAK OF *p*-ANISALDEHYDE, USEFUL FOR CHECKING THE CALIBRATION OF N.M.R. SPECTROMETERS

BY GEORGE V. D. TIERS AND DONALD R. HOTCHKISS

Contribution No. 218 from the Central Research Dept. of the Minnesota Mining and Manufacturing Co., St. Paul, 19, Minn.

Received September 18, 1961

A persistent problem in high-resolution n.m.r. spectroscopy has been the accuracy of shielding value ("chemical-shift") measurements. Commercial spectrometers¹ as supplied are inadequately calibrated, since the dial readings of the audio-oscillator which is used for precision determination of spectral position^{2,3} are well known to be rather

(1) For example the V-4300-B (40 Mc./sec.) and the HR-60 (60 Mc./sec.) spectrometers available from Varian Associates, Inc., Palo Alto, Calif.

inaccurate. Virtually all owners of these instruments recognize this problem, and most have solved it by installation of a precision frequency counter.⁴ With this addition these n.m.r. instruments truly become spectrometers, reproducibility of measurement between different laboratories being ± 0.001 p.p.m., or one part in 10^4 of the peak separation studied.⁵

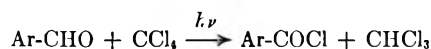
The recent introduction of the remarkable Varian A-60 spectrometer, which combines convenience of operation with very high resolution,⁶ has prompted a reconsideration of the question of spectrometer accuracy, since the calibration of this instrument is dependent on the accuracy of certain potentiometers. There is no method for internal calibration, though provision has been made for introduction of sidebands if one should have an audio-oscillator (which of course must be monitored by a frequency counter). It seems likely that most owners will not provide this accessory equipment. Inasmuch as the manufacturer does not claim initial accuracy better than ± 0.02 p.p.m., there is a reasonable chance that, with use, these instruments may develop yet more serious errors in spectral position measurement despite excellent resolution and general performance. Accordingly it should be regarded as rather important to check, occasionally, the calibration of all A-60 spectrometers.

For this purpose we recommend the formyl peak of *p*-anisaldehyde, which is at the extreme low-field end of the normal proton spectrum, $+0.197_0 \tau$ (± 0.0005). The large separation, nearly ten p.p.m., between this peak and that of the internal reference, tetramethylsilane, is desirable from the standpoint of magnifying percentage errors; however this is also a shortcoming in that the usual spectrum produced by the A-60 spectrometer does not include peaks below $+1.67 \tau$, making it necessary to use the "spectrum-offset" device to bring the formyl peak on scale. The low τ -value is not a serious limitation, however, since this offset feature is required whenever a region of the spectrum is to be expanded for more detailed investigation; therefore this unit also should be checked for accuracy. The methoxyl peak, at $6.139 \pm 0.002 \tau$, may be used as a test of linearity, and the aromatic peaks provide a convenient visual estimate of performance. A better test of resolution is seen in the formyl peak itself, which is a closely-spaced triplet having $J =$

0.57 ± 0.03 c./sec.⁷ However, for numerical evaluation of resolution, line widths at half-height are preferable.⁶

Experimental

The n.m.r. equipment and techniques have been described in detail.³ The *p*-anisaldehyde, from the Eastman Kodak Co., was distilled before use to remove oxidation products; a 4.0% (by volume) solution of it was made in "spectro grade" carbon tetrachloride (Matheson Coleman & Bell) which already contained 1.0% (by volume) of tetramethylsilane (Andersor Laboratories, Division of the Stauffer Chemical Co.). Sixteen n.m.r. tubes were filled with this solution; each tube then was sealed after having been purged with a fine stream of oxygen-free nitrogen to sweep out dissolved oxygen. Sample tubes so prepared have remained unchanged for a period of two years. *Caution:* These n.m.r. tubes should *not* be exposed to a high level of illumination over a long period of time. One of the tubes, in bright light for several weeks, was found by n.m.r. analysis to contain some chloroform and *p*-anisyl chloride, formed by the free-radical reaction



A very large number of n.m.r. measurements were made, 12 separate determinations being made on each of the 16 tubes. It thus was possible to reduce the standard deviation in the *averaged* value to ± 0.0005 p.p.m. even though the standard deviation for a single determination, namely ± 0.007 p.p.m., was much higher. The fundamental accuracy of this procedure is indicated by the remarkably good agreement, within ± 0.001 p.p.m., of our averaged value at 25.0° , $0.197_0 \tau$, ± 0.0005 , with final results from each of several other careful workers⁸; in most cases their standard deviations for a single measurement were appreciably smaller than ours.

A further series of 26 measurements was made at $+77^\circ$, the Varian variable-temperature apparatus and probe modification being employed, and the formyl peak was found to have shifted very slightly, to $+0.181 \tau$, ± 0.003 . From this observation the temperature coefficient of the τ -value for the formyl peak (assumed constant over the temperature range studied) was evaluated as -0.0003 p.p.m. per degree temperature rise. This correction was applied to certain results obtained⁶ at slightly different temperatures.

(7) First observed by C. A. Reilly at the Shell Development Co.

SOLVENT GLASSES FOR LOW TEMPERATURE SPECTROSCOPIC STUDIES

BY DONALD R. SCOTT¹ AND JEAN B. ALLISON¹

Spectroscopy Laboratory, Chemistry Department, University of Houston, Houston 4, Texas

Received September 23, 1961

We have compiled in the accompanying Table I a series of solvent systems which are particularly useful for electronic emission spectral studies at liquid nitrogen temperature, 77°K . All of these systems form transparent, rigid glasses at that temperature when proper precautions are taken to ensure that all components are anhydrous and of high purity.² Many of these glasses have been employed in this Laboratory and in others for several years for low temperature electronic spectral studies. However, several of the systems are known to be original with this Laboratory. Several of the more unusual systems are useful when one wishes to study a compound which has a limited solubility in the usual hydrocarbon or hydroxylic

(2) J. T. Arnold and M. T. Packard, *J. Chem. Phys.*, **19**, 1808 (1951).

(3) G. V. D. Tiers, *J. Phys. Chem.*, **62**, 1151 (1958).

(4) For example, the 522-B counter, manufactured by the Hewlett-Packard Co., Palo Alto, Calif.; any counter giving precision to ± 0.1 c./sec. is equivalent.

(5) A cooperative study was carried out for the NMR Subcommittee of A.S.T.M. Committee E-13 on Absorption Spectroscopy by the authors together with the following (among others). At 40 Mc./sec.: P. C. Lauterbur, Mellon Institute; C. A. Reilly, Shell Development Co.; C. M. Huggins, General Electric Research Lab.; R. E. Glick, Pennsylvania State Univ.; D. P. Ames, Monsanto Chemical Co. At 60 Mc./sec.: A. A. Bothner-By and B. L. Shapiro, Mellon Institute; J. N. Shoolery and L. F. Johnson, Varian Associates; E. D. Becker, Natl. Inst. of Health; K. J. Palmer, U.S.D.A. Western Util. Research Div.; N. F. Chamberlain, Humble Oil Co.; M. T. Rogers, Michigan State Univ. All of the above workers reported final results for the τ -value of the formyl peak of *p*-anisaldehyde (at 4.0% concn. by volume in CCl_4) within ± 0.001 p.p.m. of the "best averaged value" obtained in our measurements.

(6) G. V. D. Tiers, *J. Phys. Chem.*, **65**, 1916 (1961).

(1) Robert A. Welch Foundation Pre-doctoral Fellow.

(2) W. J. Potts, Jr., *J. Chem. Phys.*, **21**, 191 (1953).

glasses. To our knowledge no other compilation of this nature has appeared in the literature.

We wish to thank Dr. R. S. Becker for helpful suggestions and the use of the facilities of the Spectroscopy Laboratory.

TABLE I
LOW TEMPERATURE RIGID GLASS SYSTEMS

System	Composition (vol.:vol.)
Hydrocarbons	
3-Methylpentane	
Isopentane:methylcyclohexane	1:4
Pentene-2 (<i>cis</i>)-pentene-2 (<i>trans</i>) ^c	
Alcohols	
Methanol:ethanol ^a	1:4
Ethanol ^b	
Isopropyl alcohol ^b	
1-Propanol ^b	
1-Butanol ^b	
Ethers	
<i>n</i> -Butyl ether:isopropyl ether:diethyl ether	3:5:12
2-Methyltetrahydrofuran	
Alcohols:Ethers	
Ethanol:diethyl ether	1:1
Propanol:diethyl ether	2:5
Butanol:diethyl ether	2:5
Alcohol:Ether:Hydrocarbon	
Ethanol:isopentane:diethyl ether	2:5:5
Isopropyl alcohol:isopentane:diethyl ether	2:5:5
Hydrocarbons:Ethers	
Diethyl ether:isopentane	1:1
Diethyl ether:pentene-2 (<i>cis</i>)-pentene-2 (<i>trans</i>) ^c	2:1
Miscellaneous	
Diethyl ether:ethanol:toluene	2:1:1
Diethyl ether:isopentane:ethanol:dimethylformamide	12:10:6:1
Diethyl ether:isopentane:ethanol:1-chloronaphthalene	8:6:2:2
Diethyl ether:isopentane:ethanol:pyridine	12:10:6:1
Diethyl ether:isopentane:triethylamine	5:5:2
Isopentane:methylcyclopentane:methylcyclohexane:ethyl bromide	7:7:4:1

^a This glass is particularly stable for an all alcohol system. ^b If cooled slowly, these glasses can be used. They are unstable and crack easily. ^c Mixed *cis*- and *trans*-pentene-2 available from Phillips Petroleum Co., Special Products Division, Bartlesville, Oklahoma.

ULTRAVIOLET ABSORPTION SPECTRA OF *o*-, *m*-, AND *p*-NITROBENZOIC ACIDS

BY ASISH KUMAR CHANDRA

Department of Chemistry, University College of Science and Technology,
Calcutta 9, India

Received October 8, 1961

Introduction of a substituent group for hydrogen in a benzene nucleus long has been known to cause shifts in the spectrum of the original benzene derivative to longer wave lengths. The near-ultraviolet absorption spectra of some mono-substituted benzenes containing nitro, carbonyl and carboxyl groups as substituents have been interpreted by

Nagakura and Tanaka¹ in terms of the intramolecular charge-transfer involving an excitation of a bonding electron of the highest occupied energy level of benzene to the vacant energy level of the substituent group.

In this note an attempt has been made to investigate the absorption spectra of *o*-, *m*- and *p*-nitrobenzoic acids and to explain them according to the concept of intramolecular charge-transfer absorption.

Experimental

The near-ultraviolet absorption spectra of benzoic acid and nitrobenzoic acids were measured in water on a Beckman spectrophotometer Model DU using 1-cm. silica cells at room temperature (27°). In Fig. 1 are shown the absorption curves of benzoic acid and the nitrobenzoic acids. The results are recorded in Table I, where intensities and positions of the maximum absorption bands of *o*-, *m*- and *p*-nitrobenzoic acids are expressed as the logarithm of the molar extinction coefficients and as e.v. units, respectively. The materials used were all B.D.H. reagents. They were recrystallized repeatedly from ethanol and water until they gave constant melting points in agreement with those listed in the literature.

Theoretical Consideration by the Use of Energy Level Diagrams.—In order to explain the maximum absorption bands of *o*-, *m*- and *p*-nitrobenzoic acids from the concept of intramolecular charge-transfer involving excitation of a bonding electron from the highest occupied orbital of nitrobenzene to the vacant orbital of the carboxyl group, it is necessary to obtain the molecular energy level diagrams of the nitrobenzene and the substituent carboxyl group. These diagrams are determined on the basis of experimental results of the ionization potential and the electronic absorption spectrum. The energies of the highest and lower occupied orbitals of nitrobenzene were determined by Nagakura, *et al.*² The lowest vacant orbital of nitrobenzene could be estimated by adding the excitation energy to the highest occupied orbital. The vacant energy level of the carboxyl group is estimated at -4.67 e.v.² Since the lowest vacant orbital of nitrobenzene, *i.e.*, V_N and that of the carboxyl group, *i.e.*, V_{CO_2H} are nearly degenerate, as is evident in Fig. 2, there will be strong interactions between these two levels; as a result the first vacant orbital of nitrobenzoic acid will be depressed considerably. In this paper we shall attempt to explain the ultraviolet absorption spectra of nitrobenzoic acids by considering the interaction of the occupied orbital H_{n1} and the orbital V_N of nitrobenzene with the orbital V_{CO_2H} of the carboxyl group. The highest occupied orbital W_1 of nitrobenzoic acid obtained from the interaction of H_{n1} with V_{CO_2H} level is given by

$$W_1 = \frac{1}{2} [H_{n1} + V_{CO_2H} + \{(H_{n1} - V_{CO_2H})^2 + 4C_1^2 C_{CO_2H}^2 \beta^2\}^{1/2}] \quad (1)$$

while the lowest vacant orbital W_2 obtained from the interaction of V_N with V_{CO_2H} is given as

$$W_2 = \frac{1}{2} [V_N + V_{CO_2H} + \{(V_N - V_{CO_2H})^2 + 4C_2^2 C_{CO_2H}^2 \beta^2\}^{1/2}] \quad (2)$$

where H_{n1} , V_N and V_{CO_2H} are equal to the energies of the highest occupied and lowest vacant orbitals

(1) S. Nagakura and J. Tanaka, *J. Chem. Phys.*, **22**, 236 (1954).

(2) S. Nagakura, J. Tanaka and M. Kobayashi, *ibid.*, **24**, 311 (1956).

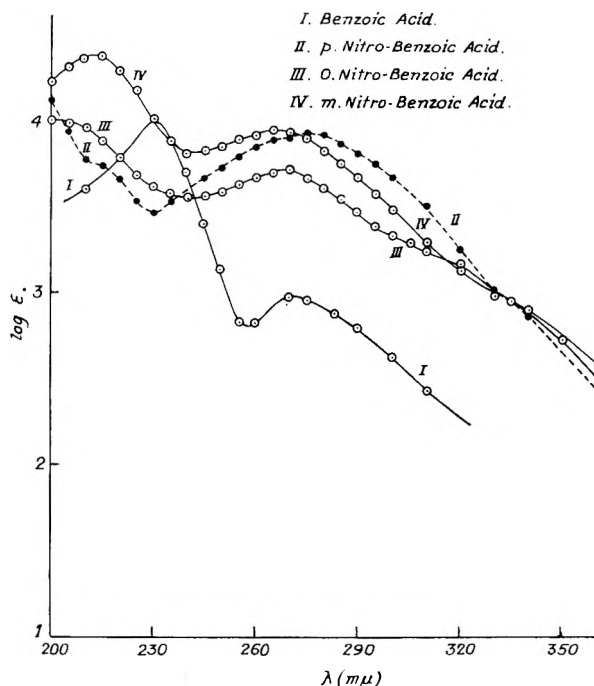


Fig. 1.—Near ultraviolet absorption spectra of nitrobenzoic acids and benzoic acids (solvent, water).

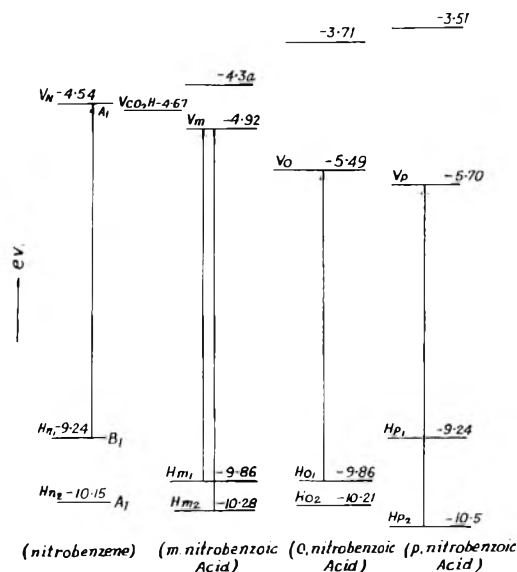


Fig. 2.—Energy level diagrams of nitrobenzene and nitrobenzoic acids.

of nitrobenzene and the lowest vacant orbital of the carboxyl group. The C_1 and C_2 are the coefficients of the atomic orbital of a carbon atom to which the substituent is attached in the molecular orbitals H_{N1} and V_N of nitrobenzene, while the C_{CO_2H} is the coefficient of the atomic orbital of the carbon atom in the molecular orbital V_{CO_2H} . The β is the resonance integral of the C-C bond joining the two conjugated systems. The value of β is taken as -3 e.v. The excitation from W_1 to W_2 gives rise to the near-ultraviolet absorption spectra of the nitrobenzoic acids.

As is well known the degeneracy of the highest occupied orbital of benzene is removed by the perturbation of a substituent and therefore for the

nitrobenzene we expect the existence of two corresponding occupied orbitals H_{n1} and H_{n2} . Since V_{CO_2H} can interact with both the levels H_{n1} and H_{n2} , for *o*- and *m*-nitrobenzoic acids we should expect two absorption bands at longer wave lengths. On substituting the carboxyl group in the *para*-position of nitrobenzene, a transition of a bonding electron from the H_{P2} level to the lowest vacant orbital V_P can be predicted to show an intense band, while the H_{n1} level of nitrobenzene remains unaffected (Fig. 2). Simple quantitative considerations were made using equations 1 and 2. The calculated results³ are shown in Table I together with the experimental ones.

TABLE I

CALCULATED AND OBSERVED SPECTRA OF NITROBENZOIC ACIDS (IN WATER)

	Calcd. spectra, e.v.	Obsd. spectra, e.v.	log ϵ
<i>o</i> -Nitrobenzoic acid	4.37	4.59	3.72
	4.72
<i>m</i> -Nitrobenzoic acid	4.94	4.67	3.95
	5.36	5.79	4.38
<i>p</i> -Nitrobenzoic acid	4.80	4.46	3.92

Discussion

Table I shows that the agreement is not very satisfactory in view of the simplicity of the theoretical treatment. Nevertheless, the observed differences in the spectra of the nitrobenzoic acids are qualitatively explained. It would be interesting to see if the absorption spectra of the nitrobenzoic acids could be explained in terms of the intramolecular charge transfer from benzoic acid to the vacant orbital of the nitro group. Since molecular energy level diagrams of benzoic acid are not known, this calculation cannot be undertaken. Moreover, it is desired that in the more exact theoretical treatment we should consider all possible configurations representing the charge-transfer and mix them.

Ortho-substituted benzene usually shows a spectrum resembling that of a *meta*-substituted benzene, but the behavior of *o*-nitrobenzoic acid is somewhat different from that of *m*-nitrobenzoic acid and shows a little broad spectrum with only one band at 268 μ . This difference may be attributed to steric hindrance by the adjacent large nitro and carboxyl groups. This steric hindrance may interfere with the coplanar arrangement of the two substituent groups with the benzene nucleus. The *p*-nitrobenzoic acid shows only one strong charge transfer band while the transition $H_P \rightarrow V_P$ at 3.5 e.v. is not observed, although this is an allowed in-plane transition. Similar transition in many other *para*-disubstituted benzenes⁴ is not observed.

The weak shoulders of the nitrobenzoic acids at 335 μ cannot be unequivocally accounted for. It may be suggested from the comparison of the

(3) The coefficients of atomic orbitals in the molecular orbitals of nitrobenzene are determined by the standard LCAO method with the same parameters used in ref. 2. To determine the coefficients of atomic orbitals in the molecular orbitals of the carboxyl group the following parameters were chosen, e.g.: Coulomb integral $\alpha_0 = \alpha_c + 2\beta$; α (carbon attached to oxygen) = $\alpha_c + 0.1\beta$ and $\beta_{co} = \sqrt{2}\beta$ where β is the C-C resonance integral.

(4) S. Nagakura and J. Tanaka, *J. Chem. Phys.*, **24**, 1274 (1956).

intensities that they correspond either to the 270 $m\mu$ band of benzoic acid or to the 290 $m\mu^5$ band of nitrobenzene.

(5) A. Venzel, *J. Chem. Phys.*, **22**, 1623 (1954).

RECOIL-FREE γ -RAY TRANSITION OF Fe^{57} IN THE BLOOD COMPONENT HEMIN

BY ULRICH GONSER

Atoms International, Division of North American Aviation, Inc.,
Canoga Park, California

Received October 5, 1961

Mössbauer¹ has shown that the nuclear recoil of an atom emitting or absorbing a γ -ray may be absent when the decaying or absorbing atom is bound in a crystal. The recoil energy of a free atom, $E_R(\text{atom})$, is given in good approximation by

$$E_R(\text{atom}) = \frac{E_\gamma^2}{2m c^2} \quad (1)$$

where E_γ is the energy of the nuclear transition, m the mass of the nucleus and c the velocity of light. If the emitting atom is bound in a crystal and $E_R(\text{atom})$ is comparatively small relative to the Debye energy, $\hbar\omega_\theta$, where ω_θ is the limiting frequency of the Debye spectrum, a finite probability exists that the entire crystal takes up the recoil momentum resulting in a negligible energy loss by the γ -ray. The fraction of recoil free events is proportional to the familiar Debye-Waller factor.

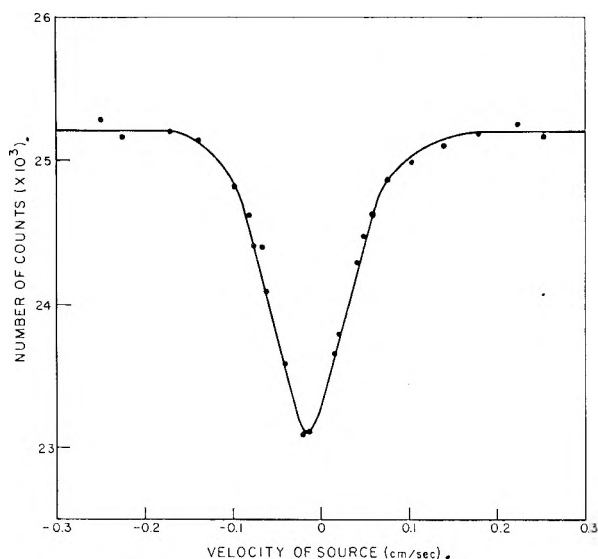


Fig. 1.—Spectrum of the 14.4 kev. γ -ray, produced by the decay of Co^{57} diffused into copper metal and a hemin absorber kept at liquid nitrogen temperature.

The class of materials available for Mössbauer experiments can be extended to organic molecules which contain the atom undergoing the nuclear transition. In order to calculate the fraction of recoil free events for this case, one has not only to consider the Debye frequencies of the organic crystal but also the fundamental vibrational frequencies, ω_f , of the emitting atom in the molecule. To get an appreciable Mössbauer effect,

(1) R. L. Mössbauer, *Z. Physik*, **151**, 124 (1958).

$\hbar\omega_f$ should be large compared to $E_R(\text{atom})$ and $\hbar\omega_\theta$ large compared to $E_R(\text{molecule})$. The ambient temperature should be low compared to the Debye temperature of the organic crystal and also low enough that the fundamental vibrational modes are not thermally excited. In such a crystal, the Debye-Waller factor consists of a term which accounts for the Debye frequencies and another term which accounts for the fundamental vibrational modes of the molecule. If the molecule is very large and the recoil momentum is taken up by the whole molecule, $E_R(\text{molecule})$ in eq. 1 becomes very small and can become of the order of the natural line width. In this case a large molecule containing the atom undergoing the transition does not have to be part of a solid crystal. A Mössbauer effect might be expected even from a large molecule in a liquid. A broadening may occur due to convection and Brownian movement (first-order Doppler effect).

An investigation was started to search for the recoil-free γ -transition of Fe^{57} in blood and in blood components. The red cells of blood consist of 32% hemoglobin with the empirical formula $[C_{738}H_{1166}O_{208}N_{203}S_2Fe]_4$. Hydrolysis of hemoglobin cleaves the molecule into two fragments: heme, which contains the Fe-atom, and the protein globin. Hemin is the chloride form of heme.² The iron is bound to four nitrogen atoms by either primary valences or coordinated links. The nitrogen atoms form a plane. The out-of-plane fundamental frequency probably is different from the in-plane frequency. Therefore, using a single crystal of hemin, a directionally dependent Mössbauer effect can be expected.

The recoil energy for a free iron atom, for a rigid hemin molecule, for a hemoglobin molecule and for one red cell emitting or absorbing a 14.4 Kev. γ -ray is according to eq. 1

$E_R(\text{Fe})$:	2×10^{-3} e.v.
$E_R(\text{hemin molecule})$:	2×10^{-4} e.v.
$E_R(\text{hemoglobin molecule})$:	2×10^{-6} e.v.
$E_R(\text{one red cell})$:	10^{-14} e.v.

These values have to be compared with the natural line width of the 14.4 kev. γ -transition of Fe^{57} which is $\Gamma = 5 \times 10^{-9}$ e.v. The natural line width is smaller than $E_R(\text{hemoglobin})$ but wide compared to $E_R(\text{red cell})$.

A source of Co^{57} diffused in Cu was used. The absorber consisted of 135 mg. hemin/cm.² held between thin aluminum foils which were mounted in a holder and connected to a liquid nitrogen cryostat.

The measured counts as a function of velocity of the source are shown in Figure 1. If these data are compared to the data for the same source with a stainless steel absorber, it is seen that the hemin curve is shifted toward the center (zero velocity) by a very small amount (about 0.01 cm./sec.) and the line width is nearly twice as large. The isomer shift (or chemical shift), which is a measure of the electron density at the nucleus, is indicative of the chemical binding of the iron atom. A large isomer shift was observed in Fe^{2+}

(2) L. F. Fieser and M. Fieser, "Organic Chemistry," D. C. Heath & Co., Boston, Mass., 2nd ed., p. 465.

and Fe³⁺ compounds but the shift was very small in K₄Fe(CN)₆·3H₂O and K₃Fe(CN)₆.³ One can assume that the iron atoms in these complexes and in hemin have similar electron configurations. A small shift may arise from a difference in the internal energy of source and absorber (including zero point energy of the oscillators in source and absorber). This temperature red-shift can be attributed to the relativistic time dilatation caused by the motion of the nuclei and molecules.⁴ The broadening could be an unresolved splitting due to the quadrupole interaction of the excited state of Fe⁵⁷ with the electric field gradient at the Fe atom. The strong absorption effect indicates that $\hbar\omega_f$ as well as $\hbar\omega_g$ of hemin is comparatively large relative to $E_R(\text{Fe})$ and $E_R(\text{molecule})$, respectively.

Measurements are in progress to investigate the temperature dependence, the line structure and larger molecules such as hemoglobin. Difficulties arise from the low concentration of Fe⁵⁷ in the specimens and the competing photoeffect. A theoretical paper will discuss the modes of vibration and chemical binding of the Fe atom which satisfies the Mössbauer absorption curve.

It came to our attention that P. G. Reizenstein and T. B. Swan reported a Mössbauer effect in hemin and hematin (International Biophysics Congress, Stockholm, Sweden, July 31–August 4, 1961).

Discussions with Dr. R. E. DeWames, Dr. A. H. Muir and Mr. C. J. Engberg are gratefully acknowledged. The author is indebted to Mr. Engberg for designing the drive system.

(3) L. R. Walker, G. K. Wertheim and V. Jaccarino, *Phys. Rev. Letters*, **6**, 98 (1961).

(4) B. D. Josephson, *ibid.*, **4**, 341 (1960).

THE VARIATION OF THE SEDIMENTATION COEFFICIENT WITH PRESSURE AND CONCENTRATION*

BY IRWIN H. BILLICK

Analytical Research Division, Esso Research & Engineering Company, Linden, New Jersey

Received October 7, 1961

Recently, Wales¹ has solved the differential equation of Fujita² relating the boundary position to time for a monodispersed species in a sector shaped cell, when the sedimentation coefficient depends on both pressure and concentration. Equation 1 shows the original relationship²

$$\frac{dy_*}{d\tau} = \frac{y_*}{1 + \alpha\theta_*} [1 - m(y_* - 1)] \quad (1)$$

where $y_* = (r_*/r_0)^2$, the boundary position; $\theta_* = C/C_0$, the dilution factor; and $\tau = 2 \omega^2 S_0^0 t$, the reduced time. The pressure and concentration dependence parameters are given by m and α , respectively.²

Equation 1 was solved¹ both numerically, using a digital computer, and analytically. In order to

* Presented at the Metropolitan Regional Meeting, A. C. S., New York, N. Y., January 22, 1962.

(1) M. Wales, *J. Am. Chem. Soc.*, **81**, 4758 (1959).

(2) H. Fujita, *ibid.*, **78**, 3598 (1956).

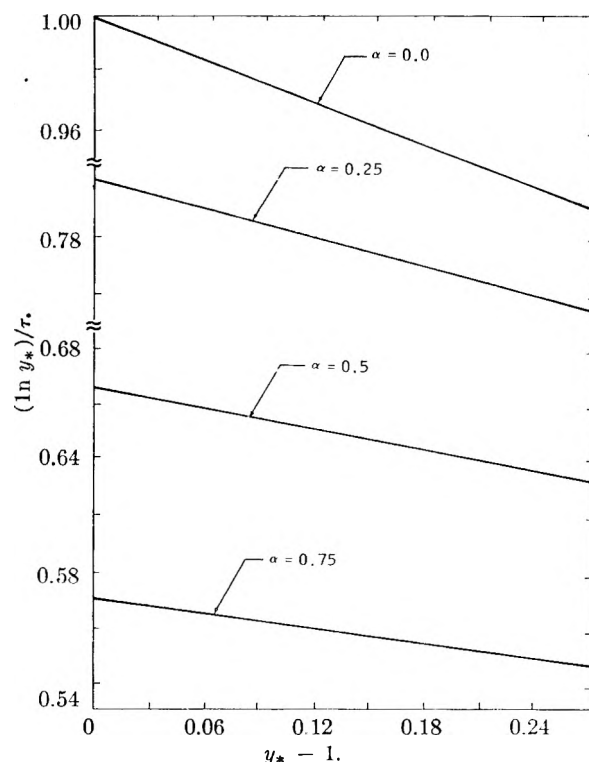


Fig. 1.—Variation of $(\ln y_*)/\tau$ with distance for various values of α . In all cases $m = 0.5$.

obtain the analytical solution the assumption was made that θ_* can be approximated by the expression at $\alpha = 0$, i.e.

$$\theta_* = \frac{1}{y_*(1 - m(y_* - 1))} \quad (2)$$

In spite of the good numerical agreement between the two solutions, the form of the analytical solution is cumbersome and difficult to apply to experimental data.

The purpose of this communication is to present alternative solutions to equation 1 which show the variation of the slope of the line relating the logarithm of the boundary position to time, i.e., the sedimentation coefficient, as a power series in time or boundary position.

A common approach for solving differential equations similar to equation 1 is "The Method of Taylor Series."³ Using this method we define a reduced sedimentation coefficient as a function of some variable $\chi - a$, as

$$S(\chi - a) \frac{\ln y_*}{\tau} = S(a) + \frac{S'(a)(\chi - a)}{1!} + \frac{S''(a)(\chi - a)^2}{2!} + \dots \quad (3)$$

where $S'(a)$ and $S''(a)$ are the first and second derivatives with respect to χ evaluated at the point a . For our purpose, we have evaluated equation 3 using

$$\chi = y_*, a = 1 \text{ and } \chi = \tau, a = 0$$

Upon attempting to obtain the coefficients using the above, one invariably obtains the indeterminate form 0/0. However, these may be readily evalu-

(3) M. R. Spiegel, "Applied Differential Equations," Prentice-Hall, Englewood Cliffs, N. J., 1950, p. 259.

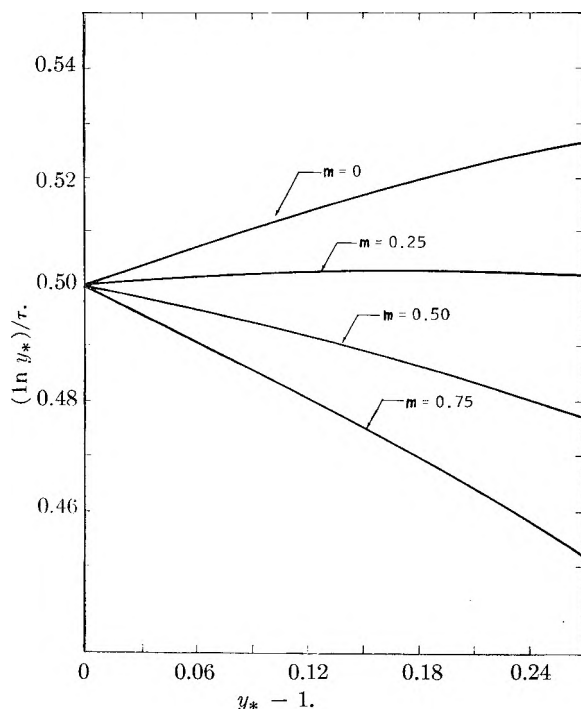


Fig. 2.—Variation of $(\ln y_*)/\tau$ with distance for various values of m . In all cases $\alpha = 1.0$.

ated by the use of the l'Hospital rule in the limit as χ approaches α . In addition, one also must have a knowledge of θ_* as a function of y_* . For the purpose of this paper, we have used the same approximation as Wales,¹ given by equation 2.

The final solutions obtained are

$$\frac{\ln y_*}{2\omega^2 t} = \frac{S_0^0}{1 + \alpha} \left[1 - \frac{1}{2} \left[\frac{m(2\alpha + 1) - \alpha}{1 + \alpha} \right] (y_* - 1) + \frac{4(1 + \alpha)^2 + 3m(m - 1)(1 + 2\alpha)^2 - 3\alpha(m - 1)}{(1 + 2\alpha) - 4(1 + \alpha)((m - 1)^2(1 + 3\alpha) + m(1 + \alpha))} \right] (y_* - 1)^2 + \dots \quad (4)$$

$$\frac{\ln y_*}{2\omega^2 t} = \frac{S_0^0}{1 + \alpha} \left[1 - \frac{1}{2} \left(\frac{m(1 + 2\alpha) - \alpha}{1 + \alpha} \right) \times \frac{S_0^0}{1 + \alpha} 2\omega^2 t + \dots \right] \quad (5)$$

When $\alpha = 0$ equation 4 reduces to the results of Fujita,² except for a reversal in sign of the third term which is unimportant. Similarly, equation 5 reduces to results obtained previously^{4,5} for the case where $m = 0$. The table given below shows a comparison between equation 4 and earlier equations describing the variation of the sedimentation coefficient when pressure and concentration effects are present. It will be noticed that the results given by equation 4 approximate the computer solution the closest.

Figures 1 and 2 show, graphically, the behavior of the sedimentation coefficient for various values of m and α . It is obvious that during a run at a single concentration the apparent sedimentation coefficient is much more sensitive to m than α , whereas the effect of α is greater as the initial concentration is varied.

Finally, it can be seen from these equations that

(4) R. A. Alberty, *J. Am. Chem. Soc.*, **76**, 3733 (1954).

(5) H. Fujita, *J. Chem. Phys.*, **23**, 1084 (1956).

for very small values of α , m , t and/or y_* , $\ln y_*$ is approximately a linear function of t and the sedimentation coefficient can be obtained in the usual manner. However, for more exact work, and to investigate the effects of pressure and radial dilution, one of the equations developed in this work should be used.

VALUES OF $(\ln y_*)/\tau$ FROM VARIOUS SOURCES FOR $\alpha = 1$, $m = 0.5$

y_*	$-\ln y_*$			
	Computer ¹	Wales eq. ¹	Oth-Desreux ⁶	Eq. 4
1.0406	0.49736	0.49723	0.49992	0.49735
1.0823	.49434	.49446	.49949	.49442
1.1250	.49074	.49121	.49759	.49117
1.2132	.48326	.48414	.49669	.48373
1.3042	.47429	.47585	.49351	.47496
1.3968	.46416	.46674	.48935	.46495

(6) J. Oth and V. Desreux, *Bull. soc. chim. Belges*, **63**, 133 (1954).

TRANSIENT SPECIES IN OXYGEN TAKE-UP BY ZINC OXIDE

BY RIMANTAS GLEMZA AND R. J. KOKES

Department of Chemistry, The Johns Hopkins University, Baltimore 18, Maryland

Received October 12, 1961

Adsorption rates often can be represented by the Elovich equation,¹ a relation requiring that the rate decreases as the time increases. Numerous theories have been devised to explain this behavior.^{1,2} With semiconductors as adsorbents, the formation of a boundary layer can lead to the observed kinetics,³⁻⁵ an alternative explanation is that two types of adsorption occur at the same time and that one of these occurs much faster than the other.¹ On zinc oxide adsorbents it is possible that both mechanisms are operating during adsorption. Recently, we have started an investigation on zinc oxide in which we have made simultaneous measurements of the amounts of adsorption and its effects on conductivity. Results with oxygen confirm earlier reports⁴ that the rate of adsorption follows the Elovich equation. Since evidence for the existence of two types of adsorption and their character has been presented,⁴⁻⁶ it seems likely that for this system the simultaneous occurrence of two types of adsorption contributes to the gross features of the kinetics. In this note, we represent experimental support for the view that oxygen adsorption on zinc oxide at elevated temperatures is a two-step consecutive process involving as an intermediate an unstable surface species.

Experimental

All measurements were made on SP 500 ZnO manufactured by the New Jersey Zinc Company. Cylindrical pellets (about 2.5 cm. long and 1.0 cm. in diameter) with four evenly spaced platinum leads perpendicular to the cylinder axis were made by compressing the loose powder and the appropriately spaced leads in a stainless steel die at 5000 p.s.i.

(1) For a recent review, see M. J. Low, *Chem. Revs.*, **60**, 267 (1961).

(2) H. A. Taylor and N. Thon, *J. Am. Chem. Soc.*, **74**, 4169 (1952).

(3) K. Hauffe, *Advances in Catalysis*, **7**, 213 (1955).

(4) T. I. Barry and F. S. Stone, *Proc. Roy. Soc. (London)*, **A355**, 124 (1960).

(5) S. R. Morrison, *Advances in Catalysis*, **7**, 259 (1955).

(6) R. J. Kokes, *J. Phys. Chem.*, **66**, 99 (1962).

The die and pellet were heated at 500° for 16 hr.; then, the pellet was removed and sintered in air at 800° for 16 hr. The sintered pill was sealed into an adsorption vessel; electrical connection to the four leads was achieved *via* four vacuum-tight metal to glass seals. Within the adsorption vessel, pure silver (without flux) was used as a solder.

D.c. resistance measurements were made by passing a known current through the outermost leads and measuring the voltage across the inner leads with a John Fluke #801 potentiometric d.c. voltmeter. Current was allowed to flow only during measurement (for about 1 sec.); reversal of the direction of current flow yielded the same measured resistance (within 1%). In order to obviate contact resistance between the leads and the semiconductor, all voltages were measured potentiometrically. Effects due to e.m.f.'s generated by temperature gradients and polarization were minimized by the method of measurement and the fact that all resistances are the average of measurements for each direction of current flow. Since the pill was ohmic for the range of currents used (30 to 0.02 mamp), the resistance reported herein is the average of several measurements and probably reliable to $\pm 1\%$.

Adsorption measurements were made on a conventional volumetric system equipped with a Pirani gage. Oxygen was prepared by fractionation of the decomposition products of degassed potassium permanganate. The pellet of zinc oxide was connected to the rest of the system *via* a trap at -78°; during evacuation the sample was protected from diffusion pump oil by a trap at -195°. In the typical initial pretreatment, the adsorption vessel and pill were heated for 16 hr. in air at 500°, and evacuated for 16 hr. at 510°; after each run the sample was evacuated for 16 hr. at 510°. This procedure yields reproducible values of the resistance; for the results reported herein the resistances at 510° after pretreatments were 37.9, 37.4, and 36.8 ohms, respectively.

Figure 1 shows a plot of $\log \sigma^2$ vs. $1/T$ (open circles) for the freshly evacuated pill. Results with other samples showed that this curve could be retraced in either direction after each pretreatment. After these data were obtained, a small amount of oxygen was admitted to the adsorption vessel at room temperature. Adsorption was virtually complete after 1 hr., at which time 0.08 μ l. of oxygen had been adsorbed. The conductivity fell, as indicated by the dotted line in Fig. 1, and remained unchanged for 5 hr. The sample then was evacuated for 5 min. and still no change in conductivity occurred even after waiting 50 hr. Then, the sample was isolated from the pumps and heated to the temperatures indicated in Fig. 1 for 1 hr., and the conductivity was measured. After the measurement at 440°, the sample was cooled and the conductivity was redetermined at the several temperatures as shown in Fig. 1. These data show that oxygen put on at room temperature has a pronounced effect on conductivity, but after treatment at elevated temperature a change occurs in which the catalyst regains its initial conductivity.

Figure 2 shows the results of two repeat kinetic runs on the same pellet. These runs were carried out by the addition of a small amount of oxygen to the pellet at 353° in a constant volume system; the kinetics were followed until all of the gas phase oxygen had adsorbed. In agreement with Barry and Stone⁴ the kinetics follow the Elovich equation until the adsorption is 90% complete. In contrast to runs at room temperature, the conductivity does not fall to a constant value; instead, the conductivity σ goes through a minimum. The position of the minimum corresponds closely to the point at which the residual pressure of oxygen becomes immeasurably small. After 25 hr., σ returns substantially to the initial value; for example, the initial value in these two runs is 10.5 ± 0.1 ohms⁻¹ and the value after 25 hr. is 10.3 ± 0.1 ohms⁻¹.

Discussion

Several investigators have postulated⁴⁻⁶ the existence of two types of oxygen adsorption on zinc oxide. On the basis of experiments on photodesorption and adsorption, Barry and Stone⁴ suggested that one form was boundary layer adsorption as O⁻ ions and the other form was O⁼ ions

(7) The conductivity σ is defined as $1000/R$ where R is the resistance measured across the inner leads.

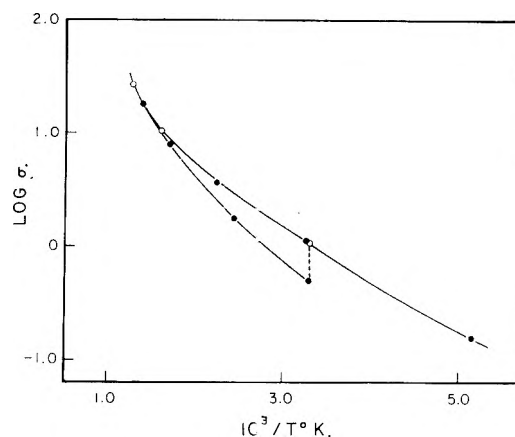


Fig. 1.—Dependence of conductivity σ on temperature with and without added oxygen: O, evacuated catalyst; ●, with 0.08 μ l. STP preadsorbed at room temperature.

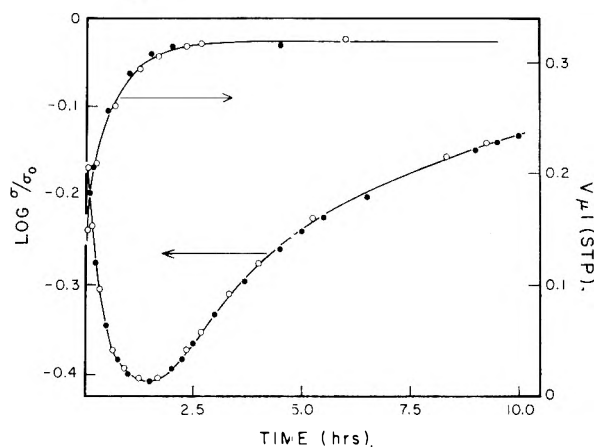
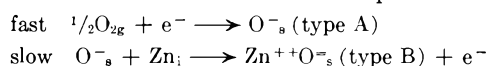


Fig. 2.—Amount of adsorption V and conductivity σ as a function of time at 353° for two duplicate runs. The first run (open circles) was made after the initial pretreatment; the second run (filled circles) was made following the first run after 16 hr. evacuation at 510°. σ_0 is the conductivity of the catalyst at 353° after pretreatment.

stabilized by the migration of interstitial zinc. Recently⁶ experimental support for this picture has been supplied by a study of the effect of oxygen chemisorption on the electron spin resonance of zinc oxide. These later investigations⁶ suggest that adsorption as O⁻ ions (type A) predominates at room temperature and adsorption as stabilized O⁼ ions (type B) predominates above 200 to 300°; furthermore, it was shown that type A adsorption has a far greater effect on the number of conduction electrons than type B-adsorption.

The results in Fig. 1 and 2 can be interpreted in the light of the above picture with the additional consistent assumption that type B adsorption always occur *via* these consecutive steps



where Zn_i stands for interstitial zinc. If we restrict our consideration to *small* amounts of adsorption, only type A oxygen should affect the conductivity; type B should have a negligible effect.^{6,8}

(8) Recent work on the decomposition of germane on germanium films (J. Kuriacose, unpublished results, reported by H. S. Taylor, *Ann. Rev. Phys. Chem.*, **12**, 147 (1961)), suggests that the presence of a metal-semiconductor contact causes a profound effect on the catalytic

The results of room temperature rate studies, wherein the conductivity falls to a steady value, suggest that the step to form type B adsorption is immeasurably slow, hence, only type A adsorption occurs at room temperature. When the catalyst with preadsorbed type A oxygen is heated to elevated temperatures, however, type A changes to type B oxygen and the conductivity returns to the initial values as shown in Fig. 1. These results are wholly consistent with conclusions based on electron spin resonance measurements.⁶

Results at 353° (Fig. 2) suggest that type B adsorption is the more stable species but that this occurs subsequent to type A adsorption. In the initial stages of adsorption, the concentration of the type A species increases and approaches a steady-state concentration; correspondingly, the conductivity falls and approaches a steady low value. Before the steady state actually is reached, however, the residual oxygen pressure falls to zero and gas phase oxygen can no longer replenish the type A species that is depleted by the formation of type B oxygen. In accord with this, the conductivity then increases and finally reaches the initial value after 25 hr., when all the type A oxygen has been converted to type B.

In conclusion, we should note that similar results have been obtained for a number of different samples of zinc oxide. In every case, catalysts pretreated in an oxidizing atmosphere yield the typical results reported above. The minimum in the σ curve (Fig. 2) is sharp and readily apparent only because the adsorption is small and the reaction is carried to completion. When larger amounts of oxygen are admitted to the sample, a steady-state concentration of type A adsorption is reached, and the conductivity levels off to a seemingly constant low value. In such runs, the conductivity does not increase unless the reaction is carried out to near completion so that the oxygen pressure drops to a very low value. Then, the concentration of type A oxygen falls off as it is converted to type B oxygen and the conductivity begins to increase. Existing data suggest that for large amounts of adsorption the return to the initial value of the conductivity is not always complete.

Acknowledgment is made to the donors of the Petroleum Research Fund, administered by the American Chemical Society, for support of this research.

efficiency of the film even though the metal by itself (after exposure to germane) is inactive. Thus the presence of inert metal electrodes seems to modify the catalytic (and adsorptive) properties of germanium semiconductors. In our interpretation of the conductivity data on zinc oxide, we assume that the presence of platinum leads does not change the qualitative features of oxygen adsorption. The fact that the present results confirm the conclusions of earlier studies based on electron spin resonance measurements⁶ on powders supports this assumption.

THE KINETICS OF THE THERMAL DECOMPOSITION OF [2,2,1]BICYCLOHEPTADIENE

BY JOHN H. BIRELY AND JOHN P. CHESICK

Contribution 1684 from the Sterling Chemistry Laboratory, Yale University, New Haven, Connecticut

Received October 13, 1961

The thermal decomposition of [2,2,1]bicycloheptadiene (BCH) was the subject of a study by Woods¹ in which he observed the simultaneous formation of both cycloheptatriene (CHT) in a rearrangement reaction, and the formation of acetylene and cyclopentadiene (CPD) in a reverse Diels-Alder reaction. Toluene formation also was observed, and was ascribed to decomposition of CHT. No attempt was made to evaluate rate constants or activation energies for the decomposition reactions of BCH. Halper, Gaertner, Swift, and Pollard² have reported a pilot plant study of these reactions using a continuous fed tube reactor but, again, the nature of the experiments did not allow them to evaluate the kinetic parameters. The possibility of heterogeneous or bimolecular reactions was not considered, and up to 20% of higher molecular weight products was obtained.

The possibility of a reactive norcaradiene as an intermediate in CHT formation has been considered,¹ and the over-all energy barrier for the process might be reduced by simultaneous bond formation if the norcaradiene formation occurs simultaneously with the methylene carbon-bridgehead carbon bond rupture in BCH. The reverse Diels-Alder reaction should involve rupture of the six-membered ring of BCH, which would be a different process from the rupture of the methylene bridge which has been suggested as the route to BCH. Hence knowledge of the activation energies would be of value in considering these processes. The study reported here therefore was undertaken to determine the kinetics of the decomposition reactions.

Experimental

The BCH used in this work was Shell Chemical material which was purified by three successive distillations through a Vigreux column keeping the middle fraction each time. Matheson Coleman and Bell 2,6-di-*t*-butyl-*p*-cresol was kept in both distillation pot and receiver as a polymerization inhibitor. This inhibitor is sufficiently non-volatile that pure BCH simply may be distilled from it for use as needed. The resulting BCH was homogeneous to gas chromatographic analyses using silicone oil on firebrick and hexamethylphosphoramide on firebrick column packings. The 60 Mc. nuclear magnetic resonance spectrum also showed that any impurities were at a level of less than 1%. The BCH was stored in the vacuum system over the inhibitor at Dry Ice or liquid nitrogen temperatures. Matheson prepurified nitrogen was used without further treatment. Matheson acetylene also was used after passage through a trap at Dry Ice temperatures to remove acetone and water. Cyclopentadiene was prepared by thermally cracking the dimer and distilling off the monomer through a Vigreux column. The resulting cyclopentadiene then was distilled into the system and kept at Dry Ice temperature. Nuclear magnetic resonance spectra taken of the stored CPD after one week showed no water or dimer. CHT for calibrations was prepared by the lithium aluminum hydride reduction of tropylium fluoroborate.³

A standard high vacuum system was used for the storage and handling of reactants and products. Reactions were carried out in a 500-ml. spherical vessel connected to the vacuum system by a mercury float valve. A gas chromatography sampling system was an integral part of the vacuum line. Quantitative analyses were performed by gas chromatography; relative peak area was obtained by weighing cut out peaks with a microbalance. Routine analyses

(1) W. G. Woods, *J. Org. Chem.*, **23**, 110 (1958).

(2) W. M. Halper, C. Gaertner, E. W. Swift, and G. E. Pollard, *Ind. Eng. Chem.*, **50**, 1131 (1958).

(3) H. J. Dauben, C. R. Honnen, and K. M. Harman, *J. Org. Chem.*, **25**, 1442 (1960).

were made using a 3-m. 0.64-cm. o.d. column packed with Dow Corning 703 silicone oil on firebrick and operated at 110°. Under these conditions, acetylene was eluted too soon for accurate measurements, and hence in a series of sixteen runs to check the cyclopentadiene to acetylene product ratio, a 30-cm. column of hexamethylphosphoramide on firebrick was used at room temperature. For this series of experiments no measurements were feasible for the other products.

The reaction vessel, equipped with thermometer wells reaching to the center, was in an air-bath thermostat controlled by a gas thermometer mercury manometer relay system. The temperature was held constant to 0.1° during a run, and temperature gradients through the vessel were less than 1°. Temperatures were monitored with four junction Chromel-Alumel thermocouples and were checked by comparison with a Leeds and Northrup certified No. 8163-C platinum resistance thermometer. L & N Mueller bridge, at each temperature employed. Precision of temperature measurement should be $\pm 0.1^\circ$. Absolute temperatures certainly should be good to $\pm 0.4^\circ$.

Mixtures for runs with added nitrogen were prepared in a mixing flask equipped with a magnetically driven paddle stirrer. Reaction products were pumped through a three turn loop of 6-mm. i.d. tubing immersed at one end in liquid nitrogen to assure complete freezeout of products and rapid removal of the nitrogen mixture from the vessel.

Results

An approximately equimolar mixture of acetylene and cyclopentadiene was prepared and heated at 360° for a time which would correspond to 50% decomposition of BCH, and at a total pressure of 1 cm. Only 0.3% of the material reacted to give a peak of the same retention time as BCH, and hence the Diels-Alder addition reaction may be ignored in considering the decomposition of BCH. No toluene or CHT, *i.e.*, less than 0.05% of the starting materials, was observed in the analysis.

Sixteen runs at BCH pressures between 0.3 and 1.2 cm. were made at 353° and were analyzed using the hexamethylphosphoramide column to check the cyclopentadiene-acetylene ratio. The reaction times corresponded to conversions of starting material ranging between 12 and 85%. The cyclopentadiene-acetylene ratio was 0.93 with a r.m.s. deviation of 2.0%. There was no significant change of this ratio with reaction time, and the deviation of the ratio from unity by 7% may be due to errors in the gas chromatography detector sensitivity calibrations. Lack of variation in the ratio with either degree of reaction or pressure would seem to rule out loss of cyclopentadiene in the reaction vessel through formation of Diels-Alder adducts with other olefins.

A plot of $-\log$ (fraction BCH unreacted) *vs.* time for a series of runs at 352.0° and another series at 356.7° gave straight lines with deviations of less than 2% from linearity except for two runs at 62 and 67% conversion which were off by 7% each. The calculation assumes CHT, CPD, and toluene account for the only reactions. Apparent first-order rate constants for BCH decomposition were computed for all runs; for a series of six runs at 340.4°, the first-order rate constants deviated from the mean by a maximum of $\pm 4\%$ for a variation in initial pressure between 1.0 and 2.7 cm. It therefore is concluded that the disappearance of BCH is a first-order reaction. A check of the material balance in this reaction and absence of important polymerization reactions is found in the total chromatogram peak areas, corrected by the appropriate detector sensitivity ratios. For a

series of runs made on one day at a constant carrier gas flow rate and detector temperature, the sum of the peak areas of BCH, CHT, toluene, and cyclopentadiene should be proportional to reactant pressure at a given reaction temperature if no other reactions are occurring. For four runs at 356.7° made consecutively with reactant conversions ranging between 24 and 74%, a plot of total corrected peak area *vs.* reactant pressure showed less than a 4% scatter of the points from a straight line going through the origin. Similar agreement was found for other sets of runs made under conditions of constant detector sensitivity.

Two runs were made at 329.8° with the reaction vessel packed with 4-mm. diameter glass beads which increased the surface to volume ratio by a factor of 55. The apparent first-order rate constant for production of cyclopentadiene plus acetylene was unchanged, and the rate constant for formation of toluene + CHT was increased by 12%. It therefore seems safe to conclude that the reaction observed in the unpacked vessel is homogeneous.

The ratio of CHT to CPD should be the ratio of rate constants for the first-order formation reactions, and should be independent of extent of reaction if there are no side reactions. The ratio shows a scatter of $\pm 8\%$ for the series of runs at 352.0° with a slight upward trend with degree of reaction which goes to 67% of completion. The ratios given in the table of data have been calculated including the toluene with the CHT. This procedure was based on the brief data of Woods which indicated that the toluene was formed from the CHT. If the toluene yield is not included with the CHT there is not a significant change in the ratio of CHT to CPD with degree of reaction.

The toluene yields ranged up to 6 or 7% of the CHT. Both of these products emerged from the chromatograph as relatively spread out peaks, which increased the uncertainty of area measurements, and the toluene peak area measurements were marginal. It therefore is difficult to sort out trends in the toluene formation except that it increased relative to CHT with an increase in temperature.

Although Woods found that toluene was formed from CHT at 475°, it also might arise from BCH by a hydrogen migration from the bridgehead carbon to the CH₂ group after a preliminary ring opening. This probably would involve a higher activation energy than the isomerization to CHT. Without knowledge of the activation energy for the CHT toluene conversion it cannot be stated positively that the toluene found at temperatures 100° or more below 475° arises from CHT decomposition.

Four runs were made with added nitrogen with results as shown in the Appendix. The chief result was the increase in CHT formation rate by 12%.

Individual rate constants for the two decomposition processes were computed for each run, including the toluene with the CHT, and the rate constants at each temperature then were averaged. These average rate constants were used in Arrhenius plots to determine the activation energies.

For the first-order formation of cyclopentadiene

plus acetylene from BCH

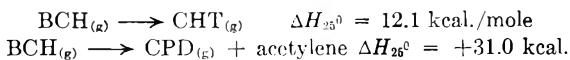
$$k_1 = 5.2 \times 10^{14} \exp(-50.5 \pm 1.2/RT) \text{ sec.}^{-1}$$

and for CHT formation from BCH

$$k_2 = 8.2 \times 10^{14} \exp(-51.6 \pm 1.8/RT) \text{ sec.}^{-1}$$

Discussion

A tentative value of 979.6 kcal./mole for the standard heat of combustion of BCH has been reported.⁴ From this and the known heats of formation of CHT, CPD, and acetylene,⁵ the heats of the following reactions may be computed. A heat of vaporization for BCH of 7.6 kcal./mole is estimated from Trouton's rule.



Although the ΔH of the first reaction probably is the same to within 1 kcal. at 350°, the ΔH for the second reaction should be increased by about 3.6 to +34.6 kcal./mole at 350°.

Subtraction of the endothermicity from the observed activation energy of 50.5 kcal. gives an activation energy for the Diels-Alder addition of acetylene to cyclopentadiene of 15.9 kcal./mole, comparable to the value of 16.7 kcal. observed⁶ for cyclopentadiene dimerization. The pre-exponential factor of $10^{14.72} \text{ sec.}^{-1}$ observed in this work for the reverse Diels-Alder reaction is higher than the A factor of $10^{13.0}$ found for the dicyclopentadiene decomposition.⁶ The BCH-CHT conversion is exothermic, and the relatively high activation energy of 51.6 kcal./mole probably indicates that the transition state for the reaction is not very similar to the product molecule and does not receive much help in reduction of the energy barrier from simultaneous bond formation steps. The pre-exponential factor of $10^{14.91} \text{ sec.}^{-1}$ is in the neighborhood of values found for the high pressure A factors of many unimolecular reactions. This high value also would indicate that any step subsequent to the initial bond rupture occurs with a high probability. The similarity of activation energies for the two modes of decomposition of BCH also hints that the rupture of a bond between a bridgehead carbon and a vinyl carbon is the initial step for both reactions. Rupture of a second such bond would lead to acetylene and cyclopentadiene; rotation of the C_2H_2 group with attack on the methylene carbon would give the alternate path to CHT. Alternatively, the valence tautomer of CHT, $\Delta^{2,6}$ -bicyclo[3,2,0]heptadiene, could be formed and would decompose rapidly under the reaction conditions to CHT.⁷

Acknowledgments.—This work was supported by the Chemical Science Division, Air Force Office of Scientific Research, under contract AF 49 (638) 722. One of us (J.H.B.) wishes to thank the National Science Foundation for an Undergraduate

(4) S. Skuratov, M. Kozina, S. Shtecher, S. Prevalova, N. Kamkina, and V. Zuko, *Bull. Chem. Thermo.*, **1A**, 21 (1958).

(5) (a) D. Scott, M. Gross, J. Messerly, and G. Waddington, *J. Am. Chem. Soc.*, **78**, 5469 (1956); (b) A.P.I. Project 44 Tables of Thermodynamic Data.

(6) J. Harkness, G. B. Kistiakowsky, and W. H. Mears, *J. Chem. Phys.*, **5**, 682 (1937); G. A. Benford and A. Wassermann, *J. Chem. Soc.*, 362 (1939).

(7) W. G. Dauben and R. L. Cargill, *Tetrahedron*, **12**, 186 (1961).

Research Participation Grant for the summer of 1961.

Appendix

A. Data for Runs without Added Nitrogen

α = fraction BCH left

T , °C.	Reactant P , cm.	α	$k_2 \times 10^4$, sec. ⁻¹	$k_1 \times 10^4$, sec. ⁻¹
327.2	1.8	0.84	1.21	1.86
	1.9	.82	1.19	1.90
	2.0	.82	1.19	2.06
340.4	1.0	.80	2.57	4.64
	1.12	.77	2.70	4.68
	1.2	.76	2.90	4.49
	1.3	.79	2.99	4.69
	1.8	.80	2.76	4.72
	2.7	.75	2.43	4.66
352.0	1.0	.74	5.77	9.13
	1.0	.83	5.54	9.86
	1.0	.81	5.36	10.4
	1.0	.33	7.23	10.9
	1.0	.50	6.75	10.2
	1.1	.60	6.65	10.0
	1.1	.61	5.97	9.83
	1.3	.72	5.99	9.91
	1.7	.65	6.05	10.2
	1.7	.84	5.28	9.72
356.7	2.2	.61	5.97	9.63
	0.8	.57	8.8	13.7
	0.9	.76	7.5	13.6
359.6	0.9	.26	9.5	14.6
	1.0	.38	9.5	13.5
	0.8	.44	10.8	16.4
370.3	0.9	.42	11.4	16.5
	1.6	.30	22.7	34.7
	1.8	.52	19.4	32.3
	2.4	.34	20.7	33.3

B. Packed Vessel

329.8	3.1	0.79	1.49	2.40
	3.2	0.78	1.68	2.21

C. Added Nitrogen

356.7	$\text{N}_2/\text{BCH} = 8.7$			
	1.4	0.36	10.1	15.0
	$\text{N}_2/\text{BCH} = 12.3$			
	0.9	0.36	9.6	14.2
	1.4	0.22	10.9	15.1
	2.0	0.29	10.2	14.4

PREPARATION AND PROPERTIES OF A VARIABLE CHARGE ION-EXCHANGE MEMBRANE

By HAROLD JACOBSON

Fundamental Research Department, The National Cash Register Company, Dayton 9, Ohio

Received October 14, 1961

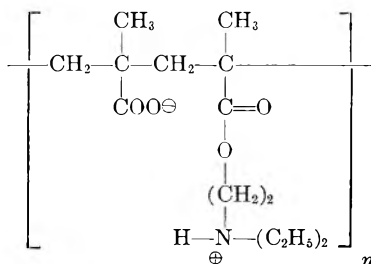
While many studies have been made of synthetic ion-exchange membranes and membrane systems, little effort has yet been made to influence directly the characteristics of a synthetic membrane itself.¹ It is our purpose to describe the fabrication and properties of a synthetic membrane that is capable of being changed both in charge density and in charge

(1) K. H. Meyer and J. F. Sievers, *Helv. Chim. Acta*, **19**, 649, 665 (1936).

sign. To achieve this, use has been made of a polyampholyte which contains weak acidic and weak basic groups, as a consequence of which the material exhibits an isoelectric point and has a charge density and polarity that are functions of pH .

Experimental

The polyampholyte was formed from the monomers methacrylic acid and *N*-diethylamino-2-ethyl methacrylate by a method described by Alfrey and Pinner.² The zwitterionic structure of this product is shown diagrammatically



A nitrogen analysis yielded a value of 4.2% as compared to a theoretical value, based on the above structure, of 5.17%.

To form the matrix of the membrane, Dynel, obtained from the Union Carbide Plastics Company, was employed. For some of the conductivity measurements requiring a large anion, purified sodium polystyrenesulfonate (NaPS) of 10,000 molecular weight was used.

Membranes were cast from an interpolymer solution made by dissolving Dynel and polyampholyte in *N,N*-dimethylformamide at 90°. The solution was 17% total solids, of which 28.6% was polyampholyte. The final membrane thickness was $50 \mu \pm 2\%$.

Concentration potentials and resistances were obtained as described elsewhere³ as a function of pH . The ambient solutions used were sodium chloride buffered with acetic acid and sodium acetate for one range of pH values (pH 4 to 5.5) and with sodium dihydrogen phosphate and disodium hydrogen phosphate for another range (pH 6 to 7.5). The buffers, prepared according to the data of Conway,⁴ were made up to 0.20 and 0.10 ionic strength (I) solutions by the addition of an appropriate amount of sodium chloride. With the former buffer the molar ratio of the sodium ions of the ambient solutions was 2.00. With the latter buffer the molar ratios of the sodium ions were 2.02, 2.04, 2.05 and 2.08, respectively, in the four pH values attained with that buffer. The chloride ion ratio was 2.25 at all the pH values.

The pH differences between the members of a pair of concentrated and dilute solutions ranged from zero to 0.09. By the use of these solutions, bi-ionic potentials were minimized, since the buffer salts were of equal concentrations (and near equal activities) on each side of the membrane, permitting the differences in sodium and chloride ion concentrations (activities) to be the principal potential determining species.

Samples of Ionics, Inc., membranes AR-111-A (anion) and CR-61 (cation) were employed for control and comparison purposes. Free diffusion potentials at each pH were measured by using a perforated rubber diaphragm. These measurements, made over a five-minute interval, were constant to within 0.06 mv.

Resistance measurements were made with buffered sodium chloride solutions (0.1 I) on conditioned membrane samples of area 0.968 cm.². Resistance measurements also were made with solutions containing 2.00 g. of NaPS made up to 100 ml. with 0.002 I buffer.

Results and Discussion

Figure 1 illustrates the results obtained of the concentration potentials as a function of pH . At low pH values, the polyampholyte membrane bears a positive charge and is, to varying degrees,

(2) T. Alfrey, Jr., and S. H. Pinner, *J. Polymer Sci.*, **23**, 533 (1957).

(3) H. P. Gregor, H. Jacobson, R. C. Shair and D. M. Wetstone, *J. Phys. Chem.*, **61**, 141 (1957).

(4) B. E. Conway, "Electrochemical Data," Elsevier Publ. Co., 1952.

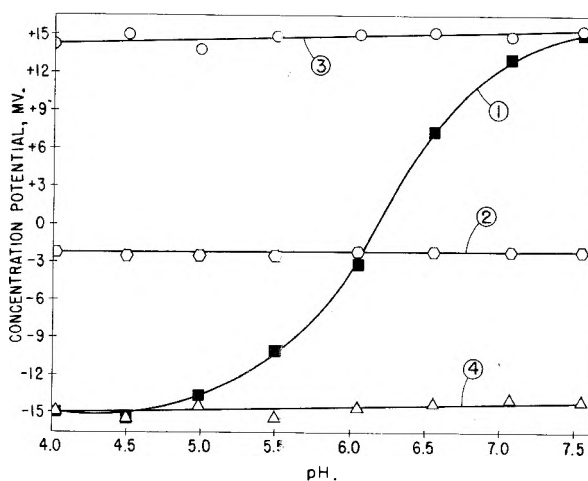


Fig. 1.—Concentration potentials as a function of pH using buffered solutions of 0.2 and 0.1 I : curve 1, polyampholyte membrane; curve 2, perforated rubber diaphragm; curves 3 and 4, Ionics, Inc., membranes CR-61 and AR-111-A, respectively.

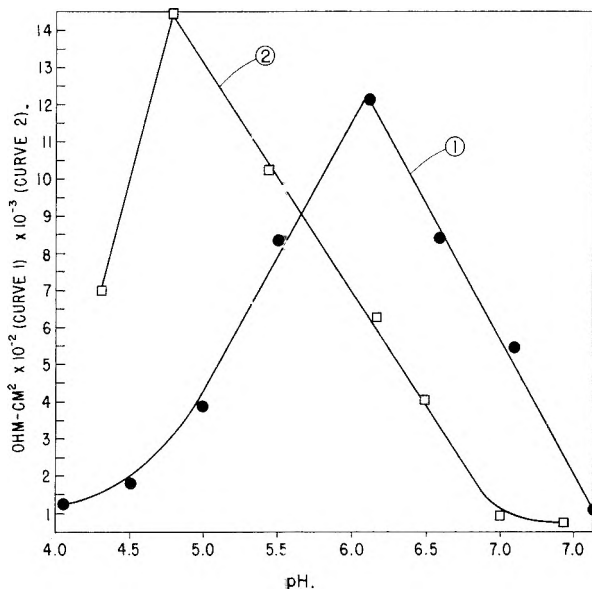


Fig. 2.—Resistance as a function of pH : curve 1, obtained with 0.1 I buffered solution of NaCl; curve 2, obtained with buffered solution containing 2% sodium polystyrenesulfonate.

anion-selective. At high pH values, the charge is negative and the membrane is cation-selective. At the pH of 6.1, there is no net charge within the membrane; the polyampholyte presumably exists in a zwitterionic form. At this point, the potential measured is essentially that of free diffusion.

The use of polyampholytes of different isoelectric points would, of course, shift the curve to different pH ranges. Obtaining potentials close to the maximum possible would depend on having available the proper charge concentration at the extreme pH values.

Concentration potentials also were measured in hydrochloric acid (0.20 N –0.10 N) and in potassium hydroxide (0.2 N –0.1 N) and values of -16.5 and $+14.9$ mv., respectively, were obtained. The theoretical maxima for the latter two systems are -16.70 and $+16.56$, respectively.

Figure 2 shows the effect of pH on the electrical resistance of the polyampholyte membrane. Curve 1, measured in 0.1 M buffered sodium chloride, exhibits an order of magnitude rise in resistance as a function of pH . The Ionics membranes were similarly measured and practically no effect on the resistance was observed.

The resistance of the polyampholyte membrane is low at pH values at the extremes of the range used, since at these pH values the concentration of fixed charges (positive at low pH and negative at high pH) with their associated gegenions is at the maximum. As the pH of 6.1 is approached from either side, the concentration of charges decreases and the resistance rises. At the isoelectric point, fixed (immobile) zwitterions exist and free charge carrying gegenions are at a minimum.

Another factor responsible for the trend illustrated in Fig. 2 is the choice of solute. Curve 2 shows the data obtained with 2% NaPS-0.002 M buffer solutions. Except for the first point, the resistance falls with increasing pH and does not show the sharp rise in resistance at or near the isoelectric point. This behavior can be explained on the basis of steric considerations. At a pH of about 4.7-4.8, the polyampholyte membrane bears fixed positive charges which hinder the transport of cations across it. Consequently, current is carried by anions. However, a large fraction of the free anions is hindered and the resistance is high. As the pH is raised, the membrane charge diminishes and the Donnan exclusion effect becomes less pronounced. The transport number of sodium ions across the membrane becomes greater and the resistance falls. At the presumed isoelectric point there is no barrier to sodium ions in contradistinction to that at lower pH . As the pH is increased further, the membrane becomes negatively charged and the transport number of the sodium ion approaches unity; thus, a larger current can be maintained and the resistance continues to fall.

It is conjectured that the initial rise in resistance is due to a decrease in the gegenion concentration (and fixed ion concentration) but not enough of a decrease to abate the Donnan effect—that is, sodium leakage remains unchanged and minimal. This is borne out by reference to the concentration potentials at the various pH values. As can be seen from Fig. 1, at pH 4.32 and 4.79, the concentration potentials are close to the maximum. The slope becomes substantial at pH values higher than 5.0. Up to this pH , ion leakage is small and the resistance is governed by the gegenion concentration. Above pH 5.0, leakage is enhanced and a greater fraction of ions becomes available for carrying current.

MISCIBILITY OF METALS WITH SALTS. VI. LITHIUM-LITHIUM HALIDE SYSTEMS¹

By A. S. DWORIN, H. R. BRONSTEIN, AND M. A. BREDIG

Chemistry Division, Oak Ridge National Laboratory, Oak Ridge, Tennessee

Received October 20, 1961

The miscibility of the alkali metals with their halides was shown to decrease rapidly in going

from the cesium systems to the sodium systems.²⁻⁶ This report covers the lithium systems which were expected to exhibit a continuation of the trend; that is, low solubility of metal in salt and high (consolute) temperatures for complete miscibility between metal and salt.

Experimental

Apparatus and Procedure.—The points on the Li-LiF phase diagram (Fig. 1) designated by open circles were obtained by means of thermal analysis (cooling curves) as described previously.⁴ A platinum wound Marshall furnace,

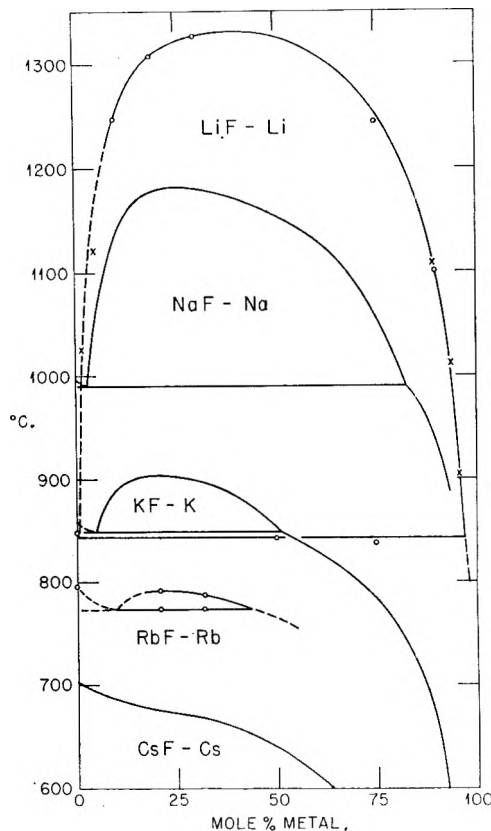


Fig. 1.—Liquid metal-salt phase equilibria in the alkali metal-fluoride systems.

stainless steel sample capsules, and a Pt-PtRh thermocouple were used at temperatures up to 1400°. At lower temperatures and at low salt or metal concentrations, where the thermal halts for liquid-liquid separation become unobservable because of the small temperature dependence of the solubility, separate sampling of the liquid metal-rich and salt-rich phases after equilibration² yielded the points designated X (Fig. 1).

For the Li-LiCl and Li-LiI systems, an apparatus was built which permitted the direct sampling of the solution at temperature, as in some measurements on the sodium-sodium halide systems.⁶ The apparatus was a smaller, modified version of the conductivity apparatus used for the alkali metal-halide systems,⁷ and has only one entry port

(1) Work performed for the U. S. Atomic Energy Commission at the Oak Ridge National Laboratory, operated by the Union Carbide Corporation, Oak Ridge, Tennessee.

(2) M. A. Bredig, J. W. Johnson, and W. T. Smith, Jr., *J. Am. Chem. Soc.*, **77**, 307 (1955).

(3) M. A. Bredig, H. R. Bronstein, and W. T. Smith, Jr., *ibid.*, **77**, 1454 (1955).

(4) J. W. Johnson and M. A. Bredig, *J. Phys. Chem.*, **62**, 604 (1958).

(5) M. A. Bredig and H. R. Bronstein, *ibid.*, **64**, 64 (1960).

(6) M. A. Bredig and J. W. Johnson, *ibid.*, **64**, 1899 (1960).

(7) H. R. Bronstein and M. A. Bredig, *J. Am. Chem. Soc.*, **80**, 2077 (1958).

on the rotatable turret. The lithium was introduced into the molten salt by means of a perforated stainless steel basket which was attached to a stainless steel rod and which acted both as a container for the lithium and a stirrer. The basket was removed after equilibration at temperature with stirring, and a sample of the molten salt-rich phase was taken by means of a sampling device described previously.⁷ (Sufficient additions of lithium were made to ensure the presence of two liquid phases at the equilibration temperatures.) The salts were held in both molybdenum and stainless steel crucibles, and no dependence on container material was noted in the measurements. The temperature limit of the apparatus was 1000°. Attempts to determine the metal-salt phase equilibria in the Li-LiCl and Li-LiI systems by thermal analysis above this temperature were unsuccessful.

Materials.—The LiF was optical grade single crystal material (Harshaw). LiCl and LiI were reagent grade materials which were purified by very slowly heating in the presence of HCl and HI, respectively, to just below the melting temperatures of the salts, melting under dry argon, and filtering while molten. The Li was analyzed for other alkali metals, as well as C, N₂, and O₂ and was found to contain less than 0.05 mole % of impurity.

Results and Discussion

The results for the Li-LiF system are shown in Fig. 1. The data obtained by the ball check valve method for the salt-rich phase are not as reliable⁶ as those obtained by the decantation method for the metal-rich phase; therefore, the salt-rich portion of the diagram is shown by a dotted line. However, both methods give results which fit very well with the data from thermal analysis.

Figure 1 shows a comparison of all five alkali metal-fluoride systems. The regular trend in the miscibility of the alkali metals with their molten fluorides, which is representative of the trend in all the alkali halides, is very apparent. This trend is a rapid increase in miscibility with increase in atomic number of the alkali metal, that is, with the decrease in internal pressure³ of both salt and metal.

The solubility of lithium in lithium chloride was found to increase from a value of 0.5 ± 0.2 mole % at 640° to 2.0 ± 0.2 mole % at 1000°. The solubility of lithium in lithium iodide increased from a value of 1.2 ± 0.5 mole % at 550° to 2.5 ± 0.5 mole % at 950°. These values are the lowest found among the alkali metal solubilities in their chlorides and iodides.

It has been demonstrated that the Li-LiF system as well as the measured portions of the Li-LiCl and Li-LiI systems follow the trend discussed above. Therefore, approximate delineation of the miscibility gap for the Li-LiCl, Li-LiBr, and Li-LiI systems can be deduced from comparison with the other alkali metal-halide systems.²⁻⁶ In light of this, further phase studies in the difficult lithium systems were not performed.

Attempts to measure the electrical conductivity of the lithium systems were unsuccessful, because of reaction between the lithium solutions and the synthetic sapphire or single crystal magnesia capillary cells used in our conductivity apparatus.⁷ No insulating material has as yet been found which will withstand attack by these solutions.

(8) J. H. Hildebrand and R. L. Scott, "The Solubility of Non-Electrolytes," Third Edition, Reinhold Publ. Corp., New York, N. Y., 1950.

THE LIQUID-LIQUID SOLUBILITY OF CYCLOHEXANE AND PERFLUOROTRIBUTYLAMINE AT 25°

BY RYOICHI FUJISHIRO AND J. H. HILDEBRAND

Department of Chemistry, University of California, Berkeley 4, California

Received October 24, 1961

The usual method for determining liquid-liquid solubility is to observe visually the separation of a mixture of known composition into two phases as the temperature is lowered. This can be done accurately only in the region around the critical point, and most composition-temperature curves have not been carried very far down the descending branches. The reliable portions of available curves for different liquid pairs extend over different ranges of temperature, and it is difficult to make a systematic comparison of such systems at a common temperature. Parameters calculated from critical temperatures are unsatisfactory also because the structure of mixtures near the critical point is extremely complex, and not amenable to model treatments that are reasonably applicable outside this region. It is very desirable to have figures for liquid-liquid solubilities at a standard temperature, preferably at 25°, by determining the composition of both phases by analysis.

We present the equilibrium compositions of the two-liquid phase of the system cyclohexane + *n*-perfluorotributylamine, analyzed by aid of the large difference in their densities. We obtained the densities of the pure components, of solutions of known composition, and of both saturated phases. Our figures are given in Table I.

TABLE I
DENSITIES AT 25° AND MOLE FRACTIONS OF C₆H₁₂, x_1 , AND (C₄F₉)₃N, x_2

Unsaturated			
x_1	d	x_2	d
0	1.8714	0	0.7741
0.1399	1.8131	0.00264	.7822
.1828	1.7972		
.2025	1.7884		
Saturated			
Phase A		Phase B	
0.218	{ 1.7827	0.00317	{ 0.7836
	{ 1.7819		{ .7842

The specific volumes corresponding to these densities plotted against mole fractions of the unsaturated solutions give straight lines which, extrapolated the short distances to specific volumes of the saturated phases, give the mole fractions in the two equilibrium phases, A and B.

The difference between the solubility parameters of the pure liquids, δ_1 and δ_2 , in the approximate solubility equation

$$\ln a_1 = \ln x_1 + v_1 \phi_2^2 (\delta_2 - \delta_1)^2 / RT \quad (1)$$

(v denotes molal volume and ϕ denotes volume fraction) can be calculated by aid of the following relations

(a) the four equations of the above form for a_1 and a_2 in phase A and in phase B.

$$(b) \quad a_{1A} = a_{1B}, \quad a_{2A} = a_{2B},$$

$$(c) \quad x_{1A} + x_{2A} = 1, \quad x_{1B} + x_{2B} = 1$$

$$\varphi_{1A} + \varphi_{2A} = 1, \quad \varphi_{1B} + \varphi_{2B} = 1$$

By combining these, one may obtain the equation

$$\frac{RT}{2} \left(\frac{1}{v_1} \ln \frac{x_{1B}}{x_{1A}} + \frac{1}{v_2} \ln \frac{x_{2A}}{x_{2B}} \right) = (\varphi_{1B} - \varphi_{1A})(\delta_2 - \delta_1)^2 \quad (2)$$

Rotariu,¹ at the suggestion of the senior author, applying the same reasoning, but starting with an equation different from eq. 1, derived a similar equation, but one in which composition is expressed in volume fractions only, now known to be inferior to eq. 1.

Substituting into this equation the molal volumes $v_1 = 108.5$ cc., $v_2 = 359$ cc., the mole fractions according to Table I, and the corresponding volume fractions, gives $\delta_1 - \delta_2 = 3.08$. The δ -values from energies of vaporization give $\delta_1 - \delta_2 = 8.2 - 5.9 = 2.3$. This mixture adds another to the many examples² of mixtures of an aliphatic hydrocarbon and a fluorocarbon that are mutually less soluble than their solubility parameters would indicate according to eq. 1.

In phase B, x_1 is 0.997, and $a_1 \approx 1$ in both phases, hence we can calculate $\delta_2 - \delta_1$ for phase A by means of eq. 1. The result is 3.03, practically identical with the figure above, calculated by eq. 2.

This work has been supported by a grant from the National Science Foundation.

(1) G. J. Rotariu, R. J. Hanrahan and R. E. Fruin, *J. Am. Chem. Soc.*, **76**, 3752 (1954).

(2) (a) J. H. Hildebrand, *J. Chem. Phys.*, **18**, 1337 (1950); (b) J. B. Hickman, *J. Am. Chem. Soc.*, **77**, 6154 (1955).

ULTRACENTRIFUGAL DETERMINATION OF THE MICELLAR CHARACTER OF NON-IONIC DETERGENT SOLUTIONS. III

BY C. W. DWIGGINS, JR., AND R. J. BOLEN

Bartlesville Petroleum Research Center, Bureau of Mines
U. S. Department of the Interior, Bartlesville, Oklahoma

Received October 25, 1961

Determinations of micellar molecular weights of non-ionic detergents in aqueous solutions by ultracentrifugal^{1,2} and light-scattering³⁻⁶ methods have shown that micellar molecular weights are highly dependent upon the types of detergents studied. In addition, ultracentrifugal studies have shown that the micellar molecular weights are highly dependent on the temperature² of detergent solutions. Thus it is likely that micellar molecular weights are dependent on the ethylene oxide chain length of the detergent molecules.

The usual polyoxyethylated alkylphenol detergents are available as high-purity surfactants, but such detergents usually have a rather wide

(1) C. W. Dwiggins, Jr., R. J. Bolen and H. N. Dunning, *J. Phys. Chem.*, **64**, 1175 (1960).

(2) C. W. Dwiggins, Jr., and R. J. Bolen, *ibid.*, **65**, 1787 (1961).

(3) A. M. Mankowich, *ibid.*, **58**, 1027 (1954).

(4) P. Debye, *ibid.*, **51**, 18 (1947).

(5) P. Debye, *J. Appl. Phys.*, **15**, 338 (1944).

(6) M. J. Schick, F. R. Eirich and S. M. Atlas, "Micellar Structure of Nonionic Detergents," 139th National Meeting, American Chemical Society, St. Louis, Missouri, March, 1961.

distribution of numbers of ethylene oxide groups. Polyoxyethylated alkylphenol detergents having no chain length distribution are very difficult to obtain, but fractions having much narrower chain length distributions than the detergents available commercially may be obtained by molecular distillation.⁷ Several properties of molecular distillation fractions of a polyoxyethylated nonylphenol detergent were studied,⁷ and physical properties were significantly different for each detergent fraction. After these fractions became available, it was decided to study the effect of ethylene oxide chain length distribution on micellar molecular weights of polyoxyethylated nonylphenol non-ionic detergent.

Experimental

The transient-state method⁸⁻¹⁰ for molecular weight determination using the analytical ultracentrifuge aided by synthetic boundary experiments,¹¹ and application of the theory to determination of micellar molecular weights of non-ionic detergents in aqueous solutions were discussed in the first two papers of this series and will not be repeated.

One set of detergent fractions was obtained from a polyoxyethylated nonylphenol having an average ethylene oxide mole ratio of 9.5. These fractions were cycles 9, 10 and 11 as described by Mayhew and Hyatt⁷ and had average mole ratios of 8.9, 9.7 and 10.7, respectively. A second set of fractions was obtained from a polyoxyethylated nonylphenol having an average ethylene oxide mole ratio of 6.0. These fractions were cycles 12 and 13 as described in ref. 7 and had average mole ratios of 7.6 and 7.7, respectively. The detergent fractions have much narrower polyoxyethylene chain length distributions than the parent detergents, but it is not claimed that they have no chain length distribution.

The ultracentrifuge experiments were performed in a 2.5°, 12-mm. double sector cell, and a matched capillary synthetic boundary cell as described.^{1,2} Great care was taken to maintain constant temperature and precise alignment, to prevent convection, and to prevent biological contamination. Values of the corrected concentration gradients at the air-liquid meniscus were used to determine micellar molecular weights.¹

Pycnometers were used to obtain partial specific volumes as described previously.^{1,2} The pycnometer water-bath was maintained constant to within 0.005°. Least-squares calculations were used to evaluate partial specific volumes as described previously.^{1,2} The average deviation of individual specific volume data from the lines fitted by least squares ranged from 0.00001 to 0.00004.

Results and Conclusions

Micellar molecular weights and partial specific volumes for the various fractions are listed in Table I. Decreasing the number of ethylene oxide groups results in increased micellar molecular weights in aqueous solutions. It is of interest that, for the lower ethylene oxide mole ratios, very small changes in the ethylene oxide mole ratio can produce quite large changes in micellar molecular weights. Cloud-point temperatures are reduced greatly when ethylene oxide mole ratios are decreased.⁷ It appears that cloud-points are dependent on the micellar character of the detergent solutions, but the correlation between cloud-point temperatures and micellar molecular weights may be the result of other, more basic factors.

(7) R. L. Mayhew and R. C. Hyatt, *J. Am. Oil Chemists Soc.*, **29**, 357 (1952).

(8) W. J. Archibald, *J. Phys. Chem.*, **51**, 1204 (1947).

(9) H. K. Schachman, "Ultracentrifugation in Biochemistry," Academic Press, New York, N. Y., 1959, pp. 181-199.

(10) J. M. Peterson and R. M. Mazo, *J. Phys. Chem.*, **65**, 566 (1961).

(11) S. M. Klainer and G. Kegeles, *ibid.*, **59**, 952 (1955).

TABLE I

PROPERTIES OF POLYOXYETHYLATED NONYLPHENOL NON-IONIC DETERGENT AS A FUNCTION OF MOLE RATIO OF ETHYLENE OXIDE AT 25.00°

Av. mole ratio of ethylene oxide	Concn., wt. %	Time of run, min.	Partial specific volume, ml./g.	Micellar mol. wt., ^a × 10 ⁻⁴
10.7 ^b	0.6255	420	0.908	4.54
	.6255	1080	...	4.69
	.6255	1262	...	4.44
	.9982	1110	...	4.46
	.9982	1440	...	4.69
	.9982	1930	...	4.68
	1.3454	1140	...	4.55
	1.3454	1830	...	4.95
	1.3454	2880	...	4.84
			Mean	
9.7 ^b	0.9939	1080	0.926	7.12
	.9939	1320	...	7.12
	1.3203	570	...	6.98
	1.3203	1380	...	6.68
			Mean	
8.9 ^b	0.9864	630	0.9265	14.3
	.9864	1320	...	14.7
	.9864	1802	...	14.2
	.9864	2880	...	14.6
			Mean	
7.7 ^c	0.9623	1440	0.932	21.7
	.9623	1680	...	22.4
	1.0386	1440	...	22.5
		Mean		22.2
7.6 ^c	1.0343	1440	0.932	96.3
	1.0343	2400	...	98.5
	1.0343	3300	...	101.3
		Mean		98.7

^a Weight-average, anhydrous micellar molecular weights.

^b Molecular distillation fractions from detergent having 9.5 mole ratio (average) of ethylene oxide; see text. ^c Molecular distillation fractions from detergent having 6.0 mole ratio (average) of ethylene oxide; see text.

Micellar molecular weights and partial specific volumes of aqueous solutions of mixtures of two of the molecular distillation fractions are listed in Table II. These results indicate that the detergent molecules having higher ethylene oxide mole ratios influence the resultant micellar molecular weights of mixtures of detergent fractions more than detergent molecules having lower ethylene oxide mole ratios. The departure from linear dependency of micellar molecular weight on composition is large.

These studies suggest that changing the ethylene oxide chain length distribution of polyoxyethylated nonylphenol detergents may produce significant variations in the micellar character of the detergent solutions. It thus is possible that changes in manufacturing conditions that produce significant variations in the shape of the chain length *versus* concentration curve as well as changes that produce variations in the average molecular weight may be of importance for synthesis of de-

TABLE II

PROPERTIES OF DETERGENT MICELLES IN AQUEOUS SOLUTIONS OF BLENDS OF MOLECULAR DISTILLATION FRACTIONS OF POLYOXYETHYLATED NONYLPHENOL AT 25.00°

Wt. % of ^a 7.6 mole ratio in blend	Wt. % of ^b blended detergent	Time of run, min.	Partial specific volume, ml./g.	Micellar mol. wt., × 10 ⁻⁴
0	See Table I		Mean	4.65
25.4	0.9347	1110	0.919	6.43
	.9347	1920	...	6.40
	.9347	2880	...	6.40
			Mean	6.41
50.1	0.9165	1110	0.919	12.6
	.9165	1500	...	12.3
	.9165	1890	...	12.2
			Mean	12.4
75.3	1.0150	1110	0.920	33.0
	1.0150	1920	...	33.0
	1.0150	2880	...	33.1
			Mean	33.0
100	See Table I		Mean	98.7

^a A series of mixed detergents was prepared by blending two of the molecular distillation fractions of polyoxyethylated nonylphenol. The fractions had ethylene oxide mole ratios of 10.7 and 7.6. The fractions were obtained from parent detergents having average ethylene oxide mole ratios of 9.5 and 6.0, respectively. ^b Weight percentages of the blended detergents, of composition given in the first column, present in the aqueous solutions.

detergents having properties most desirable for specific applications.

Acknowledgment.—The authors wish to thank the General Aniline and Film Company and especially Drs. R. L. Mayhew and R. C. Hyatt for making detergent fractions available for this investigation.

MASS SPECTROGRAPHIC DETECTION OF MOLECULAR SPECIES IN GROUP III-V COMPOUNDS

BY A. J. AHEARN AND C. D. THURMOND

Bell Telephone Laboratories, Inc., Murray Hill, New Jersey

Received October 25, 1961

Mass spectroscopy is being employed with increasing frequency in the analysis of solids. For general analytical work, the vacuum spark between electrodes of the sample is proving to be a quite satisfactory positive ion source. This is a high voltage device (50–100 kv.) and produces not only multiply charged atomic ions but also ions of molecular species. For instance, singly charged clusters as large as nine silicon atoms corresponding to mass 252 have been recorded.¹

The high sensitivity for the detection of trace components makes the vacuum spark mass spectrograph a useful instrument for the detection and identification of molecular species despite probable fragmentation of such species by the high voltage

(1) R. Brown, R. D. Craig, J. A. James, and C. M. Wilson, Conference on the Ultrapurification of Semiconductor Materials, Boston, Massachusetts, April, 1961.

spark. In the course of work on III-V compounds the familiar molecular species corresponding to two or more atoms of the Group III element were observed as well as those corresponding to two or more of the Group V element. In addition to these expected species, we wish to report the detection of new molecular species in the vapor phase—ones which we believe have not been reported previously in the literature. These molecules contain both Group III and Group V atoms.

Table I lists the molecular species observed in gallium phosphide and gallium arsenide in the order of decreasing concentration observed. The most abundant species is very roughly estimated to be at concentrations ten thousand times that of the least abundant species. It should be emphasized that these molecular species in this concentration range are revealed by their positive ions and no allowance has been made for the fragmentation of these species that may be appreciable in the vacuum spark. Furthermore, it is possible that these species are formed only as positive ions. The species reported here may or may not exist in a vapor phase in equilibrium with the solid phase.

The mass spectrometer has been used previously to study gas phase species over GaP^2 and GaAs^3

Gallium phosphide	Gallium arsenide
P_2	As_2
$\text{Ga}_2, \text{P}_3, \text{P}_4$	$\text{GaAs}, \text{Ga}_2, \text{As}_2$
GaP	Ga_2As
Ga_2P	
GaP_2	

A heated source was used rather than the vacuum spark. No compound molecular species containing Group III and V atoms were reported. Studies also have been made of InAs^2 , GaSb^2 , InP^3 , and InSb^4 . The molecular species InSb and InSb_2 were reported. In no other system was a compound molecular species observed. The species observed in GaAs and listed in Table I also were detected by J. R. Woolston⁵ by vacuum spark mass spectrometry.

(2) P. Goldfinger, M. Akerman, and M. Jeunehomme, Final Report under contract AF 61(052)-19, ARDC (January, 1959).

(3) J. Drowart and P. Goldfinger, *J. chim. phys.*, **55**, 721 (1958); also, P. Goldfinger and J. Drowart, Final Report under contract AF 61(514)-868, ARDC (October, 1957).

(4) G. DeMaria, J. Drowart, and M. G. Inghram, *J. Chem. Phys.*, **31**, 1076 (1959).

(5) J. R. Woolston, RCA Laboratories, Princeton, New Jersey, private communication.

No. **29** in the
**ADVANCES IN
CHEMISTRY
SERIES**

PHYSICAL PROPERTIES OF CHEMICAL COMPOUNDS—III

This handbook of basic data contains 456 full tables on 434 aliphatic compounds and 22 miscellaneous compounds and elements—all carefully worked out by R. R. Dreisbach of The Dow Chemical Co.

It is a sequel to **PHYSICAL PROPERTIES—II** (Advances No. 22), which covers 476 organic straight-chain compounds, and **PHYSICAL PROPERTIES—I** (Advances No. 15), which presents data on 511 organic cyclic compounds.

This series provides you with a breadth of data that you can get in no other way. For each compound 15 physical properties are given: purity—freezing point—vapor pressure—liquid density—vapor density—refractive index—rate of change of boiling point with pressure—latent heat of fusion—latent heat of evaporation—critical values—compressibility—viscosity—heat content—surface tension—solubility. Parameters are also furnished for interpolating and extrapolating determined data for almost all the compounds. To get this information by ordinary means you would have to seek out many sources.

PHYSICAL PROPERTIES—III offers the extra advantage of a cumulative index to **all three volumes** (1443 compounds and elements). Use it and the earlier compilations to save yourself hours of laboratory time, and to answer questions quickly.

489 pages.

Cloth bound.

Price: \$6.50

Physical Properties—II — 491 pages • cloth bound • price \$6.50

Physical Properties—I — 536 pages • cloth bound • price \$5.85

Order from:

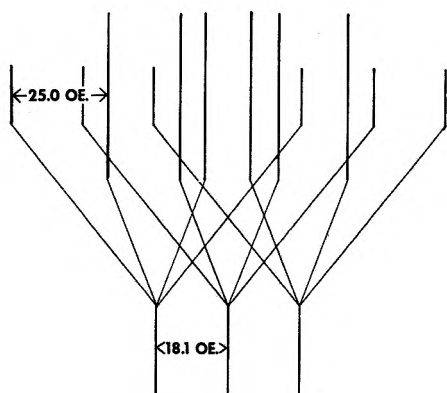
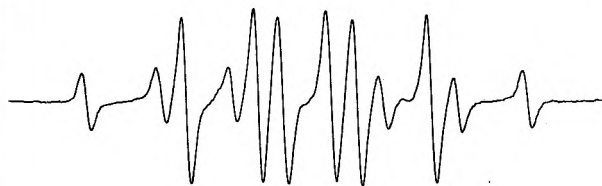
Special Issues Sales / American Chemical Society / 1155 Sixteenth Street, N.W. / Washington 6, D.C.

RADIATION DAMAGE STUDIES WITH HIGH SENSITIVITY EPR

When non-metallic solids are exposed to u-v, γ rays, x rays, electrons, etc., the electronic structure often is altered in such a way that configurations containing unpaired electrons are formed. These may be investigated by EPR and such studies often yield detailed information on structure and stability of the damage center. The Varian 100 kc EPR Spectrometer has been widely used in this type of research.

EXAMPLE

EPR observation of NH_3^+ formed by x ray irradiation of ammonium perchlorate crystals



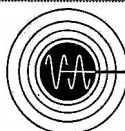
Ammonium perchlorate is a compound of particular interest in the world of missile technology. Freeman *et al.*⁽¹⁾ have reported profound changes in the stability or chemical reactivity of ammonium perchlorate crystals following x ray and γ ray irradiation. An EPR investigation was undertaken in an effort to understand the nature of the radiation damage in these crystals⁽²⁾.

The figure shows the EPR spectrum obtained at room temperature from a single crystal of irradiated ammonium perchlorate. The spectrum is that expected from hyperfine interaction with one nucleus of spin 1 and three equivalent nuclei of spin $1/2$, and almost certainly arises from an unpaired electron spin strongly localized on an NH_3 molecule. Contact with the nitrogen nucleus splits the spectrum into three lines of equal spacing and intensity, and contact with the three equivalent protons splits each of these three lines into a quartet of equally spaced lines with intensity ratios of 1:3:3:1. This analysis is illustrated in the figure. From consideration of the energies involved, it is probable that the radical is a positive ion, although the EPR technique would not distinguish it from a negative ion.

The discovery of the NH_3^+ positive ion has considerable intrinsic interest since it is a new member of the widely investigated ammonium system. Not only are the values of the splitting constants of significance to the theoretical chemist, but also the center was stable at the highest temperatures reached by Hyde and Freeman ($+125^\circ\text{C}$) and it seems likely that further work at higher temperatures will permit correlation with the reactivity studies of Freeman.

- (1) E. S. Freeman and D. A. Anderson, *J. Phys. Chem.* **63**, 1844 (1959). E. S. Freeman, D. A. Anderson, and J. J. Campisi, *J. Phys. Chem.* **64**, 1727 (1960).
- (2) J. S. Hyde and E. S. Freeman, *J. Phys. Chem.* **65**, 1636 (1961).

For literature which fully explains the 100 kc EPR Spectrometer and its application to basic and applied research in physics, chemistry, biology and medicine, write the Instrument Division.



VARIAN associates
PALO ALTO 52, CALIFORNIA